Formulation Studies and Development of Novel Anticancer Prodrugs

Asma Patel

Submitted in fulfilment of the requirements

for the degree of Doctor of Philosophy

De Montfort University

April 2007

Acknowledgements

I would like to thank both of my supervisors for affording me the privilege of working in the Cancer Drug Discovery Group, Leicester School of Pharmacy at De Montfort University. To my 1st supervisor Dr Peter Taylor thank you for your guidance, encouragement and unwavering support throughout my research. To my 2nd supervisor Prof Gerry Potter thanks for inspiring my PhD with your genius. To the past and present members of the Cancer Drug Discovery Group thank you for providing motivation, inspiration, support and laughs. Special thanks go to Dr Taeeba Ijaz, Saba Lodhi, Ketan Ruparelia, and Dr Hoon Tan for the scale-up chemistry, especially Ketan who put up with my 'requests' for compounds and guided me through the world of organic chemistry. Thanks to Dr Paul Butler and Dr Nektaria Papadopoulou for their work with the cell-lines. Finally thanks to Dyan Ankrett, Somchaiya Surichan and Dr Nicola Wilsher for HPLC training and insights into drug metabolism.

I also wish to thank Dr Walkiria Schlindwein for DSC training. Thank you to the Leicester School of Pharmacy technicians for letting me 'borrow' chemicals and equipment, a special thank you to Dr Mike Needham and Sonia Nuttall for NMR analysis and SEM imaging.

Last but not least I am immensely grateful to my parents, who have always encouraged me and nurtured my ambitions and thanks to my sisters Rizvana and Azima for listening to me through all of my most trying times.

Abstract

This thesis describes the preformulation and formulation studies of a series of novel tumour-selective anticancer prodrugs. The increased understanding of the genomics and molecular pathology of cancer has shifted the focus of cancer drug development from an empirical to a mechanistic viewpoint. The tumour-specific expression of CYP1B1 provides the opportunity for selective chemotherapy. The suitability for development of lead compounds DMU135, DMU212, DMU590, DMU949 and DMU982 was evaluated by solubility, pH-solubility profiles, log *P*, pKa, polymorphism, morphology and cytotoxicity.

The lead compound DMU212, a non-ionisable stilbene was poorly water soluble, lipophilic and thermodynamically stable with no polymorphic variants. It was possible to formulate DMU212 in oral (capsules containing sorbitol as the diluent) and topical preparations (anionic o/w cream), therefore, DMU212 was recommended for further development. The ionisable morpholine derivative of DMU212 - DMU590 was 120 times more water soluble than DMU212. Thermodynamic evaluation showed DMU590 to exist in an amorphous form. DMU590 salt screening studies yielded a phosphate salt. However, *in vivo* studies showed that it is not a candidate for further development.

The non-ionisable chalcone DMU135 was poorly water soluble, lipophilic and thermodynamically stable with no polymorphic variants. However, DMU135 underwent photo-isomerization under ambient light conditions and was therefore not a candidate for further development. The non-ionisable pyridone derivative of DMU135 – DMU949 was also poorly water soluble and lipophilic. Thermodynamic evaluation showed DMU949 to have two polymorphs. To overcome the tautomeric nature of DMU949, analogues of DMU949 were designed in a double-prodrug strategy. Metabolic evaluation of these analogues showed that the strategy was unsuccessful, since the *in vitro* re-conversion to DMU949 was not observed. Thus, DMU949 was eliminated as a lead candidate. The ionisable pyridine derivative of DMU135 - DMU982 was poorly water soluble, lipophilic and thermodynamically stable with no polymorphic variants. DMU982 salt screening studies yielded ten salts, where the maleate was recommended for further development.

The development challenges associated with non-ionisable chalcones were also addressed with the synthesis of novel ionisable chalcones, based on the recently constructed CYP1B1 pharmacophore model. The 2-imidazole positions were found to be highly important in CYP1B1 bioactivation compared to the 4-imidazole position. This structure activity relationship helped to confirm a necessary hydrogen-bonding interaction near the aromatic 'A' ring hydroxylation hotspot for CYP1B1 bioactivation. Optimum bioactivity was observed with DMU2149, which was thermodynamically stable. DMU2149 salt screening studies yielded eleven salts, but due to the lower cytotoxicity of DMU2149 compared with other lead prodrugs, it was not selected for further development.

Another strategy implemented in this study to accelerate drug preformulation and formulation assessment, was novel use of high-throughput analytical technologies. A high-throughput method using a 96-well fluorescent plate reader was successfully used for log *P* quantification. Novel uses were also successfully developed for the 96-well UV plate reader firstly in solubility and pKa quantification, and secondly in high-throughput capsule formulation screening. Finally, the MTT assay determined formulation effects on active drug CYP1 enzyme selectivity.

The current research shows DMU212 and DMU982 have the optimum potency and physicochemical properties in a series of lead compounds, and have the greatest potential for eventual clinical use.

Table of Contents

List of Figures

List of Tables

List of Symbols and Abbreviations

A	effective surface area
ADEPT	antibody-directed enzyme prodrug therapy
AhR	aryl hydrocarbon receptor
ANOVA	analysis of variance
AQ4	(1,4-bis[2-(dimethylamino)ethyl]amino-5,8-dihydroxyanthracene-9,10-dione)
AQ4N	(1,4-bis[2-(dimethylamino)ethyl]amino-5,8-dihydroxyanthracene-9,10-dione-bis-*N*-oxide)
ARNT	aryl hydrocarbon receptor nuclear translocator
Ar	aromatic
[B]	concentrations of free species of the base
[BH^+]	concentrations of protonated species of the base
BP	British Pharmacopoeia
C	drug concentration in the bulk of the dissolving medium
C_O	equilibrium concentration of drug in the organic phase (Chapter 2)
C_O	initial drug concentration in the topical vehicle (Chapter 4)
C_S	saturation solubility of the drug in the dissolution medium
C_V	concentration of drug in the topical vehicle
C_w	equilibrium concentration of drug in the aqueous phase (Chapter 2)
CA-4	combretastatin A-4
CB1954	5-(aziridin-1-yl)-2,4-dinitrobenzamide
CDDG	cancer drug discovery group
CDK	cyclin dependent kinase
cDNA	copied deoxyribonucleic acid
CMDA	4-[*N*-(2-chloroethyl)-*N*-[2-(mesyloxy)ethyl-]amino]benzoyl-L-glutamic acid
CS	critical supersaturation
CTAB	cetyltrimethylammonium bromide
CTRL	control microsomes
CYP	cytochrome P450
D	diffusion coefficient of the drug
dC/dt	rate of dissolution of the drug particles
dm/dt	cumulative amount of drug passing through a unit area of membrane as a function of time
DCM	dichloromethane
DELTA C_p/ ΔC_p	heat capacity increment
DMSO	dimethylsulfoxide
DMU	de montfort university
DNA	deoxyribonucleic acid
DPD	dihydropyrimidine dehydrogenase
DSC	differential scanning calirometry
E_2	17β-estradiol
E. coli	*Escherichia coli*
EDTA	ethylenediaminetetraacetic acid
EGFR	epidermal growth factor receptor
EGF	epidermal growth factor

EROD	7-ethoxyresorufin-*O*-deethylase
eq	equimolar
EtOH	ethanol
FACS	fluorescence activated cell sorter
FDA	Food and Drug Administration
FPR	fluorescent plate reader
FTIR	fourier transform infrared
G proteins	guanine nucleotide binding proteins
GDEPT	gene-directed enzyme prodrug therapy
GDP	guanine diphosphate
GI	gastrointestinal
Grb2	growth factor receptor-bound protein 2
GST	glutathione *S*-transferase
GTP	guanine triphosphate
h	thickness of the boundary layer adjacent to the dissolving surface (Chapter 3)
h	thickness of the membrane (Chapter 4)
HCl	hydrochloric acid
HER2	human epidermal growth factor receptor 2
HIF1α	hypoxia-inducible factor 1a
HPLC	high pressure liquid chromatography
IC_{25}	concentration that causes 25% inhibiton
IC_{50}	concentration that causes 50% inhibiton
IPA	isopropyl alcohol
IPM	isopropyl myristate
IR	infrared
J	steady-state flux
K	partition coefficient of the drug
KBr	potassium bromide
KH_2PO_4	potassium dihydrogen orthophosphate
log P	partition coefficient
LC/MS	liquid chromatography/mass spectrometer
m	cumulative amount of drug passing through a unit area of membrane
mAb	monoclonal antibody
MALDI	matrix assisted laser desorption ionisation
MAPK	mitogen-activated protein kinase
MEK	extracellular signal-regulated protein kinase
$MgCl_2$	magnesium chloride
mRNA	messenger ribonucleic acid
MTT	3-(4,5-dimethylthiazol-2-yl) 2,5-diphenyltetrazolium bromide
NADPH	β-nicotinamide adenine dinucleotide phosphate reduced tetrasodium salt
Na_2HPO_4	disodium hydrogen orthophosphate
NaOH	sodium hydroxide
NCE	new chemical entity
NMP	N-methyl pyrrolidone
NMR	nuclear magnetic resonance
o/w	oil-in-water
Q	amount of drug released per unit area

p	probability
PAH	polcyclic aromatic hydrocarbons
PCR	polymerase chain reaction
PHLM	pooled human liver microsomes
pH_{max}	pH of maximum solubility
pKa	acid dissociation constant
PTK	protein tyrosine kinase
PEG	polyethylene glycol
PDGFR	platelet derived growth factor receptor
RB	retinoblastoma
rpm	revolutions per minute
RTK	receptor tyrosine kinase
S	solubility of the drug at different pH values
S_O	solubility of the unionised form of the drug in water
S_T	total saturation solubility of drug at any given pH
SAR	structure activity relationship
SE	solution equilibrium
SEM	scanning electron micrograph
SH2	*src* homology 2 domain
SLS	sodium lauryl sulfate
SOS	guanine nucleotide release protein
t	elapsed time
TCDD	2,3,7,8 tetrachloro dibenzo-*p*-dioxin
TER286	γ-glutamyl-α-amino-β(2-ethyl-*N*,*N*,*N*',*N*'-tetrakis(2-chloroethyl)phosphoro-diamidate)-sulfonyl-propionyl)-(*R*)-(-)phenylglycine
T_g	glass transition temperature
TLC	thin layer chromatography
TP	thymidine phosphorylase
U	unsaturation point
UV	ultraviolet
UVS	ultraviolet spectrophotometer
UVPR	ultraviolet plate reader
VDEPT	virus-directed enzyme prodrug therapy
w/o	water-in-oil
δ	solubility parameter
λ_{max}	wavelength of maximum absorption
ΔH	enthalpy of fusion
2D	two dimensional
2-OHE_2	2-hydroxyestradiol
4-OHE_2	4-hydroxyestradiol
5-FU	5-Flurouracil

CHAPTER 1

Cancer and the Quest for Tumour

Selective Chemotherapy

1.1 Cancer

1.1.1 Cancer epidemiology

Cancer is a generic term for a group of more than 200 diseases characterized by uncontrolled proliferation of abnormal cells that have undergone multiple genetic changes, enabling them to negate the homeostatic regulation of normal cell division, invade nearby tissues and metastasise to distant sites in the body [1].

Cancer is the second leading cause of mortality after heart disease in the United Kingdom, contributing to more than a quarter (26%) of all deaths in 2003. Furthermore, one third of all individuals in the UK will develop cancer in their lifetime [2]. Lung (22%), colorectal (10%), breast (8%) and prostate cancer (7%) are the most prevalent forms of the disease accounting for almost half of all mortalities (Figure 1):

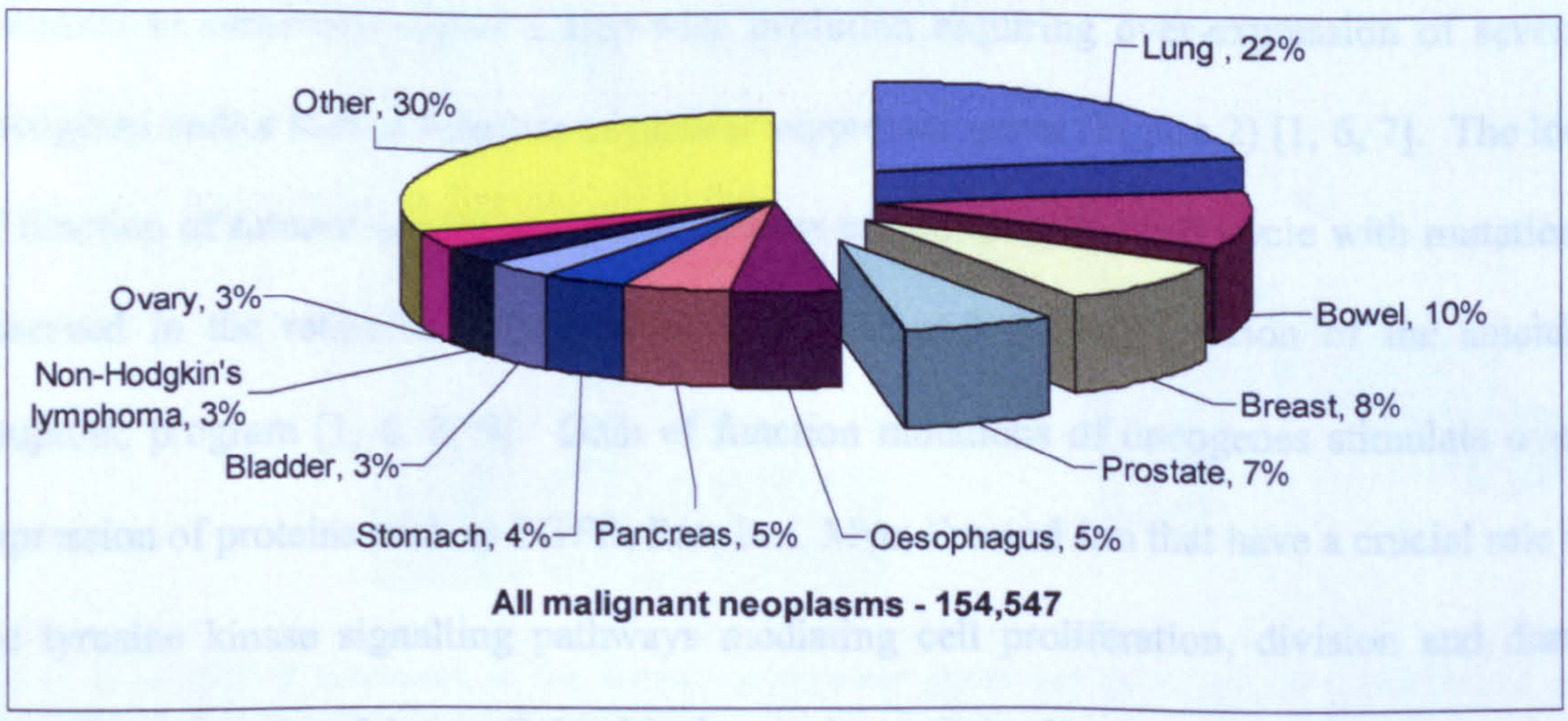

Figure 1. UK mortalities in 2003 from cancer [3].

Progressions in diagnosis, surgery, radiotherapy and chemotherapy have reduced the overall cancer mortality rate over the last 20-50 years [4], nonetheless, death rates remain

high and the chemotherapeutic realization is relatively unmet. The main reasons for this being the lack of tumour selectivity resulting in systemic toxicity; metastasis; multi-drug resistance and the heterogeneity of the disease [5]. A potential strategy to overcome these limitations is the rational and mechanistic development of drugs that target the molecular circuitry of cancer cells as opposed to normal cells. The intellectual framework provided by this phenomenon promises to deliver therapeutic agents which are less toxic and more effective than current drugs available on the market. Research from the Human Genome project could have a potential input on the effort to identify more tumour specific molecules.

1.1.2 The molecular circuitry of cancer

A single mutation alone is not enough to cause cancer, for most cancers the transition from a normal to cancerous cell is a step-wise evolution requiring over-expression of several oncogenes and/or loss of function of tumour suppressor genes (Figure 2) [1, 6, 7]. The loss of function of tumour suppressor genes reduces control over the cell cycle with mutations observed in the retinoblastoma protein (RB) and p53 causing evasion of the suicidal apoptotic program [1, 6, 8, 9]. Gain of function mutations of oncogenes stimulate over-expression of proteins such as EGFR, Ras, Raf, Myc, Fos and Jun that have a crucial role in the tyrosine kinase signalling pathways mediating cell proliferation, division and death through a cascade of intracellular biochemical reactions [1, 6, 9-11]. Both mutations ultimately result in escape from normal growth control, evasion of apoptosis, induction of angiogenesis and the ability to metastasise and invade healthy tissue [12].

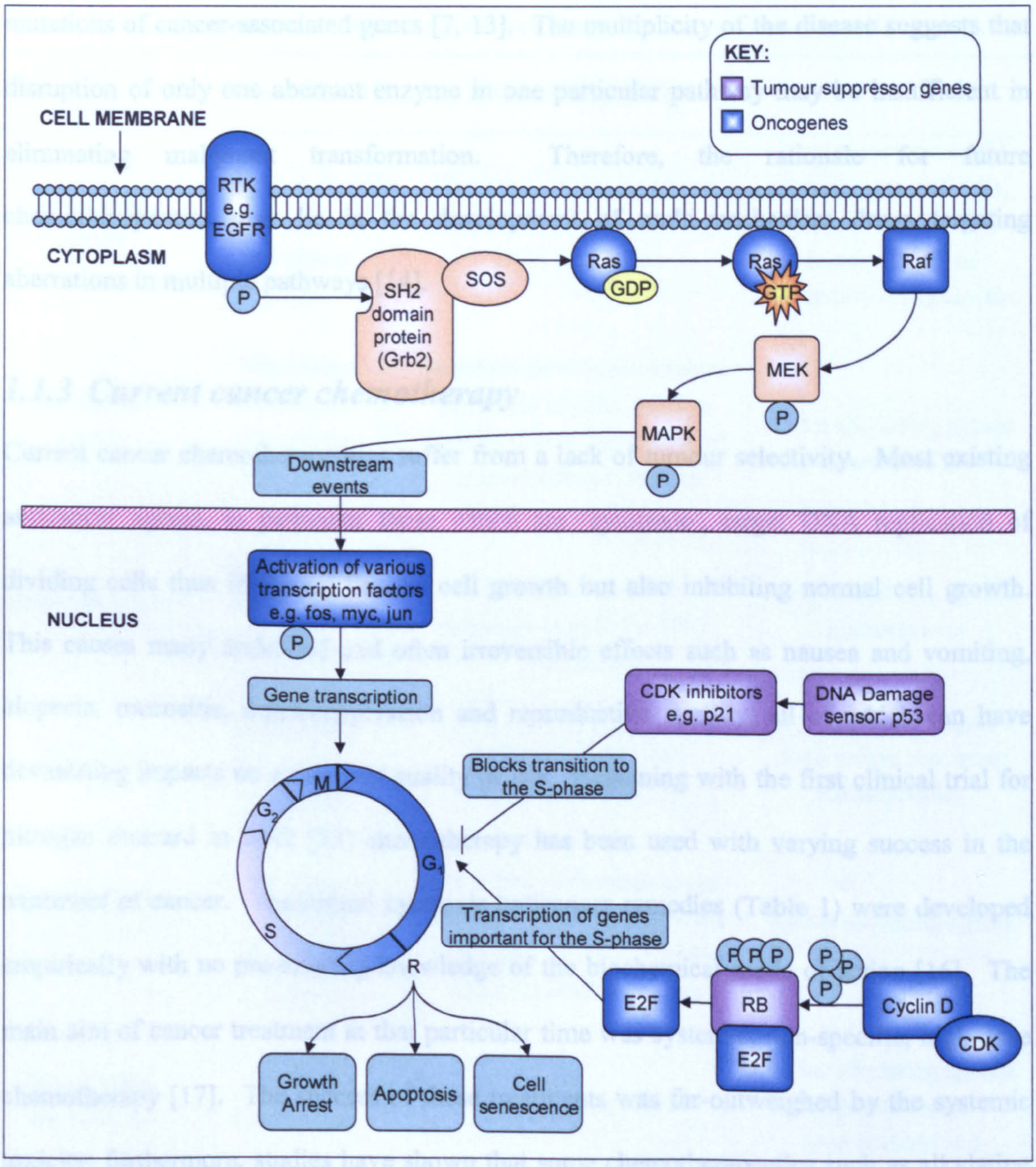

Figure 2. Simplified schematic of the tumour suppressor genes and oncogenes involved in the cell signalling cascade adapted from [1], [6] and [7].

The molecular circuitry of cancer (Figure 2), encompasses a complex architecture of signalling cascades consisting of interacting networks [12], involving multiple steps and genetic events. Studies have shown that the initiation of carcinogenesis requires at least 4-6

mutations of cancer-associated genes [7, 13]. The multiplicity of the disease suggests that disruption of only one aberrant enzyme in one particular pathway may be insufficient in eliminating malignant transformation. Therefore, the rationale for future chemotherapeutics may lie in the development of multi-mechanism drugs targeting aberrations in multiple pathways [14].

1.1.3 Current cancer chemotherapy

Current cancer chemotherapeutics suffer from a lack of tumour selectivity. Most existing anticancer agents, in particular those which are 'cytotoxic', target DNA replication of dividing cells thus inhibiting tumour cell growth but also inhibiting normal cell growth. This causes many undesired and often irreversible effects such as nausea and vomiting, alopecia, mucositis, myelosuppression and reproductive sterility, all of which can have devastating impacts on a patient's quality of life. Beginning with the first clinical trial for nitrogen mustard in 1942 [15] chemotherapy has been used with varying success in the treatment of cancer. Traditional cytotoxic anticancer remedies (Table 1) were developed empirically with no pre-existing knowledge of the biochemical mode of action [16]. The main aim of cancer treatment at that particular time was systemic, non-specific, high-dose chemotherapy [17]. The success of these treatments was far-outweighed by the systemic toxicity; furthermore, studies have shown that some chemotherapeutics such as alkylating agents are capable of inducing secondary malignancies [18, 19].

Table 1. Summary of traditional cytotoxic agents, their mode of action and side-effects [18, 20, 21].

CLASS OF DRUG	EXAMPLES	MODE OF ACTION	SIDE EFFECTS
Alkylating agents	Cyclophosphamide Chlorambucil Melphalan	Formation of covalent bonds with DNA, thus impeding DNA replication	Myelosuppression, GI disturbances, hair loss, reduced fertility and increased risk of secondary malignancies
Antimitotic agents	Vincristine Vinblastine Docetaxel Paclitaxel	Interference with microtubule assembly of cells, through stabilisation or destabilisation of microtubules, thereby blocking cell division	As for alkylating agents; neurotoxicity
Antimetabolites	Methotrexate 5-Flurouracil 6-Mercaptopurine	Inhibition of metabolic pathways involved in DNA synthesis	As for alkylating agents; nephrotoxicity
Antibiotics	Doxorubicin Mitoxantrone Mitomycin	Prevent cell division	As for alkylating agents; doxorubicin can cause cardiotoxicity
Topoisomerase inhibitors	Podophyllotoxin Etoposide Irinotecan	Inhibition of topoisomerase leading to deregulation in the unwinding of DNA, thereby blocking DNA synthesis	As for alkylating agents
Heavy Metal Derivatives	Cisplatin Carboplatin	As metallating agents	As for alkylating agents; nephrotoxicity, neurotoxicity and potential hearing loss

Over the past decade the increased understanding of the genomics and molecular pathology of cancer [14] has shifted the ethos of cancer drug development from an empirical to a mechanism based viewpoint. This has resulted in a new generation of chemotherapeutics

that act on specific molecular targets responsible for the malignant phenotype, to potentially provide tumour specific therapy (Table 2):

Table 2. Summary of currently available targeted cancer treatments [17, 20, 22, 23].

CLASS OF DRUG	EXAMPLES	MODE OF ACTION	SIDE EFFECTS
Hormonal Therapies	Tamoxifen	Blocks estrogen action in breast cancer	Endometrial cancer, blood clots, hot flushes
	Letrozole Arimidex	Inhibits aromatase, thus blocking the production of estrogen	Hot flushes, fatigue, GI disturbances
	Bicalutamide	Blocks androgen action in prostate cancer	Hot flushes, impotence
Signalling Inhibitors	Imatinib	Blocks activation of Abl, PDGFR and c-Kit to inhibit cell division in chronic myeloid leukaemia	Fluid retention, skin rashes, diarrhoea, GI disturbances
	Gefitinib	Blocks activation of the EGFR, thus inhibiting tyrosine kinase activity and ultimately cell division	Skin rashes, diarrhoea, GI disturbances
Monoclonal Antibodies	Rituximab	Antibody binds to CD20 antigen on lymphocyte derived tumours to induce cell death	Allergic response
	Trastuzumab	Blocks HER2 receptor on breast cancer cells, thus preventing activation by EGF	
	Gemtuzumab ozogamicin	Antibody binds to CD33 antigen on leukaemic cells and delivers a toxic dose of calicheamicin an anti-tumour antibody to the leukaemic cell	
Differentiating Agents	Tretinoin	Induces differentiation and death of leukaemic cells	Fever, severe respiratory distress, weight gain

Theoretically, use of these putative tumour specific chemotherapeutic agents, whether alone or in combination, should lead to an improved clinical response. However, the expression of the target proteins is not exclusive to cancer cells alone. The proteins are over-expressed in cancer cells but also expressed at a lower frequency in normal cells. A potential strategy to overcome these limitations and further the quest for tumour selective chemotherapy is the use of prodrugs [16].

1.2 Prodrugs versus active drugs

The term prodrug was first coined in the 1950s by Albert [24]. Prodrugs are inactive derivatives of drug molecules requiring chemical/biological transformation *in vivo* in order to release the active moiety. The prodrug is usually designed to improve an inadequate physicochemical property. However, prodrugs can also be designed to achieve target organ selectivity through the 'magic bullet' concept i.e. selective action. Most anticancer agents in clinical use exert their effects through anti-proliferative action interfering with DNA mechanisms; these drugs are not 'magic bullets' and have severe systemic toxic effects. Therefore, development of prodrugs has the scope for improving the safety and efficacy of chemotherapeutic agents for the treatment of cancer.

1.2.1 Design and development of anticancer prodrugs

In the last century several anticancer prodrug strategies were developed for tumour selective chemotherapy [25]. The emergence of proteomic and genomic technology has led to a better understanding of tumour biology, thereby improving chemotherapeutic

selectivity. Some of the prodrug activation mechanisms include tumour hypoxia and tumour specific exogenous or endogenous enzyme expression.

1.2.1.1 Hypoxia selective prodrugs

Hypoxia is a unique property of cells in solid tumours which have poorly developed vasculature and therefore reduced oxygen supply compared to normal tissues. This provides a unique environment which is potentially exploitable in solid-tumour selective chemotherapy such as with bioreductive prodrugs (Figure 3).

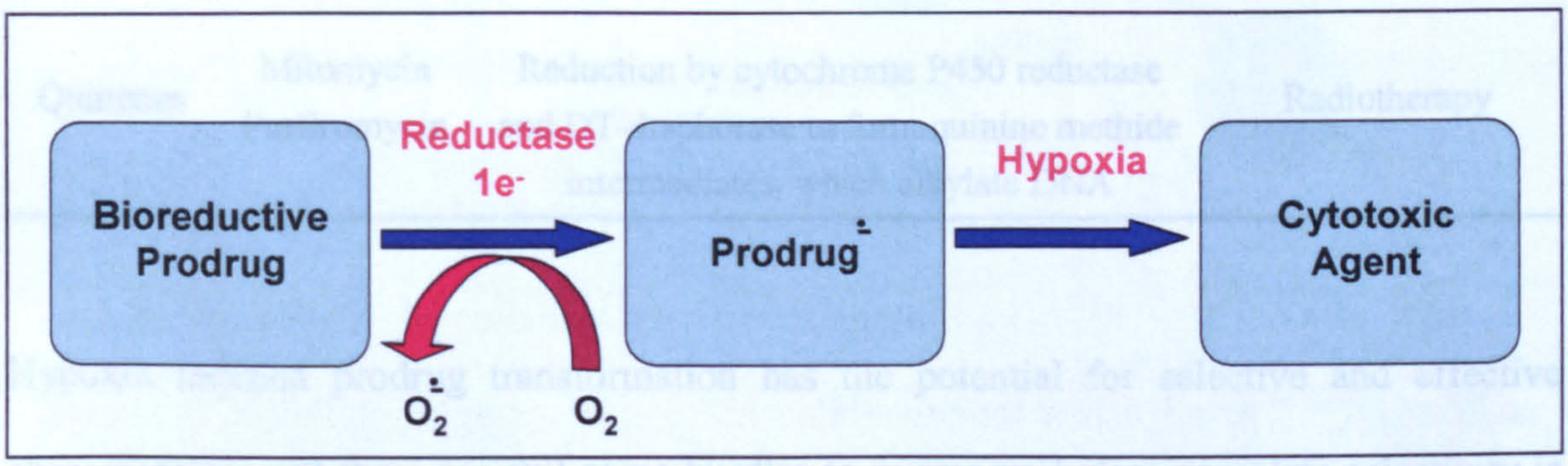

Figure 3. The hypoxia-mediated activation of bioreductive drugs to give cytotoxic compounds [26].

Bioreductive prodrugs are activated to cytotoxic agents by reductase enzymes to free radical intermediates, which are rapidly back-oxidised to the parent prodrug by molecular oxygen present in normal cells, therefore restricting prodrug activation to hypoxic cells [16, 26-28]. Currently four classes of such anticancer prodrugs are undergoing clinical or preclinical evaluation (Table 3).

Table 3. Summary of bioreductive prodrugs undergoing clinical and pre-clinical evaluation [16, 25-30].

CLASS OF DRUG	EXAMPLES	MODE OF ACTION	COMBINATION THERAPY
Nitro-aromatics	CB1954	Reduction by DT-diaphorase to a cytotoxic DNA alkylating agent	ADEPT, GDEPT in combination with *E. coli* nitroreductase
Aromatic N-oxides	Tirapazamine	Reduction by cytochrome P450 reductase to form nitroxide radicals, which alkylate DNA	Cisplatin, radiotherapy
Aliphatic N-oxides	AQ4N	Reduction by CYP3A isoforms to generate the cationic diamine AQ4 a potent topoisomerase II inhibitor	Cisplatin, Cyclophosphamide, radiotherapy
Quinones	Mitomycin Porfiromycin	Reduction by cytochrome P450 reductase and DT-diaphorase to form quinine methide intermediates, which alkylate DNA	Radiotherapy

Hypoxia induced prodrug transformation has the potential for selective and effective chemotherapy, yet there are still some hurdles to overcome before complete selectivity is achieved. One of the problems is the ubiquitous expression of the reductase enzymes, therefore prodrugs activated by these enzymes may cause side-effects [16]. Another problem is the reliance of the treatment on consistently low levels of oxygen in the tumour, which will suffer from inter-individual variance, furthermore, solid tumours generally have a hypoxia gradient, therefore, potentially a rim of tumour cells in non-hypoxic conditions may remain untreated [26, 29]. An alternative approach to directly targeting hypoxic tumours is to have the appropriate reductive enzyme transcribed or translated by a hypoxia specific-transcription factor such as HIF-1α. Therefore, the expression of that particular enzyme would be tumour specific as would the consequent prodrug bioactivation [28, 29].

1.2.1.2 Prodrugs activated by tumour targeted exogenous enzymes

Tumour specific antigens can be exploited for tumour selective cytotoxicity through antibody-directed enzyme prodrug therapy (ADEPT). A monoclonal antibody (mAb) is covalently linked to a chosen exogenous enzyme and is administered followed by a prodrug which is selectively bioactivated by the enzyme extracellularly at the tumour site (Figure 4) [16, 25, 31, 32].

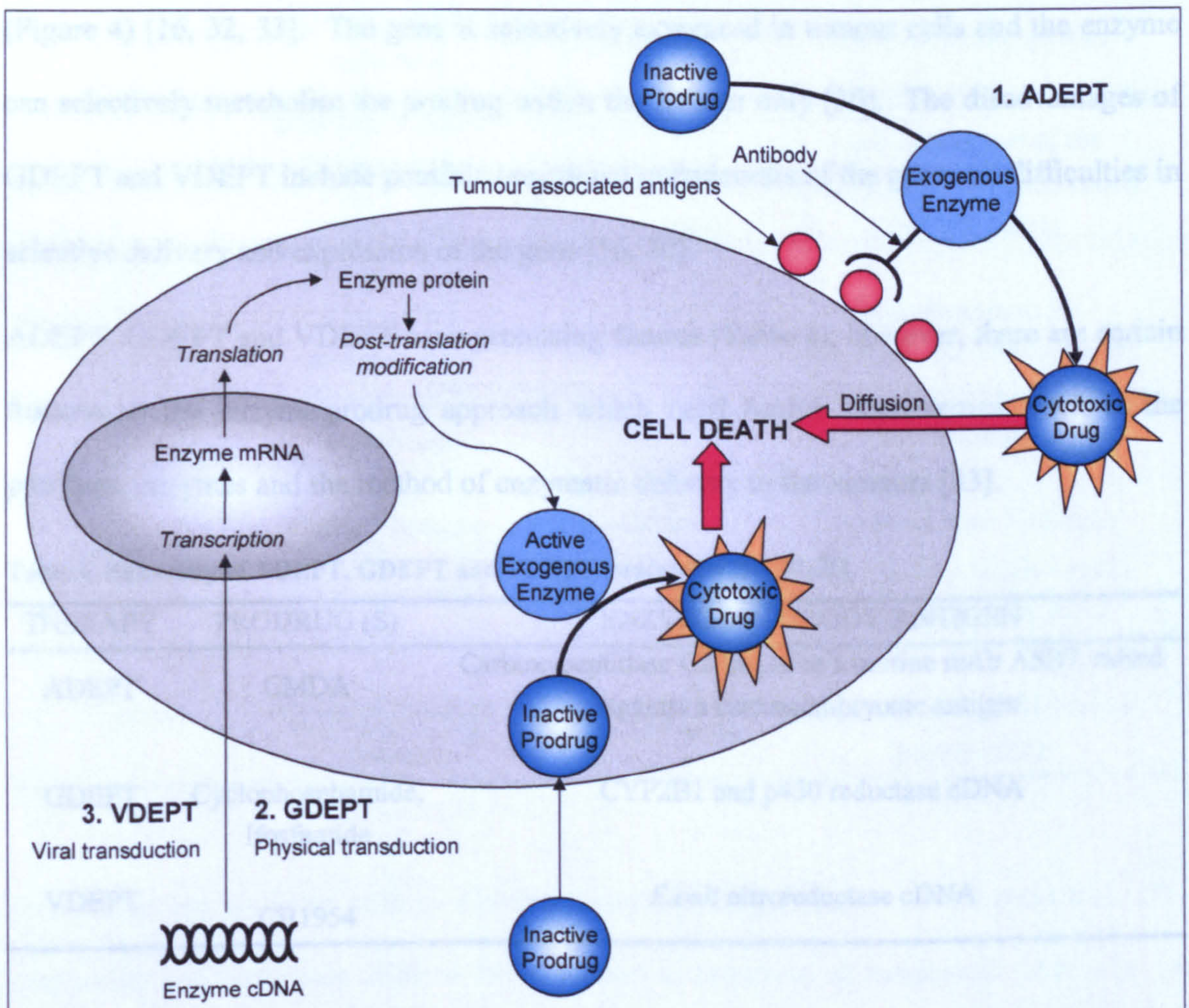

Figure 4. Principles of drug targeting, using ADEPT, GDEPT and VDEPT adapted from [16] and [33].

The disadvantages of ADEPT include possible immunogenic response to the enzyme-antibody conjugate, scarcity of tumour selective antigens and the extracellular activation of drug necessitating diffusion into the tumour [31, 32].

Other tumour-targeted exogenous enzyme approaches include gene-directed enzyme prodrug therapy (GDEPT) and virus-directed enzyme prodrug therapy (VDEPT), both of which involve incorporation of the exogenous enzyme gene into the tumour genome (Figure 4) [16, 32, 33]. The gene is selectively expressed in tumour cells and the enzyme can selectively metabolise the prodrug within the tumour only [30]. The disadvantages of GDEPT and VDEPT include possible insertional mutagenesis of the gene and difficulties in selective delivery and expression of the gene [16, 30].

ADEPT, GDEPT and VDEPT have promising futures (Table 4); however, there are certain features of the enzyme/prodrug approach which need further improvement such as the prodrugs, enzymes and the method of enzymatic delivery to the tumours [33].

Table 4. Summary of ADEPT, GDEPT and VDEPT treatments [16, 31-35].

THERAPY	PRODRUG (S)	ENZYME/ANTIBODY/ANTIGEN
ADEPT	CMDA	Carboxypeptidase G2 linked to a murine mAb A5B7, raised against a carcinoembryonic antigen
GDEPT	Cyclophosphamide, Ifosfamide	CYP2B1 and p450 reductase cDNA
VDEPT	CB1954	*E.coli* nitroreductase cDNA

1.2.1.3 Prodrugs activated by tumour specific endogenous enzymes

Endogenous tumour specific enzymes have been exploited in prodrug design to achieve selective bioactivation within the tumour resulting in selective cytotoxicity. Some of the enzymes used include oxidoreductases, transferases, hydrolases and lyases [16, 25]:

Table 5. Summary of prodrugs activated by endogenous enzymes [16, 36, 37].

CLASS	ENZYME	PRODRUG	MODE OF ACTION
Oxidoreductases	DT-diaphorase	CB1954	DNA alkylation/hypoxia
	Cytochrome P450 reductase	Tirapazamine	DNA alkylation/hypoxia
	Dihydropyrimidine dehydrogenase	5-Ethynyl-2(1H)-pyrimidinone	Inhibitor of DPD preventing the rapid breakdown of the antimetabolite 5-Fluorouracil
	Tyrosinase	Phenyl mustards	DNA alkylation
Transferases	Thymidine phosphorylase	Capecitabine	Bioactivation to the antimetabolite 5-Fluorouracil
	Glutathione *S*-transferase	TER286	Bioactivation to an aziridinium DNA alkylating agent
Hydrolases	Carboxylesterase	Irinotecan	Topoisomerase I inhibitor
	β-Glucuronidase	Paclitaxel glucuronide	Bioactivation to paclitaxel a potent antimitotic agent
Lyases	Cysteine conjugate β-lyase	SeCys conjugates	Apoptosis inducer and cancer preventative

Oxidoreductase enzymes such as dihydropyrimidine dehydrogenase, P450 reductase, DT-diaphorase and tyrosinase catalyse the oxidation or reduction of xenobiotic substrates. A major problem with dihydropyrimidine dehydrogenase is its ubiquitous expression and as such it is not an ideal target enzyme for prodrug selectivity. P450 reductase and DT-

diaphorase activate bioreductive prodrugs (Section 1.2.1.1). These enzymes are also widely distributed; however, prodrug activation requires both enzymatic reduction and hypoxic conditions, which are unique to solid tumours. Finally, tyrosinase is localised in melanoma cells and the degree of enzyme expression has been correlated with malignancy, making this enzyme a viable target for chemotherapeutic prodrug design [16].

Transferase enzymes such as thymidine phosphorylase (TP) and glutathione *S*-transferase (GST) are over-expressed in tumours relative to the host cell. However, TP is widely expressed in intestinal tissue; therefore, chemotherapeutics activated by this enzyme may instigate gastrointestinal toxicity. GST is also widely distributed in normal tissue; however, the GST polymorph GSTπ1-1 is over-expressed in tumours indicating the clinical potential of this enzyme in tumour selective therapy [16, 36, 37].

Hydrolytic enzymes such as carboxylesterase and β-glucuronidase are ubiquitous [25] and as such these enzymes cannot be used to activate prodrugs locally, except when targeted to tumours by ADEPT, GDEPT or VDEPT strategies [16]. Finally, lyase enzymes such as cysteine conjugate β-lyase are over-expressed in renal carcinoma tissue compared to normal tissue, thereby indicating their potential in kidney-tumour selective therapy [16].

Theoretically, exploitation of these tumour specific enzymes should amount to non-toxic prodrugs. However, inconsistent patterns of enzyme expression have limited the attempts to develop endogenous enzyme activated prodrugs so far [28]. Nevertheless, the cytochrome P450 (CYP) enzymes which are responsible for the majority of phase I drug (chemotherapeutic) metabolism may provide an alternative prodrug design strategy [38, 39].

1.2.1.3.1 Prodrugs activated by CYPs

Cytochrome P450 (CYP) comprises a superfamily of constitutive and inducible enzymes involved in the oxidative metabolism of xenobiotic and endogenous substrates [40]. The tumour specific over-expression of individual CYP isozymes increases the potential for tumour selective chemotherapeutic metabolism, resulting in either detoxification or bioactivation of chemotherapeutics [41, 42].

CYP mediated detoxification of anticancer prodrugs involves clearance of cytotoxics from the body [39]. The antimitotic agent taxol undergoes detoxification catalysed by CYP2C8, generating the metabolite 6-hydroxytaxol, which is 30 times less active than taxol [43]. Several clinical trials are investigating the co-administration of taxol with P450 inhibitors to alleviate drug inactivation [44]. In separate studies clearance of the anticancer prodrug irinotecan was considerably reduced when co-administered with CYP3A4 inhibitors ketoconazole or cyclosporin A [39, 44].

Some anticancer prodrugs are metabolically activated by CYPs. In particular the alkylating agents cyclophosphamide and ifosfamide are activated by CYP2B6 and CYP3A4 to yield the 4-hydroxy metabolites which undergo spontaneous degradation to generate the ultimate cytotoxins phosphoramide mustard and acrolein [16, 45]. The antiestrogen tamoxifen also undergoes 4-hydroxylation induced by CYP3A4, CYP2D6, and CYP2C9 to *trans*-4-hydroxytamoxifen, which is 100 times more potent as an estrogen inhibitor than tamoxifen [45]. These prodrugs were not actually designed as prodrugs but are serendipitously bioactivated by CYPs and as such the bioactivation is mostly systemic and non-specific

[39]. Conversely, the next generation of CYP activated anticancer prodrugs have been intentionally designed to undergo tumour specific bioactivation.

Phortress is a novel benzothiazole derivative capable of inducing CYP isozymes that mediate its bioactivation [46, 47]. It is a potent agonist of the ligand activated transcription factor aryl hydrocarbon receptor (AhR), which forms a heterodimer with the AhR nuclear translocator (ARNT) to induce CYP1A1 and CYP1B1 expression resulting in intratumoural bioactivation of Phortress and thus initiating DNA-adduct mediated cytotoxicity [39, 41, 45, 48]. Phase I clinical trials are currently underway for Phortress [49].

AQ4N is a bioreductive prodrug which is metabolised by CYP3A4, CYP1A1 and CYP2B6 in hypoxic tumour environments [45, 50, 51] to the cytotoxic metabolite AQ4 a DNA binding agent and topoisomerase II inhibitor. Moreover, AQ4 elicits a 'bystander' killing effect in surrounding tumour tissue [45] and is 1000 times more cytotoxic compared with AQ4N. AQ4N is the first CYP-activated bioreductive prodrug to enter clinical trials, although promising as a first line agent, exploitation as radio and chemo-enhancer has further clinical potential [39, 48].

Many conventional anticancer prodrugs undergo CYP mediated liver metabolism resulting in both reduced drug efficacy and toxicity. CYP-based GDEPT strategies have been developed to overcome these limitations by targeting prodrug-activating CYP genes to tumour cells, resulting in localised intratumoural prodrug activation [52]. These constructs were initially explored to overcome cyclophosphamide resistance to brain tumours resulting from hepatic CYP over-expression [16, 41]. Historically this strategy used rat CYP2B1 to chemosensitive tumours to cyclophosphamide. However, the immunological response to

rat CYP2B1 incorporation into human patients [35, 41], has resulted in the creation of constructs utilising human CYP2B6. MetXia, a novel retroviral vector encoding the human CYP2B6 gene in combination with cyclophosphamide, has recently borne fruit in phase I/II clinical trials in advanced breast cancer demonstrating both safety and efficacy [35].

The tumour-specific localisation of CYPs can also be exploited in immune-based therapy, which involves stimulation of the cancer patient's immune response against the tumour [48]. CYP1B1 is the only CYP isozyme to date found to be significantly over-expressed in tumours and as such represents an ideal target for immunotherapy [41, 53]. The novel anticancer vaccine ZYC300 is an encapsulated plasmid DNA encoding for CYP1B1 antigen. Administration of ZYC300 elicits a specific T-cell response to target and destroy CYP1B1-expressing tumours [39, 41, 48, 54]. Phase I/II clinical trials using ZYC300 are currently underway.

The ability to rationally target CYPs with prodrugs, clinical inhibitors and immunotherapy highlights the importance of these enzymes in the quest for tumour selective chemotherapy. Consequently, the Cancer Drug Discovery Group (CDDG) at De Montfort University have utilised the tumour specific expression of CYP1B1 (Table 6) to design a series of novel prodrugs that are intended to be activated by CYP1B1 only within the tumour. This groundbreaking approach has the potential for improving the safety and efficacy of chemotherapy to revolutionise the methods of cancer treatment.

1.3 CYP1B1 and cancer

CYP1B1 is the most recently cloned dioxin-inducible isozyme of the CYP1 family [55]; showing 40% sequence homology with both CYP1A1 and CYP1A2, and has also been shown to be involved in metabolism of xenobiotics and bioactivation of procarcinogens [56]. There is a general consensus that CYP1B1 is primarily expressed in extrahepatic tissue, however, there are inconsistent reports concerning CYP1B1 expression in normal human tissue. Several studies have shown the expression to be tumour specific, whereas others have reported expression in both malignant and non-malignant tissue.

The majority of studies evaluating the expression of CYP1B1 have concentrated on the expression of CYP1B1 mRNA. CYP1B1 mRNA expression has been reported in a range of extrahepatic normal tissue [57-59] including kidney [60], lung [61], brain [62], breast [63], prostate, testes [58] and foetal [64]. However, CYP1B1 mRNA expression does not correlate to the presence of CYP1B1 protein and several studies [65, 66] have demonstrated the absence of CYP1B1 protein but expression of CYP1B1 mRNA suggesting that regulation of CYP1B1 is predominantly post-transcriptional [45, 67]. In direct conflict with these findings studies by Mushkhelishvili *et al* reported the expression of both CYP1B1 mRNA and protein in a range of non-malignant tissue including brain, kidney, prostate, breast, cervix, uterus, ovary, lymph nodes and liver [59].

The discordance in the literature concerning non-malignant CYP1B1 expression may principally be due to the erroneous comparison of molecular techniques used in detecting CYP1B1 expression. CYP1B1 mRNA detection is based on PCR techniques which amplify the mRNA levels, which may generate misleading results [45]. Further confusion

is generated in the immunohistochemical techniques used in CYP1B1 protein detection [39]. The immunological similarity between isozymes in the CYP1 family may result in non-discriminate detection of CYP1 isozymes [45]. This is true for CYP1B1; the original discovery by Sutter *et al* [55] was a serendipitous breakthrough where a polyclonal antibody raised against CYP1A1 was shown to cross-react with a related CYP isozyme designated later as CYP1B1 [55]. Further studies using this antibody cannot be given much credence since the broad spectrum detection in non-malignant tissue cannot be assigned to CYP1B1 alone. Importantly, the report by Mushkhelishvili *et al* of CYP1B1 protein expression in normal human tissue used this particular antibody and as such doubts are cast on the validity of the reported data [59]. In summary, CYP1B1 protein has not been detected in normal tissue.

CYP1B1 protein expression has also been investigated in a range of cancers, utilising a variety of methods [68]. These studies have generally demonstrated absent or low level of CYP expression. However, recent immunohistochemical studies [42, 60, 68-74] have demonstrated the over-expression of CYP1B1 protein in tumour cells in a range of tumours such as bladder, brain, breast, colon, connective tissues, oesophagus, kidney, lung, lymph node, ovary, skin, stomach, testis and uterus. CYP1B1 expression was detected in all but 5 of 127 tumours investigated, but not in the corresponding normal tissue (Table 6). In contrast to previous studies Murray *et al* [68] have used validated and well characterised polyclonal and monoclonal antibodies that target a unique CYP1B1 peptide sequence [75], thereby eliminating cross-reactivity.

Table 6. Expression of CYP1B1 in different types of malignant tumours and normal tissue [68].

TISSUE	NORMAL (NO. POSITIVE/ NO. TESTED)	TUMOUR (NO. POSITIVE/ NO. TESTED)
Bladder	0/8	8/8
Brain	0/12	11/12
Breast	0/10	12/12
Colon	0/10	11/12
Connective tissue	0/9	8/9
Esophagus	0/8	8/8
Kidney	0/11	11/11
Liver	0/8	Not tested
Lung	0/8	7/8
Lymph node	0/5	9/9
Ovary	0/5	7/7
Skin	0/6	6/6
Small intestine	0/5	Not tested
Stomach	0/10	9/10
Testis	0/8	8/8
Uterus	0/7	7/7
Total	**0/130**	**122/127**

Interestingly, over-expression of the CYP1B1 protein has also been detected in pre-malignant tissue, which suggests that CYP1B1 has a role in tumour development. Studies by Stanley *et al* [76, 77] have demonstrated CYP1B1 over-expression in colon tumours, weak-expression in dysplastic tissue and no expression in normal tissue. A similar study conducted by Gibson *et al* [72] also demonstrated over-expression of CYP1B1 in colon cancer, with concomitant expression in tumour-associated vasculature. The intensity of expression was reduced with distance from the tumour. Studies by Carnell *et al* [74] give further credence to this theory, CYP1B1 over-expression was found in prostate cancer and

not in the corresponding normal tissue. However, over-expression was also detected in the associated pre-malignant and hyperplastic tissue. All of these studies implicate a possible link in malignant progression and CYP1B1 up-regulation and as such CYP1B1 could be used as a prognostic tumour marker and therapeutic target.

The endogenous function of CYP1B1, as yet, remains unknown. Recently, CYP1B1 deficient mice have been used to demonstrate its importance in modulating hypoxia-induced neovascularisation [78]. The up-regulation of CYP1B1 in vasculature surrounding colon tumours has also been described [72]. These studies implicate that CYP1B1 is up-regulated during tumour development and may be involved in angiogenesis particularly under hypoxic conditions. Interestingly, studies have indicated that the AhR pathway (the up-regulation of CYP1A1 and CYP1B1 can be induced via this pathway (Section 1.2.1.3.1)) is capable of cross-talking with the hypoxia inducible pathway [79]. In fact the ARNT can also form a heterodimer with the hypoxia-specific transcription factor HIF-1α to induce the expression of CYP1 family isozymes. This indicates that during tumour development, hypoxic conditions may induce the expression of CYP1B1 and other CYP1 family isozymes as an endogenous rescue mechanism to prevent tumour growth.

Controversially, the tumour-specific expression of CYP1B1 has been linked to carcinogenesis itself, due to the CYP1B1-mediated bioactivation of procarcinogens into carcinogenic metabolites [37, 80]. However, the formation of toxic metabolites in cancer cells can hardly be considered an issue when the cells are already cancerous. In fact exposure of cytotoxic metabolites to tumour cells would be advantageous in that these metabolites may cause mutagenic damage resulting in cancer cell death, which is actually

the goal of tumour selective chemotherapy [81]. In direct conflict with the carcinogenic theory, Potter *et al* see CYP1B1 not as the cause of cancer, but as tumour specific rescue enzyme that selectively eliminates cancer cells via metabolic activation of natural dietary components into compounds with anticancer properties (Section 1.3.2) [81]. This theory would also explain the over-expression of CYP1B1 in a range of cancers irrespective of oncogenic origin [68]. To assign CYP1B1 as the perpetrator of cancer, principally because it is present in tumours may be short-sighted, when its true nature may be as an endogenous rescue mechanism up-regulated after the cells have already undergone a malignant transformation.

Another CYP isozyme of interest for chemotherapeutic intervention is CYP1A1. CYP1A1 is an inducible CYP expressed primarily in extrahepatic tissues [82]. The expression of CYP1A1 has been extensively characterised in tumour tissue; however most studies have again focused on the mRNA expression. CYP1A1 protein expression has been less well characterised (Table 7) [83-85]:

Table 7. Protein expression of CYPs in specific tumour types (percentage of tumours staining positive by immunohistochemistry using antibodies specific to these families and isozymes as appropriate [45]).

TUMOUR TYPE	CYP1A	CYP1B1
Bladder	68	100
Breast	40	80
Colon	75	87
Ovary	Not detected	80
Kidney	100	100
Esophagus	64	100
Prostate	63	90
Sarcoma	70	90
Stomach	60	90

The CYP1A1-mediated activation of polycyclic aromatic hydrocarbons (PAH) such as those found in tobacco smoke [86, 87] and the over-expression of CYP1A1 in tumour tissue has also erroneously led to the belief that CYP1A1 is a carcinogenesis inducer [80]. Studies by Antilla *et al* [85-87] detected CYP1A1 protein over-expression in normal lung tissue from smokers compared to non-smokers, these results led them to speculate that CYP1A1 was responsible for the bioactivation of tobacco smoke carcinogens resulting in malignant transformation. An opposing viewpoint is to consider the tumoural CYP1A1 over-expression as a rescue mechanism up-regulated in response to the cellular dysfunction already caused by exposure to tobacco smoke carcinogens in an attempt to restore the *status quo* [88].

The tumour specific over-expression of CYP1 isozymes especially CYP1B1 and less-so CYP1A1, together with their proposed role as an endogenous rescue mechanism has a number of far reaching implications. Firstly they provide a putative therapeutic anticancer drug target for development of non-toxic prodrugs which can be selectively metabolised or activated within the tumour only, to form highly potent protein tyrosine kinase (PTK) inhibitors and antimitotic agents [89, 90]. The extrahepatic nature of the enzymes also helps to overcome hepatic CYP metabolism which may result in drug toxicity or decreased bioavailability. Secondly it provides an alternative strategy to overcome some drug resistance caused by CYP metabolism in tumours (e.g. taxol), through inhibition of CYP1 isozymes [43, 54, 91, 92]. However, inhibition may be futile as the role of these enzymes may be to inhibit malignant growth by acting as tumour suppressor 'rescue' enzymes, therefore, enzyme inhibition may paradoxically lead to further malignant propogation.

1.3.1 CYP1B1 and estradiol

17β Estradiol (E_2) is the only currently known endogenous substrate of CYP1B1 and has been widely implicated with carcinogenicity, possibly as a result of E_2 metabolism generating 4-hydroxyestradiol (4-OHE_2) and 2-hydroxyestradiol (2-OHE_2) [93]. 2-OHE_2 has little or no carcinogenicity and is mainly formed in the liver by CYP3A4 [94]. However 4-OHE_2 is formed mainly in extrahepatic tissues and has been shown to be highly carcinogenic in hamster kidney, showing the selective induction of carcinogenesis [93-96]:

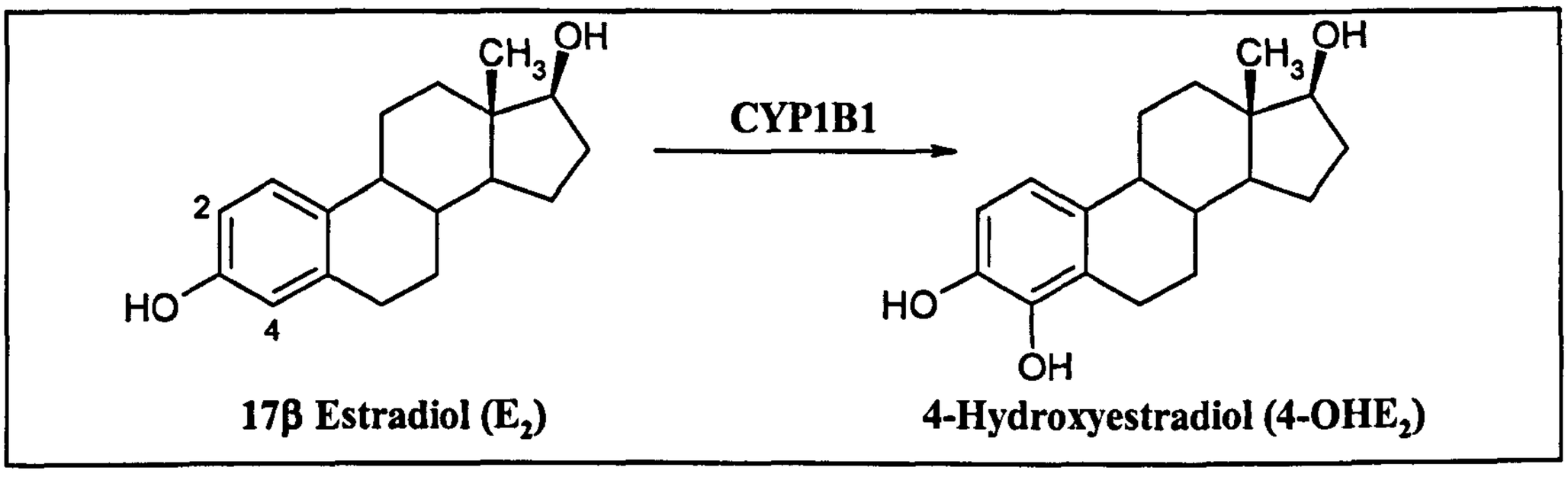

Figure 5. CYP1B1 activated 4-hydroxylation of E_2 to the carcinogenic metabolite 4-OHE_2.

4-OHE_2 can cause DNA, protein and lipid damage through CYP mediated redox cycling to semiquinone and quinone forms [97]. The selective 4-hydroxylation of E_2 by CYP1B1 has been further demonstrated by Hayes *et al* in human breast cell lines; kinetic experiments demonstrated CYP1B1 catalysed E_2 hydroxylation at the 4-position preferentially to the 2-position [98]. The fact that E_2 is selectively activated by CYP1B1 to form the carcinogenic metabolite 4-OHE_2, suggests the use of the E_2 molecular skeleton as a template for novel CYP1B1 activated anticancer prodrugs.

1.3.2 Rationale for CYP1B1 activated anticancer prodrugs

Although the expression level of CYP1 isozymes differs between tumour and corresponding normal tissue, CYP1B1 is the only CYP1 isozyme that is significantly over-expressed in tumours [39], thereby providing a rational target for anticancer drug development. Furthermore, the selective 4-hydroxylation of E_2 by CYP1B1 permits the use of the E_2 pharmacophore in providing a framework for rational and mechanistic development of CYP1B1 activated anticancer prodrugs. Potter and McCague initially pioneered this type of steroidal mapping in drug design [99]. The synthetic estrogen stilbestrol was mapped onto the E_2 pharmacophore with the two para hydroxyl groups of the A and B ring mapping onto the E_2-3 and 17β-positions respectively:

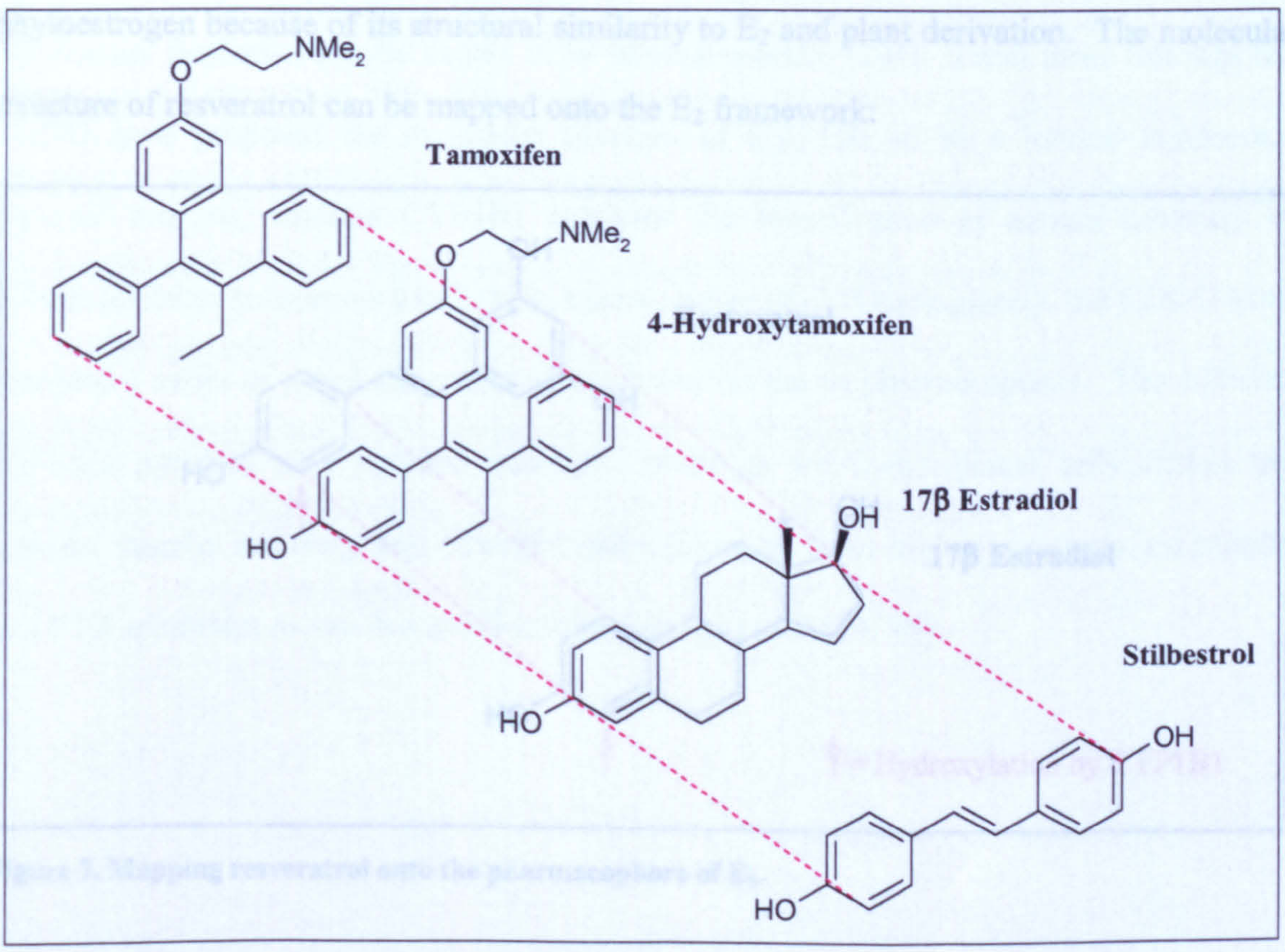

Figure 6. Mapping of the stilbenes stilbestrol and tamoxifen onto the E_2 framework.

This type of estrogenic mapping was used to explain the potency of the estrogenic metabolite *trans*-4-hydroxytamoxifen, which is 100 times more potent as an estrogen inhibitor than the parent compound tamoxifen [45, 99]. Furthermore, this led to the rational design of the tamoxifen derivative idoxifene for the treatment of metastatic breast cancer [100].

Phytoestrogens can also act as substrates for CYP1B1 given that the core structure is similar to that of E_2. This may result in aromatic hydroxylation corresponding to that of 4-OHE_2, to generate toxic species within CYP1B1-expressing tumours only. This hypothesis was partially confirmed using resveratrol; a naturally occurring anticancer agent found in red wine, broccoli and peanuts [101]. Resveratrol is a stilbene and is classified as a phytoestrogen because of its structural similarity to E_2 and plant derivation. The molecular structure of resveratrol can be mapped onto the E_2 framework:

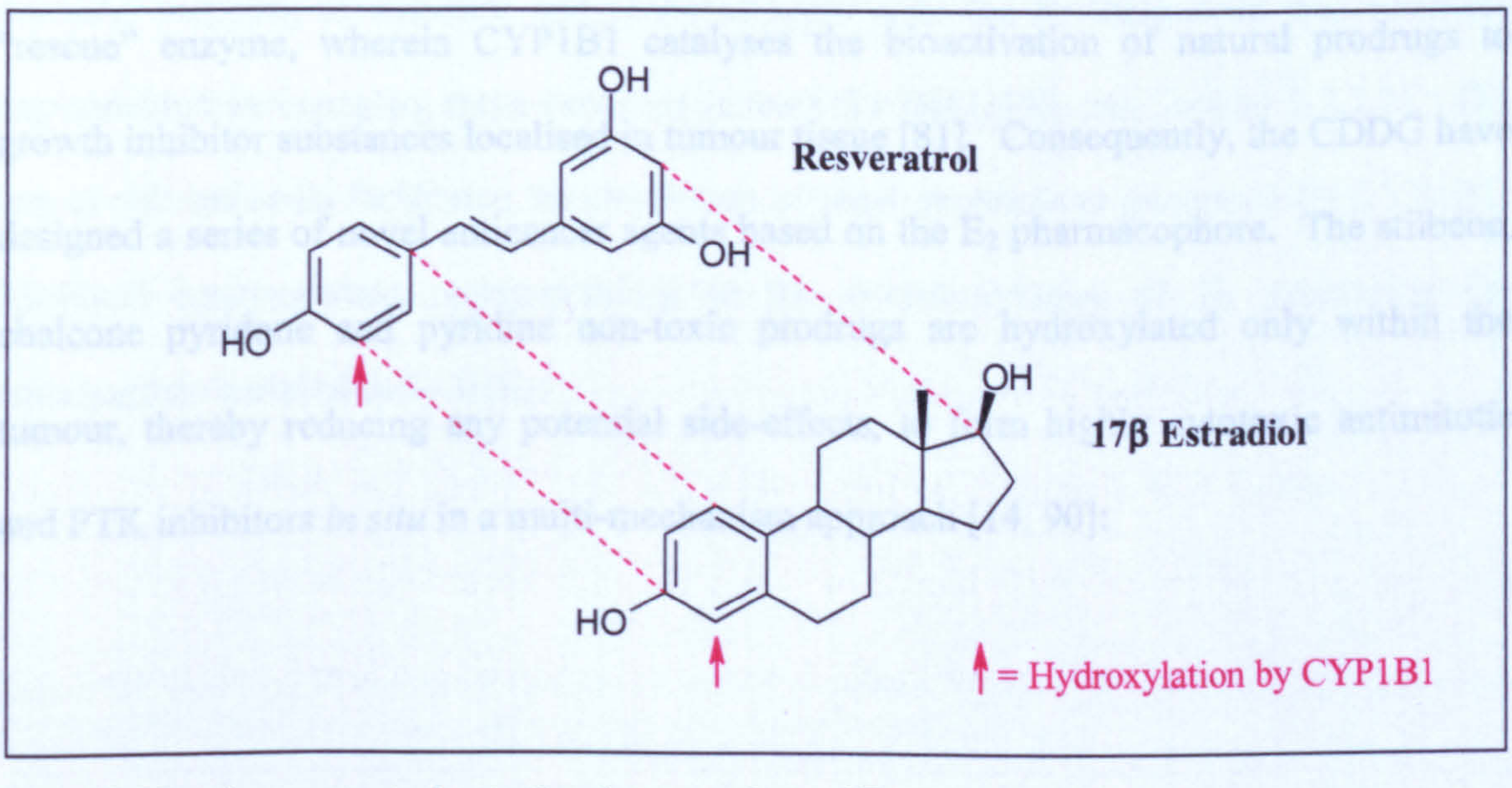

Figure 7. Mapping resveratrol onto the pharmacophore of E_2.

This relationship enabled Potter and colleagues [81] to hypothesize that resveratrol would undergo 3-hydroxylation catalysed by CYP1B1 corresponding to that of 4-OHE_2, to generate piceatannol, a known PTK inhibitor (MAPK) [102] with antileukaemic properties.

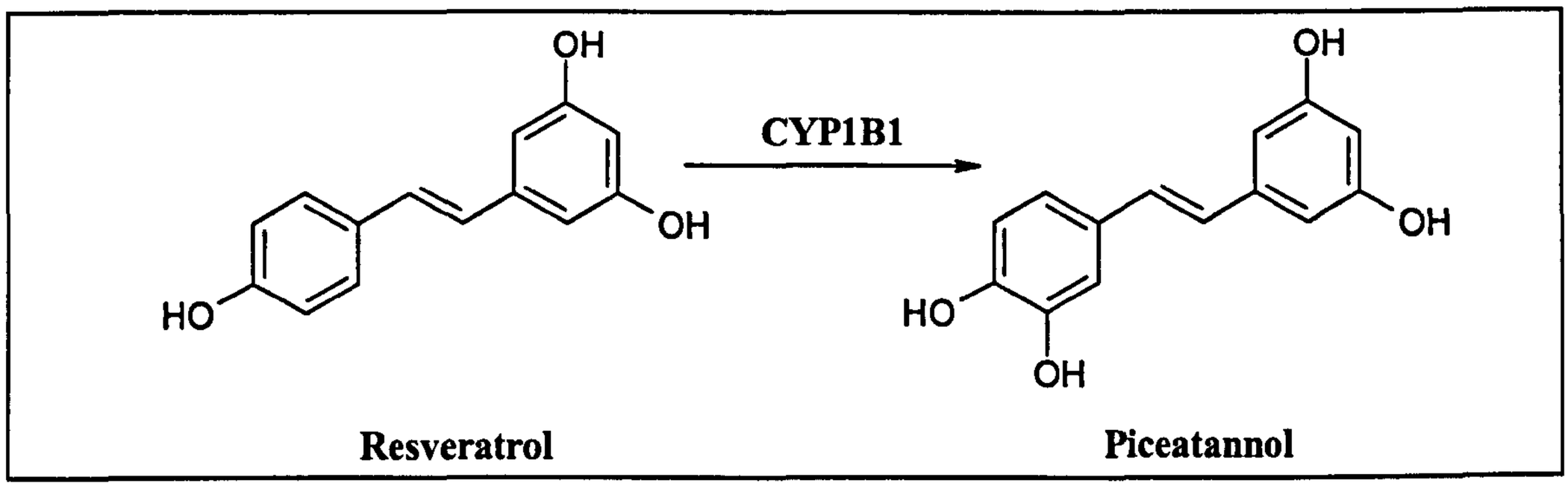

Figure 8. CYP1B1 activated 3-hydroxylation of resveratrol to the anticancer agent piceatannol.

The study demonstrated bioactivation of resveratrol to piceatannol by CYP1B1, therefore, piceatannol formation maybe shown to be tumour specific [103]. From these findings the CDDG have proposed the molecular function of CYP1B1 to be a tumour suppressor "rescue" enzyme, wherein CYP1B1 catalyses the bioactivation of natural prodrugs to growth inhibitor substances localised in tumour tissue [81]. Consequently, the CDDG have designed a series of novel anticancer agents based on the E_2 pharmacophore. The stilbene, chalcone pyridone and pyridine non-toxic prodrugs are hydroxylated only within the tumour, thereby reducing any potential side-effects, to form highly cytotoxic antimitotic and PTK inhibitors *in situ* in a multi-mechanism approach [14, 90]:

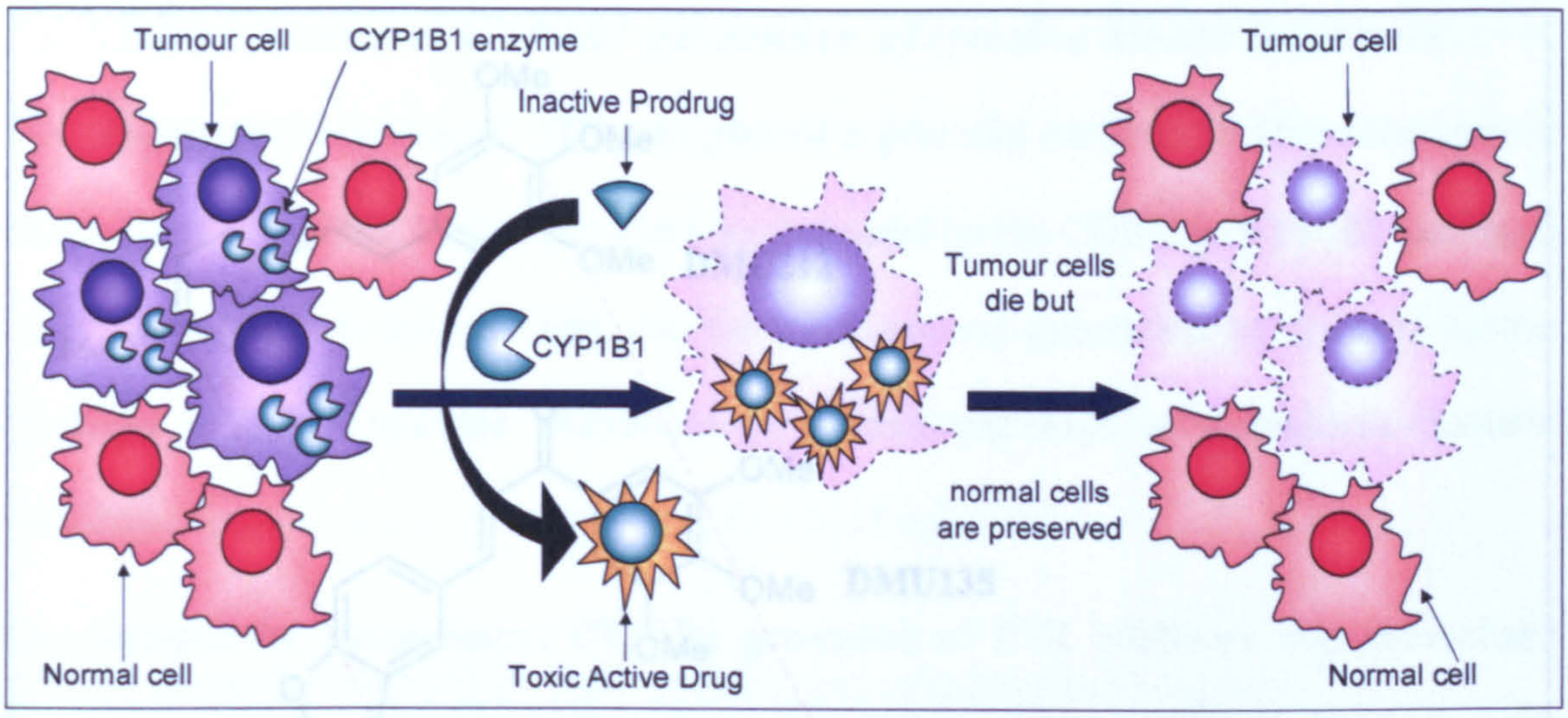

Figure 9. Rationale for prodrug design using the tumour specific expression of CYP1B1.

1.3.2.1 Mapping of lead compounds onto the estradiol framework

The potential lead hydroxylation-activated anticancer prodrugs selected to undergo preclinical evaluation are DMU135, DMU212, DMU590, DMU949 and DMU982. The steroidal mapping of stilbenes and phytoestrogens onto the E_2 framework was similarly implemented for mapping these prodrugs (except for DMU590, see Section 1.3.2.3). The use of this rationale facilitated the prediction of toxic metabolites generated by CYP1B1-mediated hydroxylation, corresponding to the 4-hydroxylation of E_2 generating the carcinogenic metabolite 4-OHE_2:

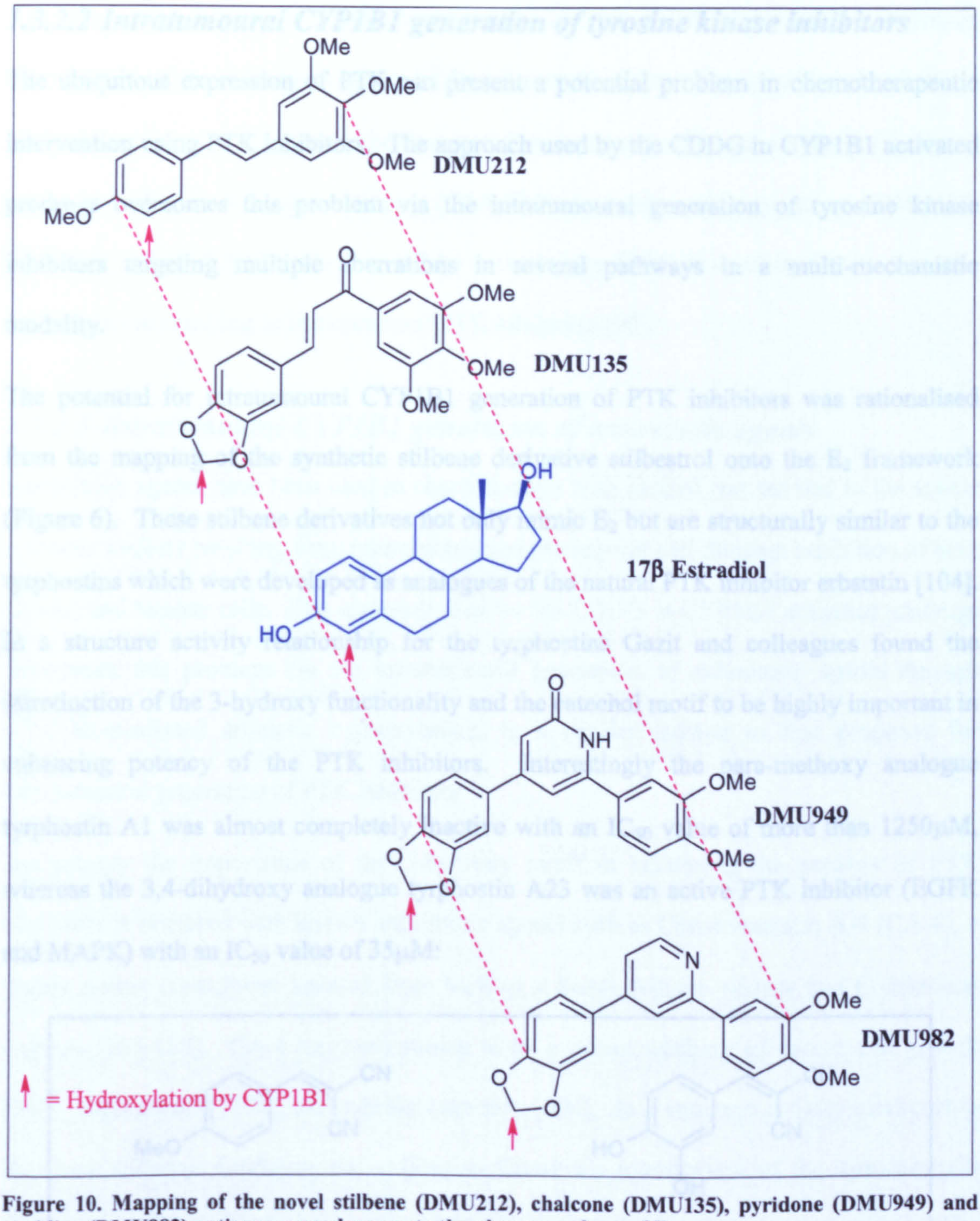

Figure 10. Mapping of the novel stilbene (DMU212), chalcone (DMU135), pyridone (DMU949) and pyridine (DMU982) anticancer prodrugs onto the pharmacophore of E_2.

1.3.2.2 Intratumoural CYP1B1 generation of tyrosine kinase inhibitors

The ubiquitous expression of PTK can present a potential problem in chemotherapeutic intervention using PTK inhibitors. The approach used by the CDDG in CYP1B1 activated prodrugs overcomes this problem via the intratumoural generation of tyrosine kinase inhibitors targeting multiple aberrations in several pathways in a multi-mechanistic modality.

The potential for intratumoural CYP1B1 generation of PTK inhibitors was rationalised from the mapping of the synthetic stilbene derivative stilbestrol onto the E_2 framework (Figure 6). These stilbene derivatives not only mimic E_2 but are structurally similar to the tyrphostins which were developed as analogues of the natural PTK inhibitor erbstatin [104]. In a structure activity relationship for the tyrphostins Gazit and colleagues found the introduction of the 3-hydroxy functionality and the catechol motif to be highly important in enhancing potency of the PTK inhibitors. Interestingly the para-methoxy analogue tyrphostin A1 was almost completely inactive with an IC_{50} value of more than 1250μM, whereas the 3,4-dihydroxy analogue tyrphostin A23 was an active PTK inhibitor (EGFR and MAPK) with an IC_{50} value of 35μM:

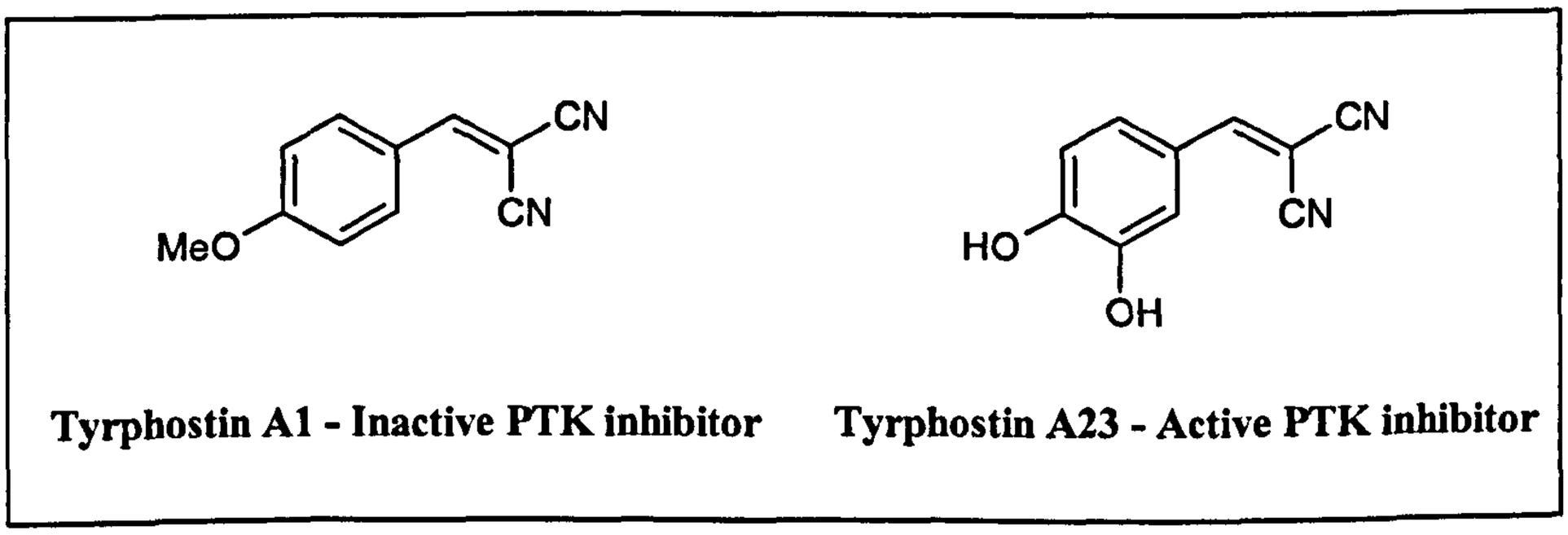

Tyrphostin A1 - Inactive PTK inhibitor **Tyrphostin A23 - Active PTK inhibitor**

Figure 11. Structures of the PTK inhibitors tyrphostin A1 and A23 [104].

Crucially this 3-hydoxy motif corresponds to the CYP1B1-mediated enzymatic introduction of the 4-hydroxy group of E_2 (Figure 5). Therefore, it was realised that a CYP1B1 activated prodrug could be designed that contained only a para-hydoxy (similar to resveratrol (Figure 8)), para-methoxy (DMU212) or methylenedioxy group (DMU135, DMU949 and DMU982), which could be activated by CYP1B1-mediated meta aromatic hydroxylation resulting in intratumoural PTK inhibition [90].

1.3.2.3 Intratumoural CYP1B1 generation of antimitotic agents

Antimitotic agents have been used in chemotherapy with limited success due to the severe systemic toxicity resulting from microtubule and consequent cell division inhibition of both normal and tumour cells. The approach used by the CDDG in CYP1B1 activated prodrugs overcomes this problem via the intratumoural generation of antimitotic agents through CYP1B1-mediated aromatic hydroxylation, in a similar fashion to that proposed for intratumoural generation of PTK inhibitors.

Intriguingly the importance of the 3-hydroxy motif in enhancing the potency of PTK inhibitors is mirrored with known antimitotic agents such as Combretastatin A-4 (CA-4), a highly potent *cis*-stilbene isolated from bark of a South African willow tree *Combretum caffrum* [105-107]. CA-4 has been shown to be a potent inhibitor of cancer cell growth [108], angiogenesis [106], and tubulin assembly [109]. In a structure activity relationship for these stilbenes Cushman and colleagues found the introduction of the 4-methoxy/3-hydroxy motif on the B-ring to be highly important in enhancing cytotoxicity. The trimethoxybenzene functionality observed in a 3,4,5 configuration on the A-ring of other antimitotic agents such as colchicine, podophyllotoxin and steganacin was also important

for the activity of these compounds [105, 110, 111]. Additionally, the CA-4 *cis*-isomer exhibited superior cytotoxicity with an IC_{50} value of 0.001μM, whereas the *trans*-isomer was less cytotoxic with an IC_{50} value of 0.01μM [105, 111]. However, the *cis*-isomer of CA-4 does not map well onto the E_2 framework (Figure 12), whereas the *trans*-isomer of CA-4 maps on very well to E_2:

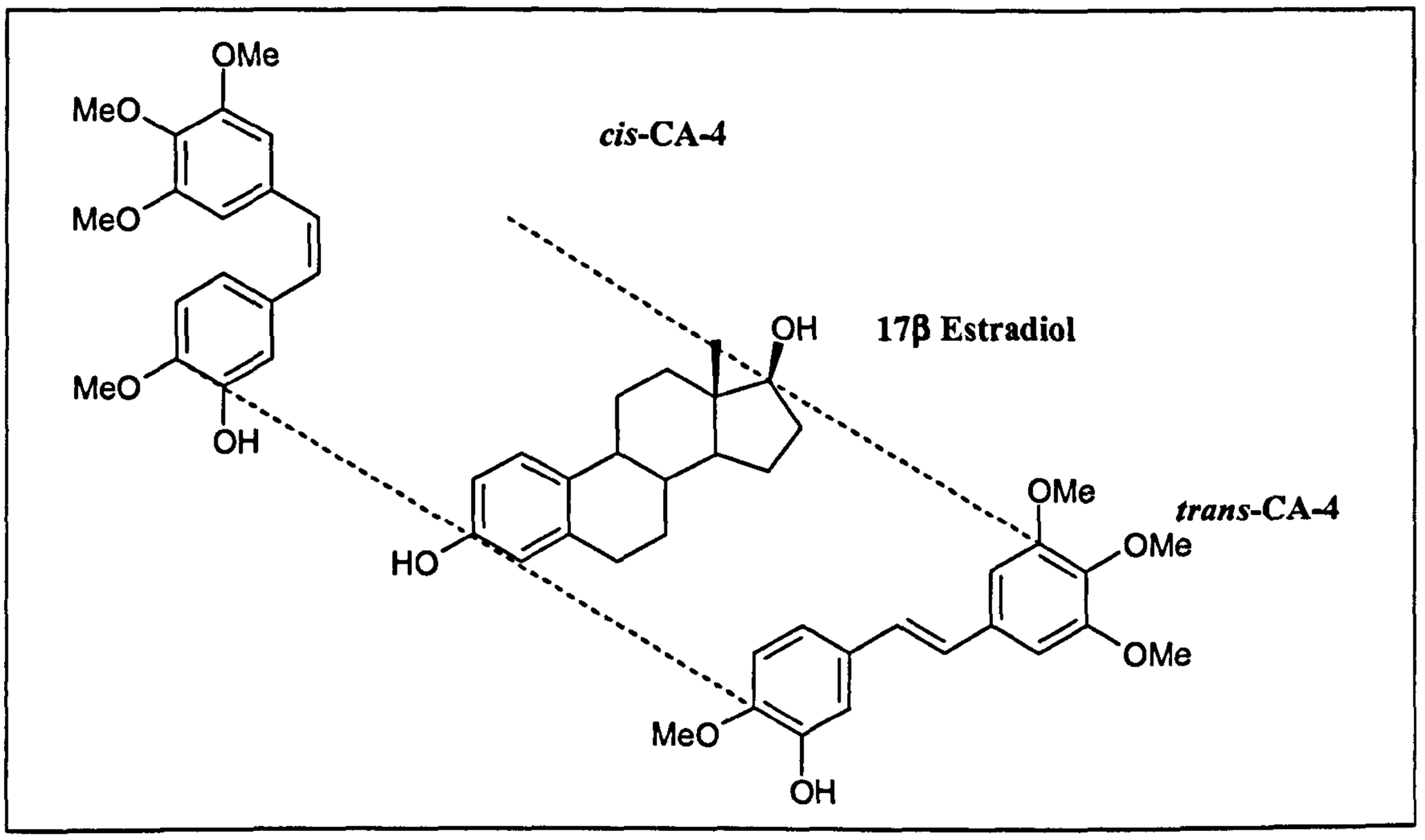

Figure 12. Mapping of the stilbenes *trans*- and *cis*-CA-4 onto the E_2 framework.

Even though the *cis*-isomer of CA-4 is the most potent, the *trans*-isomer still showed favourable potency and some of the *trans*-CDDG prodrugs are bioactivated to the *cis*-stilbene *in situ* [81]. Furthermore, studies by Cushman and colleagues demonstrated the requirement for the 3-hydroxy substituent in the B-ring for maximal antimitotic activity regardless of geometric conformation [105]. Therefore, firstly based on the structure of *trans*-CA-4, DMU212 [90, 112] was synthesised with the intention that the active 3-hydroxy functionality is introduced *in situ* by tumours to generate the PTK inhibitor and

antimitotic metabolite DMU214 or *trans*-CA-4, thus moderating any potential side-effects compared to that of CA-4 (Figure 13). Secondly, an analogue of *cis*-CA4 i.e. DMU590 was designed to potentially overcome the solubility problems associated with the parent compound [107]:

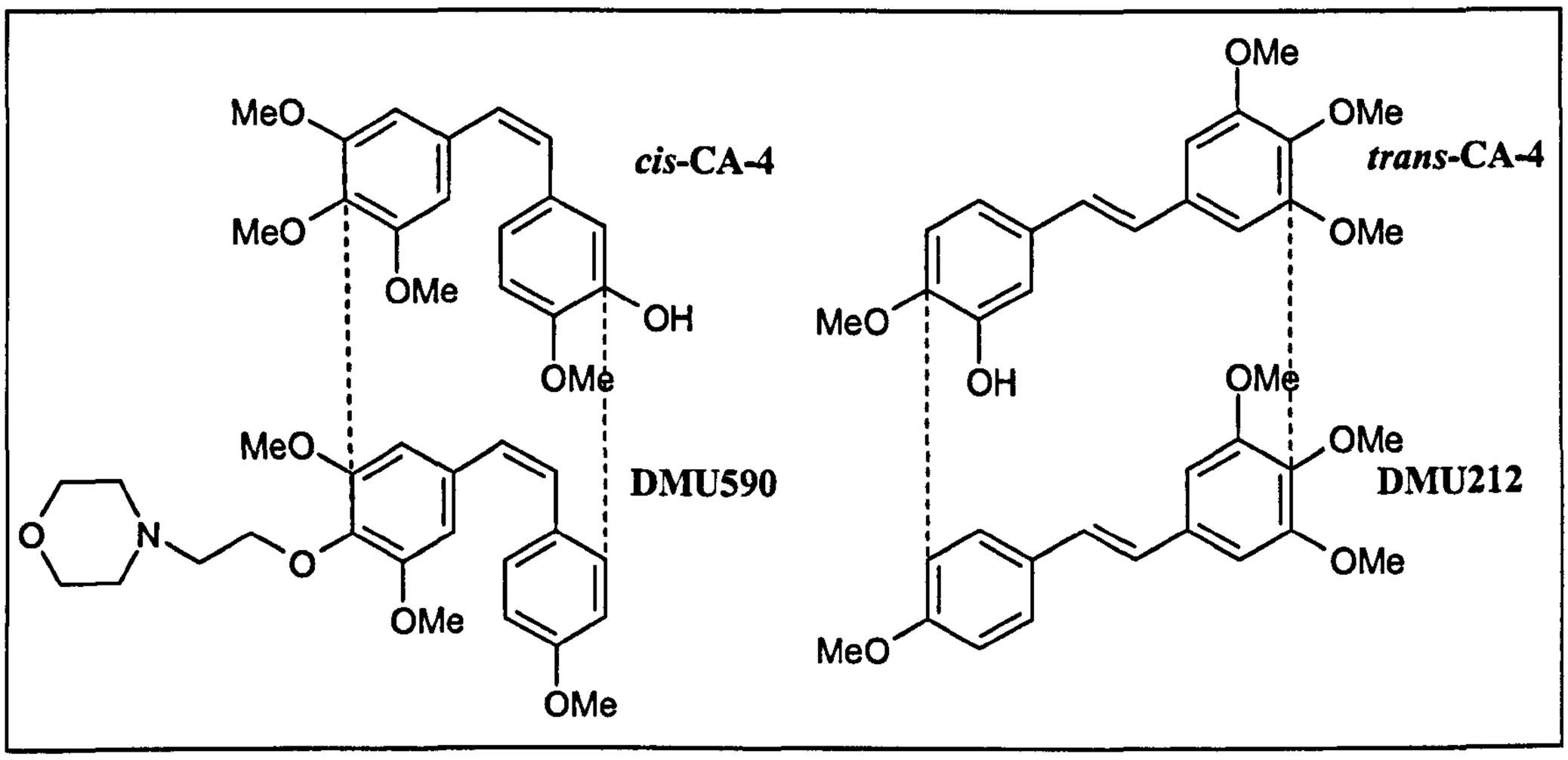

Figure 13. Mapping of the stilbenes DMU212 and DMU590 onto the *trans*- and *cis*-CA-4 framework.

Studies by Ducki *et al* [113-115] have also used the CA-4 pharmacophore in the design of antimitotic chalcones. A series of analogues were prepared and the most potent agents were found to be those possessing the 4-methoxy/3-hydroxy motif on the B-ring and the 3,4,5-trimethoxy functionality on the A-ring as with CA-4 [113, 116]. Optimum activity was found with the α-methyl chalcone (Figure 14), which had comparable and in some cases superior activity compared to CA-4 [115]. This potency is thought to arise from geometric considerations [107, 117]. The α-methyl chalcone can adopt an *s*-trans conformation, structurally similar to CA-4, whereas with a lack of steric hindrance from the methyl substitution, the chalcone prefers to adopt a less potent *s*-cis conformation.

Accordingly, the CDDG have designed a library of novel antimitotic chalcones based on the structure of *trans*-CA-4 [118], which upon CYP1B1-mediated hydroxylation result in intratumoural antimitotic activity. The most potent chalcone was identified as DMU135 [118, 119] which was predicted to undergo CYP1B1-mediated hydroxylation of the methylenedioxy group to generate the catechol metabolite DMU117 (Figure 14):

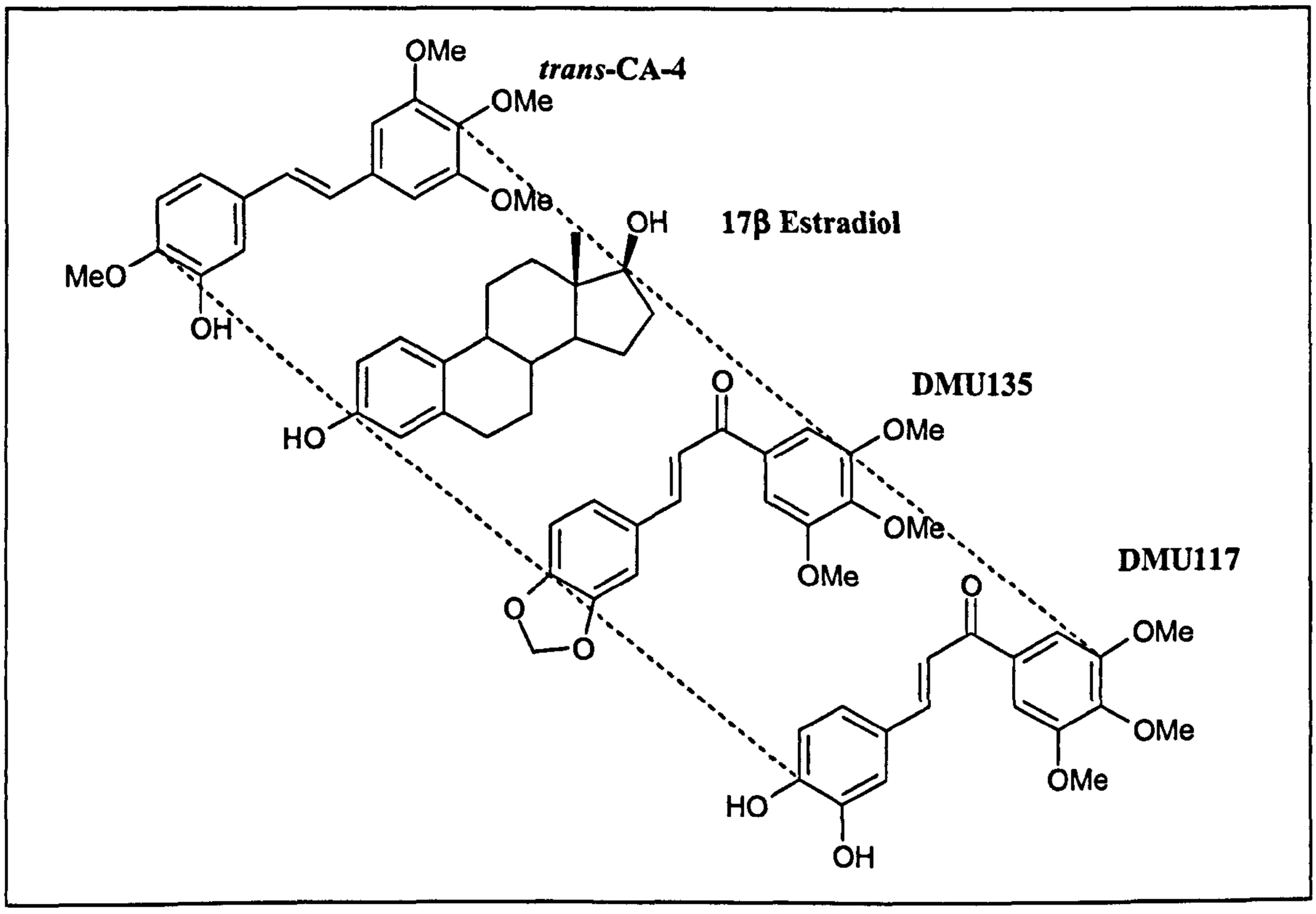

Figure 14. Mapping of the stilbene *trans*-CA-4 and the chalcones DMU135 and DMU117 (the hydroxylated form of DMU135) onto the E_2 framework.

Prediction of this metabolic activation was facilitated by the CYP1B1-mediated aromatic hydroxylation of E_2 to generate the catechol 4-OHE_2 (Figure 5) as well as the CYP1B1-mediated metabolism of phytoestrogens such as resveratrol to generate the catechol metabolite piceatannol (Figure 8).

Interestingly a striking similarity was noted between functionalities present in antimitotic agents and PTK inhibitors. The CYP1B1 metabolites of DMU212 and DMU135 i.e. DMU214 and DMU117 can both be mapped onto the tyrphostins (Figure 11) and CA-4 (Figures 13 and 14) both of which require the 3-hydroxy motif in the A-ring for maximal PTK inhibition and antimitotic activity. This relationship leads to the speculation that the CDDG prodrugs may function in a multi-mechanistic fashion once intratumourally metabolised by CYP1B1, wherein antimitotic activity may be linked to PTK inhibition.

1.4 Prodrugs: Preclinical drug development impasse?

Recent advances in proteomic and genomic technology have generated a host of high-throughput technologies enabling the identification of specific biological targets [120]. Combinatorial chemistry has been utilised to rapidly generate libraries of compounds, which can be screened rapidly through *in vitro* high-throughput assays to generate a multitude of 'hits'. This high-throughput approach was expected to accelerate the identification of lead compounds and to shorten the time to the market, ironically, high attrition rates in the later stages of drug development, have been attributed to the birth of high-throughput technology itself [121].

One of the reasons behind the high attrition rates is the almost exclusive focus on drug potency and selectivity, with insufficient focus on the pharmacokinetic and pharmaceutical properties of the drug [122, 123]. Many of these compounds exhibit physicochemical properties presenting difficulties in development, including high molecular-weight, high lipophilicity and poor aqueous solubility; all of which are a major source of failure in early

development [121]. This is corroborated by the design of CDDG prodrugs DMU135 and DMU212, which are lipophilic and have no derivatisable functional group to enable manipulation of physicochemical properties, since the active moiety is introduced *in situ*. Another reason for disconnect between discovery and pre-clinical development is the lack of available high-throughput technologies at a pre-clinical level to deal with increased output of compounds downstream of discovery [120, 123]. As such, effective tumour specific prodrugs have yet to meet the chemotherapeutic realisation despite showing preclinical promise [25].

Limitations with pre-clinical high-throughput technologies raise significant hurdles for advancement of compounds into the clinic and therefore, preclinical development is rapidly becoming a bottleneck in drug development [123]. The key to coordinating drug discovery and development, and thereby improving efficiency and reducing attrition may lie in the development of high-throughput technologies for the preformulation programme, to identify potential physicochemical problems (solubility, log *P*) at an early drug development stage [122, 124-127]; thus providing an earlier estimation of the drug pharmaceutical properties [120]. This concept will be implemented in the body of this work in novel miniaturisation of analytical assays for preformulation and formulation analysis.

Moreover, parallel optimisation of potency and pharmaceutical properties will be considered in the design and consequent synthesis of novel CYP1B1 activated prodrugs. A similar strategy was implemented by Pettit *et al* in the design of CA-4 analogues [128]. Although CA-4 has shown to be a highly potent antimitotic agent *in vitro*, the *in vivo*

efficacy was poor in comparison partly due to its very limited aqueous solubility and high lipophilicity [107]. Subsequently, a water-soluble disodium phosphate prodrug CA4P was developed [128], with improved pharmacokinetic properties thereby allowing much easier *in vivo* administration [110]. CA4P is rapidly dephosphorylated in the plasma releasing the parent compound CA-4 [107, 110] and as such is currently undergoing phase I/II clinical trials. Taking the lead from Pettit and colleagues a series of novel CYP1B1 activated prodrugs will be rationally designed as completely new entities or as analogues of existing compounds, all provided with derivatisable functional groups to potentially favour both drug potency and pharmaceutical properties in ultimately furthering the quest for tumour selective chemotherapy.

1.5 Project aims

In this thesis, the pharmaceutical development and formulation of novel anticancer prodrugs developed by the CDDG in the Leicester School of Pharmacy is presented. The development of prodrugs will include synthesis of novel entities and analogues of existing compounds, to facilitate the development of prodrugs with better pharmaceutical properties. The preformulation of lead CDDG prodrugs will quantify physicochemical properties which may influence formulation design, drug manufacture and pharmacokinetics. Formulation of lead prodrugs will enable the transition from a preclinical, discovery stage into formulated dosage forms appropriate for clinical trials. Finally, miniaturisation of assays during preformulation and formulation will also be conducted to enable efficient and high-throughput drug development. In summary the aims of this thesis were:

- To conduct preformulation studies for a series of novel lipophilic lead prodrugs synthesised by the CDDG (DMU135, DMU212, DMU590, DMU949 and DMU982). This involved the investigation of solubility, log *P*, pKa, scanning electron micrograph imaging and differential scanning calorimetry.

- To develop orally available capsule and topical formulations for a novel lipophilic lead prodrug DMU212 and subsequently demonstrate the *in vitro* activity and bioavailability of the formulated prodrugs in model systems, to be used as pre-clinical data in support of subsequent phase I clinical trials.

- To identify and characterise salt forms of DMU590 and DMU982 with the desired physicochemical properties i.e. aqueous solubility and to enable its formulation into solid dosage forms.

- To synthesise a series of novel imidazole and thiazole CYP1B1 activated prodrugs with desirable biological and physicochemical properties for subsequent salt selection and formulation.

- To synthesise novel analogues of DMU949 with desirable physicochemical properties for subsequent metabolic evaluation in a double-prodrug strategy. This will involve the investigation of CYP1A1, CYP1B1 and liver microsome mediated metabolism and identification of the metabolites formed.

- To develop novel high-throughput analytical quantification methods for log *P*, pKa and solubility determination, and measurement of dissolution samples.

CHAPTER 2

Preformulation Studies of Non-Ionisable Prodrugs

2.1 Introduction

2.1.1 Discovery of a novel stilbene prodrug

Stilbenes are found extensively in nature and as synthetic biologically active compounds, both of which are reported to exhibit a variety of therapeutic functions including antibacterial, antifungal, antioxidant, anti-inflammatory, anticancer and anti-malarial [129]. The anticancer activity in particular has garnered attention in the design of synthetic stilbenes, most notably in hormone based therapies and particularly in estrogenic cancer treatments, since the core stilbene structure can be mapped onto the E_2 framework:

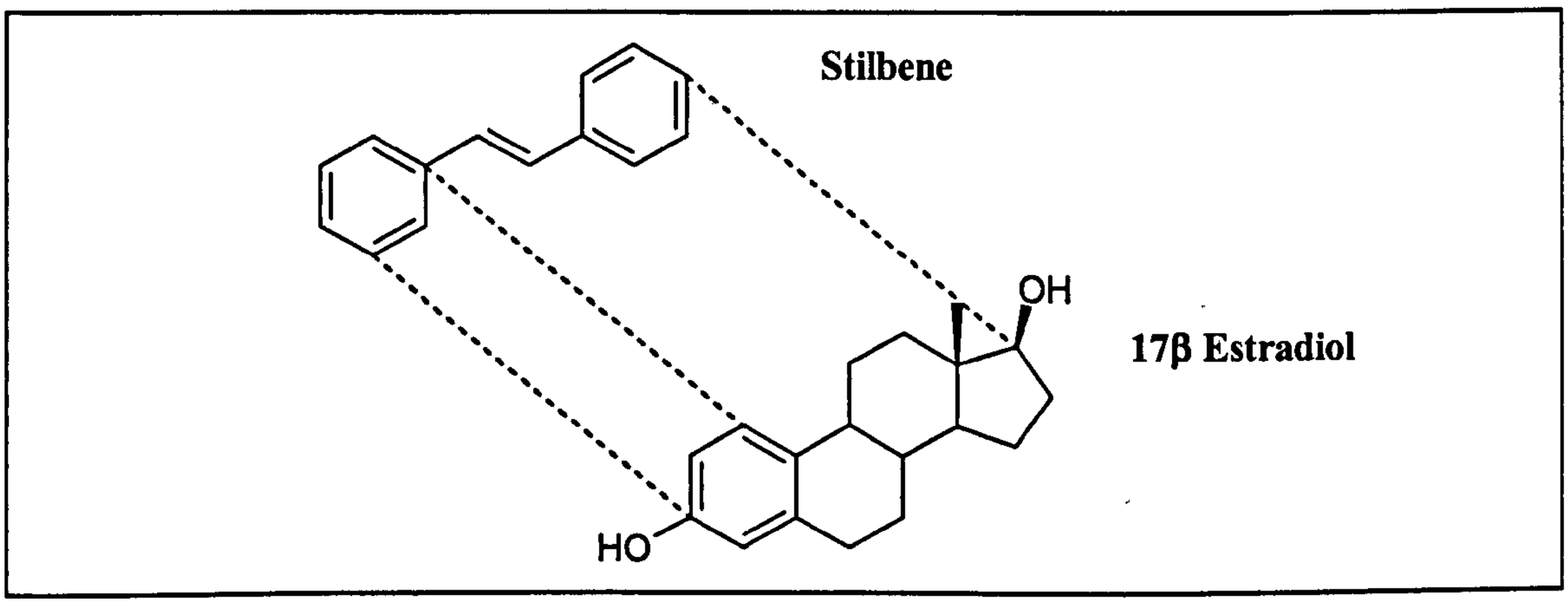

Figure 15. Mapping of the core stilbene structure onto the E_2 framework.

The antiestrogens stilbestrol and tamoxifen, used in the treatment of breast cancer, can also be mapped onto the E_2 framework (Figure 6), which would explain the potency of their respective estrogenic metabolites [99].

Interest in the use of stilbenes as anticancer agents stems from the discovery of the ability of many such natural products to act as antimitotic and antileukaemic agents [105]. The most potent natural antimitotic stilbene to date is Combretastatin A-4 (CA-4), a *cis*-stilbene

isolated from bark of the South African willow tree *Combretum caffrum* (Section 1.3.2.3) [105-107]. The CA-4 cytoskeleton has drawn wide attention in the design of novel synthetic stilbene analogues as has the phytoestrogen resveratrol.

Resveratrol (*trans*-3,5,4'-trihydroxystilbene) is a naturally occurring stilbene generated in response to environmental stress in grapes, peanuts and other Leguminosae family plants [101]. The chemopreventative activity of resveratrol has recently attracted interest because of its inhibitory activity on multiple cellular events associated with carcinogenesis (initiation, promotion and progression) [101] and its potent growth inhibitory effects on a variety of cancer cells [130]. In view of the pharmacological potential of resveratrol, the polyhydroxystilbene scaffold has served as a useful chemical platform for developing more potent and selective chemotherapeutic agents.

Accordingly, the CDDG have implemented the molecular framework provided by both combretastatin and resveratrol in the design of novel CYP1B1 activated *cis* and *trans* stilbene prodrugs. The cytotoxicity of the compounds synthesised was investigated using an in-house human breast cell-line screen with well characterised CYP1 expression. The panel consisted of MCF7, MDA-MB-468 and MCF10A cell-lines. The estrogen receptor positive cell-line MCF7 originates from the pleural cavity of a Caucasian female with malignant breast disease, when induced with 2,3,7,8 tetrachlorodibenzo-*p*-dioxin (TCDD) MCF7 cells express CYP1A1 and CYP1B1 [131], where mainly CYP1A1 is functional. The estrogen receptor negative cell-line MDA-MB-468, originates from the pleural effusion of a Black female with metastatic adenocarcinoma of the breast. This cell-line is isolated from a more aggressive tumour [132], which constitutively expresses CYP1B1 and

CYP1A1, where mainly CYP1B1 is functional. Finally, MCF10A was used in this assay for comparison with tumorigenic CYP1 expressing cell lines. MCF10A cells are immortalized from cultures of normal breast epithelial cells; they retain epithelial morphology, are non-tumorigenic and do not express any CYPs [133].

A standard MTT *in vitro* assay (see Section 3.2.6) [134] employing these cell-lines was used to study differential cytotoxicity between MCF10A and MDA-MB-468 and MCF7 with and without TCDD to identify compounds which preferentially inhibit cancer cell growth without affecting normal cell growth i.e. CYP1B1 activated compounds. The O-methylated analogue of resveratrol, DMU212 (*trans*-3,4,5,4'-tetramethoxystilbene) emerged as one of the strongest candidates for anticancer therapy:

Table 8. Summary of DMU212 *in vitro* cytotoxicity data. Data provided by P. Butler of the CDDG.

HUMAN BREAST CELL-LINE	MCF7 WITHOUT TCDD	MCF7 WITH TCDD	ACTIVATION FACTOR	MCF10A	MDA-MB-468	TUMOUR SELECTIVE FACTOR
IC_{50} VALUES (μM)	2.6	0.12	22	4.3	0.001	4300

DMU212 was found to potently inhibit the growth of MDA-MB-468 and TCDD induced MCF7 cancer cells, compared to the non-CYP expressing MCF10A and naïve MCF7 cells (Table 8). Furthermore, studies by Lu *et al* have demonstrated the potent apoptotic activity of DMU212 with preferential inhibition of virally transformed human lung-derived cells (W138VA) and little or no inhibition of the untransformed counterparts (W138) [135]. DMU212 was also reported to be 50- to 100- fold more potent than resveratrol in inhibiting

the growth of these transformed cells [136]. Studies by Sale *et al* also demonstrated superior DMU212 cytotoxicity compared with resveratrol, where DMU212 was 4 times more potent as an inhibitor of the growth of human-derived HCA-7 colon cancer cells [137, 138]. DMU212 also exhibited higher bioavailability in mouse small intestine, colon and brain compared to resveratrol [137, 138] and oral administration of DMU212 in $Apc^{Min/+}$ mouse models retarded the gastrointestinal adenoma formation by 24% [138]. Crucially, studies by Wilsher of the CDDG have recently demonstrated the selective bioactivation of DMU212 in human breast tumour clinical samples [103], indicating the clinical potential for DMU212 in tumour selective chemotherapy. In light of these findings DMU212 has recently been the subject of a successful patent application by the CDDG [90] and is about to enter phase I clinical trials in USA and as such will undergo preliminary pre-clinical evaluation within the body of this work.

2.1.2 Discovery of a novel chalcone prodrug

Chalcones are the biogenetic precursors of flavonoids found extensively in nature from ferns to higher plants [139] and they display a wide variety of biological effects including estrogenic, antibacterial, antifungal, antiviral, anti-inflammatory and anticancer activities [116, 140]. The chalcone cytoskeleton can be mapped onto the E_2 framework (Figure 16) as well as other steroidal pharmacophores; this propensity has recently borne fruit in the design of aromatase and 17β-hydroxysteroid dehydrogenase inhibitors in the treatment of hormone dependant cancers [140].

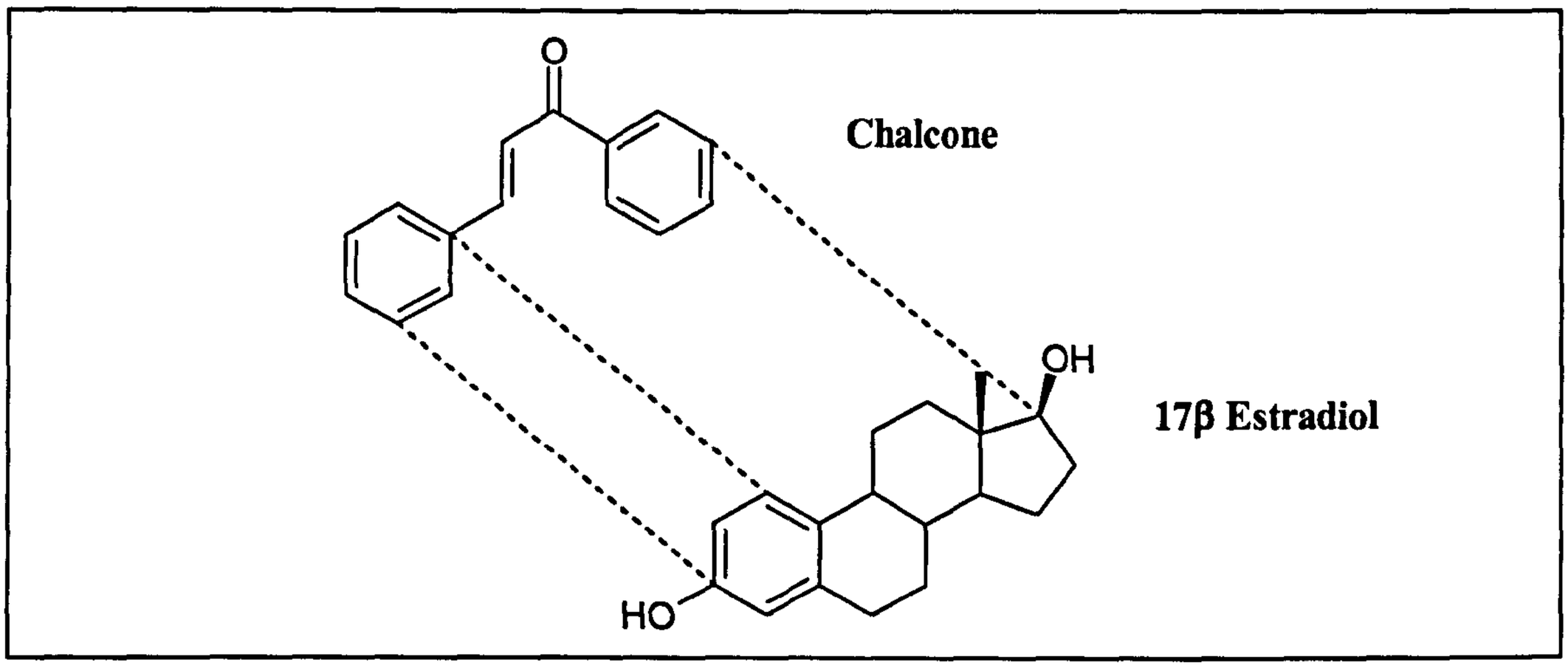

Figure 16. Mapping of the core chalcone structure onto the E_2 framework.

Chalcone derivatives have also shown cytotoxicity in the design of novel antimitotic agents possessing some of the structural functionalities present in CA-4 (Section 1.3.2.3) [113-115]. Accordingly, the CDDG have designed a library of novel synthetic chalcones based on the structure of CA-4 (Figure 14) and the hydrocarbon backbone of E_2 [118]. The cytotoxicity of these chalcones was screened in the MTT *in vitro* assay, as described in section 2.1.1, wherein the 3,4-methylenedioxy chalcone DMU135 exhibited optimum anticancer activity [118, 119]:

Table 9. Summary of DMU135 *in vitro* cytotoxicity data. Data provided by P. Butler of the CDDG.

HUMAN BREAST CELL-LINE	MCF7 WITHOUT TCDD	MCF7 WITH TCDD	ACTIVATION FACTOR	MCF10A	MDA-MB-468	TUMOUR SELECTIVE FACTOR
IC_{50} VALUES (μM)	7.0	0.08	90	2.3	0.006	380

DMU135 was found to be potently cytotoxic in MDA-MB-468 and TCDD induced MCF7 cancer cells with appreciably reduced cytotoxicity in MCF10A and naïve MCF7 cells (Table 9). Upon CYP1-mediated metabolism DMU135 is activated in the tumour to the potent tyrosine kinase inhibitor DMU117 (Figure 14). The catechol metabolite DMU117 is a potent broad spectrum tyrosine kinase inhibitor, which diminishes more than 30% of the total cellular tyrosine kinase activity [119]. The *in vivo* activity of DMU135 has also been investigated in xenograft models of human cancer (MDA-MB-468) in nude mice [141]. DMU135 was found to be well tolerated with a maximum tolerated dose of 200mg/kg. Dosing at this concentration DMU135 rapidly reached both the liver (15-170μM) and xenograft (20-75μM) 15 minutes after administration, with drug concentrations in xenografts remaining up to 10μM over the period of investigation. These results buttressed the advancement of DMU135 to pre-clinical animal studies, whereby, oral administration of DMU135 in $Apc^{Min/+}$ mouse models retarded the gastrointestinal adenoma formation by 46% [142]. In light of these findings DMU135 has recently been the subject of another successful patent application by the CDDG [118] and as such warrants further scrutiny in the preformulation of novel CYP1 activated anticancer prodrugs.

2.1.3 Preformulation of novel anticancer prodrugs

Preformulation programmes provide fundamental physicochemical characterisation for new chemical entities (NCEs), to indicate strategies for future development through identification of factors that may influence formulation design, drug manufacture, biopharmaceutics and pharmacokinetics, thereby creating an optimum drug delivery system [143, 144]. Of particular importance are the aqueous solubility and lipophilicity [145],

which influence the drug's dissolution, distribution, adsorption and bioavailability; followed by solid state properties such as crystallinity, particle size and morphology which affect drug processing and *in vivo* behaviour.

The impact of these physicochemical properties on the development (Section 1.4) of NCEs provides an impetus for in-depth preformulation at an earlier drug development stage, to minimise extensive and expensive testing of NCEs that possess unsatisfactory pharmaceutical properties, thereby reducing attrition rates in the later stages of drug development [146]. The evolution of proteomic, genomic and combinatorial synthetic technologies has enabled the rapid generation of NCEs in short periods of time and has subsequently prompted the quest for parallel high-throughput preformulation technology.

In this study the following physicochemical properties of the non-ionisable prodrugs DMU135 and DMU212 were determined; solubility, partition coefficient, scanning electron micrograph (SEM) imaging and differential scanning calorimetry (DSC). High-throughput analytical methods were also developed for solubility and partition coefficient determination.

2.1.3.1 Solubility

Solubility is defined as the concentration of solute dissolved in a solvent when equilibrium has been established between the two (i.e. a saturated solution) [147]. The aqueous solubility determines the concentration of drug in the solution (e.g. the intestinal fluid) from which the drug will be absorbed. Low aqueous solubility can lead to failure of NCEs during drug development and arises because of lipophilic substituents or strong intramolecular crystal lattice forces [124]. Drug solubility is an important physicochemical

property influencing drug bioavailability, rate of release into the dissolution medium and therapeutic efficacy. Many drugs are poorly soluble in water; therefore, measurement of drug solubility in various solvents is paramount for development of parenteral formulations. The solvents chosen for these preformulation studies were water to determine solubility in the intestinal fluids, ethanol 10% v/v, isopropyl alcohol (IPA), glycerol, propylene glycol, polyethylene glycol (PEG) and N-methyl pyrrolidone (NMP). NMP is a stable and safe solubilizer of hydrophobic drugs and solubility in NMP is comparable to dimethylsulfoxide (DMSO) but without the associated *in vivo* toxicity [148]. Several patents have elucidated improvements in drug solubility with NMP [148].

Solubility experiments are often described using the terms "kinetic solubility" and "thermodynamic solubility" [127]. For kinetic solubility measurements, the compounds are pre-dissolved in DMSO, or another suitable solvent and the solubility is measured as the concentration at which the sample precipitates from the aqueous medium [149]. For thermodynamic solubility measurements, the shake-flask method is used which measures the solubility at equilibrium. Usually the concentration at equilibrium is determined by adding excess drug into a medium, stirring the suspension for a defined time, filtering/centrifuging the suspension and quantifying the drug concentration in the supersaturated solutions [150].

Kinetic solubility measurements do not give a true measure of the drug solubility but rather an apparent solubility because crystal lattice effects are negated when the compound is dissolved in DMSO. Thus, any effects on solubility due to polymorphic variants cannot be investigated [151]. However, in the early stages of discovery, when many compounds are

synthesised in small quantities, high-throughput kinetic solubility measurements can provide an early indication of compounds that will present developmental challenges. Kinetic solubility measurements are also more amenable to automated methods, require minimal sample size and preparation, and are more appropriate in the discovery stage not only from an optimization perspective but also because most screens are run using compounds in DMSO medium [149].

Several kinetic solubility methods have been described in literature, using turbidimetry [151], nephelometry [152] and direct UV [153]. Lipinski *et al* [151] described a method to measure solubility by adding a DMSO stock solution dropwise to pH 7 phosphate buffer in a cuvette and using turbidity to detect precipitation. The solution turbidity was measured by light scattering in the 620-820 nm range with a UV detector. A high-throughput variation of this method using nephelometry was developed by Bevan *et al* [152], where DMSO stock solutions were added to phosphate buffer and serially diluted across a 96-well plate. The degree of light scattering of the dilutions was measured using a nephelometric plate reader and the concentration at which particulates appeared was used to estimate the upper limit of solubility. A high-throughput direct UV method has also been developed by Avdeef *et al* [153]. In this method DMSO stock solutions were robotically added to buffer in a 96-well plate and after an 18 hour period of equilibration, the filtered solution was analysed using a UV plate reader [153].

The drawbacks with kinetic solubility measurements are that they may be time-dependant and are most likely to use compounds pre-dissolved in DMSO [154]. The use of DMSO may increase the solubility to an unpredictable extent, since DMSO dilutions can easily

form supersaturated solutions [150, 155]. Consequently, the influence of crystal lattice energy and polymorphic variants are also completely masked in the DMSO dissolution process [151]. For compounds that are insoluble due to high crystallinity, the kinetic solubility will most likely differ significantly from the thermodynamic solubility [154]. And for compounds that exist as polymorphic variants, the precipitating form of the drug may not necessarily be the most stable one, which is a problem since polymorphs can differ greatly in solubilities [150].

For discovery scientists, solubility is used to assist in the rational selection of hits for further consideration; therefore, kinetic solubility measurements are acceptable. On the other hand, development scientists need to select amongst salt or crystalline forms, evaluate formulation excipients and determine minimum absorbable dose [155]. Therefore, development scientists generally measure the intrinsic solubility i.e. thermodynamic solubility of a compound. Traditional thermodynamic solubility measurements (shake-flask) are not feasible at an early drug discovery stage because of the large sample requirement, low throughput, and labour intensive sample preparation [149]. However, with the advances in automation, high-throughput variations of this method have also been developed. Glomme *et al* [150] have developed a miniaturised shake-flask method where the compound was weighed into a Whatman UniPrep filter chamber, buffer was added and the chamber was closed with the plunger, which has a filtration membrane on one end and a pre-attached cap on the other. The sample vials were placed in a HPLC autosampler-vial block and stirred for 24 hours, after which the block was placed in a Whatman processor that simultaneously depressed the plunger of all the devices, forcing the filtrate into the

reservoir of the plunger. HPLC was used to measure the filtrate concentration. This technique reduces the time for sample preparation for thermodynamic solubility measurement, because all of the operations are conducted in one device, and the filtration and analysis steps are automated [125].

Roy *et al* detailed the development of a 96-well plate assay, where the drug was initially introduced into the wells dissolved in acetonitrile, which was subsequently evaporated. Water was then added to the wells and the suspensions stirred for 24 hours followed by simultaneous filtration of suspensions contained in the wells and quantification on a UV plate reader [156]. The overall aim of both the high-throughput thermodynamic solubility methods discussed is to reduce the number of time-consuming steps in the shake-flask technique to improve its efficiency. This strategy was adopted within the scope of this thesis, where the traditional shake-flask method was used for sample equilibration followed by novel high-throughput assay on a UV plate reader. DMU135 and DMU212 solubility were determined and the novel technique was validated using conventional compounds (indomethacin) and a conventional assay (UV spectrophotometer).

2.1.3.2 Partition coefficients

The partition coefficient of a NCE provides a thermodynamic measure of its hydrophilic-lipophilic balance. Lipophilicity reflects the ability of the NCE to permeate biological lipid membranes in order to be absorbed, distributed into organs and tissues, and finally eliminated, so is important for pharmacokinetic properties. The relative affinity of the NCEs for aqueous and lipid environments determines the ease of solute permeation through the lipid membranes and is often represented by the octanol-water partition coefficient

[157]. A relationship exists between log *P* and aqueous solubility; highly lipophilic drugs often have poor aqueous solubility and vice-versa. A certain degree of lipophilicity is required for drug permeation of lipid membranes. However, solubility in the intestinal fluids is also a prerequisite for drug absorption from oral dosage forms. Therefore, NCE with a balance between the two parameters promise to result in optimum bioavailability.

The partition coefficient (*P*) for a non-ionisable drug is the ratio of concentrations (*C*) between two immiscible phases, e.g. organic (C_o) and aqueous (C_w), at equilibrium [158]:

$$\log P = \log\left[\frac{C_o}{C_w}\right] \tag{2.1}$$

Log *P* can be calculated experimentally using the shake-flask method to assess drug-portioning between organic (usually n-octanol) and aqueous phase. Drawbacks of this technique include time and relatively large quantities of drug needed. High-throughput log *P* methods have been developed through miniaturisation of the equilibration method in 96-well plates using robotic sample preparation combined with automated separation and analysis by reverse phase HPLC [159]. Wang *et al* have developed a modified shake-flask method, where partitioning is conducted in sealed vials and samples are quantified using LC/MS. Other high-throughput techniques include capillary electrophoresis in a 96-array format coupled with micellar electrokinetic chromatography [146] and reverse phase HPLC where test compounds partition between the polar mobile phase and the stationary non-polar phase (usually octadecane bonded to silica or polymer) [125]. The approach used in this thesis was to combine the usual shake-flask method with high-throughput analytical quantification.

Octanol is the most commonly used model for biological phospholipid membranes; because of its frequent application (i.e. convention is as important as any supposed biological relevance [160]). Considering the membrane complexities a simple isotropic solvent has served well as a model for predicting drug lipophilicity. This may be facilitated by the amphiphilic octanol structure containing eight hydrophobic C-atoms and a hydrophilic OH group, which is reflected in the octanol solubility parameter (δ=10.24) central to the range of most drugs [144]. Octanol is also able to donate hydrogen bonds and accept them almost as well as water in keeping with many biological macromolecules. Moreover, the use of alternative solvents with higher or lower polarities than octanol, may distort the measured log *P* [144]. Such that within a homologous drug series, solvents less polar than octanol e.g. hexane may be hyperdiscriminatory and exaggerate the differences in compound lipophilicity. On the other hand, solvents more polar than octanol e.g. butanol may be hypodiscriminatory resulting in log *P* values which are too close together [144].

This study details the novel application for a fluorescent plate reader (FPR) in high-throughput assay of log *P* samples which have been previously equilibrated using the traditional shake-flask method. The development of this method using DMU135 and DMU212 and the consequent validation of the novel application using conventional compounds (17β-estradiol and hydrocortisone) and a conventional assay (UV spectrophotometer) is also reported.

2.1.3.3 Thermodynamic evaluation

Thermal analytical methods such as DSC can be used to investigate thermal stability, glass transitions, polymorphism and solvation of NCE [161]. DSC measures the amount of

exothermic or endothermic energy (i.e. heat flow) required to keep the sample at the same temperature as the reference, as samples are heated or cooled at a constant rate [144]. Samples are encapsulated in aluminium pans and heated at rates of 1-400 °C/min to generate plots of sample heat flow vs. temperature:

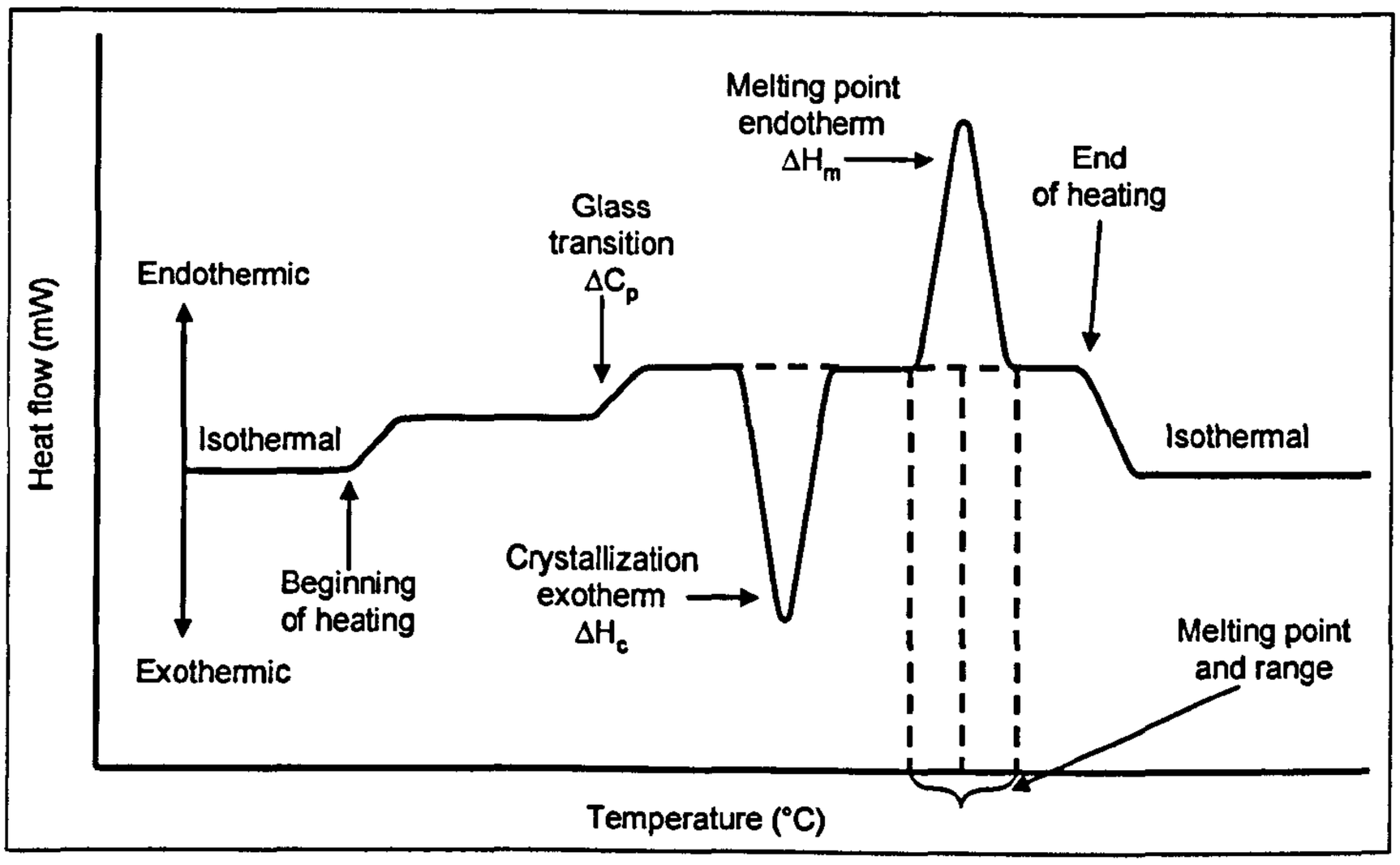

Figure 17. Schematic thermogram. Following a period of isothermal equilibration, the temperature is increased at a constant rate and the heat flow output is plotted vs. temperature [144].

These measurements provide information on glass transitions (i.e. T_g half extrapolated, which is the temperature extrapolated to the middle point of the glass transition and the change in heat capacity at a glass transition ΔC_p), crystallization (i.e. enthalpy of crystallization ΔH_c), stability and melting points (i.e. the enthalpy of fusion ΔH_m). In particular DSC is a useful tool for studying polymorphism or solvation [144, 161].

2.1.3.4 Morphological evaluation

The morphology of a drug is defined by both its structure and habit [147] and can impact both bioavailability and manufacturability. The internal structure of a crystal can exist in

cubic, tetragonal, orthorhombic, monoclinic, triclinic and hexagonal forms. The habit describes the external structure of the crystal and includes needle, columnar, blade, plate and tabular types (Figure 18) [147, 162]. The habits acquired depend on the crystallization conditions such as solvent, temperature and impurity concentration [158].

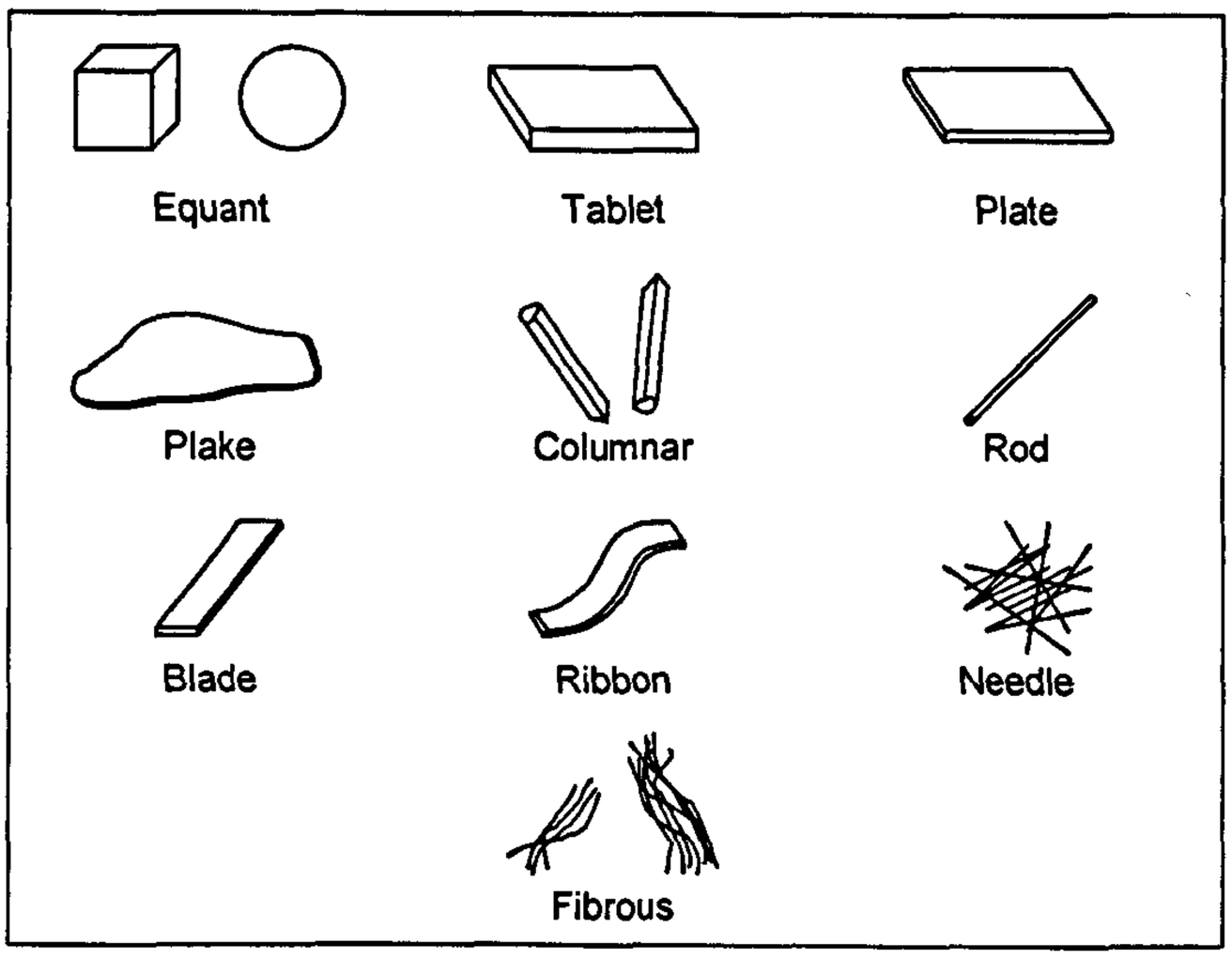

Figure 18. Illustration of crystal habit descriptions [162].

The SEM is ideal for morphological evaluation. In this technique the interrogating electron beam lies above the sample and is focused through a series of lenses to construct an image with scattered electromagnetic radiation. Samples are usually gold-coated to minimise the detrimental effects of surface charging [161]. SEM is a useful tool for distinguishing between different crystal habits with optimum bioavailability and manufacturability.

2.2 Materials and methods

Reagents were used as received from Sigma-Aldrich Chemical Company (Dorset, UK). General analytical grade ethanol, IPA, DMSO, HPLC grade water and 96-well Nunc®

plates were obtained from Fisher Scientific (Loughborough, UK). Anticancer prodrugs DMU135 and DMU212 were supplied by K. Ruparelia of the CDDG.

2.2.1 Determination of solubility

DMU135 and DMU212 drug solubility were measured in water, ethanol, IPA, NMP, glycerol, propylene glycol and PEG 400. The solubility of DMU135, DMU212 and indomethacin were determined by the shake-flask method. Excess amounts of drug (milled in a pestle and mortar beforehand) were added to test-tubes containing 10mL of different solvents. The drug suspensions were stirred continuously at 22°C ± 2°C for 24 hours to attain solubility equilibrium. The suspensions were then centrifuged in 96 deep-well plates at 3500rpm (Jouan bench-top centrifuge, model CR4i, Thermo Electron Corporation, Massachusetts, USA) for 15 minutes at 22°C to remove any particulate matter and assayed on the Heλios β UV spectrophotometer (Unicam, Cambridge, UK) and Spectramax M5 UV plate reader (Molecular Devices, California, USA) at the pre-determined wavelength. Appropriate calibration curves were conducted for all solvent-drug systems and dilutions were conducted if necessary. All experiments were conducted in triplicate.

2.2.2 Determination of log P

The log *P* values of DMU135, DMU212, 17β-estradiol and hydrocortisone were determined using the shake-flask method. The log *P* was determined at 22°C ± 2°C by preparing a 100 μg/mL drug stock solution in octanol and mixing it with an equal volume of water in 10mL test-tubes (the octanol and water were pre-saturated with each other beforehand). The two immiscible phases were stirred together for 24 hours at 22°C ± 2°C

to allow the solute to reach partition equilibrium. After allowing the mixture to stand for 24 hours, the samples were centrifuged in 96 deep-well plates for 15 minutes at 3500rpm (Jouan bench-top centrifuge) after which the two phases were separated. Aliquots of the samples were assayed either on a Heλios UV spectrophotometer at the corresponding maximum wavelength or plated out into 96-well plates and measured on the SpectraMax M5 fluorescent plate reader (Molecular Devices, California, USA) at the corresponding emission and excitation wavelengths.

Drug concentration in each phase was quantified through construction of calibration curves prepared in 96-deep well plates and log *P* was calculated using equation 2.1. Lipophilic calibration curves were prepared from a 100 μg/mL drug-octanol stock to give concentrations in the range 10-100 μg/mL and hydrophilic calibration curves were prepared from a 5 μg/mL drug-water stock to give concentrations in the range 0.5-5 μg/mL. All experiments were conducted in triplicate.

2.2.3 Differential scanning calorimetry

The samples (1-6mg) were placed in sealed aluminium pans, model number 0219-0062 (PerkinElmer) for solid samples. For oily samples (chapter 5) aluminium pans with a pin-holed lid, model number B0169317 (PerkinElmer) were used. Experiments were run in a PerkinElmer Diamond DSC (Massachusetts, USA) supplied with nitrogen and helium gas and connected to a PerkinElmer cryofill. A heating rate of 400°C/min was used over a -100 to 300°C range, immediately after heating samples were rapidly cooled to the initial temperature of -100°C using liquid nitrogen and re-heated to determine the stability of the

compounds. An empty pan served as the reference and Indium was used to calibrate the temperature. Data analysis was conducted with Pyris software.

2.2.4 Scanning electron microscopy

Samples (1-5mg) were mounted onto SEM aluminium stubs, using double-sided sticking tape (Agar Scientific Ltd., Essex, UK) and coated with gold for 60 seconds under argon using an Edwards SB150 sputter coater (Sussex, UK) in a high vacuum evaporator equipped with an omni-rotary stage. The morphologies of the samples were investigated using a Leica S430 SEM (London, UK) at 5KV with a probe current of 150 picoamps, a working distance of 25mm and magnification ranging from 25 to 9500X. The samples were analysed using Leica electron optics software version V.02.04B.

2.2.5 Statistical analysis

The data obtained in this study were subjected to statistical analysis using Microsoft Excel Software, for a one-way analysis of variance (ANOVA). A p-value of less than 0.05 was considered evidence of a significant difference.

2.3 Results

2.3.1 Solubility determination

Both DMU135 and DMU212 are slightly soluble in water; however, they were more soluble in organic solvents such as IPA and NMP. Overall, DMU135 (Table 10) was more soluble in all solvents compared to DMU212 (Table 11) and solubility values measured on the UV plate reader were comparable with those measured on the UV spectrophotometer:

Table 10. Average solubility of DMU135 in various solvents measured at 22 ± 2°C.

SOLVENT	AVERAGE SOLUBILITY OF DMU135 MEASURED ON THE UV PLATE READER (mg/mL) (n=3)	AVERAGE SOLUBILITY OF DMU135 MEASURED ON THE UV SPECTROPHOTOMETER (mg/mL) (n=3)
Water	0.001 ± 0.0001	0.001 ± 0.0001
10% v/v aqueous ethanol	0.003 ± 0.0005	0.003 ± 0.0005
Isopropyl alcohol	1.510 ± 0.085	1.642 ± 0.070
N-Methyl Pyrrolidone	388.863 ± 4.004	367.569 ± 4.286
Glycerol	0.039 ± 0.010	0.045 ± 0.012
Propylene Glycol	1.356 ± 0.005	1.282 ± 0.019
Polyethylene Glycol 400	39.880 ± 5.727	41.685 ± 1.505

Table 11. Average solubility of DMU212 in various solvents measured at 22 ± 2°C.

SOLVENT	AVERAGE SOLUBILITY OF DMU212 MEASURED ON THE UV PLATE READER (mg/mL) (n=3)	AVERAGE SOLUBILITY OF DMU212 MEASURED ON THE UV SPECTROPHOTOMETER (mg/mL) (n=3)
Water	0.001 ± 0.0001	0.001 ± 0.0001
10% v/v aqueous ethanol	0.001 ± 0.0001	0.001 ± 0.0002
Isopropyl alcohol	0.585 ± 0.025	0.656 ± 0.013
N-Methyl Pyrrolidone	150.573 ± 6.886	152.727 ± 10.496
Glycerol	0.016 ± 0.001	0.018 ± 0.002
Propylene Glycol	0.451 ± 0.133	0.492 ± 0.027
Polyethylene Glycol 400	13.508 ± 1.612	14.281 ± 0.033

In a further test of this method's validity the aqueous solubility of indomethacin was determined on both the UV spectrophotometer and plate reader and corresponded to that stated in literature of 0.015 mg/mL [163].

Table 12. Average solubility of indomethacin in water measured at 22 ± 2°C.

SOLVENT	AVERAGE SOLUBILITY OF INDOMETHACIN MEASURED ON THE UV PLATE READER (mg/mL) (n=3)	AVERAGE SOLUBILITY OF INDOMETHACIN MEASURED ON THE UV SPECTROPHOTOMETER (mg/mL) (n=3)
Water	0.010 ± 0.001	0.010 ± 0.001

2.3.2 Log P determination

Log *P* experimental values determined suggest that DMU135 (Table 13) is a more favourable candidate for preclinical evaluation than DMU212 (Table 14), which has a higher log *P* value and therefore is more lipophilic, presenting greater barriers to formulation and drug aqueous solubility.

Table 13. Concentration of DMU135 in different phases and log *P*, measured on UV spectrophotometer.

SAMPLE	MEAN CONCENTRATION OF DRUG IN WATER PHASE (μg/mL) (n=6)	MEAN CONCENTRATION OF DRUG IN OCTANOL PHASE (μg/mL) (n=6)	Log *P*
1	0.25	79.65	2.50
2	0.25	80.62	2.51
3	0.26	79.17	2.48
	MEAN log *P*		2.49 ± 0.01

Table 14. Concentration of DMU212 in different phases and log *P*, measured on UV spectrophotometer.

SAMPLE	MEAN CONCENTRATION OF DRUG IN WATER PHASE (μg/mL) (n=6)	MEAN CONCENTRATION OF DRUG IN OCTANOL PHASE (μg/mL) (n=6)	Log *P*
1	0.127	95.57	2.87
2	0.109	97.27	2.95
3	0.102	93.58	2.96
	MEAN log *P*		2.93 ± 0.05

2.3.2.1 Fluorescent plate reader method

The log *P* values for DMU135 and DMU212 determined on the fluorescent plate reader were comparable with those determined on the UV spectrophotometer, thereby confirming the usefulness of the high-throughput method:

Table 15. Concentration of DMU135 in different phases and log *P*, measured on the fluorescent plate reader.

SAMPLE	MEAN CONCENTRATION OF DRUG IN WATER PHASE (μg/mL) (n=6)	MEAN CONCENTRATION OF DRUG IN OCTANOL PHASE (μg/mL) (n=6)	Log *P*
1	0.27	71.45	2.42
2	0.29	75.56	2.41
3	0.25	73.11	2.47
	MEAN log *P*		2.44 ± 0.03

Table 16. Concentration of DMU212 in different phases and log *P*, measured on the fluorescent plate reader.

SAMPLE	MEAN CONCENTRATION OF DRUG IN WATER PHASE (μg/mL) (n=6)	MEAN CONCENTRATION OF DRUG IN OCTANOL PHASE (μg/mL) (n=6)	Log *P*
1	0.07	98.99	3.12
2	0.08	103.38	3.12
3	0.09	100.90	3.05
	MEAN log *P*		3.10 ± 0.04

2.3.2.1.1 Comparison with 17β-estradiol and hydrocortisone

In a further test of the high-throughput method validity the log *P* of 17β-estradiol and hydrocortisone determined on the UV spectrophotometer were comparable to those determined on the fluorescent plate reader:

Table 17. Concentration of 17β-estradiol in different phases and log *P*, measured on UV spectrophotometer.

SAMPLE	MEAN CONCENTRATION OF DRUG IN WATER PHASE (μg/mL) (n=6)	MEAN CONCENTRATION OF DRUG IN OCTANOL PHASE (μg/mL) (n=6)	Log *P*
1	0.15	89.86	2.78
2	0.52	90.81	2.24
3	0.22	91.43	2.61
	MEAN log *P*		2.54 ± 0.28

Table 18. Concentration of 17β-estradiol in different phases and log *P*, measured on fluorescent plate reader.

SAMPLE	MEAN CONCENTRATION OF DRUG IN WATER PHASE (μg/mL) (n=6)	MEAN CONCENTRATION OF DRUG IN OCTANOL PHASE (μg/mL) (n=6)	Log *P*
1	0.18	98.01	2.73
2	0.21	95.39	2.65
3	0.20	95.12	2.67
	MEAN log *P*		2.68 ± 0.04

Table 19. Concentration of hydrocortisone in different phases and log *P*, measured on UV spectrophotometer.

SAMPLE	MEAN CONCENTRATION OF DRUG IN WATER PHASE (μg/mL) (n=6)	MEAN CONCENTRATION OF DRUG IN OCTANOL PHASE (μg/mL) (n=6)	Log *P*
1	1.83	90.61	1.70
2	1.90	90.55	1.68
3	1.93	89.99	1.67
	MEAN log *P*		1.68 ± 0.01

Table 20. Concentration of hydrocortisone in different phases and log *P*, measured on fluorescent plate reader.

SAMPLE	MEAN CONCENTRATION OF DRUG IN WATER PHASE (μg/mL) (n=6)	MEAN CONCENTRATION OF DRUG IN OCTANOL PHASE (μg/mL) (n=6)	Log *P*
1	2.54	89.65	1.55
2	1.97	81.42	1.62
3	2.36	92.77	1.59
	MEAN log *P*		1.59 ± 0.04

Furthermore, the log *P* values for 17β-estradiol and hydrocortisone determined on both the fluorescent plate reader and UV spectrophotometer corresponded to values stated in literature [164], as shown by Figure 19:

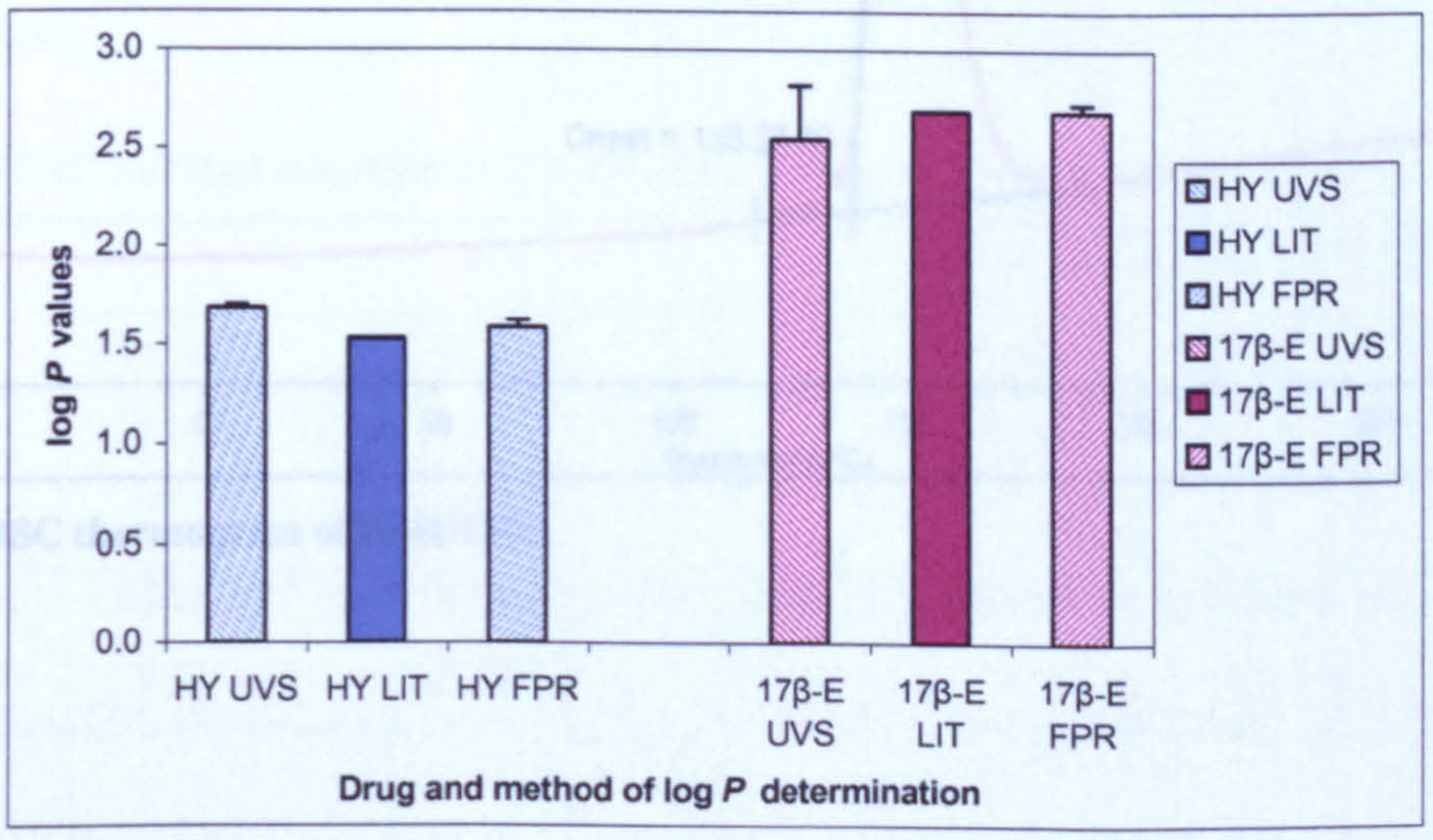

Figure 19. Correlation between experimental log *P* values measured versus values from literature for hydrocortisone and 17β-estradiol. (1) Hydrocortisone log *P* measured on the UV spectrophotometer; (2) hydrocortisone log *P* from literature; (3) hydrocortisone log *P* measured on the fluorescent plate reader; (4) 17β-estradiol log *P* measured on the UV spectrophotometer ; (5) 17β-estradiol log *P* from literature; (4) 17β-estradiol log *P* measured on the fluorescent plate reader.

2.3.3 Differential scanning calorimetry

DSC measurements for DMU135 and DMU212 do not show the presence of polymorphs, solvates and impurities, since both prodrug scans exhibited a single endotherm peak:

Table 21. DSC of DMU135 and DMU212 – initial heating from -100-300°C at 400°C/min.

DRUG	MELTING POINT ENDOTHERM		
	ONSET TEMPERATURE (°C)	PEAK TEMPERATURE (°C)	ENTHALPY OF FUSION ΔH (J/g)
DMU135	138.27	148.43	83.79
DMU212	164.96	173.49	107.27

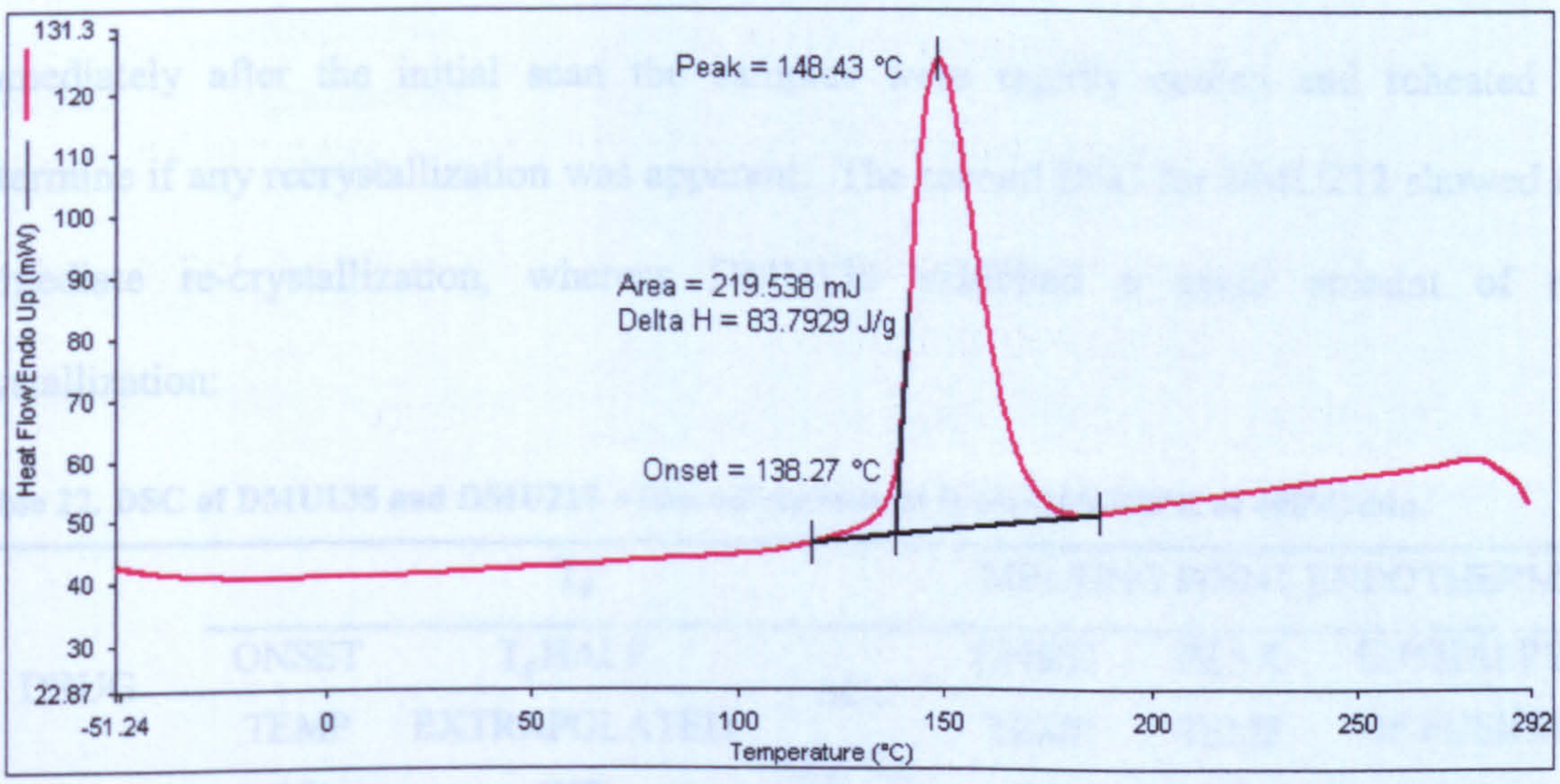

Figure 20. DSC thermogram of DMU135.

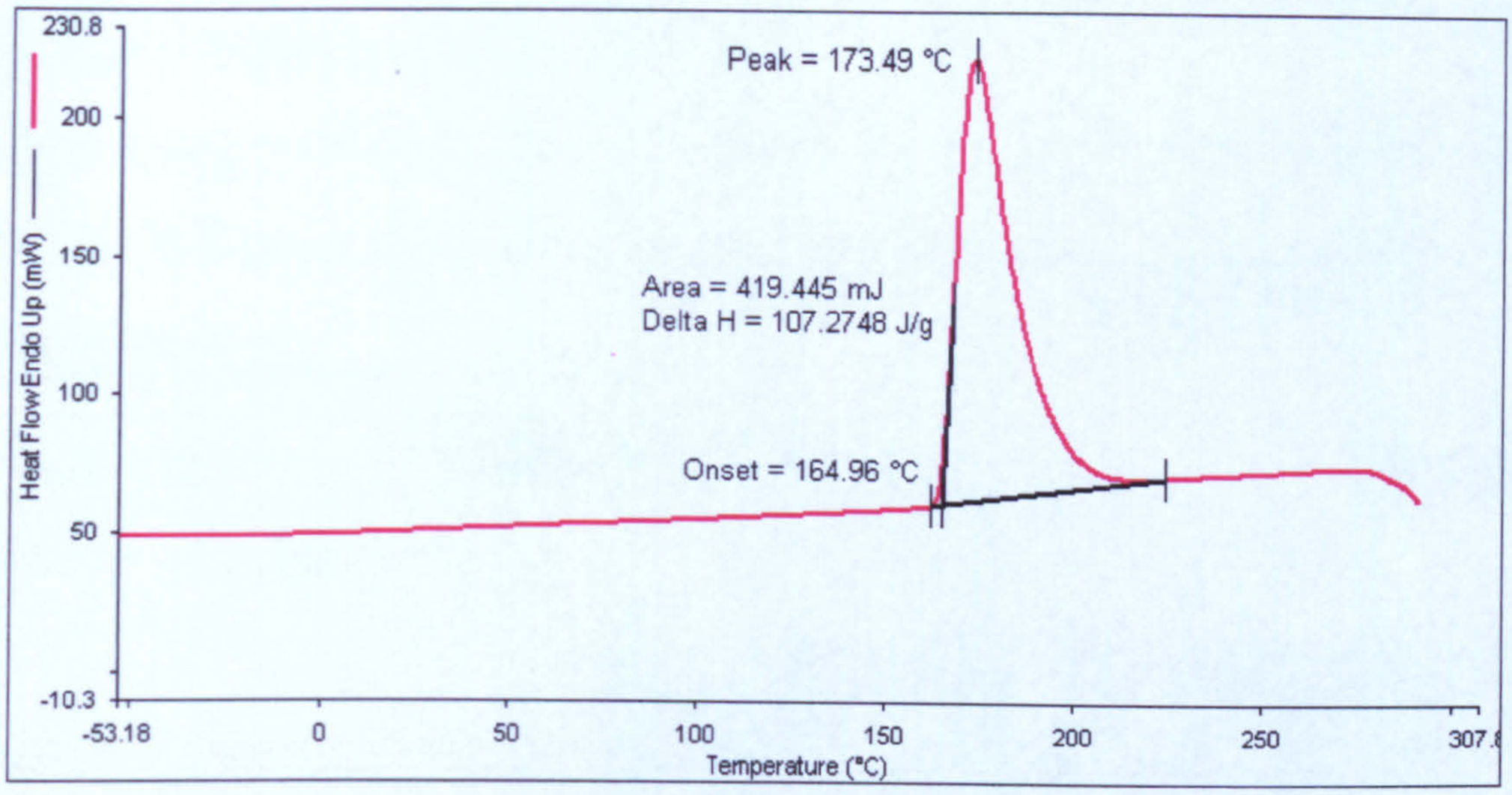

Figure 21. DSC thermogram of DMU212.

Immediately after the initial scan the samples were rapidly cooled and reheated to determine if any recrystallization was apparent. The second DSC for DMU212 showed no immediate re-crystallization, whereas DMU135 exhibited a small amount of re-crystallization:

Table 22. DSC of DMU135 and DMU212 – immediate re-heat from -100-300°C at 400°C/min.

DRUG	T_g			MELTING POINT ENDOTHERM		
	ONSET TEMP (°C)	T_g HALF EXTRAPOLATED (°C)	ΔC_p (J/g*°C)	ONSET TEMP (°C)	PEAK TEMP (°C)	ENTHALPY OF FUSION ΔH (J/g)
DMU135	25.60	32.91	0.46	138.48	147.08	1.42
DMU212	3.93	12.06	0.47	–	–	–

2.3.4 Scanning electron microscopy

SEM imaging of DMU135 showed the crystals to exist as big agglomerated blades, whereas, DMU212 crystals had large particles with a smaller surface area, in the form of columnar crystals:

Table 23. SEM imaging of DMU135 and DMU212.

DRUG	CRYSTAL SHAPE	SEM IMAGE
DMU135	Orthorhombic, Agglomerated blades	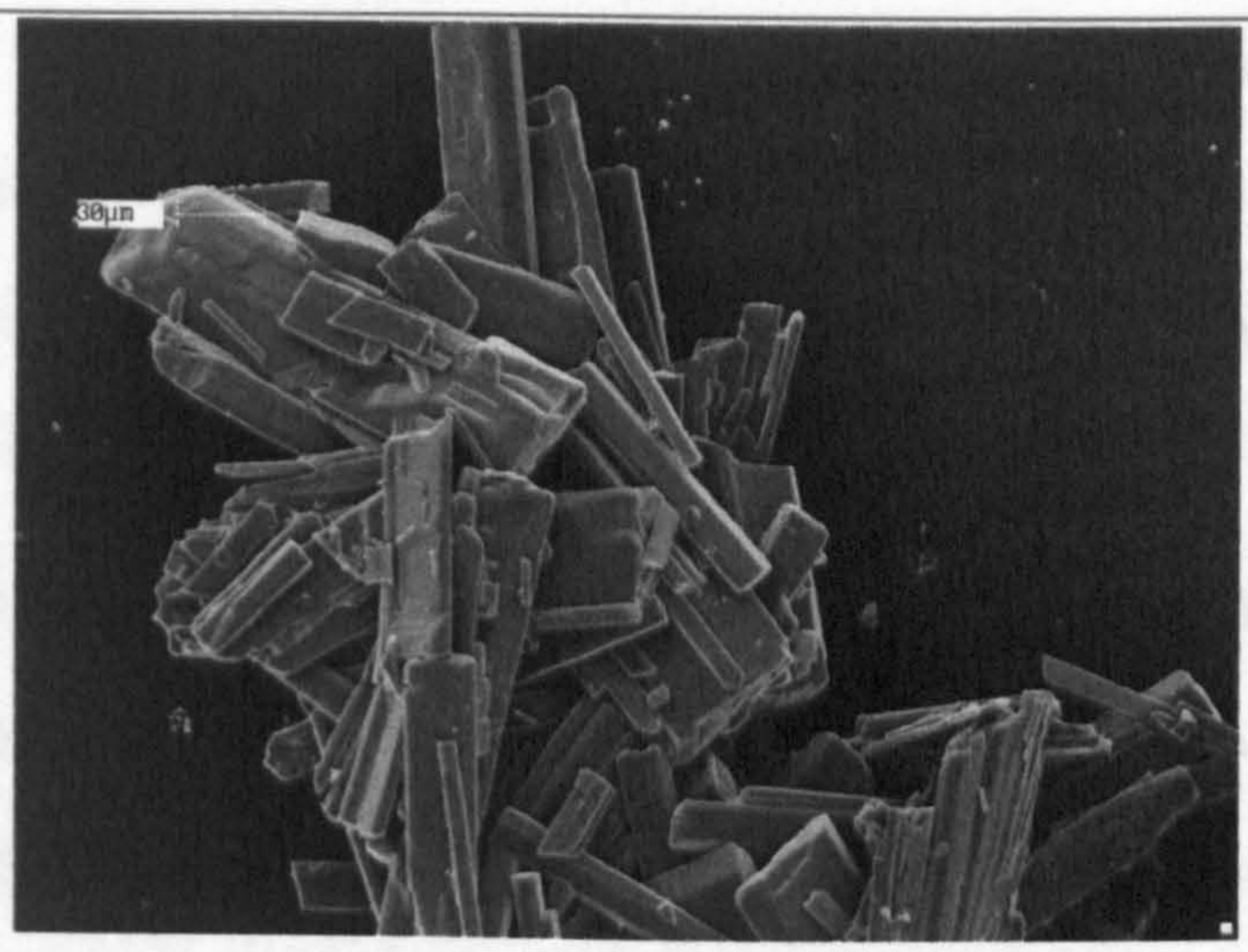
DMU212	Triclinic, columnar	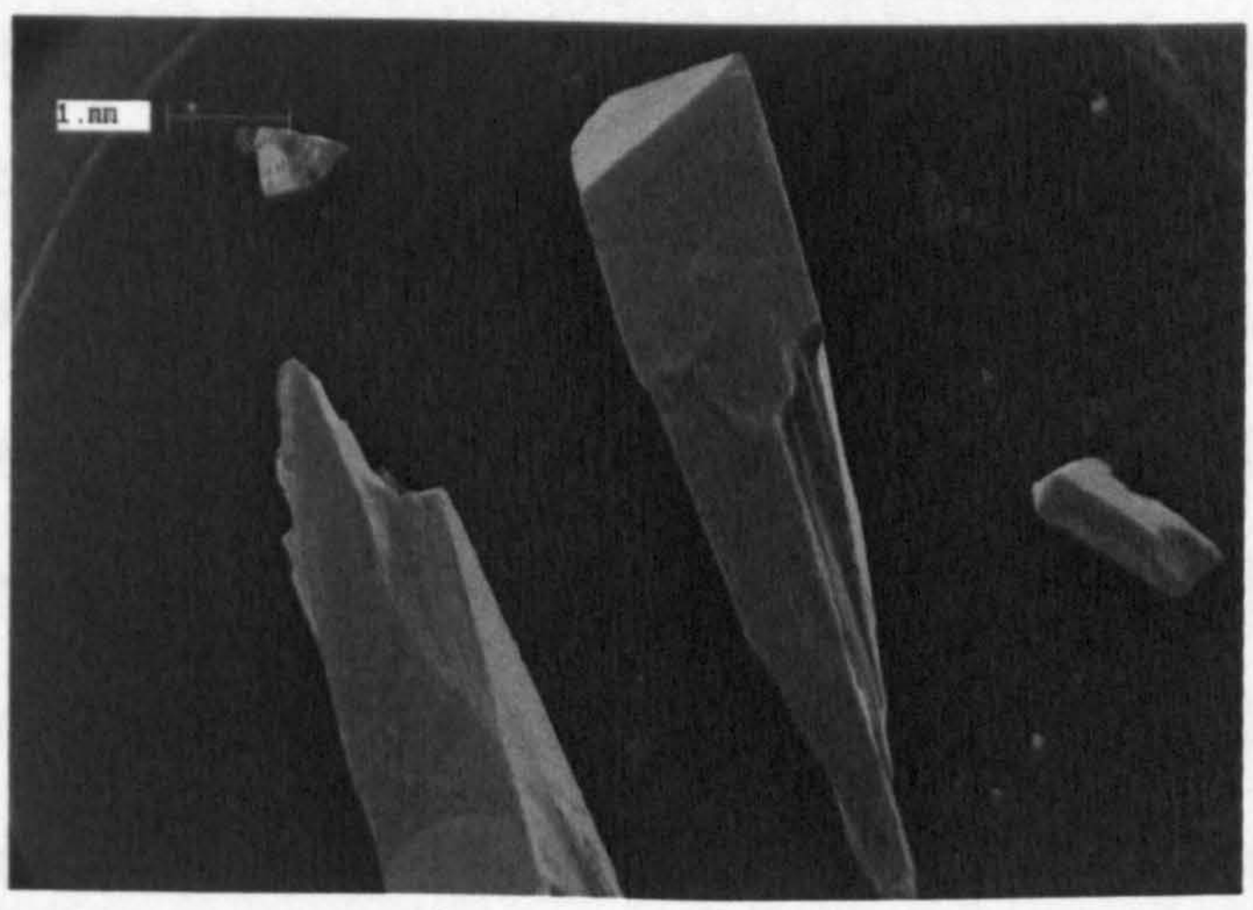

2.4 Discussion

DMU135 exhibited a slightly better solubility profile in all solvents compared with DMU212. However, both DMU135 and DMU212 exhibited poor aqueous solubility at 0.001 mg/mL. The lipophilicity of these prodrugs stems from the non-ionisable groups on the stilbene and chalcone backbones, the presence of the lipophilic methyl groups on both prodrugs is important for potency; however, the opposite effect is true for the drug pharmaceutical properties [151]. DMU135 contains three methyl groups as well as six hydrogen bond acceptor groups and DMU212 contains four of each, which is reflected in their relative solubilites as the presence of two extra polar oxygen groups and one less methyl group in DMU135 slightly increases its polarity.

Maximum solubility for both prodrugs was exhibited in NMP, probably resulting from the chemical reactions on the NMP pyrrolidone ring including hydrogen bonding and polar interactions. DMU135 NMP solubility of 388.863 ± 4.004 mg/mL on the UV plate reader and 367.569 ± 4.286 mg/mL on the UV spectrophotometer and DMU212 NMP solubility of 150.573 ± 6.886 mg/mL on the UV plate reader and 152.727 ± 10.496 on the UV spectrophotometer suggests that this may be the solvent/co-solvent of choice for future parenteral formulation and pharmacokinetic studies possibly combined with PEG 400, propylene glycol or IPA, which were the next best prodrug solubilizing agents respectively.

The solubility values determined on the UV plate reader were comparable to those determined on the UV spectrophotometer with maximum difference between the two techniques being approximately 10%. In a further test of this method's validity the aqueous solubility of indomethacin determined by both the UV plate reader and spectrophotometer

was 0.010 mg/mL and corresponded with that stated in literature of 0.015 mg/mL [163]. To determine whether the differences in solubility were a factor of the drug concentration, the solubility values for all compounds measured with both techniques were statistically compared with ANOVA (Section 2.2.5):

Table 24. Statistical comparison between DMU135, DMU212 and indomethacin solubility values as measured on the UV plate reader and spectrophotometer.

SOLVENT	DMU135 p VALUE	DMU212 p VALUE	INDOMETHACIN p VALUE
Water	0.594	0.809	0.999
10% v/v aqueous ethanol	0.682	0.716	-
Isopropyl alcohol	0.105	0.012	-
N-Methyl Pyrrolidone	0.003	0.781	-
Glycerol	0.629	0.501	-
Propylene Glycol	0.031	0.716	-
Polyethylene Glycol 400	0.708	0.568	-

The majority of solubility measurements between the two assay techniques were not found to be significantly different ($p>0.05$). However, DMU135 solubility measurements in NMP and propylene glycol and DMU212 solubility measurements in IPA were found to be significantly different ($p<0.05$). The solubility values obtained in these instances were with the higher drug concentrations, however, in most cases even at these concentrations a significant difference was not observed between the UV plate reader and UV spectrophotometer methods. On the whole, these results indicate that the 96-well UV plate reader can be successfully implemented for high-throughput, miniaturised and valid solubility quantification.

Both DMU135 and DMU212 log *P* data suggest that the prodrugs are lipophilic, DMU135 exhibited the more favourable (i.e. less lipophilic) log *P* (2.49) compared with DMU212 (2.93) which is more lipophilic presenting greater barriers to drug aqueous solubility and adsorption. The log *P* of DMU135 determined by the UV spectrophotometer was 2.49 ± 0.01, compared to that determined on the fluorescent plate reader at 2.44 ± 0.03 and the log *P* of DMU212 determined by the UV spectrophotometer was 2.93 ± 0.05, comparable to the value determined on the fluorescent plate reader at 3.10 ± 0.04, thereby confirming the usefulness of the high-throughput method. In a further test of this method's validity, the log *P* of 17β-estradiol determined by the UV spectrophotometer was 2.54 ± 0.28 compared with the value of 2.68 ± 0.04 obtained with the fluorescent plate reader, corresponding well with that stated in literature of 2.69 [164]. The log *P* of hydrocortisone determined by the UV spectrophotometer was 1.68 ± 0.01 and with the fluorescent plate reader was 1.59 ± 0.04, again both corresponding with that stated in literature of 1.53. Figure 19 illustrates the correspondence between log *P* values stated in literature to those determined experimentally with both techniques. Overall, the results as determined on the fluorescent plate reader were closer to the published log *P* values, compared to those determined by the UV spectrophotometer.

DMU135 has better aqueous solubility compared with DMU212 as reflected in the respective log *P* values. This arises because DMU212 contains more lipophilic substituents and less hydrogen-bond acceptor groups compared with DMU135. DMU135 can therefore form stronger polar interactions with water through van der Waal forces compared with DMU212, resulting in increased DMU212 lipophilicity through a stronger affinity for

octanol, which may impair permeability across phospholipid membranes, since aqueous solubility in the intestinal fluids is a prerequisite for oral drug absorption.

The effect of the different substituents on the log *P* of both DMU135 and DMU212 can be further analysed by considering the log *P* as an additive-constitutive property [160]. In fact several methods for calculating log *P* are based on the theory first proposed by Hansch and Fujita [157], that molecules can be broken down into predefined fragments and their corresponding contributions summed up to obtain the final log *P* [160]. The most widely used method for calculating log *P* is the CLOGP method developed by Hansch and Leo [165, 166]. Using this method different fragments are assigned log *P* contribution values. The fragments of interest within the context of this study were the methyl with a fragment contribution of 0.876; aliphatic oxygen with a fragment contribution of -1.820 and aromatic oxygen with a fragment contribution of -0.610. DMU135 contains three methyl substituents as well as four aliphatic and two aromatic oxygen substituents, whereas DMU212 contains four methyl and four aliphatic oxygen substituents. Therefore, theoretically the summing up of these fragment contributions, to obtain the final calculated log *P* of the core molecule, would mean that DMU212 is the more lipophilic prodrug, which is corroborated by the measured log *P*. Overall, the results indicate that the 96-well fluorescent plate reader can be successfully implemented for high-throughput, miniaturised and valid log *P* quantification.

DSC measurements for DMU135 and DMU212 do not show the presence of polymorphs, solvates and impurities, since both prodrug scans exhibited a single melting point endotherm. The onset temperature for DMU135 was 138.27°C and for DMU212 was

164.96°C. The ΔH for DMU135 and DMU212 was 83.79 and 107.27 J/g respectively. These values correlate with the overall solubility of the two drugs; DMU135 requires less energy to overcome the intermolecular crystal lattice forces (i.e. ΔH) and as such was more soluble in all solvents compared with DMU212. Immediately after the initial scan the samples were rapidly cooled and reheated to determine if recrystallization was apparent and subsequently to determine the solid-state stability of the prodrugs. In the second DSC scan the melting point endotherm for DMU212 was absent and the onset of a glass transition temperature (T_g) was observed at 3.93°C, suggesting that the crystals were in an amorphous state and no immediate recrystallization was apparent. With DMU135 a T_g was observed at 25.60°C, however, a small melting point endotherm was also observed at 138.48°C with a ΔH of 1.42 J/g. This indicates that upon immediate reheat DMU135 crystals were mostly in an amorphous state, however, a small proportion of recrystallization was apparent. The fact that DMU135 exhibited recrystallization suggests that the solid-state stability of DMU135 is superior to that of DMU212.

SEM imaging of DMU135 showed the crystals system was orthorhombic with big agglomerated blades, whereas, DMU212 crystals had very large particles with a small surface area and existed as triclinic columnar crystals. The particle size of DMU135 is difficult to assess as the aggregates have both loosely and tightly bound particles [162] and DMU212 particle size was relatively large at >1mm. The degree of agglomeration and the relatively small surface area of both drugs would account for their poor aqueous solubility.

The physicochemical properties of DMU135 and DMU212 have been evaluated and the core findings are summarised in Table 25:

Table 25. Comparison of some of the physicochemical properties of DMU135 and DMU212.

PROPERTY / DRUG	DMU135	DMU212
Activation Factor	90	22
Tumour Selective Factor	380	4300
Appearance	Pale yellow, crystalline	Yellow, crystalline
Molecular Weight	342	300
Melting Point (°C)	138.27	164.96
Enthalpy of fusion ΔH (J/g)	83.79	107.27
Crystal System	Orthorhombic, aggregated blades	Triclinic, columnar
Polymorphism	No evidence of polymorphs	No evidence of polymorphs
Hydrogen Bond Acceptor Groups	6	4
Aqueous solubility (mg/mL)	0.001 ± 0.0001	0.001 ± 0.0001
Solubility in NMP (mg/mL)	367.569 ± 4.286	152.727 ± 10.496
Log *P*	2.49 ± 0.01	2.93 ± 0.05

Generally, both DMU135 and DMU212 were found to be lipophilic, poorly soluble in water and greatly soluble in organic solvents such as NMP. The high crystallinity of both compounds significantly contributes to their non-polarity. The preformulation study conducted suggests that DMU135 has better development prospects compared to DMU212 with optimum solubility, log *P* and thermodynamic stability. On the other hand DMU212 is eleven times more potent as a CYP1B1 activated prodrug compared to DMU135. Furthermore, studies within the CDDG have found DMU135 to be unstable *in-vitro*, whereas DMU212 was relatively stable. Chalcones such as DMU135 are synthesised by Claisen-Schmidt aldol condensation reactions between acetophenone and benzaldehydes

with elimination of a water molecule to generate a α,β-unsaturated ketone. This structure is vulnerable in aqueous conditions to retro-aldol condensation reactions, where the presence of water reverses the reaction to liberate the starting materials; benzaldehyde and acetophenone. Moreover, DMU135 was also shown to undergo photo-isomerization under ambient light from the *trans* to the *cis* isomer (*unpublished results*, D. Ankrett, CDDG). As isomerisation can be extremely fast (seconds), the biological evaluation of chalcones can be fairly complicated, in that the potency and stability may differ significantly between the *trans* and *cis* isomers [167].

Overall, both DMU135 and DMU212 had the same aqueous solubility, with closely related solubilites in various organic solvents. The log *P* values were also relatively similar. DMU135 had the better thermodynamic solubility but in-house studies have shown DMU212 to have better solution stability. Accrued with the cytotoxic data these physicochemical studies buttress the advancement of DMU212 to further drug development studies. Novel high-throughput screening methods using 96-well fluorescent and UV plate readers have also been successfully implemented and validated for log *P* and solubility determination. High-throughput analytical technology can potentially accelerate the acquisition of physicochemical data for a NCE at an early stage in the drug development pipeline and miniaturisation of sample quantities can also be a benefit during preformulation where drug supplies can be limited. On the whole, 96-well plate high-throughput quantification may find use in pharmaceutics, to potentially reduce drug development times, resource requirements and the number of *in vivo* experiments.

CHAPTER 3

Oral Formulation of Non-Ionisable Prodrugs

3.1 Introduction

Synthesis of CYP1B1 non-toxic prodrugs is fruitless without the transfer of these NCEs from a preclinical, discovery stage into formulated dosage forms appropriate for clinical trials. These can vary from simple solutions through to complex drug delivery systems using numerous additives and excipients [147]. Before a NCE can be successfully formulated into a dosage form three factors are taken into consideration. These are the physicochemical properties of the drug; biopharmaceutical considerations, including factors affecting the rate and extent of drug absorption from different routes of administration and finally therapeutic considerations of the clinical indication to be treated [147].

However, the increasing adoption of high-throughput screens and combinatorial chemistry in the pharmaceutical industry has prompted the quest for the development of parallel technology in formulation [121] and more importantly fuelled the development of drugs which almost exclusively focus on drug potency and selectivity whilst compromising on pharmaceutical properties, thereby creating higher attrition rates in formulation [122, 123]. The anticancer prodrug DMU212 was designed in this manner with non-ionisable O-methyl groups which are important for potency but provide no capability for salt selection, since the active moiety is introduced *in situ*. Consequently DMU212 exhibits both lipophilicity and poor aqueous solubility which may present challenges during formulation studies.

3.1.1 Oral formulation of novel anticancer prodrugs

Oral dosage forms are one of the most frequently used for drug administration because of their convenience, simplicity and cost-effective manufacturing processes [147]. Orally

administered anticancer drugs have become increasingly abundant in chemotherapeutics, corroborated by the profusion of orally formulated agents currently in development [168]. Moreover, several new oral analogues or oral formulations of conventional cytotoxic agents such as etoposide, cyclophosphamide and 5-FU have recently been developed [169]. Oral chemotherapy is to be preferred in the first place for its convenience and its potential to improve patient quality of life. In addition, the need for infusions and consequent hospitalisation are eliminated, therefore, making this route of administration more patient compliant, practical and economically viable. Finally, the oral route also facilitates the use of more chronic treatment regimens, which result in prolonged exposure to chemotherapeutic agents [169].

3.1.1.1 Hard gelatine capsules

Capsules are one of the most popular of oral dosage forms and generally the bioavailability is better or equal to that of a tablet and unlike a tablet, no complex formulations, or techniques are needed, allowing quicker submission of the NCE for clinical trials as fewer development problems are encountered [170, 171]. There are many factors influencing release of drugs from capsules such as capsule shell disintegration and dissolution of the encapsulated product. Dissolution rate may be the most important limitation in rate of drug absorption compared with phospholipid membrane permeation, and is influenced by the capsule formulation and local conditions in the gastrointestinal tract. Therefore, formulation is an important factor in determining the release rate and bioavailability of the encapsulated product [147].

The major constituents of the powder mixture investigated for DMU212 capsule formulation were the drug and hydrophilic diluents (e.g. lactose and sorbitol) generally added to increase powder bulk; however, addition of hydrophilic diluents can also improve the solubility of poorly soluble drugs by improving the drug-water affinity, through optimisation of effective drug surface area [172]. Cyclodextrins were also used as diluents to potentially improve the solubility of DMU212 through formation of inclusion complexes, acting as drug carriers by masking drug hydrophobicity [173]. Incorporation of surfactants as wetting agents e.g. sodium lauryl sulphate (SLS) was also studied for possible dissolution enhancement, through reduction of interfacial tension between the drug and medium. Glidants/lubricants such as magnesium stearate were also incorporated to improve powder flow in high-speed capsule filling machinery, however, as the capsules will initially be produced by hand, such materials will not be needed in the immediate future [147, 174].

3.1.1.2 In vitro release of drugs from capsules

Formulation efficacy was determined using the BP paddle dissolution method [175], a simple *in vitro* test, which has been well standardised and is a regulatory requirement submitted for pre-clinical data and used to ensure batch to batch uniformity. Before a drug is absorbed into the gastrointestinal tract it has to be released and dissolved first. These variables are evaluated with the *in vitro* dissolution test which quantifies the rate of active drug release into the dissolution medium and consequently the effects of excipient variability can be assessed.

The basic principles underlying the dissolution process can be identified by the Noyes-Whitney equation [176]:

$$\frac{dC}{dt} = \frac{DA(C_S - C)}{h} \quad \textbf{(3.1)}$$

Where *dC/dt* is the rate of dissolution of the drug particles, *D* is the diffusion coefficient of the drug, *A* represents the effective surface area, *h* is the thickness of the boundary layer adjacent to the dissolving surface, C_S is the saturation solubility of the drug in the dissolution medium and *C* is the drug concentration in the bulk of the dissolving medium [147]. There are many physicochemical and experimental factors which can influence Equation 3.1 and therefore the dissolution rate. Physicochemical factors include the particle size, dispersibility and porosity of the drug particles [147].

The experimental factors that can influence the dissolution rate are the composition and volume of dissolution media, type of apparatus and the temperature and agitation of the media [147]. The degree of media agitation dictates the thickness of the boundary layer (*h*), where an increase in agitation can reduce the thickness of the stagnant film surrounding the capsule to result in an increased dissolution rate [177]. The drug saturation solubility in the dissolution medium (C_S) can also influence the dissolution rate. If the concentration of drug dissolved in the dissolution medium (*C*) does not exceed 10% of the drug saturation concentration, then 'sink conditions' are said to exist. Under sink conditions saturation solubility is mostly responsible for determining the drug concentration gradient across the boundary layer, which is the driving force behind dissolution. The standard methods of

controlling the saturation solubility are to alter the dissolution media volume or to change the media composition [177].

Most studies use water, buffers, acids or alkalis as dissolution media [178]. However, for poorly soluble drugs dissolution in the aforementioned media may be challenging especially if they are lipophilic and non-ionisable like DMU212. In developing a dissolution test for poorly soluble drugs such as DMU212, a variety of media have been used to increase drug solubility such as alcohols or other organic solvents, these media have no physiological relevance and as such may result in poor *in vivo-in vitro* correlations [179]. Consequently, potential solubility improvements in aqueous media may be facilitated through inclusion of surfactants in the dissolution medium. Poorly soluble drugs can be solubilized in the body by endogenous surfactants e.g. bile and lecithin, therefore, inclusion of natural surfactants in the dissolution media simulates the gastrointestinal fluid milieu [180], thereby exhibiting test conditions more useful in evaluating drug quality. However, the expense of natural surfactant media has led to the employment of synthetic ionic and non-ionic surfactants such as SLS, cetyltrimethylammonium bromide (CTAB) and the polysorbates (or Tweens) [177, 179-181], all of which are more cost-effective. Moreover, the physiological relevance of synthetic surfactants has been approved by the FDA for sparingly water-soluble drug dissolution methods [178].

Within the scope of this thesis DMU212 capsule formulations were developed and subsequently evaluated using the BP paddle dissolution method [175]. A high-throughput assay on a UV plate reader was also developed for dissolution sample measurement and the novel technique was validated using indomethacin and UV spectrophotometry. A novel

application for the standard MTT *in vitro* assay [134] was also used to demonstrate the retention of DMU212 CYP1 enzyme selectivity after capsule formulation, and to determine whether the excipients had any effect on the drug's cytotoxicity.

3.2 Materials and methods

Reagents were used as received from Sigma-Aldrich Chemical Company (Dorset, UK) or Alfa Aesar (Lancashire, UK). Tween 80 was obtained from Thornton and Ross Ltd. (Huddersfield, UK) and size 2 hard gelatine capsule shells were purchased from Davcaps (Hertfordshire, UK). TCDD (2,3,7,8 tetrachlorodibenzo-*p*-dioxin) was obtained from British Greyhound Chromatography (Birkenhead, UK). HPLC grade water, 2.5mL eppendorf tubes, 96-well Nunc® plates, 96 deep square well polypropylene plates and SLS were obtained from Fisher Scientific (Loughborough, UK). Human breast cell lines were obtained from the American Type Culture Collection and DMU212 was supplied by K. Ruparelia of the CDDG.

3.2.1 Dissolution media preparation

All dissolution media were prepared using the following reagents: HPLC grade water, hydrochloric acid (HCl), sodium hydroxide (NaOH), potassium phosphate (KH_2PO_4), disodium hydrogen orthophosphate (Na_2HPO_4), Tween 80 and SLS. All media were degassed by sonication before use. Buffer solutions were prepared as described in the British Pharmacopoeia 2003 (Volume IV, Appendix ID, A130). Depending on the initial pH, either 1M NaOH or HCl was used to adjust the pH appropriately using a SevenEasy™ benchtop pH meter (Mettler-Toledo Inc., Ohio, USA).

3.2.2 Capsule formulations

Powder blends containing DMU212 or indomethacin and the chosen excipients were prepared by trituration in a pestle and mortar. The formulations were manually packed into size 2 hard gelatine capsule shells using bench scale capsule filling equipment. The effect of particle size on DMU212 dissolution was also studied with cap1/50D, where samples were passed through a series of sieves with different aperture sizes (Endecotts Ltd., London, UK). The following particle size fractions were collected and encapsulated: <150μM, 150-250μM and 250-500μM. The following capsules were prepared for other dissolution studies:

Table 26. Summary of DMU212 capsule formulations:

INGREDIENT / CAPSULE FORMULATION	DMU212 (mg)	Sorbitol (mg)	Lactose (mg)	SLS (mg)	Magnesium Stearate (mg)	α-Cyclo-dextrin (mg)	β-Cyclo-dextrin (mg)
Cap1/50D	50						
Cap2/50D/L	50		150				
Cap3/50D/S	50	150					
Cap4/50D/MS/L	50		140				10
Cap5/50D/MS/S	50	140					10
Cap6/50D/SLS/L	50		140	10			
Cap7/50D/SLS/S	50	140		10			
Cap8/50D/SLS/L	50		50	100			
Cap9/50D/SLS/S	50	50		100			
Cap10/100D	100						
Cap11/100D/L	100		100				
Cap12/100D/S	100	100					
Cap13/50D/ACYC	50					150	
Cap14/50D/BCYC	50						150

Table 27. Summary of indomethacin capsule formulations:

INGREDIENT / CAPSULE FORMULATION	Indomethacin (mg)	Sorbitol (mg)	Lactose (mg)
Cap1/100D	100		
Cap2/100D/L	100		100
Cap3/100D/S	100	100	

3.2.3 Determination of saturation concentration

It is highly important to determine the saturation concentration of the drug in the dissolution medium to ensure that sink conditions are maintained. The saturation concentration of DMU212 was determined in 1% w/v SLS (i.e. optimum dissolution conditions) by adding excess drug to 900mL of dissolution medium, which was stirred using a paddle stirrer at 100 rpm over 24 hours at 37.5°C (±0.5°C) (section 3.2.4). Afterwards, 1mL of the suspension was centrifuged for 1 minute at 13,000 rpm and assayed for DMU212 using the UV spectrophotometer and UV plate reader at λmax of 326nm.

3.2.4 In vitro dissolution studies

The BP paddle dissolution test was used for all *in vitro* dissolution studies (2003, Volume IV, Appendix X XIID, A249). Experiments were carried out using a manual Erweka Dissolution System (Heusenstamm, Germany) equipped with paddle stirrers fixed at depth of 23-27mm from the bottom of the dissolution vessel whilst rotating at 50-100 rpm. The capsules were placed in steel wire springs to weigh them down and introduced into 900mL of the dissolution medium maintained at a temperature of 37.5°C (±0.5°C) [175]:

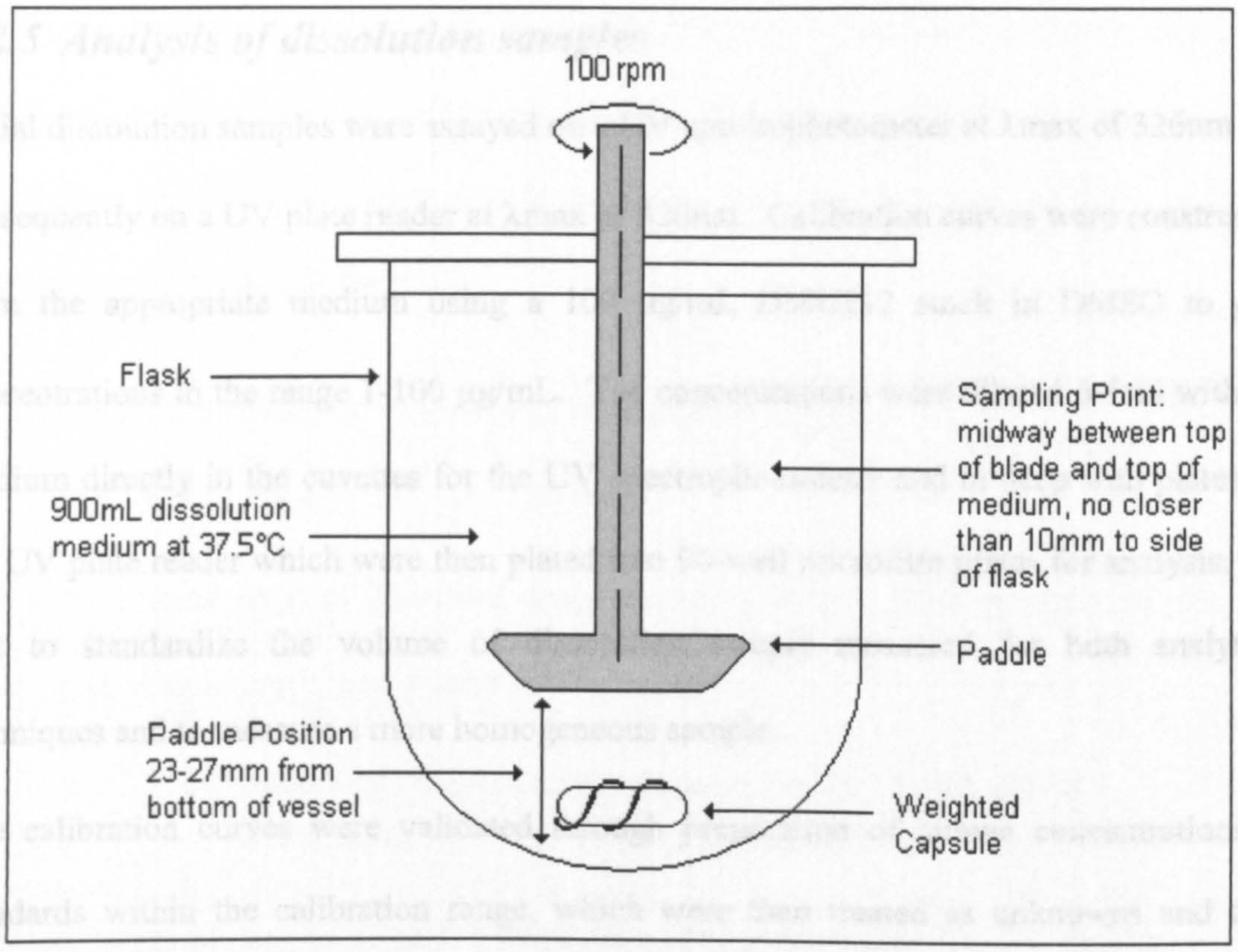

Figure 22. Schematic of the BP paddle method used for dissolution studies.

At specified time intervals 1mL of dissolution medium was taken and centrifuged for 1 minute at 13,000 rpm (the samples were not filtered due to adsorption of drug onto the cellulose nitrate membrane filters, which would have been otherwise used). An equal volume of fresh dissolution medium was added after each removal to maintain a constant volume. The samples were then assayed using the UV spectrophotometer (Heλios β) and the UV plate reader (Spectramax M5) at λmax of 326nm. The method variables evaluated were the stirring speed and dissolution medium and after method development a range of capsule formulations were evaluated (Tables 26 and 27).

3.2.5 Analysis of dissolution samples

Initial dissolution samples were assayed on a UV spectrophotometer at λmax of 326nm and subsequently on a UV plate reader at λmax of 326nm. Calibration curves were constructed from the appropriate medium using a 100 μg/mL DMU212 stock in DMSO to give concentrations in the range 1-100 μg/mL. The concentrations were diluted 5-fold with the medium directly in the cuvettes for the UV spectrophotometer and in deep well plates for the UV plate reader which were then plated into 96-well microtitre plates for analysis; this was to standardize the volume of dissolution sample measured for both analytical techniques and to measure a more homogeneous sample.

The calibration curves were validated through preparation of known concentrations of standards within the calibration range, which were then treated as unknowns and their concentrations were back calculated from the calibration curves constructed. The excipients did not affect drug absorbance, which was demonstrated through comparison of standards prepared in neat dissolution media and standards prepared in solutions containing the maximum concentration of powder blends in the appropriate dissolution media.

3.2.5.1 Calculations for drug release data

The equation of the line for corresponding calibration curves were rearranged to convert absorbance into apparent drug concentration in the corresponding sample of dissolution medium removed at time t:

$$\text{Apparent Concentration of DMU212 (mg/mL)} = \frac{(\text{Absorbance} - \text{y Intercept})}{\text{Slope}} \qquad (3.2)$$

Corrected concentration of DMU212 was calculated to correct for error caused by replacement of 1mL samples withdrawn from the dissolution medium. Also the volume of dissolution medium was constantly 900mL, therefore, the equation used for corrected concentration of DMU212 was:

$$\underset{\text{at time t (mg/mL)}}{\text{Corrected Concentration}} = \underset{\text{at time t}}{\text{Apparent Concentration}} + \frac{1}{900}\left(\begin{array}{c}\Sigma \text{ of previous apparent} \\ \text{concentrations}\end{array}\right) \quad \textbf{(3.3)}$$

The total amount (mg) of dissolved drug present in 900mL of dissolution medium at a given time of sampling t, was given by:

$$\underset{\text{Released (mg)}}{\text{Total Amount of Drug}} = \underset{\text{of drug released at time t}}{\text{Corrected concentration (mg/mL)}} \times 900 \quad \textbf{(3.4)}$$

The percentage of drug released at a given time of sampling t, was then calculated.

3.2.6 MTT in vitro cytotoxicity assay

The MTT assay (Section 2.1.1) performed by P. Butler was employed to demonstrate the CYP1 enzyme selectivity of DMU212 after capsule formulation, and to determine whether the excipients had any effect on cytotoxicity. The human breast cell-lines used included MCF7, MDA-MB-468 and MCF10A. MCF7 cells were cultured in RPMI 1640 medium, MDA-MB-468 cells were cultured in RPMI 1640 medium without phenol red, MCF10A cells were cultured in DMEM:HAM's F-12 medium with 10 μg/mL insulin, 500 ng/mL hydrocortisone and 20 ng/mL epidermal growth factor. All media were supplemented with glutamine and 10% v/v heat inactivated foetal calf serum. Cells were incubated at 37°C,

5% CO_2/95% air with 100% humidity and passaged at subconfluence using 0.5% trypsin/0.2% EDTA.

The cells cultured in medium were plated out at $2x10^4$ cells per well in 96-well plates and allowed to attach for 4 hours before treatment. MCF7 cells were induced with 100µl of medium containing 20nM TCDD or without TCDD (vehicle control, 0.2% v/v DMSO) for 24 hours to allow CYP expression. The medium was then aspirated and the cells were resuspended in 100µL of fresh medium. Serial dilutions of the test compounds (DMU212, cap3/50D/S and sorbitol) were added to the 96-well plates. All test compound concentrations (0.0003-100µM) were examined in quadruplicate. After a 96 hour incubation period 50µL of MTT at 2 mg/mL in RPMI 1640 without phenol red was added to each well followed by incubation for a further 2 hours. All medium was aspirated and the formazan product generated by viable cells was solubilized with 100µl DMSO. Plates were vortexed and the absorbance at 540nm determined using a Labsystems Multiskan MS plate reader (Helsinki, Finland). Results were expressed as the percentage of 100% (control) proliferation and the IC_{50} calculated from the linear regression analysis of experimental data using GraphPad Prism version 4 software. The activity of the drugs in the cell-lines was calculated using the tumour selective factor (Equation 3.5) and the activation factor (Equation 3.6):

$$\text{Tumour selective factor} = \frac{(IC_{50} \text{ in MCF10A})}{(IC_{50} \text{ in MDA - MB - 468})} \quad \textbf{(3.5)}$$

$$\text{Activation factor} = \frac{(IC_{50} \text{ in MCF7})}{(IC_{50} \text{ in TCDD induced MCF7})} \quad \textbf{(3.6)}$$

3.2.7 Statistical analysis

See Section 2.2.5.

3.3 Results

3.3.1 Dissolution quantification on the UV spectrophotometer

Initial dissolution studies were conducted with water as the medium:

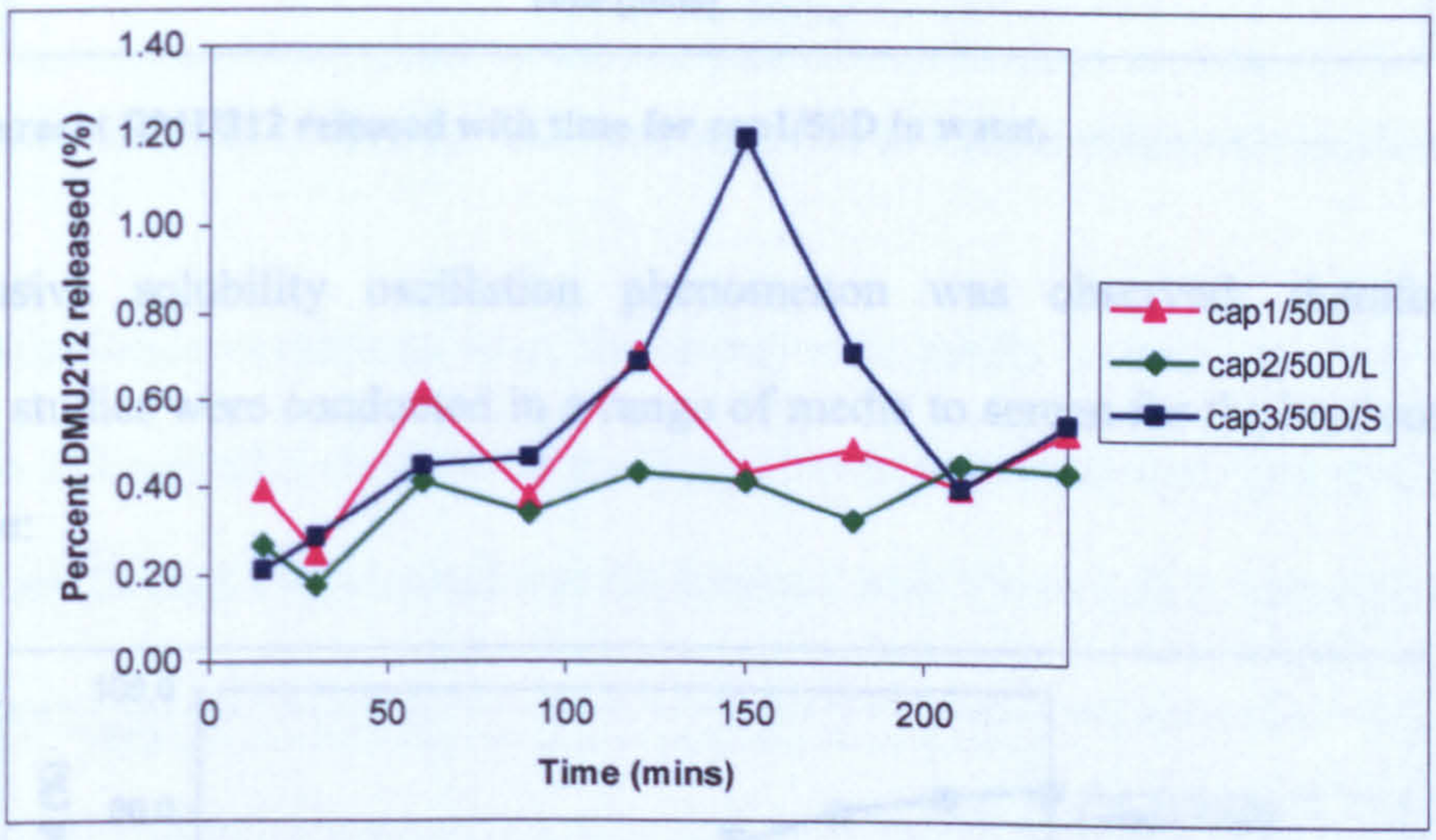

Figure 23. Percent DMU212 released with time for a range of capsule formulations in water.

DMU212 aqueous dissolution was very poor, however, the drug released appeared to be oscillating with time. The observed oscillation may be a factor of the drug solubility where the drug molecules may be dissolving and crystallizing out of the dissolution medium, until the thermodynamic solubility level is reached. To prove or disprove this theory, tighter time points were measured in the aqueous dissolution of cap1/50D:

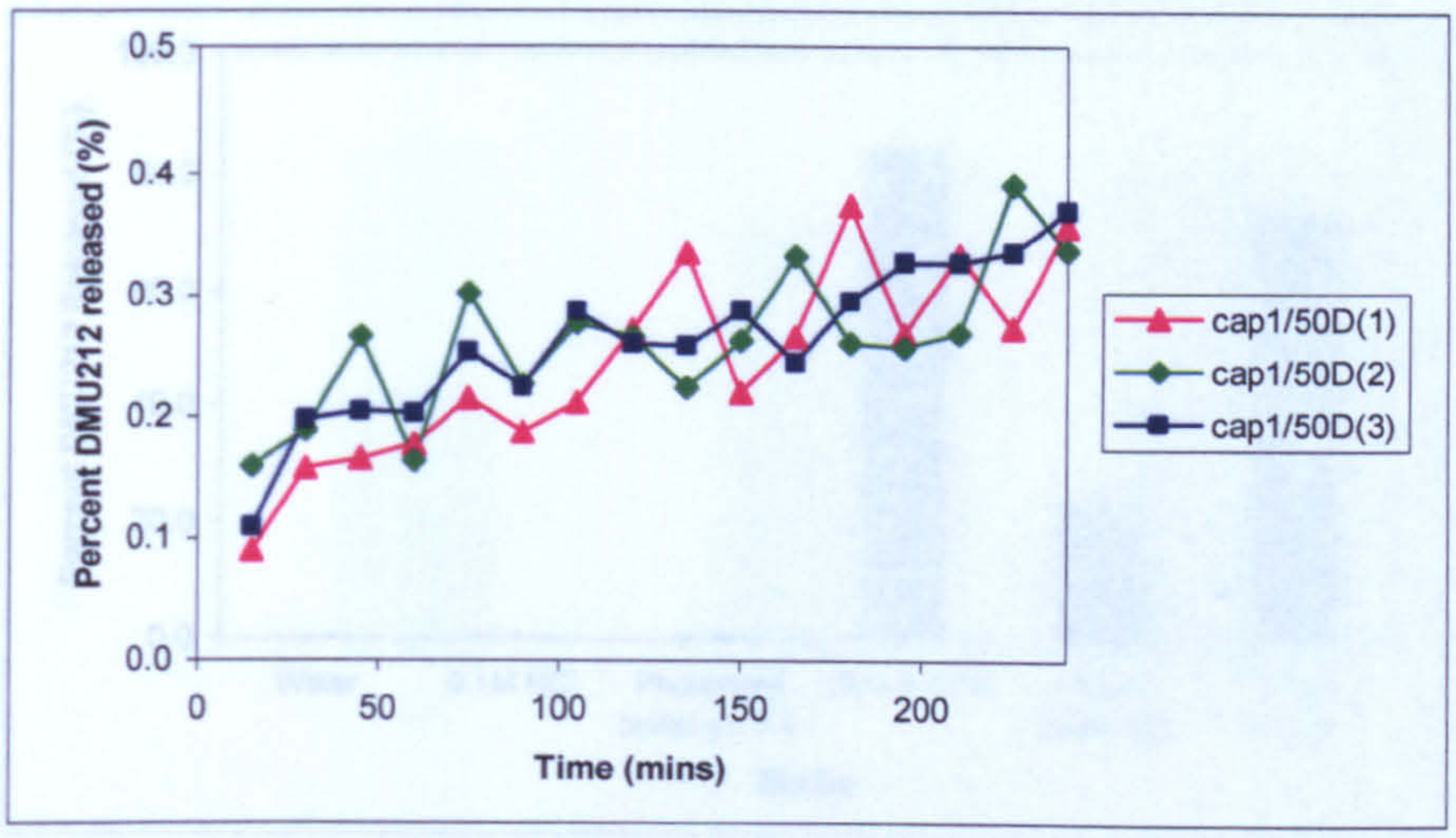

Figure 24. Percent DMU212 released with time for cap1/50D in water.

No conclusive solubility oscillation phenomenon was observed; therefore, further dissolution studies were conducted in a range of media to screen for the best conditions for drug release:

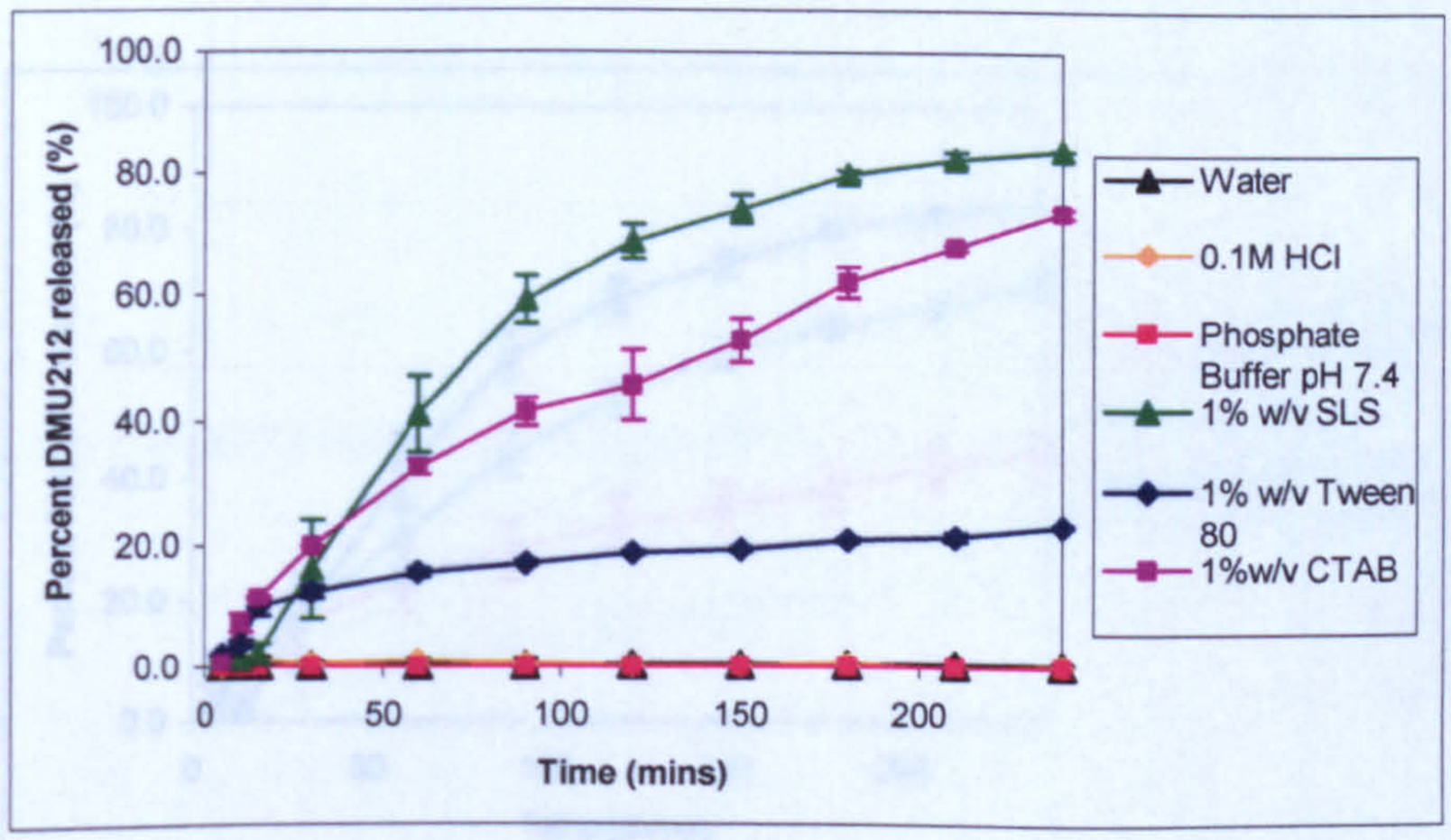

Figure 25. Percent DMU212 released with time for cap1/50D in various media at 100 rpm and 37.5°C (n=3).

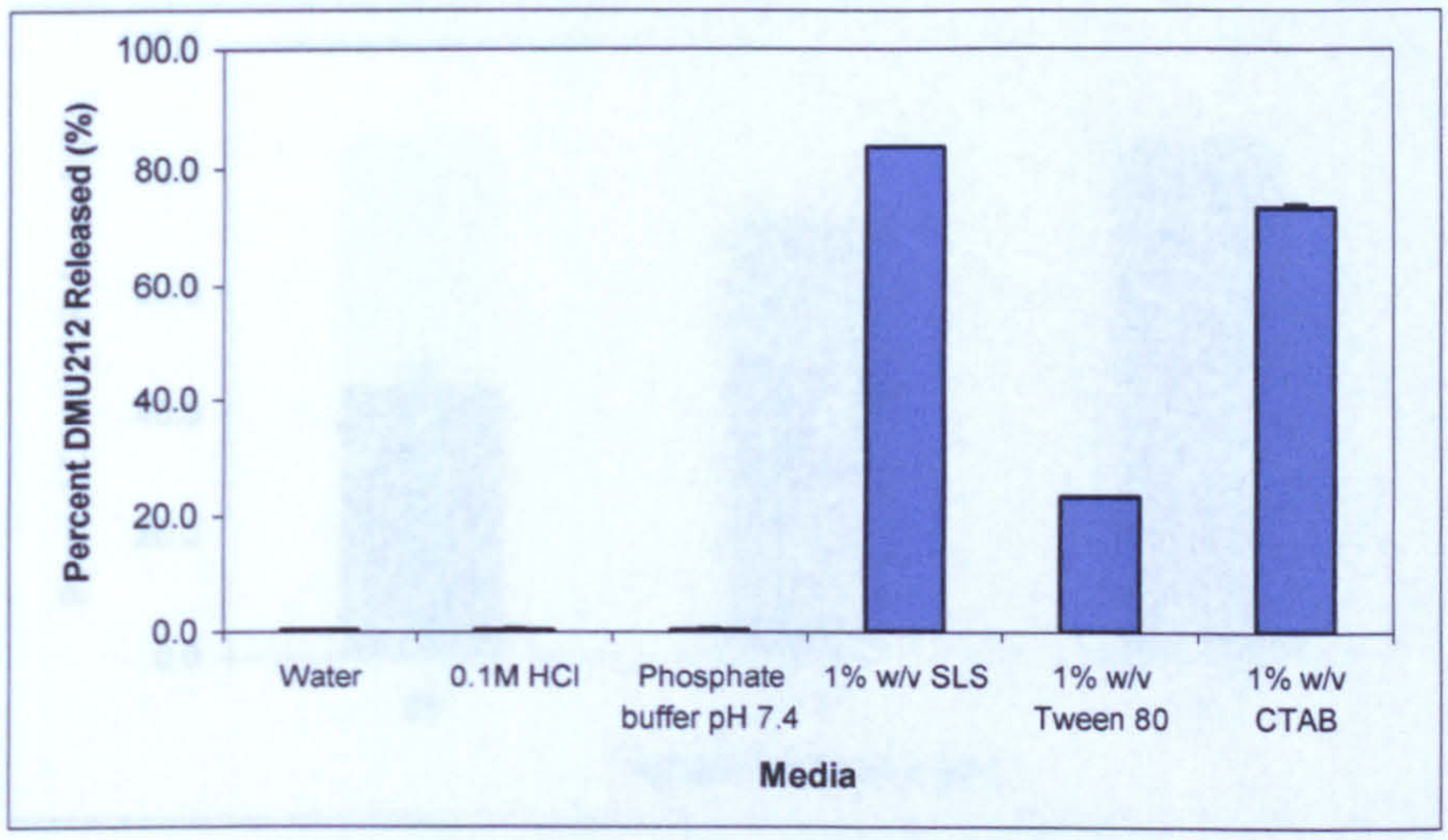

Figure 26. Total percent DMU212 released from cap1/50D in various dissolution media over 4 hours (n=3).

The best dissolution conditions were observed with media containing surfactants most notably with 1% w/v SLS dissolution medium. To further maximise the sensitivity of the test conditions the best rotary speed was determined with 1% w/v SLS and cap1/50D:

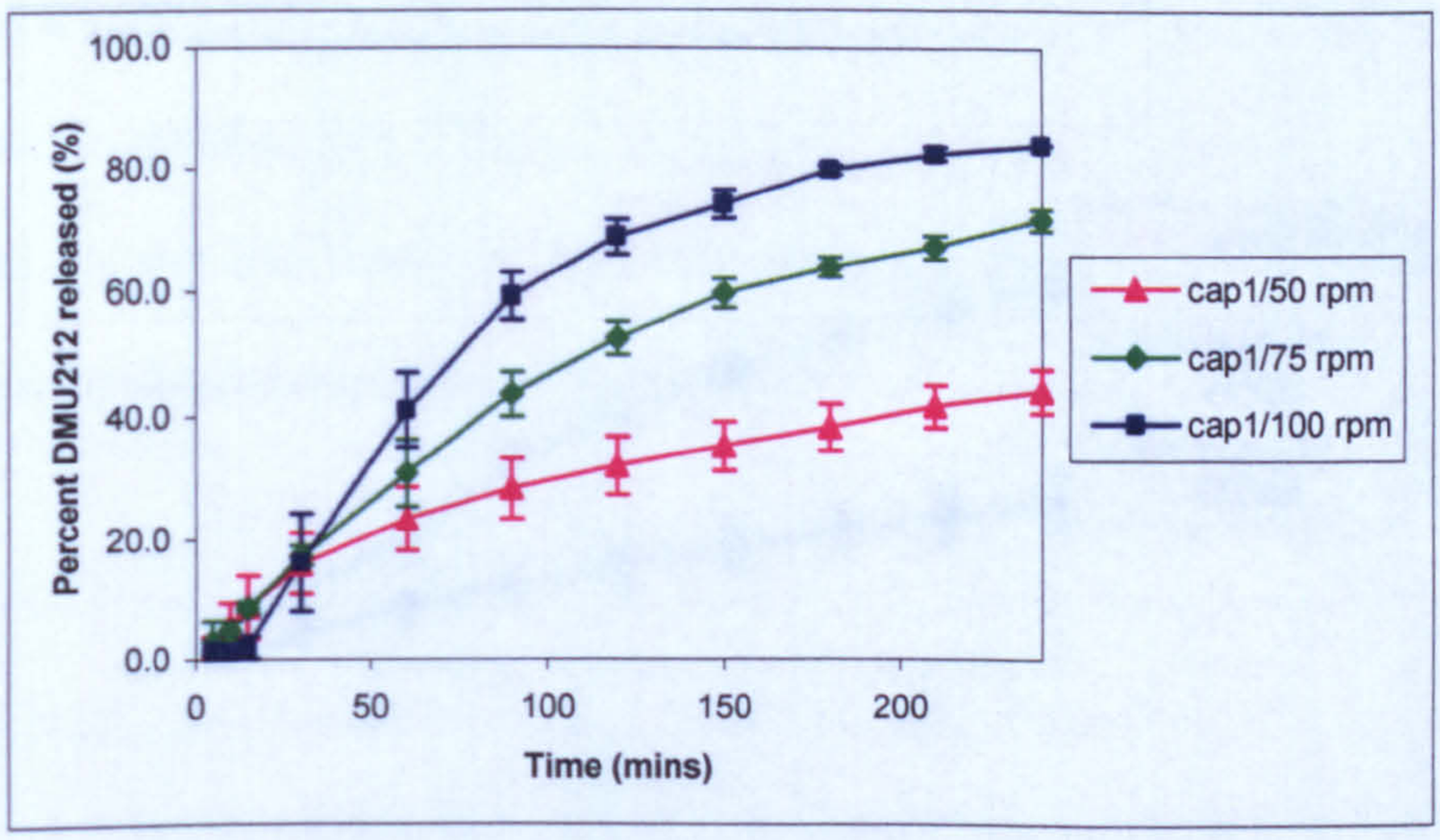

Figure 27. Percent DMU212 released with time for cap1/50D in 1% w/v SLS dissolution medium at different stirring speeds (n=3).

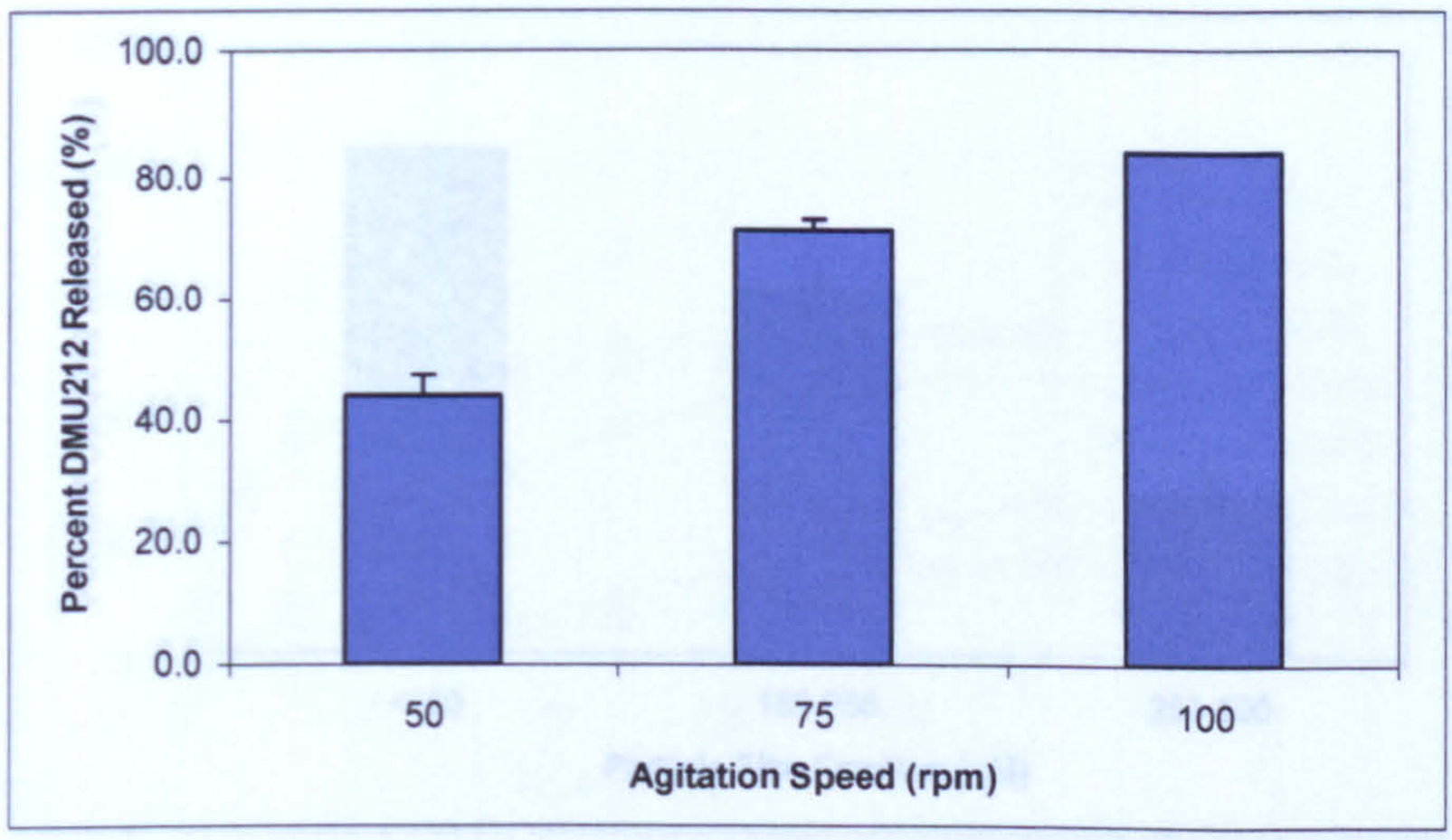

Figure 28. Total percent DMU212 released from cap1/50D at different agitation speeds in 1% w/v SLS dissolution medium over 4 hours (n=3).

The highest dissolution rate was observed with a rotary speed of 100 rpm and the lowest was with 50 rpm. Prior to formulation screening studies the effect of drug particle size on DMU212 dissolution rate was also evaluated using cap1/50D:

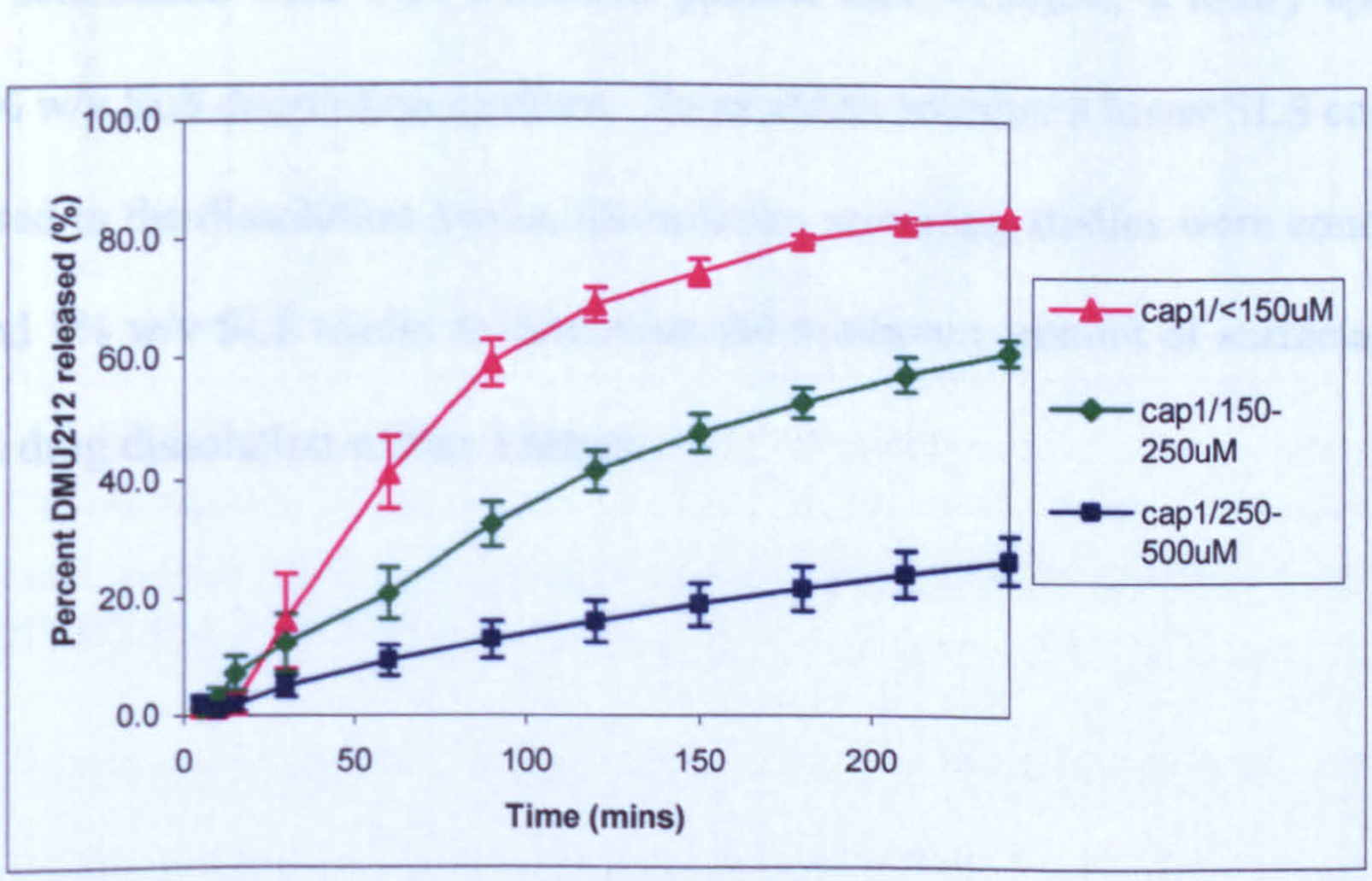

Figure 29. Percent DMU212 released with time for cap1/50D at different particle sizes in 1% w/v SLS dissolution medium (n=3).

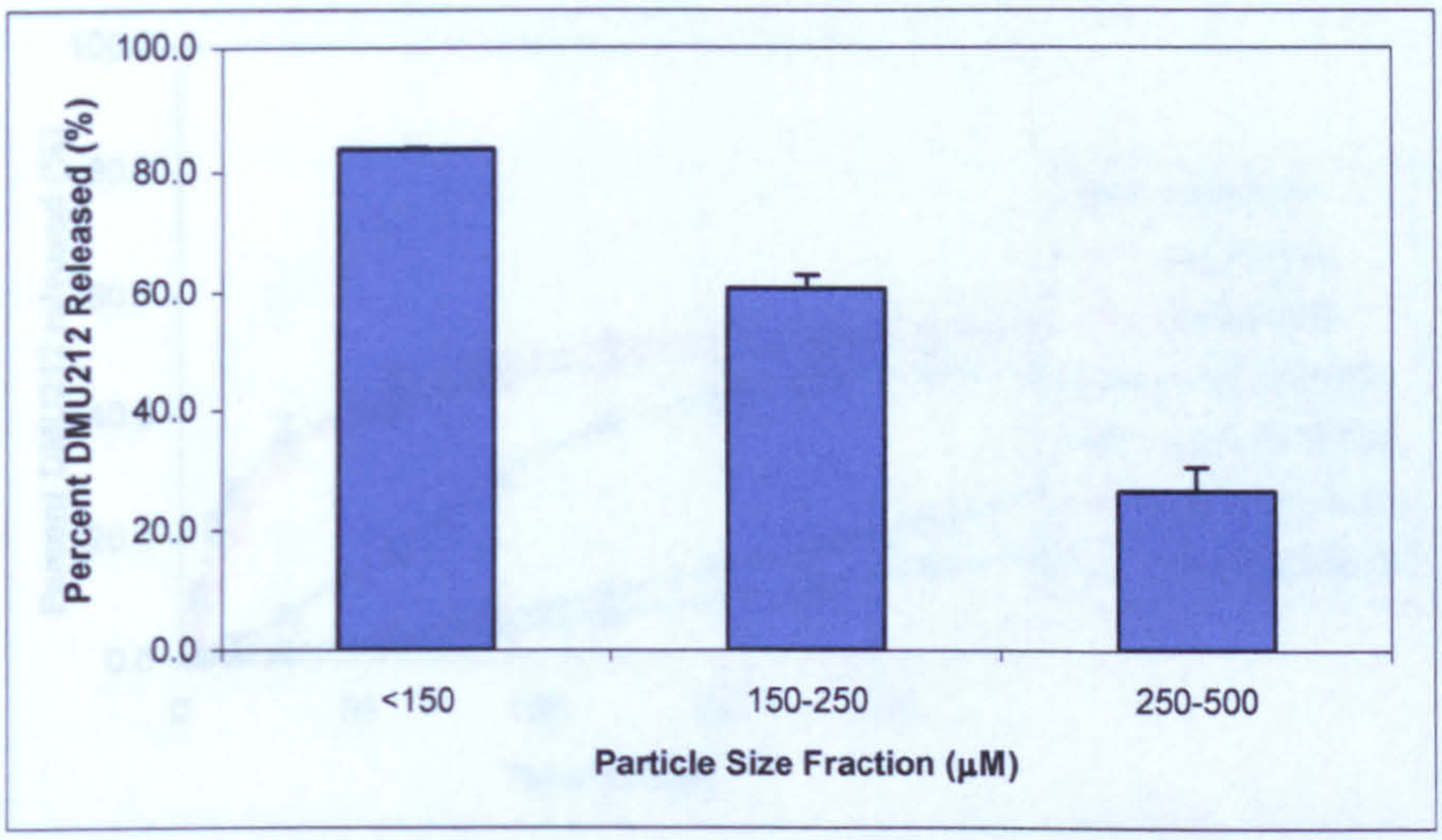

Figure 30. Total percent DMU212 released from cap1/50D at different particle sizes in 1% w/v SLS dissolution medium over 4 hours (n=3).

The fastest drug release for cap1/50D was with drug particle size at <150µM and the slowest release was with particle size at 250-500µM. Overall, the best dissolution test conditions determined were with DMU212 particle size <150µM, a rotary speed of 100 rpm and 1% w/v SLS dissolution medium. To establish whether a lower SLS concentration could be used in the dissolution media, formulation screening studies were conducted with both 0.5 and 1% w/v SLS media to determine the minimum amount of surfactant required for 75-80% drug dissolution within 4 hours:

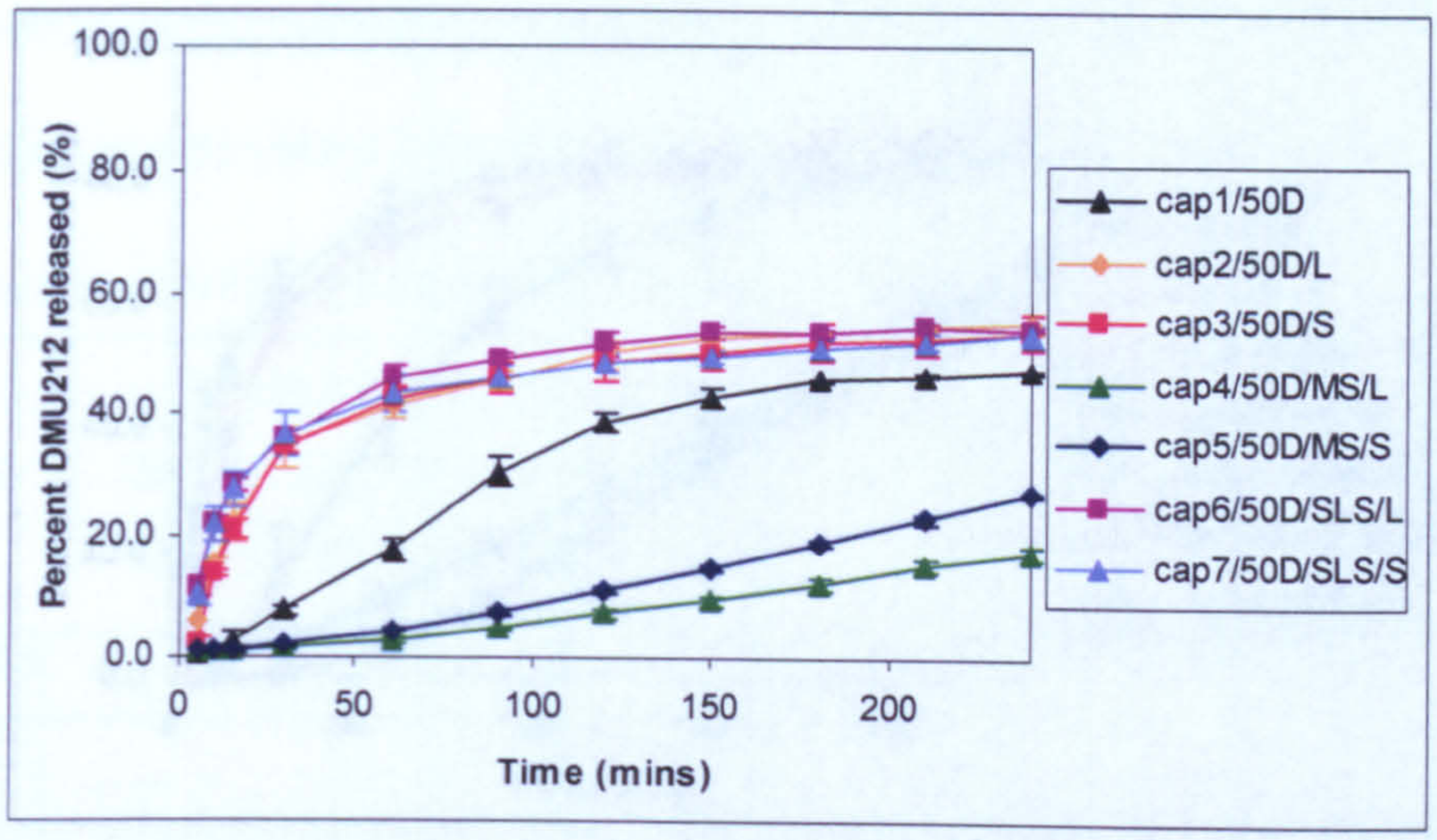

Figure 31. Percent DMU212 released with time for capsule formulations in 0.5% w/v SLS dissolution medium (n=3).

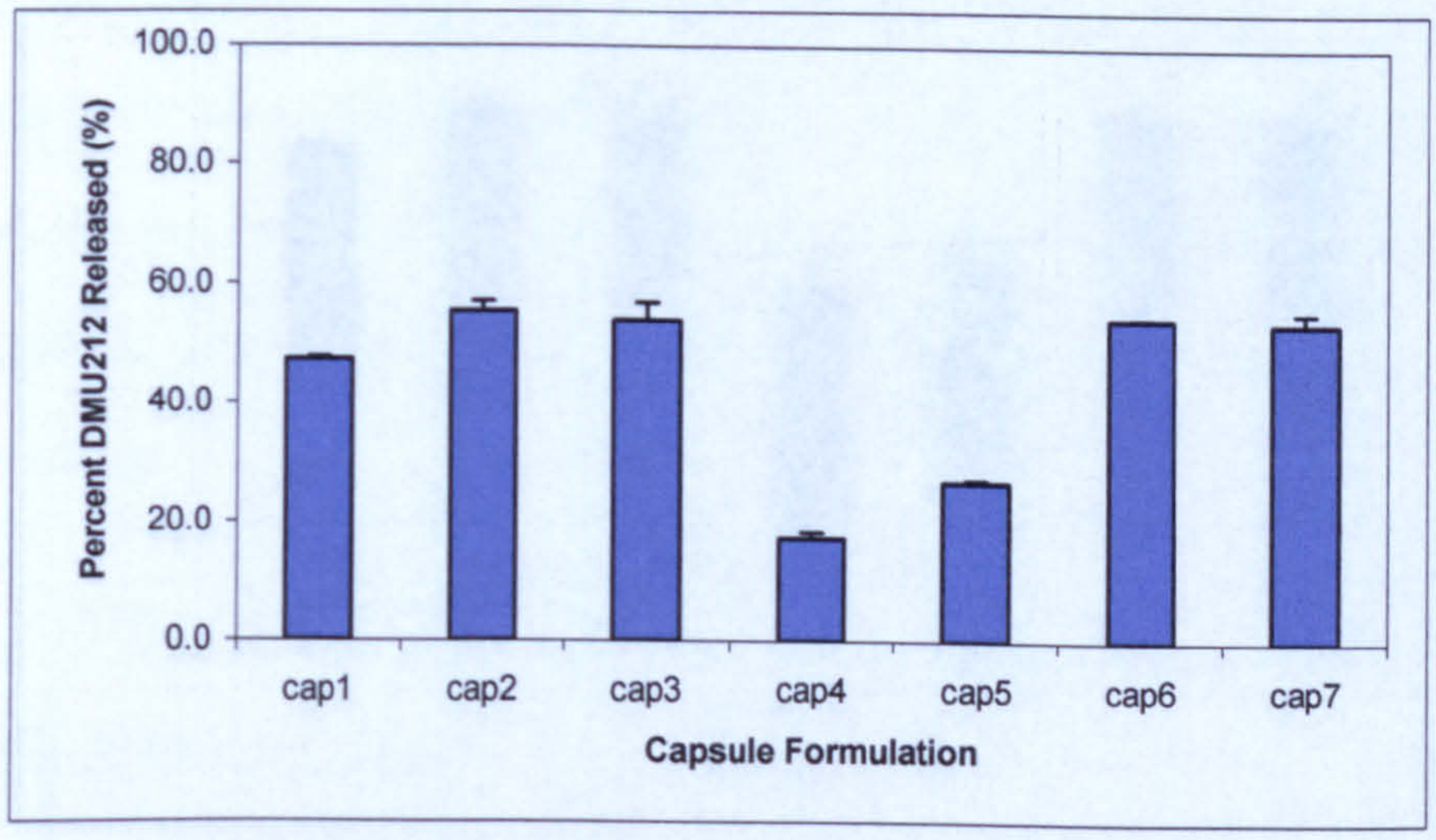

Figure 32. Total percent DMU212 released from different capsule formulations in 0.5% w/v SLS dissolution medium over 4 hours (n=3).

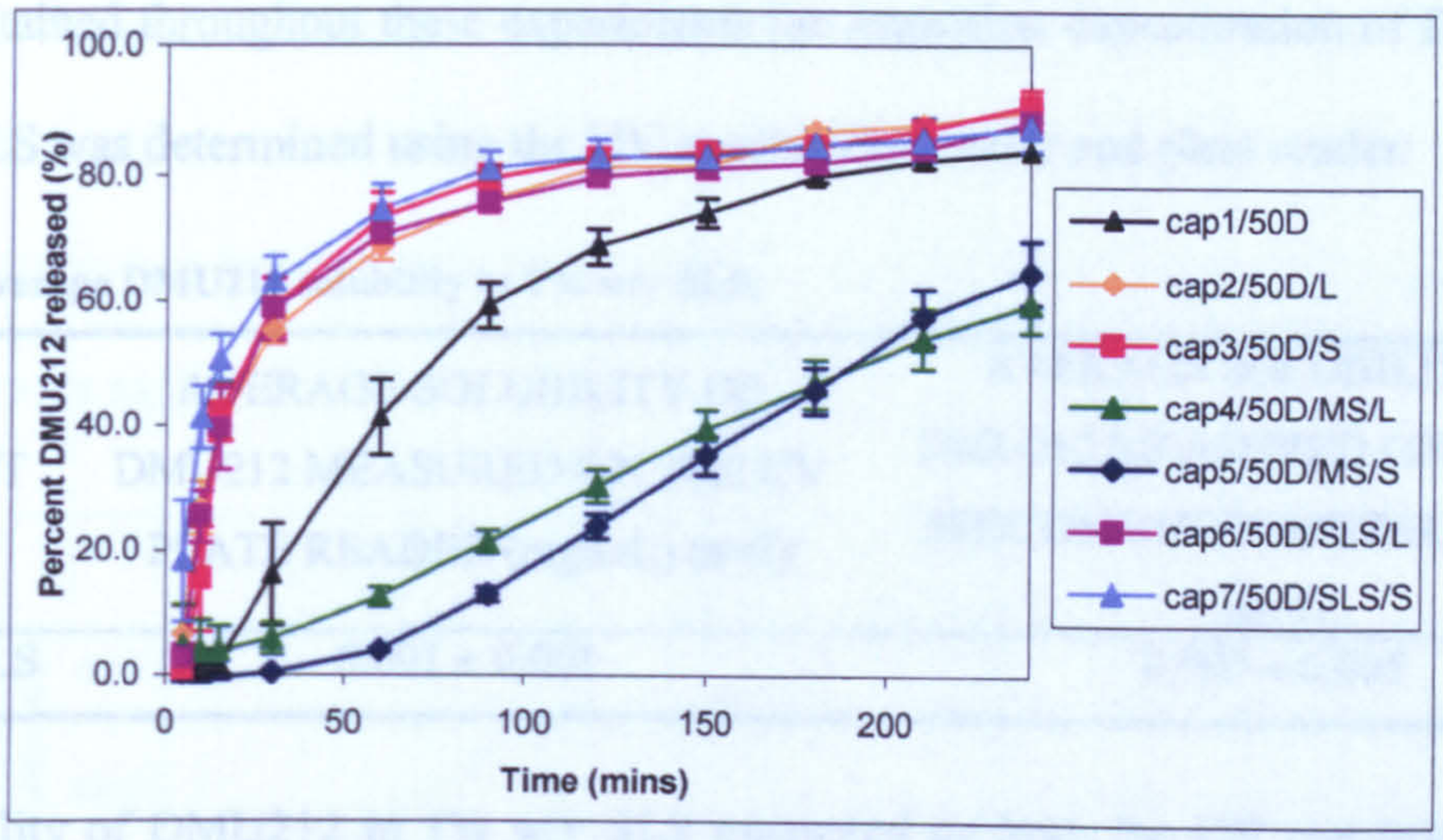

Figure 33. Percent DMU212 released with time for capsule formulations in 1% w/v SLS dissolution medium (n=3).

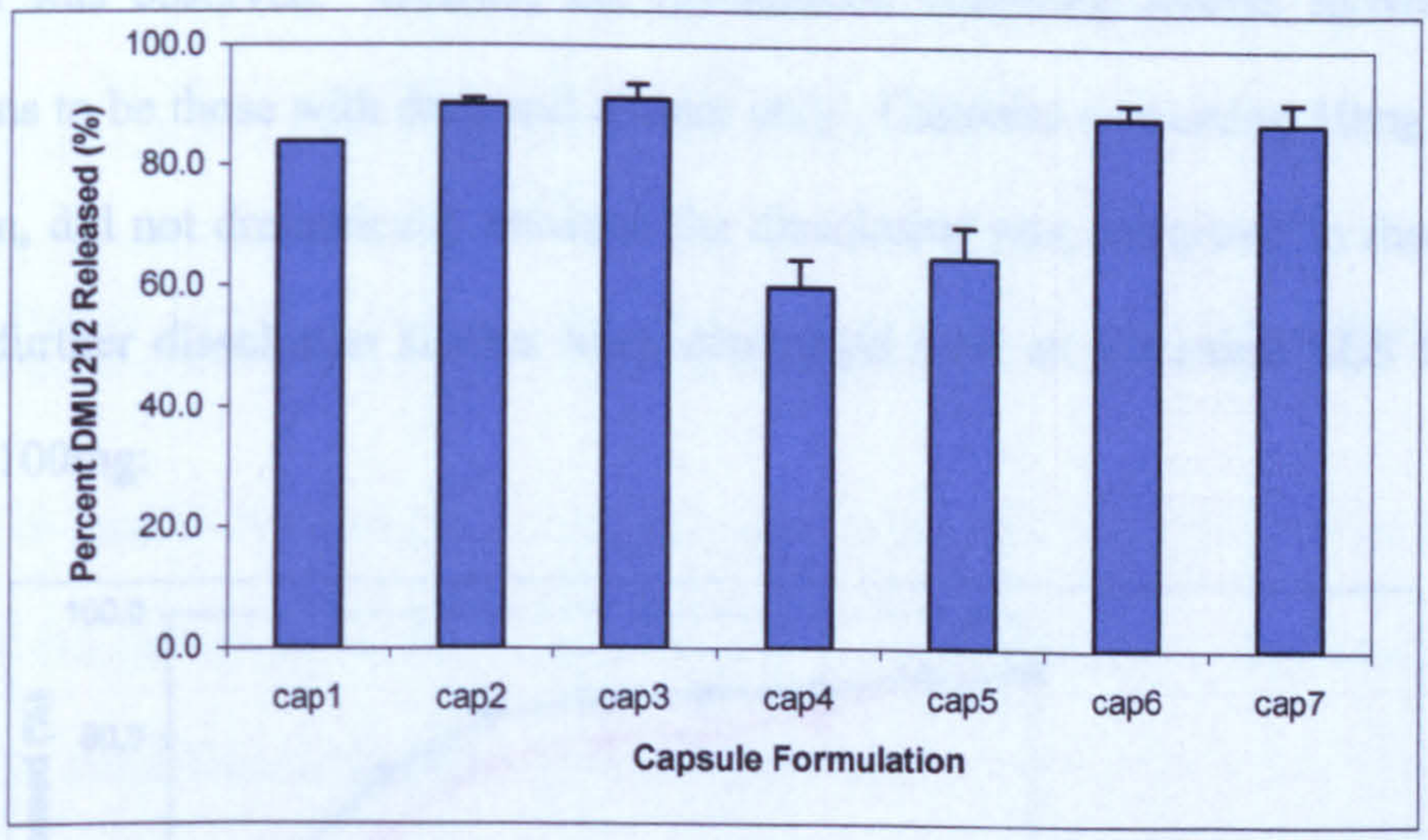

Figure 34. Total percent DMU212 released from different capsule formulations in 1% w/v SLS dissolution medium over 4 hours (n=3).

The highest drug release was observed with cap2/50D/L and cap3/50D/S and the lowest was with cap4/50D/MS/L and cap5/50D/MS/S with both 0.5 and 1% w/v SLS media. The fastest dissolution was with 1% w/v SLS medium, therefore, to establish if sink conditions

were maintained throughout these experiments the saturation concentration of DMU212 in 1% w/v SLS was determined using the UV spectrophotometer and plate reader:

Table 28. Average DMU212 solubility in 1% w/v SLS.

SOLVENT	AVERAGE SOLUBILITY OF DMU212 MEASURED ON THE UV PLATE READER (mg/mL) (n=3)	AVERAGE SOLUBILITY OF DMU212 MEASURED ON THE UV SPECTROPHOTOMETER (mg/mL) (n=3)
1% w/v SLS	0.091 ± 0.001	0.095 ± 0.005

The solubility of DMU212 in 1% w/v SLS measured on both the UV spectrophotometer and plate reader is two times the concentration of DMU212 that would be observed if 100% dissolution was observed. Overall, the formulation screening studies showed the best formulations to be those with drug and diluent only. Capsules containing 10mg SLS in the formulation, did not dramatically enhance the dissolution rate compared to those without, therefore, further dissolution studies were conducted with an increased SLS formulation content of 100mg:

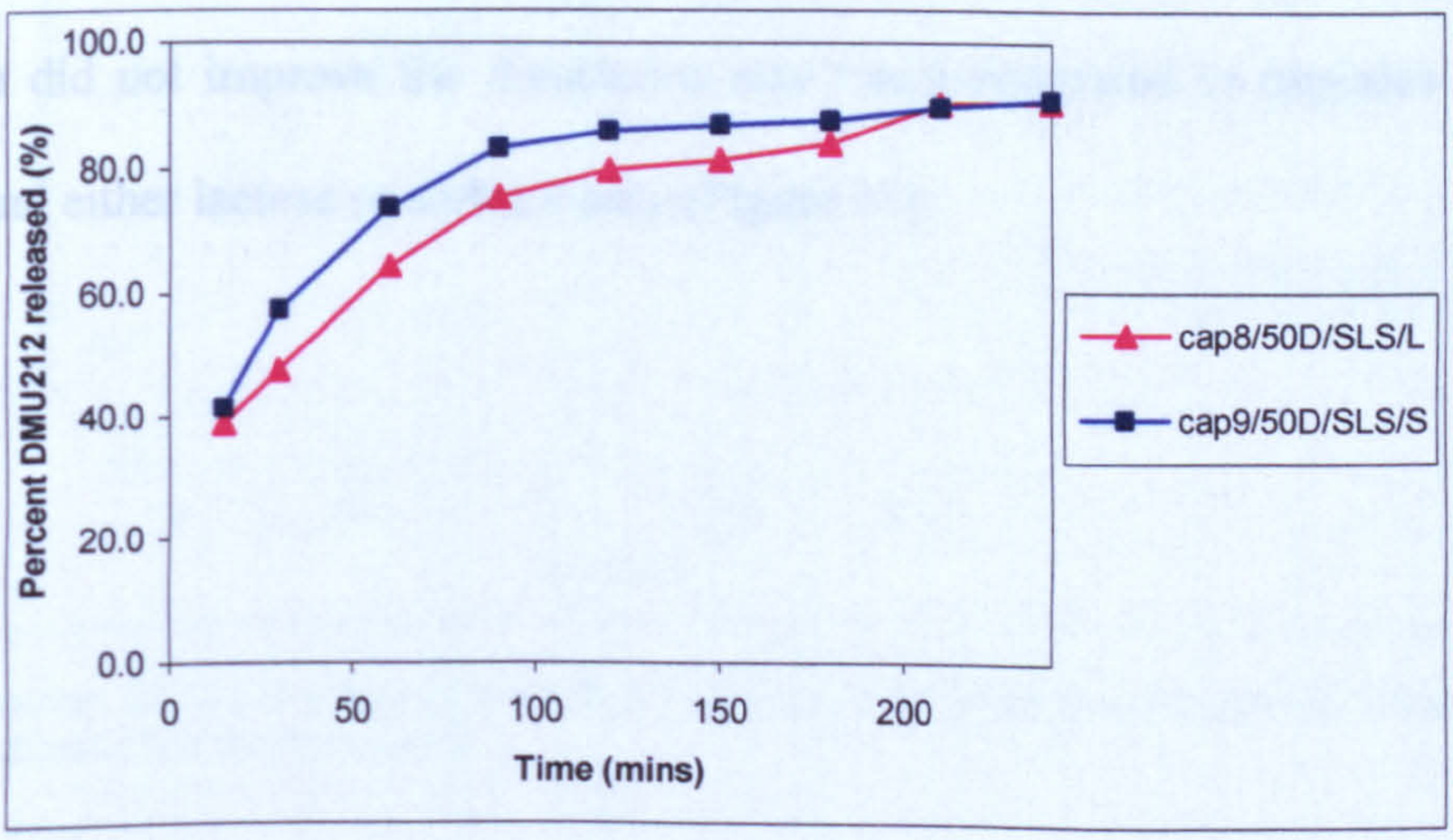

Figure 35. Percent DMU212 released with time for different capsule formulations containing diluent and 100mg of SLS in 1% w/v SLS dissolution medium.

However, inclusion of 100mg SLS in the formulation still did not enhance the drug release profile extensively compared to formulations containing drug and diluent only. Therefore, another strategy was implemented to potentially improve the dissolution rate using α- and β-cyclodextrins as the diluents:

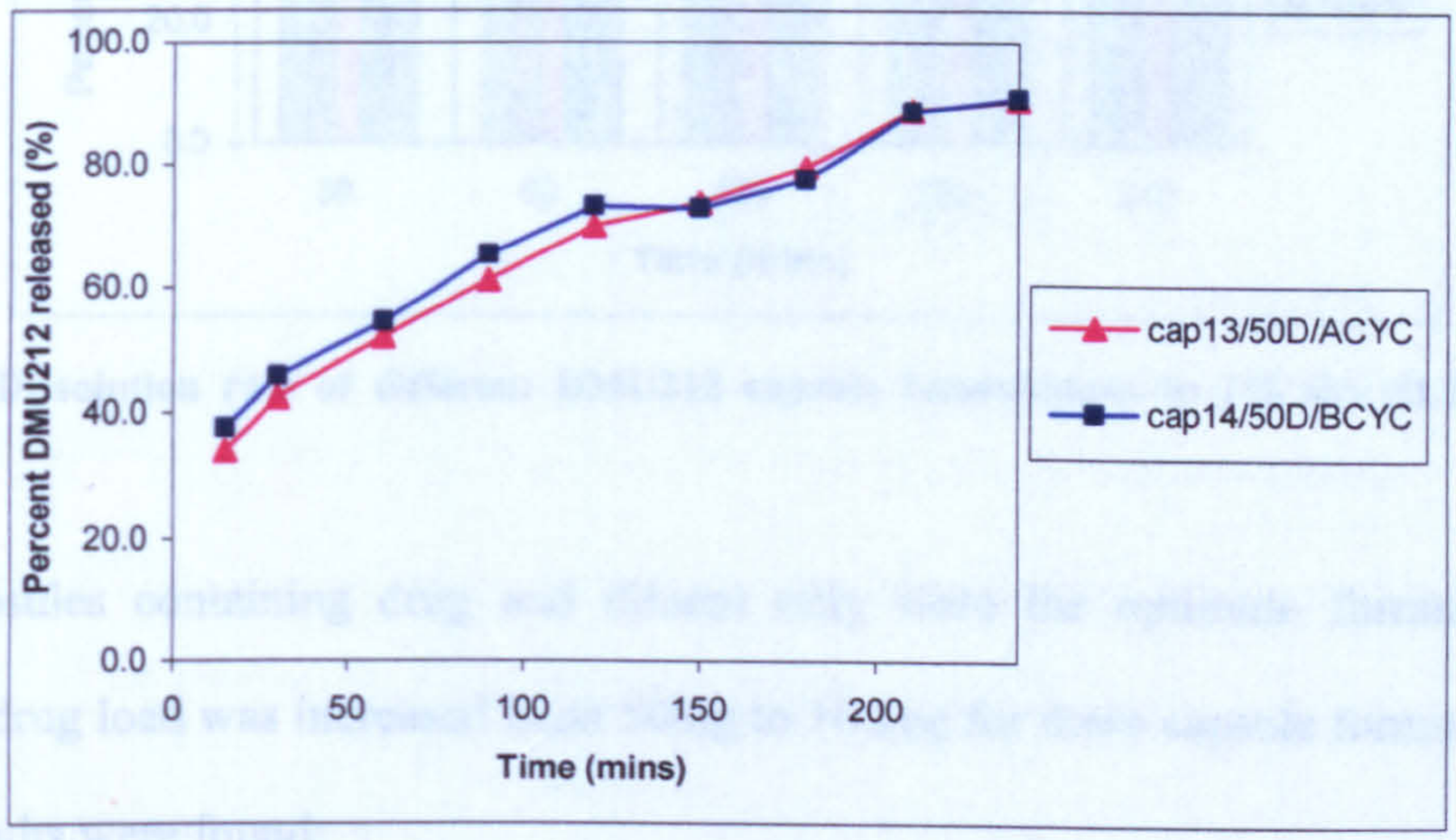

Figure 36. Percent DMU212 released with time for different capsule formulations containing cyclodextrins as the diluent in 1% w/v SLS dissolution medium.

The use of α- and β-cyclodextrin as diluents and larger quantities of SLS in the capsule formulation did not improve the dissolution rate much compared to capsules containing DMU212 and either lactose or sorbitol only (Figure 37):

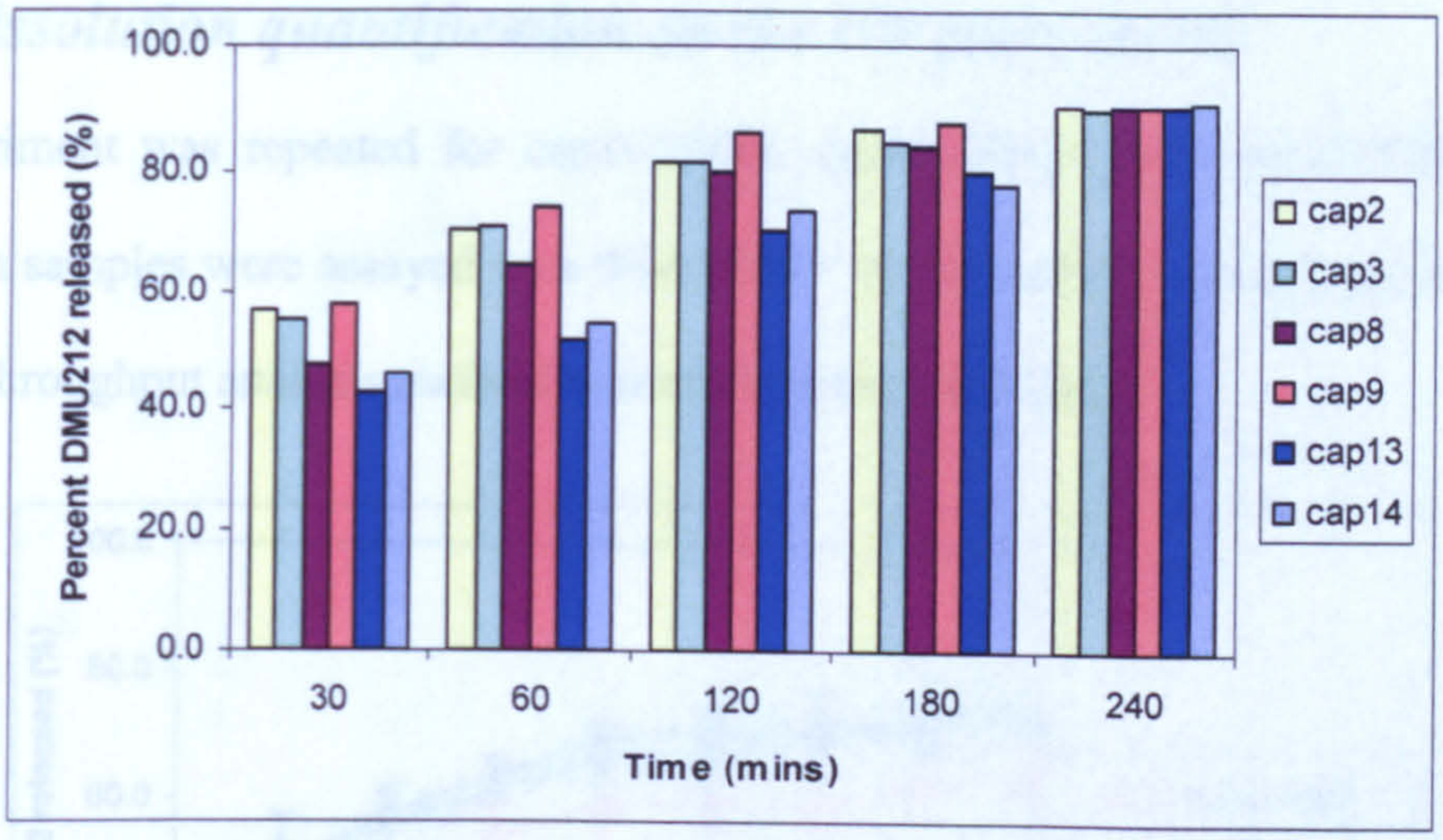

Figure 37. Dissolution rate of different DMU212 capsule formulations in 1% w/v SLS dissolution medium.

Since, capsules containing drug and diluent only were the optimum formulations the DMU212 drug load was increased from 50mg to 100mg for these capsule formulations and similar results were found:

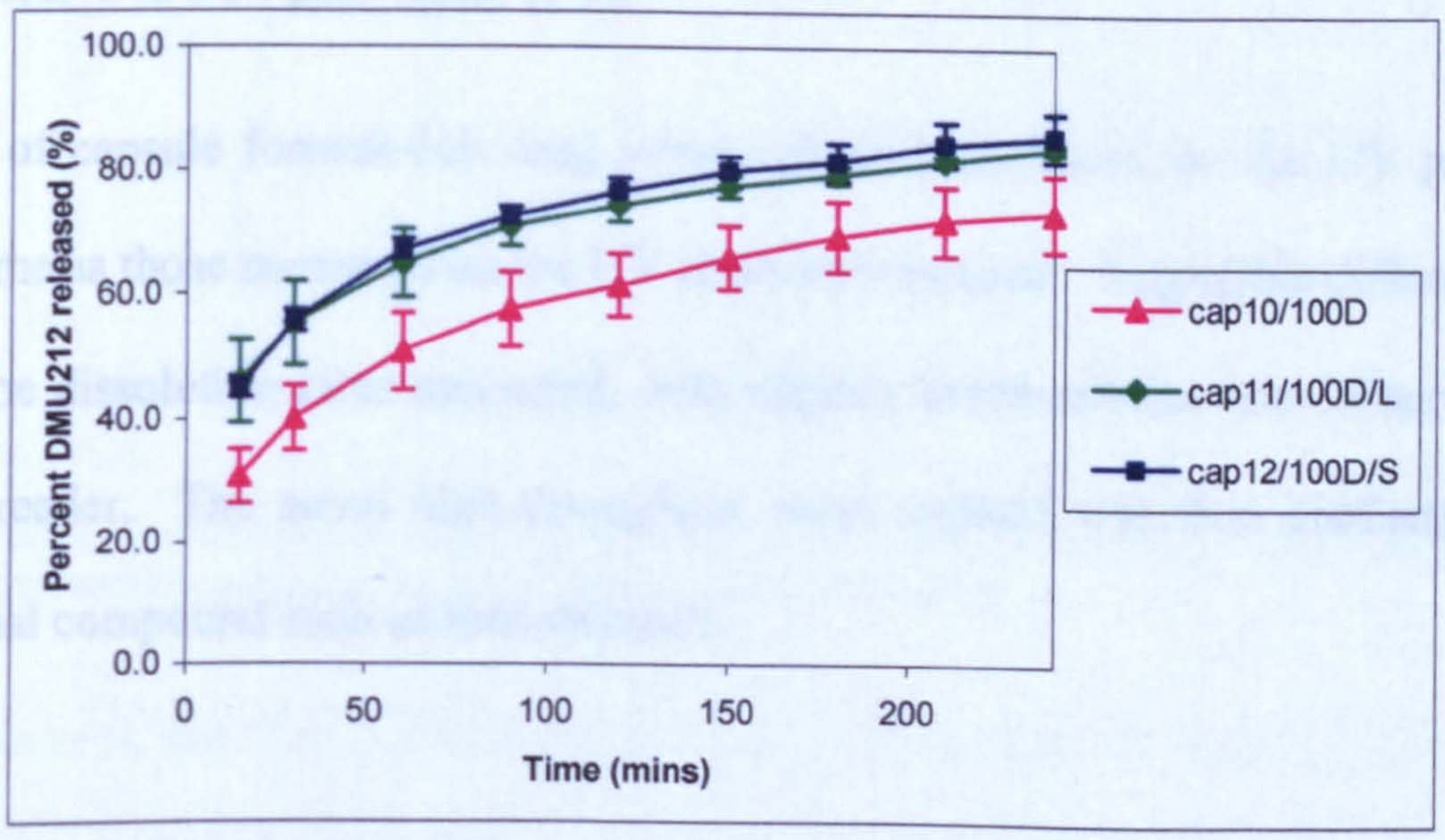

Figure 38. Percent DMU212 released with time for capsule formulations containing 100mg of drug in 1% w/v SLS dissolution medium (n=3).

3.3.2 Dissolution quantification on the UV plate reader

The experiment was repeated for cap10/100D, cap11/100D/L and cap12/100D/S where dissolution samples were assayed on a 96-well UV plate reader to attempt the construction of a high-throughput analysis method to improve assay efficiency:

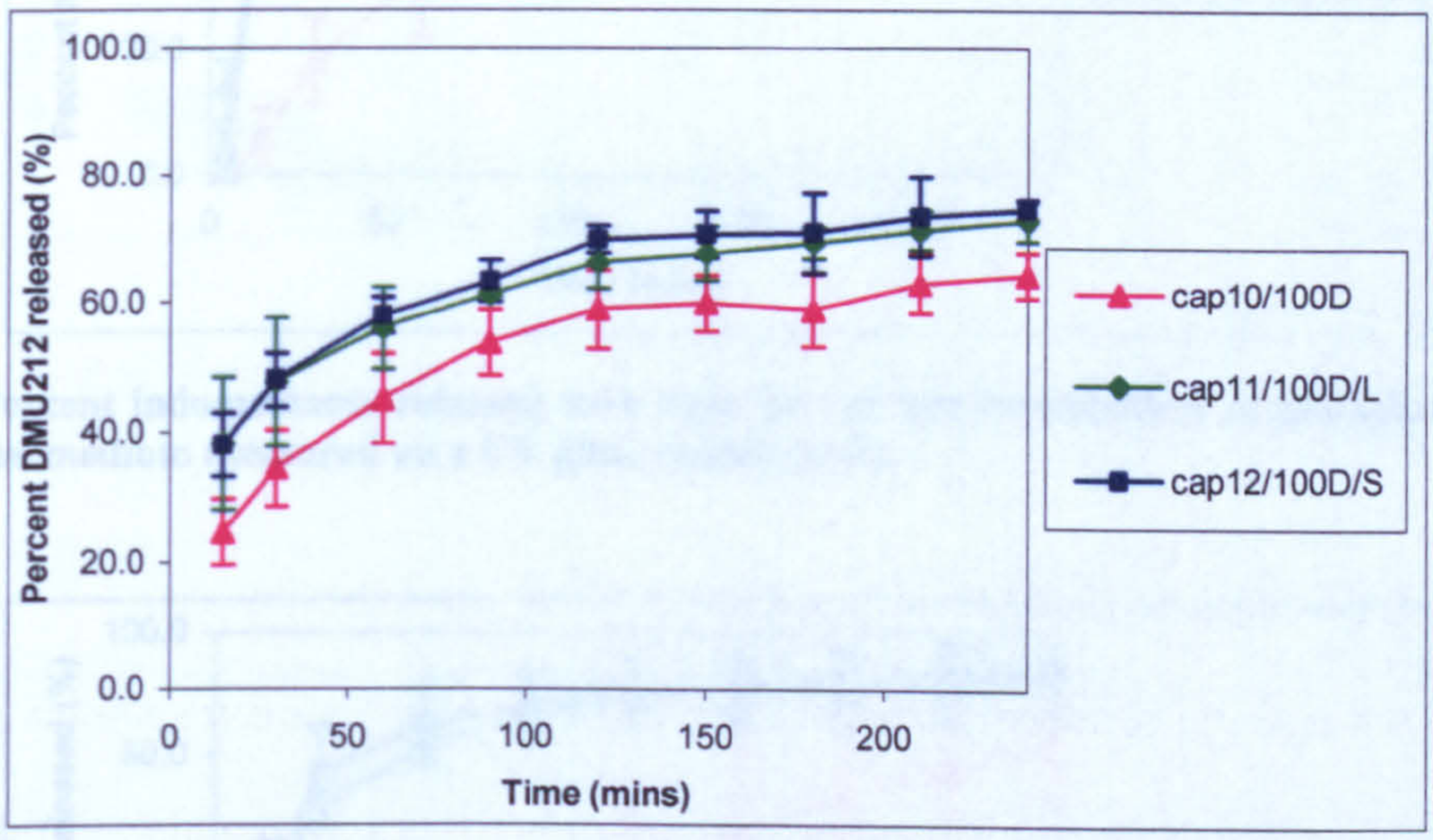

Figure 39. Percent DMU212 released with time for capsule formulations in 1% w/v SLS dissolution medium measured on a UV plate reader (n=3).

The order of capsule formulation drug release profiles measured on the UV plate reader was the same as those measured on the UV spectrophotometer. Negligible differences were found in the dissolution rates measured, with slightly lower release rates observed on the UV plate reader. The novel high-throughput assay method was then challenged with a conventional compound such as indomethacin:

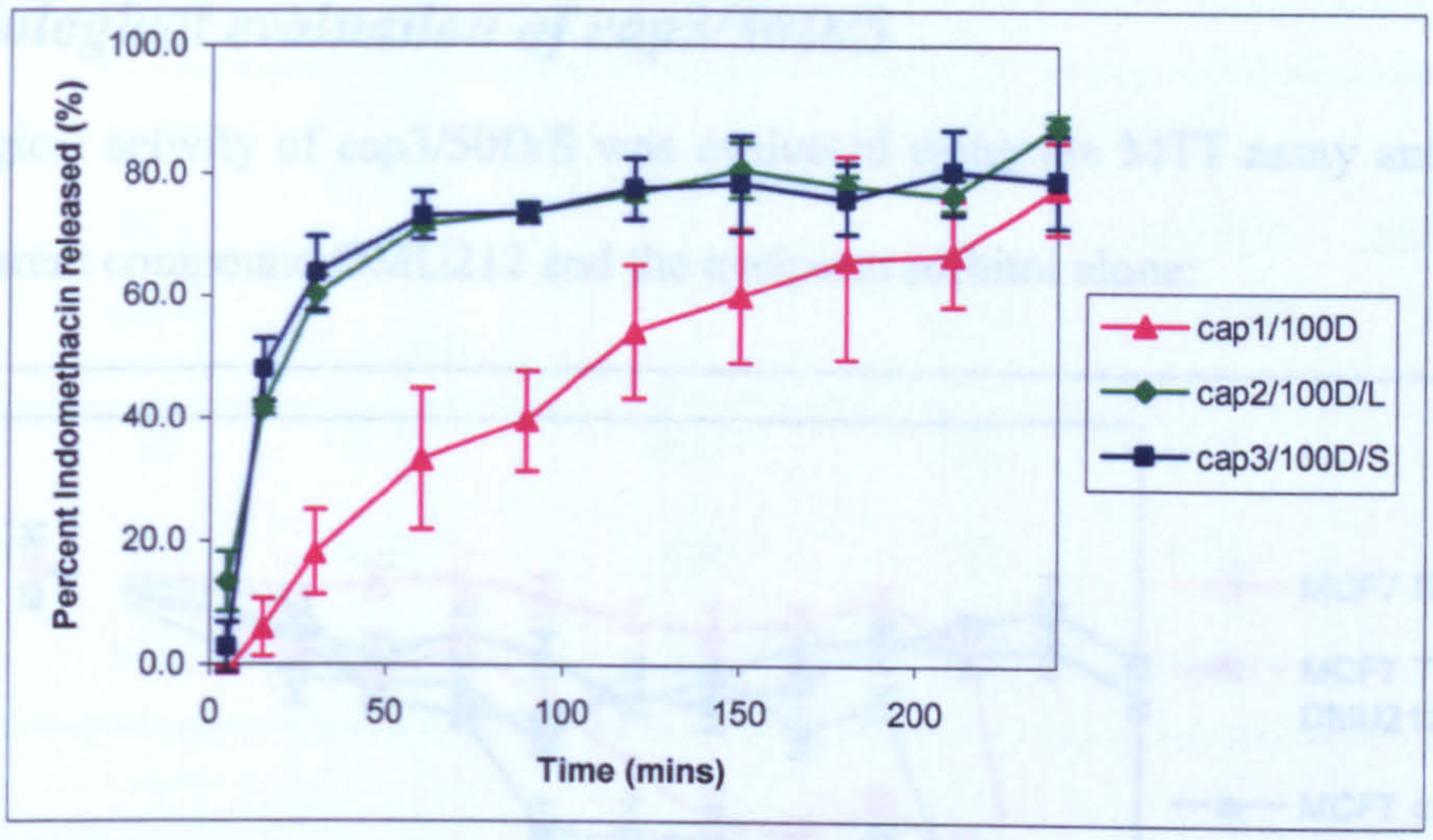

Figure 40. Percent indomethacin released with time for capsule formulations in phosphate buffer pH 6.4 dissolution medium measured on a UV plate reader (n=3).

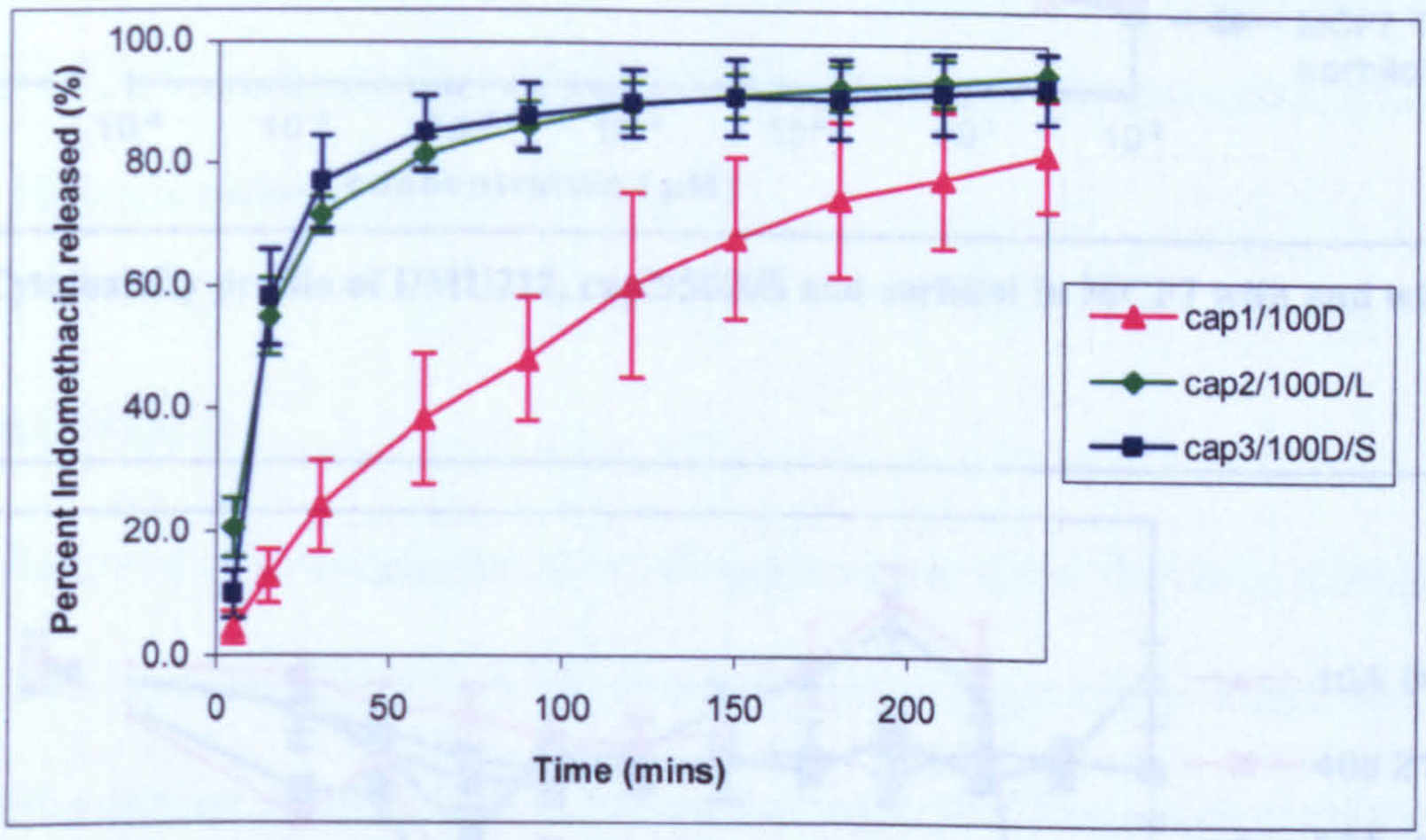

Figure 41. Percent indomethacin released with time for capsule formulations in phosphate buffer pH 6.4 dissolution medium measured on a UV spectrophotometer (n=3).

The difference in the drug release profiles measured on the UV spectrophotometer and plate reader was also apparent with indomethacin; however, the rank order of dissolution profiles remained consistent, regardless of the assay method.

3.3.3 Biological evaluation of cap3/50D/S

The biological activity of cap3/50D/S was evaluated using the MTT assay and compared with the parent compound DMU212 and the excipient sorbitol alone:

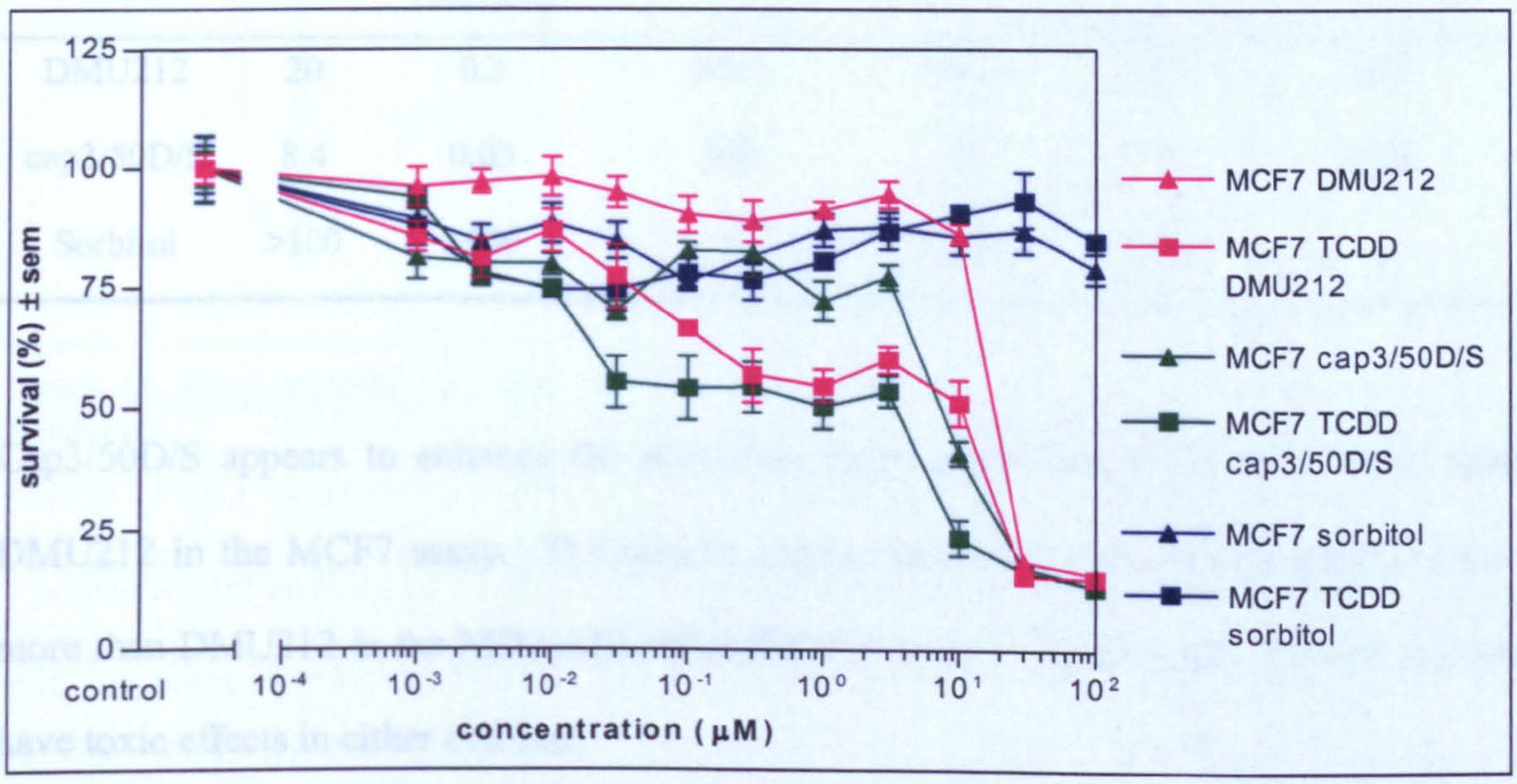

Figure 42. Cytotoxicity profile of DMU212, cap3/50D/S and sorbitol in MCF7 with and without TCDD induction.

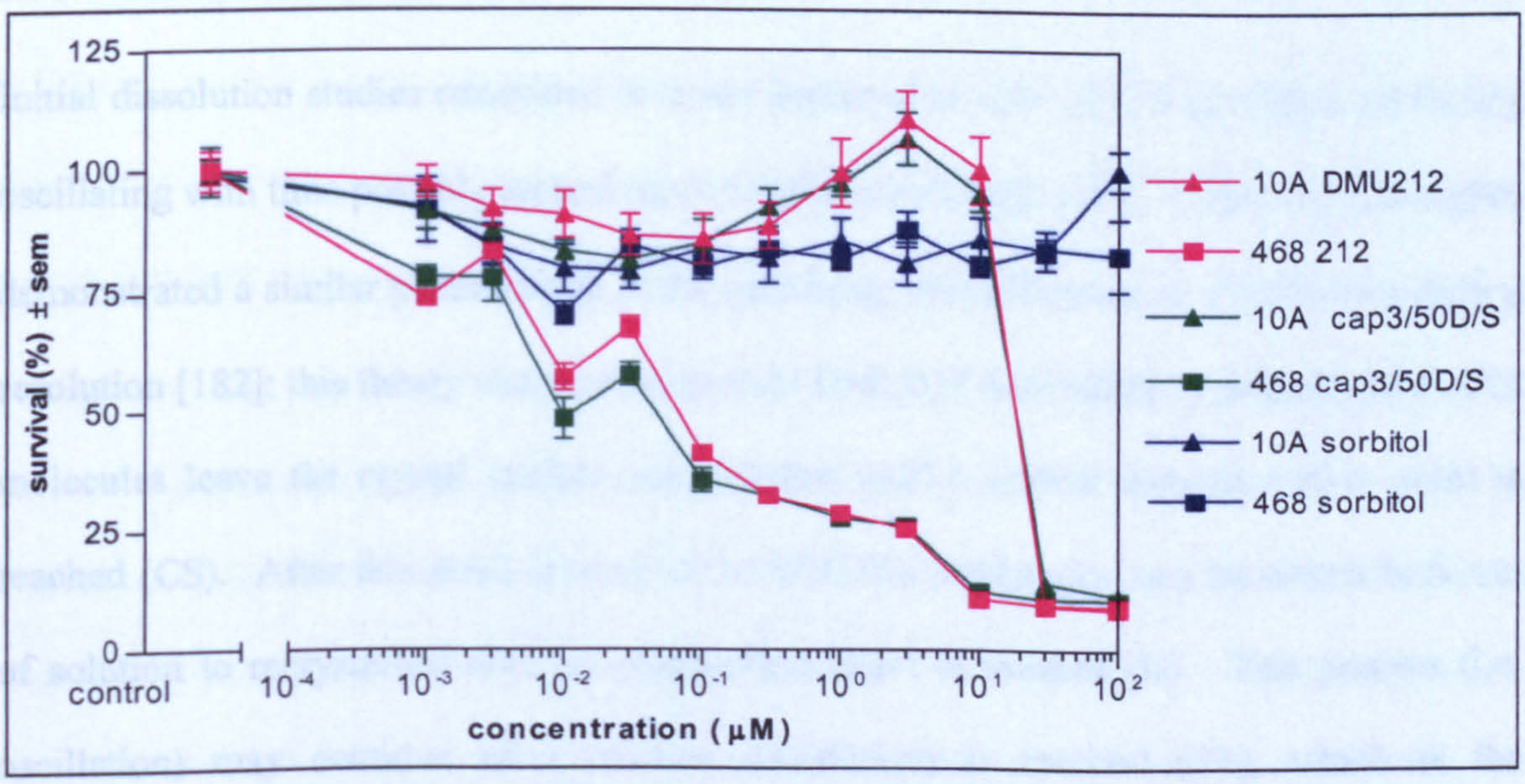

Figure 43. Cytotoxicity profile of DMU212, cap3/50D/S and sorbitol in MDA-MB-468 and MCF10A cell lines.

Table 29. Biological evaluation of DMU212, cap3/50D/S and sorbitol.

DRUG	MCF7 IC_{50} (μM)	MCF7 TCDD INDUCED IC_{50} (μM)	ACTIVATION FACTOR	MCF10A IC_{50} (μM)	MDA-MB-468 IC_{50} (μM)	TUMOUR SELECTIVE FACTOR
DMU212	20	0.3	66.7	20	0.05	400
cap3/50D/S	8.4	0.03	280	20	0.01	2000
Sorbitol	>100	>100	1	>100	>100	1

Cap3/50D/S appears to enhance the activation factor approximately 4 times more than DMU212 in the MCF7 assay. The tumour selectivity factor was also enhanced 5 times more than DMU212 in the MDA-MB-468/MCF10A assay. The excipient sorbitol did not have toxic effects in either cell-line.

3.4 Discussion

Initial dissolution studies conducted in water appeared to show the drug release uniformly oscillating with time possibly around the solubility level (Figure 23). Potter and colleagues demonstrated a similar phenomenon in the oscillating crystallization of enantiomers during resolution [182]; this theory was used to explain DMU212 oscillation i.e. initially DMU212 molecules leave the crystal surface and dissolve until a critical supersaturation point is reached (CS). After this point is reached the DMU212 molecules may be driven back out of solution to recrystallize until an unsaturation point is reached (U). This process (i.e. oscillation) may continue until solution equilibrium is reached (SE), which is the thermodynamic solubility level:

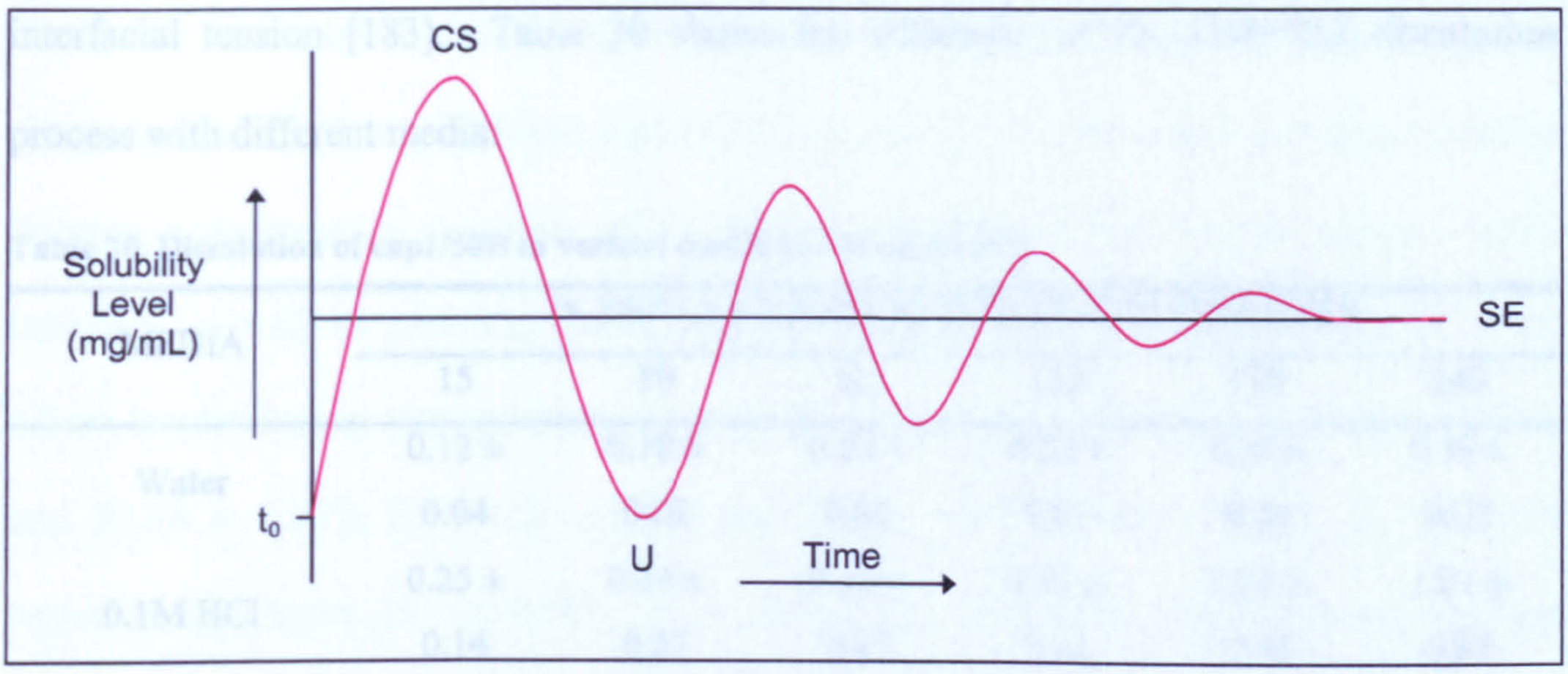

Figure 44. Drug solubility vs. time for the theoretical solubility oscillation of DMU212 during dissolution.

To confirm this observation the dissolution study was repeated in water with cap1/50D whilst observing tighter time points. However, no substantial continuous oscillation patterns were observed (Figure 24), suggesting the perceived oscillations were random fluctuations attributed to experimental noise, rather than any theoretical solubility configuration. Further studies were conducted with standard dissolution media, including 0.1M HCl and pH 7.4 phosphate buffer (Figure 25). However, dissolution studies were not possible with these media because of DMU212 lipophilicity coupled with its non-ionisable nature and poor aqueous solubility (Table 30).

Dissolution rates were significantly enhanced in media containing surfactants; this is because the surfactant acts to lower the interfacial tension and increase the wetting between hydrophobic DMU212 and the aqueous dissolution medium to improve media penetration into the capsule mass [172]. In fact it has been suggested that use of surfactant media is more representative of *in vivo* dissolution rates for poorly soluble drugs because of these reasons i.e. bile salts and lecithin also act as wetting agents in gastric fluid by lowering the

interfacial tension [183]. Table 30 shows the efficiency of the DMU212 dissolution process with different media:

Table 30. Dissolution of cap1/50D in various media at 100 rpm (n=3).

MEDIA	% DMU212 DISSOLVED IN STATED MINUTES					
	15	30	60	120	180	240
Water	0.12 ± 0.04	0.18 ± 0.02	0.18 ± 0.02	0.27 ± 0.01	0.31 ± 0.06	0.36 ± 0.02
0.1M HCl	0.25 ± 0.14	0.34 ± 0.27	0.53 ± 0.27	0.53 ± 0.11	1.01 ± 0.40	1.01 ± 0.67
Phosphate Buffer pH 7.4	0.10 ± 0.00	0.20 ± 0.08	0.28 ± 0.09	0.31 ± 0.12	0.37 ± 0.21	0.39 ± 0.15
1% w/v SLS	2.03 ± 1.87	16.08 ± 8.14	41.16 ± 6.04	68.78 ± 2.84	79.81 ± 0.75	83.88 ± 0.06
1% w/v Tween 80	9.97 ± 1.58	12.35 ± 1.02	15.63 ± 0.63	18.80 ± 0.40	20.78 ± 0.31	23.21 ± 0.16
1% w/v CTAB	11.43 ± 0.30	19.84 ± 0.01	32.68 ± 1.19	45.62 ± 5.51	62.03 ± 2.53	73.60 ± 0.74

Dissolution studies conducted in 1% w/v non-ionic Tween 80 resulted in the lowest dissolution rates with regards to surfactant media, followed by 1% w/v cationic CTAB. During the first 30 minutes of dissolution fastest release was with 1% w/v CTAB medium, thereafter and overall the fastest dissolution for cap1/50D was exhibited in 1% w/v SLS media. Overall, dissolution efficiency with 1% w/v SLS was more than 200-fold better when compared with aqueous media such as water, buffers and acids ($p<0.05$). This improvement in solubility may be attributed to SLS lowering the interfacial tension and improving the wettability of DMU212, which in turn increases the drug dissolution rate [184].

To further maximise the sensitivity of the test conditions the optimum rotary speed was determined with 1% w/v SLS and cap1/50D (Figure 27). Generally an increase in agitation induces a decrease in thickness of the diffusion boundary layer at the capsule-media interface, as well as providing better mixing to prevent the development of static areas where localised drug concentrations may arise. A total of 43.98 ± 3.56%, 71.59 ± 1.71% and 83.88 ± 0.06% DMU212 was released using stirring speeds of 50, 75, and 100 respectively (Figure 28) ($p<0.05$). At a rotor speed of 50 rpm the lowest release was observed, probably since the boundary layers at the capsule-media interface were stagnant, thereby, providing additional resistance to drug diffusion from the capsule mass, since a lower drug concentration gradient exists across the boundary layer i.e. non-sink conditions exist (Section 3.1.1.2). Optimum drug release rate was observed with a speed of 100 rpm and since the dissolution rate for DMU212 appears to be quite slow this agitation speed was implemented to potentially increase the rate for future dissolution studies.

The effect of particle size on DMU212 dissolution rate was also studied (Figure 29) with cap1/50D at 100 rpm in 1% w/v SLS dissolution medium. A total of 83.88 ± 0.06%, 60.87 ± 2.20% and 26.54 ± 4.05% DMU212 was released using particle size fractions of <150μM, 150-250μM and 250-500μM respectively (Figure 30) ($p<0.05$). These results demonstrate the discriminatory power of the developed dissolution method, since differences in drug characteristics such as particle size exhibited measurable differences. DMU212 drug release was shown to be particle size dependent, with greatest drug release at <150μM, followed by 150-250μM and finally 250-500μM. These results can be explained using the Noyes-Whitney equation (Equation 3.1), in which the dissolution rate

is directly proportional to the surface area of the drug. In turn the surface area to volume ratio increases with decreasing particle size depending on the amount of drug used and providing that the drug particles are intimately wetted by the dissolution medium [147], which is applicable for DMU212 dissolution.

Initial formulation screening studies were conducted in both 0.5 and 1% w/v SLS to determine the lowest surfactant concentration necessary for 75-80% dissolution within a reasonable period of time. The optimum dissolution rates were observed with 1% w/v SLS dissolution medium for all formulations and as such DMU212 saturation concentration in this medium was determined. The saturation solubility of DMU212 in 1% w/v SLS at 0.091 mg/mL measured on the UV plate reader and 0.095 mg/mL on the UV spectrophotometer is twice the concentration of DMU212 that would be observed if 100% dissolution was observed i.e. 0.056 mg/mL. Although sink conditions state that the solubility of drug in the media should be five times the intended dose, studies by Brown *et al* state that non-sink conditions are justifiable if the medium provides sufficient discriminatory power and reliable data which can only be obtained with addition of surfactants [181], both of which are true for DMU212 dissolution. Furthermore, it is more important that the proposed dissolution test closely simulate the gastrointestinal milieu than necessarily produce sink conditions.

Nonetheless, in both SLS media, drug release from cap1/50D was much lower compared with other capsule formulations, thereby indicating the need for other excipients in DMU212 capsule formulation to aid drug release. Inclusion of hydrophilic diluents e.g. sorbitol or lactose in the formulation enhanced the dissolution rate (Figures 31-34), since

the hydrophilic particles in the capsule mass dissolved first in the dissolution medium to leave a porous mass of dispersed hydrophobic drug through which the medium could penetrate much more easily compared with clumped cap1/50D drug particles [172], thereby improving the effective drug surface area and therefore the dissolution rate [147]. The best dissolution rate was observed with cap3/50D/S followed by cap2/50D/L.

The addition of SLS to the formulation did not significantly improve the dissolution rate compared with capsules containing drug and diluent only ($p>0.05$), even with 50% w/w SLS incorporation (cap8/50D/SLS/L and cap9/50D/SLS/S) ($p>0.05$). Therefore, incorporation of such a high SLS formulation concentration, which could potentially cause patient side effects (Figure 35) was unjustified. The inclusion of magnesium stearate in the formulation reduced the dissolution rate significantly even when compared with cap1/50D i.e. drug alone ($p<0.05$). These results suggest that strong interactions are formed between DMU212 and magnesium stearate (i.e. magnesium stearate may coat the DMU212 particles); such that the hydrophobic nature of the drug is further enhanced by a hydrophobic excipient, therefore, incorporation of magnesium stearate in the capsule formulations was disregarded. Finally capsules containing cyclodextrins (cap13/50D/ACYC and cap14/50D/ACYC) did not exhibit faster (Figure 36) dissolution rates compared with capsules containing drug and sorbitol/lactose (Figure 37) ($p>0.05$). Overall, capsules containing sorbitol as the diluent gave the optimum release profile with the fastest dissolution rate, validated with a DMU212 dose increase from 50mg to 100mg to give the same results with a maximum drug release of 85.74 ± 3.89% (Figure 38). These

results also demonstrated the robustness of the dissolution method, since the drug release profile was more or less the same independent of drug loading.

The dissolution samples assayed on the UV plate reader (Figure 39) were comparable to those determined on the UV spectrophotometer (Figure 38) with optimum difference between the two assay techniques being ±10% ($p>0.05$):

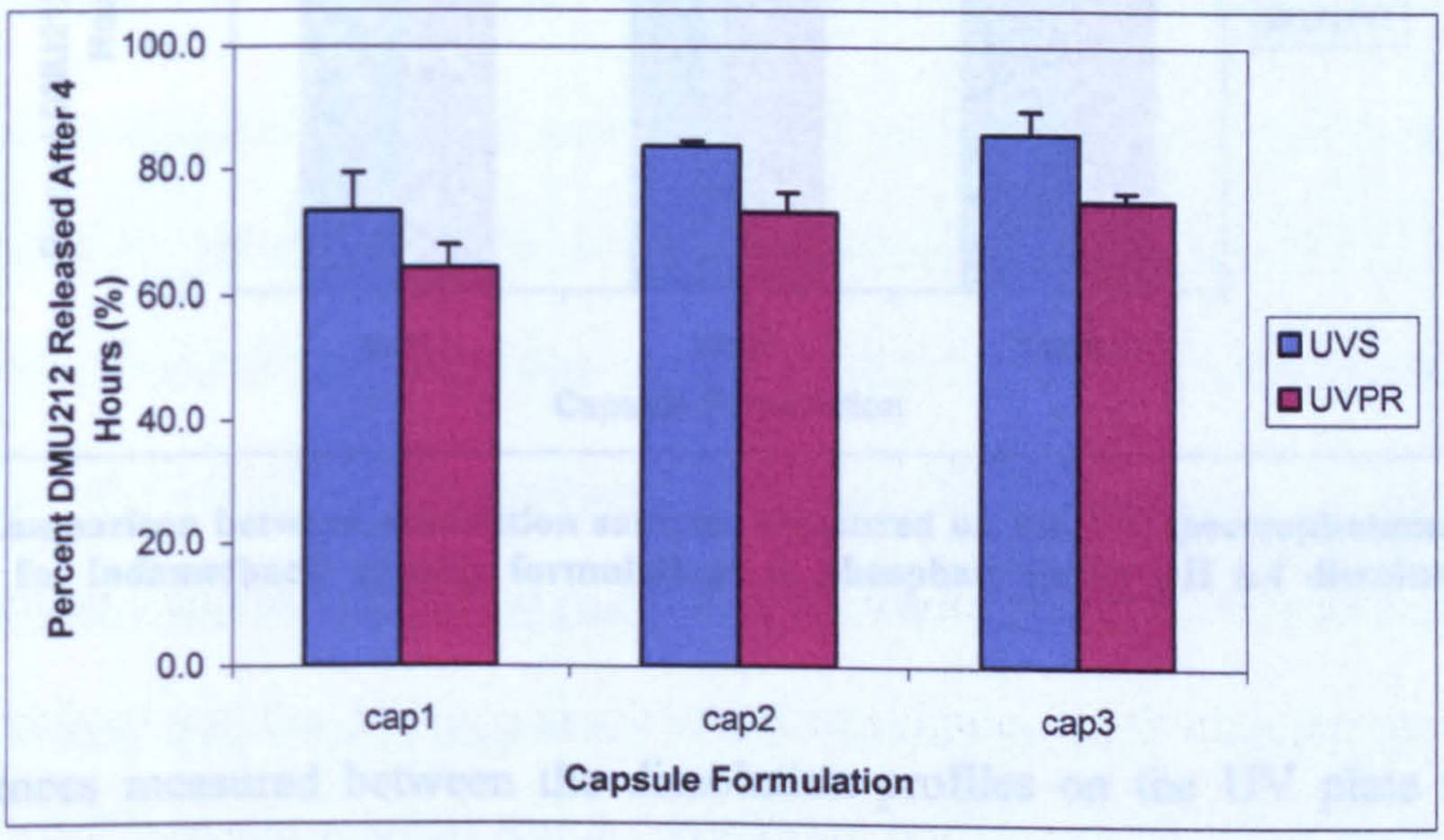

Figure 45. Comparison between dissolution samples measured on the UV spectrophotometer and UV plate reader for DMU212 capsule formulations in 1% w/v SLS dissolution medium (n=3).

Capsules assayed on the 96-well UV plate reader exhibited slightly lower dissolution rates compared to measurements on the UV spectrophotometer. Initial differences were thought to arise from miniaturisation of dissolution sample volumes; therefore, sample volumes used for both assay methods were standardised, however, the results still indicated a difference in sensitivity between the two methods of assay. Regardless of the sensitivity differences, the order of capsule formulation drug release profiles measured on the UV plate reader was the same as those measured on the UV spectrophotometer. This

phenomenon was also observed with dissolution studies of a conventional compound such as indomethacin:

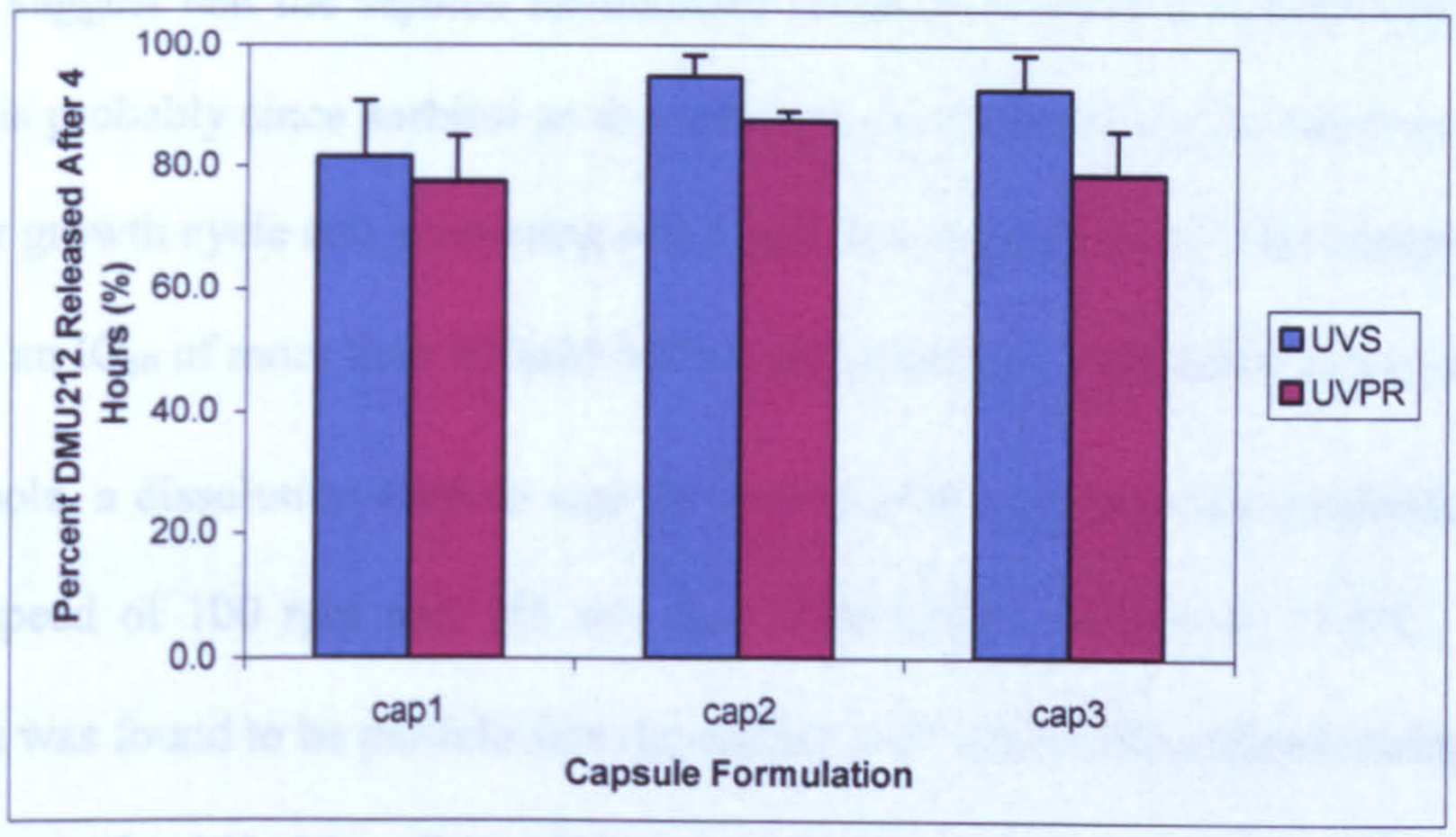

Figure 46. Comparison between dissolution samples measured on the UV spectrophotometer and UV plate reader for indomethacin capsule formulations in phosphate buffer pH 6.4 dissolution medium (n=3).

The differences measured between the dissolution profiles on the UV plate reader and spectrophotometer were not found to be statistically significantly ($p>0.05$) for either DMU212 or indomethacin capsule formulations. Therefore, it is proposed that the UV plate reader method be utilised as a high-throughput capsule formulation screening method, from which candidate formulations may be determined as validated by the dissolution and consequent assay of the conventional compound indomethacin (Figures 40-41). The dissolution rate for these formulations can then be validated through conventional UV spectrophotometry.

Biological evaluation of cap3/50D/S compared to DMU212 (Figures 42-43) showed a 4-fold increase in the activation factor with a 2.5-fold toxicity enhancement against non-induced MCF7 cells and a considerable 10-fold increase in induced cells. The tumour

selective factor was also enhanced 5-fold; MDA-MB-468 cytotoxicity was again enhanced 5-fold, however in the normal cell line MCF10A there was no alterations in toxicity. These results all suggest that the capsule formulation increases DMU212 cytotoxicity to tumour cells; this is probably since sorbitol as the excipient is a nutrient and is therefore enhancing the tumour growth cycle and promoting cell death as a consequence. The excipient sorbitol alone with an IC_{50} of more than 100μM had no influence on cytotoxicity in any cell line.

On the whole, a dissolution method was developed with optimum test conditions using an agitation speed of 100 rpm and 1% w/v SLS dissolution medium at 37.5°C. DMU212 dissolution was found to be particle size dependant with fastest drug release using a particle size fraction of <150μM. Formulation screening studies assayed on both the UV spectrophotometer and plate reader showed capsules containing DMU212 and sorbitol only to give the fastest drug release, regardless of the initial drug load. Overall, use of the UV plate reader for high-throughput capsule formulation screening was also validated from which candidate formulations may be determined and a novel application for the MTT assay was developed to determine capsule formulation effect on DMU212 cytotoxicity.

CHAPTER 4

Topical Formulation of Non-Ionisable prodrugs

4.1 Introduction

In addition to oral administration, another route for administration of chemotherapeutic agents is through topical application. The need for topically administered anticancer agents has gathered momentum along with the increasing incidence of skin cancer [169]; current cytotoxic agents most commonly administered topically include 5-FU [185]. The advantages of topical chemotherapy include high local drug concentrations for optimum therapeutic efficacy, low systemic toxicity, and avoidance of first pass metabolism [169]. The major factors which determine the pharmacological response to topically applied drugs are the regional differences in skin permeability, the concentration gradient and the partition coefficient, all of which drive the release of drugs from topical formulations and most importantly the topical vehicle which influences skin penetration and topical bioavailability [169].

4.1.1 Topical formulation

Topically applied formulations can be classified into liquid (emulsions, solutions and suspensions), solid (powders) or semisolid systems [186]. Semisolid formulations are the most popular of topically applied preparations and are characterised by their rheological behaviour which allows them to reside on the skin for longer periods to allow prolonged drug delivery at the application site. Advantages of semisolid formulations are ease of application and the capacity for topical delivery of a wide variety of drugs [187].

Semisolids are available as a wide variety of formulation types such as ointments, creams, gels and pastes, each having unique characteristics. Ointments are greasy, semisolid

preparations intended for external application to the skin, they are often anhydrous and the drug may be either dissolved or dispersed in the vehicle [186-189]. Ointment bases can be broadly classified into hydrocarbons, absorption and emulsifying bases. Hydrocarbon bases mostly consist of paraffins, are lipophilic, anhydrous and form an occlusive layer on the skin, thereby making them useful for dry scaly conditions. Absorption bases, in addition to lipophilic components, contain emulsifiers which allow the formulation to incorporate water resulting in the formation of water-in-oil (w/o) emulsions. Emulsifying bases are similar to absorption bases but can form oil-in-water (o/w) emulsions which make them miscible with water.

Patients prefer creams to ointments as creams are less greasy and easier to apply; they consist of medicaments dissolved or suspended in water soluble or vanishing cream bases [186-188]. Creams can be defined as ointments which incorporate an aqueous phase to form either o/w or w/o emulsions, if the oil droplets are dispersed in water, then the system is described as an o/w emulsion; conversely if the disperse phase is water and the continuous phase is oily then a w/o emulsion exists. Gels are two-phase systems consisting of a continuous liquid phase such as water or ethanol thickened by a disperse phase such as carbopol and hydroxypropylmethylcellulose to form a three-dimensional structure that can entrap large amounts of solvent [147]. Gels can be either water-based (aqueous gels) or organic solvent based (organogels). Pastes are stiff ointments which contain a high proportion of powder suspended in a fatty base. Because of their consistency, pastes are useful in treating highly localised areas of the body; furthermore, they are less greasy than ointments since the powder adsorbs some of the fluid hydrocarbons [186, 188].

The appropriate choice of semisolid vehicle not only involves delivery of the compound to the target tissue but also maximises therapeutic efficacy by considering the aetiology of the disease and the mechanism of action of the drug [190]. In this context, the formulation clearly influences skin penetration and topical bioavailability, therefore, selection of an appropriate vehicle is one of the most important parameters in increasing efficacy of a topically applied drug [191]. In order to study the influence of the semisolid vehicle on the drug release of DMU212, various hydrophilic and lipophilic vehicles were evaluated in this study. These included anhydrous absorption and anhydrous washable (emulsifying) ointments, since ointments are occlusive and so are useful for dry lesions [186]. Anionic, cationic and non-ionic o/w creams and a w/o cream were also evaluated, since creams are generally preferred by patients.

4.1.2 In vitro release of drugs from topical formulations

The formulation efficacy was determined using an *in vitro* release test, which serves to ensure batch to batch uniformity, to act as a guide for topical formulation during product development and possibly to predict *in vivo* performance. Before a topically applied product can be efficacious, it must release the active moiety from the vehicle in order to penetrate the skin and exert its effect; these processes are influenced by the physicochemical properties of the drug, the vehicle and the skin [191]. With respect to skin/membrane permeation this process is most often described by Fick's first law of diffusion [147, 186]:

$$J = \frac{dm}{dt} = \frac{DC_V K}{h} \qquad (4.1)$$

Where J is the steady-state drug flux and dm/dt is the cumulative amount of drug, m, passing through a unit area of membrane as a function of time t, D is the diffusion coefficient of the drug, C_V is the concentration of drug in the topical vehicle (concentration in the dissolution medium is assumed to be zero with maintenance of sink conditions), K is the partition coefficient of the drug between the membrane and the topical vehicle and h is the thickness of the membrane. The steady-state flux J can be estimated from the slope of the linear portion of a plot of dm/dt against time.

The scenario in which the transport of a drug within the vehicle is the rate-determining step can be described by Higuchi's equations, which are derived from Fick's law [192, 193]. Higuchi proposed two equations, one in which the drug exists as a solution in the vehicle:

$$Q = 2C_O\sqrt{\frac{Dt}{\pi}} \qquad \textbf{(4.2)}$$

and one in which the drug exists as a suspension in the vehicle:

$$Q = \sqrt{2DC_OC_St} \qquad \textbf{(4.3)}$$

Where Q is the amount of drug released per unit area, D is the diffusion coefficient of the drug, C_O is the initial drug concentration in the topical vehicle, C_S is the saturation concentration of drug in the dissolution medium and t is the elapsed time. Irrespective of whether the drug is solubilized or suspended in the vehicle, the release should be proportional to the square root of time, if the release is governed by Higuchi kinetics.

The assumptions made in deriving Higuchi's equations were as follows: (1) the drug particles are much smaller in diameter than the thickness of the applied layer such that

dissolution of the particles is not rate-limiting, (2) the initial concentration of the drug in the topical vehicle C_V or C_O is much larger than its saturation concentration C_S, (3) the drug solubility in the receptor fluid is rapid enough such that dissolution is not rate-limiting, (4) sink conditions are maintained, (5) the diffusion coefficient is invariant with respect to time or position within the vehicle and (6) only a single drug is present in the vehicle and only the drug molecules diffuse into the receptor fluid [147, 191, 193]. There are many physicochemical and experimental factors which can influence Equations 4.1-4.3 and therefore the drug release rate. Physicochemical factors include the solubility, diffusion and partition coefficient, molecular size and shape and concentration of the drug [147].

The experimental factors that can influence the drug release rate are the composition of the topical vehicle, temperature, agitation and composition of the dissolution medium and the membrane [186, 191]. The composition of the topical vehicle will directly influence the diffusion, partitioning and solubility of the drug within the vehicle, and therefore the drug release rate [194]. For example, studies by Rege *et al* showed that hydrophobic drugs have a higher affinity for oleaginous vehicles and therefore have a slower release rate into aqueous media [195]. Another major influence on the drug release rate is the thermodynamic activity of the drug in the topical vehicle, whereby the maximum release is obtained when the drug is saturated (i.e. suspended) in the topical vehicle [186, 191]. Only the dissolved drug molecules can penetrate the skin, however, as the drug is released from the vehicle the suspended drug particles dissolve to replenish the donor phase and therefore maintain the driving force for drug release. For this approach to be successful the suspended drug particles have to rapidly dissolve in the topical vehicle, and since the

dissolution rate is inversely proportional to the particle size (Noyes-Whitney equation), then smaller size particles are more likely to replenish the donor phase without introducing a dissolution rate-limiting barrier to drug release [186].

The temperature at which the *in vitro* release studies are conducted can influence the drug release rate from formulations by altering the viscosity of the vehicle as well as the solubility/partition coefficient of the drug all of which may affect the diffusion of the drug through the vehicle. The experiments are typically conducted at 32°C to reflect ambient skin temperature [196]. The degree of media agitation dictates the thickness of the diffusion layer at the interface between the dissolution medium and the membrane, an increase in agitation can reduce the thickness of this stagnant film to result in an increased drug release rate. Another factor that can influence the drug release rate is the drug saturation solubility in the dissolution medium (C_S). If the concentration of drug dissolved in the dissolution medium does not exceed 10% of the drug saturation concentration, then 'sink conditions' are said to exist (Section 3.1.1.2), in which a favourable driving force for drug release from the vehicle and through the skin is maintained. The standard methods of controlling the saturation solubility are to alter the dissolution medium volume and more commonly to change the medium composition [191].

Most studies use physiologically relevant media such as water or phosphate buffer, however, it is also important that the drug has sufficient solubility in the dissolution medium to maintain sink conditions and that the medium has sufficient partitioning characteristics to receive the drug. Therefore, lipophilic drugs such as DMU212 are not suitable for measurement in this type of media, since they will not readily dissolve or

partition into aqueous media [186, 191]. In developing an *in vitro* release test for such compounds, dissolution media containing surfactants, aqueous or organic solvents can be used [197]. For many studies, the latter option has been the most popular, and a wide range of compositions of ethanol/water co-solvent systems has been used. Recently, *in vitro* release from corticosteroid ointments was studied using this co-solvent dissolution medium with the addition of isopropyl myristate (IPM) in a mixture consisting of IPM/water/ethanol in a ratio of 10:5:85 [198]. Several investigators have studied the use of IPM as a dissolution medium since it has been recognised as a good model compound representing skin lipids [194], therefore, when used in combination with ethanol and water the medium is more representative of the skin whilst simultaneously acting as a sink [191].

The membrane used for *in vitro* release studies can also dictate the drug release rate from topical vehicles. Commonly, skin (i.e. the stratum corneum) is used as the membrane to separate the formulation and dissolution medium. However, the constraints in availability, together with the variability associated with animal and human skin has instigated the use of synthetic membranes [199]. The synthetic membrane selected should not impede or control drug diffusion from the formulation to the dissolution medium, but should only provide an inert support. It should be sufficiently permeable to the test drug with minimal thickness, and exhibit no binding to offer the lowest diffusional resistance, such that the only rate-limiting factor, and therefore the measurable one is drug release from the semisolid [200, 201]. Synthetic membranes can be used to compare drug release from different vehicles; however, to ultimately determine drug absorption, skin would still need to be used.

To date no universal apparatus, methods or test conditions for *in vitro* release from semisolid dosage forms have been described in any relevant Pharmacopoeias [202]. However, general guidelines given by the FDA [203] describe a method using an open chamber diffusion cell system, fitted usually with a synthetic membrane. The semisolid dosage form is placed in the open chamber of the diffusion cell and is separated from the dissolution medium by a synthetic membrane. Diffusion of the drug from the topical formulation and across the membrane is determined by assay of sequentially collected samples of dissolution medium to give a time-dependent release profile.

Currently the most popular method for conducting *in vitro* release studies is with the use of Franz diffusion cells, which consist of a donor and receptor compartment between which a horizontally mounted membrane is clamped. The test formulation is applied to the donor side of the compartment and the receptor compartment is maintained at the skin surface temperature of 32°C. The dissolution medium is agitated with a magnetic stirrer and samples are withdrawn from a side-arm located on the receptor compartment at regular intervals [186]. This technique tends be complicated and the method does not lend itself easily to full automation [204].

An alternative technique is the BP paddle-over-disk dissolution apparatus [175] modified to accommodate a release cell, where the release cell rests at the bottom of a dissolution vessel, with a paddle stirring the dissolution medium above it. The release cell generally consists of a sample reservoir and an open screw-on cap to secure the membrane over the sample reservoir. One such device is the newly developed Enhancer cell™ composed entirely of Teflon® containing an adjustable-capacity sample reservoir, a washer for

controlling the exposure of the surface area, and an open screw-on cap to secure the washer and the membrane over the sample reservoir [187, 195, 204]. Crucially, studies by Sanghvi *et al* have demonstrated higher cumulative drug release from ointments and greater ease of use with the Enhancer cell™ compared with the Franz diffusion cells [205], furthermore, similar results were also found by Fares *et al* who compared the release from in-house gel formulations [206]. This technique lends itself to full automation, whilst generating reliable release data and using commercially available apparatus, at a relatively low cost with better temperature and stirring control than the Franz diffusion cell technique.

Within the scope of this thesis the drug release of DMU212 from six topical bases each possessing different physicochemical properties was studied using a modified BP paddle-over-disk dissolution method [175] with an in-house release cell. The method variables evaluated were the composition of dissolution medium, agitation speed and the choice of the synthetic membrane.

4.2 Materials and methods

Reagents were used as received from Sigma-Aldrich Chemical Company (Dorset, UK) or Alfa Aesar (Lancashire, UK). HPLC grade water, ethanol, SLS, white soft paraffin, liquid paraffin, hard paraffin and cellulose acetate membrane (44μm thickness) were obtained from Fisher Scientific (Loughborough, UK). Hydrous wool fat BP and wool alcohol BP were obtained from J. M. Loveridge Ltd. (Hampshire, UK). Silicone membrane (thickness 300μm) was obtained from Samco Silicone Products Ltd. (Nuneaton, UK). DMU212 was supplied by K. Ruparelia of the CDDG.

4.2.1 Topical formulations

All formulations were prepared manually whereby the oily phase of the formulation (DMU212 (passed through a 150μM sieve), cetostearyl alcohol, white soft paraffin, liquid paraffin, hard paraffin, wool alcohol and hydrous wool fat BP) was melted at 60°C in a porcelain dish over a steam bath. For cream formulations the appropriate aqueous phase (sodium propyl *p*-hydroxybenzoate, sodium methyl *p*-hydroxybenzoate, phenoxyethanol, emulsifier e.g. SLS, cetrimide or tween 60 and water) was also heated at 60°C in a porcelain dish and added to the molten oily phase. The formulation was stirred continuously to room temperature and the final weight of product was checked and adjusted with water if necessary. The following formulations were prepared for *in vitro* studies:

Table 31. Summary of DMU212 topical formulations:

FORMULATION / INGREDIENT	TOP1 (%w/w)	TOP2 (%w/w)	TOP3 (%w/w)	TOP4 (%w/w)	TOP5 (%w/w)	TOP6 (%w/w)
DMU212	1	1	1	1	1	1
Sodium Propyl *p*-Hydroxybenzoate			0.05	0.05	0.05	0.05
Sodium Methyl *p*-Hydroxybenzoate			0.15	0.15	0.15	0.15
Phenoxyethanol			0.8	0.8	0.8	0.8
Sodium Lauryl Sulphate		2	2			
Cetrimide				2		
Tween 60					2	
Cetostearyl Alcohol	4	27	9	9	9	
Wool Alcohol						6
Hard Paraffin						15
Liquid Paraffin		35	6	6	6	40
White Soft Paraffin	70	35	15	15	15	8
Hydrous Wool Fat BP	25					
Purified Water (freshly boiled and cooled)			66	66	66	29

4.2.2 Dissolution media preparation

See Section 3.2.1.

4.2.3 In vitro dissolution studies

The modified BP paddle-over-disk dissolution test (2003, Volume IV, Appendix X XIID A249) [175] with an in-house release cell was used for all *in vitro* dissolution studies. Experiments were carried out using a fully automated Pharmatest dissolution flow-through system (PT-DT7, Pharmatest Apparatebau GmbH, Hainburg, Germany), equipped with paddle stirrers fixed at distance of 23-27mm from the top of the release cell whilst rotating at a known fixed speed in the range of 50-200 rpm:

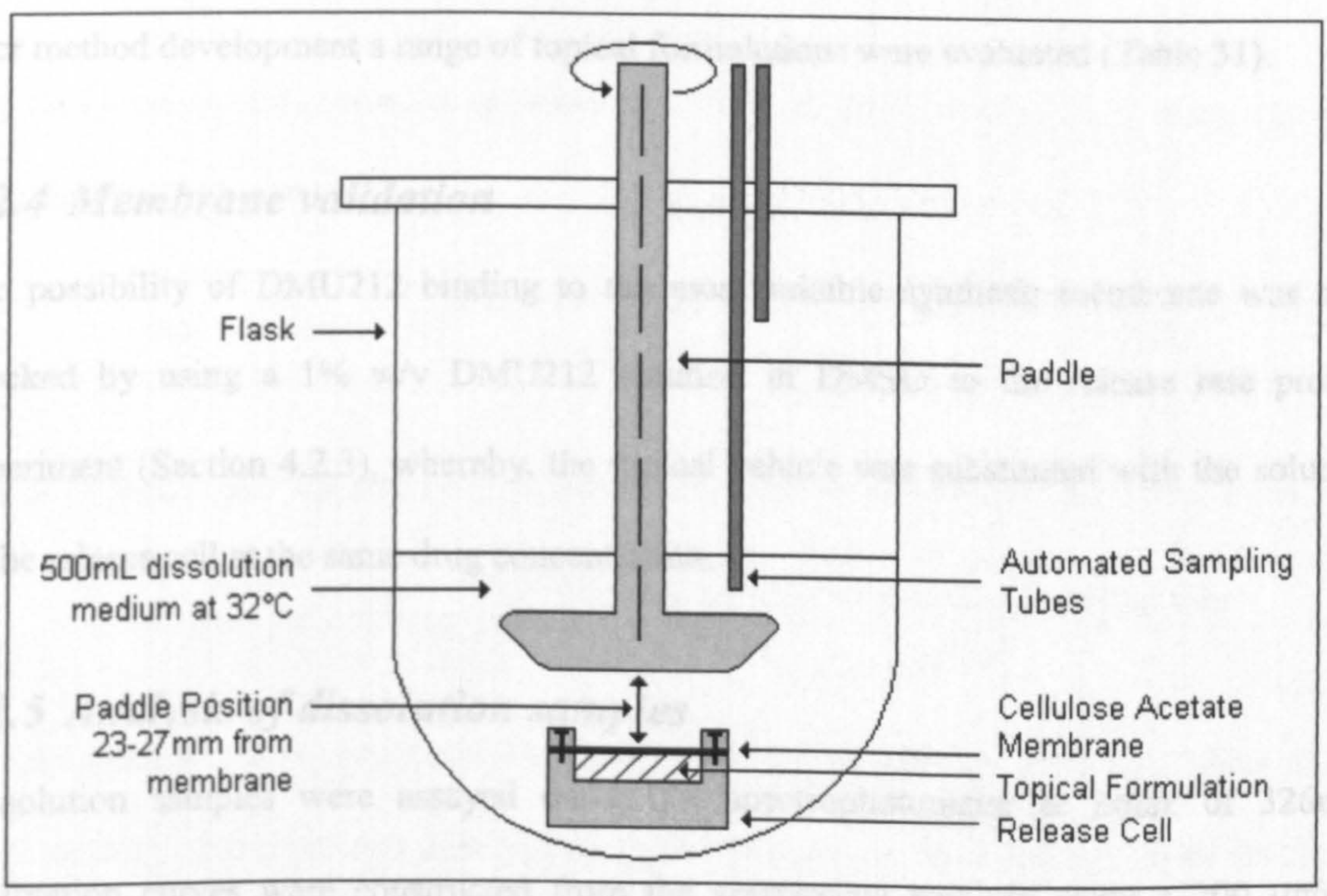

Figure 47. Schematic of the dissolution apparatus.

An 8g sample of the test formulation was placed in the reservoir of the release cell. The membrane (previously wetted with the dissolution medium for 10 minutes and then patted dry) was mounted over the sample and the screw cap secured in place to give a release area of 12.6cm^2. Care was taken to ensure that no entrapped air was present at the membrane-formulation interface. The loaded cell was then introduced into 500mL of the dissolution medium maintained at a temperature of 32.0°C (±0.5°C). At specified time intervals samples of the dissolution medium were withdrawn using a peristaltic pump (Pharmatest-P80), assayed automatically on a UV spectrophotometer (Cecil CE 3021, Cecil Instruments Ltd., Cambridge, UK) at λmax of 326nm and then fed back into the system. The method variables controlled were the dissolution media, stirring speed and choice of membrane and after method development a range of topical formulations were evaluated (Table 31).

4.2.4 Membrane validation

The possibility of DMU212 binding to the most suitable synthetic membrane was also checked by using a 1% w/v DMU212 solution in DMSO to the release rate profile experiment (Section 4.2.3), whereby, the topical vehicle was substituted with the solution in the release cell at the same drug concentration.

4.2.5 Analysis of dissolution samples

Dissolution samples were assayed on a UV spectrophotometer at λmax of 326nm. Calibration curves were constructed from the appropriate medium using a 200 μg/mL DMU212 stock in DMSO to give concentrations in the range 2-20 μg/mL. The calibration curves were validated through preparation of known concentrations of standards within the

calibration range, which were then treated as unknowns and their concentrations were back calculated from the calibration curves constructed. The topical vehicle excipients did not contribute to the drug absorbance and therefore the drug release, this was demonstrated through release studies with all of tested vehicles (Table 31) containing no DMU212.

4.2.5.1 Calculations for drug release data

The equation of the line for corresponding calibration curves were rearranged to convert absorbance into apparent drug concentration in the corresponding sample of dissolution medium removed at time t:

$$\text{Apparent Concentration of DMU212 (mg/mL)} = \frac{(\text{Absorbance} - \text{y Intercept})}{\text{Slope}} \qquad \textbf{(4.3)}$$

The total amount of dissolved drug present in 500mL of dissolution medium at a given time of sampling t was given by:

$$\text{Total Amount of Drug Released } (\mu g) = \left(\begin{array}{c}\text{Apparent concentration (mg/mL)} \times 500 \\ \text{of drug released at time t}\end{array}\right) \times 1000 \qquad \textbf{(4.4)}$$

The drug release per unit area of the membrane at a given time of sampling t was given by:

$$\text{Drug Released per unit area } (\mu g/cm^2) = \frac{\text{Total amount of drug released at time t}}{12.6cm^2} \qquad \textbf{(4.5)}$$

The drug release rate ($\mu g/cm^2 min$) or ($\mu g/cm^2 min^{0.5}$) was calculated from the slope of the graph of drug release per unit area plotted against time or the square root of time, according to Fick's and Higuchi's equations respectively (Equation 4.1-4.3).

4.2.6 Determination of DMU212 saturation concentration in dissolution media

It is important to determine the saturation concentration of the drug in the dissolution medium to ensure that sink conditions are maintained. The saturation concentration of DMU212 was determined in ethanol/water/IPM solvent mixtures to ensure favourable partitioning of DMU212 from a lipophilic topical vehicle to a lipophilic dissolution medium. A ternary phase diagram was constructed for the three-phase solvent mixture, to determine the optimum mixture for dissolution studies:

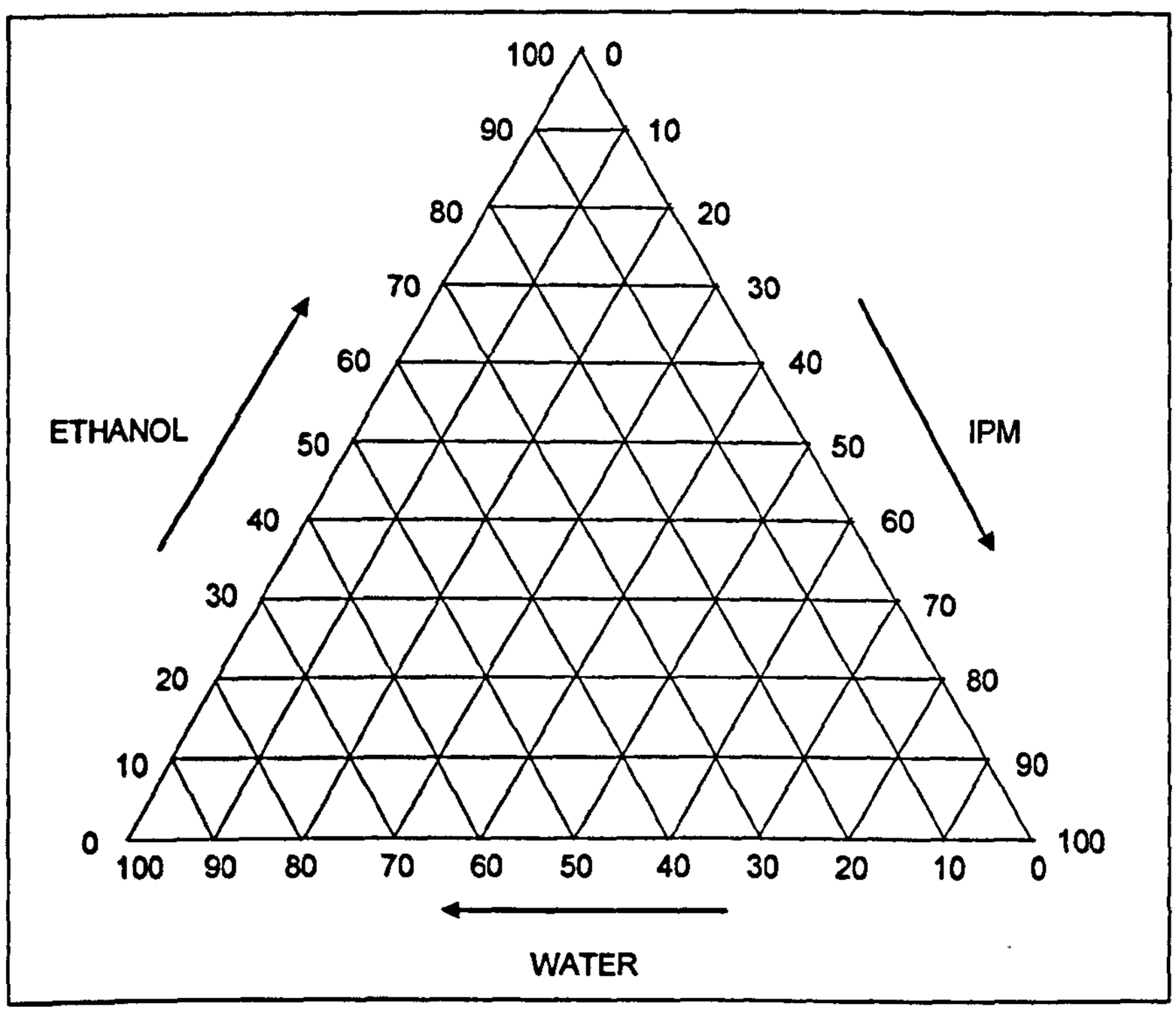

Figure 48. A diagram to show the co-ordinates used when plotting a ternary phase diagram to determine the optimum DMU212 solubility in mixtures of ethanol, water and IPM.

The saturation concentration of DMU212 at each solvent mixture was determined by the shake-flask method (Section 2.2.1).

4.2.7 Determination of DMU212 saturation concentration in topical formulations

The formulations were prepared with a definite concentration of DMU212 (0.25-2% w/w), after having been left for 3 days at room temperature the formulations were examined for the presence of DMU212 crystals using a Leica DMIL microscope (London, UK). The first concentration at which crystals were observed was taken as the saturation concentration [207].

4.2.8 Determination of emulsion type of cream formulations

The emulsion type was determined by incorporation of a water-soluble dye (methylene blue) into the aqueous phase of the cream (TOP3-6); the preparations were examined under a Leica DMIL microscope. The dye stained the corresponding aqueous phase of the o/w or w/o cream i.e. disperse or continuous phase.

4.2.9 Statistical analysis

See Section 2.2.5.

4.3 Results

Linear data plots for the *in vitro* drug release studies were obtained by fitting the dissolution data to Fick's law (Equation 4.1). The cumulative amount of drug release per unit area ($\mu g/cm^2$) was plotted as a function of time (min). The regression coefficients were greater than 0.99 in most cases. Initial drug release studies were conducted using a range of media to screen for the optimum conditions for drug release:

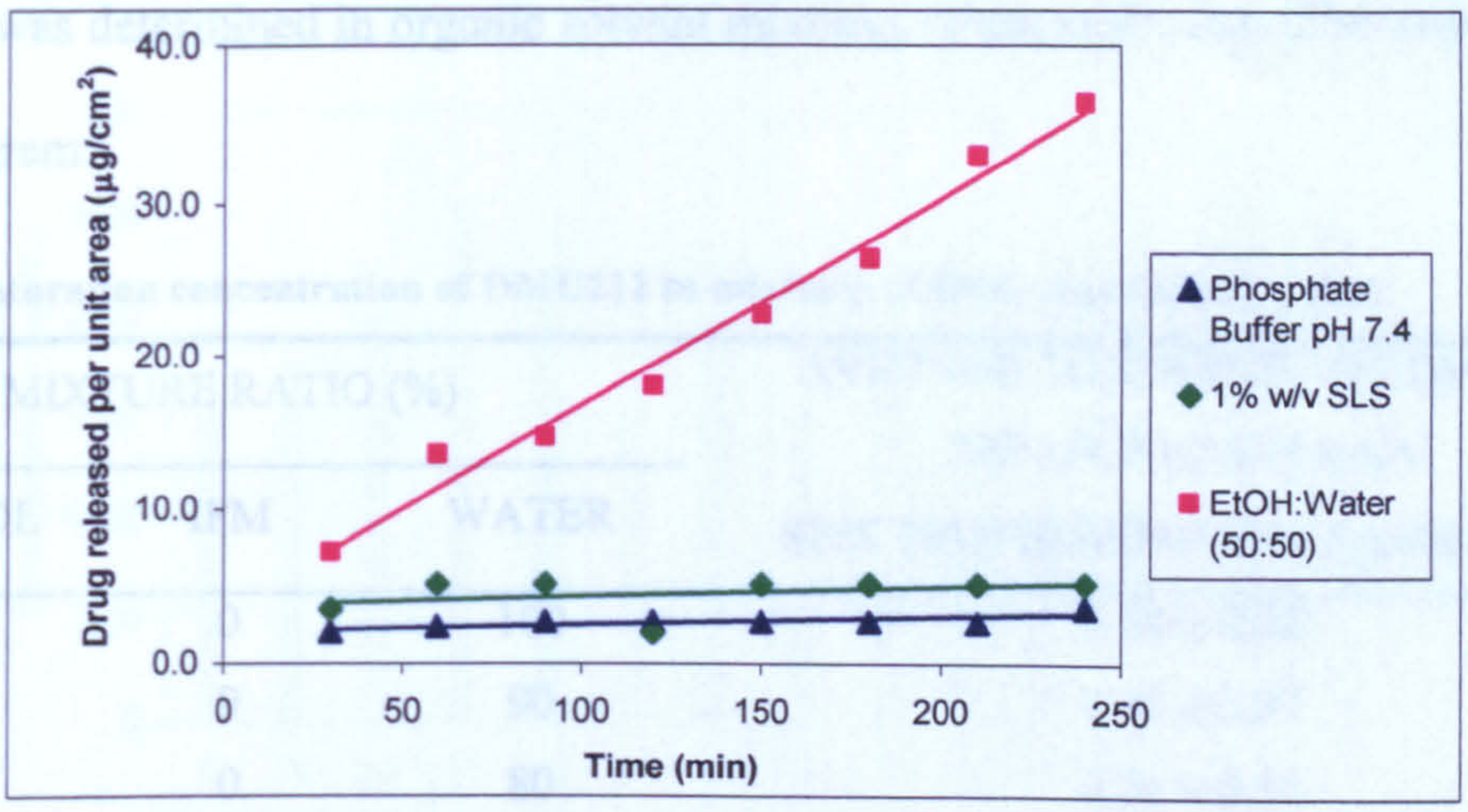

Figure 49. Release of DMU212 from TOP3 in various dissolution media at 50 rpm and 32°C.

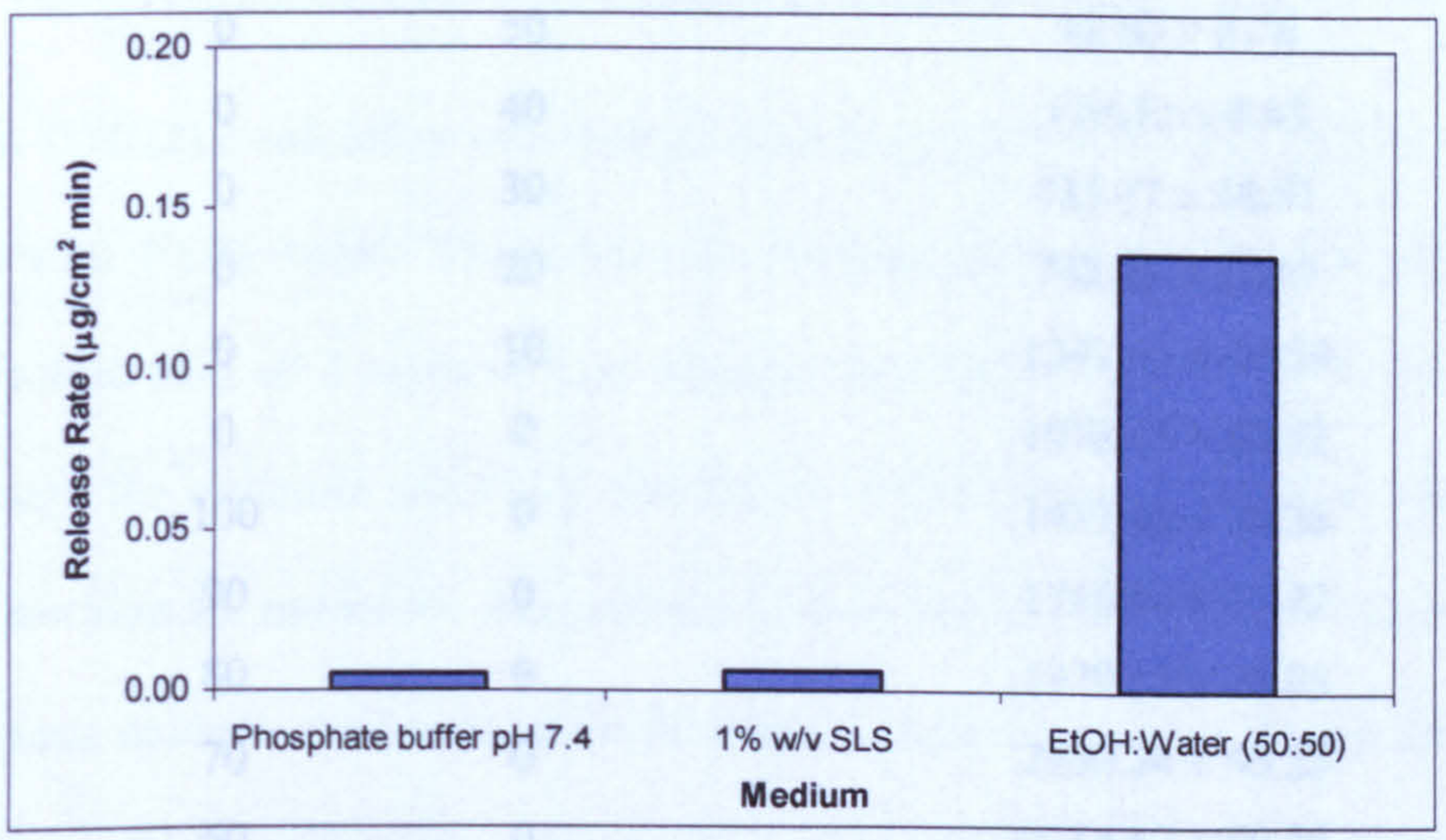

Figure 50. Release rate (slope of the release/area vs. time plots) of DMU212 from TOP3 in various dissolution media over 4 hours.

DMU212 drug release was minimal with aqueous media such as phosphate buffer pH 7.4 and 1% w/v SLS. The highest drug release was observed from organic dissolution media i.e. ethanol/water and even then only a total amount of $36.47 \pm 3.84 \mu g/cm^2$ or $0.57 \pm 0.06\%$ was released. Therefore, to develop a method with favourable sink conditions and sufficient partitioning characteristics to receive the drug, the saturation concentration of

DMU212 was determined in organic solvent mixtures of ethanol/water/IPM using a ternary phase diagram:

Table 32. Saturation concentration of DMU212 in mixtures of IPM, ethanol and water.

MIXTURE RATIO (%)			AVERAGE SOLUBILITY OF DMU212 MEASURED ON A UV SPECTROPHOTOMETER (μg/mL) (n=3)
ETHANOL	IPM	WATER	
0	0	100	1.34 ± 0.22
10	0	90	1.42 ± 0.07
20	0	80	2.21 ± 0.24
30	0	70	4.96 ± 0.41
40	0	60	24.14 ± 1.47
50	0	50	92.90 ± 0.76
60	0	40	196.32 ± 4.93
70	0	30	435.17 ± 18.81
80	0	20	742.32 ± 27.67
90	0	10	1341.63 ± 44.59
100	0	0	1078.45 ± 62.52
0	100	0	1477.45 ± 26.38
10	90	0	1716.96 ± 35.72
20	80	0	1979.15 ± 24.88
30	70	0	2530.24 ± 45.25
40	60	0	2054.87 ± 80.38
50	50	0	1981.58 ± 86.98
60	40	0	1939.27 ± 15.56
70	30	0	1780.03 ± 69.33
80	20	0	1707.74 ± 84.57
80	10	10	1591.14 ± 61.91
90	10	0	1103.77 ± 19.54

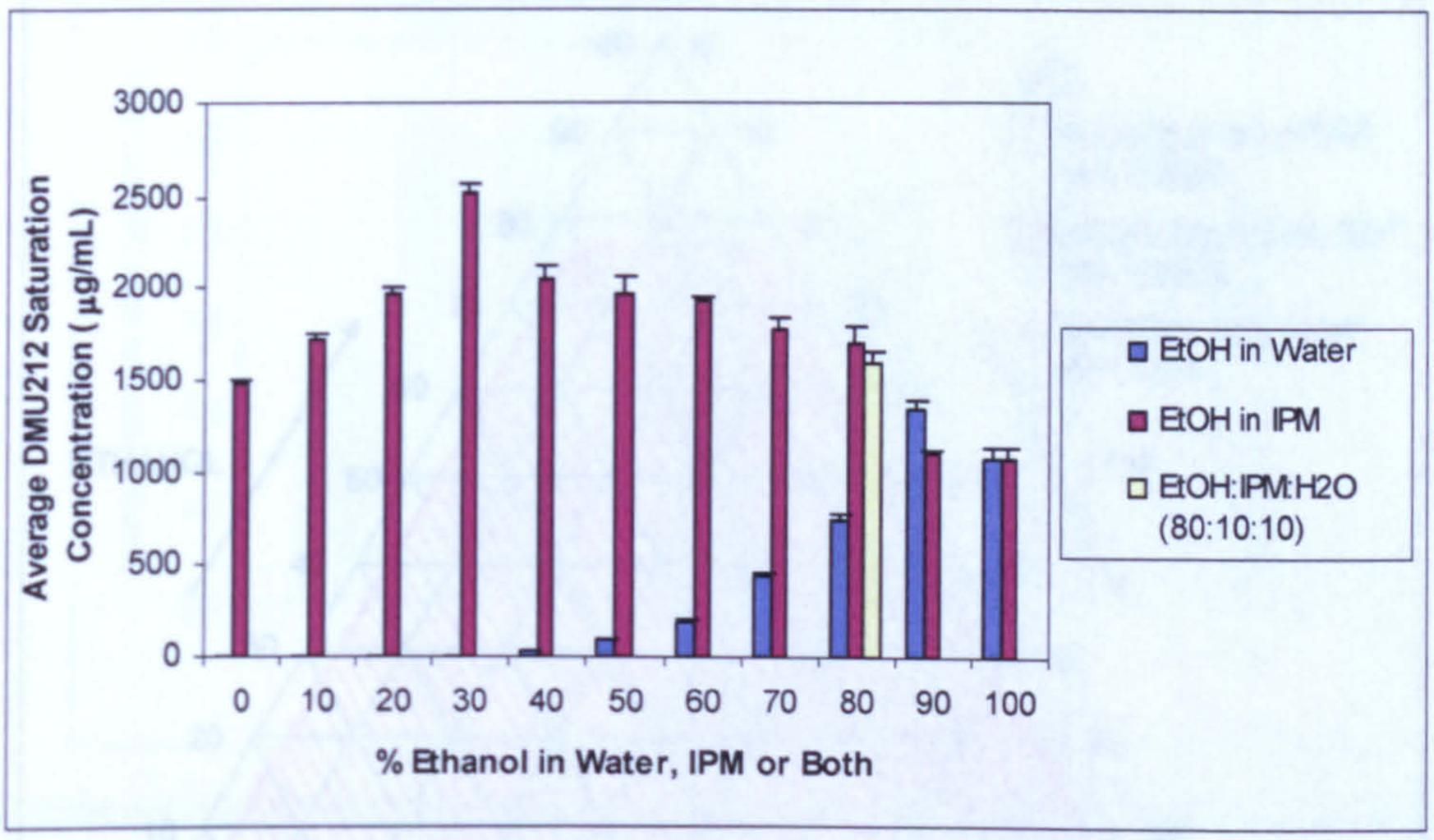

Figure 51. DMU212 Saturation concentration in mixtures of IPM, ethanol and water (n=3).

The highest DMU212 solubility was with ethanol/water/IPM in a ratio of 30:0:70 and the lowest was with 100% water. There were 22 combinations of miscible solvents; the only mixture miscible with all 3 solvents was ethanol/water/IPM in a ratio of 80:10:10 (Figure 52). Although the optimum solubility was found with a mixture of 30% ethanol in IPM, use of this medium for numerous drug release studies would be expensive. However, there were numerous solvent combinations with saturation concentrations above 1500 µg/mL, therefore, the solvent combination chosen was ethanol/water/IPM in a ratio of 80:10:10, since all 3 solvents were utilised, and previous topical studies with corticosteroids by Shah *et al* [198] used a similar combination of ethanol/water/IPM in a ratio of in a ratio of 85:5:10.

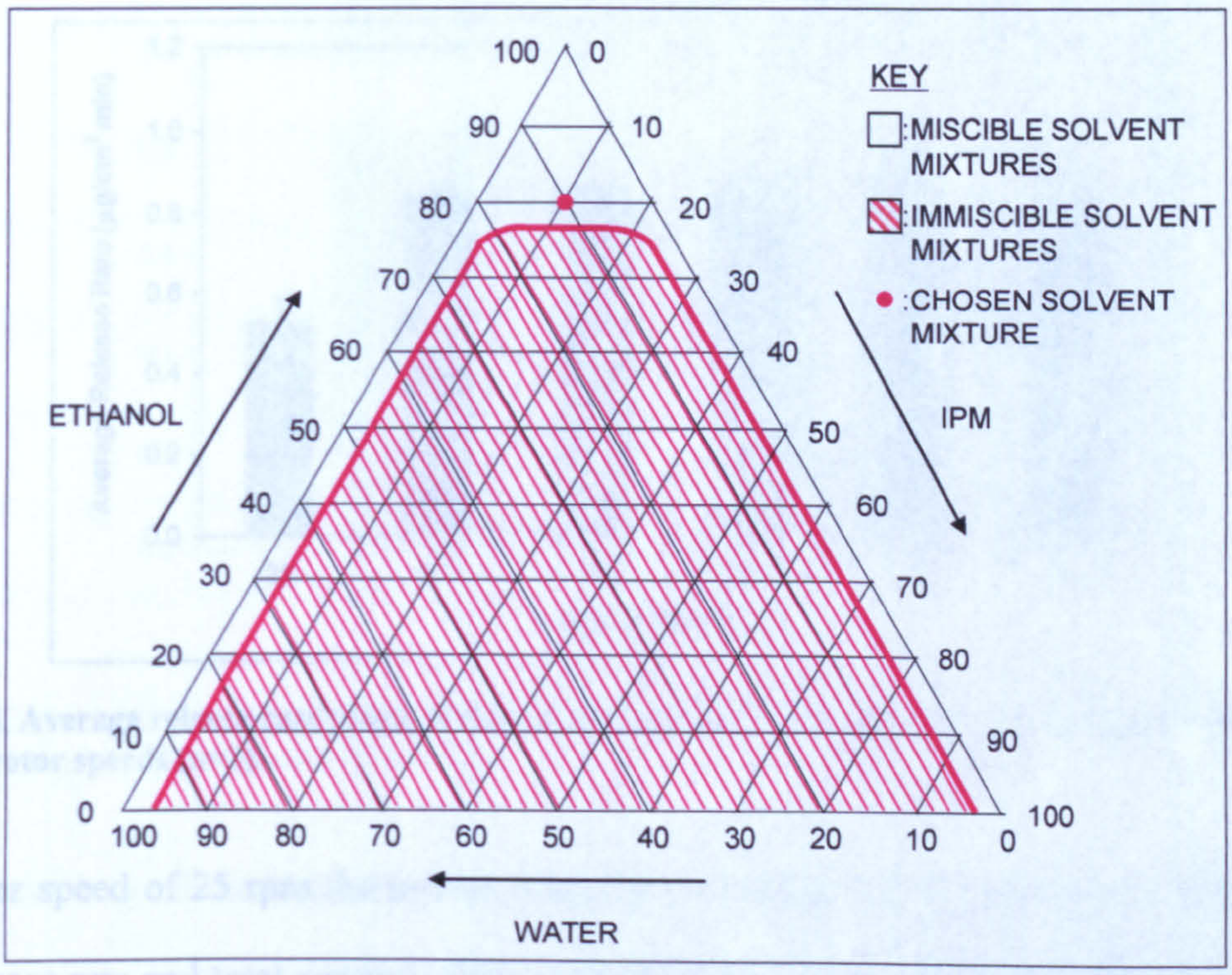

Figure 52. A ternary phase diagram to show the mixture of ethanol, water and IPM chosen for DMU212 topical release studies.

To further maximise the sensitivity of the test conditions the optimum rotary speed was determined using ethanol/water/IPM in a ratio of 80:10:10 and TOP3:

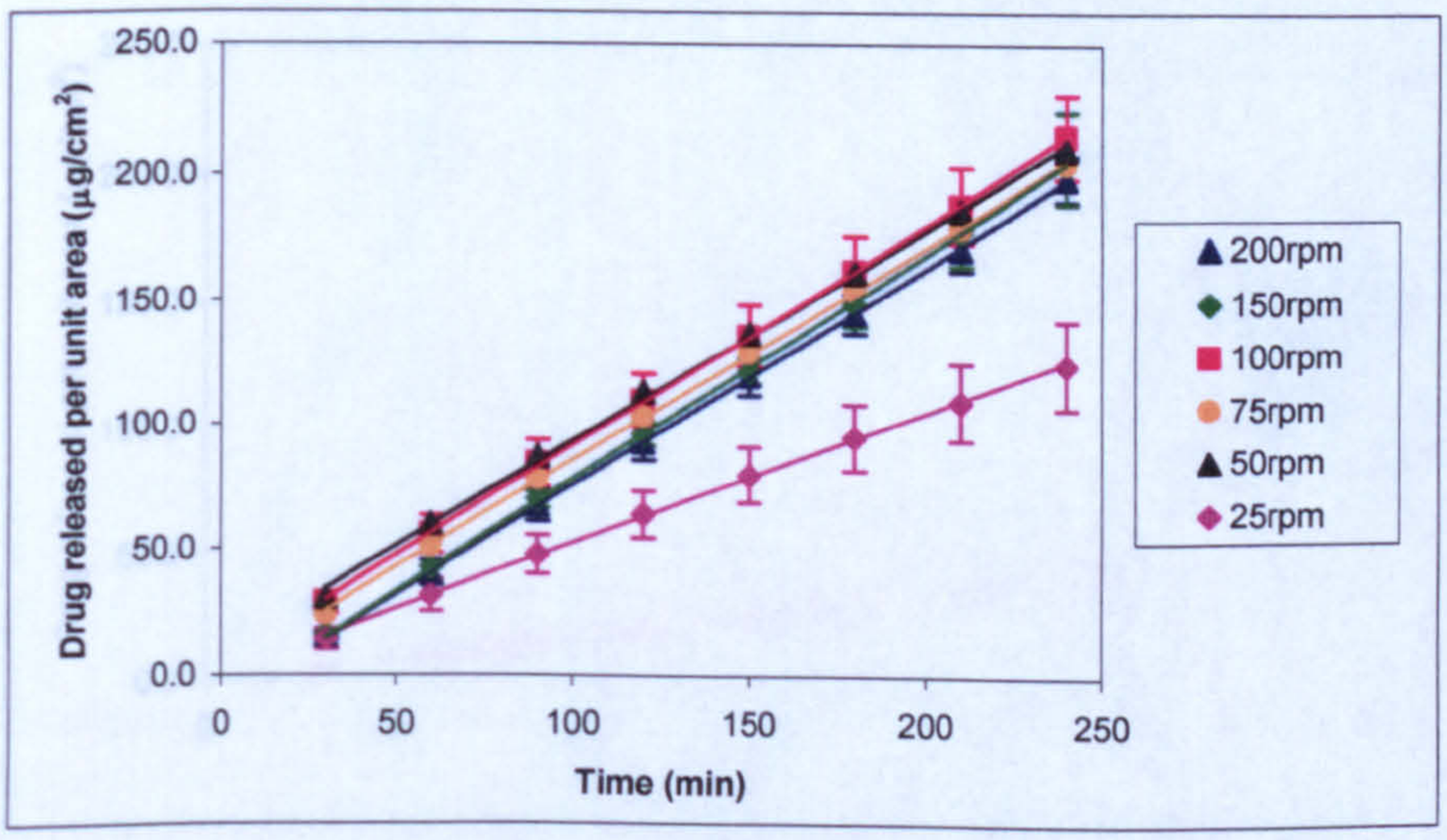

Figure 53. Release of DMU212 from TOP3 in EtOH:IPM:H_2O [80:10:10] at different stirring speeds (n=3).

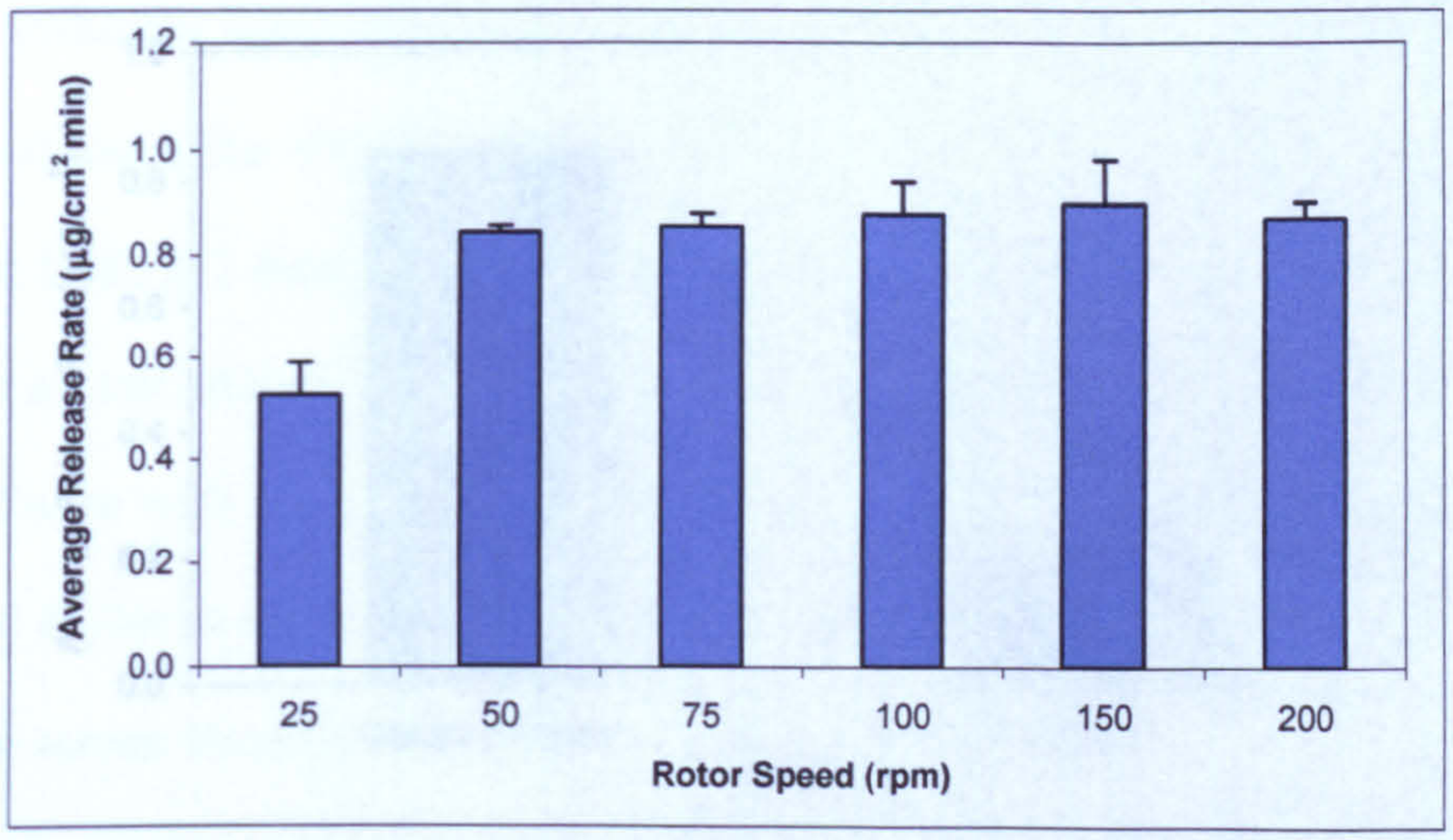

Figure 54. Average release rate (slope of the release/area vs. time plots) of DMU212 from TOP3 over a range of rotor speeds (n=3).

At a rotor speed of 25 rpm the lowest drug release was observed, from 50 to 200 rpm the drug release rate and total amount of drug released were not significantly different. A rotor speed of 50 rpm is recommended by BP standards for the paddle-over disk method for semisolid formulations; therefore, this speed was implemented. The effect of membrane selection on DMU212 drug release rate was also evaluated using TOP3:

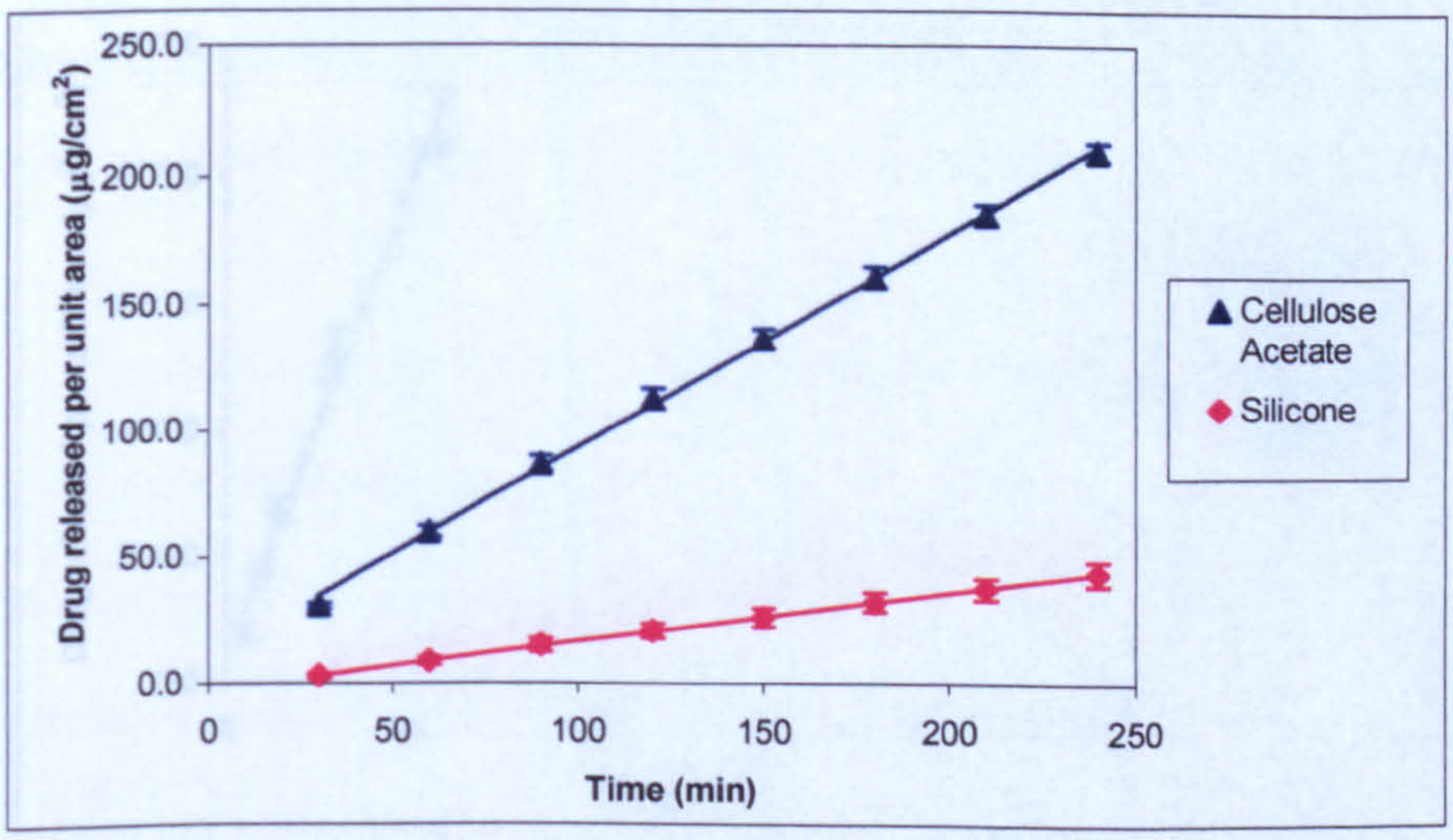

Figure 55. Release of DMU212 from TOP3 in EtOH:IPM:H_2O [80:10:10] through different membranes (n=3).

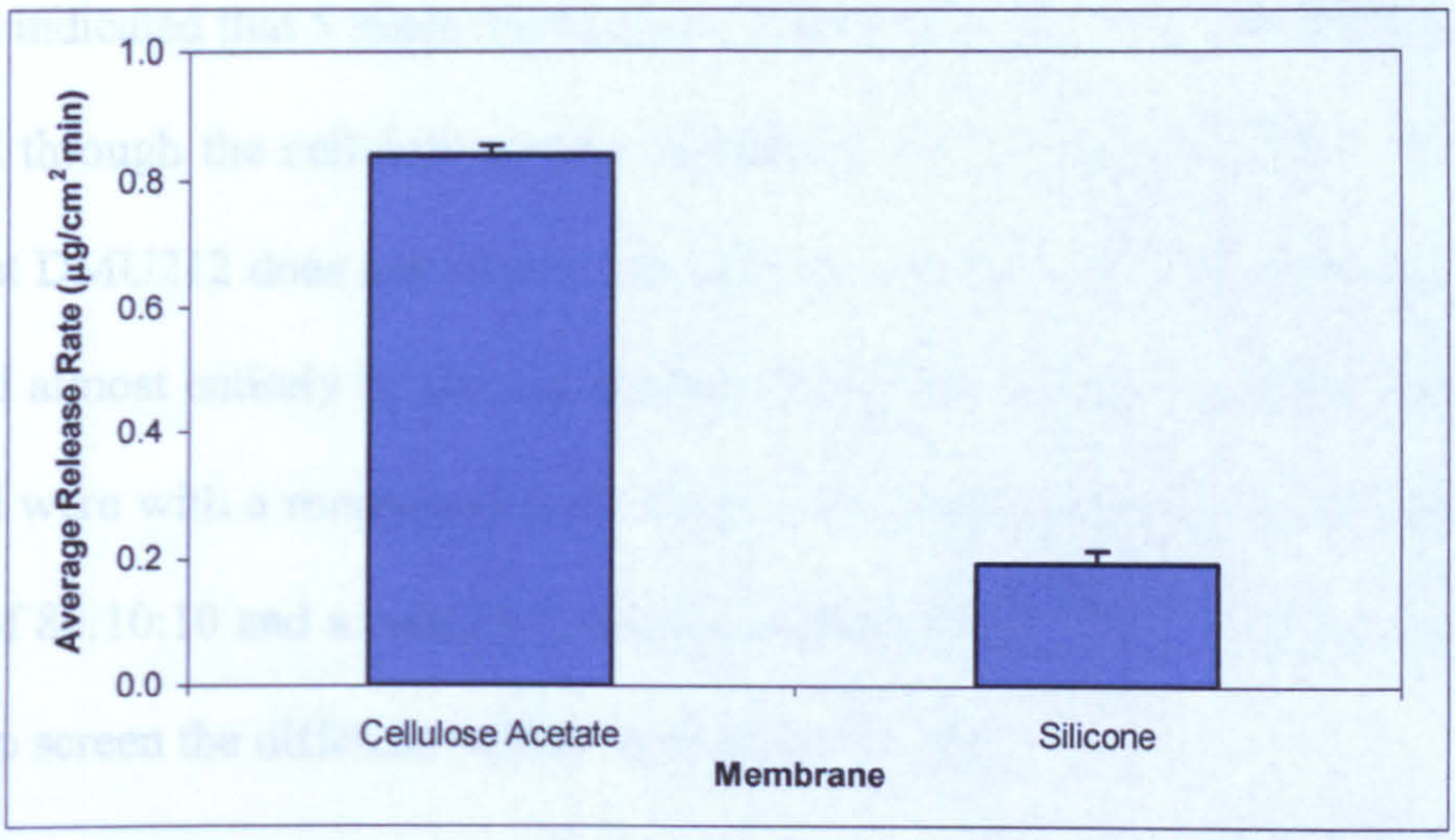

Figure 56. Average release rate (slope of the release/area vs. time plots) of DMU212 from TOP3 through various artificial membranes (n=3).

The highest drug release was observed with the cellulose acetate membranes and the lowest with the silicone membranes and as such the cellulose acetate membrane was chosen as the support membrane. In order to ensure that the drug release observed was a factor of the formulation only and that the membrane was not rate-limiting a 1% w/v DMU212 solution in DMSO was tested in the *in vitro* set-up:

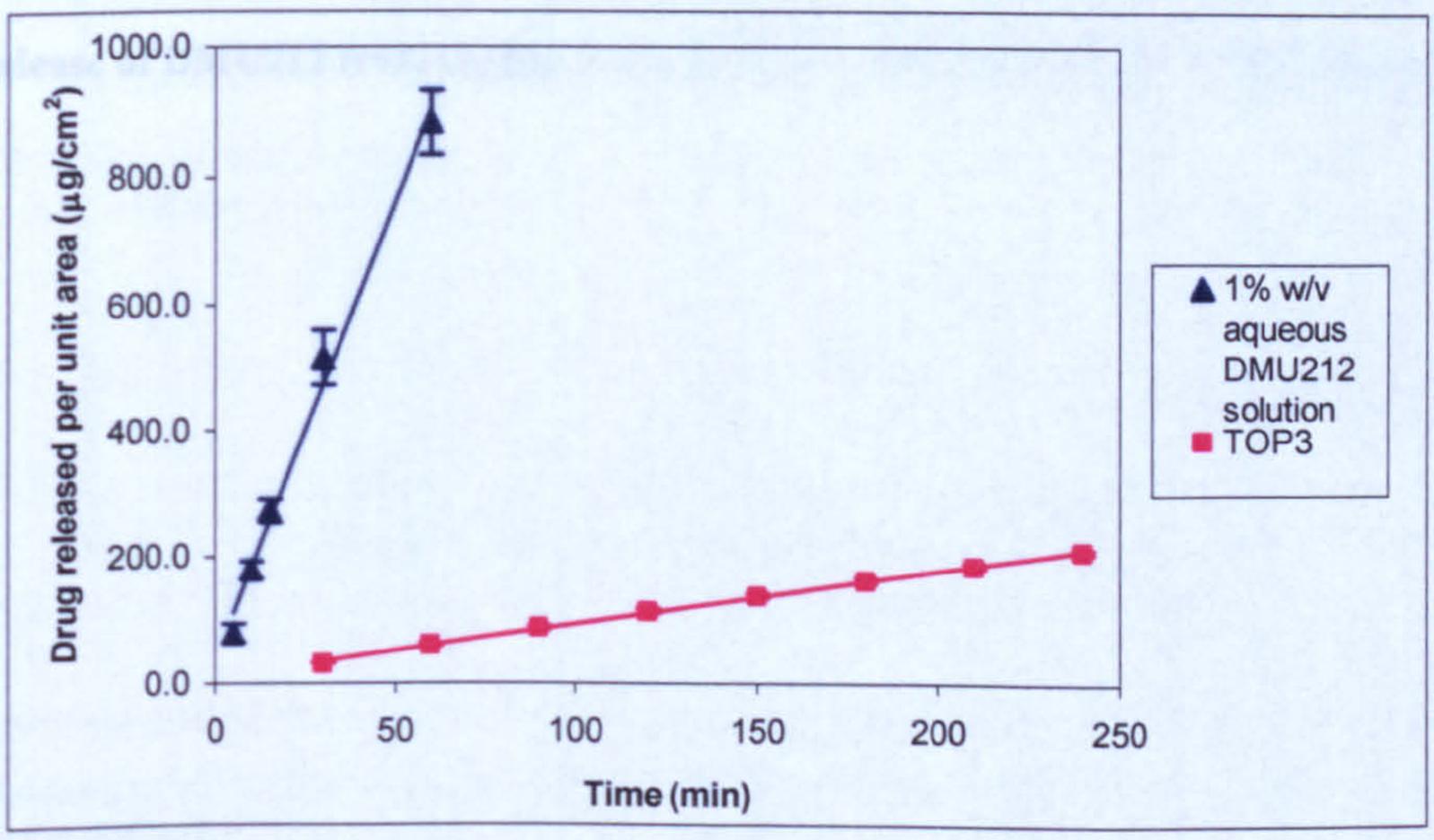

Figure 57. Release of DMU212 from a 1% w/v aqueous solution and TOP3 in EtOH:IPM:H_2O [80:10:10] (n=3).

The results indicated that 5 times the amount of DMU212 applied from the 1% w/v solution had passed through the cellulose acetate membrane, compared with TOP3. These results suggest that DMU212 does not bind to the cellulose acetate membrane and that the release is governed almost entirely by the formulation itself. Overall, the preferred test conditions determined were with a rotary speed of 50 rpm, dissolution medium of ethanol/water/IPM in a ratio of 80:10:10 and a cellulose acetate support membrane. This release method was then used to screen the different topical formulations (Table 31):

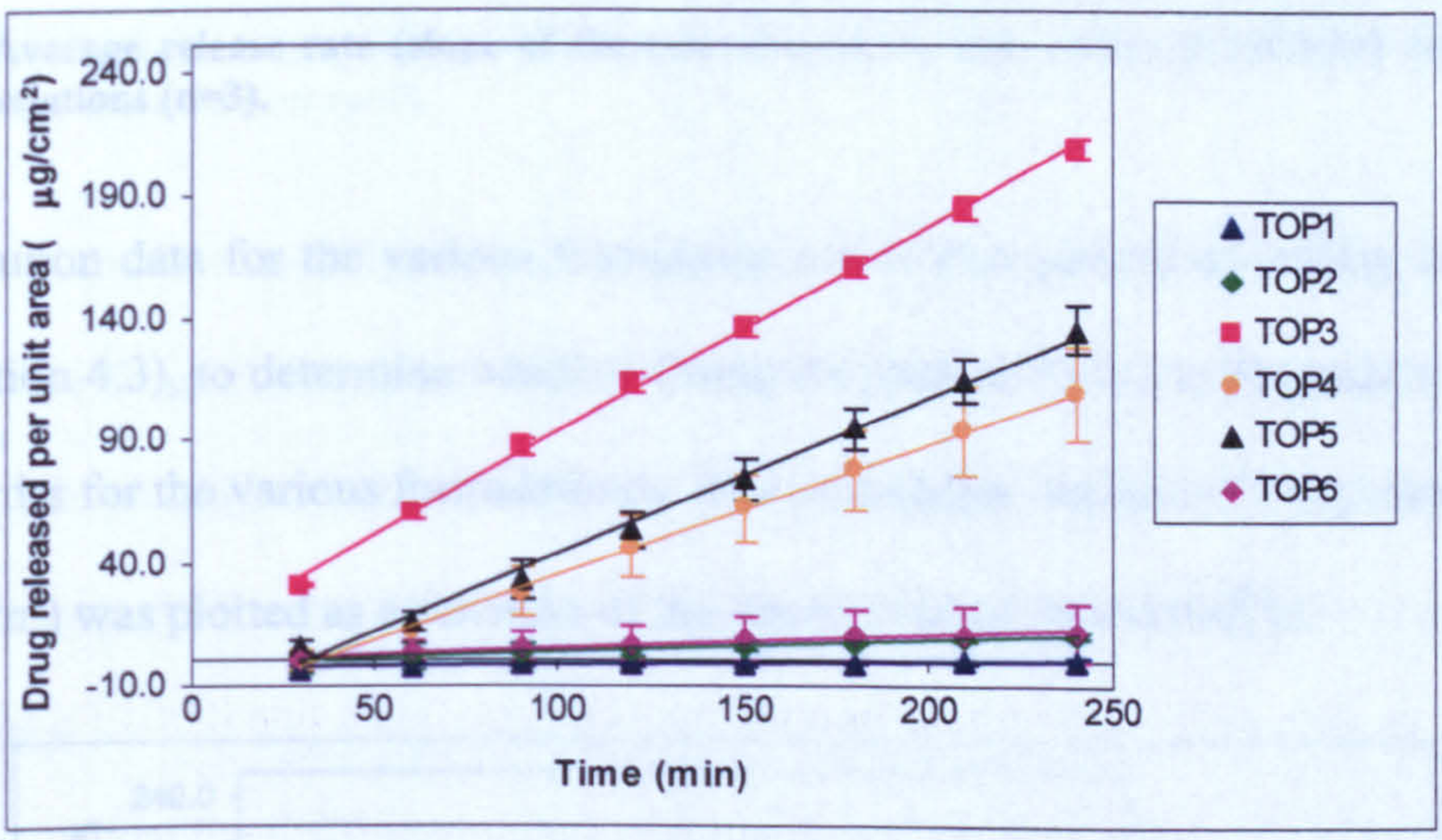

Figure 58. Release of DMU212 from topical formulations in EtOH:IPM:H_2O [80:10:10] (n=3).

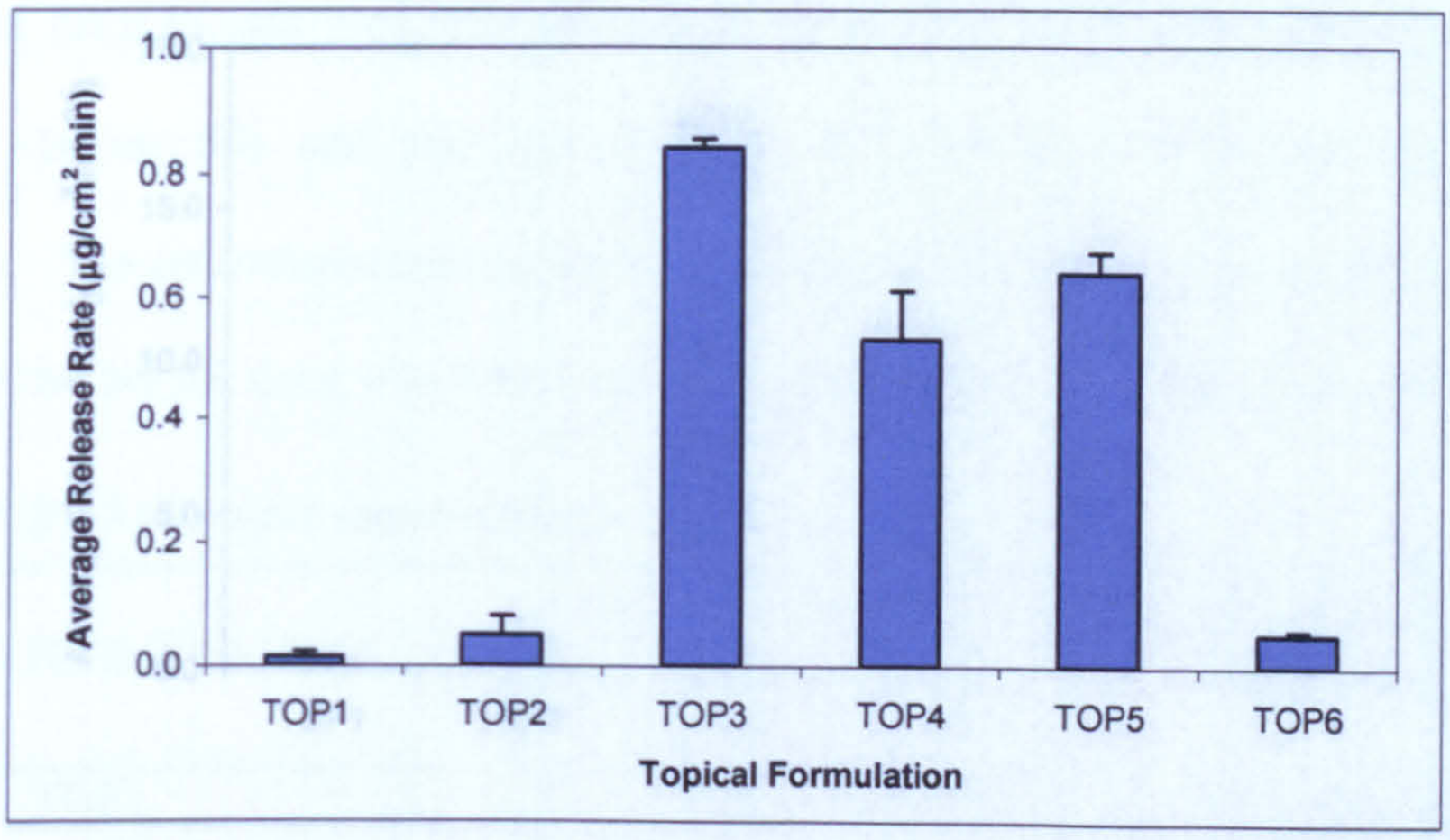

Figure 59. Average release rate (slope of the release/area vs. time plots) of DMU212 from different topical formulations (n=3).

The dissolution data for the various formulations was also plotted according to Higuchi's law (Equation 4.3), to determine whether fitting the data to Fick's or Higuchi's law affects the rank order for the various formulations. The cumulative amount of drug release per unit area ($\mu g/cm^2$) was plotted as a function of the square root of time ($min^{0.5}$):

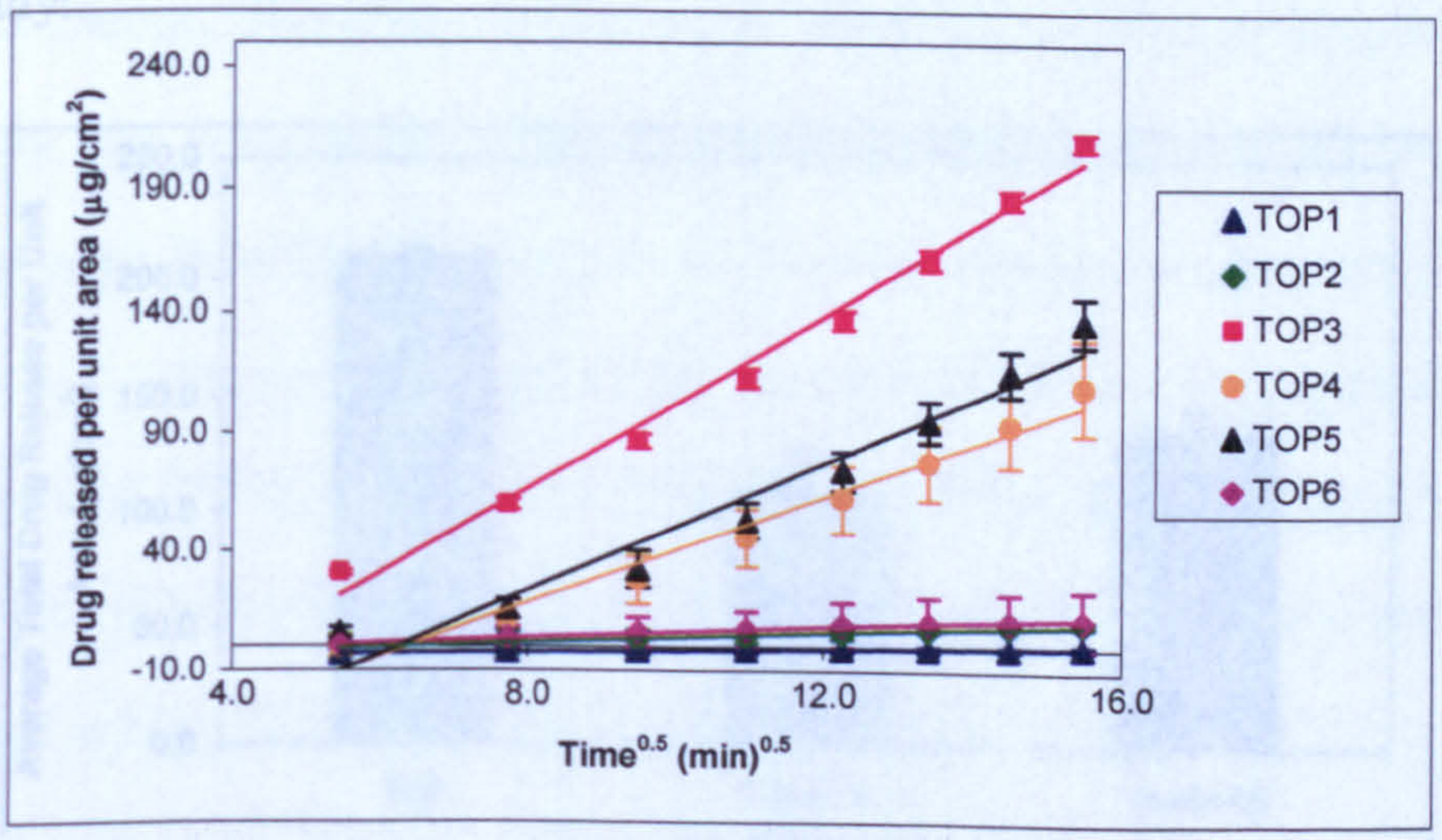

Figure 60. Release of DMU212 from topical formulations in EtOH:IPM:H_2O [80:10:10], plotted vs. the square root of time (n=3).

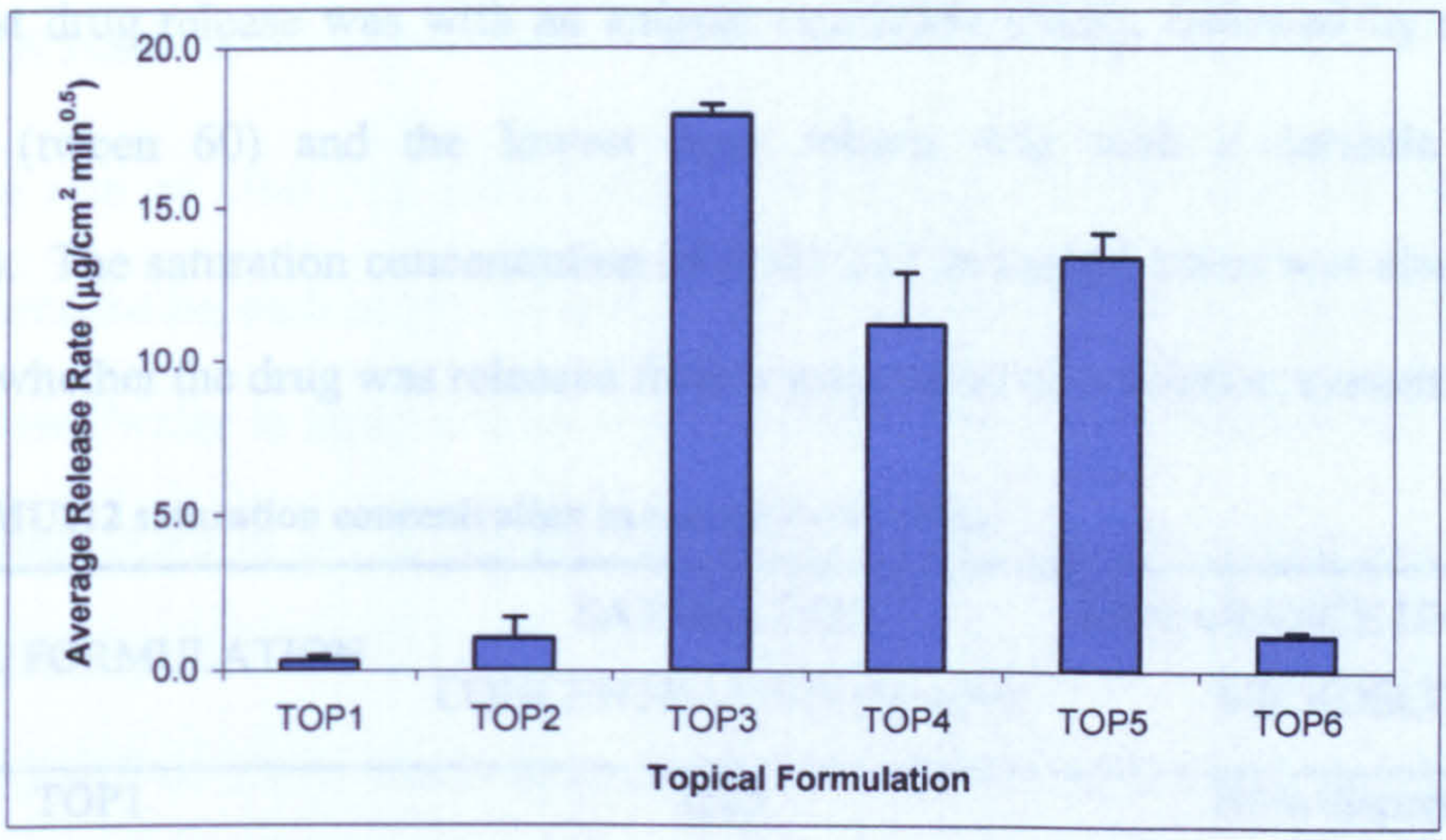

Figure 61. Average release rate (slope of the release/area vs. square root of time plots) of DMU212 from different topical formulations (n=3).

Regardless of the law used the highest drug release was observed from TOP3, 4 and 5 and the lowest was from TOP1, 2 and 6 respectively. TOP3, 4 and 5 have the same formulae apart from the emulsifier (SLS for the anionic o/w cream, cetrimide for the cationic o/w cream and tween 60 for the non-ionic o/w cream), however the differences in drug release varied greatly:

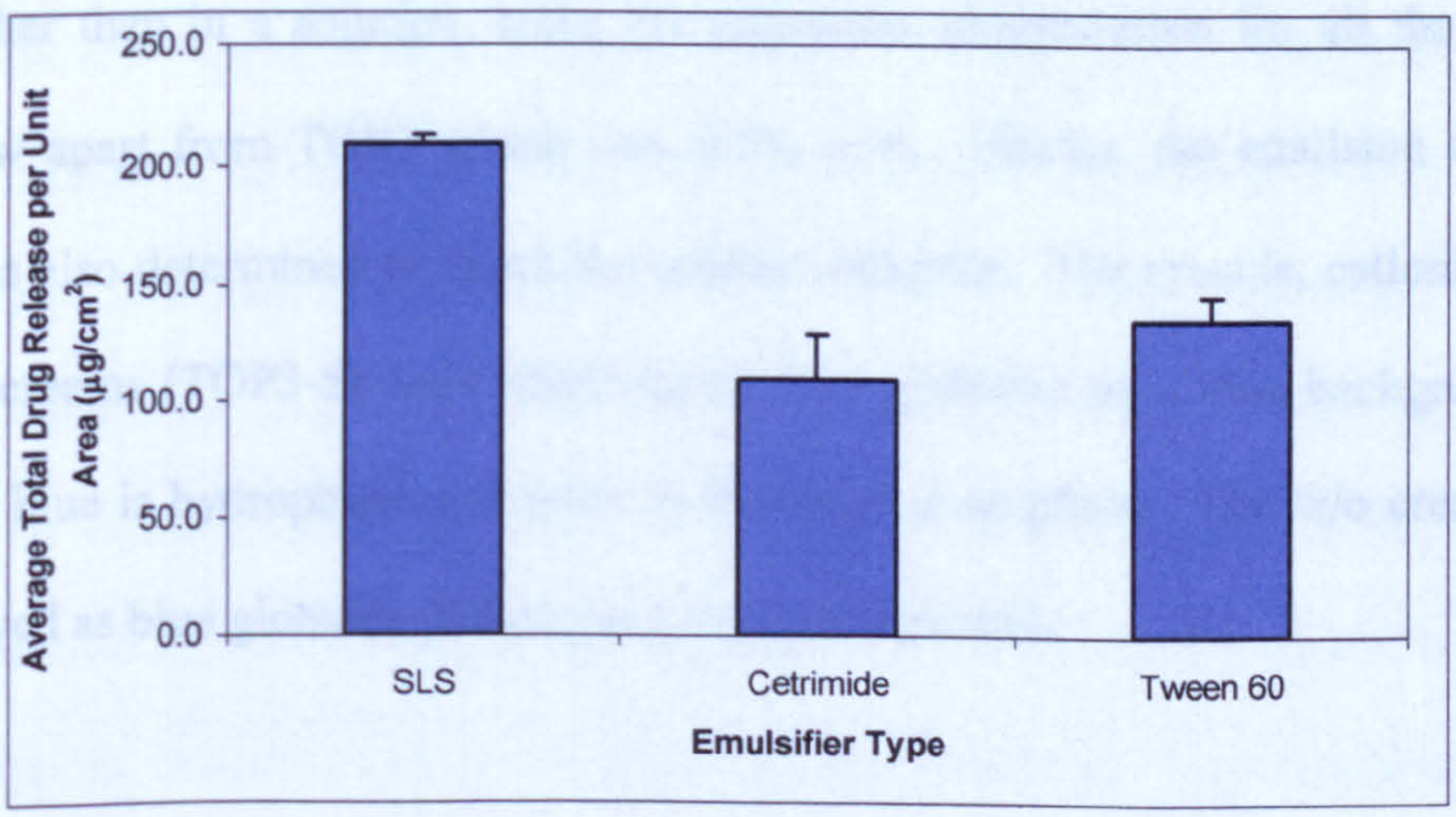

Figure 62. Average DMU212 total drug release per unit area from topical formulations as a function of emulsifier type (n=3).

The highest drug release was with an anionic emulsifier (SLS), followed by a non-ionic emulsifier (tween 60) and the lowest drug release was with a cationic emulsifier (cetrimide). The saturation concentration of DMU212 in topical bases was also studied to determine whether the drug was released from a suspension or a solution system:

Table 33. DMU212 saturation concentration in topical bases (n=3).

TOPICAL FORMULATION	SATURATION CONCENTRATION (% w/w)	APPEARANCE UNDER THE MICROSCOPE
TOP1	0.25	Even dispersion
TOP2	0.25	Strand-like
TOP3	0.50	Droplets
TOP4	0.25	Droplets
TOP5	0.25	Droplets
TOP6	0.25	Droplets

The release rate of DMU212 measured in all *in vitro* studies was from 1% w/v DMU212 topical formulations. Therefore, the drug release observed was from the drug suspended in a base rather than in a solution, since the saturation concentration for all the bases was 0.25% w/w apart from TOP3 which was 0.5% w/w. Finally, the emulsion type of the creams was also determined to check the product integrity. The anionic, cationic and non-ionic o/w creams (TOP3-5) were observed as clear globules on a blue background, since methylene blue is hydrophilic and water is the continuous phase. The w/o cream (TOP6) was observed as blue globules (water) on a clear background.

4.4 Discussion

The release rate of DMU212 from topical formulations was initially determined using either aqueous media such as pH 7.4 phosphate buffer and 1% w/v SLS, or organic media such as ethanol/water in equal concentrations (Figures 49-50). However, no release was observed from TOP3 in any of the aqueous media. This is primarily because of the poor aqueous solubility of DMU212 (1.34 ± 0.22 μg/mL in water) coupled with its high partition coefficient (log *P* of 2.93), which does not thermodynamically favour its release/partition from a lipophilic topical vehicle into an aqueous dissolution media. Use of organic media such as ethanol/water in a 50:50 ratio does increase the drug release rate significantly (0.14 ± 0.01μg/cm^{2}min) compared to aqueous media ($p<0.05$), and small amounts of DMU212 were detected in the dissolution medium (36.47 ± 3.84μg/cm^2 over 4 hours). However, this quantity is too small to detect any significant differences between the topical formulations. Therefore, other organic solvents were evaluated for use as the dissolution medium.

The saturation concentration of DMU212 was determined in organic solvent mixtures of ethanol/water/IPM using a ternary phase diagram (Figure 52). Among the different solvents evaluated, a mixture consisting of ethanol/water/IPM in a ratio of 30:0:70 resulted in the highest saturation concentration (2530.24 ± 45.25 μg/mL), however, use of this media for numerous drug release studies would be expensive. Therefore, a mixture consisting of ethanol/water/IPM in a ratio of 80:10:10 was chosen as the dissolution medium, because firstly a saturation concentration of 1591.14 ± 61.91 μg/mL was obtained with this system, secondly this was the only mixture where all 3 solvents were used and thirdly previous topical studies with corticosteroids by Shah *et al* [198] used a similar

combination of ethanol/water/IPM in a ratio of 85:5:10. The saturation concentration measured in this medium was also 300 times the maximum drug concentration measured in the drug release studies at 5.27 ± 0.09 μg/mL, therefore, sink conditions were maintained since the total drug dissolved in the dissolution medium did not exceed 10% of the drug saturation concentration.

To further maximise the sensitivity of the test conditions the optimum rotary speed was determined with ethanol/water/IPM in a ratio of 80:10:10 and TOP3 (Figures 53-54). Generally an increase in agitation induces a decrease in thickness of the diffusion boundary layer at the membrane-receptor interface, as well as providing better mixing to prevent the development of static areas where localised drug concentrations may arise. A total of 124.81 ± 17.64, 209.67 ± 3.51, 204.03 ± 3.38, 214.21 ± 16.14, 206.10 ± 17.51 and 198.26 ± 8.88μg/cm^2 was released using stirring speeds of 25, 50, 75, 100, 150 and 200 rpm, respectively. At a rotor speed of 25 rpm the lowest drug release rate of 0.53 ± 0.07μg/cm^{2}min was observed, since the boundary layers at the membrane-receptor interface were stagnant and thick, thereby, providing additional resistance to drug diffusion from the donor ($p<0.05$). However from 50 to 200 rpm the drug release rate (Figure 54) and total amount of drug released were not significantly different ($p>0.05$), thereby illustrating the ruggedness and reproducibility of the *in vitro* test system used. At a rotor speed of 50 rpm the drug release rate was 0.84 ± 0.01μg/cm^{2}min, this speed is recommended by BP standards for the paddle-over disk method for semisolid formulations and was therefore implemented in the *in vitro* set-up.

Release as a function of membrane selection was studied to implement the use of a membrane which does not affect drug release, but simply acts as an inert support, therefore, ensuring that drug release is dependent on the formulation only (Figures 55-56). A total of 43.81 ± 4.78 and 209.67 ± 3.51μg/cm^2 was released using silicone and cellulose acetate membranes respectively ($p<0.05$). The slower drug release of 0.19 ± 0.02μg/cm^{2}min, observed with the silicone membranes was probably due to the increased thickness of the membrane at 300μM compared to cellulose acetate at 44μM, with which the drug release rate was 4 times faster at 0.84 ± 0.01μg/cm^{2}min. Silicone membranes are also hydrophobic in nature, which may affect the diffusion coefficient of the drug [186], whereas cellulose acetate membranes are hydrophilic with hydrophobic properties imparted from pre-treatment with IPM, therein more closely reflecting the nature of skin and providing justification for use [208].

In order to ensure that the drug release characteristics observed were a function of the formulation only and that the membrane was not rate-limiting a 1% w/v DMU212 solution in DMSO was tested in the *in vitro* set-up (Figure 57). The experiment was terminated after 60 minutes since the maximum possible absorbance on the UV spectrophotometer was observed. The total drug release observed was 1095.81 ± 99.22μg/cm^2, 5 times greater than the maximum drug release observed from TOP3 at 209.67 ± 3.51μg/cm^2 ($p<0.05$). The drug release rate at 14.46 ± 1.10μg/cm^{2}min was again 17 times higher than for TOP3. These results indicate that DMU212 does not adsorb onto the cellulose acetate membrane and that the release is governed almost entirely by the formulation itself.

Based on these studies the optimal release method determined was with dissolution medium of ethanol/water/IPM in a ratio of 80:10:10, using an agitation speed of 50 rpm and a cellulose acetate support membrane. This release method was used to compare the release rate of DMU212 from a lipophilic/anhydrous absorption ointment (TOP1), hydrophilic/anhydrous washable ointment (TOP2), anionic o/w cream (TOP3), cationic o/w cream (TOP4), non-ionic o/w cream (TOP5) and w/o cream (TOP6) (Figures 58-59). A total of 0.62 ± 0.58, 10.66 ± 1.33, 209.67 ± 3.51, 109.68 ± 19.5, 136.09 ± 9.89 and 12.17 ± 3.94μg/cm^2 was released using TOP1, TOP2, TOP3, TOP4, TOP5 and TOP6 respectively ($p<0.05$).

The solubility of DMU212 in the topical vehicles can help to explain the different drug release rates. Although, the maximum release is obtained when the drug is saturated (i.e. suspended) in the topical vehicle [186, 191], only the dissolved drug can diffuse through the membrane. Therefore, it was important to determine the saturation concentration of DMU212 in the topical vehicles to determine its effect on drug release:

Table 34. DMU212 saturation concentration in and average drug release rate from the topical vehicles (n=3).

TOPICAL FORMULATION	SATURATION CONCENTRATION (% w/w)	AVERAGE RELEASE RATE OF DMU212 FROM DIFFERENT BASES (μg/cm^{2}min)
TOP1	0.25	0.33 ± 0.17
TOP2	0.25	1.05 ± 0.65
TOP3	0.50	17.93 ± 0.33
TOP4	0.25	11.23 ± 1.69
TOP5	0.25	13.45± 0.75
TOP6	0.25	1.16 ± 0.14

The drug release observed was from the drug suspended in a base rather than in a solution, since the saturation concentration for all the bases was 0.25% w/w apart from TOP3 which was 0.5% w/w. TOP3 exhibited the greatest solubilizing capacity for DMU212, probably due to the presence of SLS in the formulation which can solubilize the drug. Furthermore, the optimal release of DMU212 was also from TOP3, suggesting that the release of DMU212 is dependent on the concentration of dissolved drug in the topical vehicles.

Considering the microstructure of the topical vehicles also helps to explain the different drug release rates. TOP3, 4 and 5 are o/w creams, which have a similar microstructure. They can have a complex structure such as a 4-phase system consisting of a hydrophilic gel phase, a lipophilic gel phase, an aqueous bulk phase and an internal dispersed lipophilic phase [207]. Since, DMU212 is a lipophilic drug thermodynamically its release would be favoured from this hydrophilic base. The poor solubility of the drug in the external aqueous environment would lead to fewer drug-vehicle interactions thereby pushing the equilibrium towards the drug partitioning out of the vehicle. TOP6 is a w/o cream, where water droplets are dispersed throughout a continuous oily phase. The internal water phase has less of an affinity for the drug and has no significant influence on the drug diffusion and solubility. Therefore, the activity in the external phase drives the diffusion, however, the increased drug-vehicle interactions in the external phase negate the high thermodynamic activity require for drug partitioning, leading to a lower drug release rate.

TOP2 is a hydrophilic/anhydrous washable ointment, consisting of cetostearyl alcohol and SLS which form a three-dimensional network to immobilise the liquid and white soft paraffin. The solubilization of the drug may occur inside emulsifying cetostearyl alcohol

[207]. TOP1 is a hydrophobic/absorption ointment consisting mainly of white soft paraffin, in which the wool fat alcohols are partly suspended and partly dissolved. In this vehicle the wool fat alcohol acts as a lyotropic solubilizing agent [207]. The lower thermodynamic activity and therefore slower release rate of DMU212 from both ointments is because of the high affinity between the drug and the lipophilic vehicle, which hinders partition of the drug from the vehicle to the dissolution medium. Overall the release rate of DMU212 was much higher from hydrophilic vehicles incorporating water (TOP3-5), compared to lipophilic vehicles (TOP6) containing water, which had little effect on the drug release rate compared to the anhydrous bases (TOP1-2). The drug release from TOP3 ($209.67 \pm 3.51 \mu g/cm^2$) was about 300 times higher compared with release from TOP1 ($0.62 \pm 0.58 \mu g/cm^2$) and about 20 times higher compared with TOP2 ($10.66 \pm 1.33 \mu g/cm^2$) and TOP6 ($12.17 \pm 3.94 \mu g/cm^2$).

Taking into consideration that TOP3, 4 and 5 probably have a similar microstructure and the same formulae apart from the emulsifier the differences in total drug released varied greatly (Figure 62) ($p<0.05$). TOP3 contained the anionic emulsifying agent SLS, TOP4 contained the cationic emulsifying agent cetrimide and TOP5 contained the non-ionic emulsifying agent tween 60. The highest drug release was with TOP3 ($209.67 \pm 3.51 \mu g/cm^2$), followed by TOP5 ($136.09 \pm 9.895 \mu g/cm^2$) and the lowest drug release was with TOP4 ($109.68 \pm 19.5 \mu g/cm^2$). The difference in drug release between TOP3 and TOP4 is almost double showing the greater solubilizing capacity of SLS for DMU212.

All of the dissolution data were initially plotted according to cumulative amount of drug release per unit area vs. time. The plots showed that the cumulative amount of drug

released varied in direct proportion with time. Therefore, the release was governed by Fick's first law of diffusion (Equation 4.1), where all of the drug release profiles followed zero-order kinetics (Figures 49-50 and 53-59), suggesting that the drug release was controlled by the membrane. The dissolution data were also plotted according to cumulative amount of drug release per unit area vs. the square root of time (Figures 60-61). The cumulative amounts of drug released did not vary in direct proportion to the square root of time, but were manifest as curves. Therefore, Higuchi's laws (Equation 4.2-4.3) were not applicable, suggesting that drug release into the dissolution medium was not controlled by the formulation [209]. Regardless of the model used to plot the data the rank order for the formulations remained unchanged (Figures 58-61). Overall, a TOP3 > TOP5 > TOP4 > TOP6 > TOP2 > TOP1 rank order was set for release of DMU212 from the topical vehicles, based on the total drug released and the release rate of the drug measured from the vehicles.

On the whole, a robust *in vitro* release test was developed using a modified BP paddle-over-disk dissolution method [175] with an in-house release cell, dissolution medium of ethanol/water/IPM in a ratio of 80:10:10, agitation speed of 50 rpm and a cellulose acetate support membrane at 32°C. Formulation screening studies showed the optimum drug release of DMU212 to be from an anionic o/w cream.

CHAPTER 5

Synthesis of Ionisable Prodrugs

5.1 Introduction

Development of a universal CYP1B1 pharmacophore model that unites known chemotherapeutics, CDDG anticancer drugs, natural anticancer compounds and inhibitors is advantageous for the design of next generation anticancer prodrugs and may provide a better understanding for prodrug mechanism of action.

5.1.1 CYP1B1 pharmacophore construction

Most studies attempting the construction of pharmacophores use molecular modelling/protein sequence homology. Molecular modelling is only functional if the three-dimensional crystal structure of the target enzyme is known through X-ray crystallography. Once the crystal structure is known, protein sequences with strong sequence homology to that of the target protein are compared and aligned onto the crystal structure using computer simulations to build a structural model. However, the quality of the model is dependent upon the resolved X-ray structure and sequence comparison and alignment quality.

Early attempts to build CYP models were based on the X-ray crystal structure of P450cam originating from *Pseudomonas putida* [40]. However, models based on P450cam are unreliable since there is only 15~20% sequence homology with mammalian CYPs leading to incorrect sequence alignment with the target protein. Another shortcoming is the assumption that the P450cam binding site is identical for all CYPs when actually this is the most variable CYP region and specific to each isozyme [210]. A significant step forward in the reliability of these models was taken by Williams and colleagues in resolving the crystal structure of the first mammalian CYP, rabbit CYP2C5 [211]. Consequently, many CYP

models were re-modelled using this crystallographic template, due to its increased sequence identity to the target protein compared with P450cam [212]. More recently the availability of crystal structures of human CYPs such as CYP2D6 [213], CYP2C8 [214] and CYP3A4 [215], will likely help to further improve these models [216].

The only known CYP1B1 model to date, has been developed by Lewis *et al* [217]. The three-dimensional model was based on primary sequence homology with mammalian CYP2C5. The relative flatness of the resolved structure led Potter and Tan of the CDDG to develop a two-dimensional CYP1B1 model [218]. The model was constructed firstly by mapping a range of known anticancer compounds, CDDG prodrugs, flavones, chalcones and stilbenes with predefined drug metabolism data. And secondly by mapping a range of CDDG inhibitors, whose ability to inhibit CYP1B1 was studied using the 7-ethoxyresorufin-*O*-deethylase (EROD) assay. This assay evaluates the ability of CYP enzymes to deethylate 7-ethoxyresorufin to form resorufin, which is highly fluorescent and can be quantified. Using both these parameters all of the compounds were mapped to delineate the CYP1B1 pharmacophore model structure.

The drug molecules were mapped out following two rules: (i) minimal space and (ii) mapping the molecules all to one side of the haem to reduce the complexity of the model. Both rules were based on the assumption that the compound site of metabolism or for inhibitors the pyridine ring coordinated to the haem. The minimal space rule involved mapping out chalcone compounds as flavanoid conformers to occupy minimal space i.e. in the s-*trans* conformation rather than the s-*cis* conformation, which is also reported to be the more potent chalcone conformation [113]:

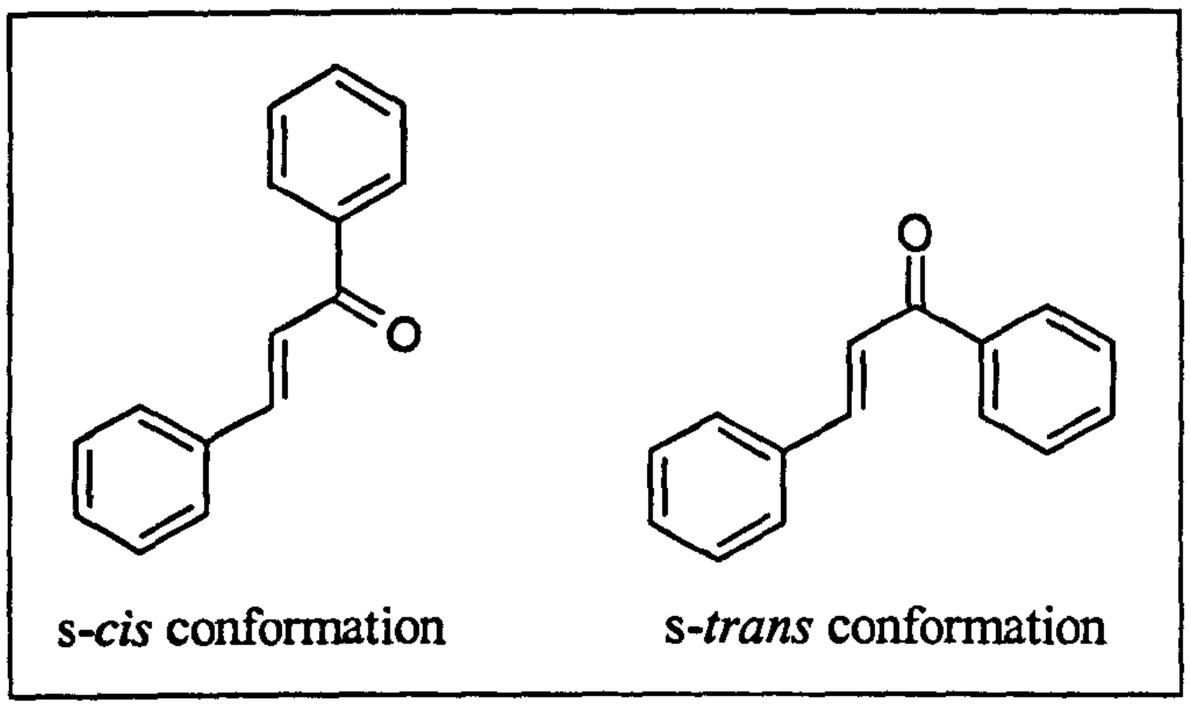

Figure 63. The chalcone conformations.

The second rule also utilised the minimal space rule to some degree, where the molecules were all mapped out to the left or right of the haem, which is located at the base of the pharmacophore. Within the CDDG all compounds studied were mapped to the right of the haem; therefore, the variability of molecular mapping was reduced to result in a less complex pharmacophore model. After mapping all of the compounds, the delineated CYP1B1 pharmacophore model was shown to contain common areas/hotspots for compounds with desirable biological activity. Firstly, two distinct binding pockets i.e. horizontal and vertical were identified, where the compounds can bind to the CYP1B1 active site in a horizontal or vertical binding mode:

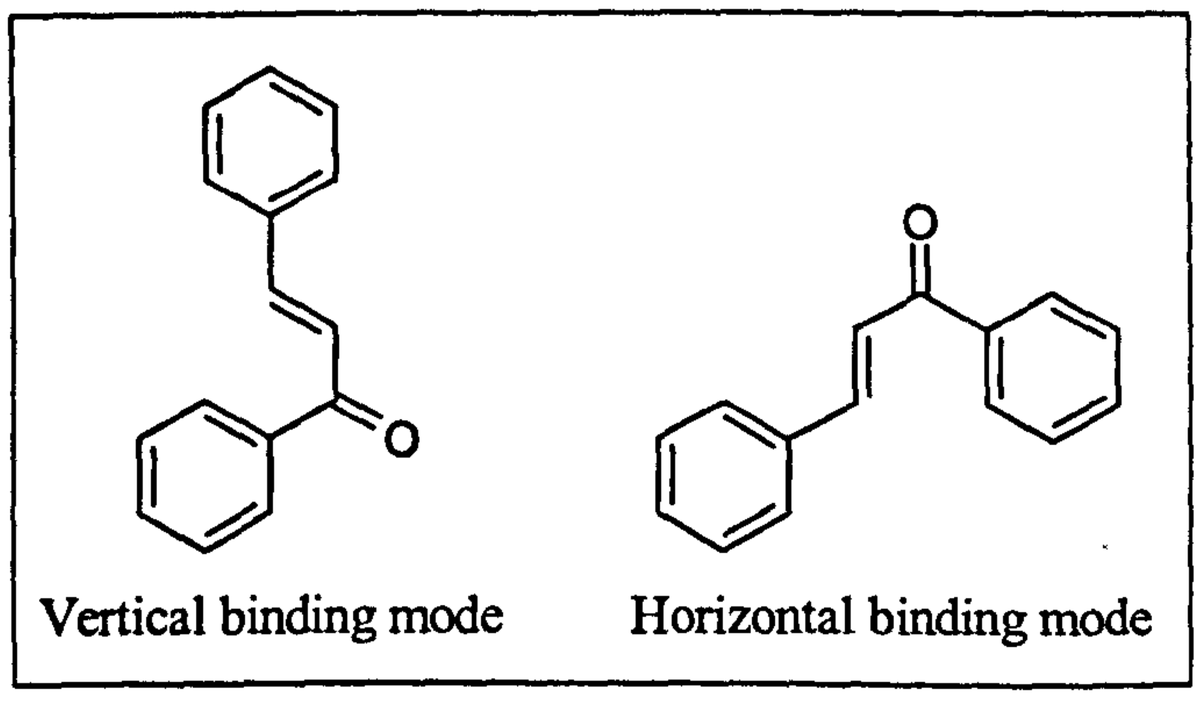

Figure 64. The horizontal and vertical binding modes of chalcones.

Secondly, within the horizontal binding pocket a hydrophobic region was identified, and thirdly five hydrogen-bonding residues penetrating into the active site were identified. With the discovery of hotspots exclusion zones with common areas of no catalytic significance were also defined as 'cold spots':

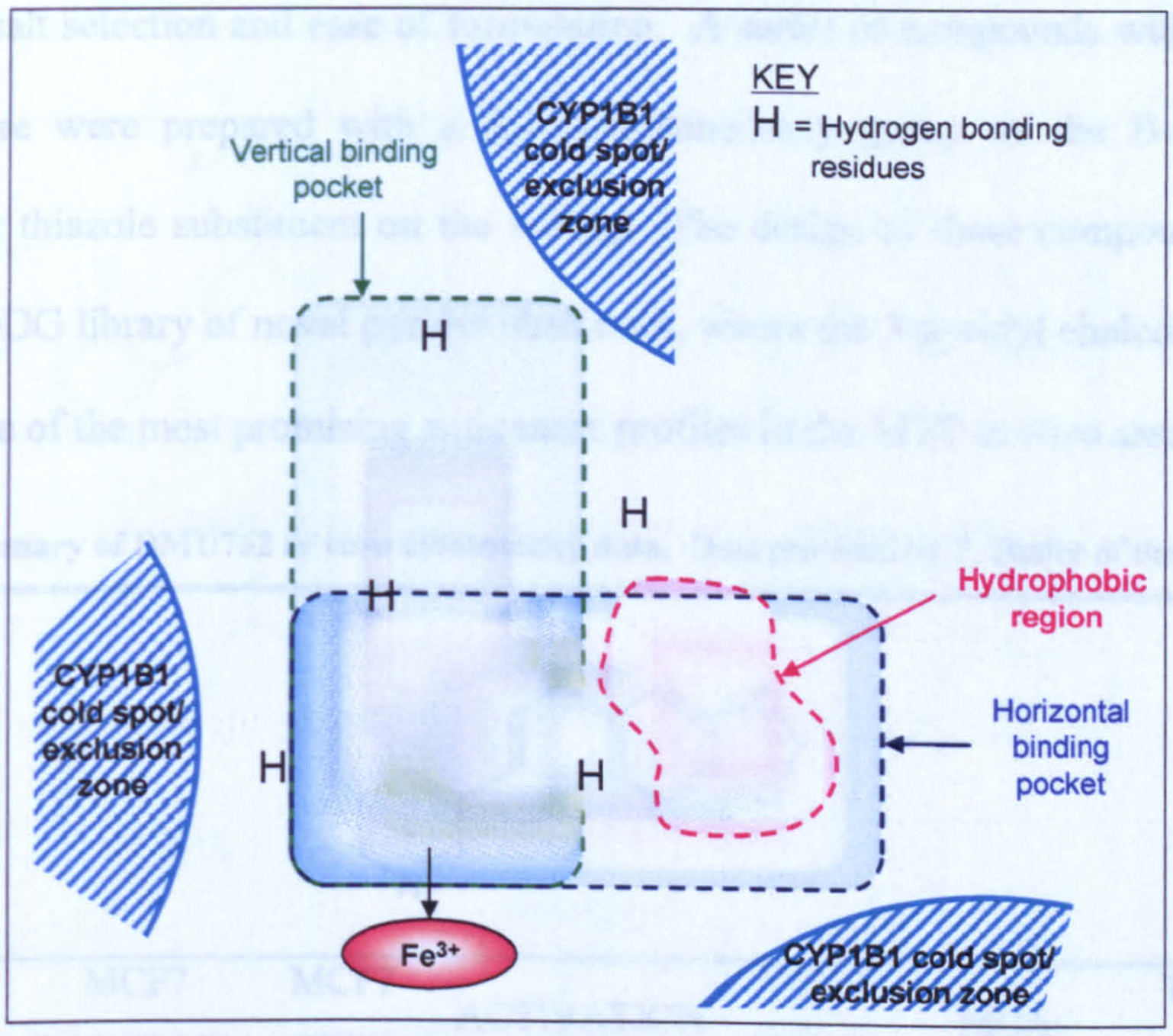

Figure 65. CYP1B1 CDDG pharmacophore model [218].

The construction of such a pharmacophore model is advantageous for the design of next generation prodrugs, by acting as a tool to predict whether a drug candidate will interact with a particular CYP isozyme. This could significantly reduce the failure rate in clinical trials by identifying potential problems at an early stage of development, to potentially reduce the time and money required to bring a new drug to market [216]. This model still remains under investigation and continuous refinement as more data is acquired.

5.1.2 Selection, design and synthesis of CYP1B1 activated prodrugs

The compounds chosen for synthesis and subsequent assay in this study were designed from the CYP1B1 pharmacophore model (Figure 65). The rationale behind the design was selective CYP1B1 activation as well as use of derivatisable functional groups to enable subsequent salt selection and ease of formulation. A series of compounds with a chalcone core structure were prepared with a 3,4-methylenedioxy group on the B-ring and an imidazole or thiazole substituent on the A-ring. The design of these compounds evolved from the CDDG library of novel pyridyl chalcones, where the 3-pyridyl chalcone DMU762 exhibited one of the most promising anticancer profiles in the MTT *in vitro* assay:

Table 35. Summary of DMU762 *in vitro* cytotoxicity data. Data provided by P. Butler of the CDDG.

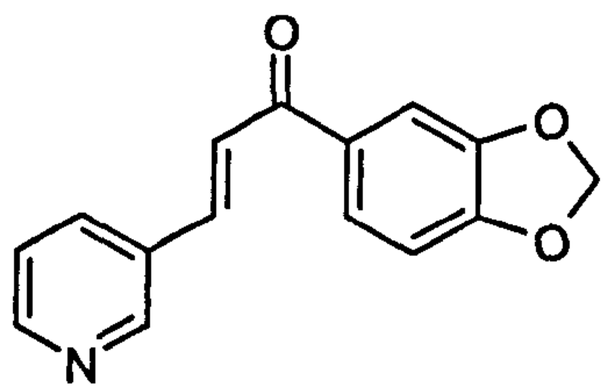

HUMAN BREAST CELL-LINE	MCF7 WITHOUT TCDD	MCF7 WITH TCDD	ACTIVATION FACTOR	MCF10A	MDA-MB-468	TUMOUR SELECTIVE FACTOR
IC_{25} VALUES (μM)	6.0	6.0	1	5.0	0.002	2500

DMU762 was found to be potently cytotoxic in MDA-MB-468 cancer cells with appreciably reduced cytotoxicity in MCF10A and MCF7 cells with and without TCDD induction (Table 35). Both DMU762 and the imidazole and thiazole substituents should

theoretically enable salt selection through protonation of the nitrogen to potentially enhance the drug physicochemical properties compared to non-ionisable chalcones such as DMU135 (Chapter 2). Furthermore, differences in the position of lone pair of electrons on the nitrogen will allow the determination of the optimum angle for the nitrogen lone pair of electrons to coordinate to the hydrogen bonding residues (Figure 65):

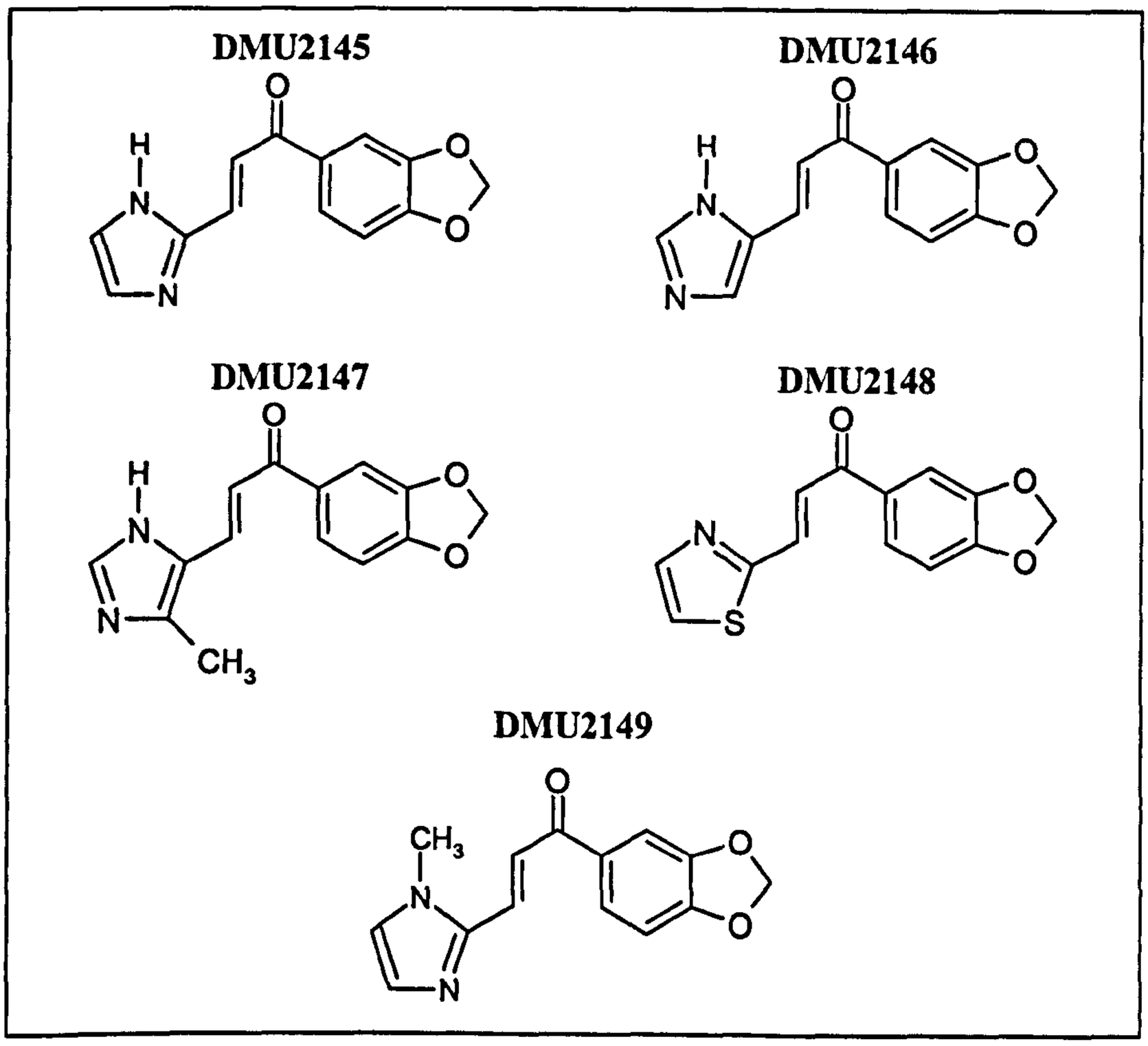

Figure 66. Chemical structures of potential CYP1B1 activated prodrugs.

Chalcones can be readily synthesised by the Claisen-Schmidt aldol condensation reaction [219]. This is a base catalysed condensation reaction, which results in the elimination of water to yield an α,β-unsaturated ketone:

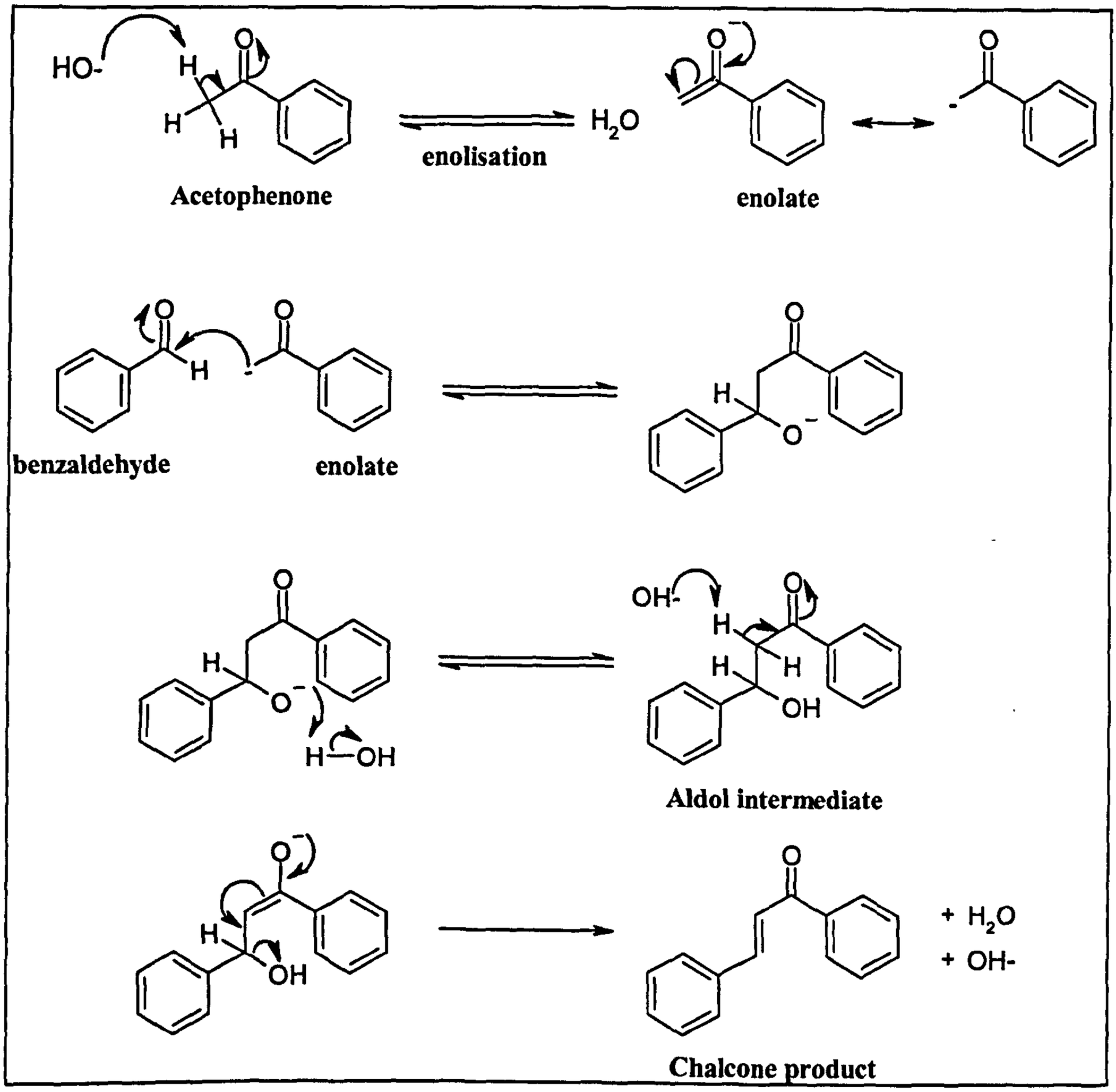

Figure 67. Reaction mechanism for Claisen-Schmidt aldol condensation.

There first step of the reaction involves proton abstraction, where the acetophenone is deprotonated by the base (NaOH) to yield an enolate anion. Secondly, nucleophilic addition of the enolate ion to benzaldehyde leads to the formation of an aldol intermediate. The final step of the reaction involves dehydration of the aldol intermediate where the elimination of a water molecule gives the α,β-unsaturated chalcone.

5.1.3 Selection, design and synthesis of a potentially specific CYP1B1 prodrug

The design of the imidazole and thiazole chalcones was based on the CYP1B1 pharmacophore (Figure 65). These compounds bind to CYP1B1 via the vertical binding pocket, since the 3,4-methylenedioxy group on the chalcone B-ring co-ordinates to the haem, as this is the site of metabolism via dealkylation to generate the catechol metabolite. As a result these chalcones cannot bind to the CYP1B1 active site in the horizontal binding mode as this would place the hydrophilic imidazole/thiazole substituted ring in the hydrophobic region. The design of a compound in this series, which can bind to both the horizontal and vertical binding pockets and the hydrophobic region, could potentially form a completely specific CYP1B1 activated prodrug with favourable anticancer properties:

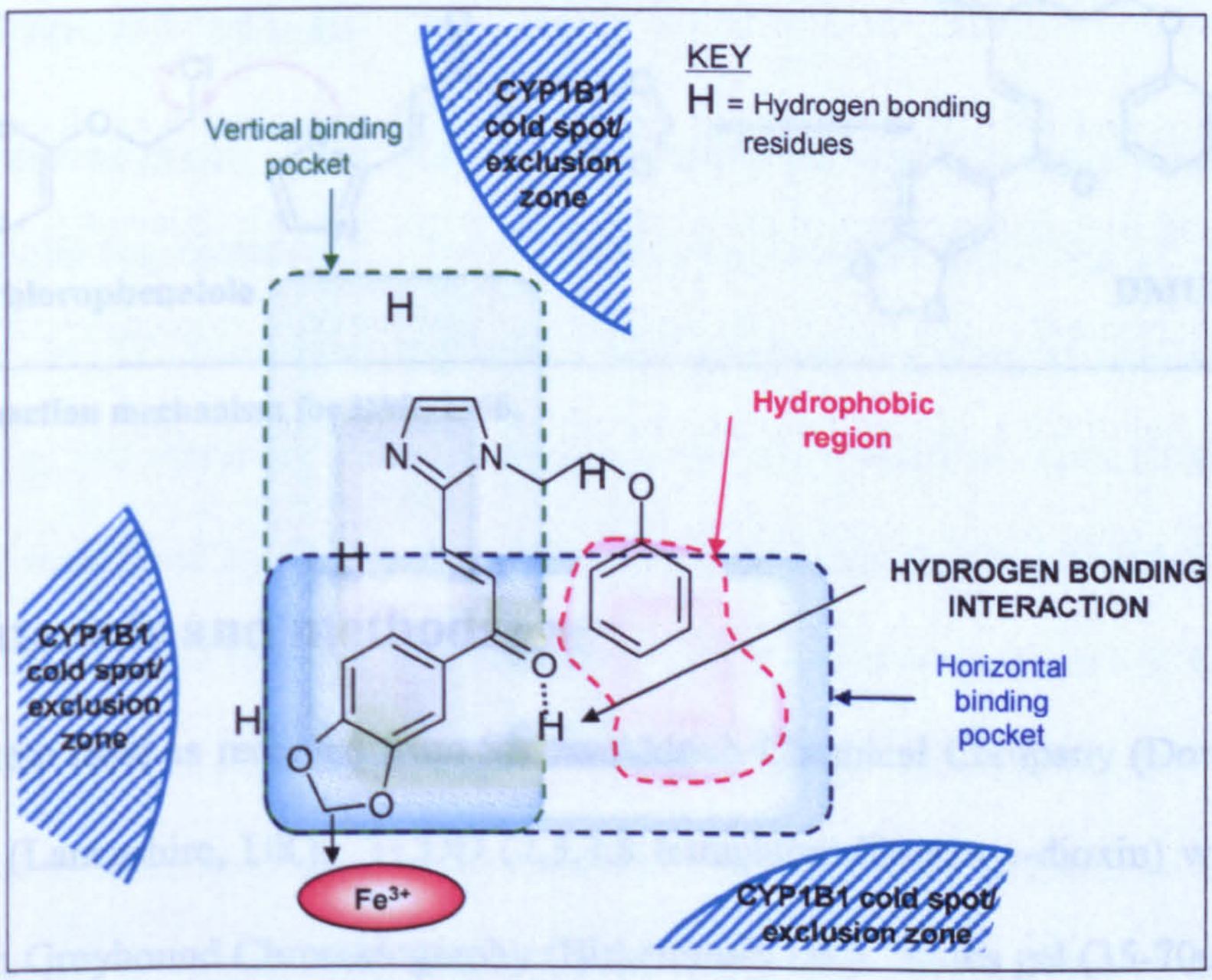

Figure 68. Mapping of DMU2306 onto the CYP1B1 pharmacophore.

DMU2306 was synthesised via Claisen-Schmidt condensation of 3,4-methylenedioxy acetophenone with imidazole-2-carboxaldehyde to generate DMU2145. This was followed by proton abstraction, where the imidazole ring was deprotonated by the base (2.5M n-butyllithium in hexane). Resulting in a resonance stabilised anion, which underwent a nucleophilic substitution reaction with β-chlorophenetole to generate the potentially

CYP1B1 specific anticancer prodrug DMU2306:

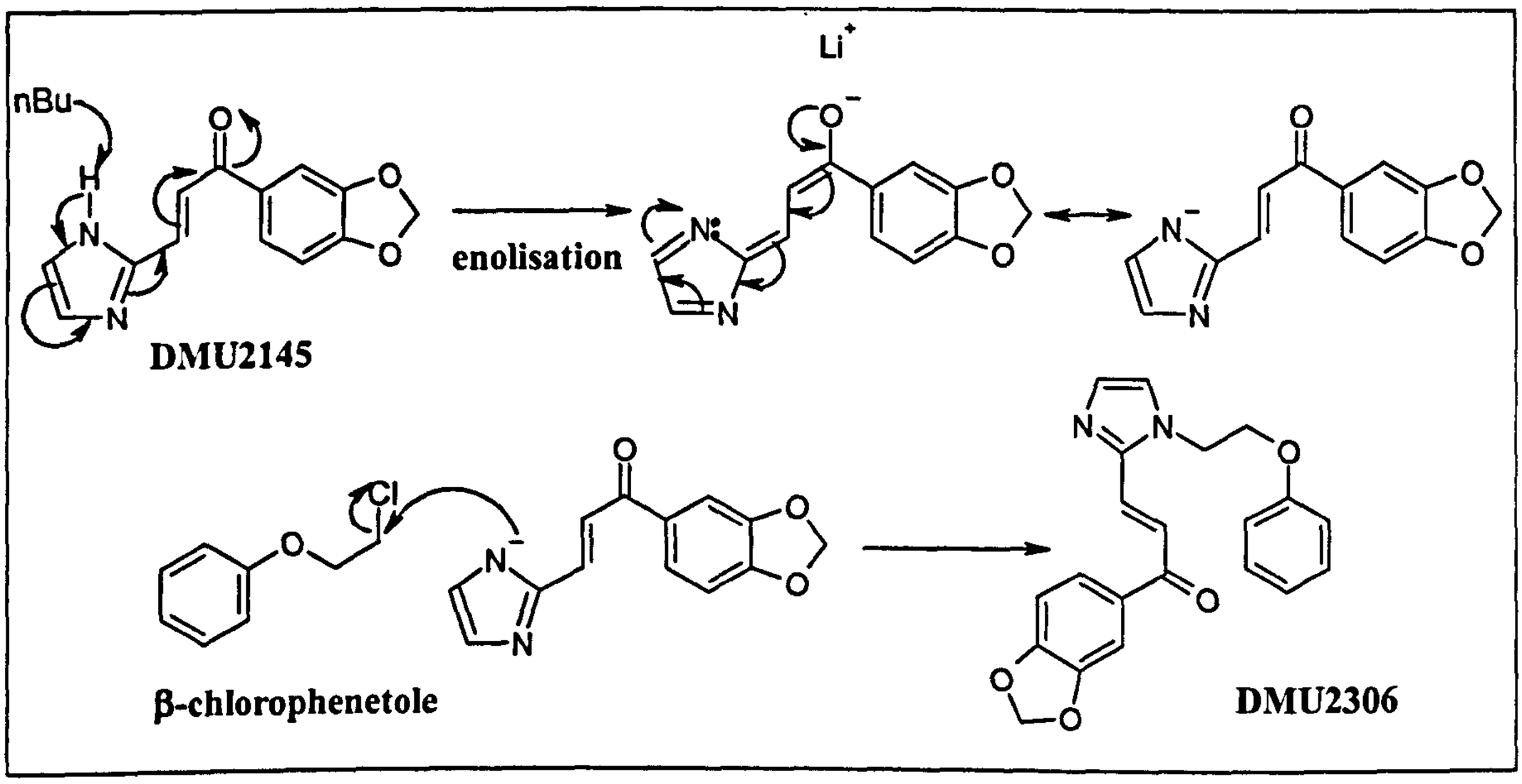

Figure 69. Reaction mechanism for DMU2306.

5.2 Materials and methods

Reagents were used as received from Sigma-Aldrich Chemical Company (Dorset, UK) or Alfa Aesar (Lancashire, UK). TCDD (2,3,7,8 tetrachlorodibenzo-*p*-dioxin) was obtained from British Greyhound Chromatography (Birkenhead, UK). Silica gel (35-70μm) and 96-well Nunc® plates were obtained from Fisher Scientific (Loughborough, UK). Human breast cell lines were obtained from the American Type Culture Collection.

5.2.1 Analytical methods

The ^{1}H and ^{13}C-NMR spectra were recorded on a 400MHz super-conducting Bruker Spectrometer (Karlsruhe, Germany) at 30°C. Infrared spectra were recorded in potassium bromide disks on a Perkin-Elmer 298 FTIR spectrophotometer (Massachusetts, USA). Mass spectra were recorded on a Finnigan Lasermat 2000 MALDI spectrometer (Thermo Bioanalysis, Hemel Hempstead, UK). Melting points were determined on a Gallenkamp melting point apparatus (Leicestershire, UK). Thin layer chromatography (TLC) was performed on aluminium sheets pre-coated with silica gel $60f_{254}$ (Merck, Darmstadt, Germany) observed under UV light (450nm) and stained with 2,4-dinitrophenylhydrazine (to stain for the carbonyl group).

5.2.2 Chemical synthesis

5.2.2.1 General method for synthesis of imidazole and thiazole chalcones

To an equimolar (eq) quantity of 3,4-methylenedioxyacetophenone (2.00g, 12.18mmol) and carboxaldehyde (12.18mmol) in methanol (20mL) was added 20eq of sodium hydroxide pellets (9.75g, 243.66mmol). The resulting mixture was stirred at room temperature and sequentially monitored by TLC (ethyl acetate/petroleum ether/methanol (15:5:1) with 3% triethylamine) until the reaction was complete. The reaction was quenched with distilled water (20mL) and extracted with ethyl acetate (3×50mL). The combined organic layers were washed with saturated brine (50mL), dried with anhydrous magnesium sulphate and concentrated under *vacuo*. The crude product was purified by column chromatography

with an isocratic solvent system (ethyl acetate/petroleum ether/methanol (15:5:1) with 3% triethylamine).

5.2.2.2 Synthesis of DMU2306

DMU2145 (0.20g, 0.83mmol) was dissolved in dry dimethylformamide (10mL) under nitrogen and the solution cooled to -20°C. A solution of 2.5M n-butyllithium in hexane (0.18mL, 0.45mmol) was added slowly and the reaction mixture was stirred for 20 minutes. A solution of β-chlorophenetole (43.83g, 279.90mmol) in dry dimethylformamide (10mL) was added. The resulting mixture was stirred at room temperature and sequentially monitored by TLC (ethyl acetate/petroleum ether/methanol (15:5:1) with 3% triethylamine) until the reaction was complete. The reaction was quenched with distilled water (20mL) and extracted with ethyl acetate (3×50mL). The combined organic layers were washed with saturated brine (50mL), dried with anhydrous magnesium sulphate and concentrated under *vacuo*. The crude product was purified by column chromatography with an isocratic solvent system (ethyl acetate/petroleum ether/methanol (3:7:1) with 3% triethylamine).

5.2.3 MTT in vitro cytotoxicity assay

See Section 3.2.6.

5.3 Results

A total of 6 imidazole and thiazole prodrugs were synthesised. They were chemically evaluated using the techniques described in Section 5.2.1 and their chemical structures, physical characteristics and yields are described below:

5.3.1 Chemical analysis of imidazole and thiazole chalcones

1-(3,4-Methylenedioxyphenyl)-3-(1*H*-2-imidazolyl)-prop-2-en-1-one (DMU2145)

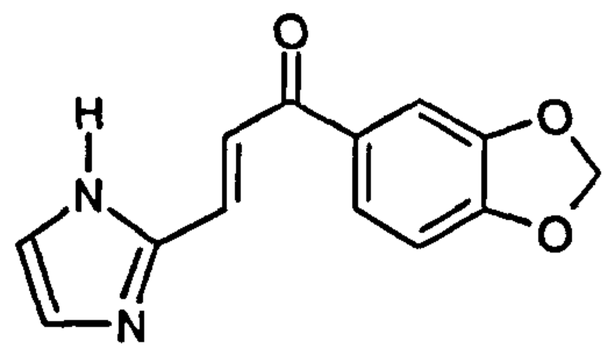

Yellow solid, yield (1.07g, 36%); m.p. 220°C; mass spectrum (MALDI) m/z 243.61 (M^+ + 1); IR spectrum υmax (KBr)/cm^{-1} 3225 (N–H), 1653 (C=O); ^{1}H-NMR (DMSO) δ 6.10 (s, 2H), 7.10 (d, 1H, J=17Hz), 7.40 (s, 1H), 7.45 (m, 2H), 7.70 (d, 1H, J=17Hz), 7.80 (s, 1H), 7.85 (s,1H), 12.80 (s, 1H); ^{13}C-NMR (DMSO) δ 102.28, 107.66, 108.35, 121.41, 124.33, 130.35, 131.41, 132.31, 143.73, 147.84, 148.03, 152.03, 186.76.

1-(3,4-Methylenedioxyphenyl)-3-(1*H*-4-imidazolyl)-prop-2-en-1-one (DMU2146)

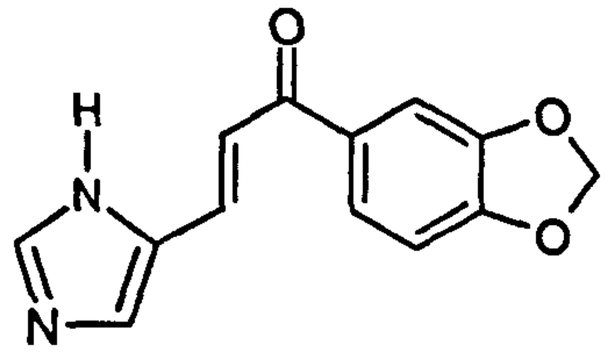

Yellow solid, yield (0.67g, 23%); m.p. 180°C; mass spectrum (MALDI) m/z 243.93 (M^+ + 1); IR spectrum υmax (KBr)/cm^{-1} 3182 (N–H), 1648 (C=O); ^{1}H-NMR (DMSO) δ 6.15 (s, 2H), 7.05 (d, 1H, J=14Hz), 7.50 (s, 1H), 7.63 (d, 3H), 7.70 (d, 1H, J=13Hz), 7.85 (s, 1H), 12.50 (s, 1H); ^{13}C-NMR (DMSO) δ 102.14, 107.66, 108.24, 117.98, 124.46, 132.81, 134.45, 138.16, 142.81, 148.13, 148.73, 151.38, 187.02.

1-(3,4-Methylenedioxyphenyl)-3-(5-methyl-1*H*-4-imidazolyl)-prop-2-en-1-one

(DMU2147)

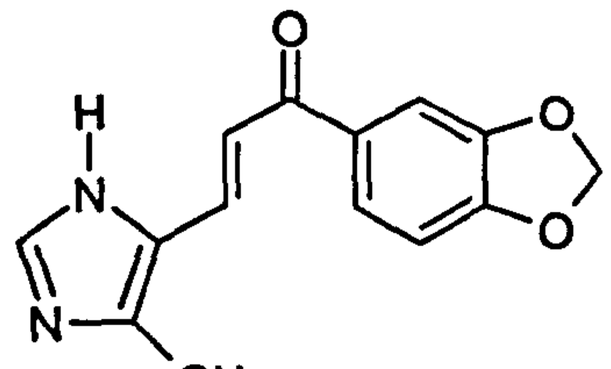

Yellow solid, yield (0.66g, 21%); m.p. 207°C; mass spectrum (MALDI) m/z 257.21 (M^+ + 1); IR spectrum υmax (KBr)/cm^{-1} 3196 (N–H), 1647 (C=O); ^{1}H-NMR (DMSO) δ 2.55 (s, 3H), 6.25 (s, 2H), 7.15 (d, 1H, J=12Hz), 7.65 (s, 1H), 7.75 (d, 1H), 7.85 (d, 1H, J=14Hz), 7.90 (m, 1H), 7.95 (d, 1H), 12.40 (s, 1H); ^{13}C-NMR (DMSO) δ 102.14, 107.66, 108.24, 117.98, 124.46, 132.81, 134.45, 138.16, 142.81, 148.13, 147.92, 151.15, 186.60.

1-(3,4-Methylenedioxyphenyl)-3-(2-thiazolyl)-prop-2-en-1-one (DMU2148)

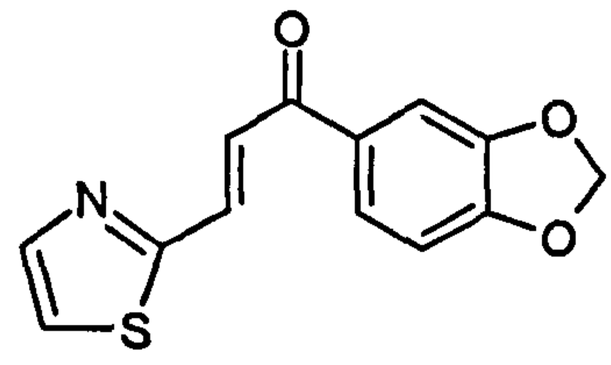

Pale orange solid, yield (1.13g, 49%); m.p. 143°C; mass spectrum (MALDI) m/z 261.24 (M^+); IR spectrum υmax (KBr)/cm^{-1} 1655 (C=O); ^{1}H-NMR ($CDCl_3$) δ 6.05 (s, 2H), 6.90 (d, 1H, J=15Hz), 7.45 (d, 1H), 7.55 (d, 1H), 7.70 (d, 1H, J=17Hz), 7.85 (s, 2H), 7.95 (s, 1H); ^{13}C-NMR ($CDCl_3$) δ 101.80, 107.79, 108.33, 121.64, 124.46, 125.11, 132.08, 134.33, 144.83, 148.12, 151.76, 164.01, 187.18.

1-(3,4-Methylenedioxyphenyl)-3-(1-methyl-2-imidazolyl)-prop-2-en-1-one (DMU2149)

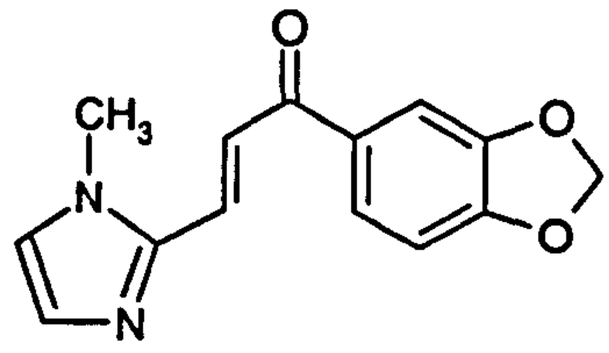

Yellow solid, yield (1.80g, 77%); m.p. 147°C; mass spectrum (MALDI) m/z 257.70 (M^+ + 1); IR spectrum υmax (KBr)/cm^{-1} 1652 (C=O); ^{1}H-NMR ($CDCl_3$) δ 3.80 (s, 3H), 6.05 (s, 2H), 6.60 (d, 1H), 7.00 (s, 1H), 7.20 (s, 1H), 7.58 (d, 1H), 7.65 (d, 1H, J=14Hz), 7.75 (m, 1H), 7.95 (d, 1H, J=14Hz); ^{13}C-NMR ($CDCl_3$) δ 32.96, 101.91, 107.90, 108.23, 123.14, 123.86, 125.03, 127.03, 130.32, 132.55, 143.80, 148.33, 151.93, 187.25.

5.3.2 Chemical analysis of DMU2306

1-(3,4-Methylenedioxyphenyl)-3-[(2-phenoxy-ethyl)-2-imidazolyl]-prop-2-en-1-one (DMU2306)

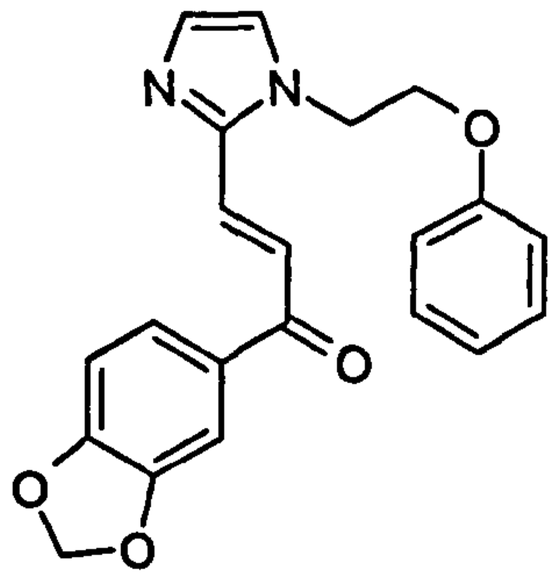

Pale yellow solid, yield (0.06g, 20%); m.p. 174°C; mass spectrum (MALDI) m/z 363.20 (M^+ + 1); IR spectrum υmax (KBr)/cm^{-1} 1663 (C=O); ^{1}H-NMR ($CDCl_3$) δ 4.20 (t, 2H), 4.60 (t, 2H), 6.00 (s, 2H), 6.80 (d, 1H), 6.85 (t, 2H), 6.90 (d, 1H), 7.20 (t, 3H), 7.40 (s, 1H), 7.55 (d, 1H), 7.75 (d, 1H), 7.85 (d, 1H, J=14Hz), 7.95 (d, 1H, J=14Hz); ^{13}C-NMR ($CDCl_3$)

δ 44.62, 64.34, 99.27, 105.43, 105.76, 111.66, 111.68, 118.60, 122.41, 123.24, 125.50, 126.78, 126.98, 127.08, 127.84, 142.84, 145.57, 149.28, 155.20, 155.33, 193.60.

5.3.3 Biological evaluation of imidazole and thiazole chalcones

All synthesised compounds were biologically evaluated with the *in vitro* MTT assay using the CDDG in-house breast cell panel of MCF7, MDA-MB-468 and MCF10A:

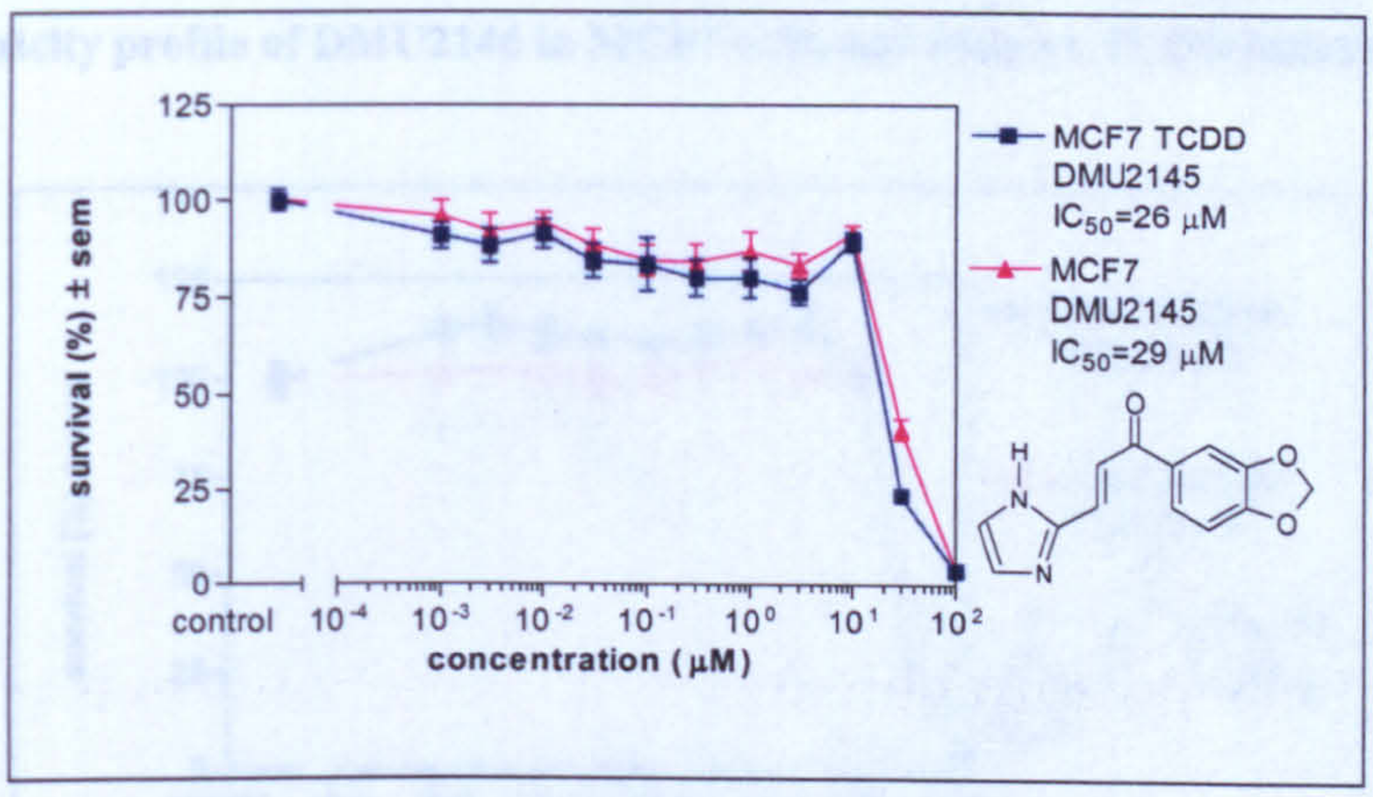

Figure 70. Cytotoxicity profile of DMU2145 in MCF7 with and without TCDD induction.

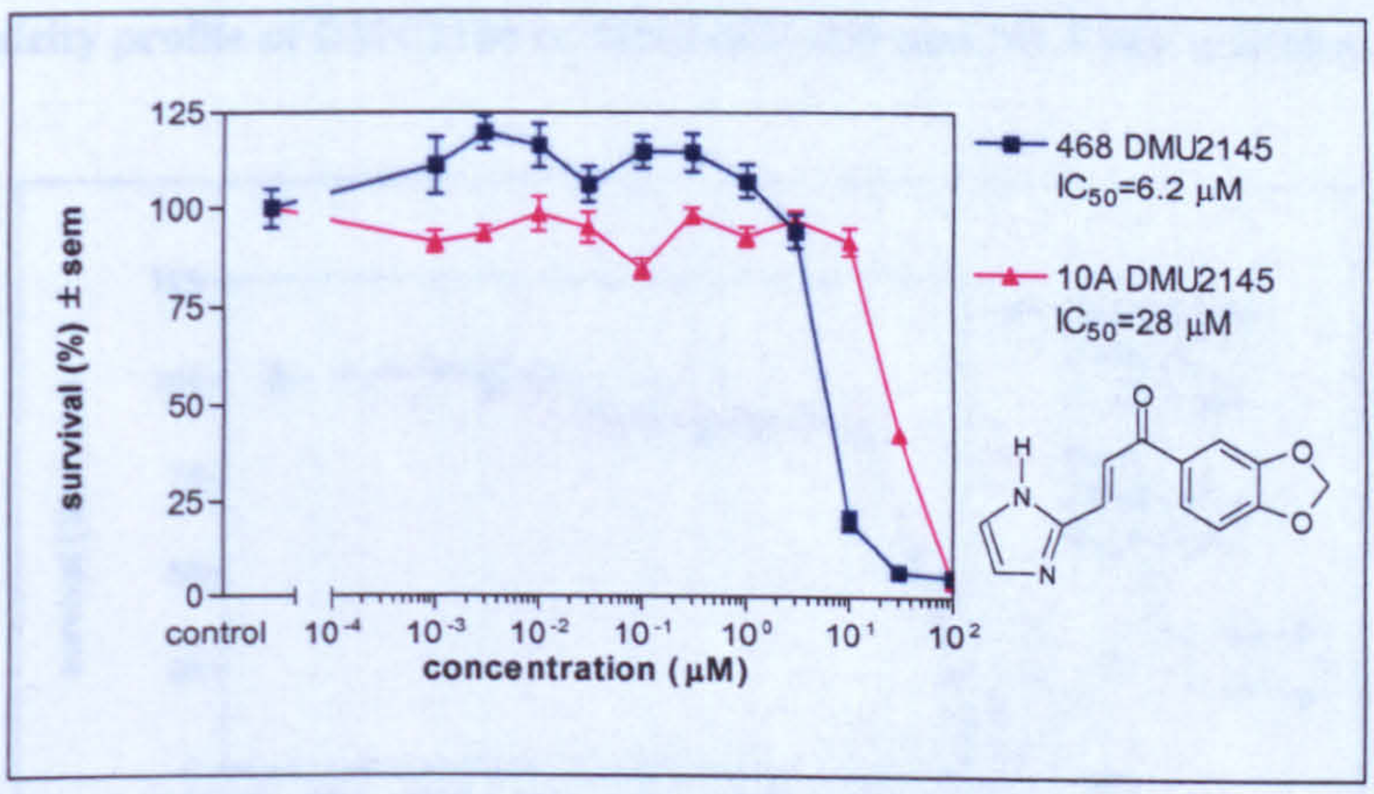

Figure 71. Cytotoxicity profile of DMU2145 in MDA-MB-468 and MCF10A cell lines.

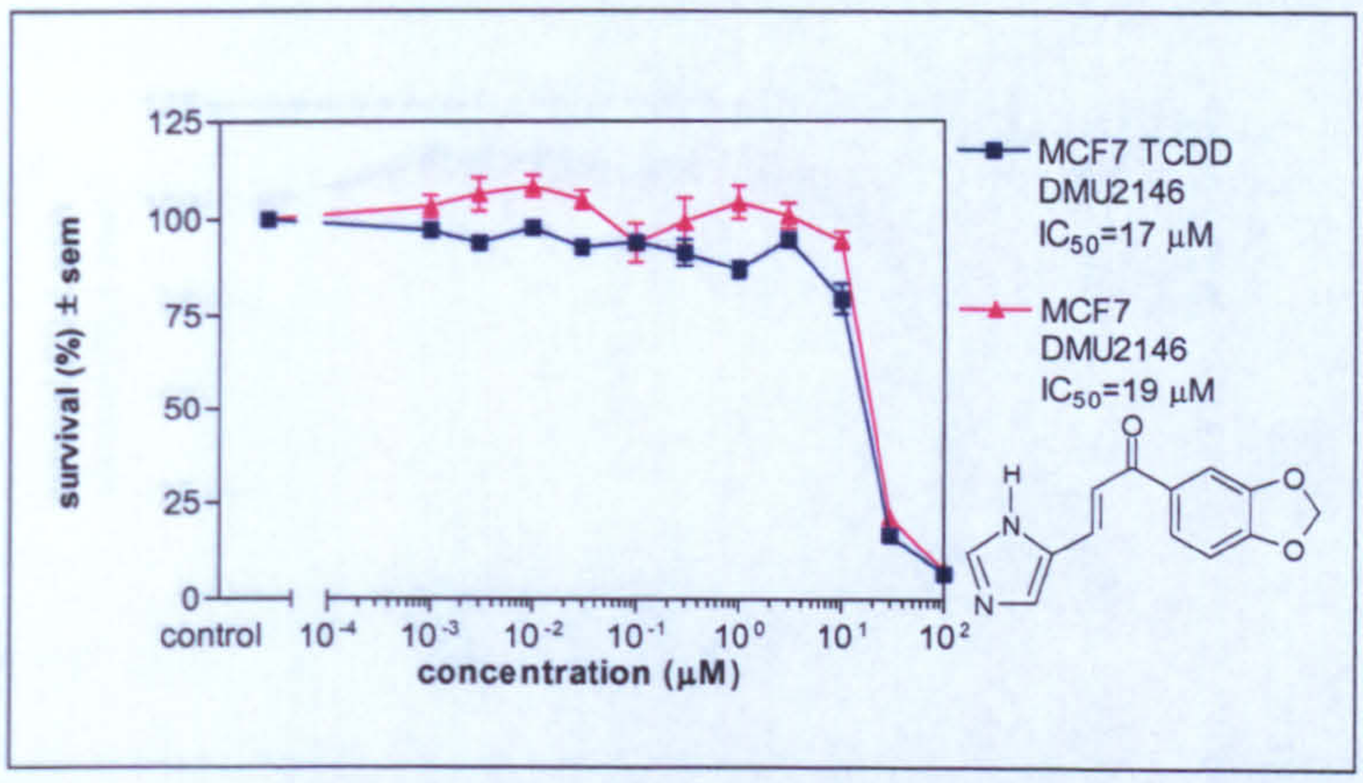

Figure 72. Cytotoxicity profile of DMU2146 in MCF7 with and without TCDD induction.

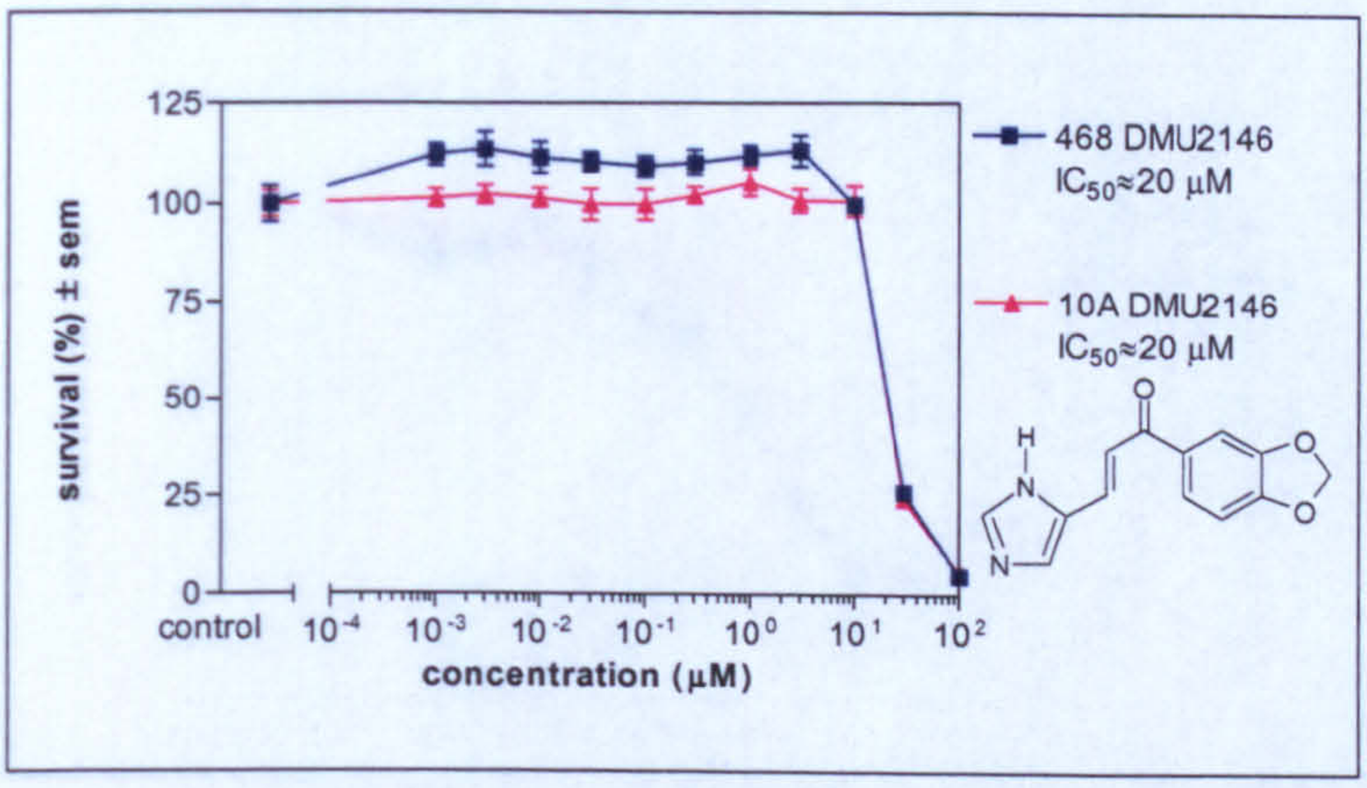

Figure 73. Cytotoxicity profile of DMU2146 in MDA-MB-468 and MCF10A cell lines.

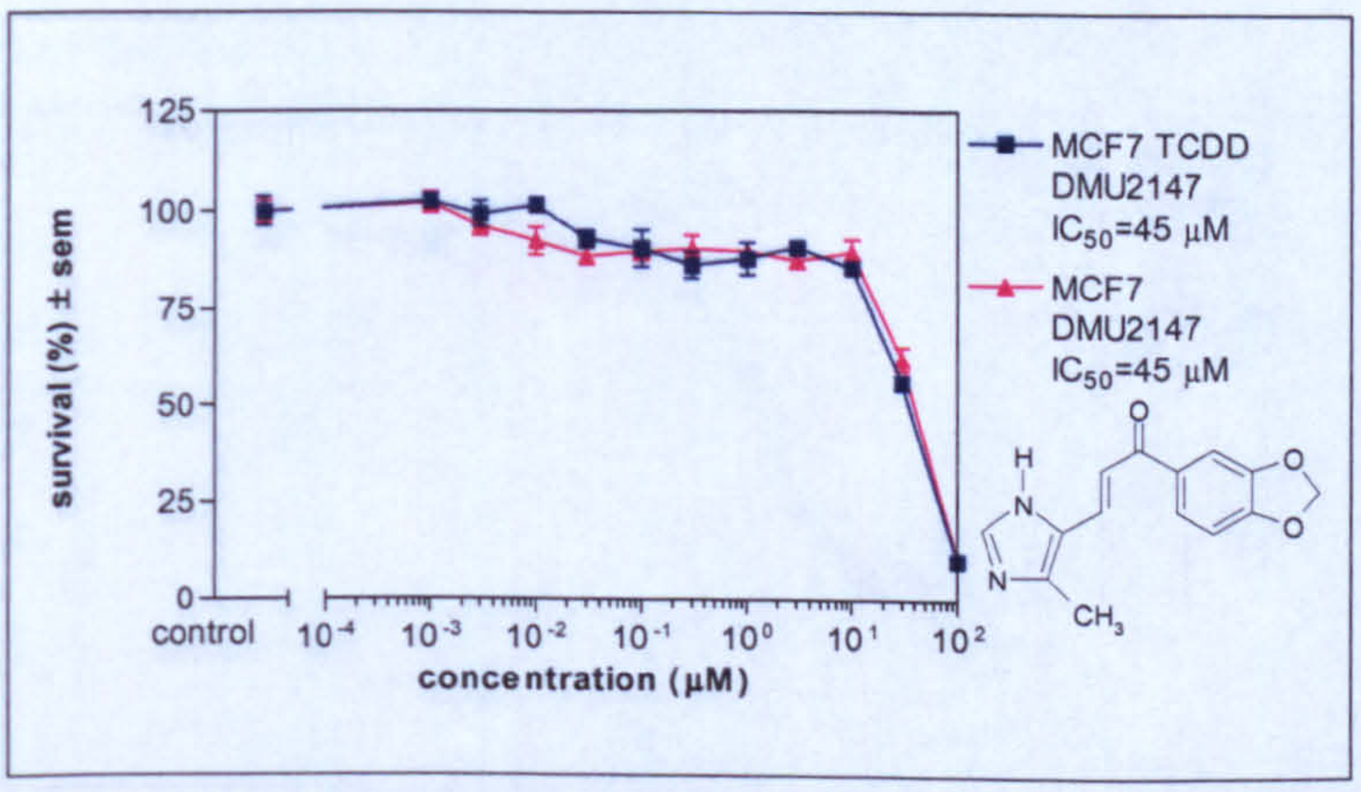

Figure 74. Cytotoxicity profile of DMU2147 in MCF7 with and without TCDD induction.

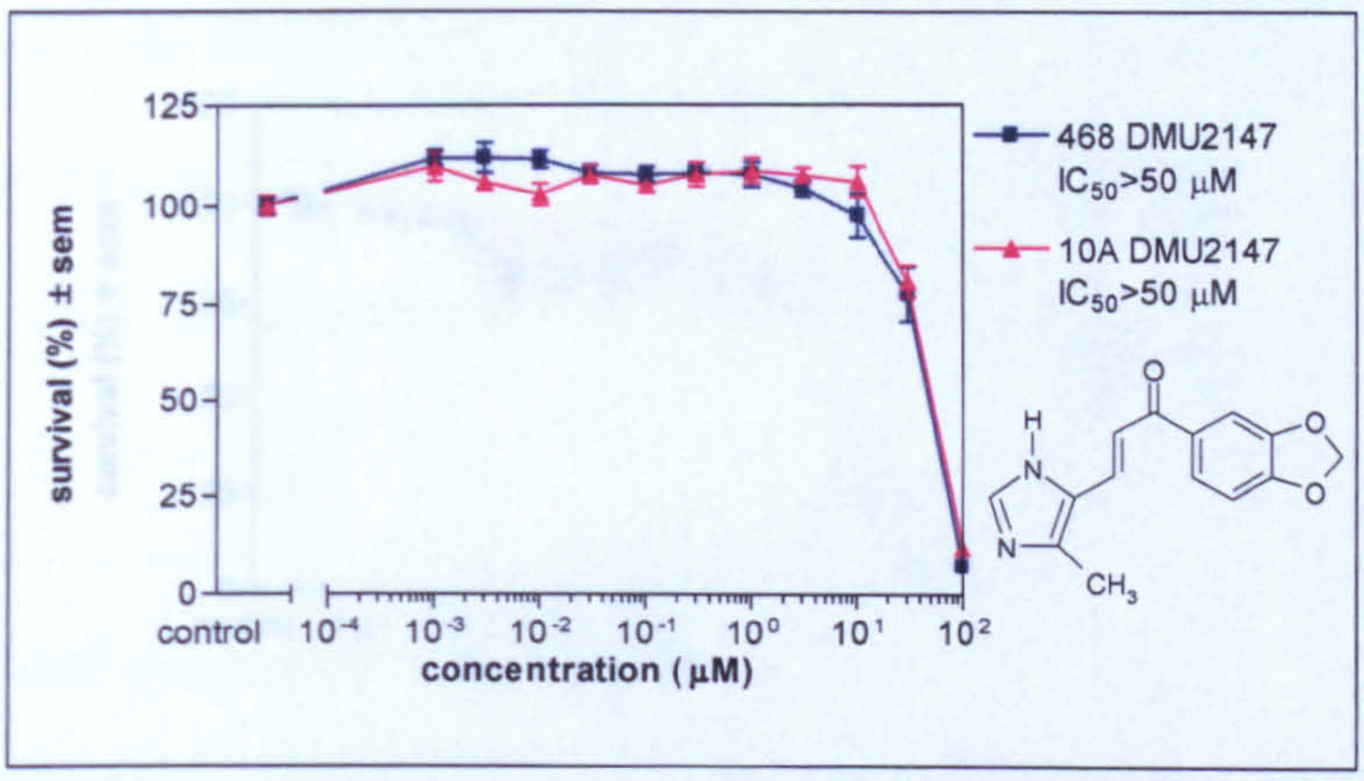

Figure 75. Cytotoxicity profile of DMU2147 in MDA-MB-468 and MCF10A cell lines.

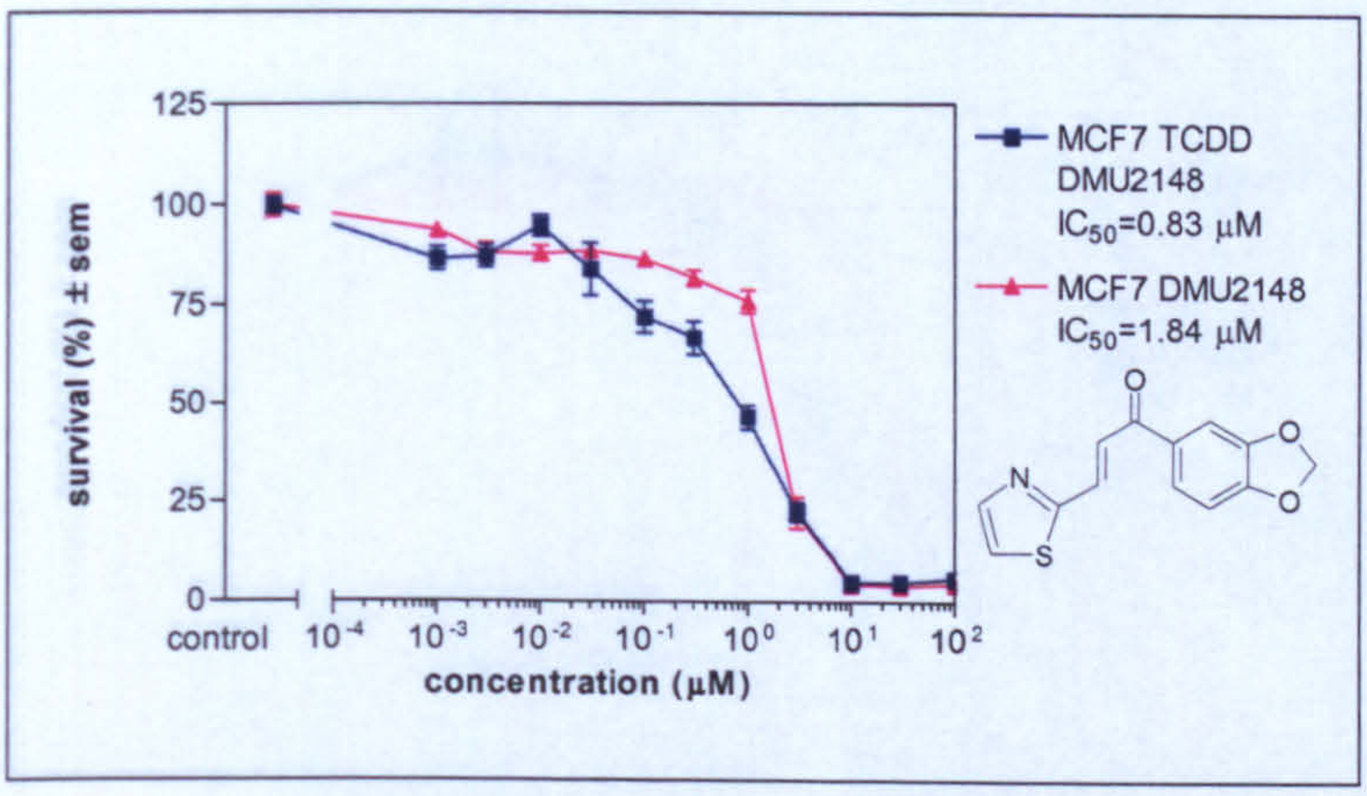

Figure 76. Cytotoxicity profile of DMU2148 in MCF7 with and without TCDD induction.

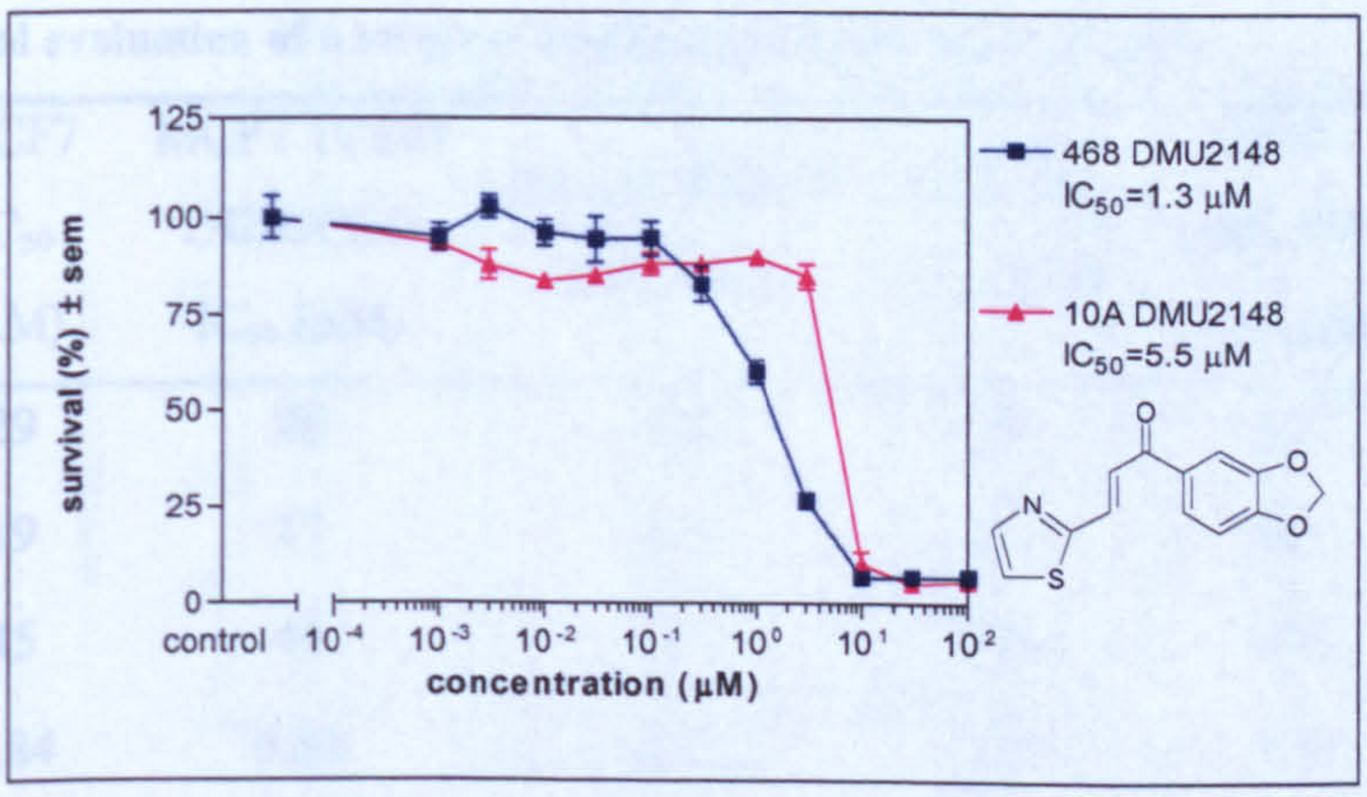

Figure 77. Cytotoxicity profile of DMU2148 in MDA-MB-468 and MCF10A cell lines.

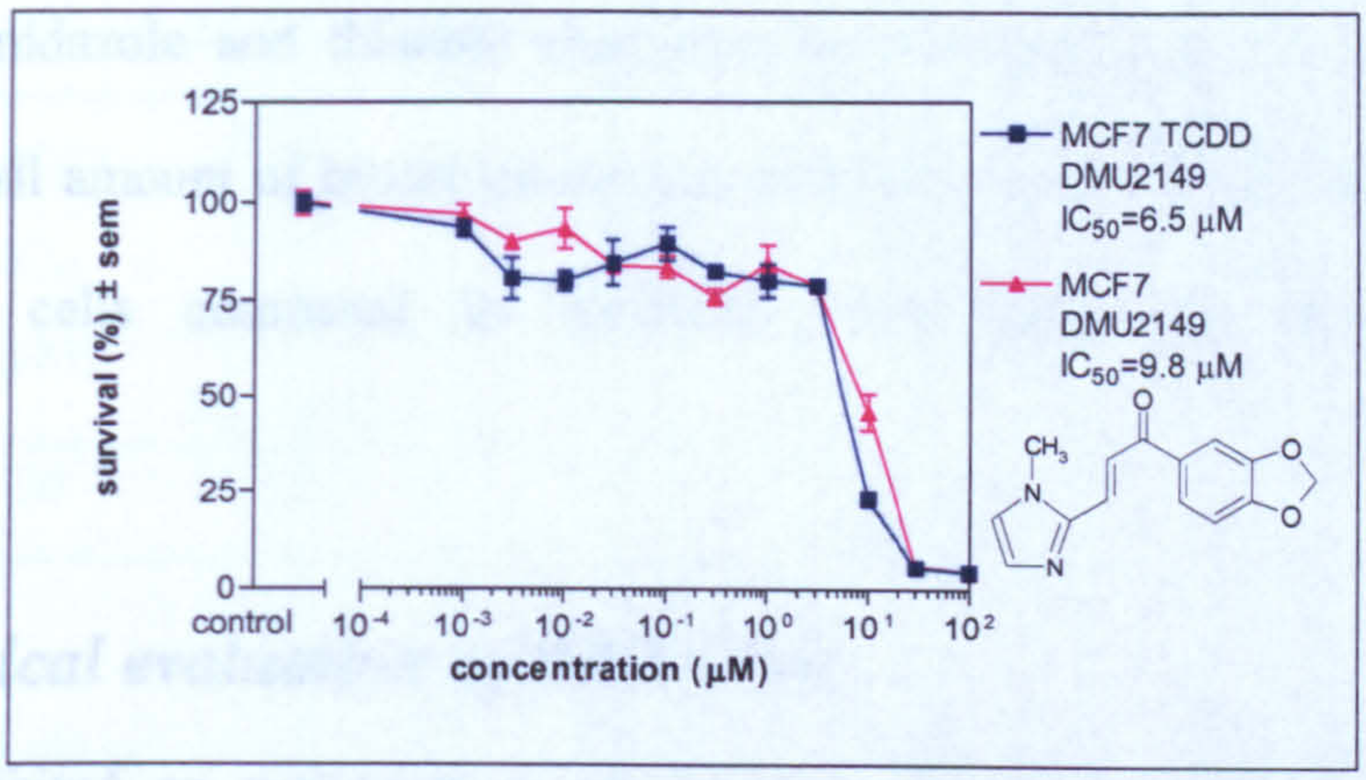

Figure 78. Cytotoxicity profile of DMU2149 in MCF7 with and without TCDD induction.

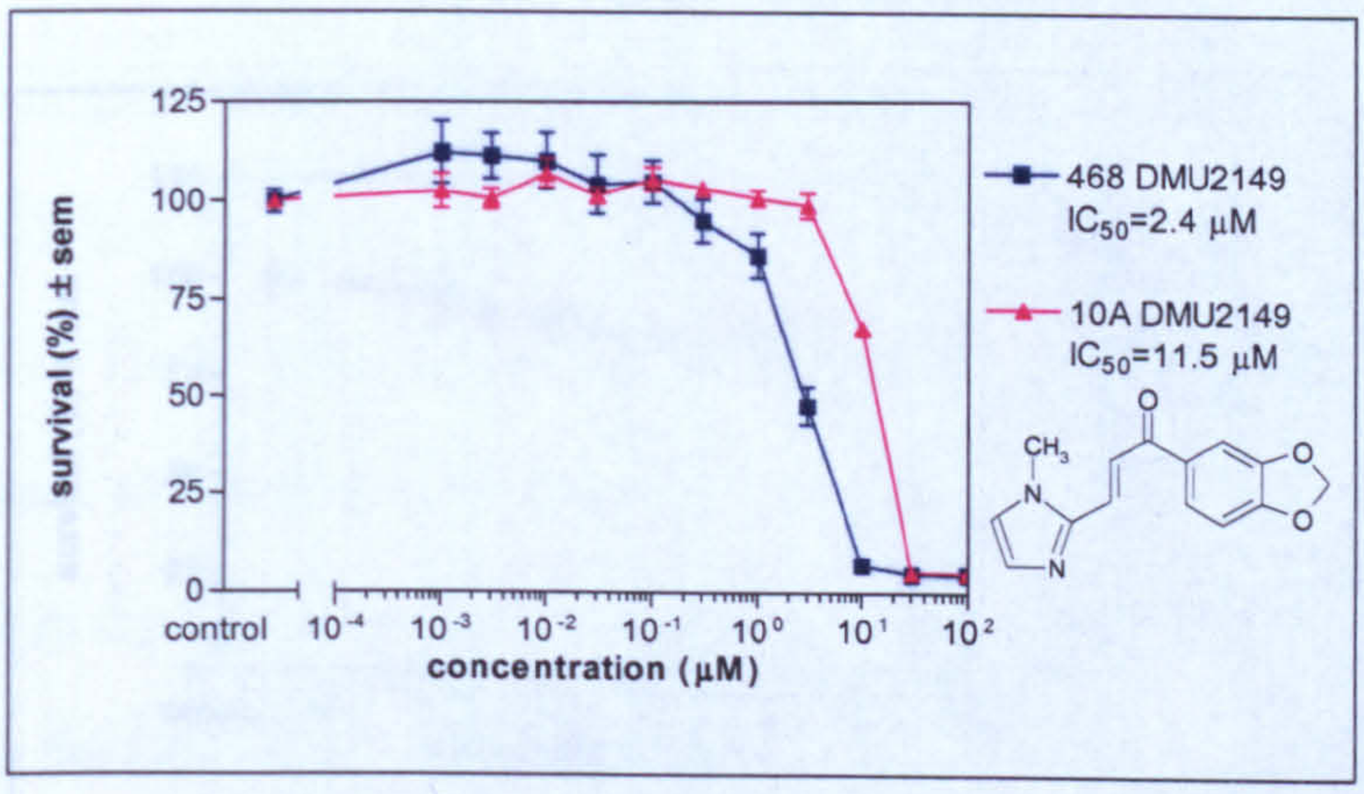

Figure 79. Cytotoxicity profile of DMU2149 in MDA-MB-468 and MCF10A cell lines.

Table 36. Biological evaluation of a series of imidazole and thiazole chalcones.

DRUG	MCF7 IC_{50} (μM)	MCF7 TCDD INDUCED IC_{50} (μM)	ACTIVATION FACTOR	MCF10A IC_{50} (μM)	MDA-MB-468 IC_{50} (μM)	TUMOUR SELECTIVE FACTOR
DMU2145	29	26	1.1	28	6.2	4.5
DMU2146	19	17	1.1	20	20	1
DMU2147	45	45	1	>50	>50	1
DMU2148	1.84	0.83	2.2	5.5	1.3	4.2
DMU2149	9.8	6.5	1.5	11.5	2.4	4.8

None of the imidazole and thiazole chalcones showed activation in the MCF7 assay. However, a small amount of bioactivation was observed for DMU2145 and DMU2149 in MDA-MB-468 cells compared to MCF10A cells suggesting selective CYP1B1 bioactivation.

5.3.4 Biological evaluation of DMU2306

DMU2306 exhibited no activation in MCF7 cells, however, slight bioactivation was observed in MDA-MB-468 cells compared to MCF10A cells:

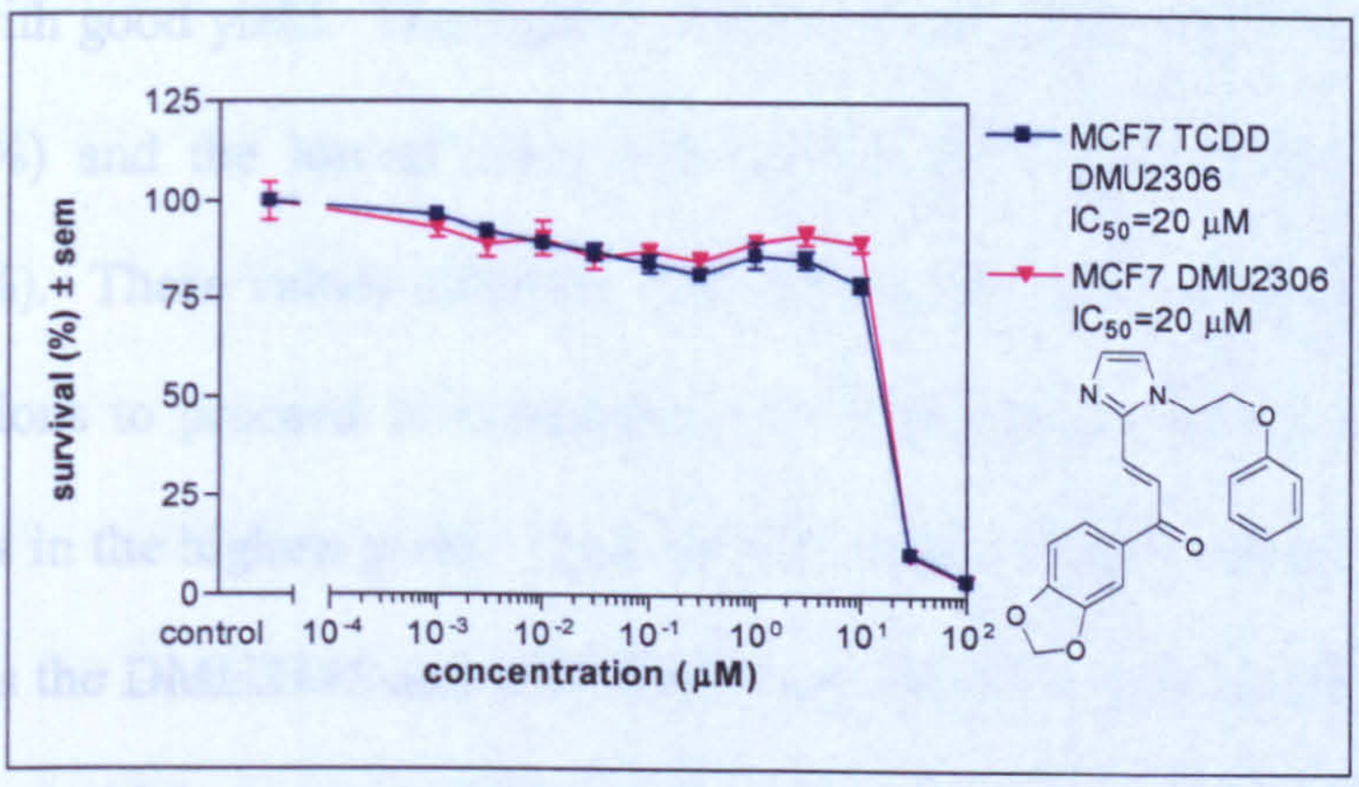

Figure 80. Cytotoxicity profile of DMU2306 in MCF7 with and without TCDD induction.

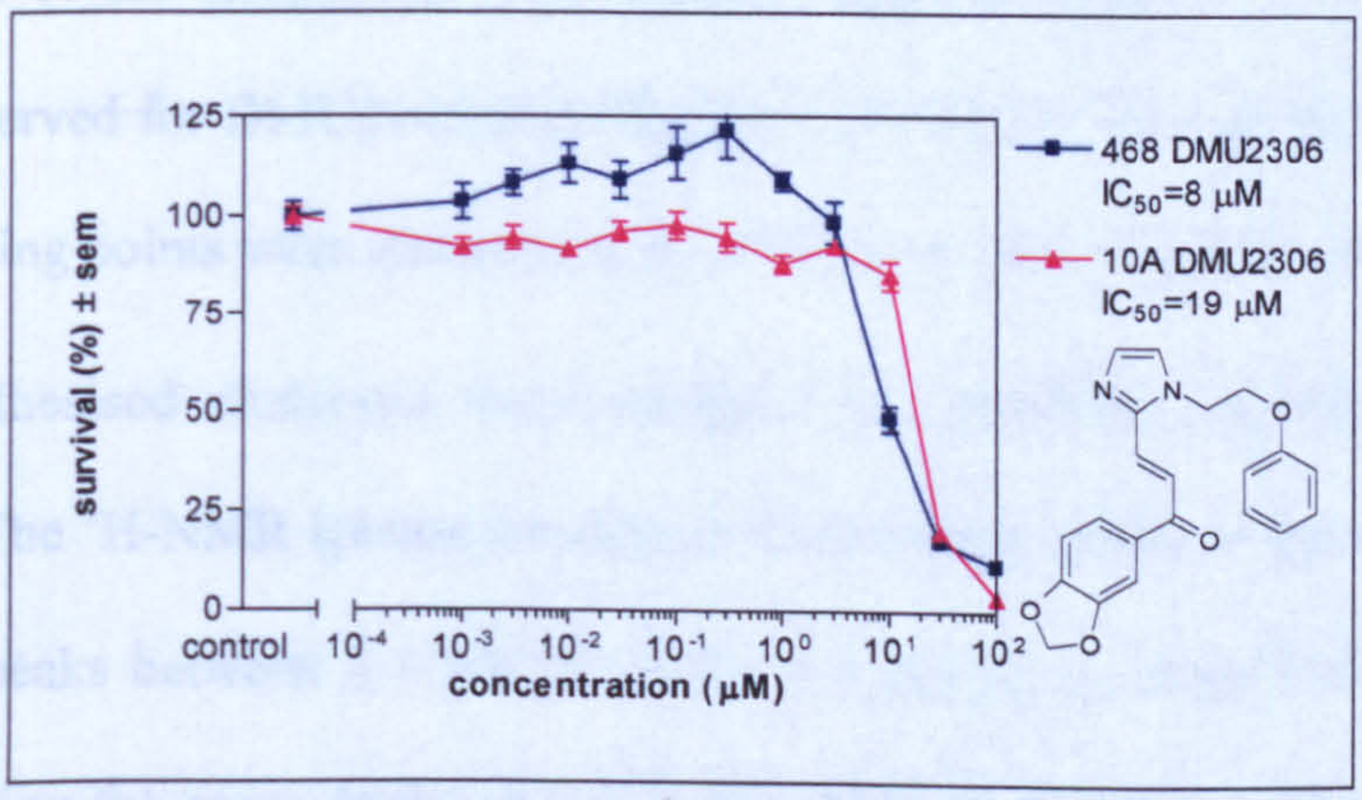

Figure 81. Cytotoxicity profile of DMU2306 in MDA-MB-468 and MCF10A cell lines.

Table 37. Biological evaluation of DMU2306.

DRUG	MCF7 IC_{50} (μM)	MCF7 TCDD INDUCED IC_{50} (μM)	ACTIVATION FACTOR	MCF10A IC_{50} (μM)	MDA-MB-468 IC_{50} (μM)	TUMOUR SELECTIVE FACTOR
DMU2306	20	20	1	19	8	2.4

5.4 Discussion

Five *imidazole/thiazole* prodrugs were synthesised successfully using Claisen-Schmidt condensation, with good yield. The highest yields were obtained for DMU2149 (77%) and DMU2148 (49%) and the lowest were with DMU2147 (21%), DMU2146 (23%) and DMU2145 (36%). These values correlate with the overall reaction times required for the individual reactions to proceed to completion where reactions that proceeded the fastest gave compounds in the highest yield. Both DMU2149 and DMU2148 reaction times were 4 hours, whereas the DMU2145 and DMU2146 reactions proceeded within 24 hours. The slowest reaction at 28 hours and consequently the lowest yield were both observed for DMU2147. All of the compounds were afforded as yellow solids. The highest melting points were observed for DMU2145 (220°C), DMU2147 (207°C) and DMU2146 (180°C). The lowest melting points were observed with DMU2148 (143°C) and DMU2149 (147°C).

All of the synthesised chalcones were analysed by ^{1}H-NMR, ^{13}C-NMR and infrared spectroscopy. The ^{1}H-NMR spectra confirmed the enone structure of the chalcones with a set of doublet peaks between δ 6.90-7.95, with a coupling constant J between 12-17Hz, thereby confirming the *trans* double bond in the chalcone structure. The presence of the 3,4-methylenedioxy group was confirmed by a characteristic singlet peak observed between

δ 6.00-6.25 and the NH groups in DMU2145, DMU2146 and DMU2147 were confirmed with broad peaks between δ 12.40-12.60. The ^{13}C-NMR spectra showed a characteristic carbonyl peak between δ 187.25-186.60. Infrared spectroscopy also demonstrated the characteristic carbonyl peaks between 1647-1655cm^{-1} and characteristic NH peaks between 3225-3182 cm^{-1}. Mass spectroscopy of the chalcones showed that the desired compounds were synthesised as they all showed M^+ or M^++1 peaks.

DMU2306 was synthesised successfully by deprotonation of DMU2145 followed by nucleophilic substitution with β-chlorophenetole, the overall reaction proceeded fairly slowly with a reaction time of 45 hours. The product was synthesised in a 20% yield as a pale yellow solid with a melting point of 147°C. ^{1}H-NMR spectra confirmed the enone structure of the chalcone with a set of doublet peaks between δ 7.85-7.95, with a coupling constant J of 14Hz, thereby confirming the *trans* double bond in the chalcone structure. The presence of the 3,4-methylenedioxy group was confirmed by a characteristic singlet peak observed at δ 6.00. The ^{13}C-NMR spectra showed a characteristic carbonyl peak at δ 193.60; infrared spectroscopy also demonstrated the characteristic carbonyl peak at 1652cm^{-1}. Mass spectroscopy of the compound showed that the desired compound was synthesised with an M^++1 peak.

The rationale for selective CYP1B1 prodrug bioactivation was substantiated to some degree as none of the prodrugs exhibited any discernible activation in MCF7 cells with or without CYP1A1 induction. However, in MDA-MB-468 cells DMU2145 and DMU2149 showed enhanced cytotoxicity towards tumour cells 5-fold compared to MCF10A non-tumour cells. But, the tumour selectivity factor was reduced compared to DMU762, which has a 2,500-

fold selectivity factor at IC_{25} suggesting that the 3-pyridyl substituent in the 'A' ring instigates superior biological activity compared to the 2-imidazole substituent.

The other imidazole prodrugs DMU2146 and DMU2147 were non-toxic in all breast cell-lines at pharmacologically acceptable dosages. Comparison of these 4-imidazole prodrugs to the 2-imidazole versions (DMU2145 and DMU2149) led to the generation of a structure activity relationship (SAR). Where, the translocation of nitrogen from 2 to 4-imidazole resulted in elimination of CYP1B1 mediated tumour cytotoxicity. Mapping DMU2145 onto the pharmacophore may explain this; alignment of the prodrug to the hotspots shows that the lone pair of electrons on the nitrogen form hydrogen-bonding associations with one of the hydrogen-bonding residues. Translocation of the nitrogen to the 4 position in DMU2146 changes the alignment to eradicate this hydrogen-bonding association:

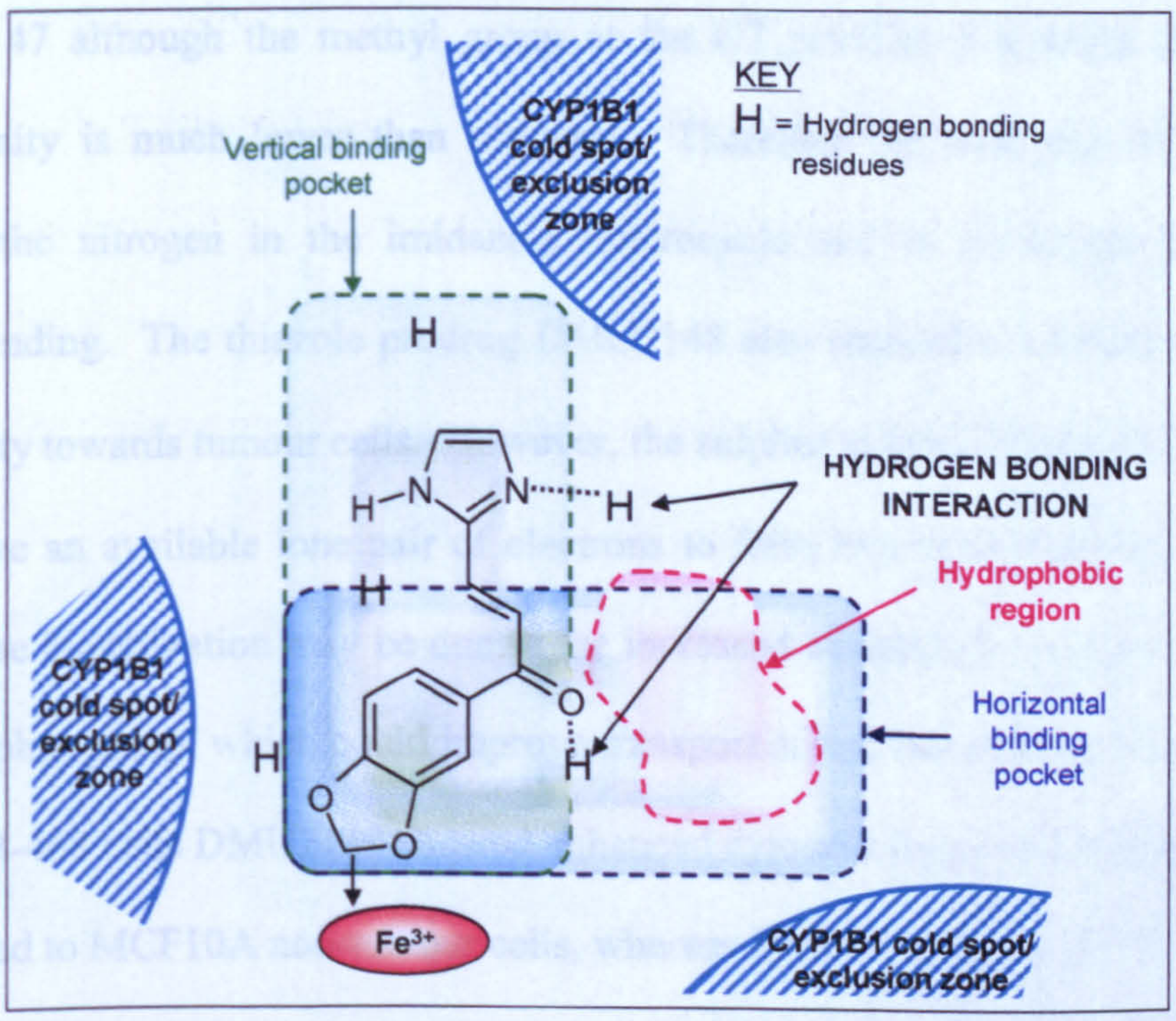

Figure 82. DMU2145 mapping to show hydrogen-bonding interaction associated with 2-imidazoles.

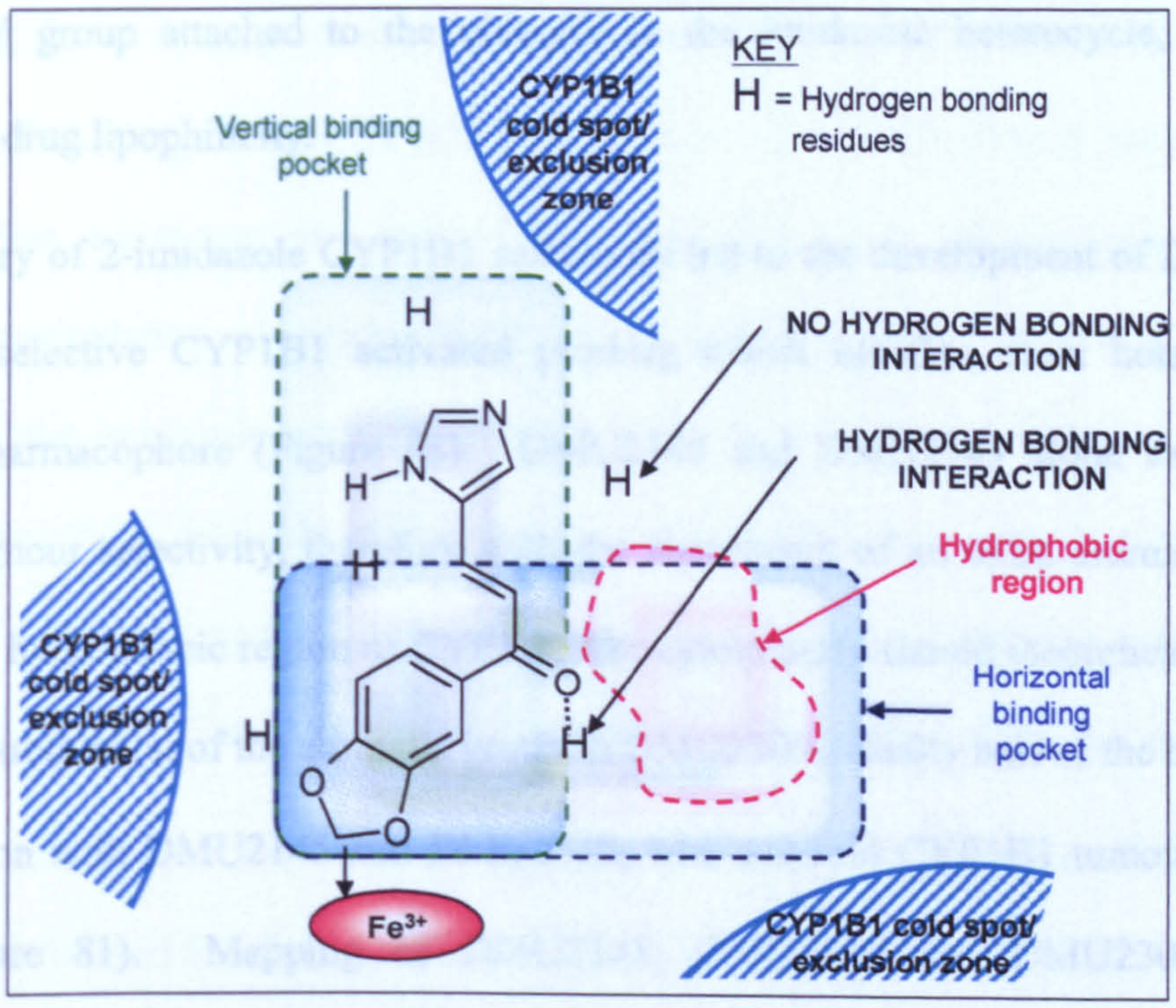

Figure 83. DMU2146 mapping to show no hydrogen-bonding interaction associated with 4-imidazoles.

For DMU2147 although the methyl group at the C2 position is electron donating, the electron-density is much lower than nitrogen. Therefore the lone pair of electrons is donated to the nitrogen in the imidazole heterocycle and is no longer available for hydrogen-bonding. The thiazole prodrug DMU2148 also showed a 4.2-fold enhancement in cytotoxicity towards tumour cells. However, the sulphur at the C2 position in DMU2148 does not have an available lone pair of electrons to form hydrogen-bonding associations. Therefore, the bioactivation may be due to the increased lipophilicity incurred on the drug from the sulphur group, which could improve transport across the cell membrane. Overall, in MDA-MB-468 cells DMU2149 showed enhanced cytotoxicity towards tumour cells 4.8-fold compared to MCF10A non-tumour cells, whereas DMU2145 had a CYP1B1 activation factor of 4.5. The slight enhancement in cytotoxicity for DMU2149 could be due to the

extra methyl group attached to the nitrogen in the imidazole heterocycle, which may enhance the drug lipophilicity.

The discovery of 2-imidazole CYP1B1 selectivity led to the development of DMU2306, a potentially selective CYP1B1 activated prodrug which satisfies most hotspots in the CYP1B1 pharmacophore (Figure 68). DMU2145 and DMU2149 alone exhibit 5-fold CYP1B1 tumour selectivity, therefore with the attachment of an extra aromatic group to locate in the hydrophobic region of CYP1B1, the cytotoxicity should theoretically improve. However, introduction of the aromatic group in DMU2306 actually halved the bioactivation in comparison with DMU2145 and DMU2149, with a 2-fold CYP1B1 tumour selectivity factor (Figure 81). Mapping of DMU2145, DMU2149 and DMU2306 onto the pharmacophore may explain this:

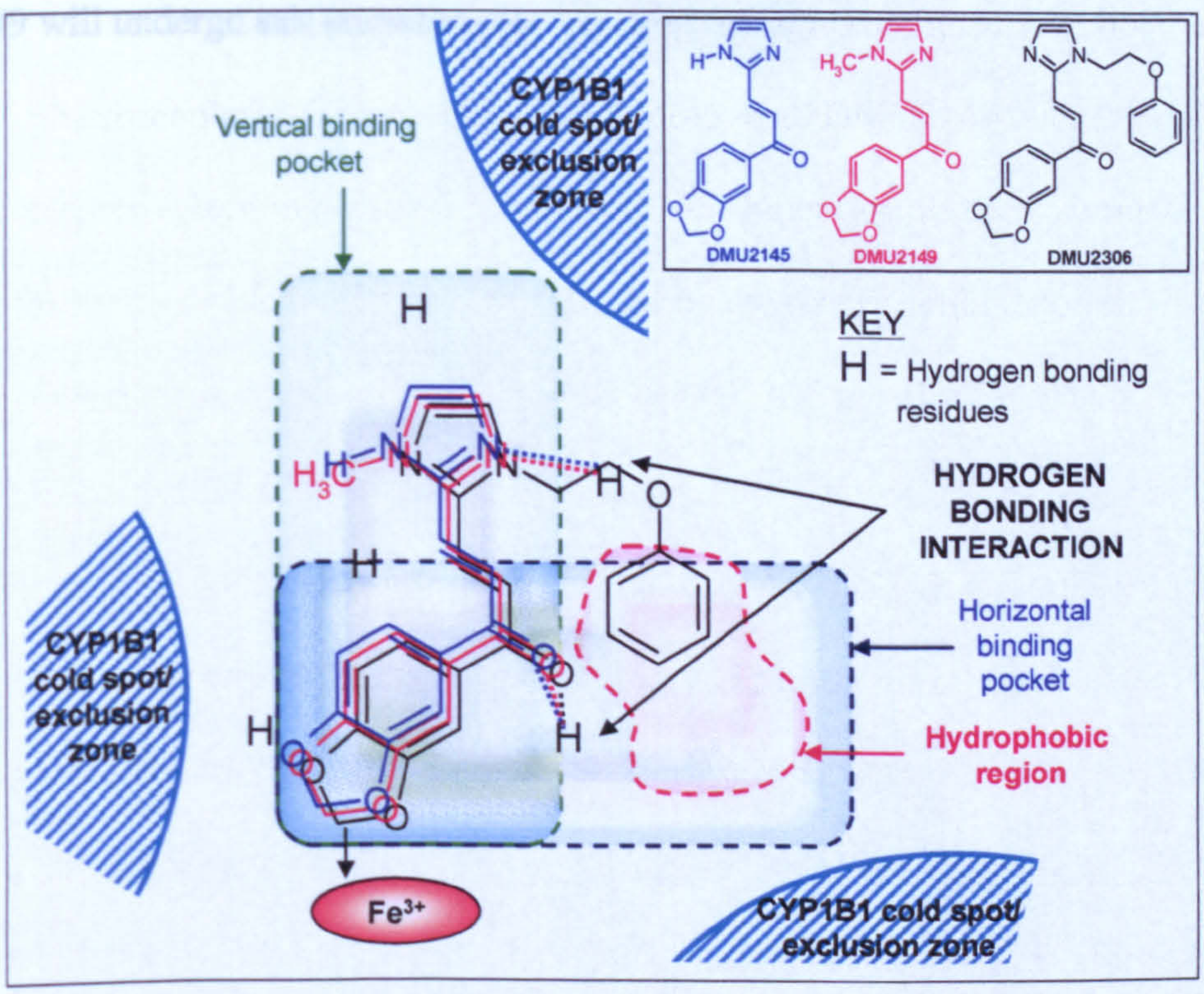

Figure 84. Mapping of DMU2145, DMU2149 and DMU2306 onto the CYP1B1 pharmacophore.

The mapping shows the importance of the hydrogen bonding interaction near the upper part of the hydrophobic region for CYP1B1 bioactivation. In fact this interaction is even more important than satisfying the hydrophobic region, as was shown with DMU2306. However, manipulation of either DMU2145 or DMU2149 such that the lone pair of electrons on the imidazole nitrogen is still available for hydrogen-bonding associations, whilst also satisfying the hydrophobic region may result in a more potent compound. An example of such a compound may be DMU2149 with a hydrophobic aromatic group attached to the carbon-2 atom of the enone structure as described by Ducki *et al* [113].

Overall, optimum bioactivity was shown with the 2-imidazole prodrug DMU2149 and since rationale behind the design of these compounds was selective CYP1B1 activation as well as use of derivatisable functional groups to enable subsequent salt selection, DMU2149 will undergo salt screening studies (Chapter 6).

CHAPTER 6

Salt Selection Studies of Ionisable Prodrugs

6.1 Introduction

Rarely do NCEs possess the desired physicochemical properties such as solubility, dissolution rate, stability and hygroscopicity to enable formulation for a therapeutic effect. If the NCE contains ionisable functional groups, salt form selection can be considered to optimise these properties, consequently it is frequently an essential component of the preformulation process [220].

Salt selection as a means of improving solubility and bioavailability is considered when drug solubility is less than 1 mg/mL. The salt usually renders the parent compound ionised in water i.e. water-soluble and therefore suitable for pharmacokinetic studies using parenteral formulations [221]. Salt synthesis involves reaction between an acid and a base where proton transfer or neutralisation occurs, the strength of the components determines the probability of salt formation. 43% of FDA approved weakly basic drugs are marketed as hydrochlorides and 63% of weakly acidic drugs are marketed as sodium salts [222].

The salt forming species are often chosen based on the acidity/basicity of the NCE. For a basic compound studying the pH-solubility relationship can indicate whether it will exist as the free base or form a salt under certain pH conditions [221]. The pH-solubility profile of a basic drug can be expressed as two independent curves where the point of intersection is described as the pH of maximum solubility (pH_{max}) [223]. This relationship can be explained by Equations 6.1 and 6.2 [221, 224]:

$$pH > pH_{max}: \quad S_T = [BH^+] + [B]_s = [B]_s\left(1 + \frac{[H_3O^+]}{K_a}\right) \tag{6.1}$$

$$\text{pH} < \text{pH}_{max}: \quad S_T = [BH^+]_s + [B] = [BH^+]_s \left(1 + \frac{K_a}{[H_3O^+]}\right) \tag{6.2}$$

Where S_T is the total saturation solubility of the drug at any given pH, [B] and [BH^+] are concentrations of free and protonated species of the base, respectively and the subscript s represents a saturated species. Each of these equations represents an independent curve in the pH-solubility profile for a monobasic drug:

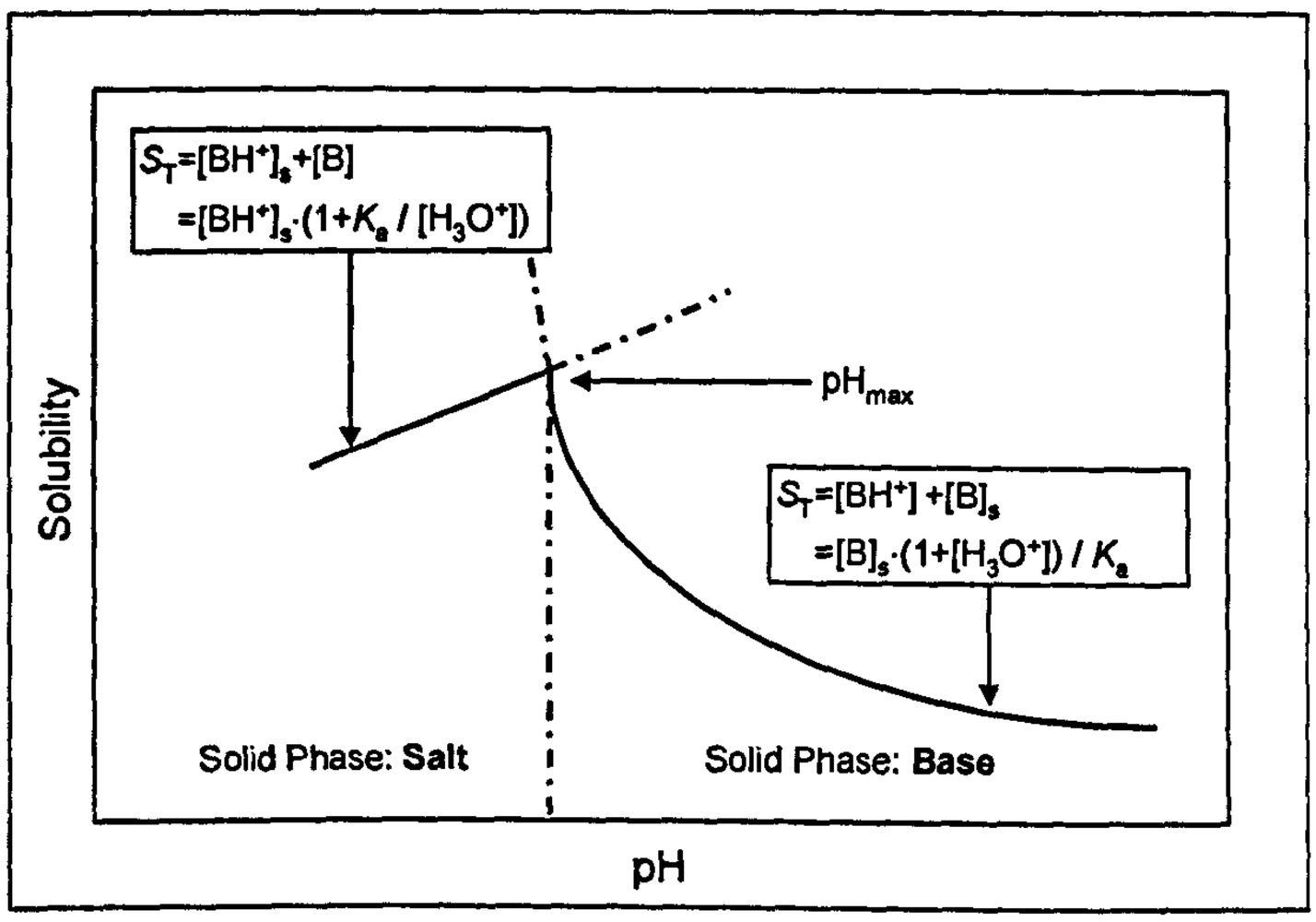

Figure 85. Schematic representation of the pH-solubility profile of a monobasic drug, showing that the solubilities of the base and salt can be expressed by two independent curves corresponding to two independent equations [221].

There are two key regions in the pH-solubility profile described above, salt formation will only occur if the pH of the aqueous solution of basic drug is adjusted below its pH_{max}, and if the pH of the saturated salt solution is raised above this level the salt will be reconverted to the free base. Therefore, the counter-ion chosen for salt selection must be suitable to achieve pH conditions below the pH_{max}, for a basic compound the pKa of the chosen conjugate acid should be lower than the parent compound. The most common criterion for selection of counter-ions was proposed by Tong *et al* [224], who recommended that, for the

preparation of salts of a basic drug, the pKa of the conjugate acid should be at least two pH units lower than the pKa of the drug. Empirical selection can also be used as described by Gould [225] in the preparation of salts from planar, high melting point aromatic sulfonic or hydrocarboxylic acids which yielded high melting crystalline salts, whereas flexible aliphatic acids yielded oils. However, in general no guidelines exist for salt selection during drug development, literature range is limited and selection is normally based on experience. Within the scope of this thesis, salt screening studies were conducted for the anticancer prodrugs DMU590 and DMU2149. The salt screening method used in this study was a three-tiered approach, with progression to the next stage resulting from failure of the previous stage i.e. (i) inorganic mineral acids, (ii) organic aliphatic and olefinic acids and (iii) organic aromatic acids.

6.1.1 DMU590: A morpholino prodrug

The clinical potential of the novel *trans*-stilbene prodrug DMU212 has led to the evolution of a library of novel CDDG prodrugs with the core DMU212 molecular skeleton. The cytotoxicity of these compounds was screened in the MTT *in vitro* assay, where the *cis*-stilbene analogue of DMU212 – DMU590 exhibited optimum anticancer activity:

Table 38. Summary of DMU590 *in vitro* cytotoxicity data. Data provided by P. Butler of the CDDG.

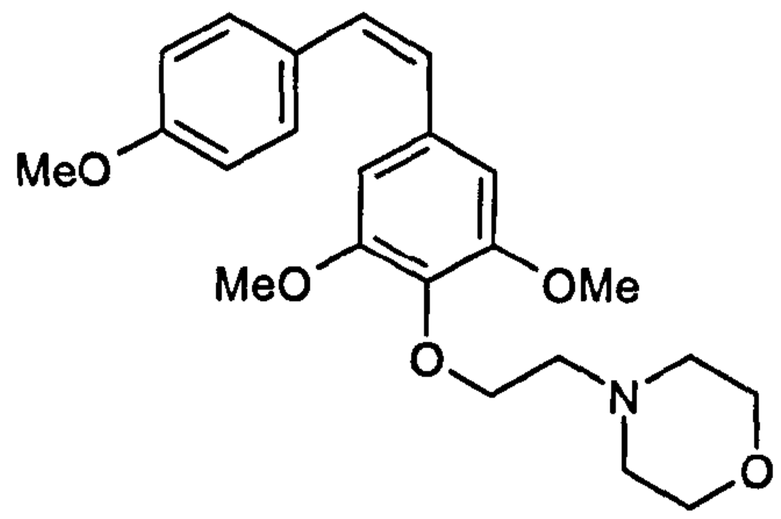

HUMAN BREAST CELL-LINE	MCF7 WITHOUT TCDD	MCF7 WITH TCDD	ACTIVATION FACTOR	MCF10A	MDA-MB-468	TUMOUR SELECTIVE FACTOR
IC_{50} VALUES (μM)	0.7	0.08	8.6	50	0.01	5000

DMU590 was found to be potently cytotoxic in MDA-MB-468 cancer cells with appreciably reduced cytotoxicity in MCF10A and MCF7 cells with and without TCDD induction (Table 38). DMU590 was a more potent anticancer prodrug than DMU212, with CYP1B1-activation factors of 5000 and 4300 respectively. This improvement in cytotoxicity may correspond to the increased likeness in structure between DMU590 and the antimitotic stilbene CA-4, which would theoretically increase its antimitotic activity (Figure 13). Furthermore, the morpholine substituent on DMU590 should theoretically improve the solubility and also enable salt selection through protonation of the nitrogen to enhance the drug physicochemical properties compared to DMU212.

6.1.2 DMU2149: An imidazole prodrug

A library of imidazole/thiazole chalcones were prepared to enable salt selection of a specific CYP1B1 activated prodrug (Chapter 5). The compounds were designed from the CDDG designated CYP1B1 pharmacophore model (Figure 65) and the core structure of the 3-pyridyl chalcone DMU762. The cytotoxicity of these compounds was screened in the MTT *in vitro* assay, where the 2-imidazole chalcone DMU2149 exhibited optimum anticancer activity:

Table 39. Summary of DMU2149 *in vitro* cytotoxicity data. Data provided by P. Butler of the CDDG.

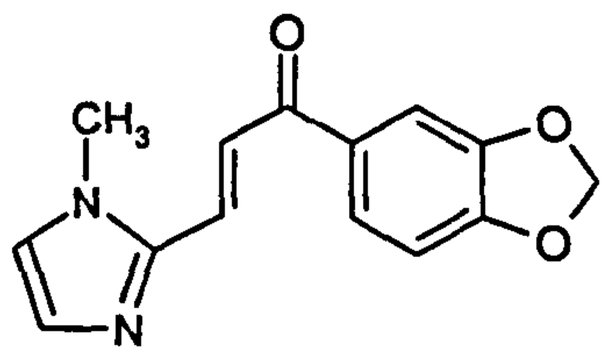

HUMAN BREAST CELL-LINE	MCF7 WITHOUT TCDD	MCF7 WITH TCDD	ACTIVATION FACTOR	MCF10A	MDA-MB-468	TUMOUR SELECTIVE FACTOR
IC_{50} VALUES (μM)	8	8	1	11.5	2.4	4.8

DMU2149 was specifically bioactivated in MDA-MB-468 cells, with no activation observed in MCF7 cells with or without CYP induction. Moreover, protonation of the nitrogen in the imidazole heterocycle can facilitate its salt selection to enhance the drug physicochemical properties compared to DMU762. Although DMU2149 is significantly less active compared to all of the other lead CDDG prodrugs, it was synthesised specifically within this thesis to enable salt selection. Within the scope of this thesis salt

selection studies were conducted for both DMU590 and DMU2149. The aqueous solubility of the salts was determined to consider the feasibility for further development and the salts with the lowest solubility were eliminated. A comprehensive physicochemical and biological analysis of the selected salts was conducted using pH-solubility profiles, DSC, SEM and the MTT assay. High-throughput analytical quantification methods were also developed for pKa determination of DMU590 and DMU2149 using a UV plate reader. The novel technique was corroborated using conventional compounds (indomethacin) and a conventional assay (UV spectrophotometer).

6.2 Materials and methods

Reagents were used as received from Sigma-Aldrich Chemical Company (Dorset, UK) or Alfa Aesar (Lancashire, UK). TCDD (2,3,7,8 tetrachlorodibenzo-*p*-dioxin) was obtained from British Greyhound Chromatography (Birkenhead, UK). 96-well Nunc® plates were obtained from Fisher Scientific (Loughborough, UK). Human breast cell lines were obtained from the American Type Culture Collection and DMU590 was supplied by T. Ijaz of the CDDG.

6.2.1 Salt preparation

The general salt formation procedure was to prepare an equimolar quantity of prodrug and salt forming species i.e. acid in an appropriate solvent (ethanol, methanol, acetone, acetonitrile, 2-propanol, toluene, ethyl acetate or dichloromethane) and allow the mixture to react/stir for a defined time to allow crystallization. If this did not occur within a reasonable time further techniques were used to initiate crystallization e.g. cooling the

mixture, evaporation of solvent and addition of anti-solvents e.g. diethyl ether and hexane to decrease solubility [221, 226]. The following acids were employed for attempted DMU590 and DMU2149 salt formation:

Table 40. Acids used in attempting DMU590 and DMU2149 salt selection. *pKa values obtained from [221].

ACID	ACID TYPE	pKa(s)*	DMU590 SALT?	DMU2149 SALT?
HCl Hydrochloric Acid	Mineral, inorganic	-6.0	No	**Yellow solid formed in 70% (0.08g) yield**
H_3PO_4 Phosphoric Acid	Mineral, inorganic	1.96, 7.12, 12.32	**White solid formed in 84% (0.52g) yield**	**Yellow solid formed in 65% (0.09g) yield**
H_2SO_4 Sulphuric Acid	Mineral, inorganic	-3.0, 1.92	No	**Yellow solid formed in 87% (0.12g) yield**
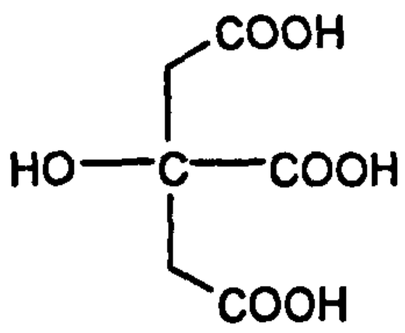 Citric Acid	Organic, aliphatic	3.13, 4.76, 6.40	No	No
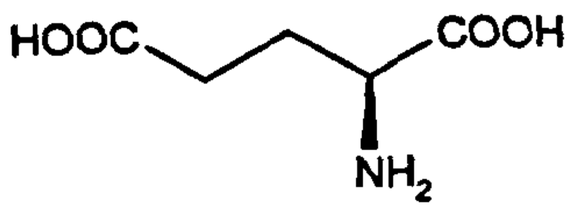 L-Glutamic Acid	Organic, aliphatic	2.19, 4.25, 9.67	No	No
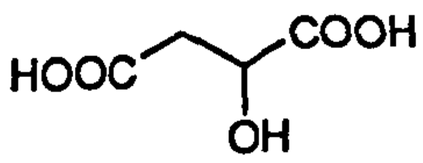 (–)-L-Malic Acid	Organic, aliphatic	3.46, 5.10	No	No

CH_3SO_3H Methanesulphonic Acid	Organic, aliphatic	-1.20	No	**Yellow solid formed in 80% (0.11g) yield**
 Oxalic Acid	Organic, aliphatic	1.27, 4.27	No	**Pale yellow solid formed in 67% (0.09g) yield**
 Stearic Acid	Organic, aliphatic	4.90	No	No
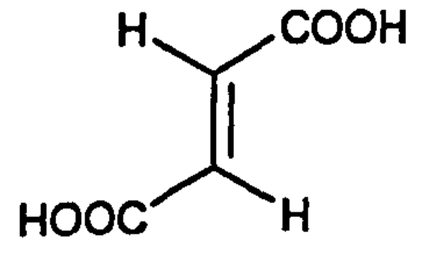 Succinic Acid	Organic, aliphatic	4.21, 5.64	No	No
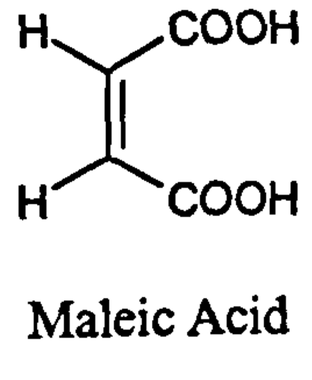 L-Tartaric Acid	Organic, aliphatic	3.02, 4.36	No	**Yellow solid formed in 54% (0.09g) yield**
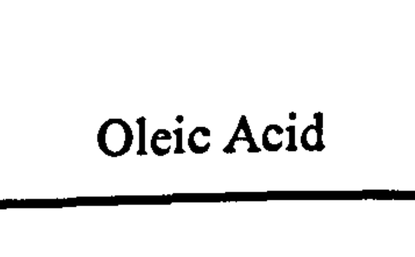 Fumaric Acid	Organic, olefinic	3.03, 4.38	No	**Yellow solid formed in 55% (0.08g) yield**
 Maleic Acid	Organic, olefinic	1.92, 6.23	No	**Yellow solid formed in 75% (0.11g) yield**
 Oleic Acid	Organic, olefinic	4.0	No	No

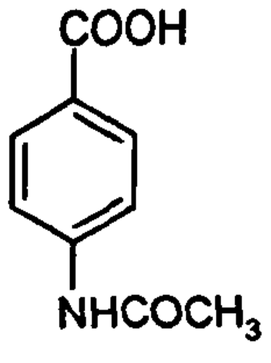 4-acetamidobenzoic acid	Organic, aromatic	4.30	No	No
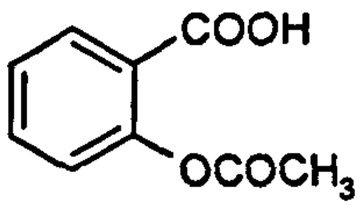 Acetyl Salicylic Acid	Organic, aromatic	3.50	No	No
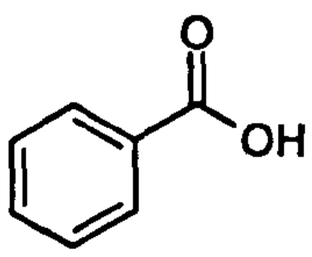 Benzoic Acid	Organic, aromatic	4.19	No	No
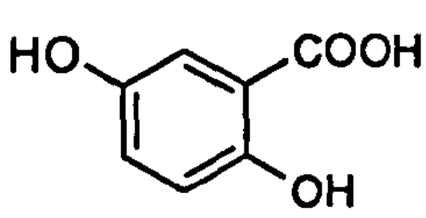 Gentisic Acid	Organic, aromatic	2.93	No	**Yellow solid formed in 30% (0.02g) yield**
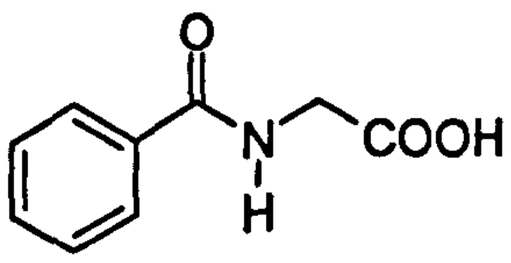 Hippuric Acid	Organic, aromatic	3.55	No	No
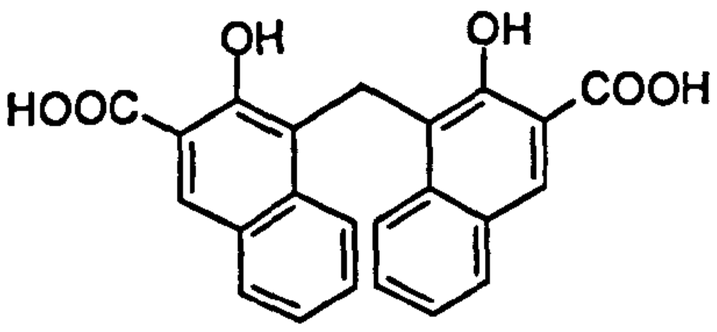 Pamoic Acid	Organic, aromatic	2.51, 3.10	No	No

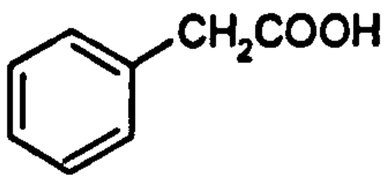 Phenyl Acetic Acid	Organic, aromatic	4.28	No	No
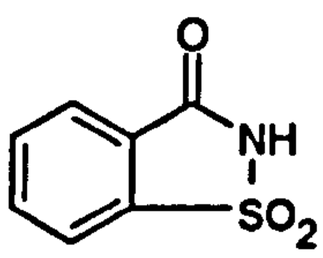 Saccharin	Organic, aromatic	1.80	No	No
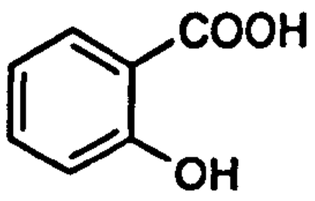 Salicylic Acid	Organic, aromatic	2.97, 13.82	No	No
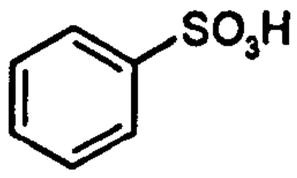 Benzenesulphonic Acid	Organic, aromatic	0.70	No	**Yellow solid formed in 43% (0.07g) yield**
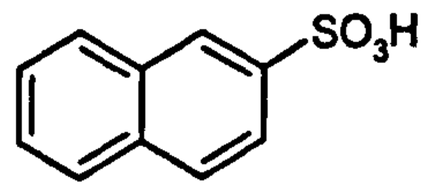 Naphthalene-2-sulfonic Acid	Organic, aromatic	0.17	No	No
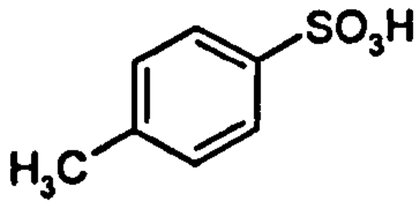 para-Toluenesulfonic Acid	Organic, aromatic	-1.34	No	**Yellow solid formed in 69% (0.12g) yield**

6.2.2 Determination of solubility

See Section 2.2.1.

6.2.2.1 Determination of the pH-solubility profile

The buffer systems used for the pH-solubility profile were 10mM acetate with pH range 2-4, 10mM phosphate with pH range 4-8 and 10mM glycine with pH range 8-12. Depending on the initial pH, either 1M NaOH or HCl was used to adjust the pH measured using a SevenEasy™ benchtop pH meter (Mettler-Toledo Inc., Ohio, USA). The saturation concentration in these buffer systems was determined by the shake-flask method.

6.2.2.2 Determination of the pKa

The measurement of the pH-solubility profiles was also used to determine the pKa of the ionisable compounds. The equations used for pKa determination for the acids and bases respectively were as follows [227]:

$$\mathrm{pH} = \mathrm{p}K_a + \log\left(\frac{S - S_0}{S_0}\right) \tag{6.3}$$

$$\mathrm{pH} = \mathrm{p}K_a - \log\left(\frac{S - S_0}{S_0}\right) \tag{6.4}$$

Where S_0 is the solubility of the unionised form of the drug in water and S is the observed solubility of the drug at different pH values. Plots of pH versus log $[(S - S_0)]/ S_0]$ were constructed and the intercept on the pH axis was taken as the pKa value.

6.2.3 Differential scanning calorimetry

See Section 2.2.3.

6.2.4 Scanning electron microscopy

See Section 2.2.4.

6.2.5 MTT in vitro cytotoxicity assay

See Section 3.2.6.

6.3 Results

6.3.1 Determination of solubility and pKa

6.3.1.1 Determination of DMU590 solubility and pKa

The aqueous solubility of DMU590 was 120 times higher compared with DMU212 and the solubility values measured on the UV plate reader and spectrophotometer were the same:

Table 41. Average solubility of DMU590 in water measured at 22± 2°C.

SOLVENT	AVERAGE SOLUBILITY OF DMU590 MEASURED ON THE UV PLATE READER (mg/mL) (n=3)	AVERAGE SOLUBILITY OF DMU590 MEASURED ON THE UV SPECTROPHOTOMETER (mg/mL) (n=3)
Water	0.120 ± 0.004	0.120 ± 0.009

Table 42. Solubility of DMU590 in different buffers measured at 22± 2°C.

pH	AVERAGE SOLUBILITY OF DMU590 MEASURED ON THE UV PLATE READER (mg/mL) (n=3)	AVERAGE SOLUBILITY OF DMU590 MEASURED ON THE UV SPECTROPHOTOMETER (mg/mL) (n=3)
2.0	0.678 ± 0.062	0.635 ± 0.073
3.0	0.648 ± 0.059	0.626 ± 0.026
4.0	0.568 ± 0.021	0.572 ± 0.016
5.0	0.716 ± 0.060	0.754 ± 0.005
5.5	0.642 ± 0.104	0.622 ± 0.132
6.0	0.297 ± 0.014	0.293± 0.009
6.5	0.203 ± 0.008	0.206 ± 0.002
7.0	0.150 ± 0.005	0.158 ± 0.007
8.0	0.103 ± 0.009	0.093 ± 0.004
9.0	0.108 ± 0.018	0.098 ± 0.007
10.0	0.107 ± 0.009	0.106 ± 0.003
11.0	0.130 ± 0.014	0.129 ± 0.025
12.0	0.137 ± 0.016	0.124 ± 0.011

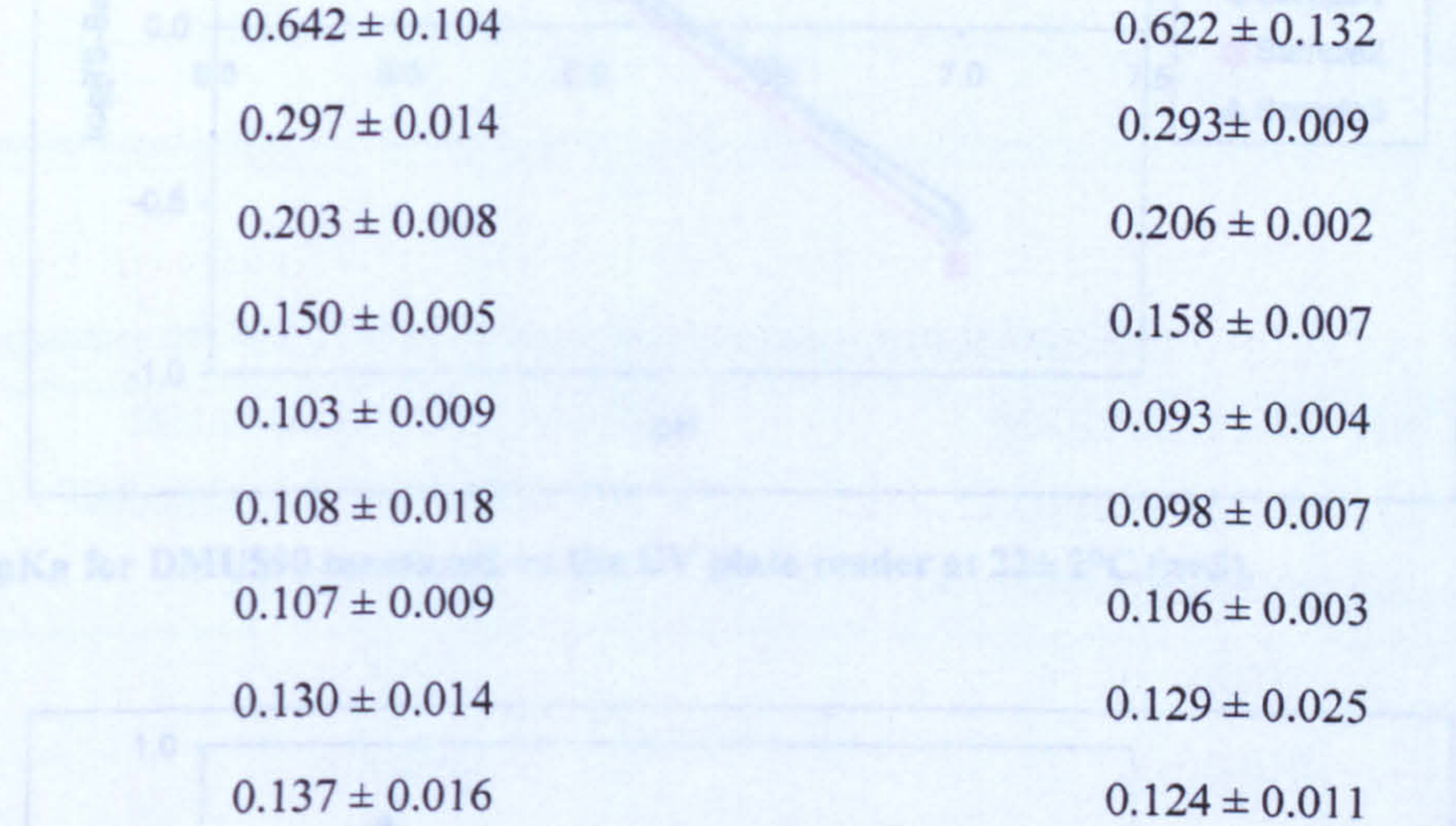

Figure 86. pH solubility profile for DMU590 measured on the UV plate reader and spectrophotometer at 22± 2°C (n=3).

The pH-solubility profile of DMU590 showed the free base to be most soluble at low pH values between pH 2-5.5. Above pH 5.5 the solubility began to drop off. The pKa of DMU590 was also determined from the pH-solubility profile:

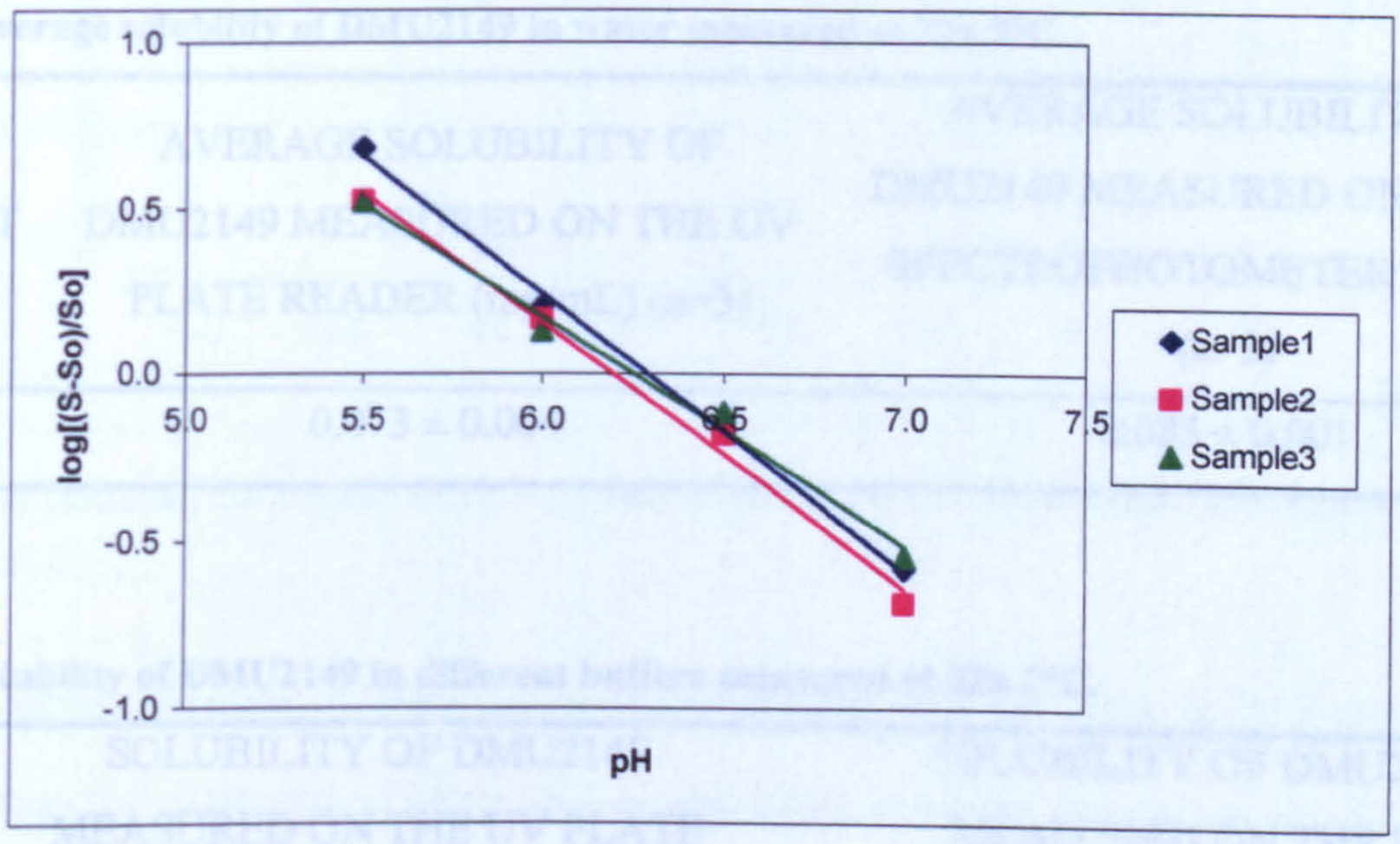

Figure 87. pKa for DMU590 measured on the UV plate reader at 22± 2°C (n=3).

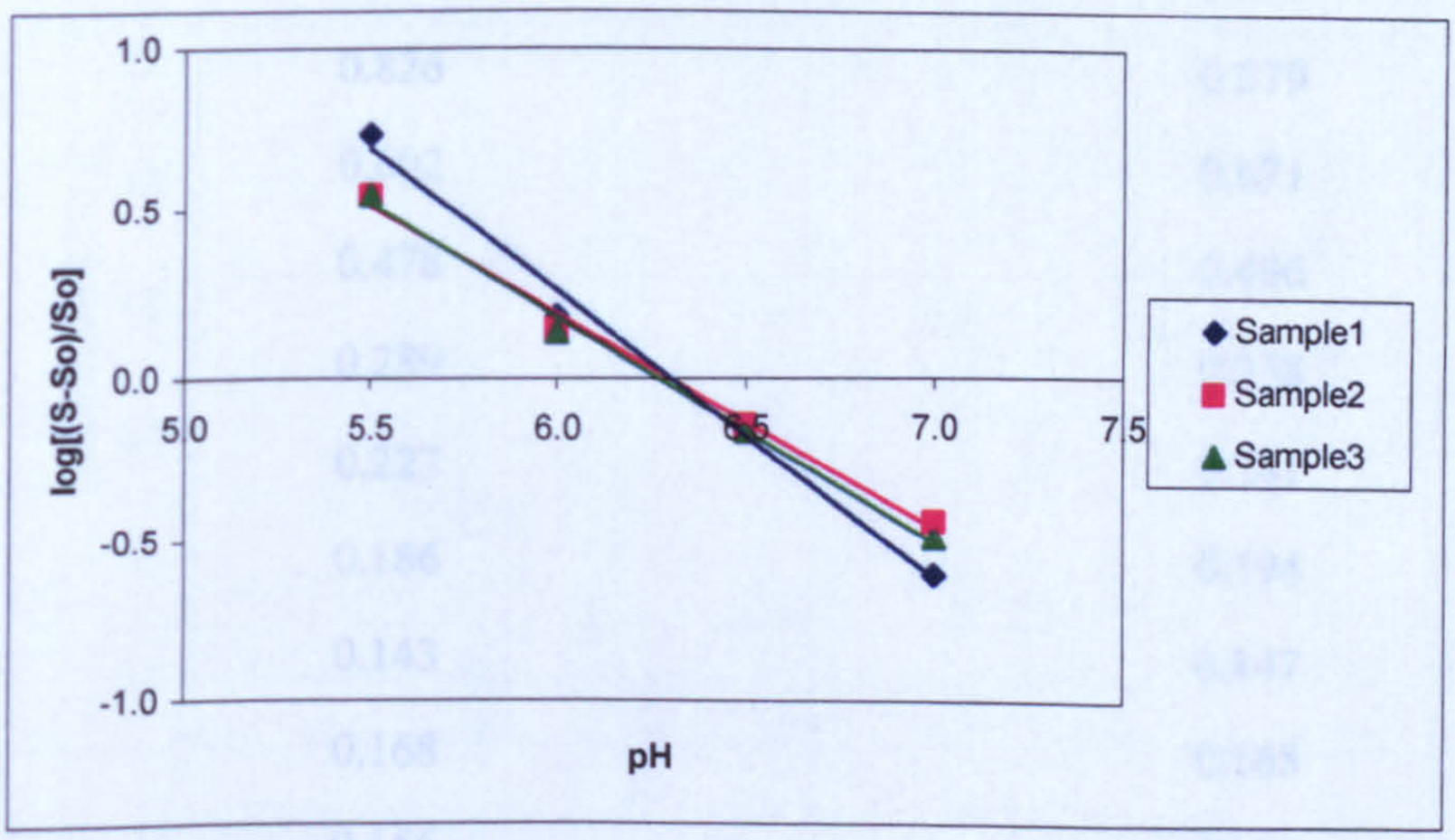

Figure 88. pKa for DMU590 measured on the UV spectrophotometer at 22± 2°C (n=3).

The pKa of DMU590 calculated using both its pH-solubility profile and aqueous solubility was 6.23 from the UV plate reader and 6.29 from the UV spectrophotometer.

6.3.1.2 Determination of DMU2149 solubility and pKa

The aqueous solubility of DMU2149 was measured at 0.073 mg/mL on the UV plate reader and 0.085 mg/mL on the UV spectrophotometer:

Table 43. Average solubility of DMU2149 in water measured at 22± 2°C.

SOLVENT	AVERAGE SOLUBILITY OF DMU2149 MEASURED ON THE UV PLATE READER (mg/mL) (n=3)	AVERAGE SOLUBILITY OF DMU2149 MEASURED ON THE UV SPECTROPHOTOMETER (mg/mL) (n=3)
Water	0.073 ± 0.004	0.085 ± 0.001

Table 44. Solubility of DMU2149 in different buffers measured at 22± 2°C.

pH	SOLUBILITY OF DMU2149 MEASURED ON THE UV PLATE READER (mg/mL)	SOLUBILITY OF DMU2149 MEASURED ON THE UV SPECTROPHOTOMETER (mg/mL)
2.00	3.731	3.697
3.00	0.826	0.879
3.25	0.602	0.671
3.50	0.478	0.486
3.75	0.289	0.338
4.00	0.227	0.241
5.00	0.186	0.194
7.00	0.143	0.147
9.00	0.168	0.165
11.00	0.156	0.152

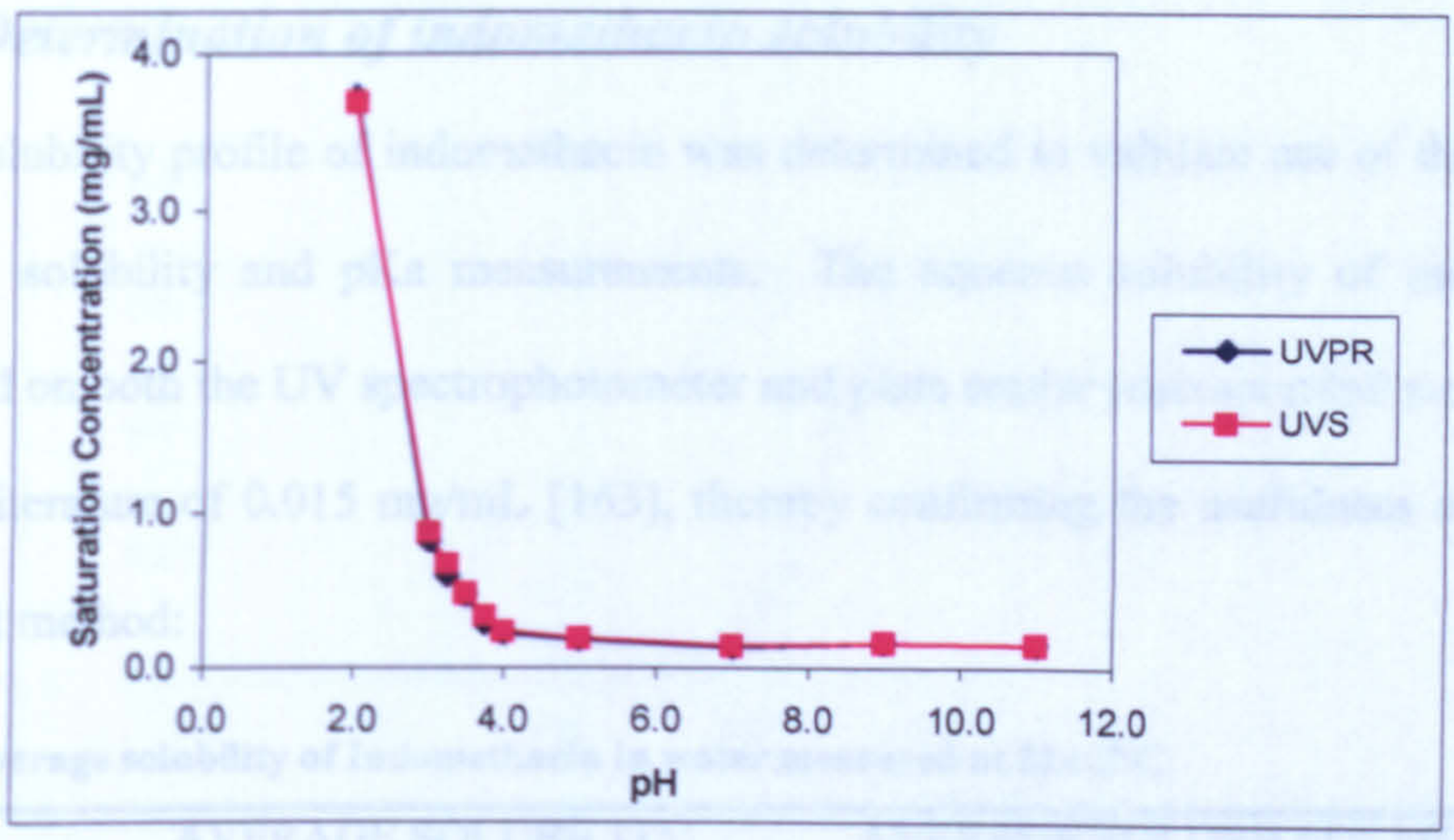

Figure 89. pH solubility profile for DMU2149 measured on the UV plate reader and spectrophotometer at 22± 2°C.

The pH-solubility profile of DMU2149 again showed the free base to be most soluble at low pH values, in particular at pH 2 above which the solubility began to steadily decrease.

The pKa of DMU2149 was also determined from the pH-solubility profile:

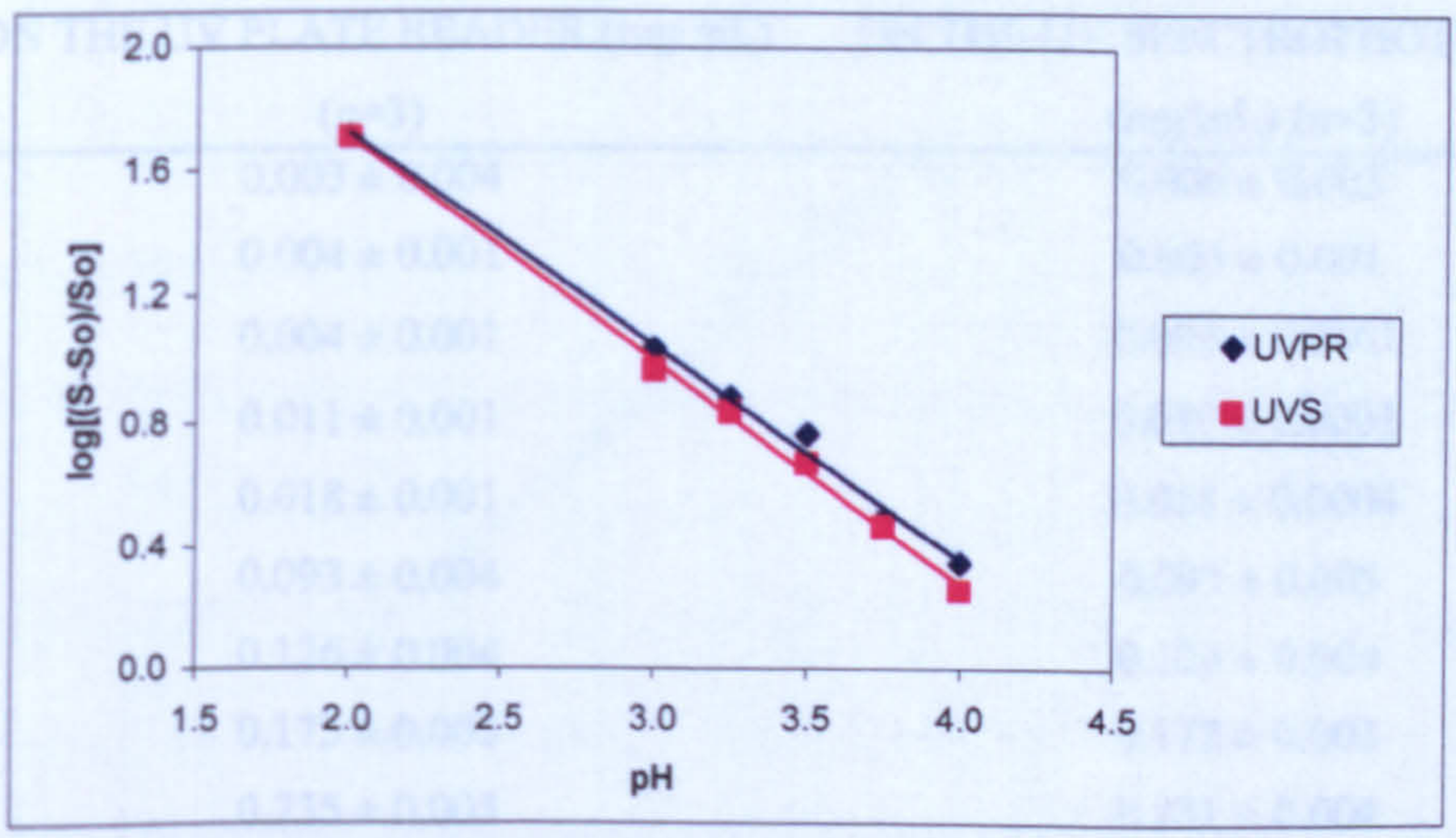

Figure 90. pKa for DMU2149 measured on the UV plate reader and spectrophotometer at 22± 2°C.

The pKa of DMU2149 calculated using both its pH-solubility profile and aqueous solubility was 4.53 from the UV plate reader and 4.40 from the UV spectrophotometer.

6.3.1.3 Determination of indomethacin solubility

The pH-solubility profile of indomethacin was determined to validate use of the UV plate reader for solubility and pKa measurements. The aqueous solubility of indomethacin determined on both the UV spectrophotometer and plate reader corresponded well with that stated in literature of 0.015 mg/mL [163], thereby confirming the usefulness of the high-throughput method:

Table 45. Average solubility of Indomethacin in water measured at 22± 2°C.

SOLVENT	AVERAGE SOLUBILITY MEASURED ON THE UV PLATE READER (mg/mL) (n=3)	AVERAGE SOLUBILITY MEASURED ON THE UV SPECTROPHOTOMETER (mg/mL) (n=3)
Water	0.010 ± 0.001	0.010 ± 0.001

Table 46. Solubility of indomethacin in different buffers measured at 22± 2°C.

pH	AVERAGE SOLUBILITY MEASURED ON THE UV PLATE READER (mg/mL) (n=3)	AVERAGE SOLUBILITY MEASURED ON THE UV SPECTROPHOTOMETER (mg/mL) (n=3)
2.00	0.003 ± 0.004	0.006 ± 0.003
4.00	0.004 ± 0.001	0.005 ± 0.001
4.50	0.004 ± 0.001	0.003 ± 0.0001
5.00	0.011 ± 0.001	0.010 ± 0.0001
5.50	0.018 ± 0.001	0.018 ± 0.0004
6.00	0.093 ± 0.004	0.093 ± 0.005
6.25	0.126 ± 0.004	0.124 ± 0.004
6.50	0.173 ± 0.005	0.172 ± 0.003
6.75	0.235 ± 0.005	0.231 ± 0.004
7.00	0.408 ± 0.009	0.372 ± 0.013
7.50	0.614 ± 0.069	0.589 ± 0.050
8.00	0.655 ± 0.034	0.641 ± 0.019
9.00	0.704 ± 0.008	0.643 ± 0.019

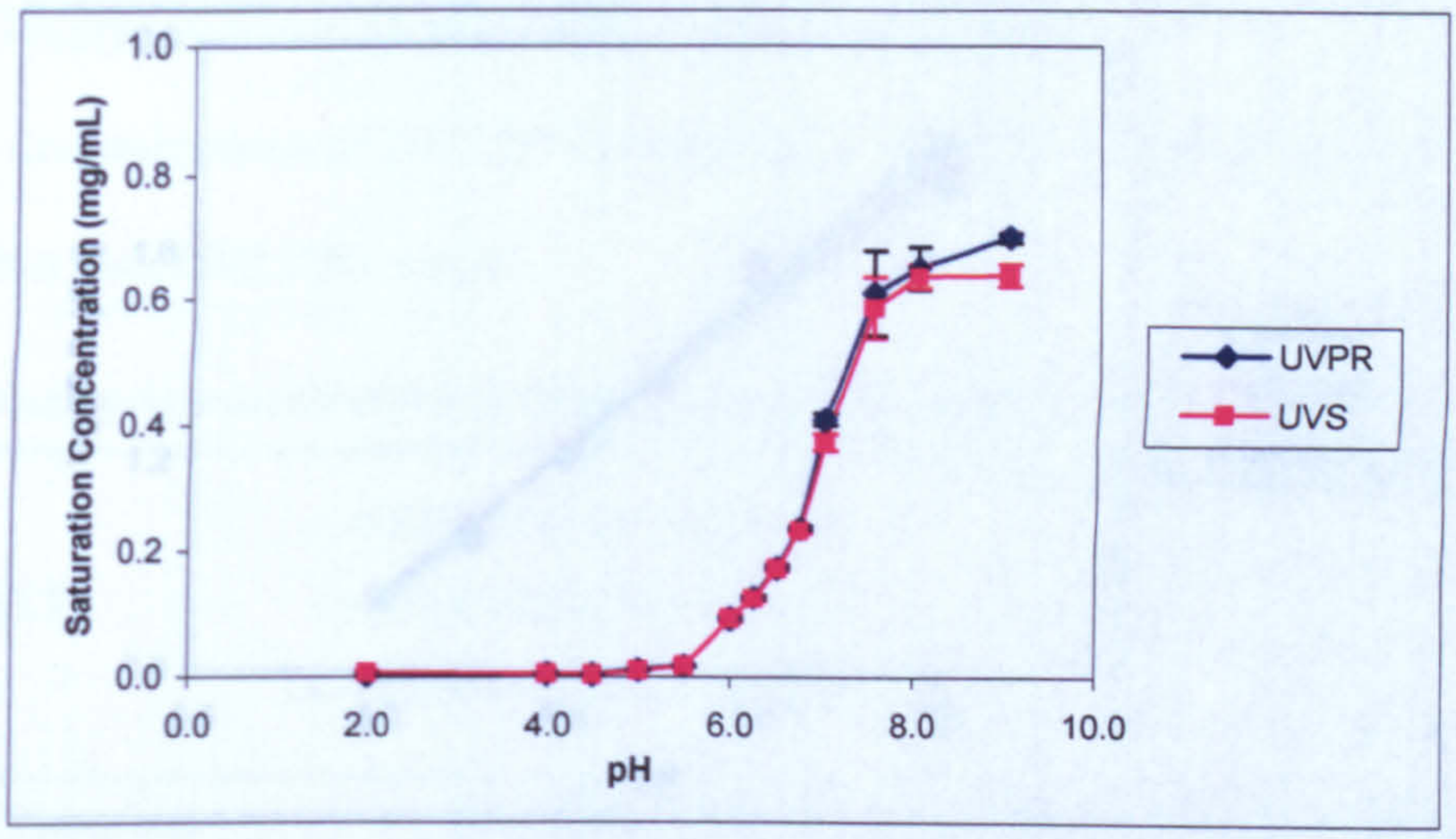

Figure 91. pH solubility profile for indomethacin measured on the UV plate reader and spectrophotometer at 22± 2°C (n=3).

The pH-solubility profile of indomethacin showed the free acid to be most soluble at high pH values between pH 6-9. Below pH 6 the solubility began to drop off. The pKa of indomethacin was also determined from the pH-solubility profile:

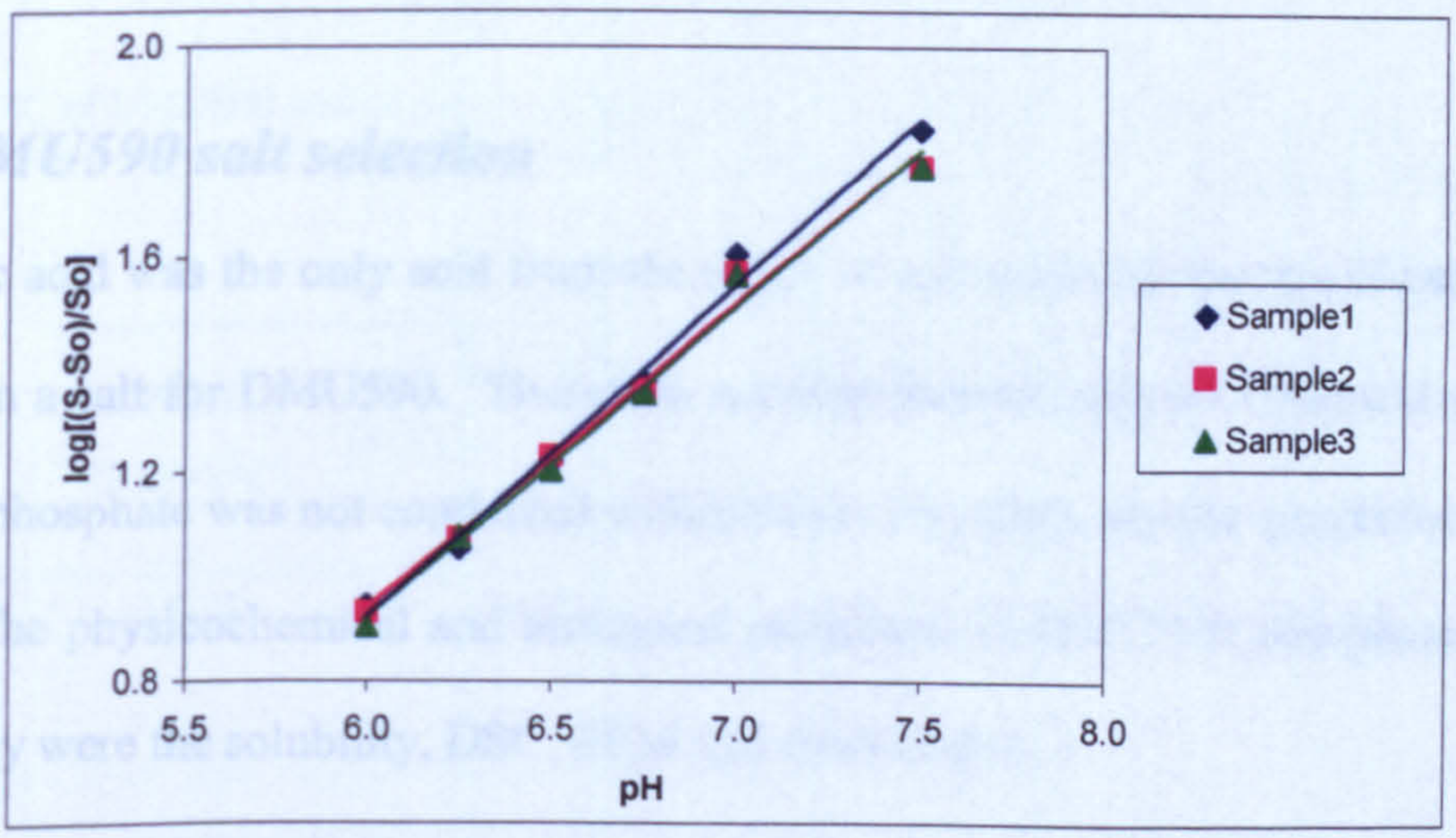

Figure 92. pKa for indomethacin measured on the UV plate reader at 22± 2°C (n=3).

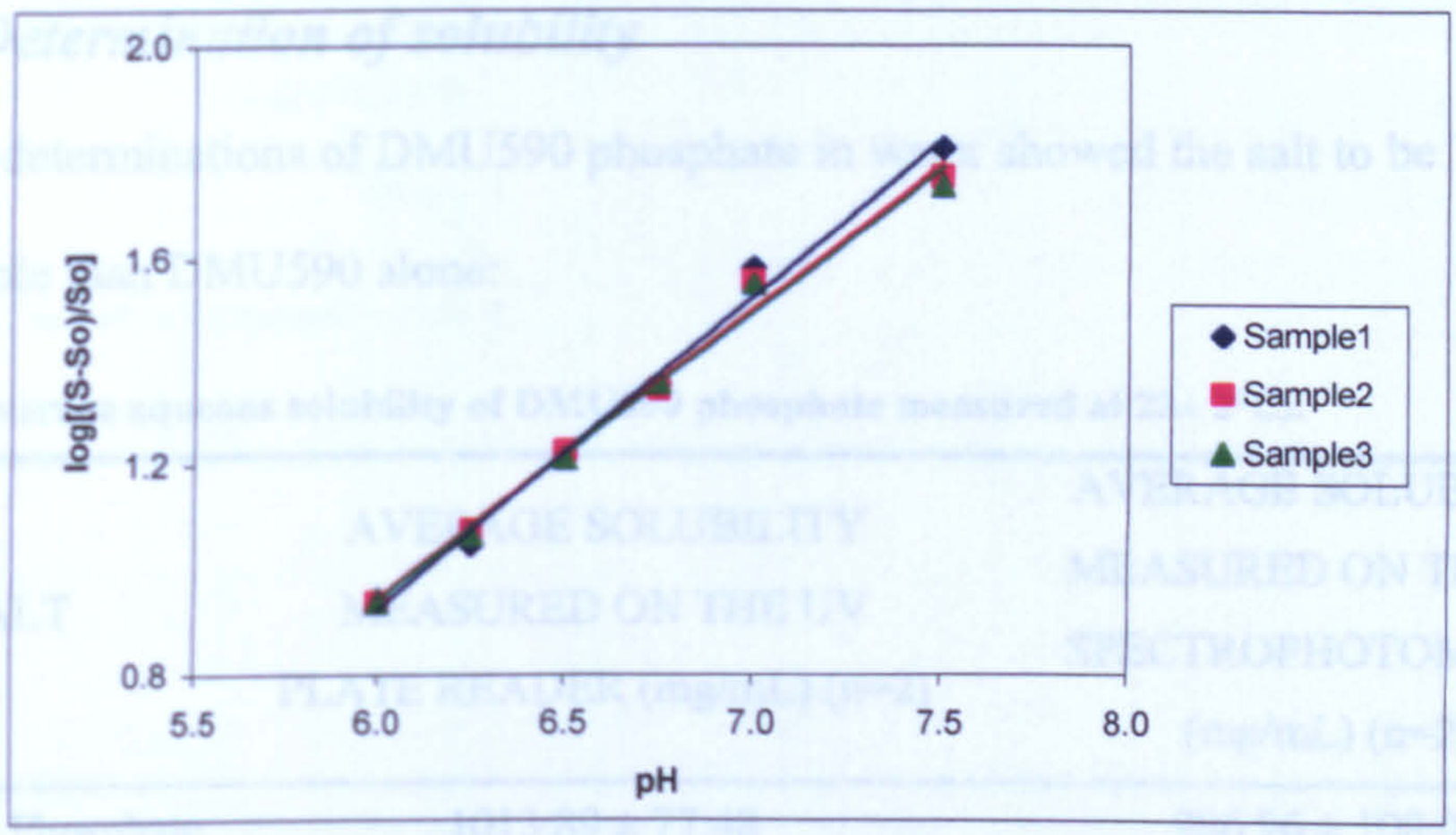

Figure 93. pKa for indomethacin measured on the UV spectrophotometer at 22± 2°C (n=3).

The pKa of indomethacin calculated using both its pH-solubility profile and aqueous solubility was 4.43 from the UV plate reader and 4.37 from the UV spectrophotometer. These values compare favourably with the value of 4.5 stated in literature [228], thereby justifying the use of the UV plate reader for pKa measurement.

6.3.2 DMU590 salt selection

Phosphoric acid was the only acid from the range of salt selecting species screened (Table 40) to form a salt for DMU590. Therefore, a comprehensive physicochemical analysis of DMU590 phosphate was not conducted within this study, since sample quantities were very limited. The physicochemical and biological properties of DMU590 phosphate measured in this study were the solubility, DSC, SEM and cytotoxicity.

6.3.2.1 Determination of solubility

Solubility determinations of DMU590 phosphate in water showed the salt to be 10,000-fold more soluble than DMU590 alone:

Table 47. Average aqueous solubility of DMU590 phosphate measured at 22± 2°C..

SALT	AVERAGE SOLUBILITY MEASURED ON THE UV PLATE READER (mg/mL) (n=2)	AVERAGE SOLUBILITY MEASURED ON THE UV SPECTROPHOTOMETER (mg/mL) (n=2)
DMU590 Phosphate	1013.89 ± 77.48	986.96 ± 108.09

6.3.2.2 Differential scanning calorimetry

DSC measurements for DMU590 showed the drug to exist in an amorphous form, with no melting point endotherms. However, DMU590 phosphate was crystalline, but there were no polymorphs, solvates and impurities, since a single endotherm peak was detected:

Table 48. DSC of DMU590 and its salts – initial heating from -100-300°C at 400°C/min.

DRUG	T_g			MELTING POINT ENDOTHERM		
	ONSET TEMP (°C)	T_g HALF EXTRAPOLATED (°C)	DELTA C_p (J/g*°C)	ONSET TEMP (°C)	PEAK TEMP (°C)	DELTA H (J/g)
DMU590	-15.88	-11.65	0.30	–	–	–
DMU590 Phosphate	–	–	–	165.12	171.38	81.96

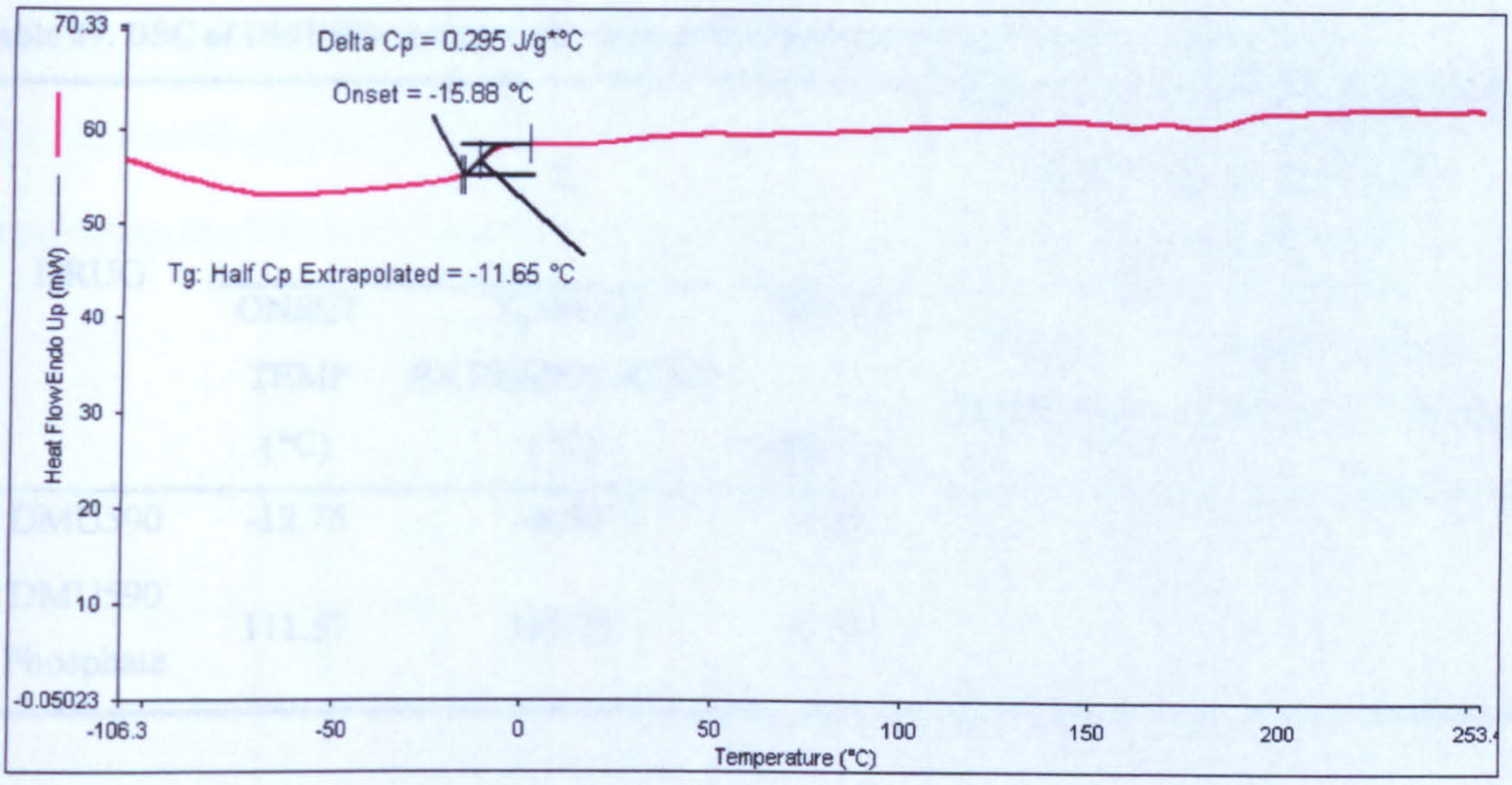

Figure 94. DSC thermogram for DMU590.

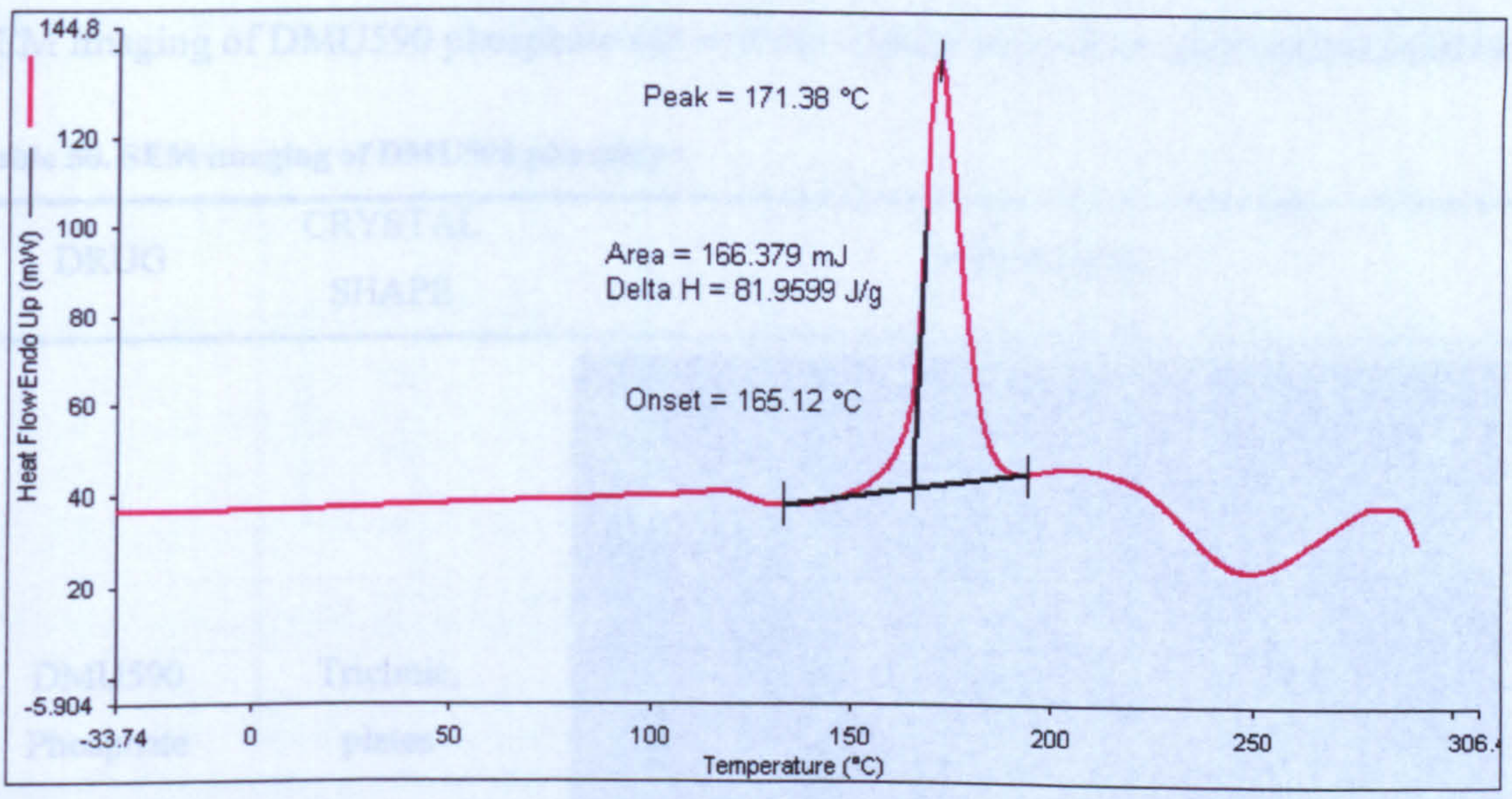

Figure 95. DSC thermogram for DMU590 phosphate.

Immediately after the initial scan the samples were rapidly cooled and reheated to determine if any recrystallization was apparent. The second DSC scan for both compounds did not show immediate recrystallization:

Table 49. DSC of DMU590 and its salts –immediate re-heat from -100-300°C at 400°C/min.

DRUG	T_g			MELTING POINT ENDOTHERM/ RE-CRYSTALLIZATION EXOTHERM		
	ONSET TEMP (°C)	T_g HALF EXTRAPOLATED (°C)	DELTA C_p (J/g*°C)	ONSET TEMP (°C)	PEAK TEMP (°C)	DELTA H (J/g)
DMU590	-12.76	-6.50	0.34	–	–	–
DMU590 Phosphate	111.57	135.75	0.72	–	–	–

6.3.2.3 Scanning electron microscopy

SEM imaging of DMU590 phosphate showed the crystals to exist as agglomerated plates:

Table 50. SEM imaging of DMU590 phosphate.

DRUG	CRYSTAL SHAPE	SEM IMAGE
DMU590 Phosphate	Triclinic, plates	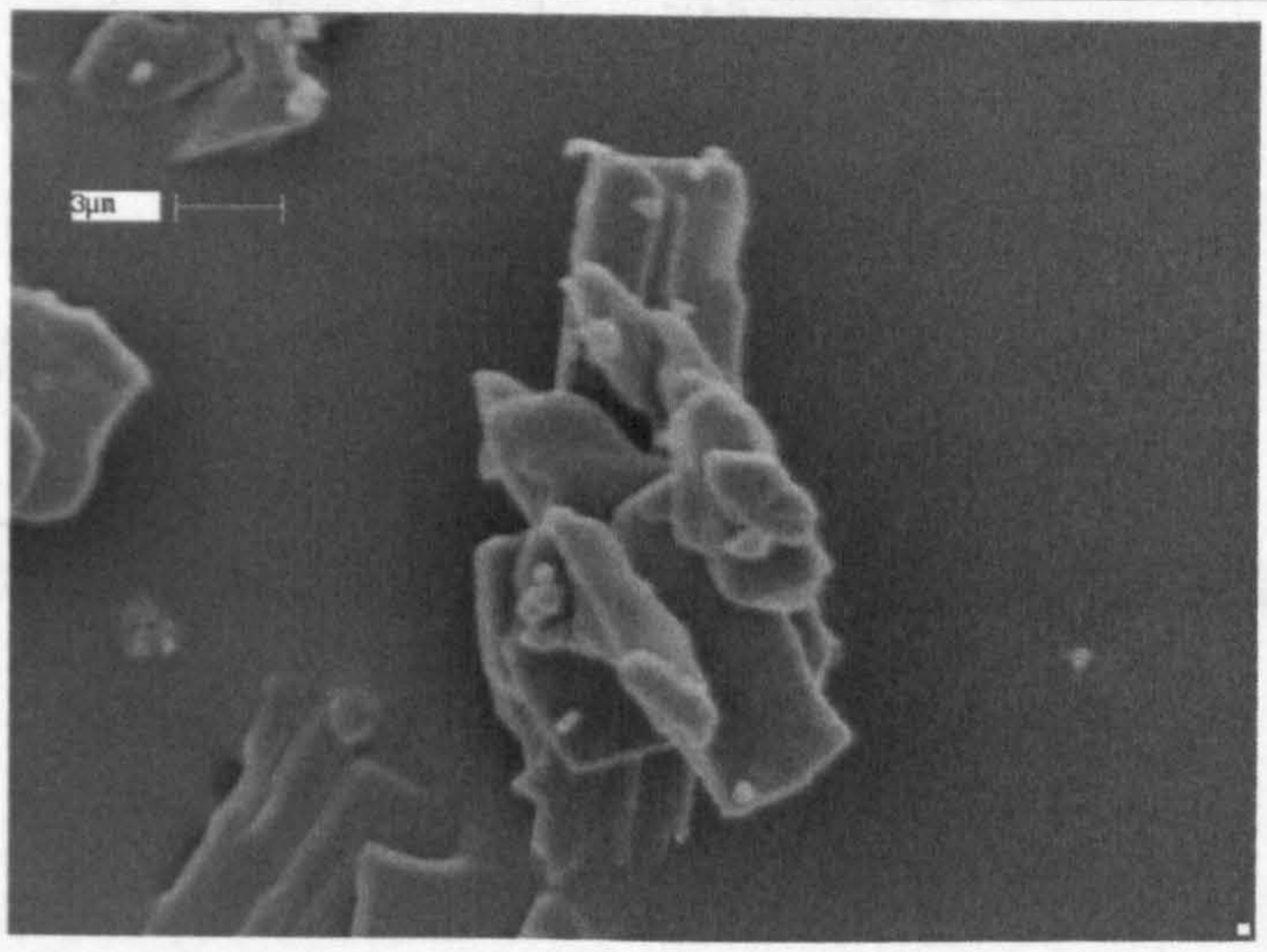

6.3.2.4 Biological evaluation of DMU590 salts

The biological activity of DMU590 and DMU590 phosphate was evaluated with the MTT assay using the CDDG in-house breast cell panel of MCF7, MDA-MB-468 and MCF10A:

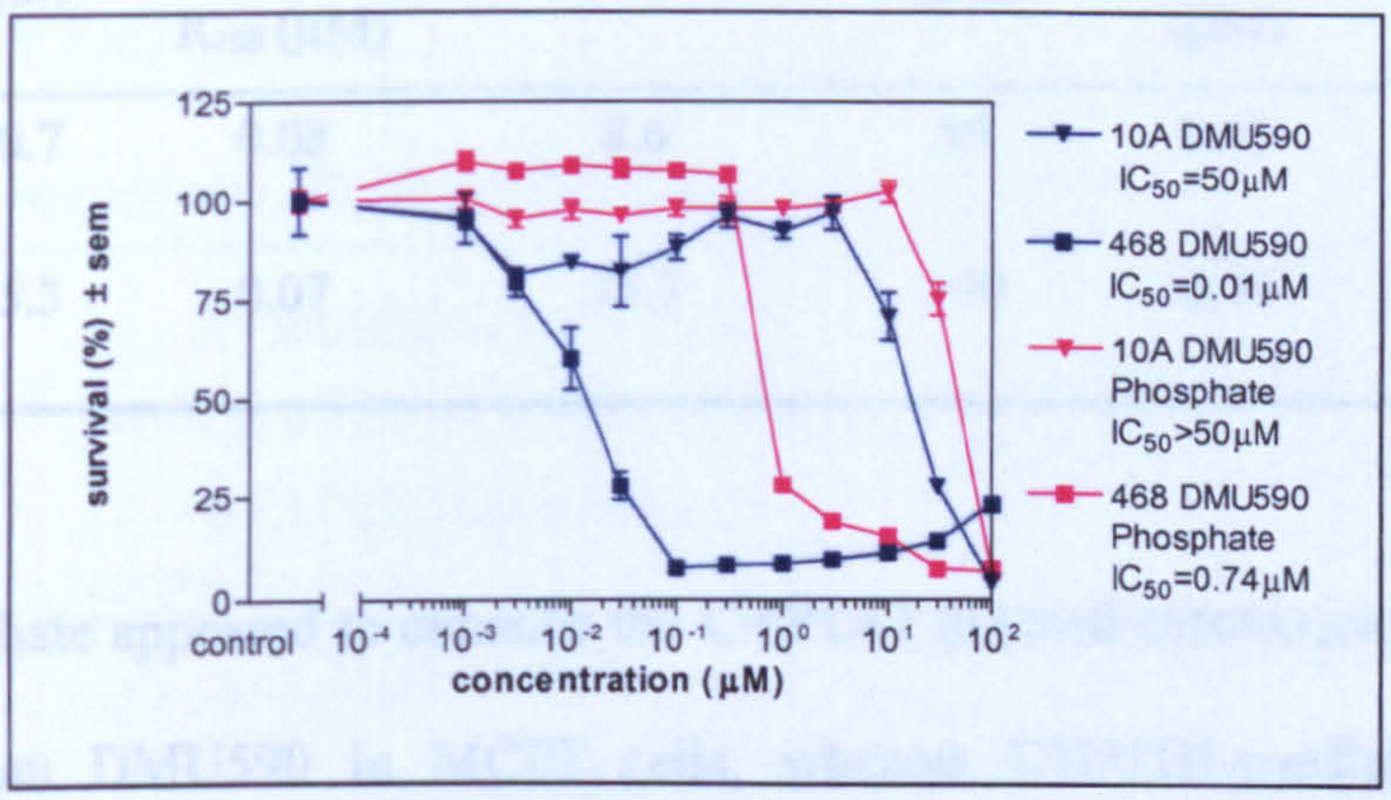

Figure 96. Cytotoxicity profile of DMU590 and DMU590 phosphate in MDA-MB-468 and MCF10A cell lines.

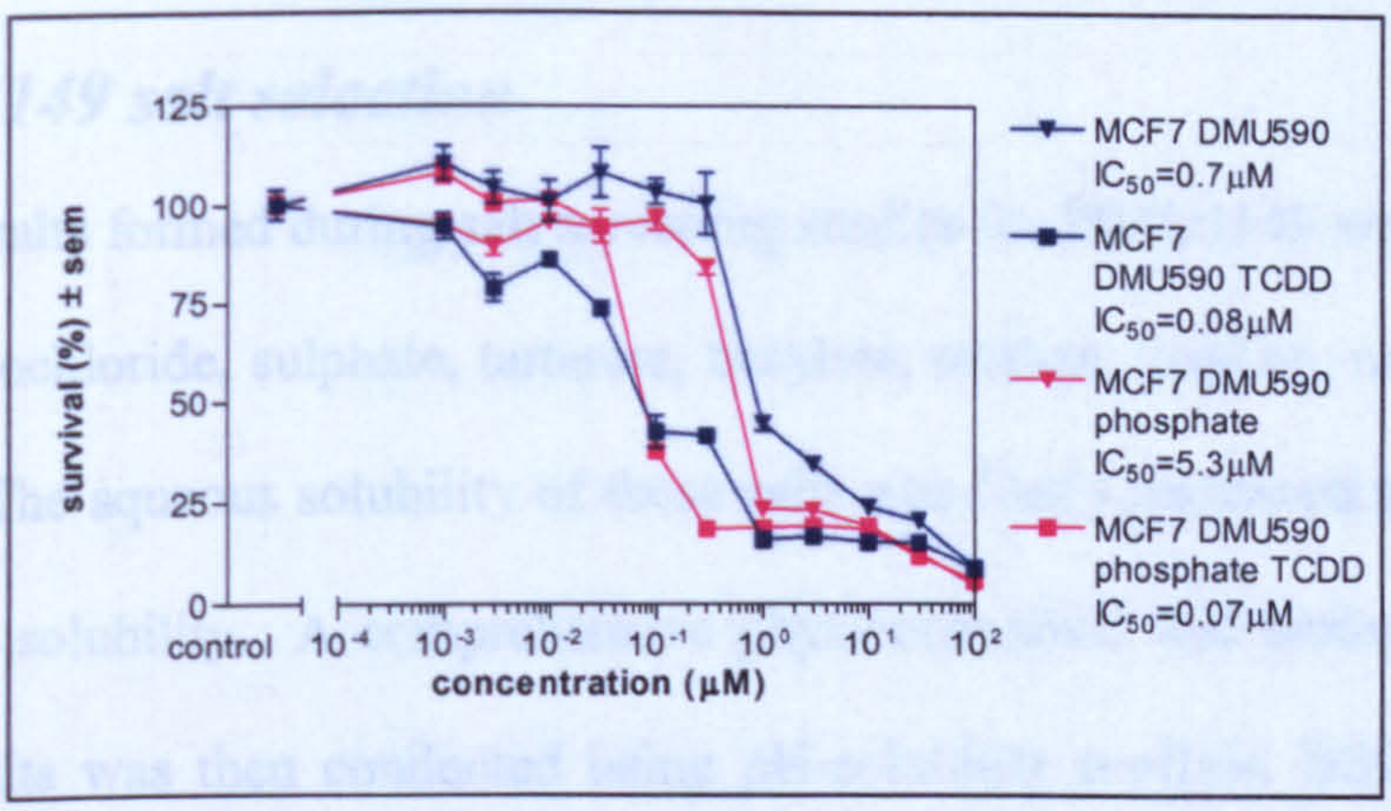

Figure 97. Cytotoxicity profile of DMU590 and DMU590 phosphate in MCF7 with and without TCDD induction.

Table 51. Biological evaluation of DMU590 and the corresponding phosphate salt.

DRUG	MCF7 IC_{50} (μM)	MCF7 TCDD INDUCED IC_{50} (μM)	ACTIVATION FACTOR	MCF10A IC_{50} (μM)	MDA-MB-468 IC_{50} (μM)	TUMOUR SELECTIVE FACTOR
DMU590	0.7	0.08	8.6	50	0.01	5000
DMU590 phosphate	5.3	0.07	75.7	>50	0.74	67.6

DMU590 phosphate appeared to enhance the CYP1A1 induced cytotoxicity approximately 9-fold more than DMU590 in MCF7 cells, whereas CYP1B1-mediated cytotoxicity demonstrated a 75-fold decrease in salt potency compared to the parent compound.

6.3.3 DMU2149 salt selection

The crystalline salts formed during salt screening studies for DMU2149 were the mesylate, phosphate, hydrochloride, sulphate, tartarate, besylate, oxalate, tosylate, maleate, fumarate and gentisate. The aqueous solubility of these salts was firstly measured to eliminate salts with the lowest solubility. A comprehensive physicochemical and biological analysis of the optimum salts was then conducted using pH-solubility profiles, DSC, SEM and the MTT assay.

6.3.3.1 Determination of solubility

The best DMU2149 salt forms in terms of aqueous solubility were the mesylate, phosphate, hydrochloride and sulphate respectively, and as such a comprehensive preformulation study was conducted for each of them:

Table 52. Average aqueous solubility of DMU2149 salts measured at 22± 2°C.

SALT	AVERAGE SOLUBILITY MEASURED ON THE UV PLATE READER (mg/mL) (n=2)	AVERAGE SOLUBILITY MEASURED ON THE UV SPECTROPHOTOMETER (mg/mL) (n=2)
Mesylate	27.740 ± 0.068	27.794 ± 2.226
Phosphate	18.547 ± 0.471	19.475 ± 0.071
Hydrochloride	16.044 ± 0.258	17.011 ± 0.486
Sulphate	15.094 ± 0.589	13.355 ± 0.628
Tartarate	9.747 ± 0.699	10.302 ± 0.600
Besylate	8.883 ± 0.069	9.126 ± 0.226
Oxalate	6.010 ± 1.750	5.676 ± 1.700
Tosylate	2.647 ± 0.305	3.308 ± 0.015
Maleate	1.066 ± 0.059	1.132 ± 0.117
Fumarate	0.908 ± 0.161	0.883 ± 0.169
Gentisate	0.301 ± 0.023	0.293 ± 0.022

To further evaluate the DMU2149 salt forms with the highest aqueous solubility, their pH-solubility profiles were determined:

Table 53. Solubility of DMU2149 salts in different buffers measured at 22± 2°C.

SALT	pH	SOLUBILITY MEASURED ON THE UV PLATE READER (mg/mL)	SOLUBILITY MEASURED ON THE UV SPECTROPHOTOMETER (mg/mL)
Mesylate	2	32.435	31.657
Mesylate	4	24.042	23.559
Mesylate	7	4.120	4.100
Mesylate	10	1.597	1.554
Mesylate	12	0.156	0.175
Hydrochloride	2	12.836	12.794
Hydrochloride	4	4.870	4.943
Hydrochloride	7	7.647	7.631
Hydrochloride	10	2.323	2.149
Hydrochloride	12	0.104	0.124
Phosphate	2	12.728	13.418
Phosphate	4	12.705	12.525
Phosphate	7	11.389	11.232
Phosphate	10	6.356	5.480
Phosphate	12	0.261	0.282
Sulphate	2	14.395	15.581
Sulphate	4	13.844	13.871
Sulphate	7	17.554	17.856
Sulphate	10	12.312	13.284
Sulphate	12	0.133	0.156

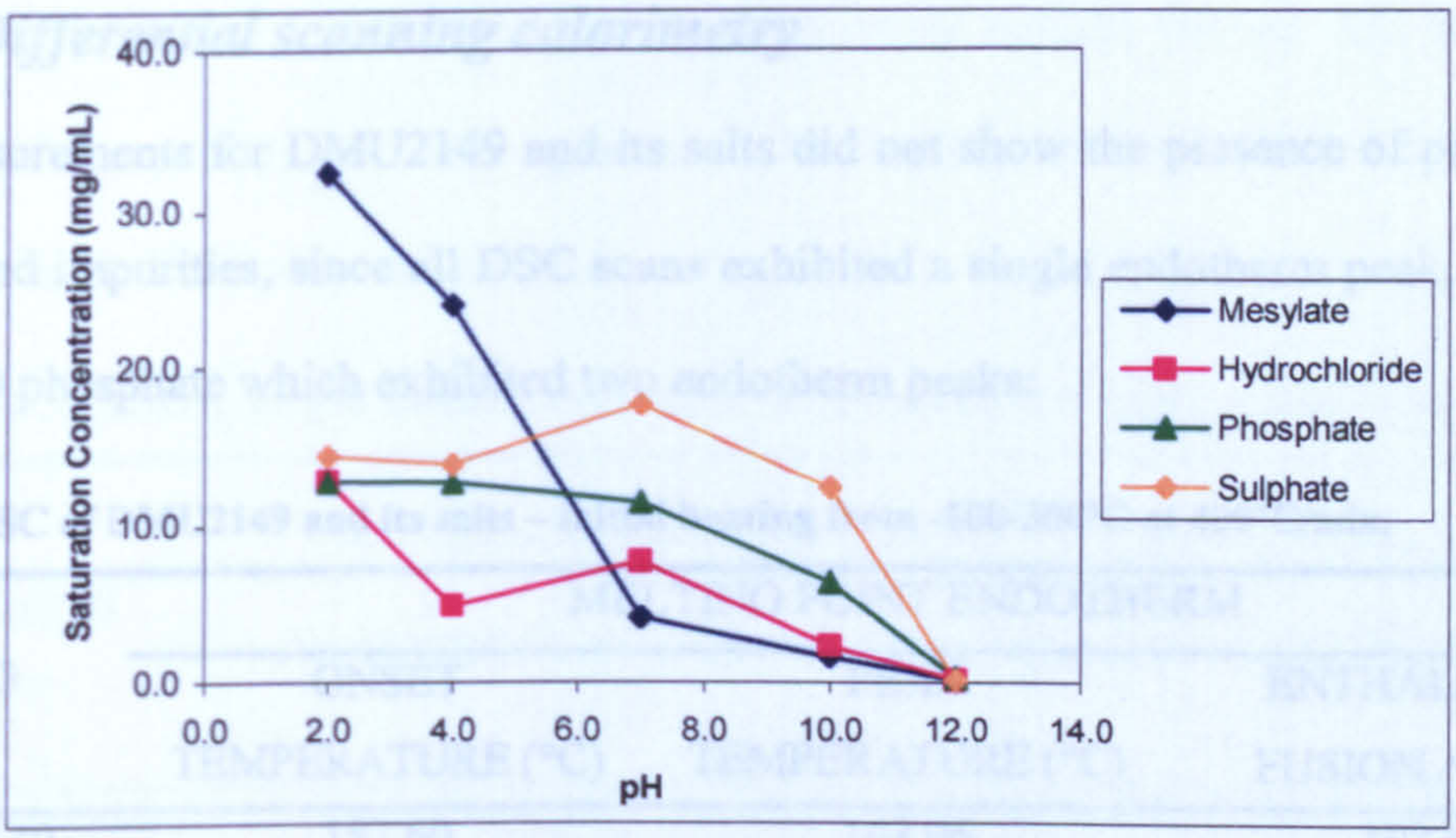

Figure 98. pH solubility profiles for DMU2149 salts measured on the UV plate reader at 22± 2°C.

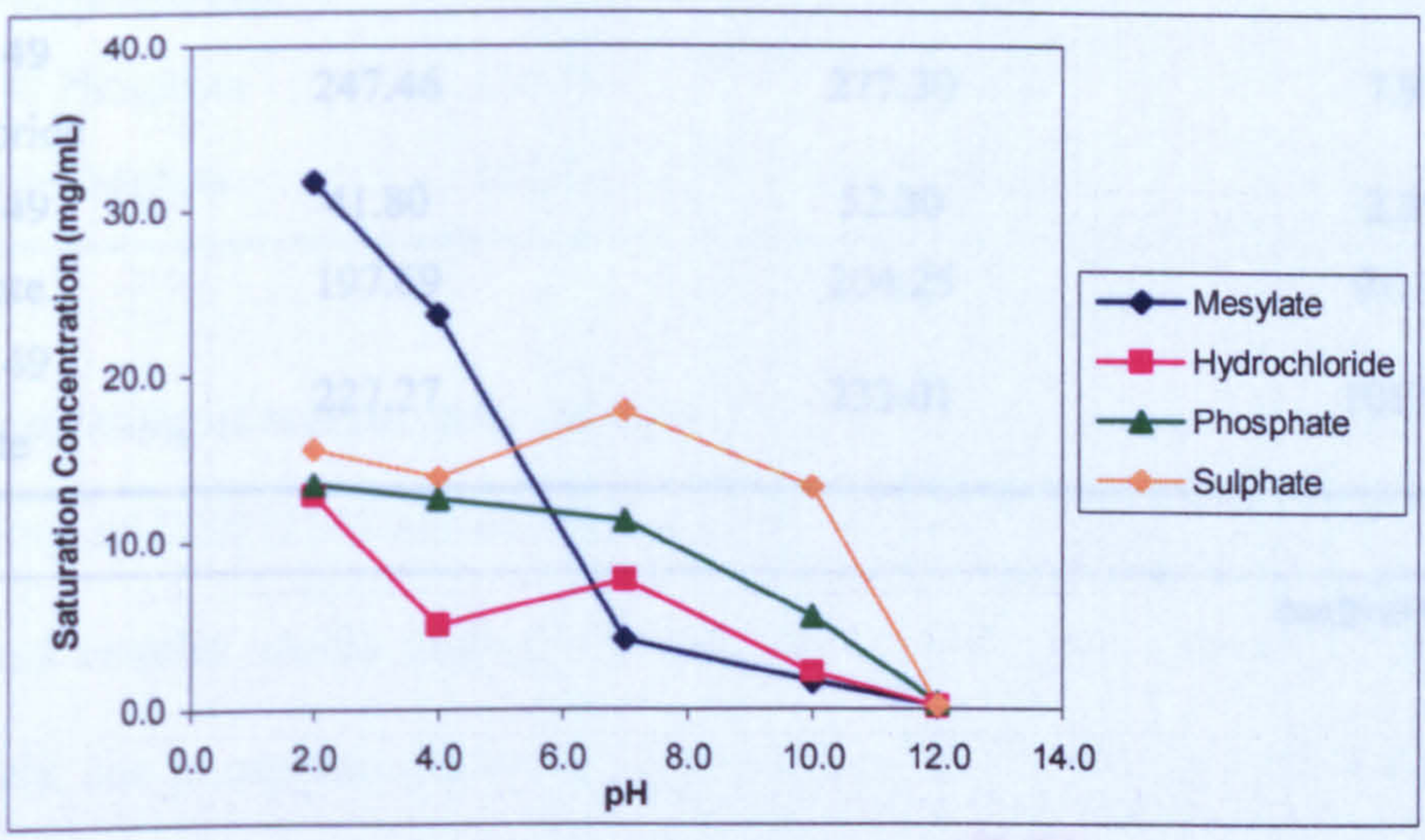

Figure 99. pH solubility profiles for DMU2149 salts measured on the UV spectrophotometer at 22± 2°C.

The pH-solubility profile of DMU2149 salts showed the salts to be most soluble at low pH values between pH 2-4 where the mesylate had the highest solubility at pH 2. DMU2149 sulphate had the highest solubility over a wide pH range of 2-10.

6.3.3.2 Differential scanning calorimetry

DSC measurements for DMU2149 and its salts did not show the presence of polymorphs, solvates and impurities, since all DSC scans exhibited a single endotherm peak, except for DMU2149 phosphate which exhibited two endotherm peaks:

Table 54. DSC of DMU2149 and its salts – initial heating from -100-300°C at 400°C/min.

DRUG	MELTING POINT ENDOTHERM		
	ONSET TEMPERATURE (°C)	PEAK TEMPERATURE (°C)	ENTHALPY OF FUSION ΔH (J/g)
DMU2149	157.60	163.06	102.58
DMU2149 Mesylate	257.74	264.50	160.96
DMU2149 Hydrochloride	247.46	277.30	7.97
DMU2149 Phosphate	41.80	52.30	2.30
	197.69	204.25	91.71
DMU2149 Sulphate	227.27	233.01	101.88

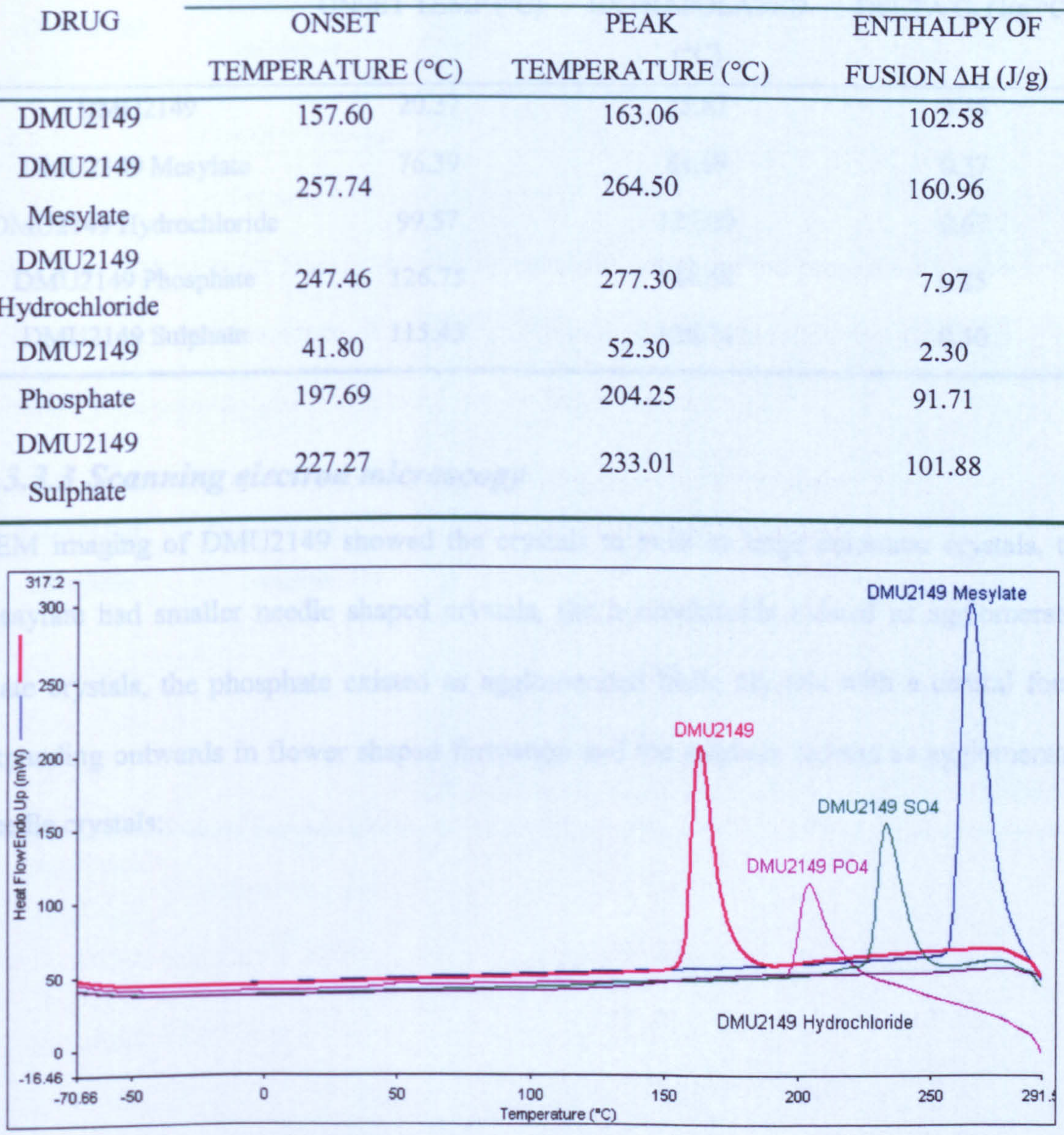

Figure 100. DSC thermograms of DMU2149 salts compared to the free base.

Immediately after the initial scan the samples were rapidly cooled and reheated to determine if recrystallization was apparent. The second DSC scan for all compounds showed no immediate recrystallization:

Table 55. DSC of DMU2149 and its salts –immediate re-heat from -100-300°C at 400°C/min.

DRUG	T_g ONSET TEMP (°C)	T_g HALF EXTRAPOLATED (°C)	DELTA C_p (J/g°°C)
DMU2149	20.37	25.87	0.55
DMU2149 Mesylate	76.39	81.69	0.37
DMU2149 Hydrochloride	99.57	125.00	0.67
DMU2149 Phosphate	126.75	144.68	0.85
DMU2149 Sulphate	115.43	126.74	0.50

6.3.3.3 Scanning electron microscopy

SEM imaging of DMU2149 showed the crystals to exist as large columnar crystals, the mesylate had smaller needle shaped crystals, the hydrochloride existed as agglomerated plate crystals, the phosphate existed as agglomerated blade crystals with a central focus expanding outwards in flower shaped formation and the sulphate existed as agglomerated needle crystals:

Table 56. SEM imaging of DMU2149 and its salts.

DRUG	CRYSTAL SHAPE	SEM IMAGE
DMU2149	Orthorhombic, columnar	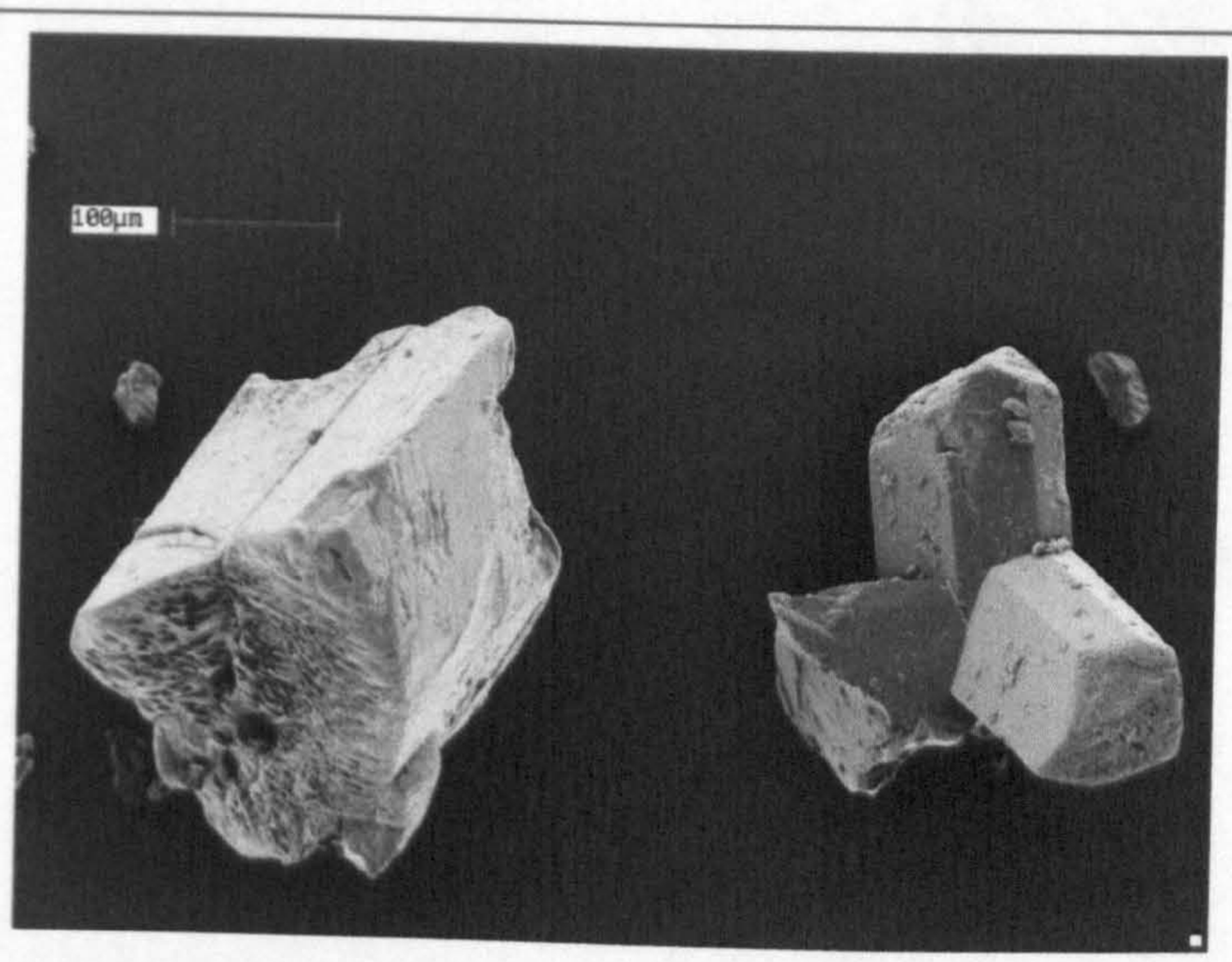
DMU2149 Mesylate	Orthorhombic, Needles	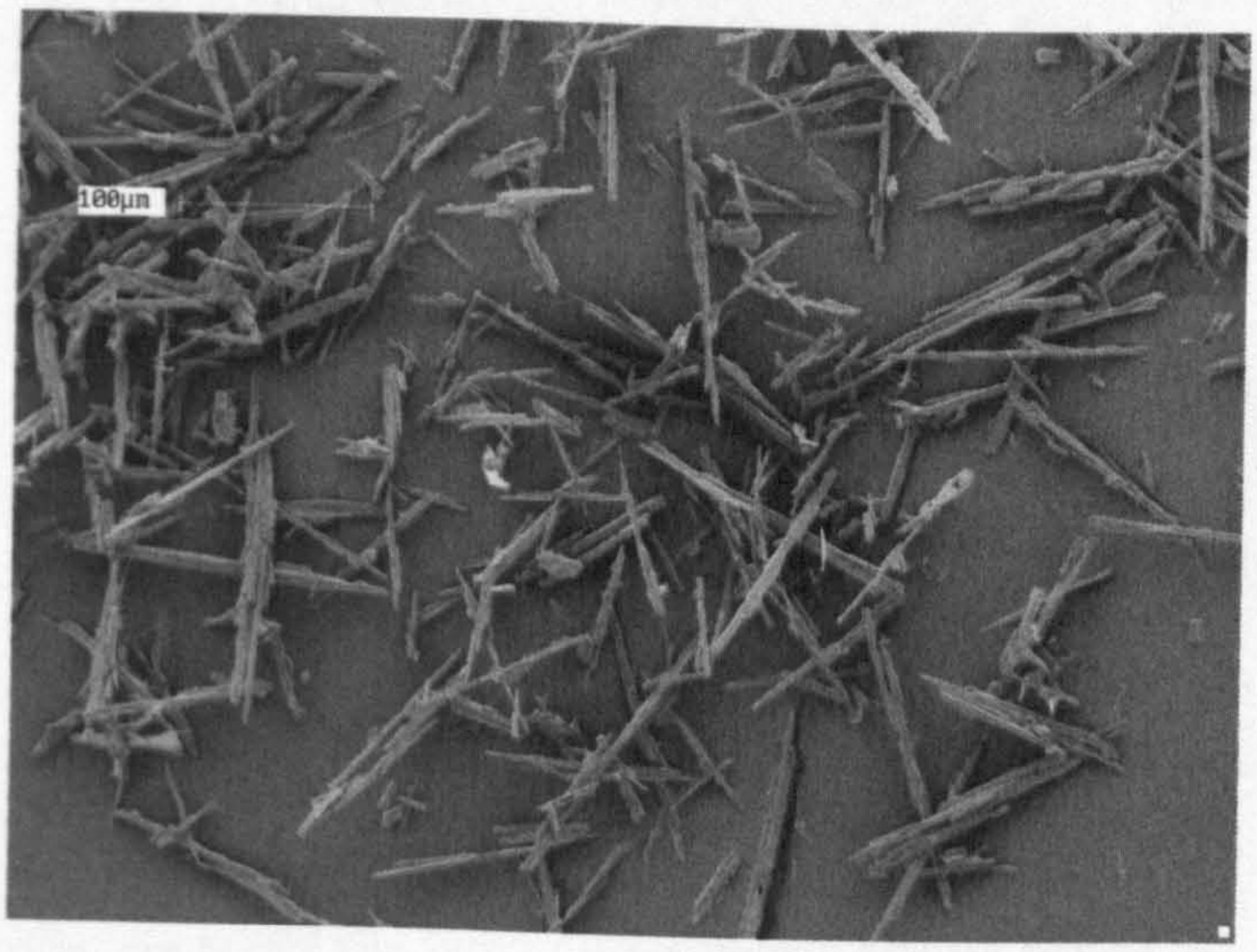

DMU2149 Hydrochloride	Triclinic, Agglomerated plates	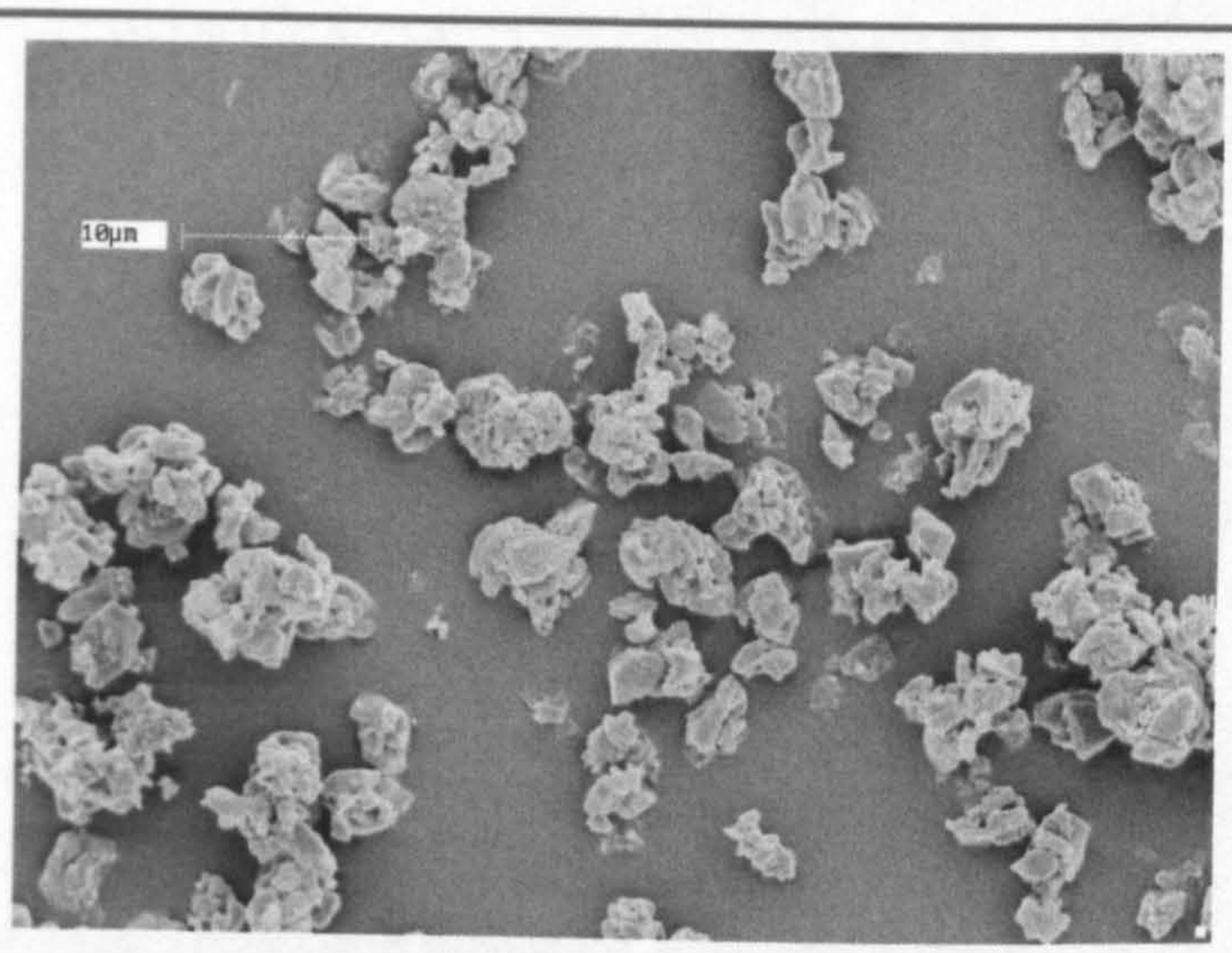
DMU2149 Phosphate	Triclinic, Agglomerated blades	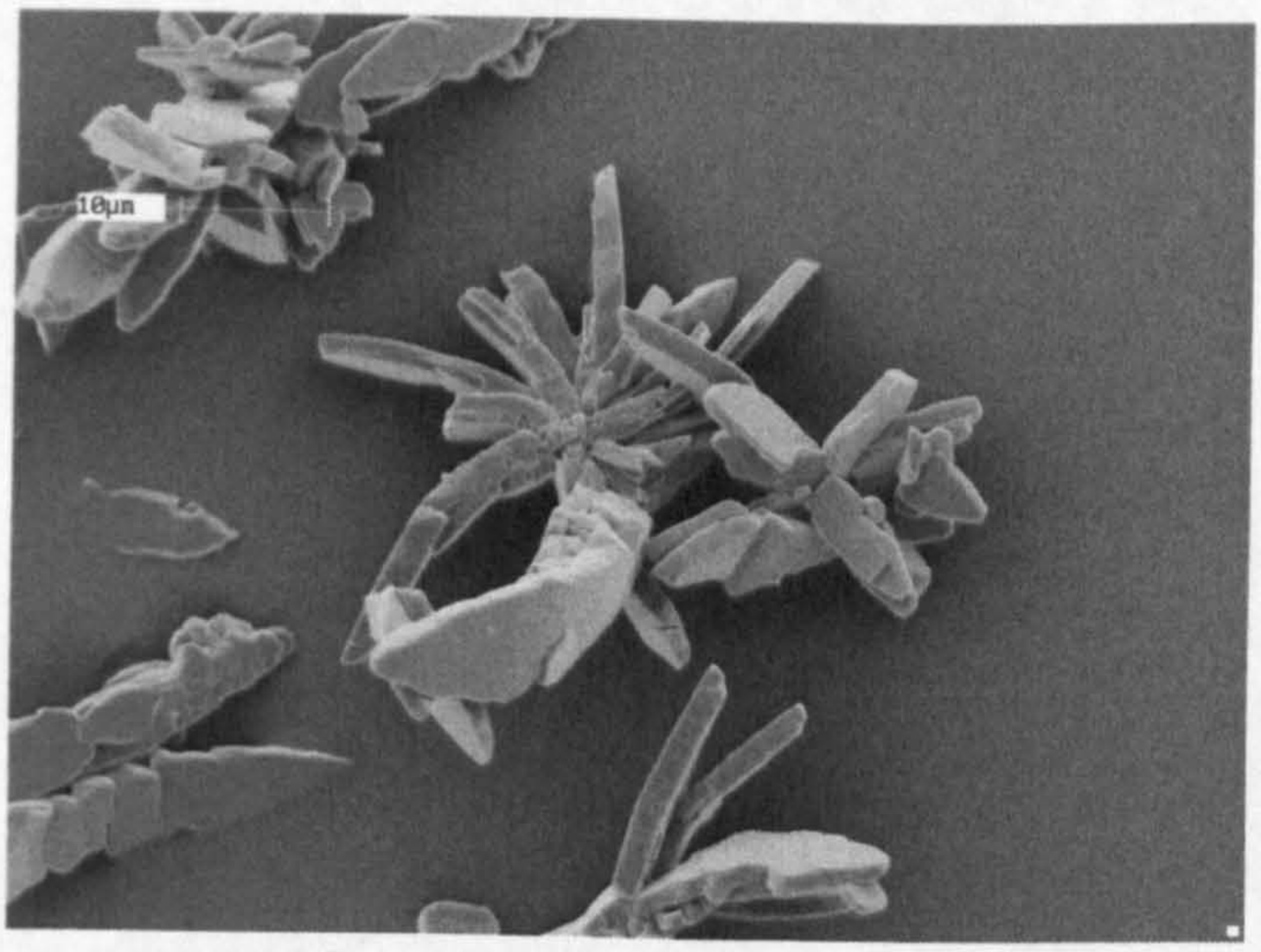
DMU2149 Sulphate	Triclinic, Agglomerated rods	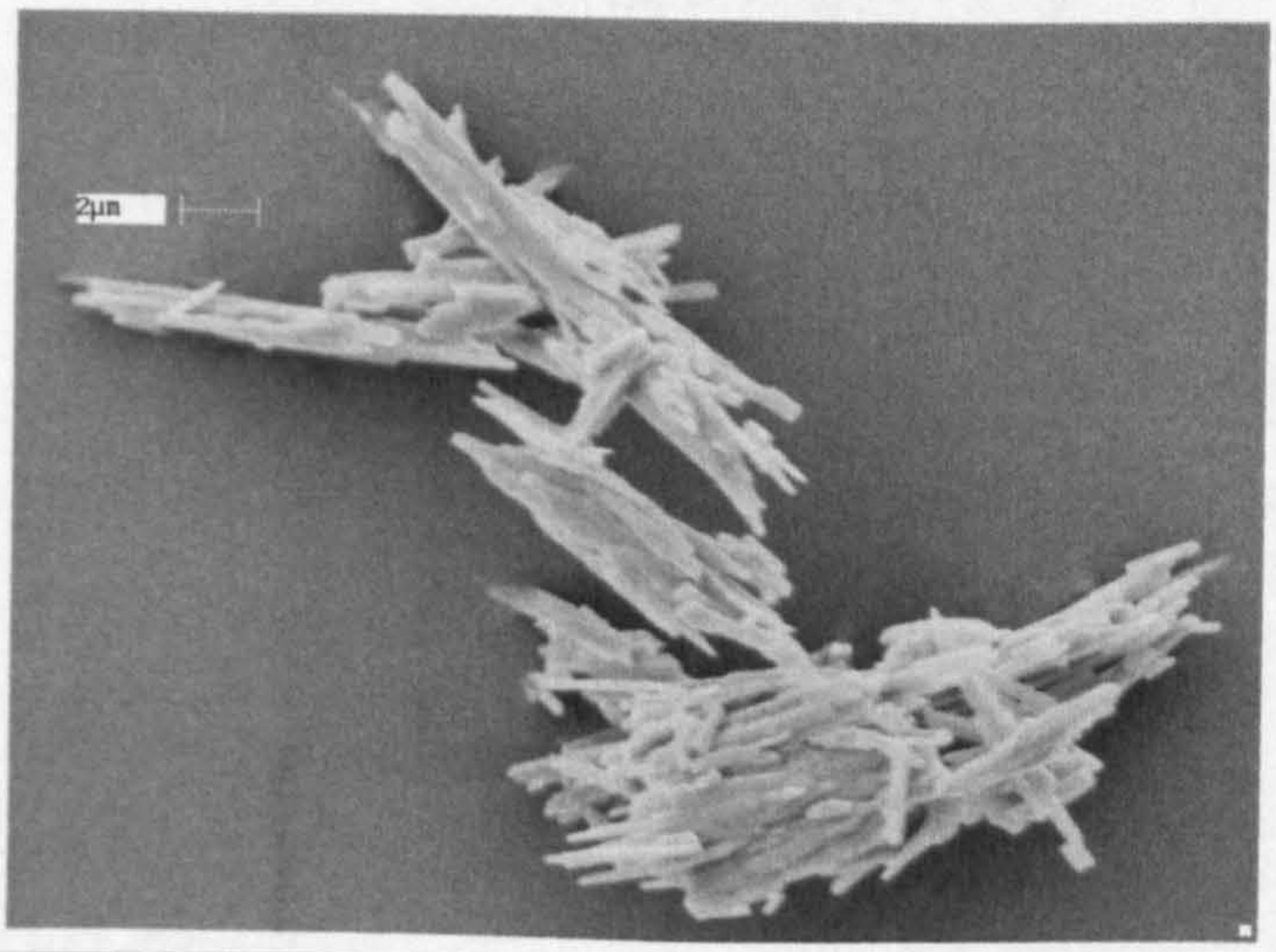

6.3.3.4 Biological evaluation of DMU2149 salts

The biological activity of DMU2149 and its salts was evaluated with the MTT assay using the CDDG in-house breast cell panel of MCF7, MDA-MB-468 and MCF10A:

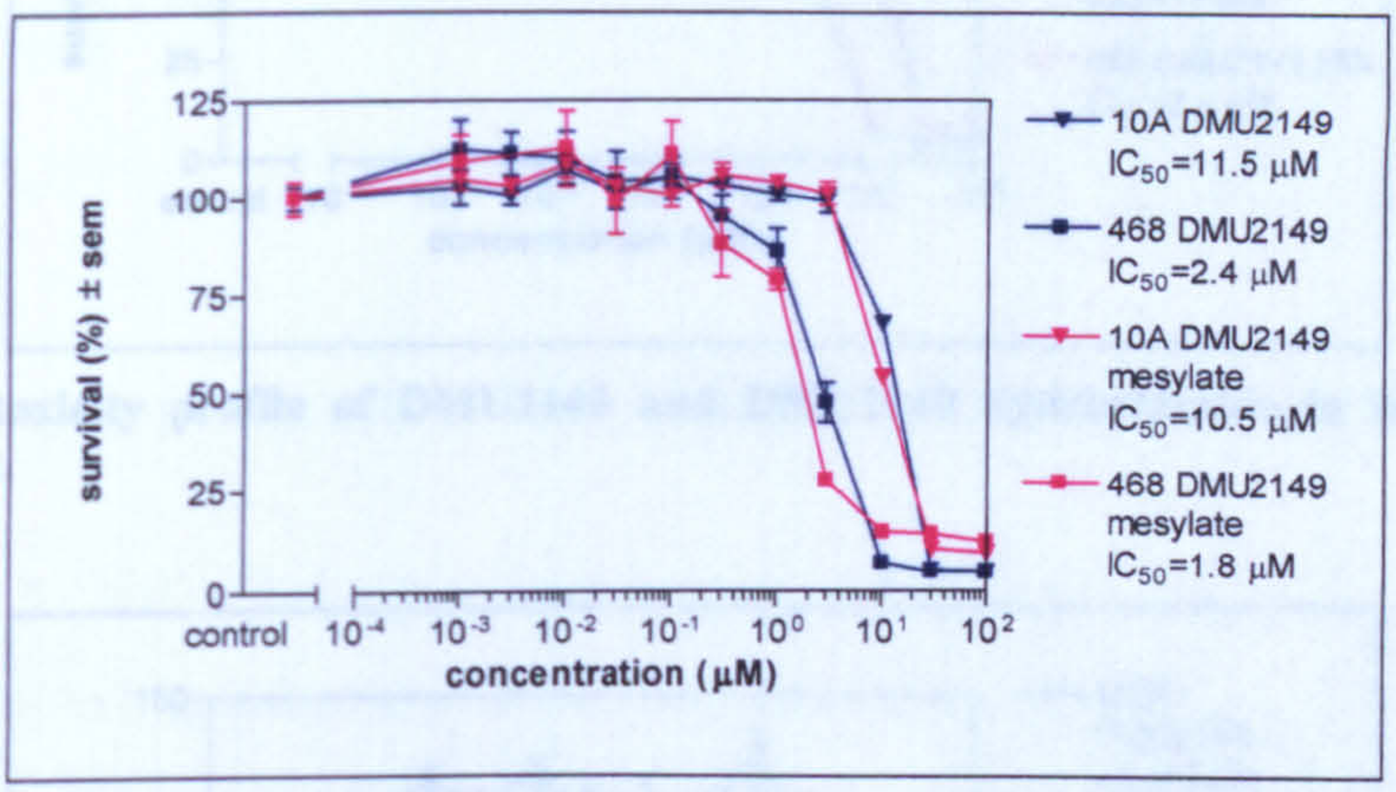

Figure 101. Cytotoxicity profile of DMU2149 and DMU2149 mesylate in MDA-MB-468 and MCF10A cell lines.

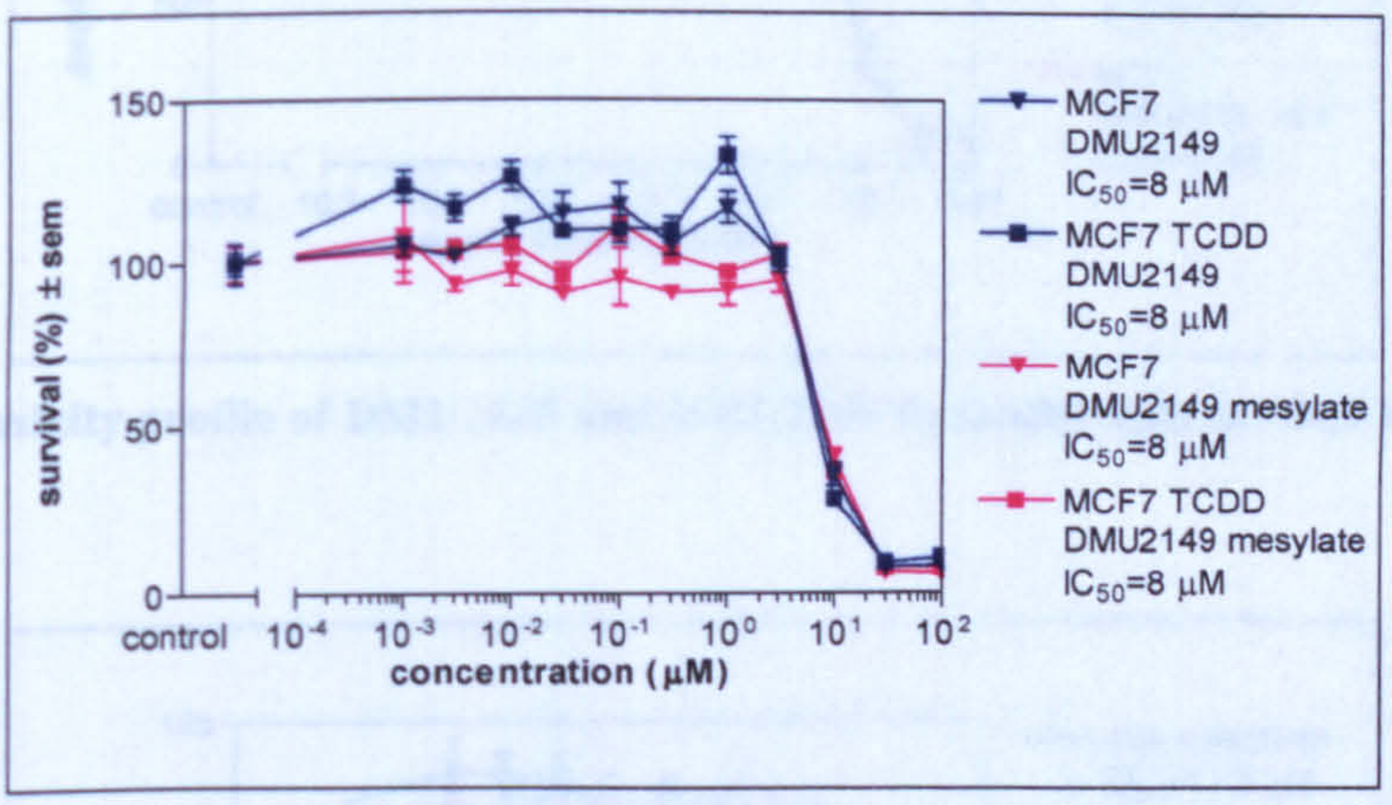

Figure 102. Cytotoxicity profile of DMU2149 and DMU2149 mesylate in MCF7 with and without TCDD induction.

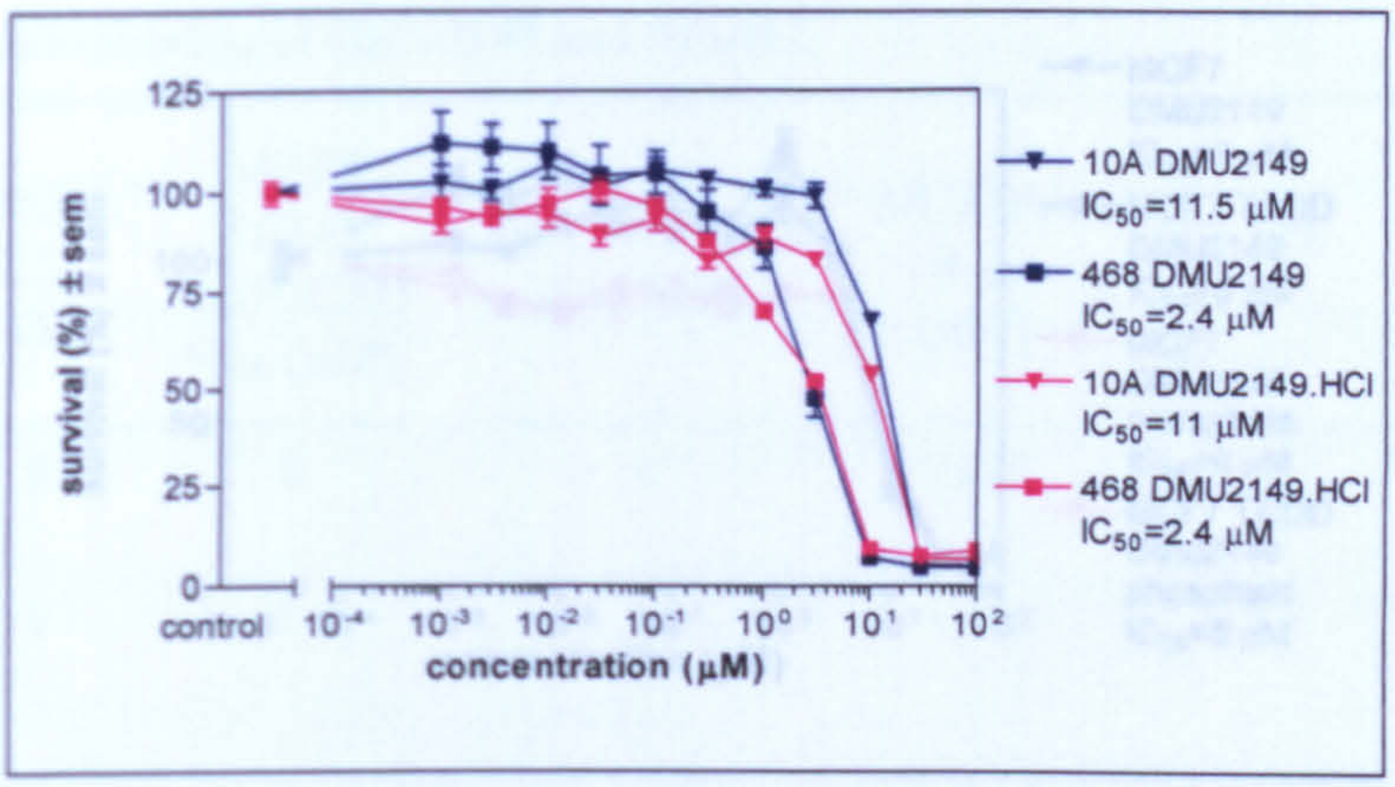

Figure 103. Cytotoxicity profile of DMU2149 and DMU2149 hydrochloride in MDA-MB-468 and MCF10A cell lines.

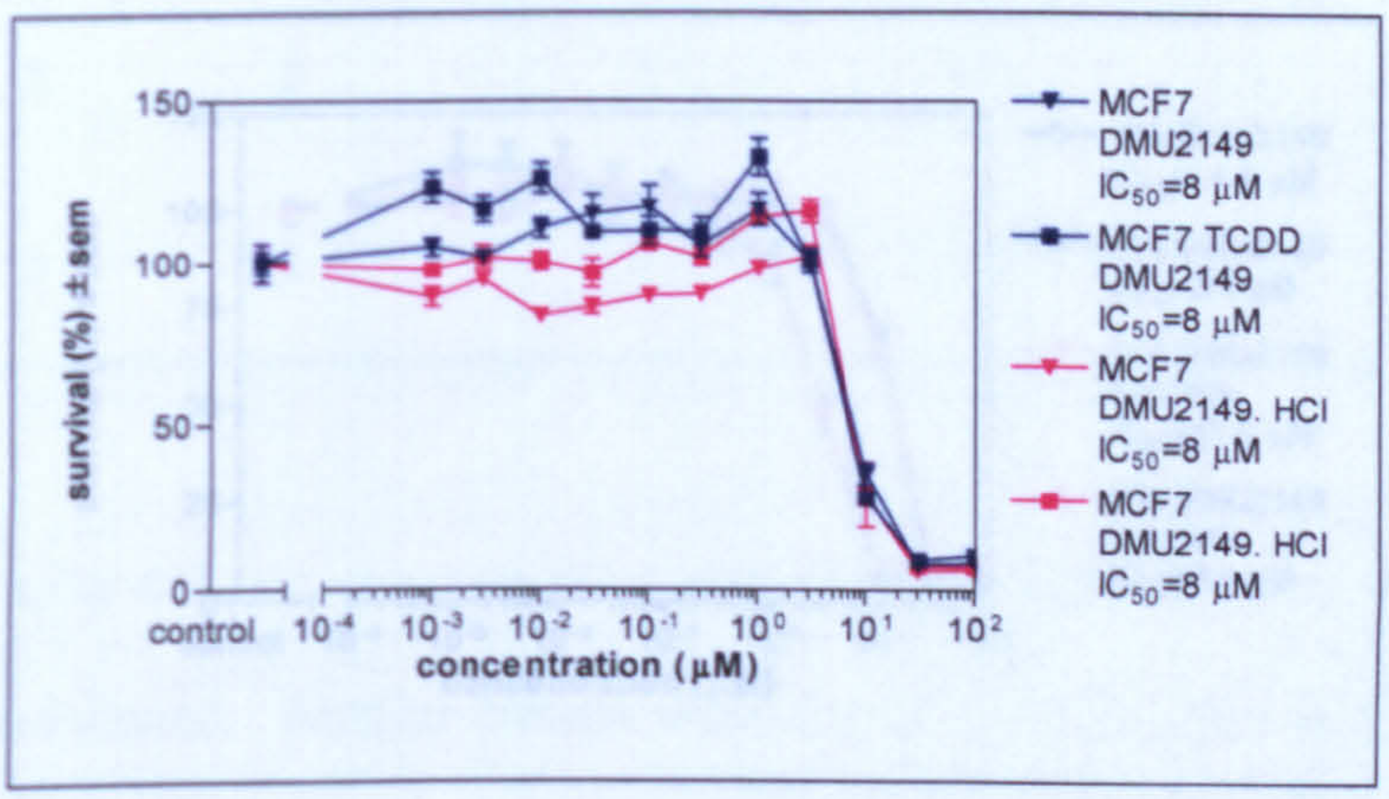

Figure 104. Cytotoxicity profile of DMU2149 and DMU2149 hydrochloride in MCF7 with and without TCDD induction.

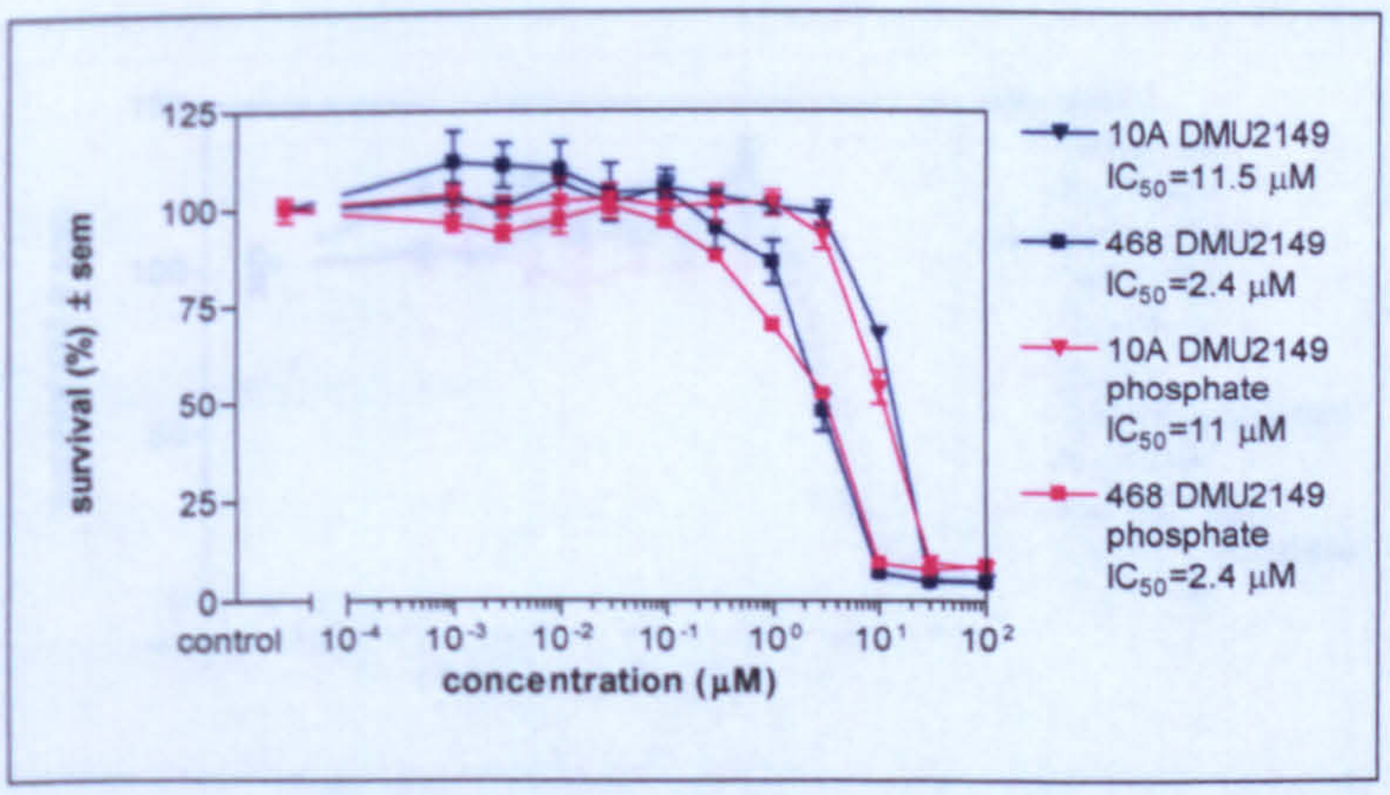

Figure 105. Cytotoxicity profile of DMU2149 and DMU2149 phosphate in MDA-MB-468 and MCF10A cell lines.

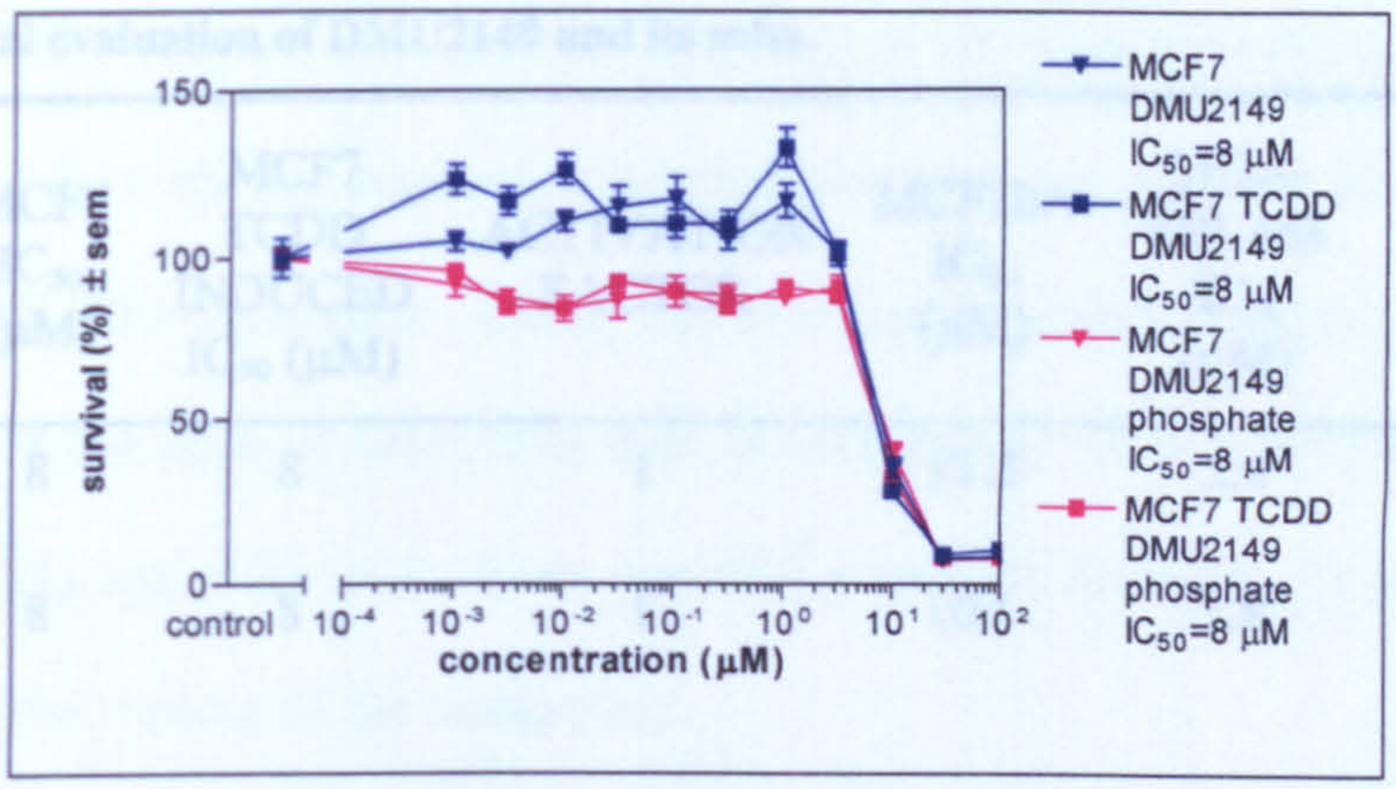

Figure 106. Cytotoxicity profile of DMU2149 and DMU2149 phosphate in MCF7 with and without TCDD induction.

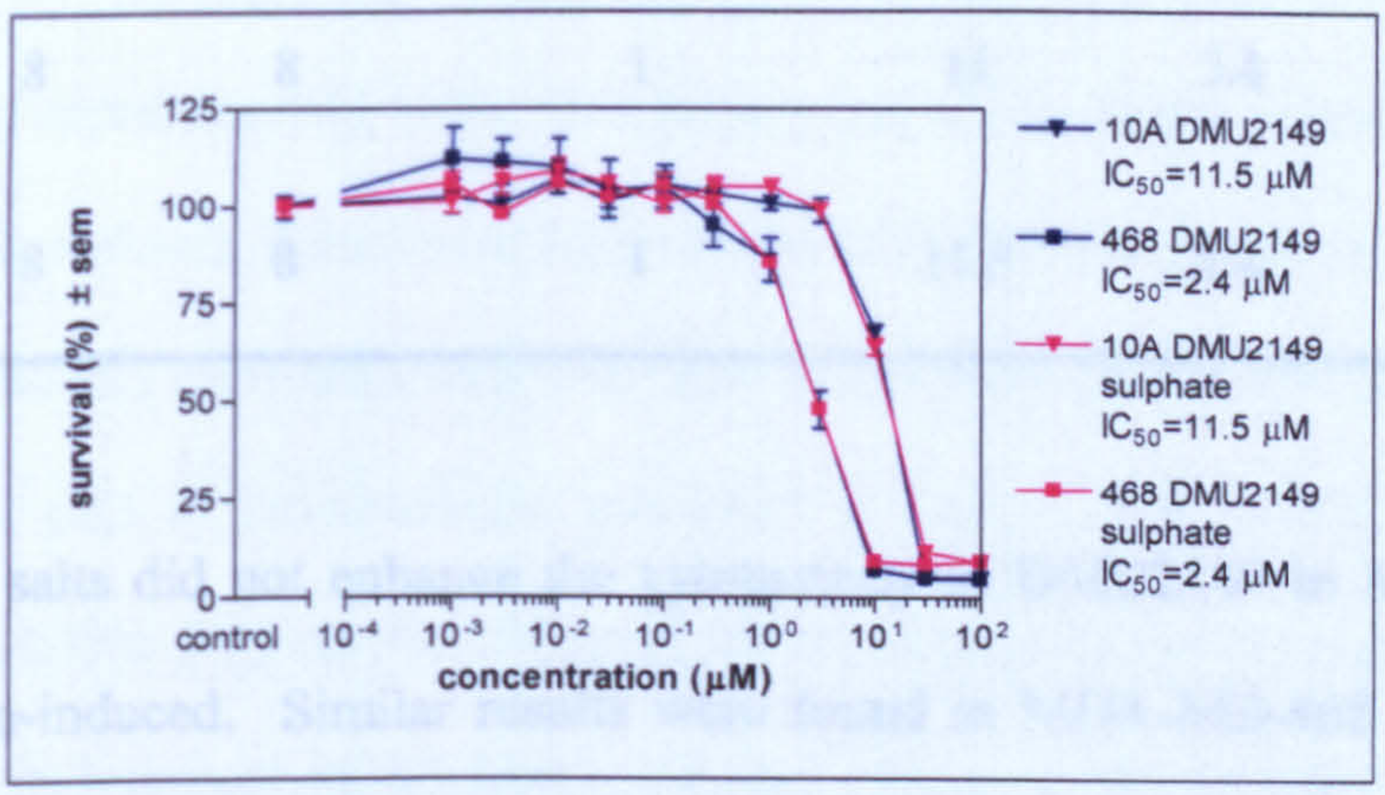

Figure 107. Cytotoxicity profile of DMU2149 and DMU2149 sulphate in MDA-MB-468 and MCF10A cell lines.

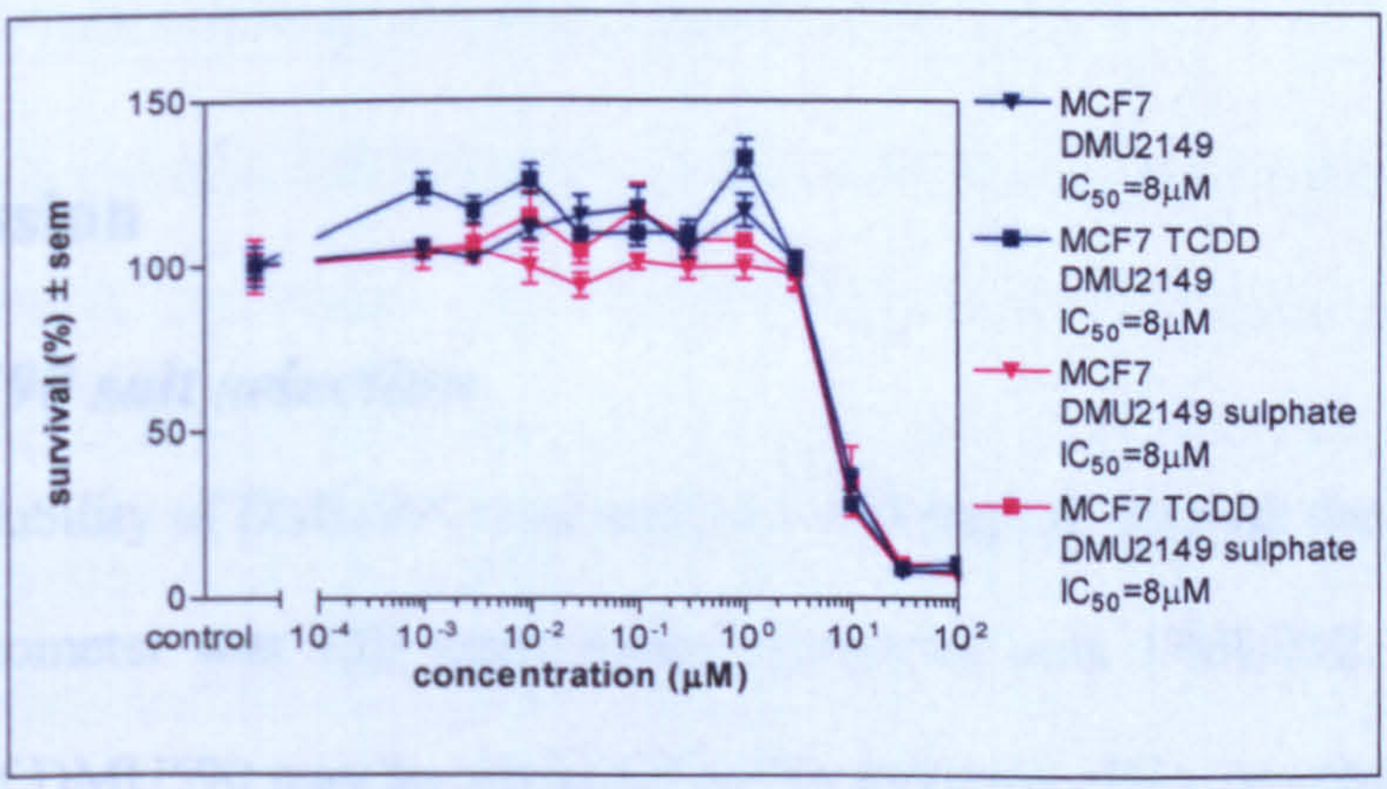

Figure 108. Cytotoxicity profile of DMU2149 and DMU2149 sulphate in MCF7 with and without TCDD induction.

Table 57. Biological evaluation of DMU2149 and its salts.

DRUG	MCF7 IC_{50} (μM)	MCF7 TCDD INDUCED IC_{50} (μM)	ACTIVATION FACTOR	MCF10A IC_{50} (μM)	MDA-MB-468 IC_{50} (μM)	TUMOUR SELECTIVE FACTOR
DMU2149	8	8	1	11.5	2.4	4.8
DMU2149 Mesylate	8	8	1	10.5	1.8	5.8
DMU2149 Hydrochloride	8	8	1	11	2.4	4.6
DMU2149 Phosphate	8	8	1	11	2.4	4.6
DMU2149 Sulphate	8	8	1	11.5	2.4	4.8

The DMU2149 salts did not enhance the cytotoxicity of DMU2149 in MCF7 cells both induced and non-induced. Similar results were found in MDA-MB-468 cells except for DMU2149 mesylate which demonstrated a slight increase in potency compared to DMU2149.

6.4 Discussion

6.4.1 DMU590 salt selection

The aqueous solubility of DMU590 measured at 0.120 mg/mL on both the UV plate reader and spectrophotometer was 120 times better compared with DMU212. The increased hydrophilicity of DMU590 may be attributed to the presence of the morpholine substituent, which counteracts the lipophilic nature of the methyl substituents. The pH-solubility

profile of DMU590 (Figure 86) showed the drug to be most soluble at low pH values between pH 2-5.5, with the highest solubility observed at pH 2. Above pH 5.5 the solubility of DMU590 decreased. Using the aqueous solubility, the pH-solubility profile and Equation 6.4 the pKa of DMU590 was determined at 6.23 ± 0.05 on the UV plate reader (Figure 87) and 6.29 ± 0.02 on the UV spectrophotometer (Figure 88), thereby confirming the basic nature of the compound.

The solubility and pKa values determined on the UV plate reader were comparable to those determined on the UV spectrophotometer with maximum difference between the two techniques being approximately 10%. In a further test of this methods validity the aqueous solubility of indomethacin determined by both the UV plate reader and spectrophotometer was 0.010 mg/mL and correlated well with that stated in literature of 0.015 mg/mL [163]. Furthermore, the pKa of indomethacin measured at 4.43 ± 0.08 on the UV plate reader (Figure 92) and 4.37 ± 0.01 on the UV spectrophotometer (Figure 93) also correlated well with that stated in literature of 4.5 [228]. Overall, these results indicate that the 96-well automated UV plate reader can be successfully implemented for high-throughput, miniaturised and valid solubility and pKa quantification.

Initial salt screening studies with DMU590 using strong inorganic mineral acids (Table 40) were unsuccessful on the whole, generally resulting in the formation of an amorphous mass. However, reaction with phosphoric acid did yield a white crystalline salt. Theoretically, reaction with hydrochloric and sulphuric acid should have also resulted in salt formation, since the pKa of these conjugate acids are 2 pH units lower than DMU590. The pKa of phosphoric acid at 1.96 is higher than for hydrochloric acid at -6.0 and

sulphuric acid at -3.0, therefore making it a weaker acid, which may have enabled its salt selection with DMU590. This may be because the double bond in the DMU590 structure may be highly sensitive to strong acids and could readily undergo protonation causing isomerisation to the *trans* isomer leading to degradation:

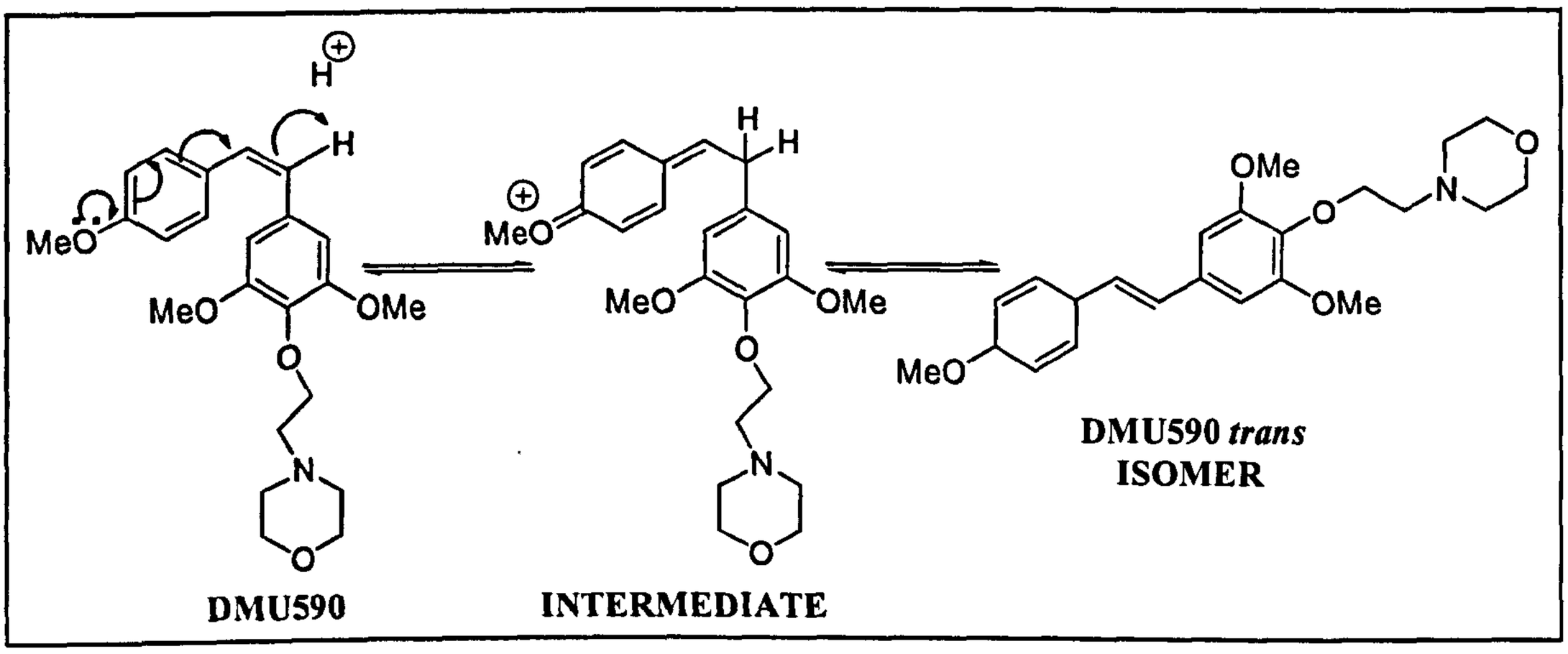

Figure 109. Isomerisation of DMU590 resulting from salt selection with strong acids.

As such the next salt screening screen consisted of organic aliphatic and olefinic acids; however, salt formation was fruitless, corroborating Gould who suggested that aliphatic acid conjugation often yielded oils, which would be unsuitable because of the practical difficulties associated in working with oils [225]. Gould explained that planar symmetry of the anion was important for the maintenance of high crystal lattice forces, so the next screening consisted of organic aromatic acids. Theoretically, aromatic acids should yield crystalline salts because of π-electron sharing between benzene rings in the anions and DMU590, which could lead to stacking of the molecules to form a better crystalline structure. However, in this instance this theory was unsubstantiated as salt crystallization was unsuccessful.

The phosphate was the only salt formed in salt screening studies with DMU590. Physicochemical and biological evaluation of DMU590 phosphate involved measurement of the aqueous solubility, DSC, SEM and cytotoxicity. The aqueous solubility of DMU590 phosphate was 10,000-fold higher than for DMU590 alone (Table 47). DSC measurements for DMU590 showed the drug to exist in an amorphous form, the onset of a glass transition temperature (T_g) was observed at -15.88°C, with a ΔC_p of 0.30 J/g.°C. DSC measurements for DMU590 phosphate did not show the presence of polymorphs, solvates and impurities, since a endotherm peak was detected with an onset temperature of 165.12°C and ΔH of 81.96 J/g. These values correlate with the overall crystallinity of the two compounds DMU590 exists as a highly viscous oil, with no crystalline form, whereas, DMU590 phosphate exists as a crystalline solid. Immediately after the initial scan the samples were rapidly cooled and reheated to determine if any recrystallization was apparent and subsequently to determine the solid-state stability of the prodrugs. In the second DSC scan for DMU590 a T_g was again observed at -12.76°C, with a ΔC_p of 0.34 J/g.°C. For DMU590 phosphate the melting point endotherm was absent and the onset of a glass transition temperature (T_g) was observed at 111.57°C, suggesting that the solid was in an amorphous state and no immediate re-crystallization was apparent.

SEM imaging of DMU590 was not attempted, since it has no crystalline structure to evaluate. SEM imaging of DMU590 phosphate showed the crystal system was triclinic with small agglomerates of plate shaped crystals. The exact particle size of DMU590 phosphate is difficult to assess as the aggregates have both loosely and tightly bound particles [162]. However, the overall particle size is relatively small at <20μM, offering a

large surface area: volume ratio for dissolution, which may explain its relatively high aqueous solubility.

The biological data of DMU590 compared to DMU590 phosphate showed a significant reduction in CYP1B1 induced cytotoxicity i.e. a 75-fold decrease in tumour selectivity factor. However, DMU590 phosphate still enhanced cytotoxicity towards tumour cells 68-fold compared to MCF10A normal cells and so a therapeutic window still exists for preclinical evaluation. However, in the MCF-7 cell-line there was a 9-fold increase in activation factor compared to the parent compound and an *in vitro* therapeutic window of 76-fold.

Overall, DMU590 salt screening studies yielded a single crystalline salt, where phosphoric acid was used as the conjugate acid. DMU590 phosphate was 10,000-fold more soluble in water compared with DMU590. DMU590 phosphate was also more thermodynamically stable as a crystalline compound compared with DMU590, which exists as a highly viscous oil. DMU590 phosphate also exhibited a lower CYP1B1-activation factor compared with DMU590. The physicochemical properties of DMU590 and DMU590 phosphate have been evaluated and the core findings are summarised in Table 58. A novel high-throughput screening method using a 96-well automated UV plate reader has also been successfully implemented and validated for pKa quantification.

Table 58. Comparison of some of the physicochemical properties of DMU590 and its salt.

PROPERTY \ DRUG	DMU590	DMU590 Phosphate
Activation Factor	9	76
Tumour Selective Factor	5000	68
Appearance	Pale yellow oil	White, crystalline
Molecular Weight	399	497
Melting Point (°C)	-	165.12
Enthalpy of fusion ΔH (J/g)	-	81.96
Glass Transition Temperature (°C)	-15.88	-
Heat Capacity Increment ΔC_p ($J/g^{\bullet}°C$)	0.30	-
Crystal System	-	Triclinic, blades
Polymorphism	No evidence of polymorphs	No evidence of polymorphs
Aqueous solubility (mg/mL)	0.120 ± 0.009	986.963 ± 108.094
pKa	6.29 ± 0.02	-

6.4.2 DMU2149 salt selection

The aqueous solubility of DMU2149 (Table 43), was much improved compared with the lipophilic chalcone DMU135; which may be attributed to the presence of the imidazole substituent in the chalcone backbone. The pH-solubility profile of DMU2149 (Figure 89) showed the drug to be most soluble at low pH values between pH 2-4, with the highest solubility observed at pH 2 (Table 44). Above pH 4 the solubility of DMU2149 decreased. Using the aqueous solubility, the pH-solubility profile and Equation 6.4 the pKa of DMU2149 was determined at 4.53 on the UV plate reader and 4.40 on the UV spectrophotometer (Figure 90), thereby confirming the basic nature of the compound.

Initial salt screening studies with DMU2149 using strong inorganic mineral acids (Table 40) yielded the phosphate, sulphate and hydrochloride salts, since the pKa of the respective conjugate acids were 2 pH units lower than DMU2149. The second salt-forming group using organic aliphatic and olefinic acids yielded the fumarate, maleate, mesylate, oxalate and tartarate salts. The conjugate acids used for these salts had pKa values lower than that of DMU2149, moreover, the aliphatic and olefinic conjugate acids used which did not yield salts had pKa values higher than of DMU2149. The final salt-forming group using organic aromatic acids yielded the besylate, tosylate and gentisate salts. The conjugate acids used for these salts also had pKa values lower than that of DMU2149. The aqueous solubility of all these salts was firstly measured to eliminate salts with the lowest solubility.

Overall, all of the salts had better aqueous solubility than DMU2149 alone (Table 52). The salt with the lowest aqueous solubility was the gentisate. The highest solubilities were observed with the mesylate, phosphate, hydrochloride and sulphate respectively, all of which were formed from strong low molecular weight conjugate acids. Determination of the pH-solubility profile for these salts may provide an indication of the salt behaviour *in vivo* as well as providing valuable information for intravenous and oral formulations. The pH-solubility profile of the DMU2149 salts (Figures 98-99) showed all of the salts to be more soluble at low pH values between pH 2-4, where the highest solubilities were observed at pH 2. DMU2149 sulphate was the most soluble salt over a wide pH range of 2-10, followed by DMU2149 phosphate. The highest solubility at pH 2 was observed with DMU2149 mesylate. At pH 7 the highest solubility was with DMU2149 sulphate, followed

by DMU2149 phosphate. The lowest solubility at pH 7 was with the DMU2149 mesylate, followed by DMU2149 hydrochloride.

DSC measurements for DMU2149 and it salts except for the phosphate did not show the presence of polymorphs, solvates and impurities, since all thermograms showed a single endotherm peak (Figure 100). DMU2149 had an onset temperature of 157.60°C with a ΔH of 102.58 J/g, DMU2149 mesylate had an onset temperature of 257.74°C with a ΔH of 160.96 J/g, DMU2149 hydrochloride had an onset temperature of 247.46°C with a ΔH of 7.97 J/g and DMU2149 sulphate had an onset temperature of 227.27°C with a ΔH of 101.88 J/g. The DSC trace for DMU2149 phosphate exhibited two melting point endotherms with onset temperatures of 41.80 and 197.69°C and ΔH values of 2.30 and 91.71 J/g respectively, suggesting the presence of solvates, polymorphs or hydrates. However, the broad nature of the endotherm suggests that presence of a solvate, since polymorphic variants generally exhibit sharper peaks. This theory is supported by the peak temperature at which this endotherm was observed i.e. 52.30°C, which coincides with the boiling point of the solvent used for phosphate salt selection i.e. acetone, which has a boiling point of 56.3°C.

Immediately after the initial scan the samples were rapidly cooled and reheated to determine if recrystallization was apparent and subsequently to determine the solid-state stability of the prodrugs. In the second DSC scan the melting point endotherm for DMU2149, DMU2149 mesylate, DMU2149 hydrochloride, DMU2149 sulphate and DMU2149 phosphate was absent and the T_g's were observed at 20.37, 76.39, 99.57, 126.75

and 115.43°C respectively, suggesting that the crystals were in an amorphous state and no immediate recrystallization was apparent.

SEM imaging of DMU2149 showed the crystal system was orthorhombic with large columnar crystals that have a relatively large particle size of >200μM and a relatively small surface area: volume ratio. The mesylate had an orthorhombic crystal system with needle crystals, a small surface area and particle size of <10μM. The hydrochloride had a triclinic crystal system with agglomerated plate crystals and a small particle size of <10μM. The phosphate had a triclinic crystal system with agglomerated blade crystals with a central focus expanding outwards in flower shaped formation and a particle size of <30μM. Finally, the sulphate had a triclinic crystal system with agglomerated rod crystals and a particle size of <30μM.

DMU2149 alone had the lowest aqueous solubility corresponding to the largest crystal shapes, with little surface area available for dissolution. DMU2149 mesylate has the optimum solubility correlating with the crystals which exist as individualised crystals offering a large surface area for dissolution. The next most soluble salt was the phosphate salt, which has flower shaped plate like crystals with a large surface area. The hydrochloride salt was the next most soluble with a crystal-aggregate existence offering little surface area to aid dissolution. The lowest salt solubility was observed with the sulphate which has a highly aggregated rod shaped crystal formation, with the lowest surface area available for dissolution.

The biological data of DMU2149 compared to DMU2149 salts was fairly similar, with no significant enhancement in CYP induced cytotoxicity. The greatest enhancement in tumour

selectivity was observed with DMU2149 mesylate, which had a 5.8 fold tumour selective factor compared to 4.8-fold with DMU2149.

Overall, DMU2149 salt screening studies yielded eleven crystalline salts, the mesylate, phosphate, hydrochloride, sulphate, tartarate, besylate, oxalate, tosylate, maleate, fumarate and gentisate. Initially the aqueous solubility of the salts was determined to consider the feasibility for further development and the salts with the lowest solubility were eliminated. The optimum salt forms in terms of aqueous solubility were the mesylate, phosphate, hydrochloride and sulphate respectively. A preformulation study was conducted on each of these salts so as to select a salt with optimum physicochemical and biological properties. Table 59 lists the physicochemical properties of these salts and DMU2149. All the salts showed a better pH-solubility profile than DMU2149, the sulphate and phosphate being the best, with optimum buffering capacity. The mesylate and hydrochloride salts had a lower buffering capacity and thus were discarded for further studies. DSC measurements showed none of the salts to exhibit polymorphic variants apart from DMU2149 phosphate, which was found to exist in more than one form and thus was discarded for future studies. None of the salts significantly altered the biological activity of DMU2149. SEM imaging of the salts showed all of the salts to have a relatively small particle size, however, the mesylate salt had needle shaped crystals which may result in poor powder flow properties [221], providing a further reason for its elimination. On the basis of these results DMU2149 sulphate is recommended for further development.

Table 59. Comparison of some of the physicochemical properties of DMU2149 and its salts.

PROPERTY \ DRUG	DMU2149	DMU2149 Mesylate	DMU2149 Phosphate	DMU2149 Hydrochloride	DMU2149 Sulphate
Activation Factor	1	1	1	1	1
Tumour Selective Factor	4.8	5.8	4.6	4.6	4.6
Appearance	Yellow, crystalline	Yellow, crystalline	Yellow, crystalline	Yellow, crystalline	Yellow, crystalline
Molecular Weight	256	352	354	293	354
Melting Point (°C)	157.60	257.74	41.80 197.69	247.46	227.27
Enthalpy of fusion ΔH (J/g)	102.58	160.96	2.30 91.71	7.97	101.88
Crystal System	Orthorhombic, columnar	Orthorhombic, needles	Triclinic, aggregated blades	Triclinic, aggregated plates	Triclinic, aggregated rods
Polymorphism	No evidence of polymorphs	No evidence of polymorphs	At least two forms detected	No evidence of polymorphs	No evidence of polymorphs
Aqueous solubility (mg/mL)	0.085 ± 0.001	27.794 ± 2.226	18.547 ± 0.471	16.044 ± 0.258	15.094 ± 0.589
pKa	4.40	-	-	-	-

CHAPTER 7

Formulation Studies of Pyridone and Pyridine Prodrugs

7.1 Introduction

A potential problem with using chalcone prodrugs such as DMU135 is their high lipophilicity and poor aqueous solubility, which presents problems during drug formulation. Moreover, the lack of derivatisable functional groups, does not allow manipulation of the drug physicochemical properties as a salt form. One possible strategy to overcome these problems is to incorporate the chalcone functionality into a nitrogen containing heterocycle, to form pyridone or pyridine anticancer prodrugs:

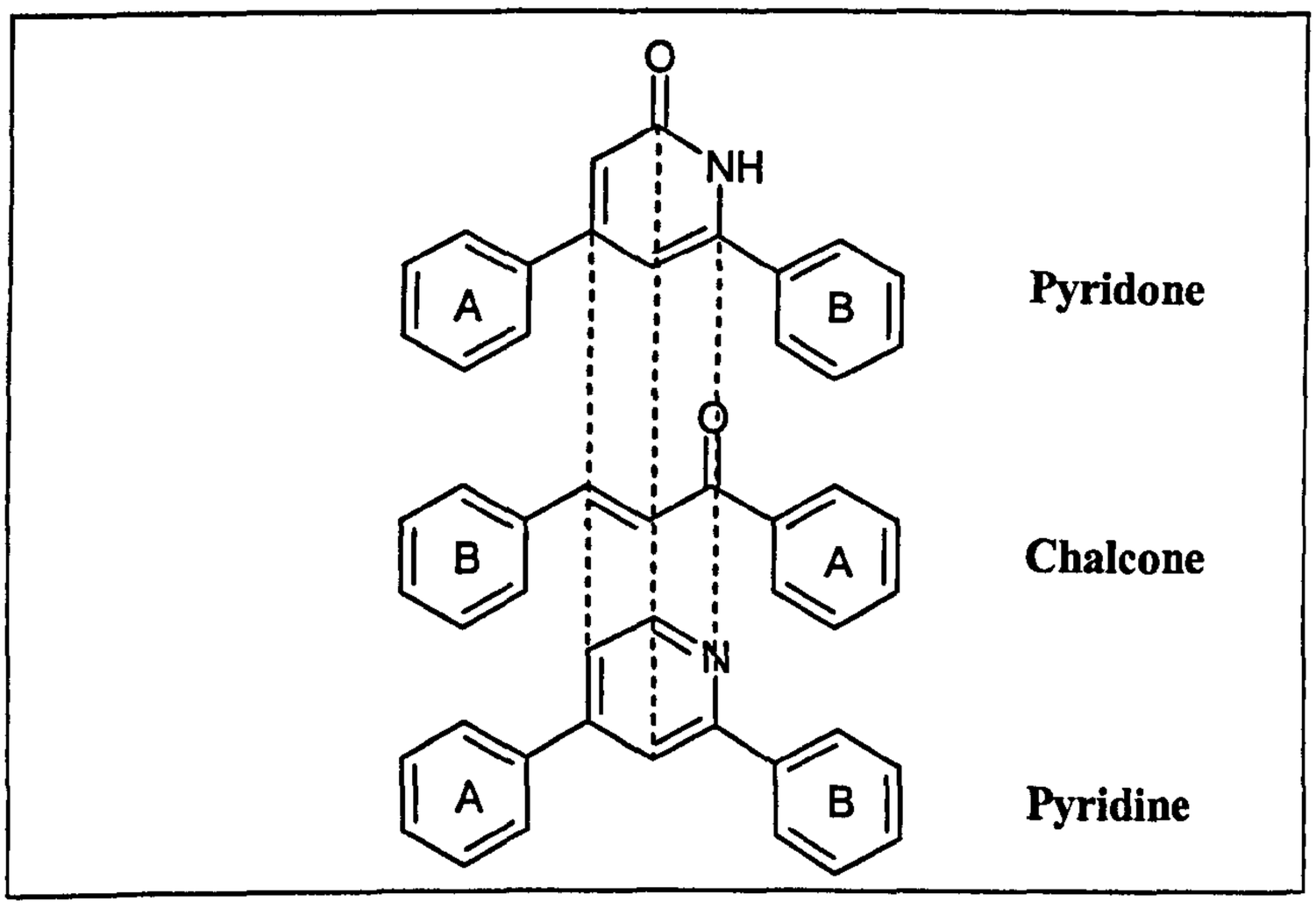

Figure 110. Mapping of pyridones and pyridines onto the chalcone structure.

This strategy should theoretically improve drug solubility and enable salt selection through protonation of the nitrogen to enhance the drug physicochemical properties compared to chalcones, whilst simultaneously retaining their anticancer properties. The chalcone stability should also improve with an increase in rigidity of the heterocyclic structure, thereby, avoiding the tendency for chalcones to undergo retro-aldol condensation reactions.

7.1.1 Discovery of a novel pyridone prodrug

A library of pyridone prodrugs had been previously prepared by S. Lodhi of the CDDG, to develop compounds with favourable physicochemical and biological properties compared with chalcones. The cytotoxicity of these compounds was screened in the MTT *in vitro* assay, where the pyridone DMU949 with a 3,4-methylenedioxy substituent on the A-ring and a 3,4-dimethoxy functionality on B-ring, exhibited one of the optimum anticancer profiles:

Table 60. Summary of DMU949 *in vitro* cytotoxicity data. Data provided by P. Butler of the CDDG.

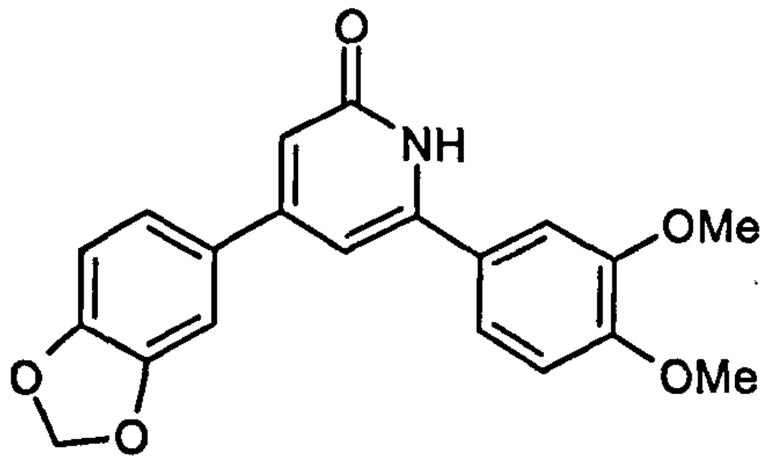

HUMAN BREAST CELL-LINE	MCF7 WITHOUT TCDD	MCF7 WITH TCDD	ACTIVATION FACTOR	MCF10A	MDA-MB-468	TUMOUR SELECTIVE FACTOR
IC_{50} VALUES (μM)	100	100	1	>100	0.04	2500

DMU949 was found to potently inhibit the growth of MDA-MB-468 cancer cells, compared to MCF10A and MCF7 cells with and without TCDD induction. The structural similarity between DMU949 and GTP (Figure 110) has led the CDDG to hypothesise that the activated catechol metabolite of the prodrug may function as a GTP competitive inhibitor:

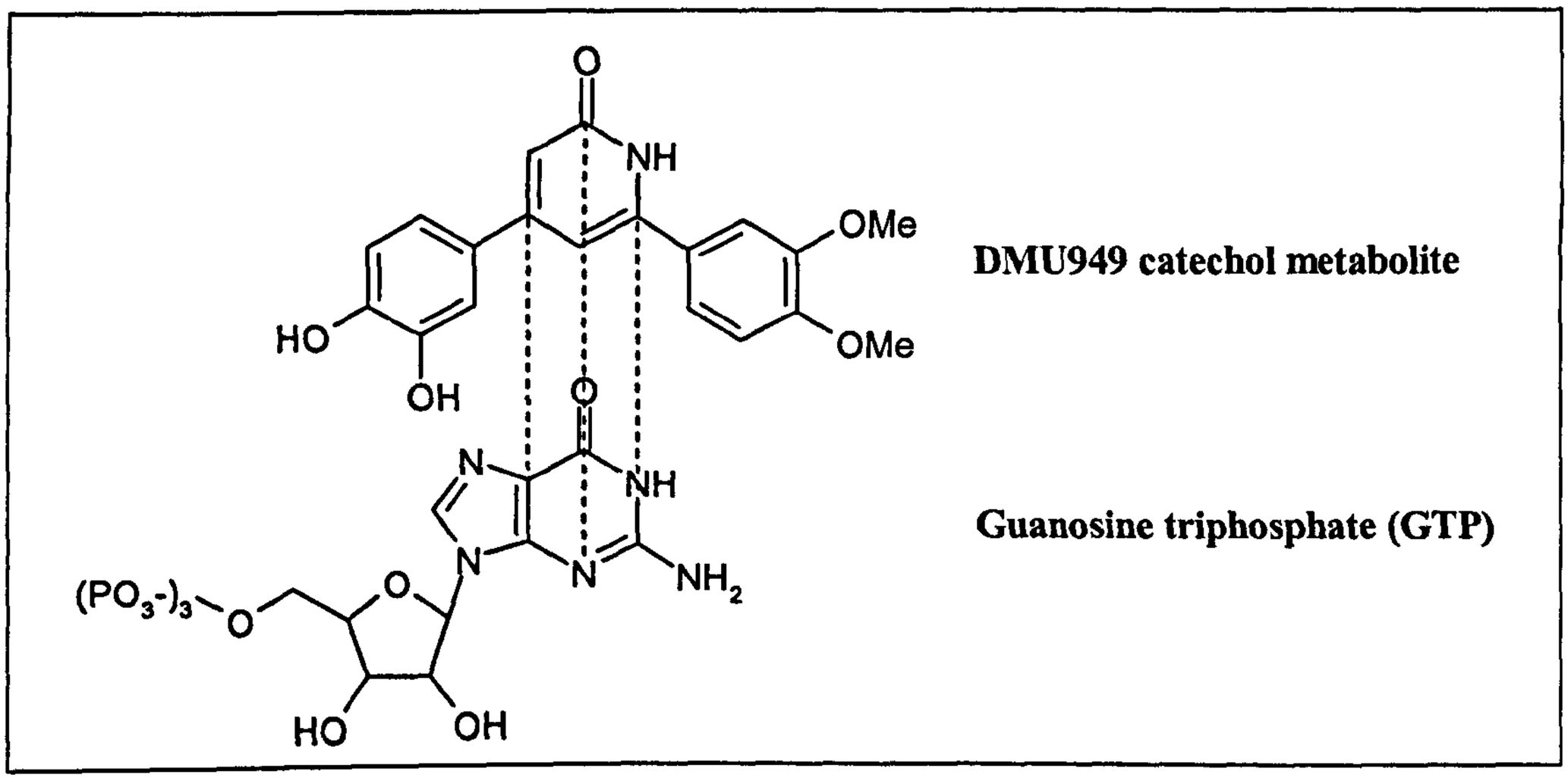

Figure 111. Mapping of DMU949 onto GTP.

GTP is an essential component in the cell signalling cascade (Figure 2), controlling the activity of membrane bound G-proteins such as Ras. Ras proteins that are oncogenically mutated do not attain a stabilised GTP transition state, and therefore fail to hydrolyse their GTP-bound form to a regulated, inactive GDP-bound form [229], resulting in uncontrolled cell proliferation and cancer [1]. The structural similarities between pyridones and GTP, suggests that they may be able to occupy the GTP binding site of G-proteins to prevent this unregulated cell proliferation.

Although DMU949 has an excellent cytotoxicity profile, the tautomeric nature of the drug may present potential problems during drug development. The predominant tautomer in solid state is the 2-pyridone (tautomer 1); however, the hydrogen bond to the nitrogen is also suitable to move to the oxygen to give a second tautomer as 2-hydroxypyridine (tautomer 2) [230]:

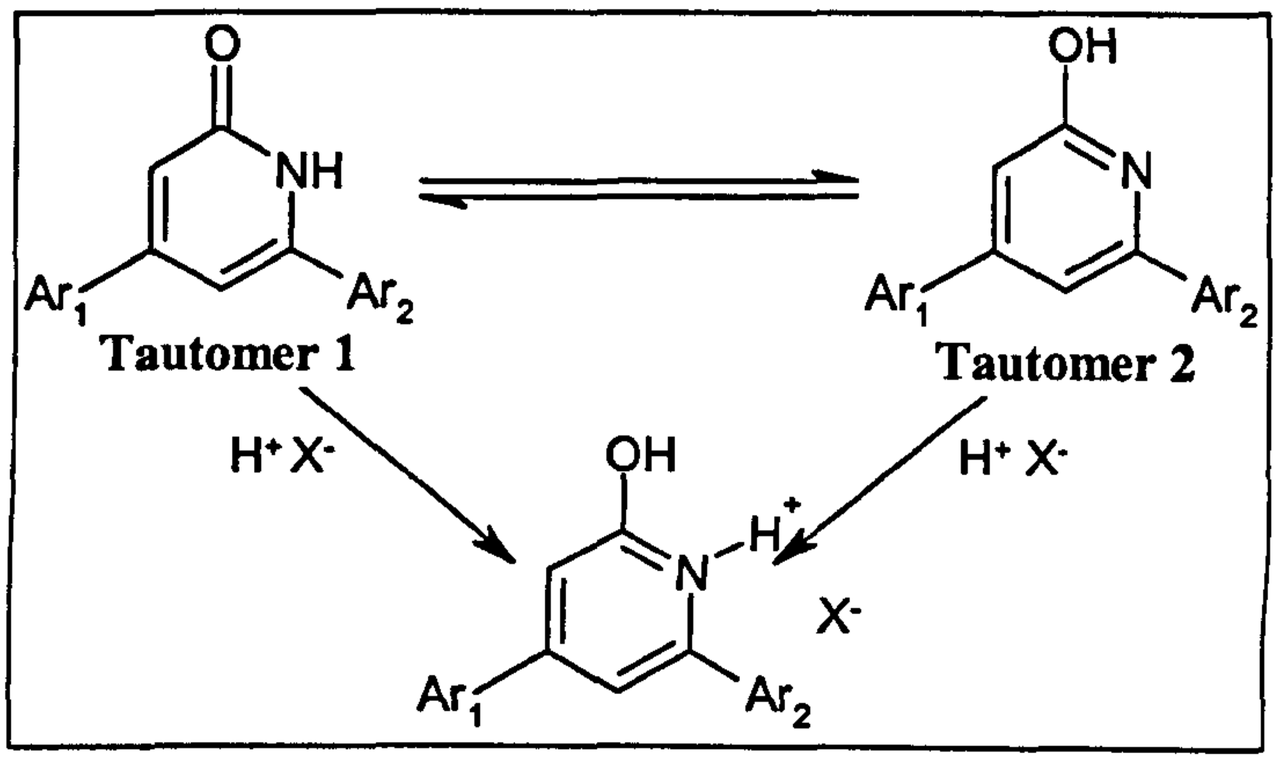

Figure 112. The tautomeric forms of DMU949.

Unfortunately, the tautomeric nature of the drug does not allow for salt selection. This is because the predominant tautomer (2-pyridone) is already protonated at the nitrogen and to further protonate the oxygen would require a much stronger acid, which would not form useful salts. Two strategies were undertaken to overcome this problem, firstly derivatives of DMU949 were designed in a double-prodrug strategy and secondly the pyridone prodrug was synthesised as its pyridine counterpart, which would enable salt selection.

A promising means of optimising the properties of prodrugs and overcoming drawbacks such as solubility, lipophilicity and stability involves the double-prodrug concept (pro-prodrugs) [231]. Therefore, it should be possible to overcome the salt selection problems of DMU949 by derivatising it in such manner that a handle is provided for salt synthesis. Salt selection of the pro-prodrug should improve the delivery of DMU949, since theoretically the handle would be enzymatically cleaved systemically *in vivo* to release the prodrug DMU949, which would then be specifically bioactivated in tumours by CYP1B1. Within the scope of this thesis DMU2297 and DMU2298 were designed as analogues of DMU949:

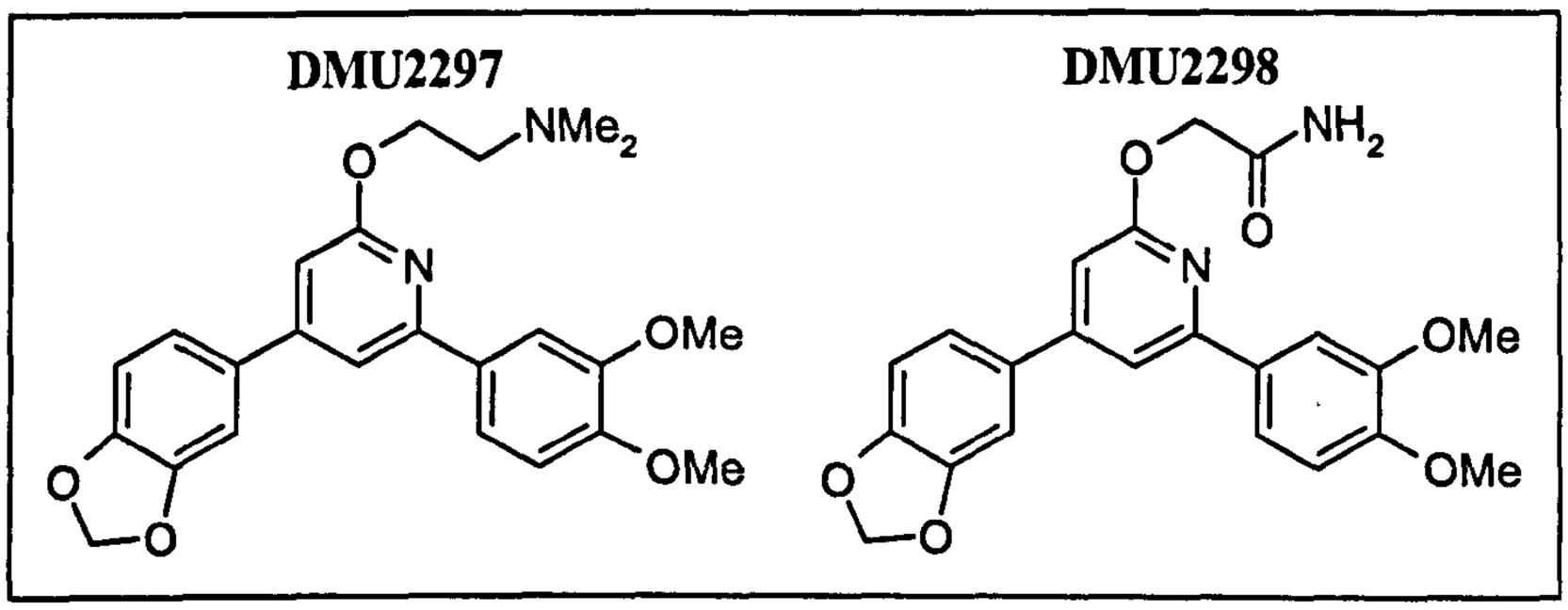

Figure 113. Chemical structures of potential pro-prodrugs of DMU949.

7.1.1.1 Synthesis of DMU2297

DMU2297 was prepared according to the protocol described by Top *et al* [232]. The pro-prodrug was synthesised by deprotonation of DMU949 using sodium hydride to generate the enolate ion, which was then alkylated with 2-dimethylaminoethyl chloride hydrochloride in a nucleophilic substitution reaction to generate DMU2297:

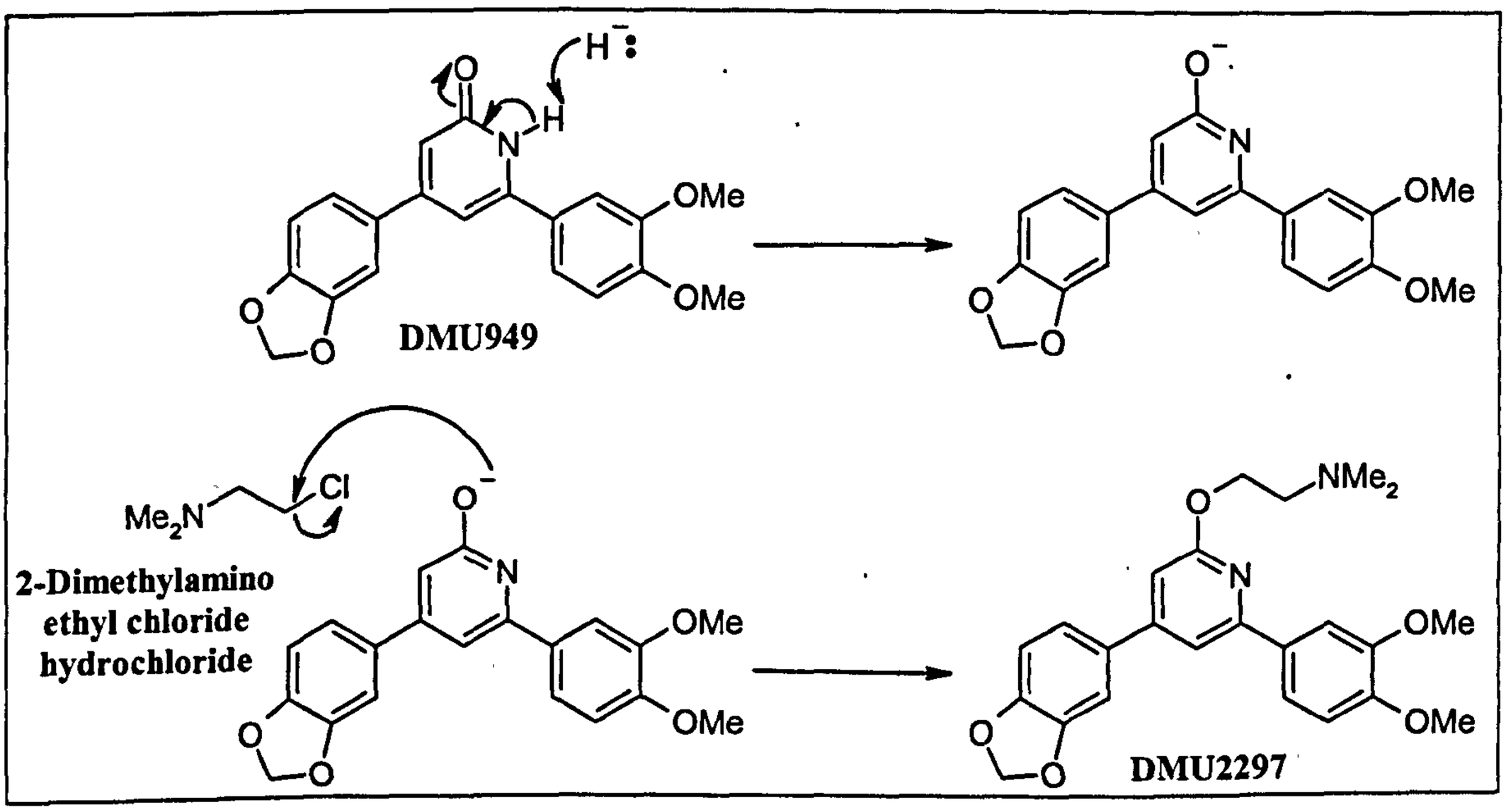

Figure 114. Reaction mechanism for DMU2297.

7.1.1.2 Synthesis of DMU2298

DMU2298 was prepared according to the protocol described by Tyvorskii *et al* [233]. The pro-prodrug was synthesised by proton abstraction, where DMU949 was deprotonated by the base (potassium carbonate) to yield an enolate ion. Finally, the O^- anion in the enolate attacked the electron deficient carbon in the 2-bromoacetamide in a nucleophilic substitution reaction to generate DMU2298:

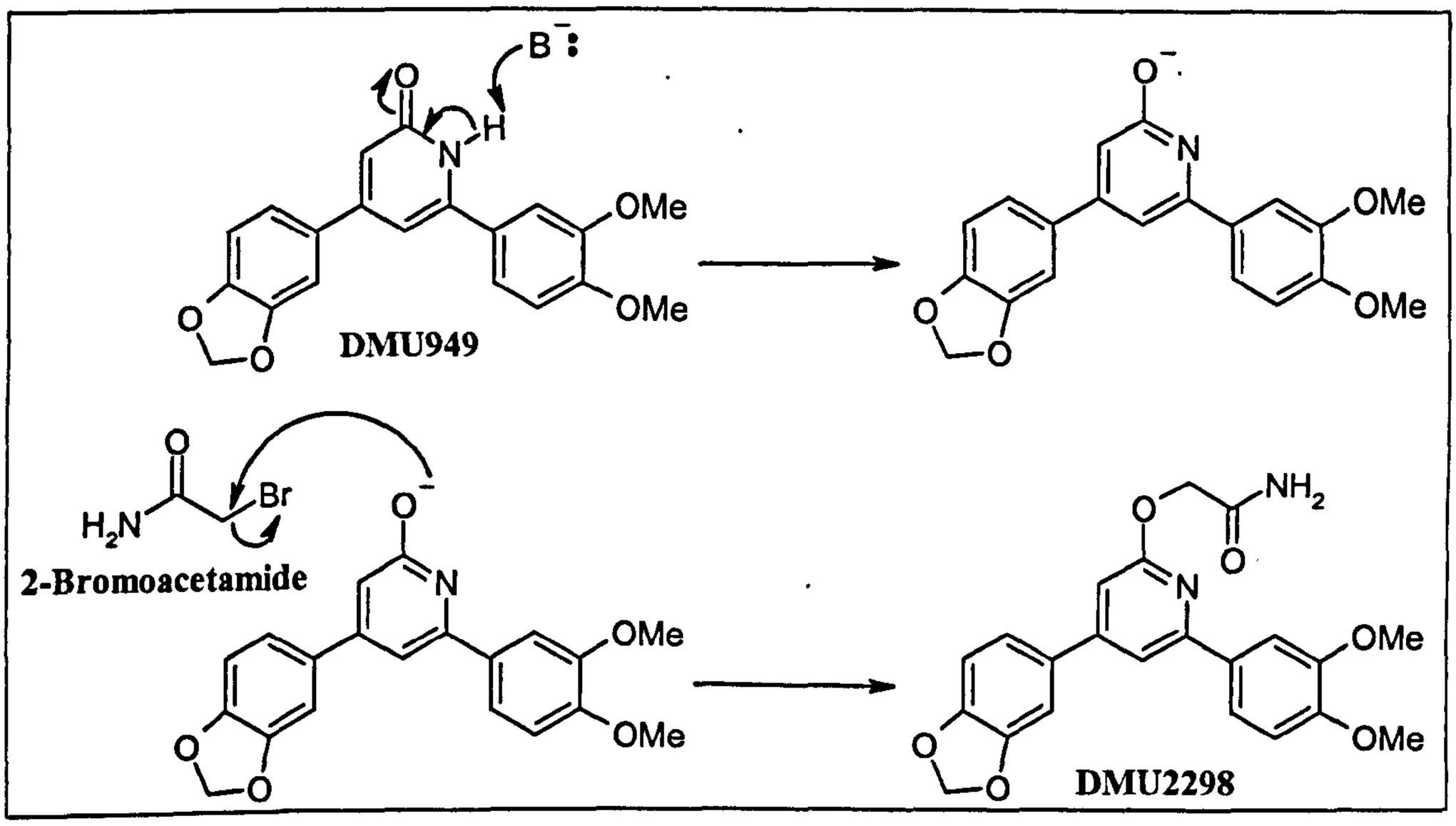

Figure 115. Reaction mechanism for DMU2298.

7.1.2 Discovery of a novel pyridine prodrug

A library of pyridine prodrugs had also been previously prepared by S. Lodhi of the CDDG to overcome the tautomeric nature of pyridones and to enable salt selection of a potent anticancer prodrug. The cytotoxicity of these compounds was screened in the MTT *in vitro* assay, where the pyridine version of DMU949 - DMU982 exhibited one of the optimum anticancer profiles:

Table 61. Summary of DMU982 *in vitro* cytotoxicity data. Data provided by P. Butler of the CDDG.

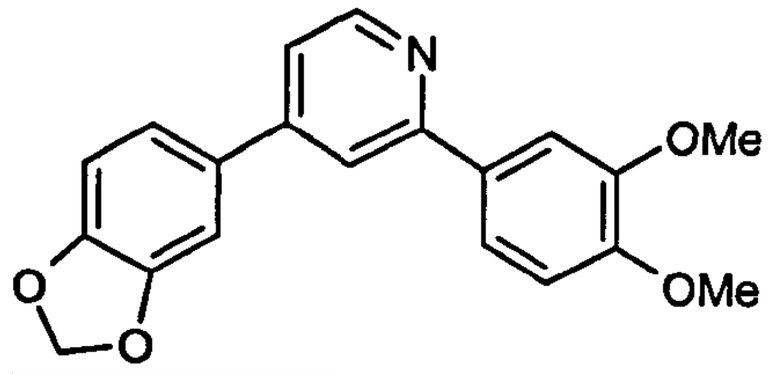

HUMAN BREAST CELL-LINE	MCF7 WITHOUT TCDD	MCF7 WITH TCDD	ACTIVATION FACTOR	MCF10A	MDA-MB-468	TUMOUR SELECTIVE FACTOR
IC_{50} VALUES (μM)	0.09	0.06	1.5	30	0.01	3000

DMU982 was found to be potently cytotoxic in MDA-MB-468 cancer cells with appreciably reduced cytotoxicity in MCF10A and MCF7 cells with and without TCDD induction. Moreover, the pyridine heterocycle of DMU982 should theoretically improve the solubility and also enable salt selection through protonation of the nitrogen to enhance the drug physicochemical properties compared to DMU949.

In this study the following physicochemical properties of the prodrugs DMU949 and DMU982 were determined; solubility, pH-solubility profile, pKa, partition coefficient, pH-partition coefficient profile, SEM and DSC. Salt selection studies were also conducted for DMU982. The aqueous solubility of the salts was performed to consider the feasibility for further development and the salts with the lowest solubility were eliminated. A comprehensive physicochemical and biological analysis of the selected salts was conducted using pH-solubility profiles, DSC, SEM and the MTT assay. Analogues of DMU949 were also synthesised in a double-prodrug strategy and metabolic evaluation of the analogues was undertaken to determine if the double-prodrug strategy was successful.

7.2 Materials and methods

Reagents were used as received from Sigma-Aldrich Chemical Company (Dorset, UK) or Alfa Aesar (Lancashire, UK). TCDD (2,3,7,8 tetrachlorodibenzo-*p*-dioxin) was obtained from British Greyhound Chromatography (Birkenhead, UK). General analytical grade ethanol, IPA, DMSO, HPLC grade water and 96-well Nunc® plates were obtained from Fisher Scientific (Loughborough, UK). Pooled human liver microsomes (20mg microsomal protein/mL, 410pmol total CYP/mg protein), human recombinant CYPs (CYP1A1 and 1B1) expressed in baculovirus-infected insect cells with co-expression of human NADPH-CYP reductase (Supersomes™) and wild-type baculovirus-infected insect cell microsomes (control microsomes) were obtained from Gentest Corporation (Woburn, USA). HPLC analytical columns were supplied by Phenomenex (Cheshire, UK). Human breast cell lines were obtained from the American Type Culture Collection. Anticancer prodrugs DMU949 and DMU982 were supplied by K. Ruparelia and S. Lodhi of the CDDG.

7.2.1 Synthesis of DMU949 derivatives

7.2.1.1 Synthesis of DMU2297

Sodium hydride in oil (0.34g, 8.54mmol) was washed 3 times with anhydrous petroleum ether under nitrogen to remove the oil phase. DMU949 (1.00g, 2.85mmol) in anhydrous tetrahydrofuran (30mL) was added slowly. After the reaction mixture had been stirred for 20 minutes, anhydrous dimethylformamide (30mL) was added, followed by 2-dimethylaminoethyl chloride hydrochloride (0.41g, 2.85mmol). The resulting mixture was

stirred at reflux temperature and sequentially monitored by TLC (ethyl acetate/petroleum ether/methanol (5:5:1) with 3% triethylamine) until the reaction was complete. The reaction was quenched with distilled water (60mL) and extracted with ethyl acetate (3×50mL). The combined organic layers were washed with saturated brine (50mL), dried with anhydrous magnesium sulphate and concentrated under *vacuo*. The crude product was purified by column chromatography with an isocratic solvent system (ethyl acetate/petroleum ether/methanol (5:5:1) with 3% triethylamine).

7.2.1.2 Synthesis of DMU2298

DMU949 (0.10g, 0.28mmol) was dissolved in dry dimethylformamide (5mL) under nitrogen. 2-Bromoacetamide (0.04g, 0.28mmol), potassium carbonate (0.01g, 0.71mmol) and sodium iodide (0.001g, 0.007mmol) were added to the mixture. The resulting mixture was stirred at 50-60°C and sequentially monitored by TLC (dichloromethane with 3% ethanol) until the reaction was complete. The reaction was quenched with distilled water (20mL) and extracted with dichloromethane (3×50mL). The combined organic layers were washed with saturated brine (50mL), dried with anhydrous magnesium sulphate and concentrated under *vacuo*. The crude product was purified by column chromatography with an eluent of dichloromethane and an increasing gradient of ethanol (3-4%).

7.2.2 Metabolism of DMU949 derivatives

7.2.2.1 Buffer preparations

All buffers were prepared using the following reagents: HPLC grade water, hydrochloric acid (HCl), sodium hydroxide (NaOH), potassium phosphate (KH_2PO_4), disodium

hydrogen orthophosphate (Na_2HPO_4), magnesium chloride ($MgCl_2.6H_2O$) and β-nicotinamide adenine dinucleotide phosphate reduced tetrasodium salt (NADPH). Sodium/potassium phosphate buffer (100mM) was prepared by the addition of 8.375g of Na_2HPO_4 and KH_2PO_4 to 900mL of HPLC grade water. Depending on the initial pH, either 1M NaOH or HCl was used to adjust the pH to 7.4, measured using a SevenEasy™ benchtop pH meter (Mettler-Toledo Inc., Ohio, USA). The buffer volume was adjusted to 1L and the pH re-checked and adjusted if necessary. A solution of 15mM magnesium chloride was prepared by the addition of 30.75g of $MgCl_2.6H_2O$ to 1L of distilled water. The 15mM stock solution was diluted appropriately to give a 5mM $MgCl_2$ solution. A solution of NADPH (5mM) was prepared immediately before each experiment. NADPH (1-3mg) was weighed out into an eppendorf tube and an appropriate volume of HPLC grade water was added to give a final concentration of 5mM. The solution was stored on ice until required.

7.2.2.2 Authentic standard preparation

The authentic standards DMU2297 and DMU2298 were dissolved in DMSO to provide 10mM stock solutions. Serial dilutions of the stock solutions were prepared to give concentrations of 100, 10, 5 and 2μM as required. Standard solutions were stored at 4°C until required. The purity of the solutions was assessed by HPLC analysis prior to experiments, where the highest measurable concentration for DMU2297 was 5μM and for DMU2298 was 2μM using the lowest gain setting on the fluorescence detector, and as such these concentrations were used for compound incubations.

7.2.2.3 HPLC analytical method for DMU949 derivatives

Separation of DMU2297 and DMU2298 and their potential metabolites was achieved using the following analytical method: Phenomenex Synergi Max-RP (250×4.6mm) analytical column at 40°C. The mobile phase (flow rate of 1mL/min) consisted of 80% solvent A (water) and 20% of solvent B (acetonitrile). On sample analysis a gradient was initiated with solvent B rising to 80% over 15 minutes. Solvent B was held at 80% for 3 minutes before returning to the initial conditions. A re-equilibration time of 6 minutes was allowed between each sample analysis. The DMU949 derivatives and their potential metabolites were detected by fluorescence using an excitation wavelength of 337nm and an emission wavelength of 420nm. Analysis was conducted on a PerkinElmer (Massachusetts, USA) analytical system consisting of a Series 200 autosampler and pump coupled with a FP-1520 fluorescence detector (Jasco, Essex, UK), DG-4400 in-line degasser (Phenomenex, Cheshire, UK) and a column heater-chiller (Jones Chromatography, California, USA). Analytical data was collected on TotalChrom HPLC software (PerkinElmer).

7.2.2.4 Quantification of DMU949 derivatives

The DMU949 derivatives were quantified in incubate samples by preparation of the appropriate calibration curves. Denatured, pooled microsomes (0.1 mg/mL) were spiked with appropriate volumes of DMU2297 (5μM) or DMU2298 (2μM) in DMSO, to give final concentrations of each in the ranges of 0.5-5μM and 0.2-2μM respectively. Calibration standards were treated in an identical manner to incubate samples (Section 7.2.2.5) prior to HPLC analysis and all calibration curves were linear in the concentration ranges used with correlation coefficients of >0.995.

7.2.2.5 Microsomal incubations and sample preparations

Compounds were incubated with CYP1A1, CYP1B1, control microsomes and pooled human liver microsomes (PHLM) under the following conditions: DMU2297 (5μM) or DMU2298 (2μM), CYP and control Supersomes™ (20pmol/mL), PHLM (164pmol/mL), NADPH (0.5mM), $MgCl_2$ (0.5mM) and sodium/potassium phosphate buffer (20mM, pH 7.4) at 37°C in a humidified incubator. Samples (100μL) were taken at 5 minute intervals between 0 and 25 minutes after the enzymatic reaction was initiated by the addition of the enzyme. The reactions were terminated by addition of an equal volume of ice-cold acetonitrile. Following centrifugation (3500 rpm, 15 minutes, 4°C) aliquots (100 μL) of the supernatants were analysed by HPLC. Control incubations were prepared by exclusion of either the compound, NADPH, enzyme or through using non-CYP expressing CTRL Supersomes™. All samples were prepared in triplicate.

7.2.2.6 Co-elution studies

To confirm the identity of the metabolites co-elution studies were performed. Incubations were prepared as previously described (Section 7.2.2.5). Samples were either analysed directly after centrifugation or if metabolism was observed samples were spiked with a 0.05 or 0.5μM solution of authentic DMU949 prior to analysis. If any of the metabolites produced corresponded to DMU949, an increase in peak area for that particular metabolite should have been observed.

7.2.3 Determination of solubility

See Section 2.2.1.

7.2.3.1 Determination of the pH-solubility profile

See Section 6.2.2.1.

7.2.3.2 Determination of the pKa

See Section 6.2.2.2.

7.2.4 Determination of log P

See Section 2.2.2.

7.2.4.1 Determination of the pH-log P profile

The buffer systems used for the pH-log *P* profile were 10mM acetate with pH range 1.75-4, 10mM phosphate with pH range 4-8 and 10mM glycine with pH range 8-12 (Section 3.2.1). The log *P* in these buffers was determined by the shake-flask method (Section 2.2.2).

7.2.5 Differential scanning calorimetry

See Section 2.2.3.

7.2.6 Scanning electron microscopy

See Section 2.2.4.

7.2.7 Salt preparation for DMU982

See Section 6.2.1.

7.3 Results

7.3.1 Chemical analysis of DMU949 derivatives

A total of two DMU949 derivatives were synthesised. They were chemically evaluated using the techniques described in Section 5.2.1 and their chemical structures, physical characteristics and yields are described below:

2-[4-(3,4-Methylenedioxyphenyl)-6-(3',4'-dimethoxyphenyl)-2-pyridyloxyl]-dimethylaminoethyl (DMU2297)

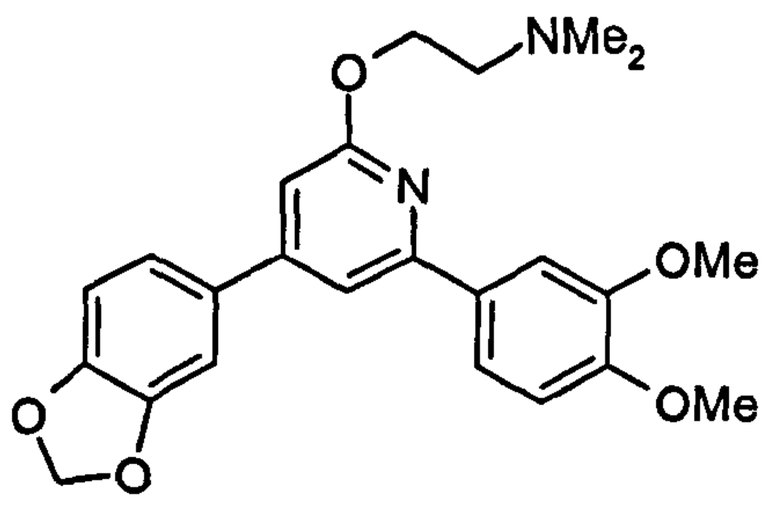

White solid, yield (0.05g, 4%); m.p. 129°C; mass spectrum (MALDI) m/z 432.20 ($M^+ + 1$); IR spectrum υmax (KBr)/cm^{-1} 1607 (O–CH3), 1506 (N–C); ^{1}H-NMR (CD_3OD) δ 2.40 (s, 6H), 2.80 (t, 2H), 3.90 (s, 3H), 3.95 (s, 3H), 4.55 (t, 2H), 6.00 (s, 2H), 6.80 (s, 1H), 6.90 (d, 1H), 7.05 (d, 1H), 7.25 (d, 2H), 7.50 (s, 1H), 7.70(d, 1H), 7.75 (s, 1H); ^{13}C-NMR (CD_3OD) δ 45.71, 45.83, 56.40, 56.50, 59.10, 64.04, 102.85, 106.71, 108.25, 109.61, 111.54, 111.78, 112.60, 120.83, 122.08, 133.36, 133.88, 149.86, 149.96, 150.43, 151.49, 153.19, 156.10, 165.14.

2-[4-(3,4-Methylenedioxyphenyl)-6-(3',4'-dimethoxyphenyl)-2-pyridyloxyl]-acetamide (DMU2298)

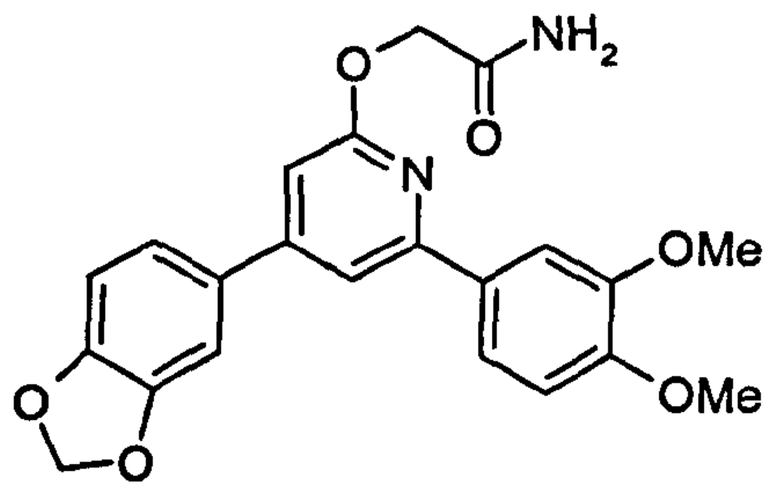

White solid, yield (0.09g, 80%); m.p. 188°C; mass spectrum (MALDI) m/z 408.40 (M^+ + 1); IR spectrum υmax (KBr)/cm^{-1} 3367 and 3182 (N–H), 1670 (C=O), 1607 (O–CH_3); ^{1}H-NMR (DMSO) δ 3.90 (s, 3H), 4.00 (s, 3H), 5.00 (s, 2H), 5.60 (s, 1H), 6.00 (s, 2H), 6.40 (s, 1H), 6.85 (s, 1H), 6.90 (s, 1H), 6.95 (d, 1H), 7.20 (t, 2H), 7.50 (s, 1H), 7.60 (d, 1H), 7.70 (s, 1H); ^{13}C-NMR (DMSO) δ 55.72, 55.79, 64.13, 101.57, 105.44, 107.44, 108.88, 110.38, 110.70, 111.76, 119.55, 121.29, 131.04, 131.69, 148.23, 148.38, 148.96, 149.99, 151.19, 154.02, 162.73, 170.76.

7.3.2 Metabolism of DMU949 derivatives

The *in vitro* metabolism of DMU2297 and DMU2298 by PHLM and control microsomes was investigated using HPLC, to determine whether the double-prodrugs were systemically cleaved to DMU949. The metabolism by CYP1A1 and CYP1B1 was also investigated:

7.3.2.1 Metabolism of DMU2297

DMU2297 was not metabolised by CYP1B1, control microsomes or PHLM, however, disappearance of the parent compound was observed with CYP1A1:

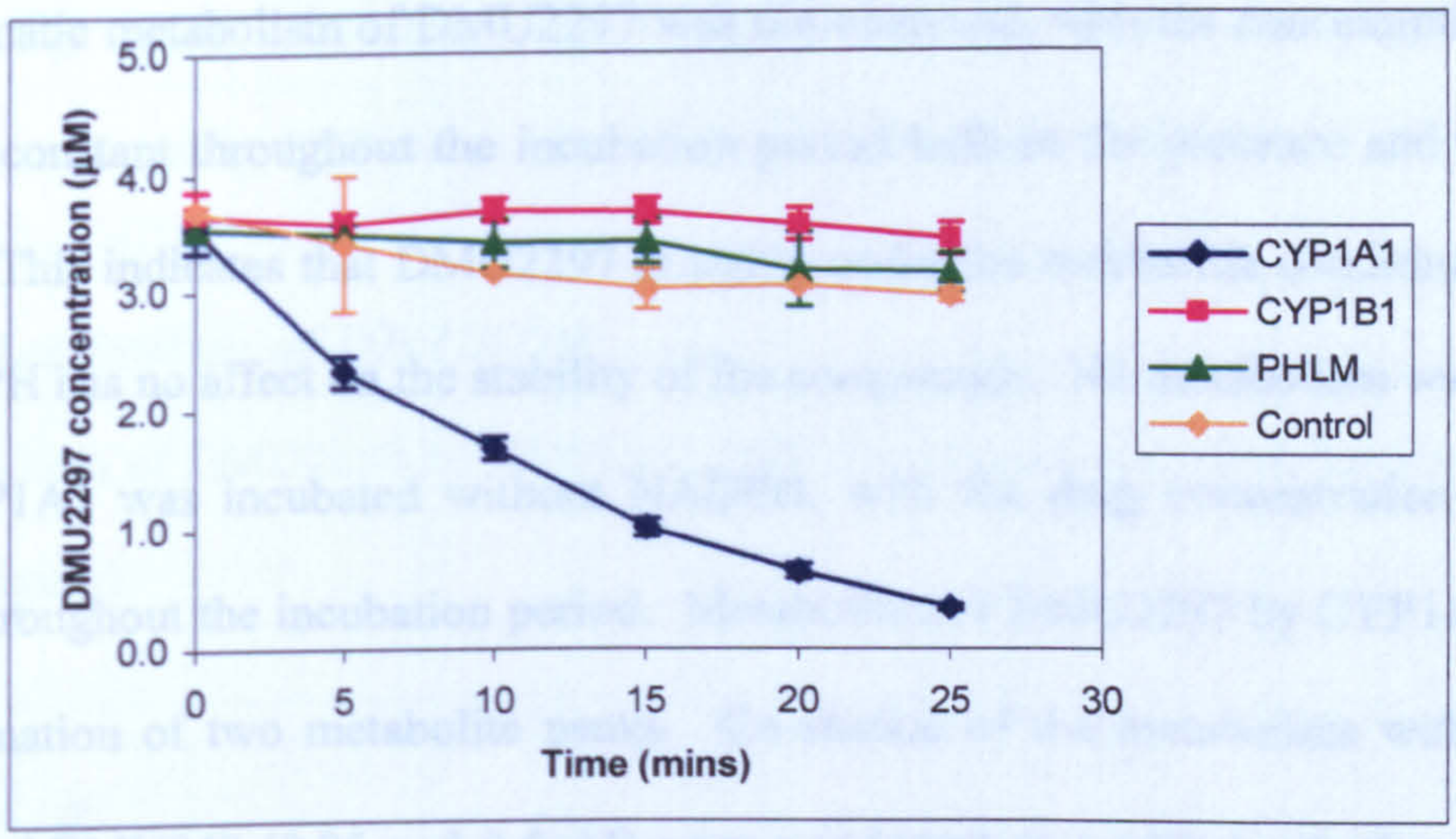

Figure 116. Time profile incubation of DMU2297 with CYP1A1, CYP1B1, control and PHLM (n=3).

To ensure that the CYP1A1-mediated disappearance of DMU2297 was metabolism and not non-enzymatic degradation of the compound in the incubate; the stability of DMU2297 was assessed under the incubation conditions. Incubations of the compound without enzyme and incubations of the compound with CYP1A1 were undertaken, both in the presence and absence of NADPH:

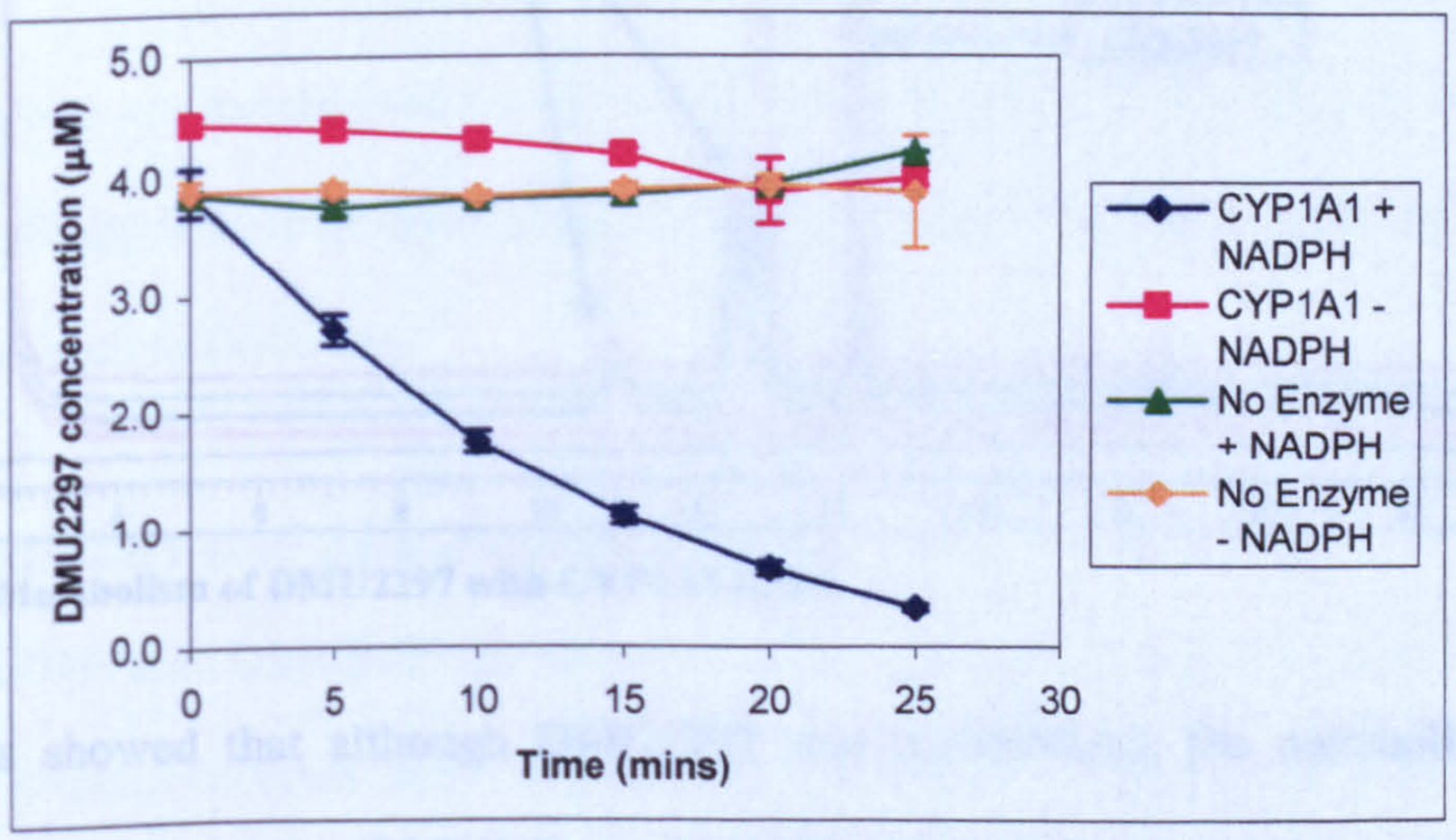

Figure 117. Time profile incubation of DMU2297 with CYP1A1 ± NADPH and no enzyme ± NADPH (n=3).

Non-enzymatic metabolism of DMU2297 was not observed, with the concentration of drug remaining constant throughout the incubation period both in the presence and absence of NADPH. This indicates that DMU2297 is stable under the incubation conditions and also that NADPH has no affect on the stability of the compounds. No metabolism was observed when CYP1A1 was incubated without NADPH, with the drug concentration remaining constant throughout the incubation period. Metabolism of DMU2297 by CYP1A1 resulted in the formation of two metabolite peaks. Co-elution of the metabolites with authentic standards of DMU949 (0.05 and 0.5μM) were conducted to establish whether DMU2297 was re-converted to DMU949:

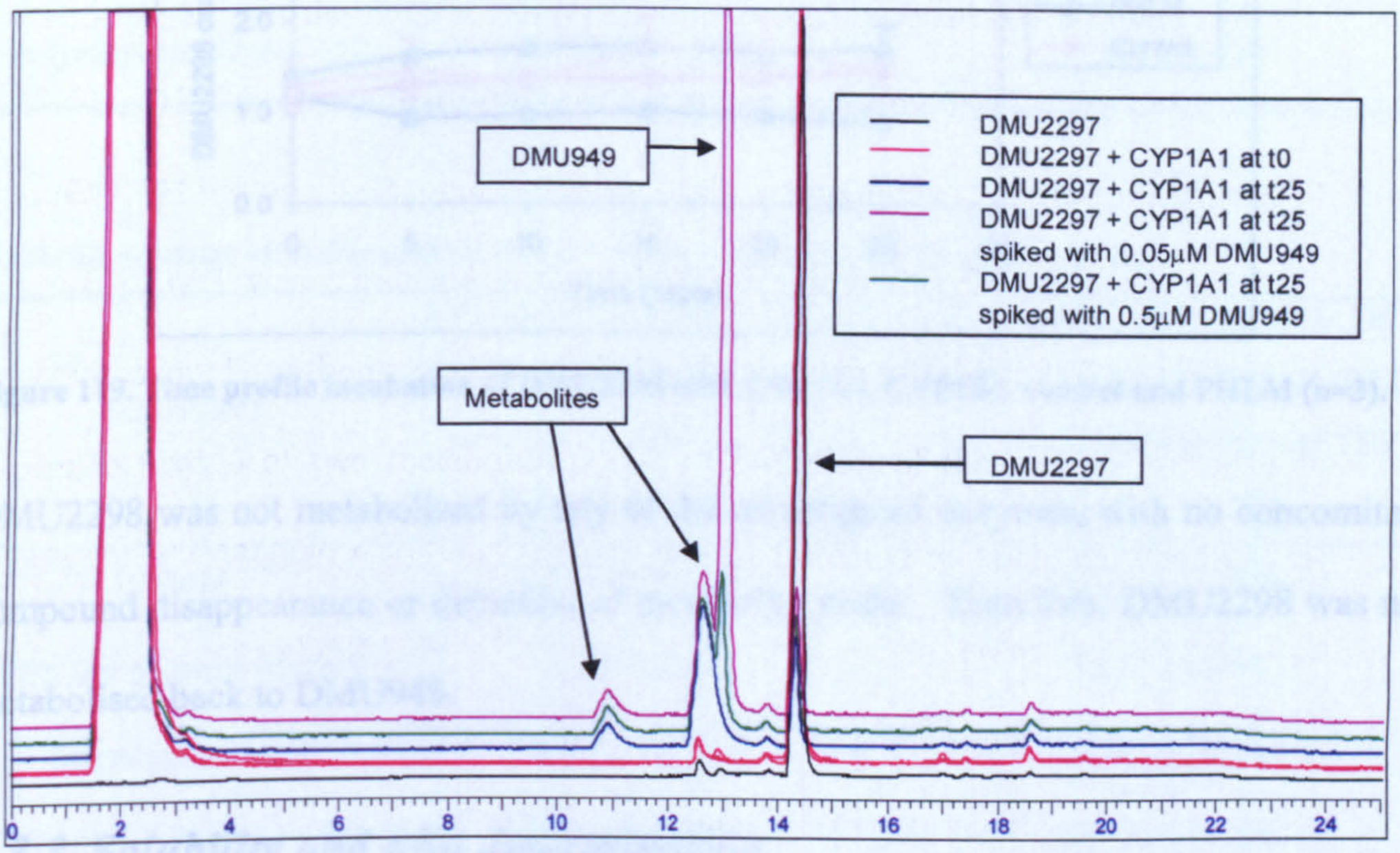

Figure 118. Metabolism of DMU2297 with CYP1A1 (n=3).

The results showed that although DMU2297 was metabolised, the metabolite peak at retention time 12.3 was not DMU949, as the DMU949 spike had a retention time of 12.5.

The similarity in retention times for DMU949 and the metabolite suggest that the metabolite produced by CYP1A1 is structurally very similar to DMU949.

7.3.2.2 Metabolism of DMU2298

The metabolism of DMU2298 by CYP1A1, CYP1B1, PHLM and control microsomes was also investigated:

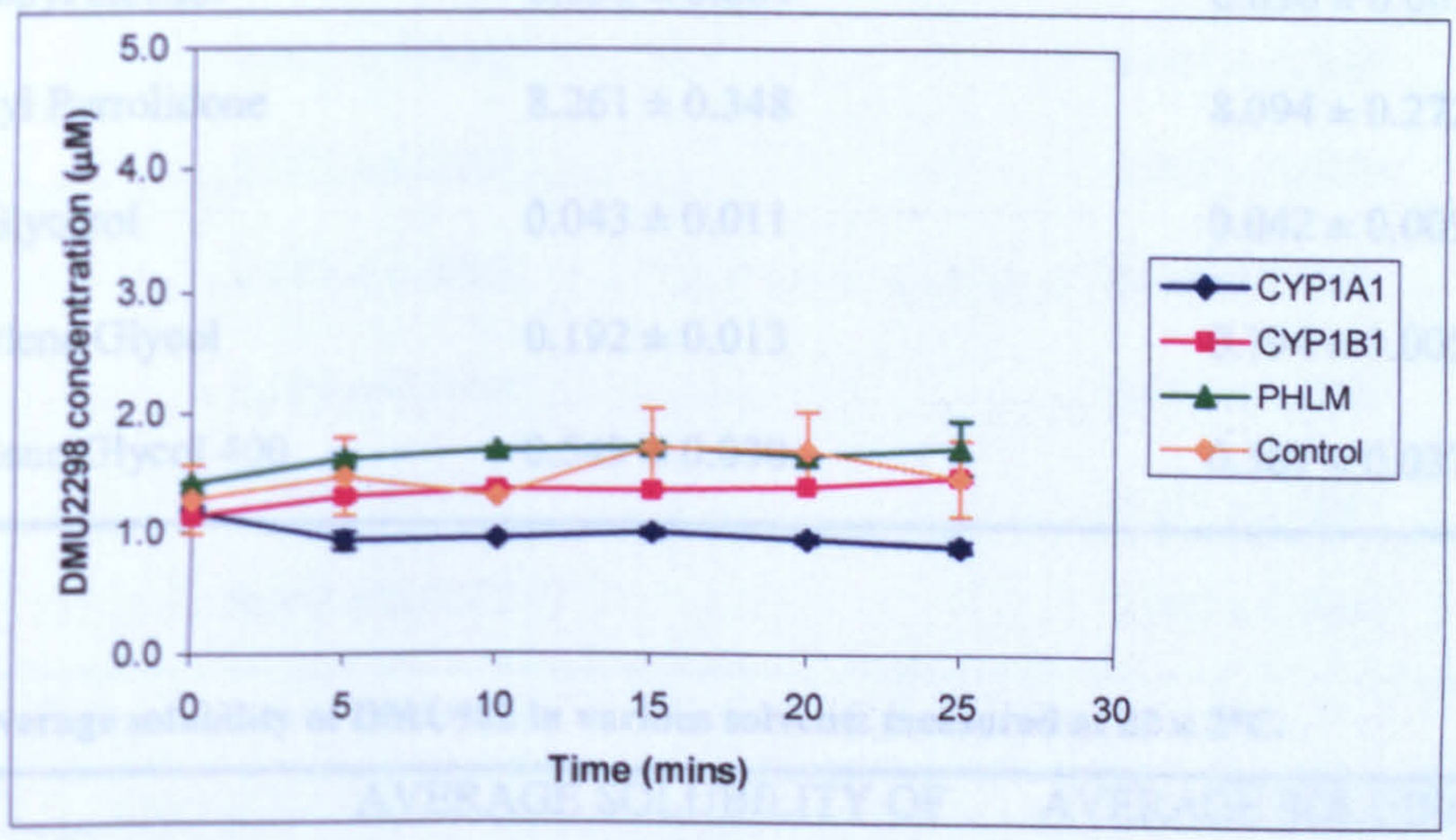

Figure 119. Time profile incubation of DMU2298 with CYP1A1, CYP1B1, control and PHLM (n=3).

DMU2298 was not metabolised by any of the investigated enzymes, with no concomitant compound disappearance or detection of metabolite peaks. Therefore, DMU2298 was not metabolised back to DMU949.

7.3.3 Solubility and pKa determination

Both DMU949 and DMU982 are slightly soluble in water; however, they were more soluble in organic solvents such as PEG 400 and NMP. Overall, DMU982 was more soluble in all solvents compared to DMU949:

Table 62. Average solubility of DMU949 in various solvents measured at 22 ± 2°C.

SOLVENT	AVERAGE SOLUBILITY OF DMU949 MEASURED ON THE UV PLATE READER (mg/mL) (n=3)	AVERAGE SOLUBILITY OF DMU949 MEASURED ON THE UV SPECTROPHOTOMETER (mg/mL) (n=3)
Water	0.003 ± 0.001	0.003 ± 0.0004
10% v/v aqueous ethanol	0.002 ± 0.001	0.002 ± 0.001
Isopropyl alcohol	0.030 ± 0.004	0.030 ± 0.003
N-Methyl Pyrrolidone	8.261 ± 0.348	8.094 ± 0.272
Glycerol	0.043 ± 0.011	0.042 ± 0.009
Propylene Glycol	0.192 ± 0.013	0.194 ± 0.005
Polyethylene Glycol 400	0.549 ± 0.030	0.567 ± 0.037

Table 63. Average solubility of DMU982 in various solvents measured at 22 ± 2°C.

SOLVENT	AVERAGE SOLUBILITY OF DMU982 MEASURED ON THE UV PLATE READER (mg/mL) (n=3)	AVERAGE SOLUBILITY OF DMU982 MEASURED ON THE UV SPECTROPHOTOMETER (mg/mL) (n=3)
Water	0.001 ± 0.001	0.001 ± 0.0004
10% v/v aqueous ethanol	0.002 ± 0.001	0.001 ± 0.001
Isopropyl alcohol	0.174 ± 0.011	0.179 ± 0.011
N-Methyl Pyrrolidone	93.146 ± 1.909	86.183 ± 5.766
Glycerol	0.031 ± 0.005	0.028 ± 0.002
Propylene Glycol	0.421 ± 0.044	0.434 ± 0.004
Polyethylene Glycol 400	17.176 ± 2.080	18.024 ± 1.031

The pH-solubility profile of DMU949 was also determined, over a pH range of 2-12:

Table 64. Solubility of DMU949 in different buffers measured at 22 ± 2°C.

pH	AVERAGE SOLUBILITY OF DMU949 MEASURED ON THE UV PLATE READER (mg/mL) (n=3)	AVERAGE SOLUBILITY OF DMU949 MEASURED ON THE UV SPECTROPHOTOMETER (mg/mL) (n=3)
2	0.002 ± 0.0002	0.003 ± 0.0003
4	0.003 ± 0.0003	0.003 ± 0.0004
7	0.001 ± 0.0002	0.001 ± 0.0001
8	0.001 ± 0.0001	0.001 ± 0.0005
9	0.001 ± 0.0005	0.001 ± 0.0007
11	0.002 ± 0.0009	0.001 ± 0.0001
10	0.001 ± 0.0002	0.001 ± 0.0001
12	0.002 ± 0.0003	0.002 ± 0.0005

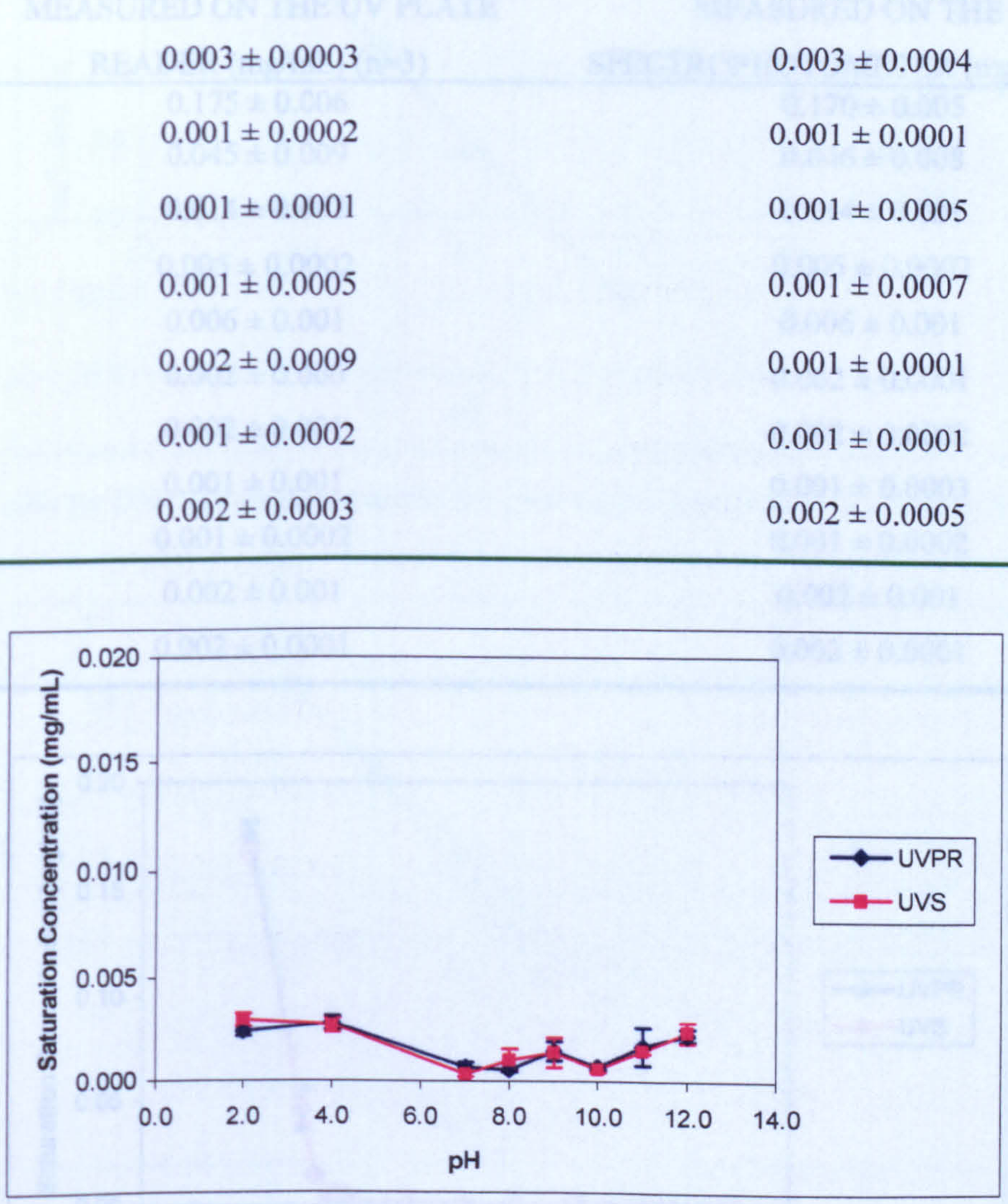

Figure 120. pH solubility profile for DMU949 measured on the UV plate reader and spectrophotometer at 22 ± 2°C. (n=3).

The pH-solubility profile of DMU949 showed that the drug solubility does not significantly change with pH, thereby indicating that DMU949 is a non-ionisable compound. The pH-solubility profile of DMU982 was also determined over a pH-range of 2-11:

Table 65. Solubility of DMU982 in different buffers measured at 22 ± 2°C.

pH	AVERAGE SOLUBILITY OF DMU982 MEASURED ON THE UV PLATE READER (mg/mL) (n=3)	AVERAGE SOLUBILITY OF DMU982 MEASURED ON THE UV SPECTROPHOTOMETER (mg/mL) (n=3)
2.00	0.175 ± 0.006	0.170 ± 0.005
3.00	0.045 ± 0.009	*0.046 ± 0.008*
3.25	0.014 ± 0.002	0.014 ± 0.001
3.50	0.005 ± 0.0002	0.005 ± 0.0002
3.75	0.006 ± 0.001	0.006 ± 0.001
4.00	0.002 ± 0.000	0.002 ± 0.0001
5.00	0.002 ± 0.001	0.002 ± 0.0002
6.00	0.001 ± 0.001	0.001 ± 0.0003
7.00	0.001 ± 0.0002	0.001 ± 0.0002
8.00	0.002 ± 0.001	0.002 ± 0.001
11.00	0.002 ± 0.0001	0.002 ± 0.0001

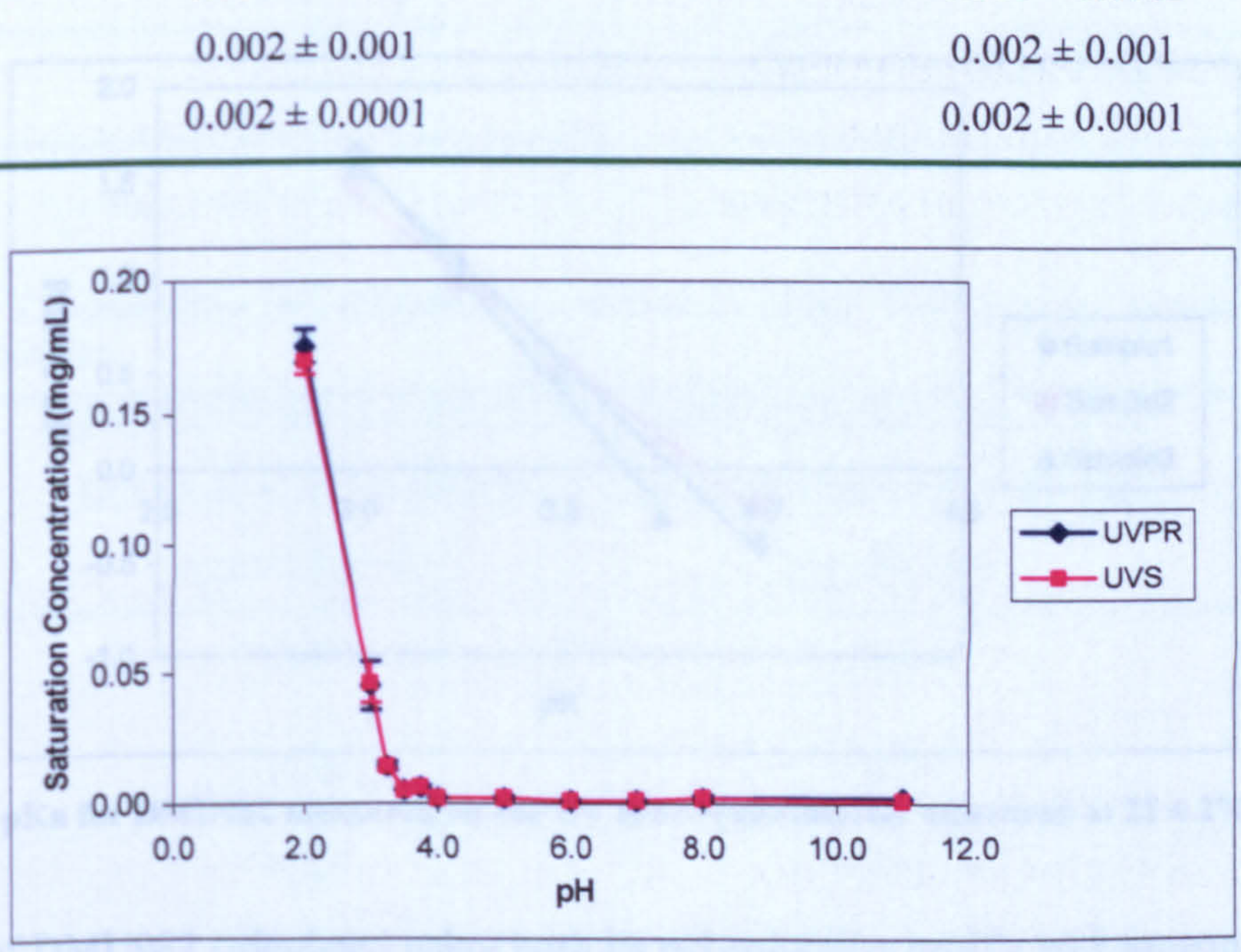

Figure 121. pH solubility profile for DMU982 measured on the UV plate reader and spectrophotometer at 22 ± 2°C. (n=3).

The pH-solubility profile of DMU982 showed the free base to be most soluble at low pH values between pH 2-4. Above pH 4 the solubility began to drop off. The pKa of DMU982 was also determined from the pH-solubility profile:

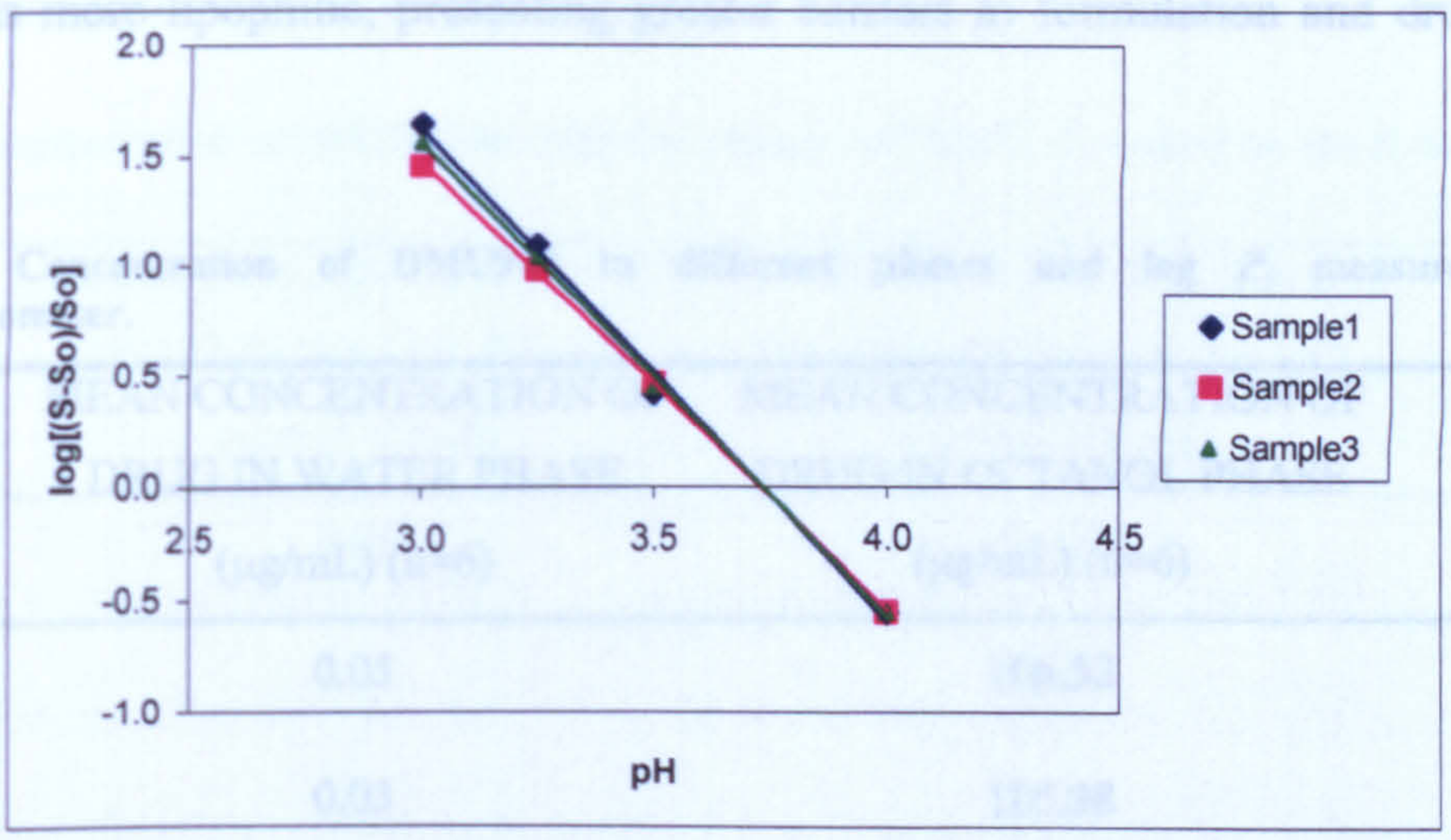

Figure 122. pKa for DMU982 measured on the UV plate reader measured at 22 ± 2°C (n=3).

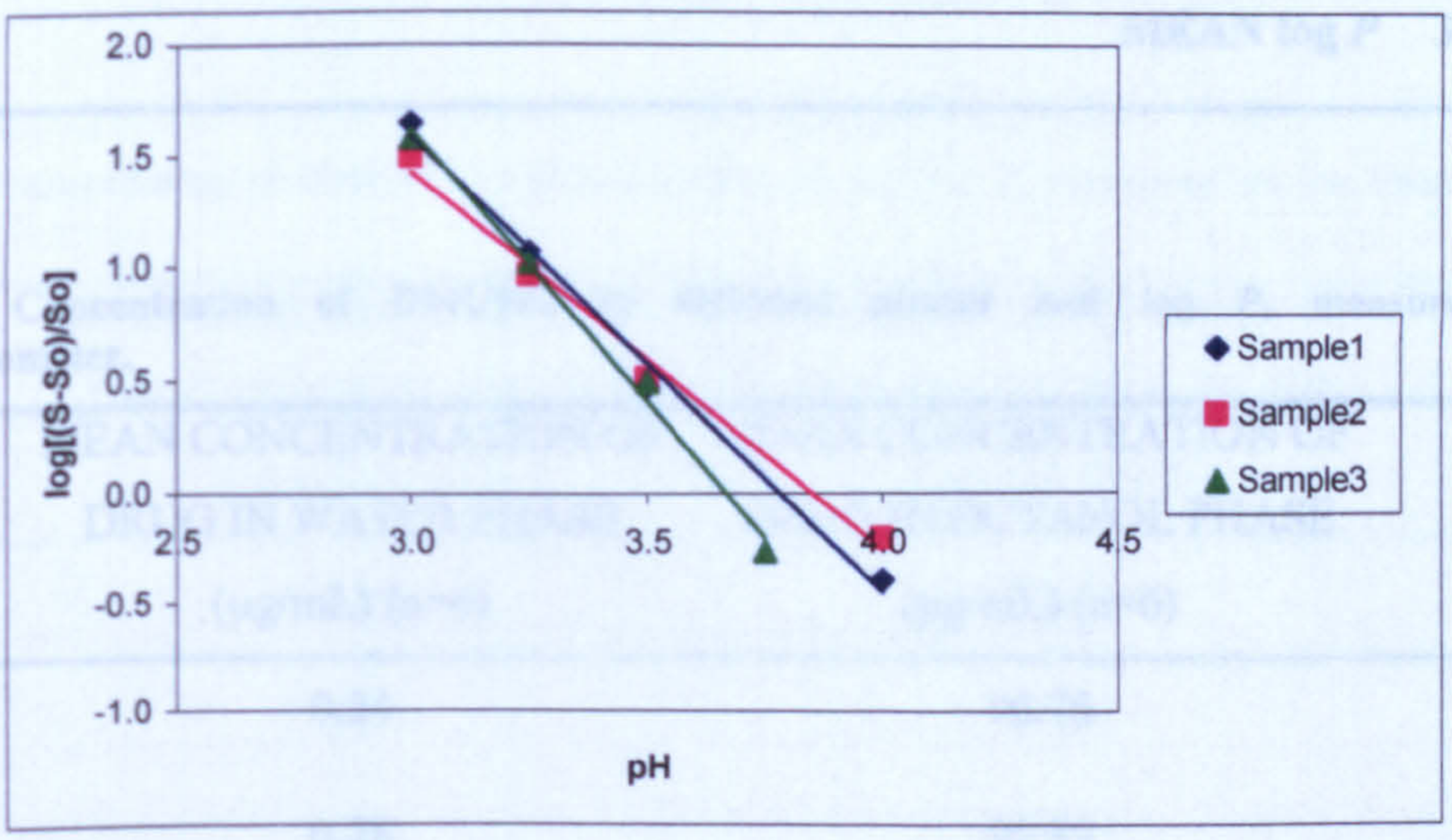

Figure 123. pKa for DMU982 measured on the UV spectrophotometer measured at 22 ± 2°C (n=3).

The pKa of DMU982 calculated using both its pH-solubility profile and aqueous solubility was 3.73 from the UV plate reader and 3.77 from the UV spectrophotometer.

7.3.4 Log P determination

Log *P* experimental values determined suggest that DMU982 is a more favourable candidate for preclinical evaluation than DMU949, which has a higher log *P* value and therefore is more lipophilic, presenting greater barriers to formulation and drug aqueous solubility.

Table 66. Concentration of DMU949 in different phases and log *P*, measured on UV spectrophotometer.

SAMPLE	MEAN CONCENTRATION OF DRUG IN WATER PHASE (μg/mL) (n=6)	MEAN CONCENTRATION OF DRUG IN OCTANOL PHASE (μg/mL) (n=6)	Log *P*
1	0.05	106.52	3.30
2	0.03	105.38	3.49
3	0.11	100.31	2.95
		MEAN log *P*	3.25 ± 0.28

Table 67. Concentration of DMU982 in different phases and log *P*, measured on UV spectrophotometer.

SAMPLE	MEAN CONCENTRATION OF DRUG IN WATER PHASE (μg/mL) (n=6)	MEAN CONCENTRATION OF DRUG IN OCTANOL PHASE (μg/mL) (n=6)	Log *P*
1	0.24	96.76	2.61
2	0.28	95.89	2.53
3	0.40	95.89	2.38
		MEAN log *P*	2.51 ± 0.12

7.3.4.1 Fluorescent plate reader method

The log *P* values for DMU949 and DMU982 determined on the fluorescent plate reader were comparable with those determined on the UV spectrophotometer, thereby confirming the usefulness of the high-throughput method:

Table 68. Concentration of DMU949 in different phases and log *P*, measured on the fluorescent plate reader.

SAMPLE	MEAN CONCENTRATION OF DRUG IN WATER PHASE (μg/mL) (n=6)	MEAN CONCENTRATION OF DRUG IN OCTANOL PHASE (μg/mL) (n=6)	Log *P*
1	0.06	95.48	3.17
2	0.04	92.01	3.33
3	0.08	85.65	3.05
		MEAN log *P*	3.18 ± 0.14

Table 69. Concentration of DMU982 in different phases and log *P*, measured on the fluorescent plate reader.

SAMPLE	MEAN CONCENTRATION OF DRUG IN WATER PHASE (μg/mL) (n=6)	MEAN CONCENTRATION OF DRUG IN OCTANOL PHASE (μg/mL) (n=6)	Log *P*
1	0.14	85.65	2.78
2	0.35	87.29	2.40
3	0.26	88.61	2.54
		MEAN log *P*	2.57 ± 0.20

7.3.4.2 Determination of the pH-log P profile

The pH-log *P* profile of DMU982 showed that between pH 4.75-8.75 the log *P* was maintained at the level determined with water as the aqueous phase. Below pH 4.75 partitioning into the octanol phase decreased:

Table 70. Log *P* of DMU982 in different buffers.

pH	AVERAGE log *P* OF DMU982 MEASURED ON THE FLUORESCENT PLATE READER (mg/mL) (n=3)	AVERAGE log *P* OF DMU982 MEASURED ON THE UV SPECTROPHOTOMETER (mg/mL) (n=3)
1.75	0.81 ± 0.05	0.60 ± 0.01
2.75	1.72 ± 0.04	1.70 ± 0.01
3.75	2.13 ± 0.08	2.20 ± 0.06
4.75	2.42 ± 0.12	2.44 ± 0.08
5.75	2.52 ± 0.17	2.38 ± 0.05
6.75	2.37 ± 0.06	2.48 ± 0.12
8.75	2.24 ± 0.07	2.32 ± 0.11

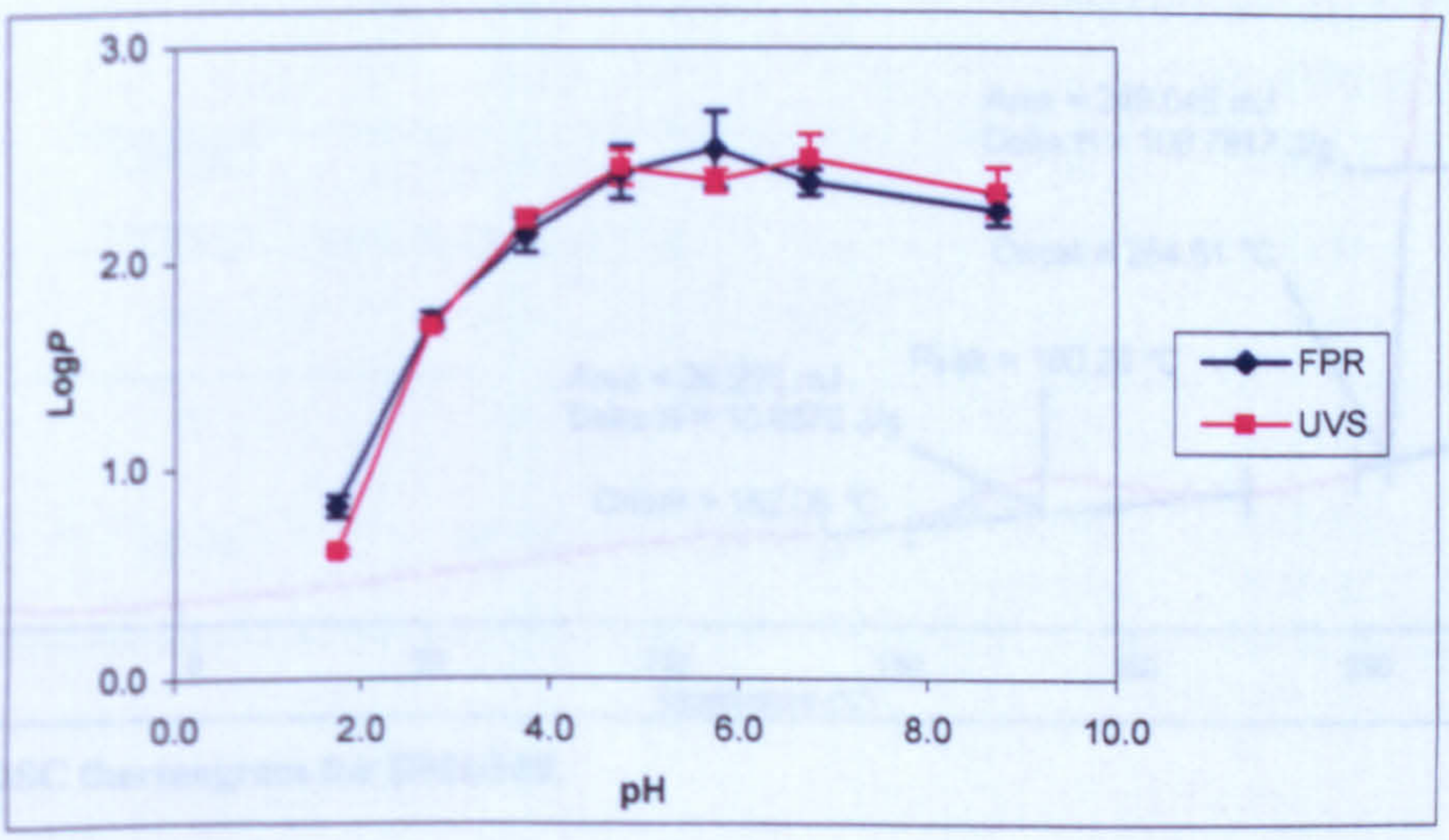

Figure 124. pH-log *P* profile for DMU982 in the octanol-buffer system measured on the fluorescent plate reader and UV spectrophotometer.

7.3.5 Differential scanning calorimetry

DSC measurements for DMU982 did not show the presence of polymorphs, solvates and impurities, since all prodrug scans exhibited a single endotherm peak. DMU949 exhibited two endotherm peaks:

Table 71. DSC of DMU949 and DMU982 – initial heating from -100-300°C at 400°C/min.

DRUG	T_g			MELTING POINT ENDOTHERM		
	ONSET TEMP (°C)	T_g HALF EXTRAPOLATED (°C)	DELTA C_p (J/g*°C)	ONSET TEMP (°C)	PEAK TEMP (°C)	DELTA H (J/g)
DMU949	–	–	–	152.06 254.51	180.20 267.01	10.66 108.79
DMU982	–	–	–	167.20	176.65	77.33

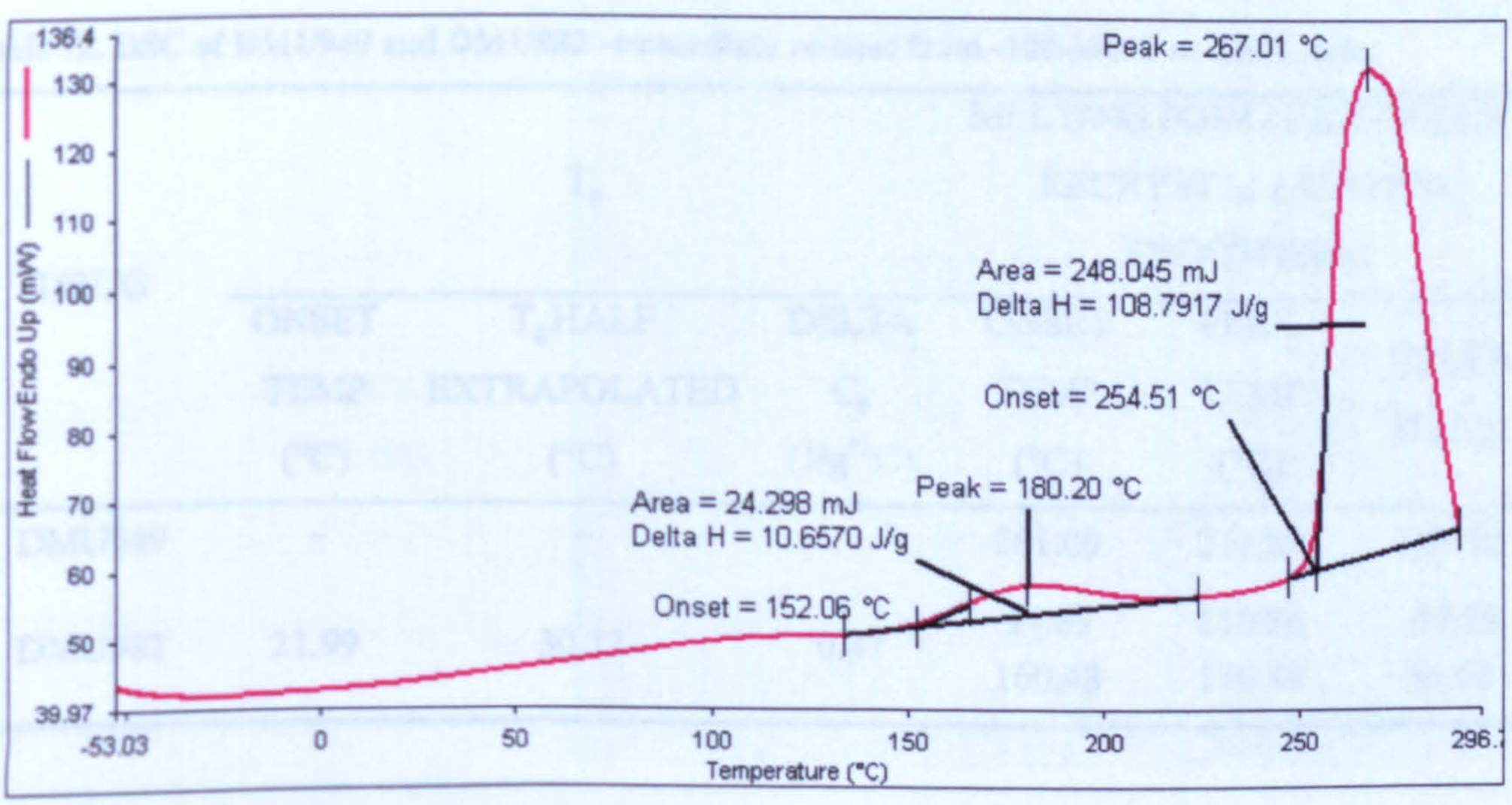

Figure 125. DSC thermogram for DMU949.

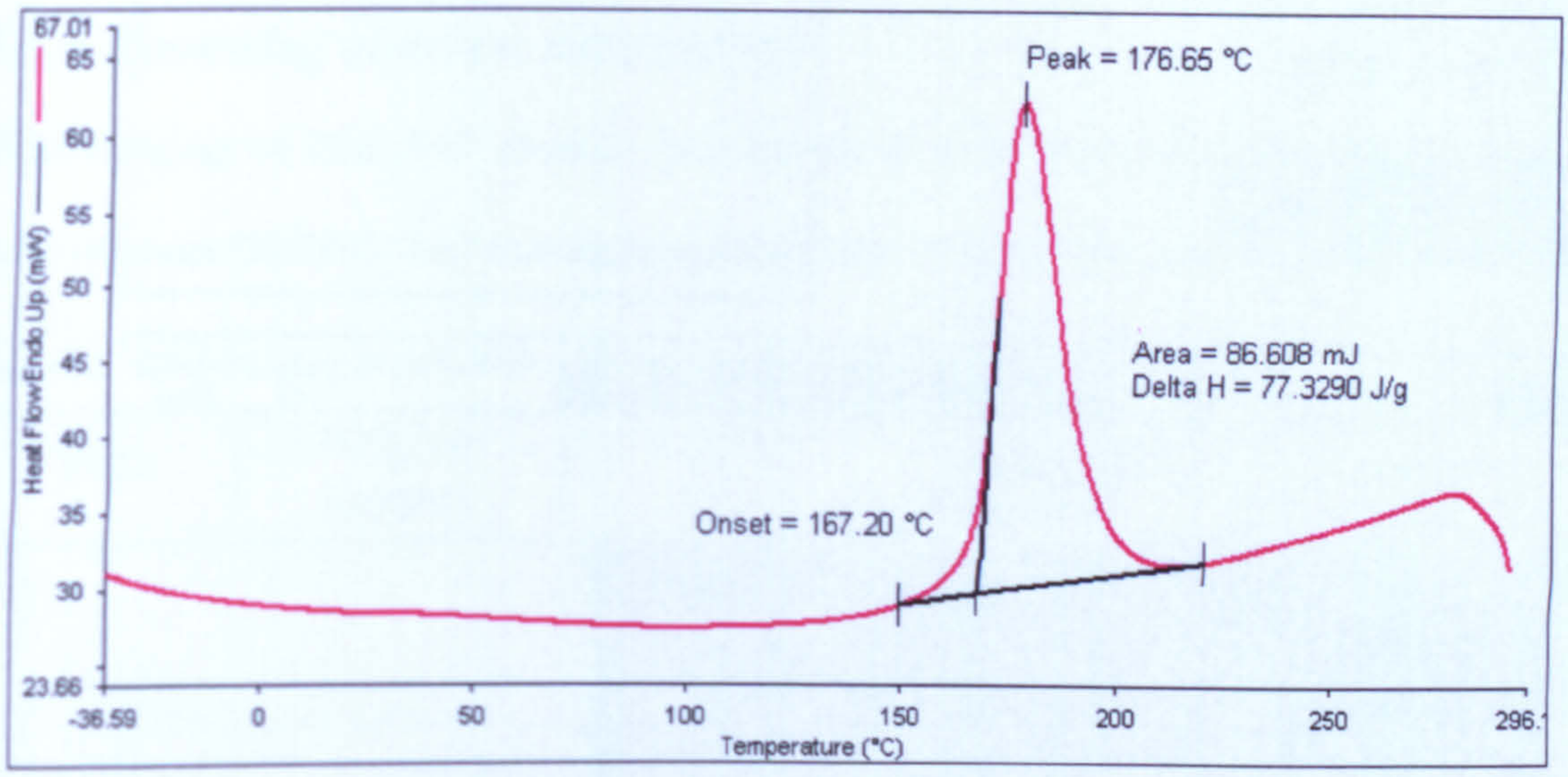

Figure 126. DSC thermogram for DMU982.

Immediately after the initial scan the samples were rapidly cooled and reheated to determine if any recrystallization was apparent. The second DSC scan for both compounds showed some recrystallization:

Table 72. DSC of DMU949 and DMU982 –immediate re-heat from -100-300°C at 400°C/min.

DRUG	T_g			MELTING POINT EXOTHERM / RECRYSTALLIZATION ENDOTHERM		
	ONSET TEMP (°C)	T_g HALF EXTRAPOLATED (°C)	DELTA C_p (J/g*°C)	ONSET TEMP (°C)	PEAK TEMP (°C)	DELTA H (J/g)
DMU949	–	–	–	261.09	271.89	107.10
DMU982	21.99	30.13	0.47	94.69 160.48	110.86 170.48	-57.25 64.66

7.3.6 Scanning electron microscopy

SEM imaging of DMU949 showed the crystals to exist as large compact agglomerated rods, whereas DMU982 had non-agglomerated blade shaped crystals:

Table 73. SEM imaging of DMU949 and DMU982.

DRUG	CRYSTAL SHAPE	SEM IMAGE
DMU949	Triclinic, Agglomerated rods	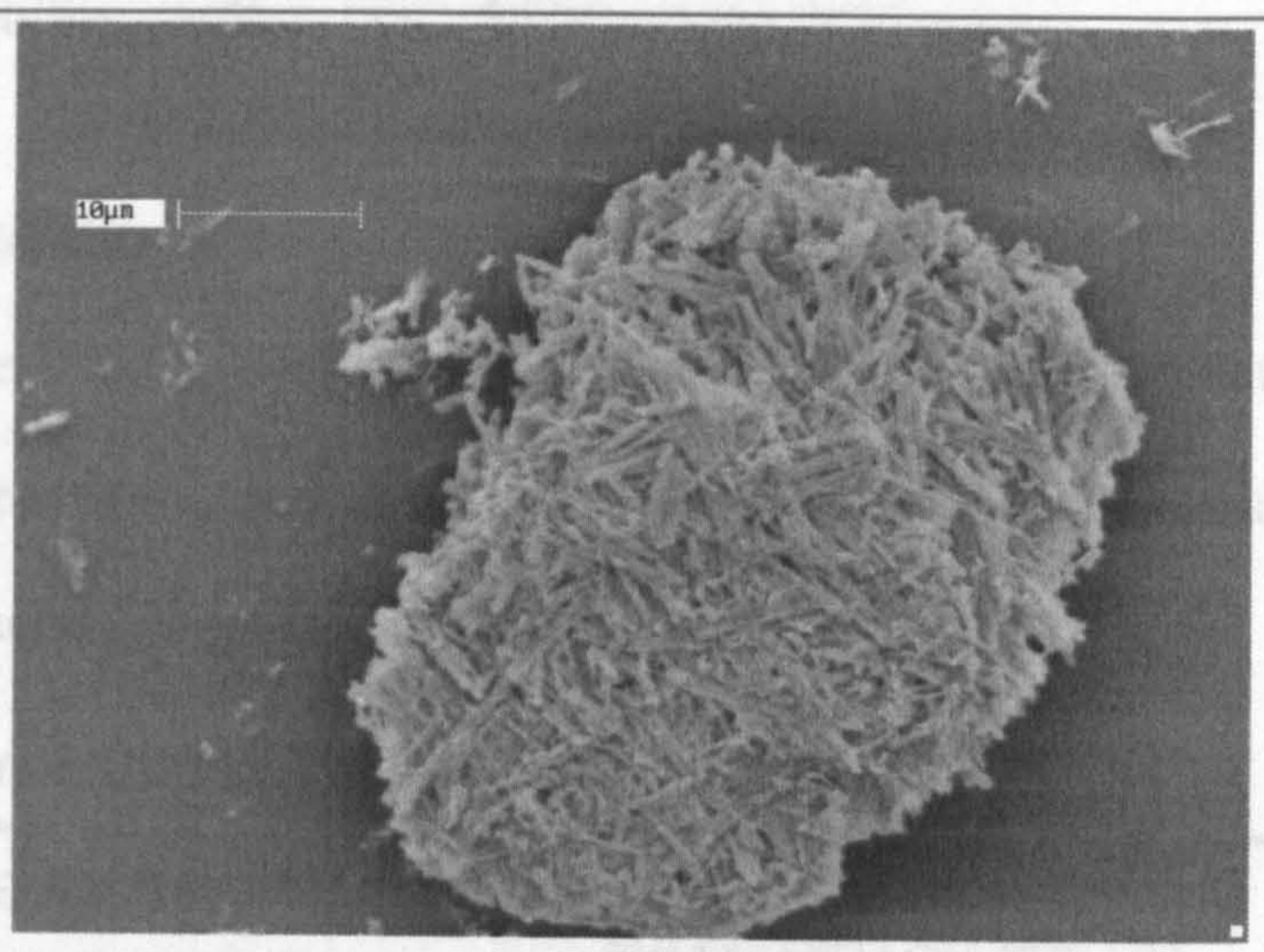
DMU982	Orthorhombic, Blades	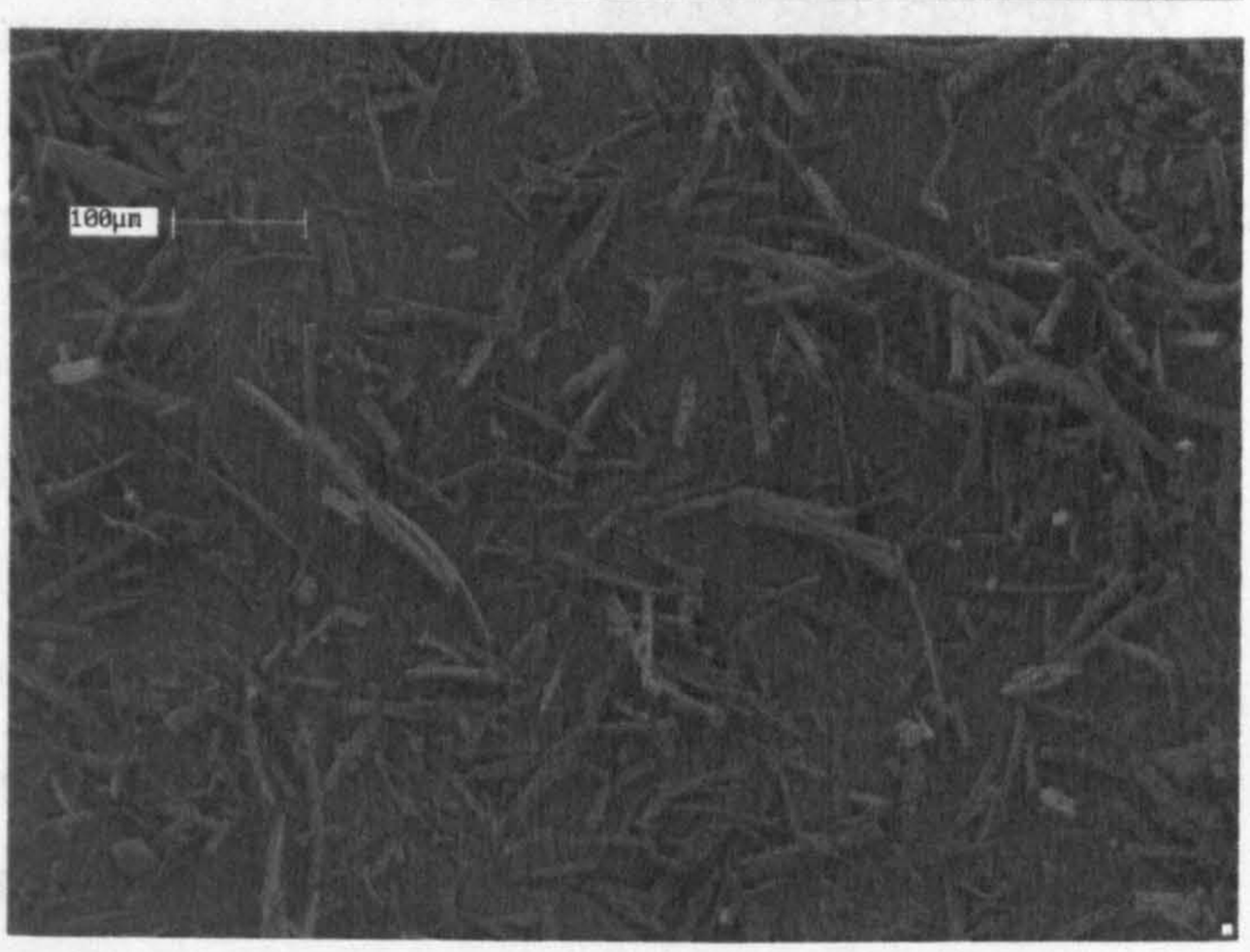

7.3.7 Salt selection

The crystalline salts formed during salt selection for DMU982 were the sulphate, maleate, phosphate, hydrochloride, mesylate, tartarate, oxalate, besylate, tosylate and saccharinate. The aqueous solubility of these salts was firstly measured to eliminate salts with the lowest solubility. A comprehensive physicochemical and biological analysis of the optimum salts was then conducted using pH-solubility profiles, DSC, SEM and the MTT assay.

7.3.7.1 Determination of solubility

The DMU982 salt forms with the highest aqueous solubility were the sulphate, maleate, phosphate and hydrochloride respectively, and as such a comprehensive preformulation study was conducted for each of them:

Table 74. Average aqueous solubility of DMU982 salts measured at 22 ± 2°C.

SALT	AVERAGE SOLUBILITY MEASURED ON THE UV PLATE READER (mg/mL) (n=3)	AVERAGE SOLUBILITY MEASURED ON THE UV SPECTROPHOTOMETER (mg/mL) (n=3)
Sulphate	0.210 ± 0.002	0.202 ± 0.001
Maleate	0.184 ± 0.001	0.184 ± 0.005
Phosphate	0.083 ± 0.002	0.087 ± 0.001
Hydrochloride	0.061 ± 0.001	0.065 ± 0.0004
Mesylate	0.039 ± 0.004	0.045 ± 0.002
Tartarate	0.019 ± 0.001	0.021 ± 0.002
Oxalate	0.015 ± 0.0003	0.015 ± 0.0001
Besylate	0.014 ± 0.003	0.014 ± 0.002
Tosylate	0.007 ± 0.001	0.006 ± 0.0002
Saccharinate	0.006 ± 0.002	0.006 ± 0.0004

To further investigate the best salt form for future studies the pH-solubility profiles of these salt forms was determined:

Table 75. Solubility of DMU982 salts in different buffers measured at 22 ± 2°C.

SALT	pH	AVERAGE SOLUBILITY MEASURED ON THE UV PLATE READER (mg/mL) (n=3)	AVERAGE SOLUBILITY MEASURED ON THE UV SPECTROPHOTOMETER (mg/mL) (n=3)
Sulphate	2	0.155 ± 0.007	0.160 ± 0.004
Sulphate	4	0.076 ± 0.001	0.080 ± 0.001
Sulphate	7	0.014 ± 0.0001	0.016 ± 0.0001
Sulphate	10	0.002 ± 0.0001	0.002 ± 0.001
Sulphate	12	0.004 ± 0.001	0.004 ± 0.001
Maleate	2	0.219 ± 0.001	0.223 ± 0.0001
Maleate	4	0.006 ± 0.001	0.009 ± 0.0004
Maleate	7	0.007 ± 0.002	0.005 ± 0.0001
Maleate	10	0.002 ± 0.0001	0.002 ± 0.001
Maleate	12	0.006 ± 0.001	0.006 ± 0.001
Phosphate	2	0.138 ± 0.001	0.143 ± 0.001
Phosphate	4	0.038 ± 0.002	0.043 ± 0.001
Phosphate	7	0.003 ± 0.0001	0.003 ± 0.0001
Phosphate	10	0.001 ± 0.0002	0.001 ± 0.0001
Phosphate	12	0.006 ± 0.0003	0.004 ± 0.001
Hydrochloride	2	0.115 ± 0.001	0.122 ± 0.001
Hydrochloride	4	0.009 ± 0.001	0.020 ± 0.002
Hydrochloride	7	0.002 ± 0.001	0.001 ± 0.001
Hydrochloride	10	0.001 ± 0.0001	0.001 ± 0.0002
Hydrochloride	12	0.003 ± 0.0002	0.003 ± 0.0002

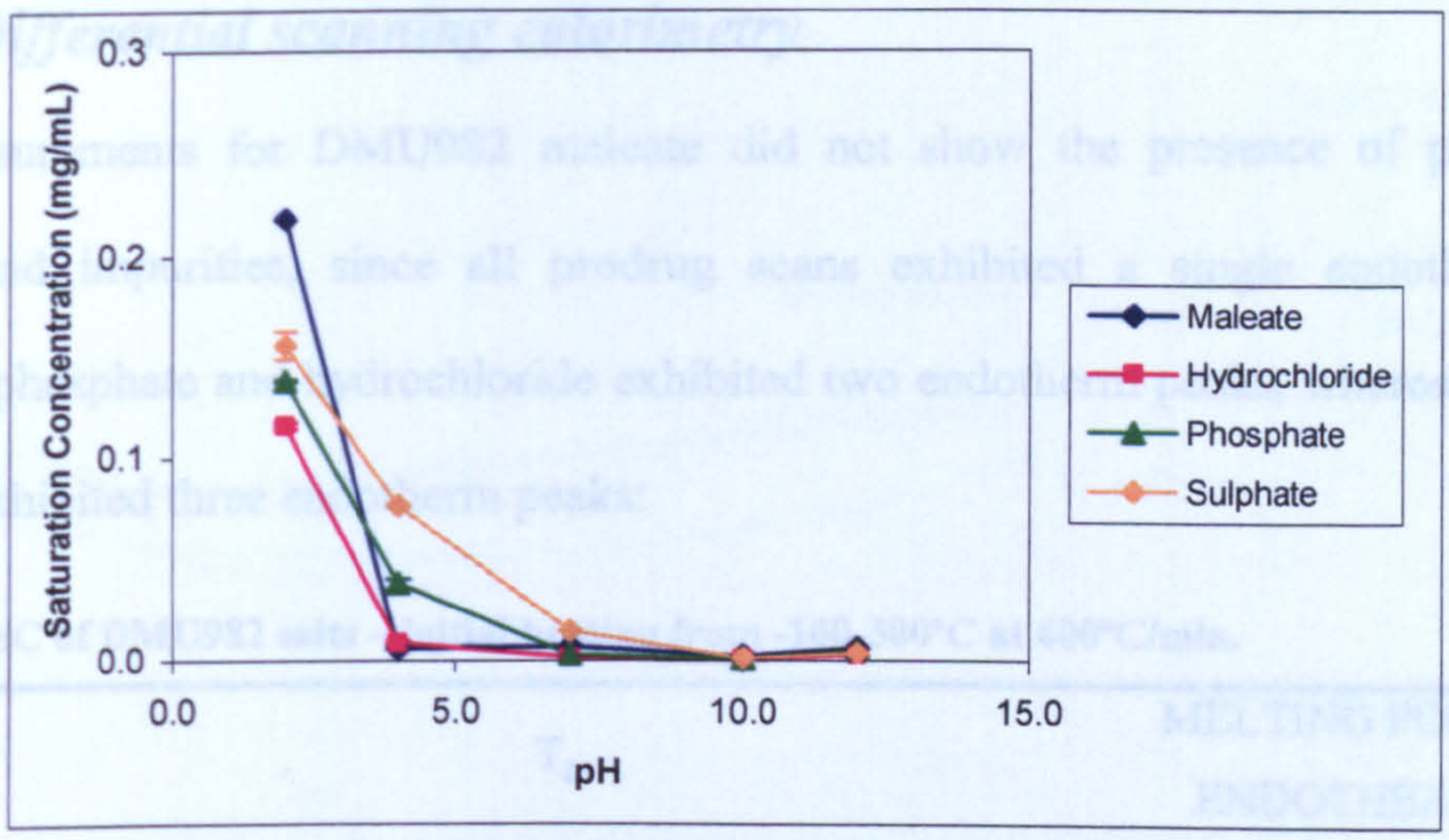

Figure 127. pH solubility profiles for DMU982 salts measured on the UV plate reader at 22 ± 2°C (n=3).

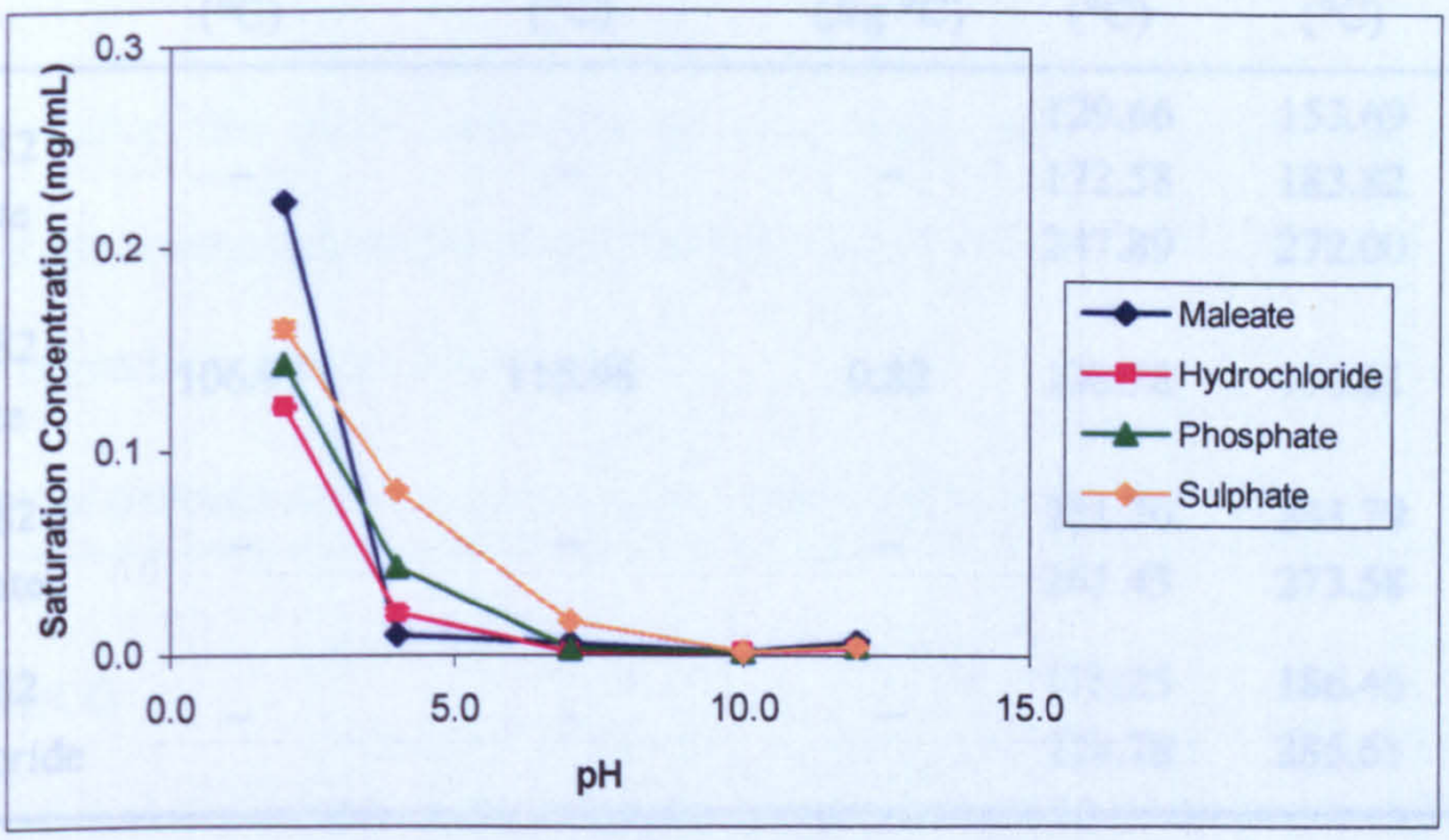

Figure 128. pH solubility profiles for DMU982 salts measured on the UV spectrophotometer at 22 ± 2°C (n=3).

DMU982 sulphate had the highest solubility over a wide pH range of 2-10. The highest solubility at pH 2 was observed with DMU982 maleate and at pH 7 the highest solubility was with DMU982 sulphate.

7.3.7.2 Differential scanning calorimetry

DSC measurements for DMU982 maleate did not show the presence of polymorphs, solvates and impurities, since all prodrug scans exhibited a single endotherm peak. DMU982 phosphate and hydrochloride exhibited two endotherm peaks, whereas DMU982 sulphate exhibited three endotherm peaks:

Table 76. DSC of DMU982 salts – initial heating from -100-300°C at 400°C/min.

DRUG	T_g			MELTING POINT ENDOTHERM		
	ONSET TEMP (°C)	T_g HALF EXTRAPOLATED (°C)	DELTA C_p (J/g*°C)	ONSET TEMP (°C)	PEAK TEMP (°C)	DELTA H (J/g)
DMU982 Sulphate	–	–	–	129.66 172.58 247.89	153.69 183.82 272.00	22.79 4.79 98.31
DMU982 Maleate	106.97	115.98	0.82	138.78	150.01	20.32
DMU982 Phosphate	–	–	–	231.76 261.43	243.79 273.58	19.55 59.10
DMU982 Hydrochloride	–	–	–	175.25 278.78	186.46 285.61	17.61 50.89

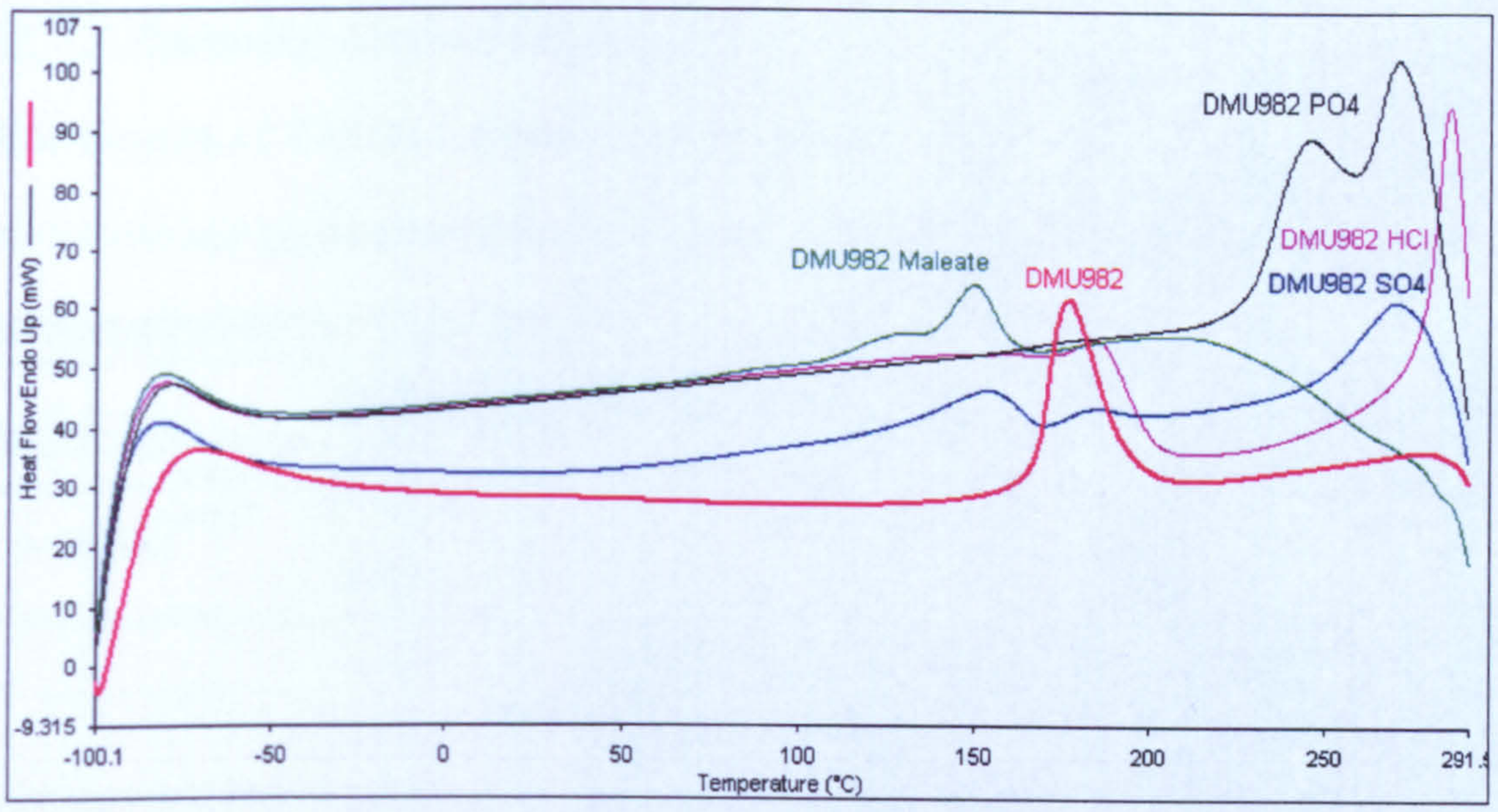

Figure 129. DSC thermograms of DMU982 salts compared to the free base.

Immediately after the initial scan the samples were rapidly cooled and reheated to determine if any recrystallization was apparent. The second DSC scan for all compounds showed no immediate recrystallization:

Table 77. DSC of DMU982 salts –immediate re-heat from -100-300°C at 400°C/min.

DRUG	T_g		
	ONSET TEMP (°C)	T_g HALF EXTRAPOLATED (°C)	DELTA C_p (J/g*°C)
DMU982 Sulphate	95.10	111.27	0.76
DMU982 Maleate	23.92	33.63	0.58
DMU982 Phosphate	66.55	103.60	0.10
DMU982 Hydrochloride	75.44	86.08	0.62
	169.00	186.73	0.87

7.3.7.3 Scanning electron microscopy

SEM imaging of DMU982 sulphate showed agglomerated rod and plate shaped crystals, the maleate had agglomerated fibrous crystals, the phosphate had agglomerated rod crystals and the hydrochloride existed as agglomerated needle and fibrous crystals:

Table 78. SEM imaging of DMU982 salts.

DRUG	CRYSTAL SHAPE	SEM IMAGE
DMU982 Sulphate	Triclinic, Agglomerated rods and plates	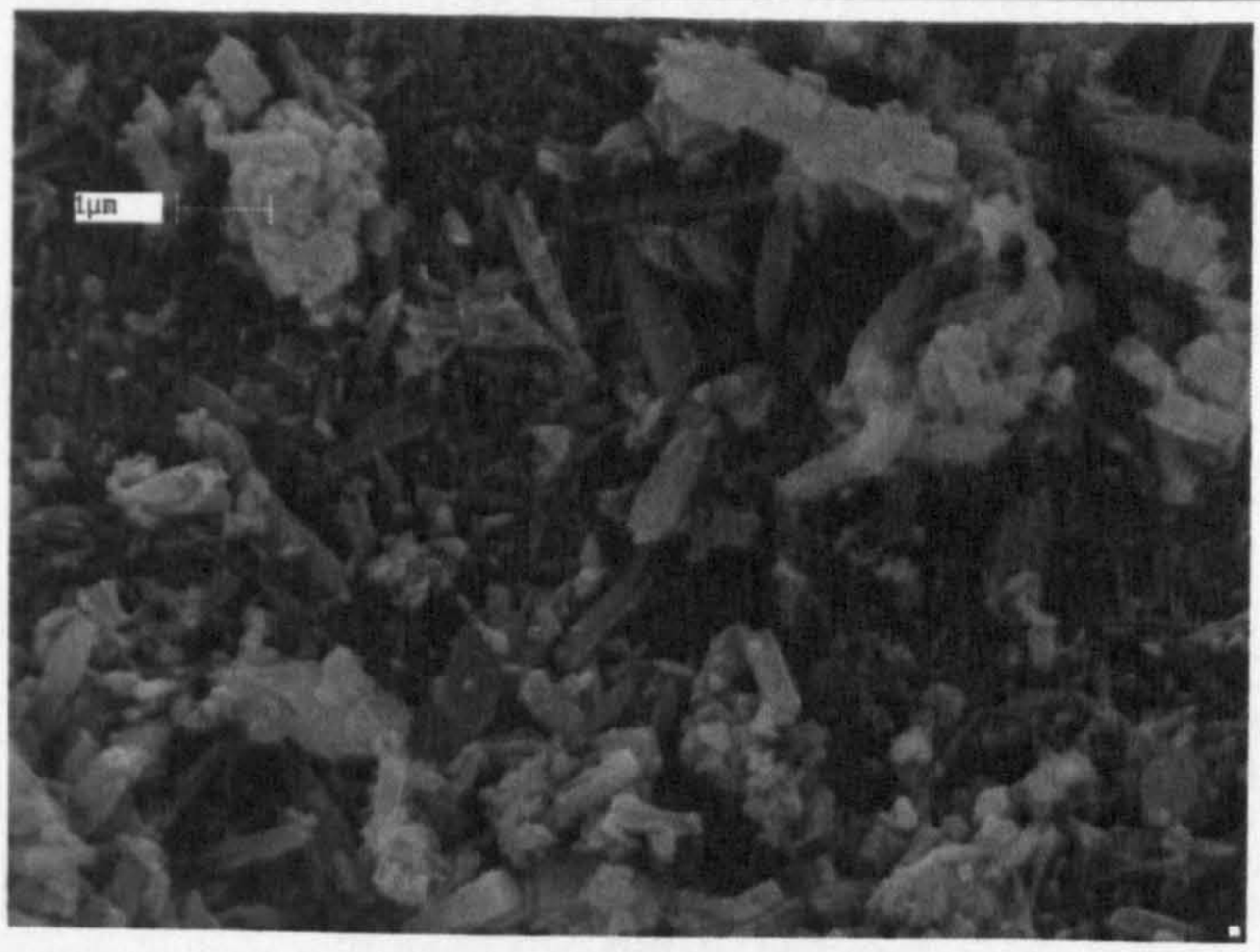
DMU982 Maleate	Triclinic, Agglomerated fibrous	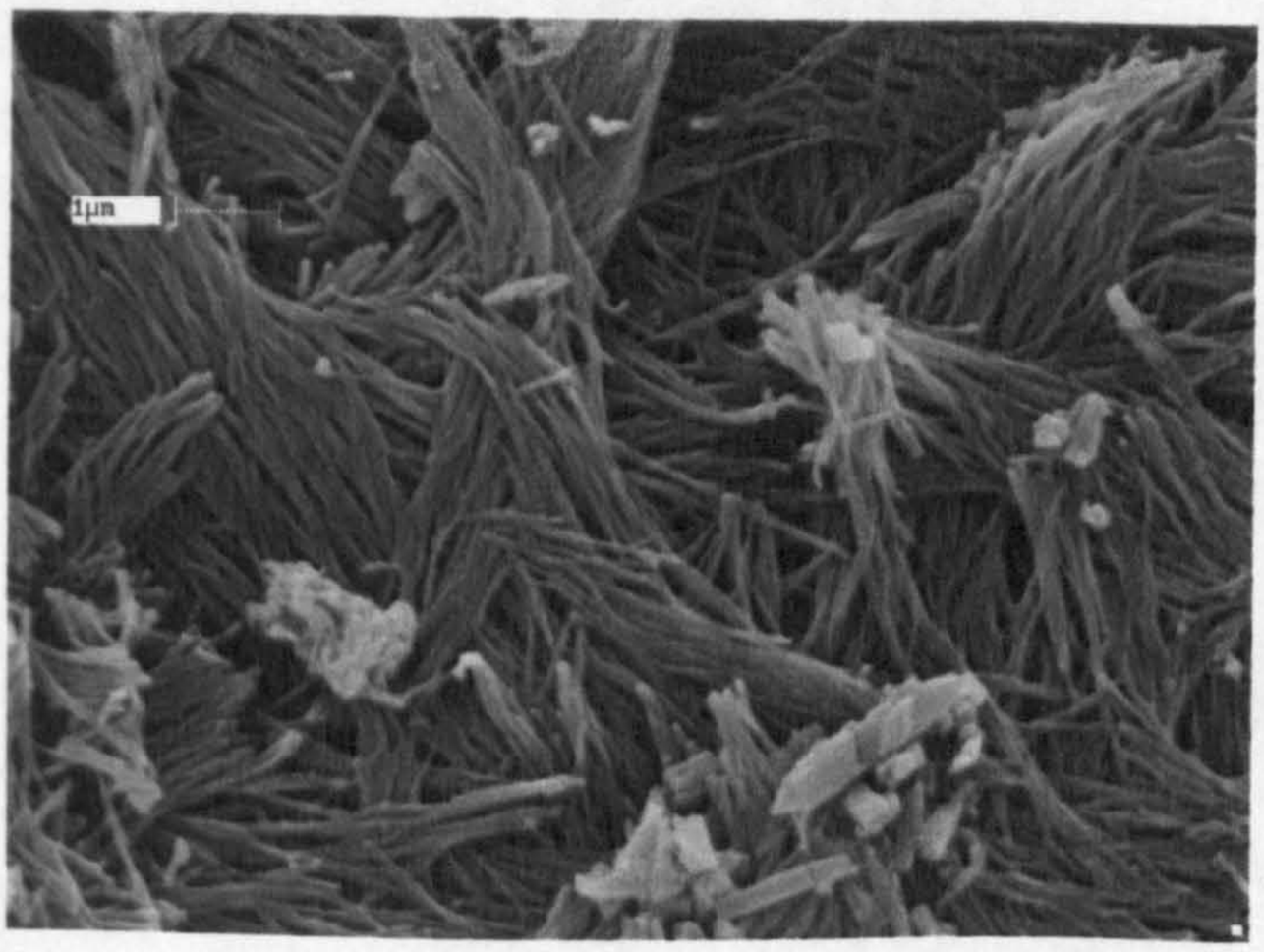

DMU982 Phosphate	Triclinic, Agglomerated rods	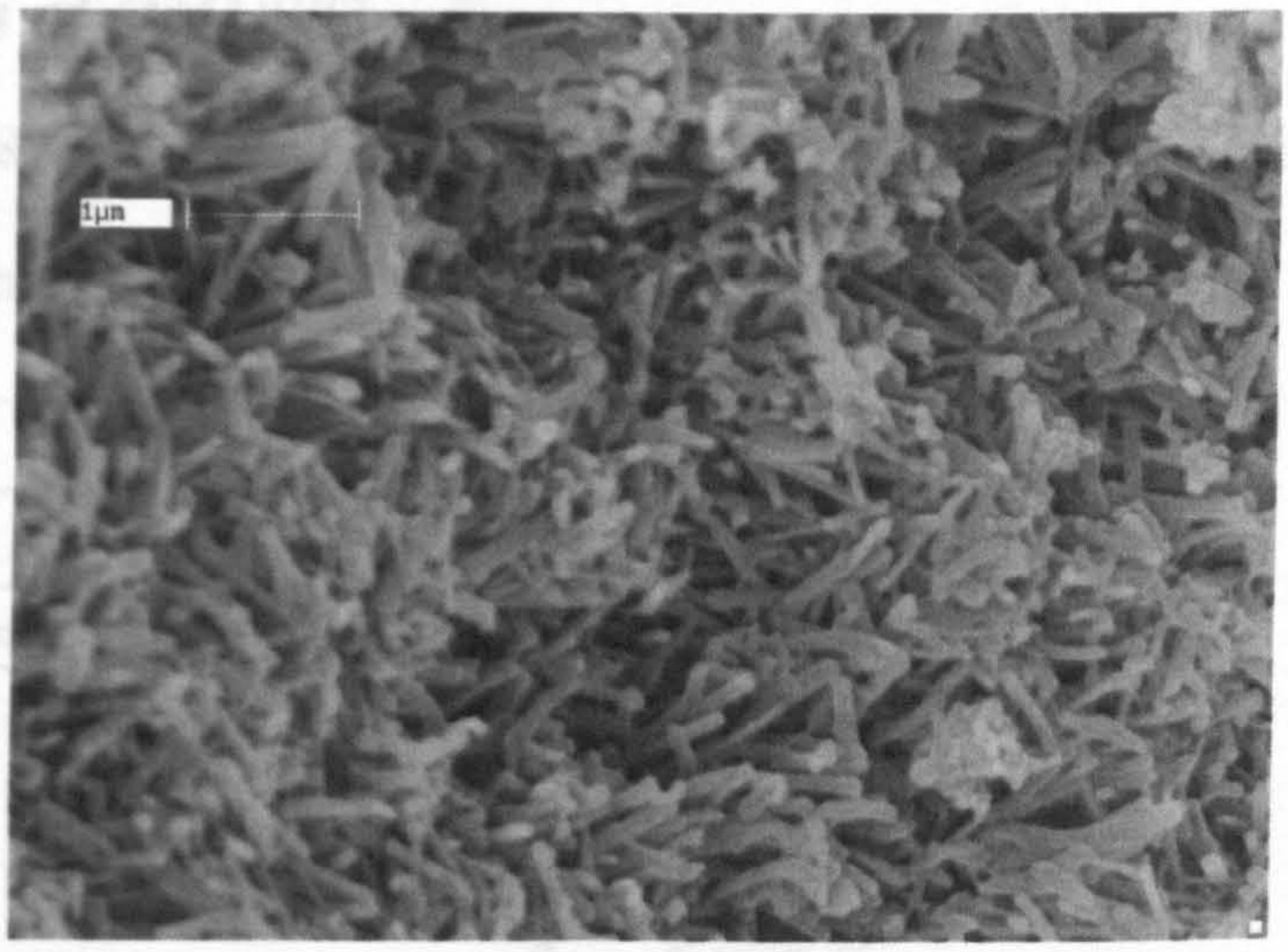
DMU982 Hydrochloride	Triclinic, Agglomerated needles and fibrous	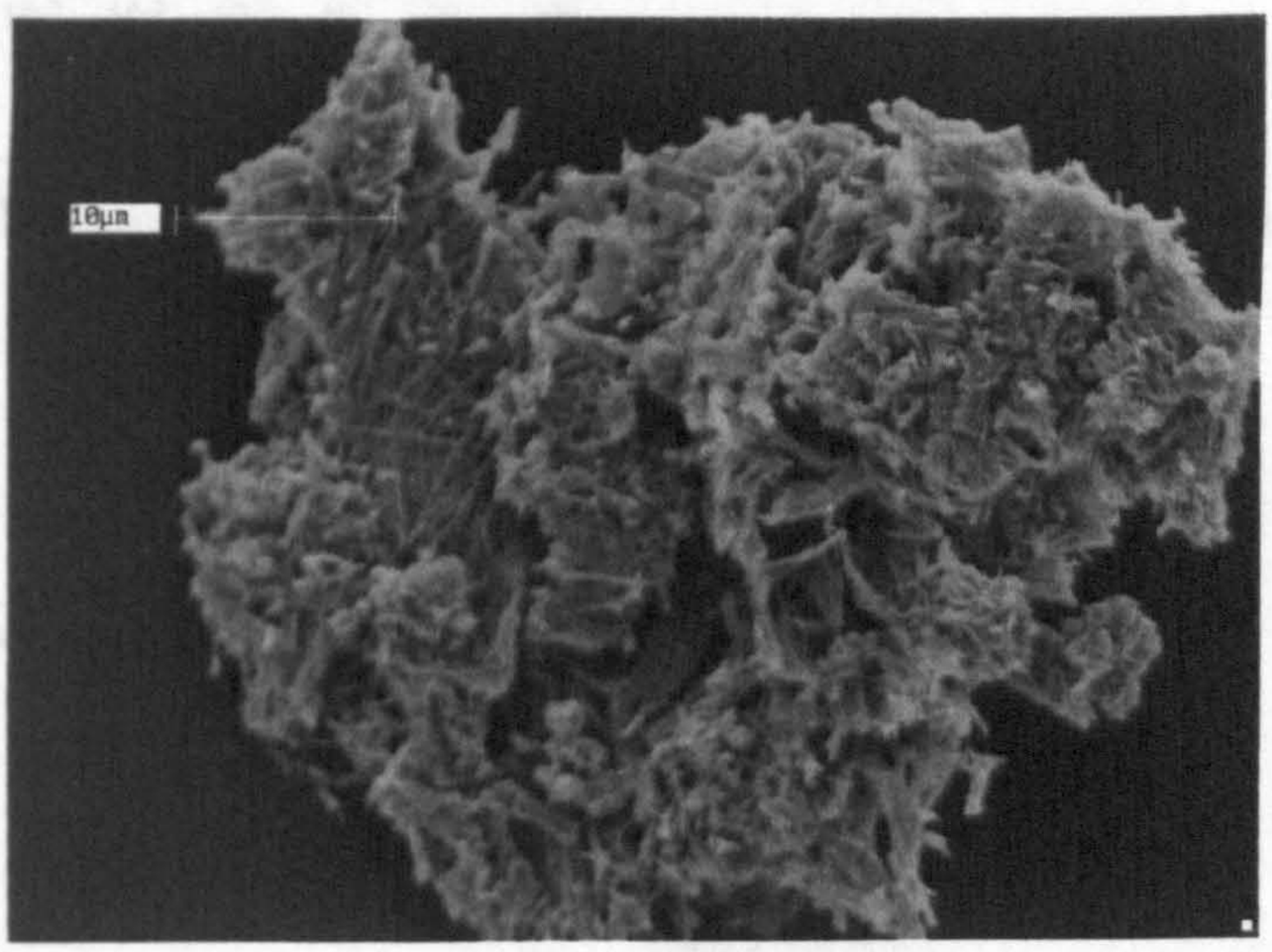

7.3.7.4 Biological evaluation of DMU982 salts

The biological activity of DMU982 and its salts was evaluated with the MTT assay using the CDDG in-house breast cell panel of MCF7, MDA-MB-468 and MCF10A:

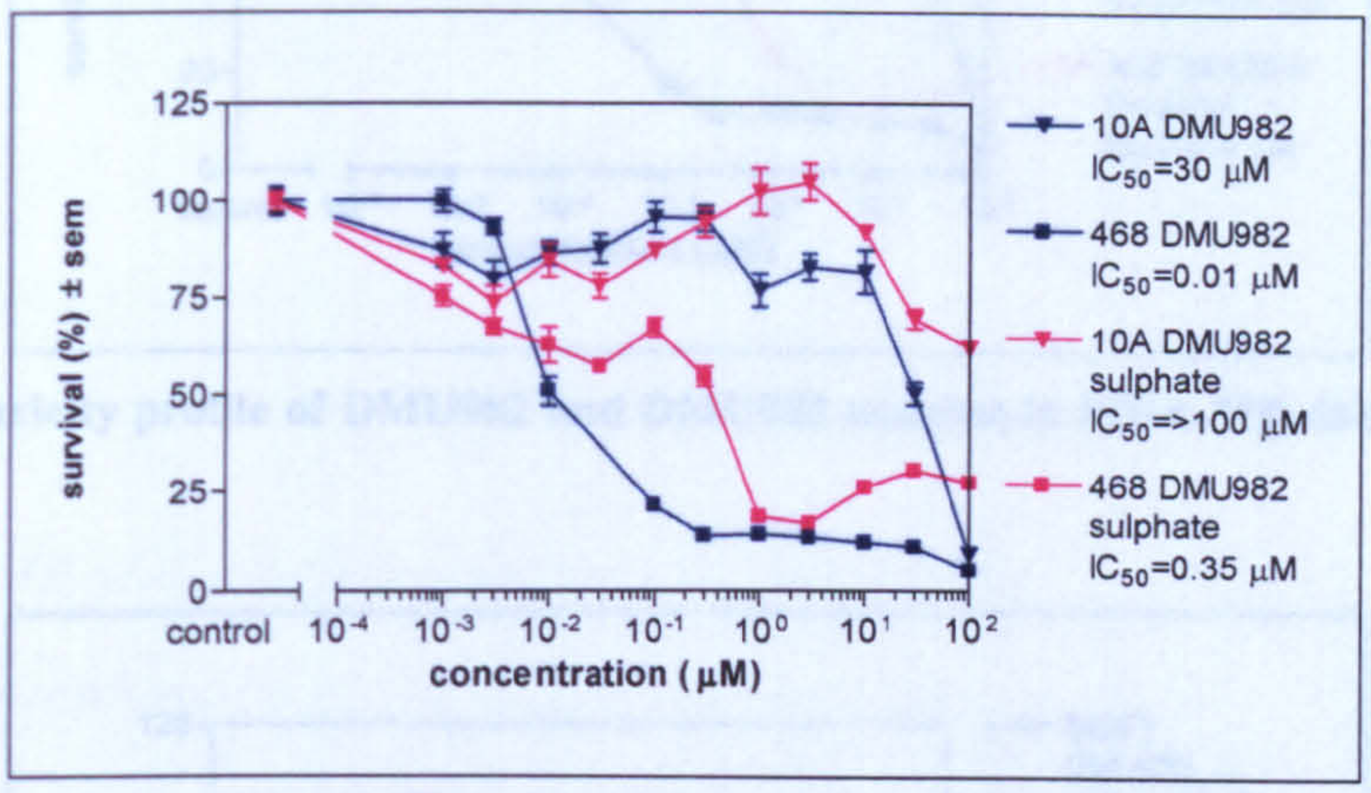

Figure 130. Cytotoxicity profile of DMU982 and DMU982 sulphate in MDA-MB-468 and MCF10A cell lines.

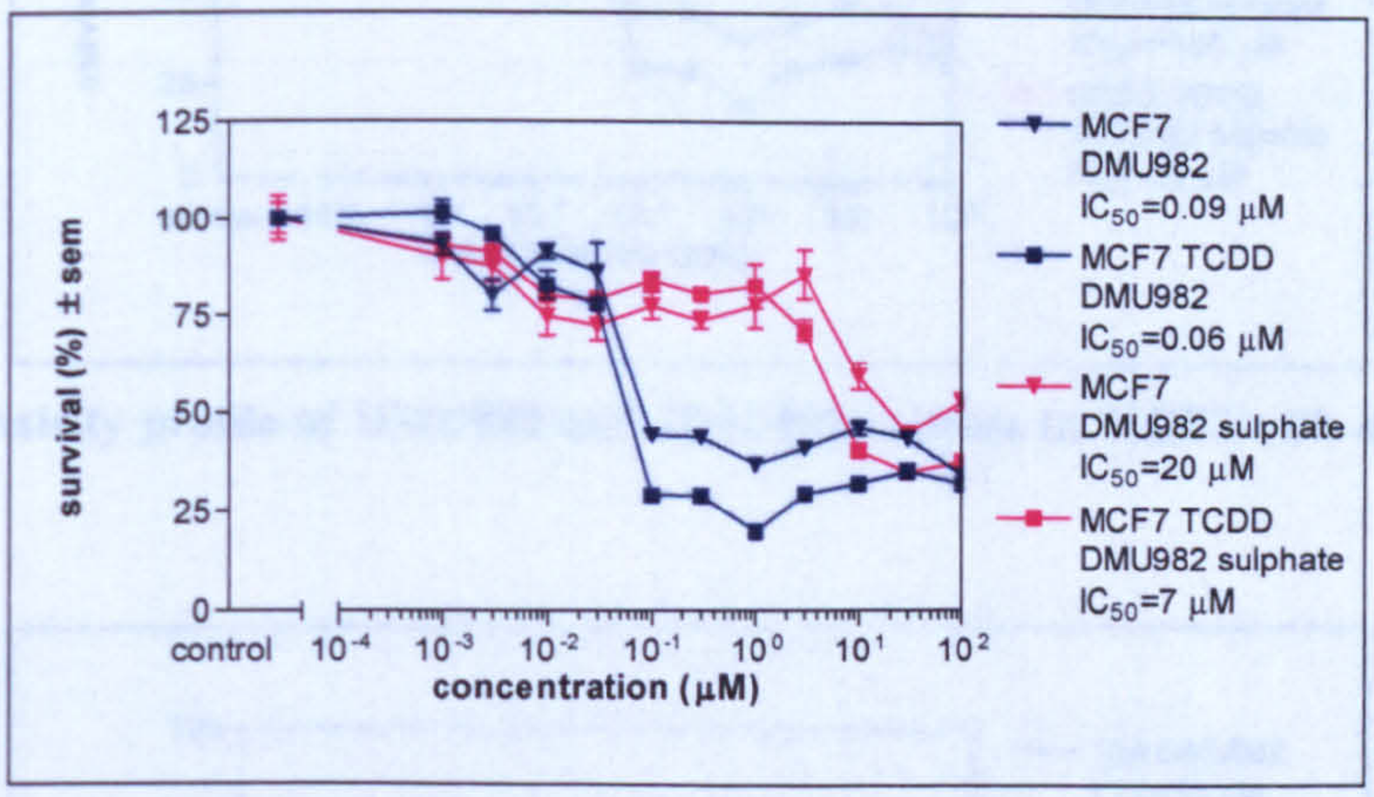

Figure 131. Cytotoxicity profile of DMU982 and DMU982 sulphate in MCF7 with and without TCDD induction.

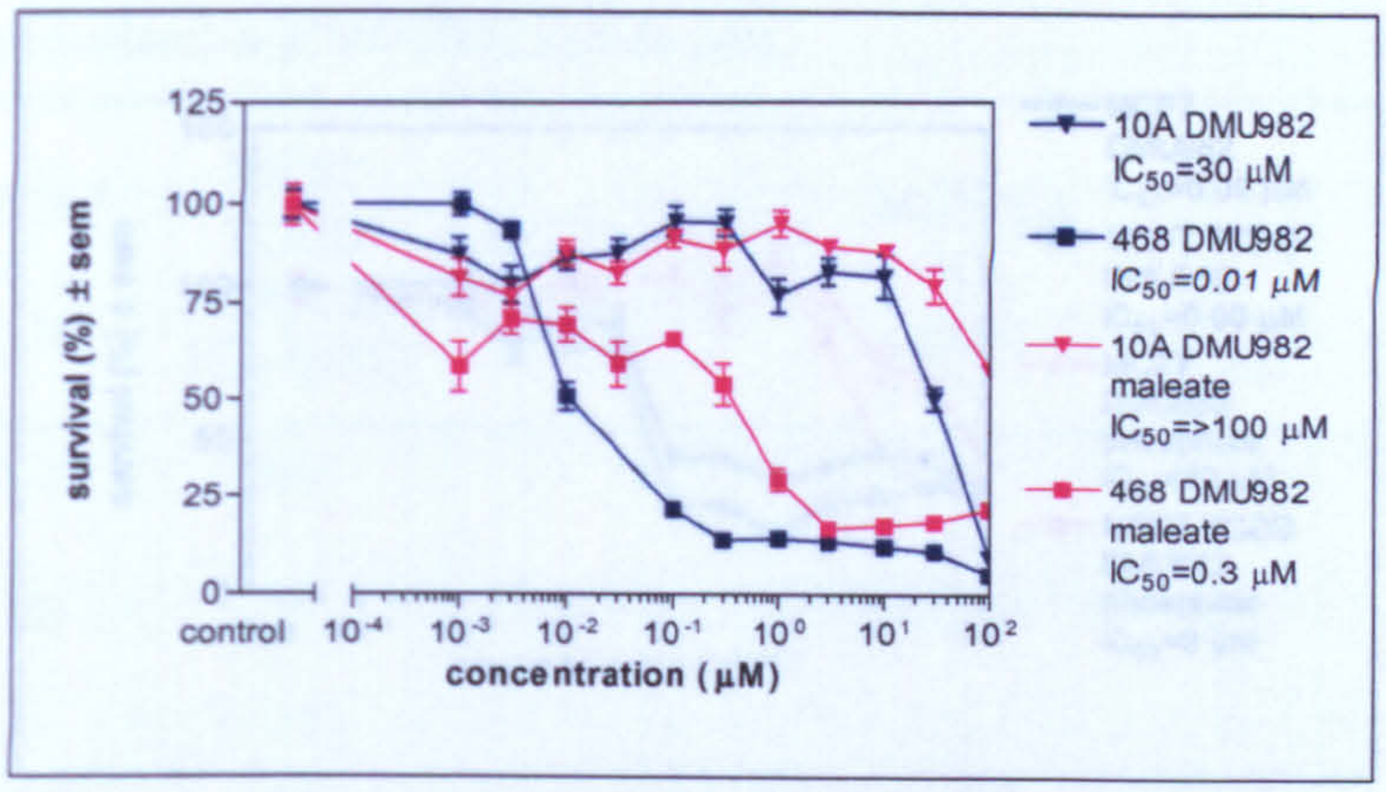

Figure 132. Cytotoxicity profile of DMU982 and DMU982 maleate in *MDA-MB-468* and MCF10A cell lines.

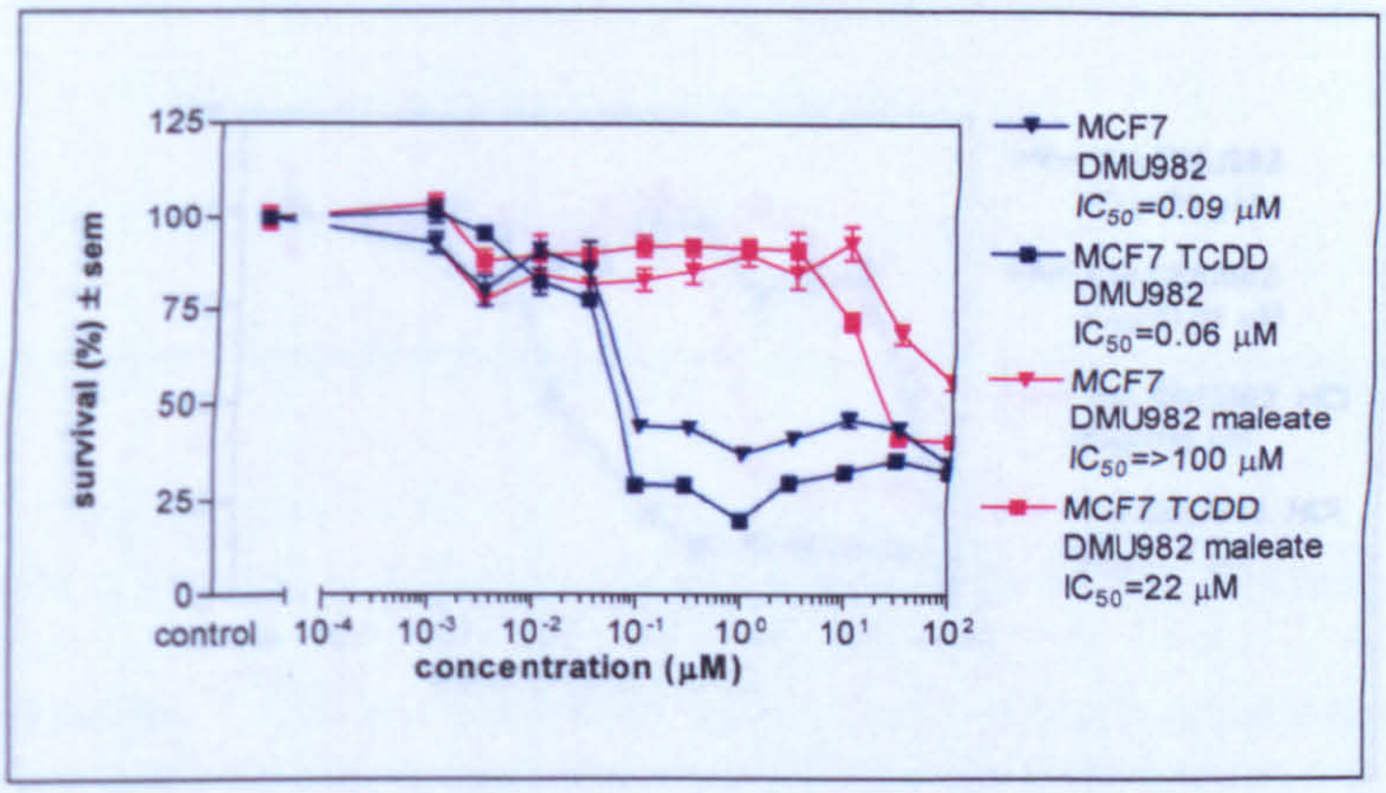

Figure 133. Cytotoxicity profile of DMU982 and DMU982 maleate in MCF7 with and without TCDD induction.

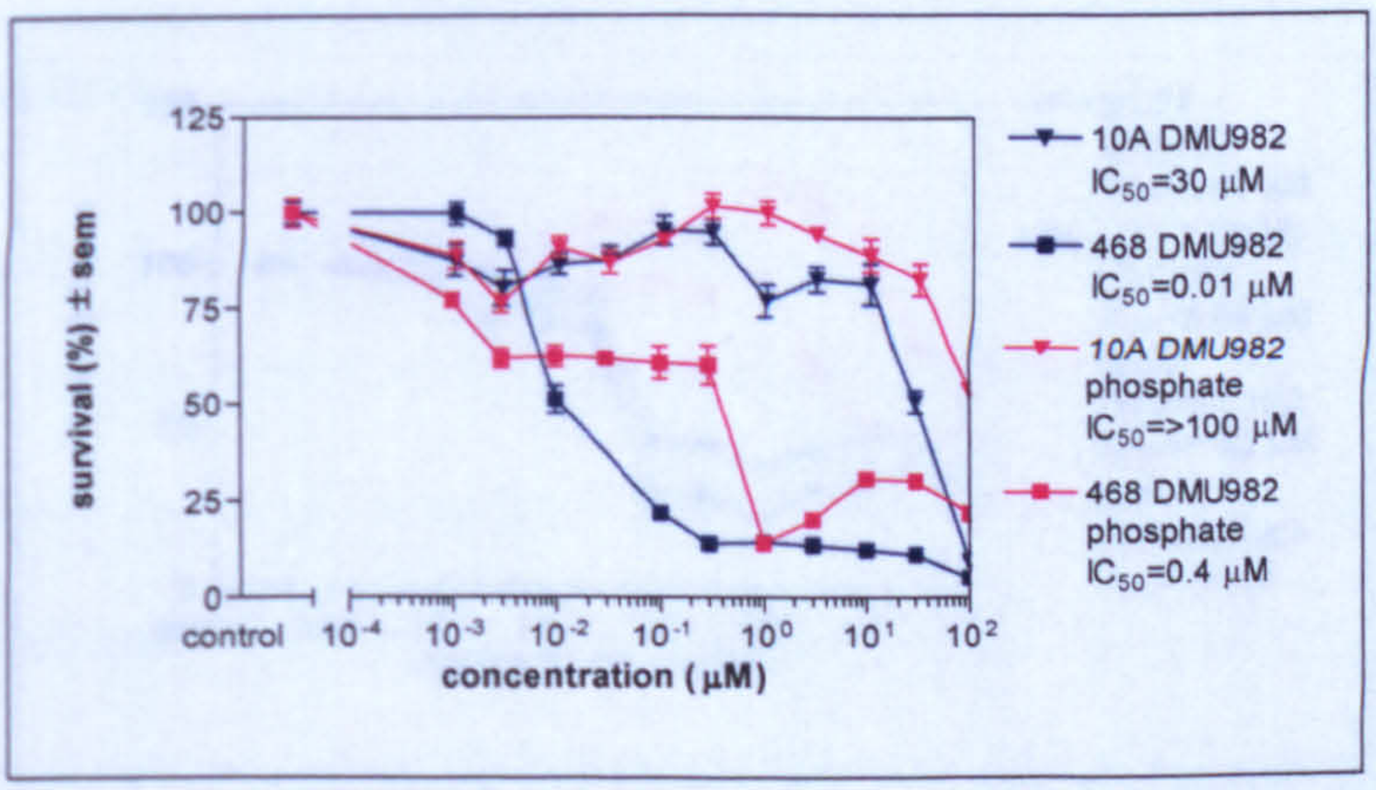

Figure 134. Cytotoxicity profile of DMU982 and DMU982 phosphate in MDA-MB-468 and MCF10A cell lines.

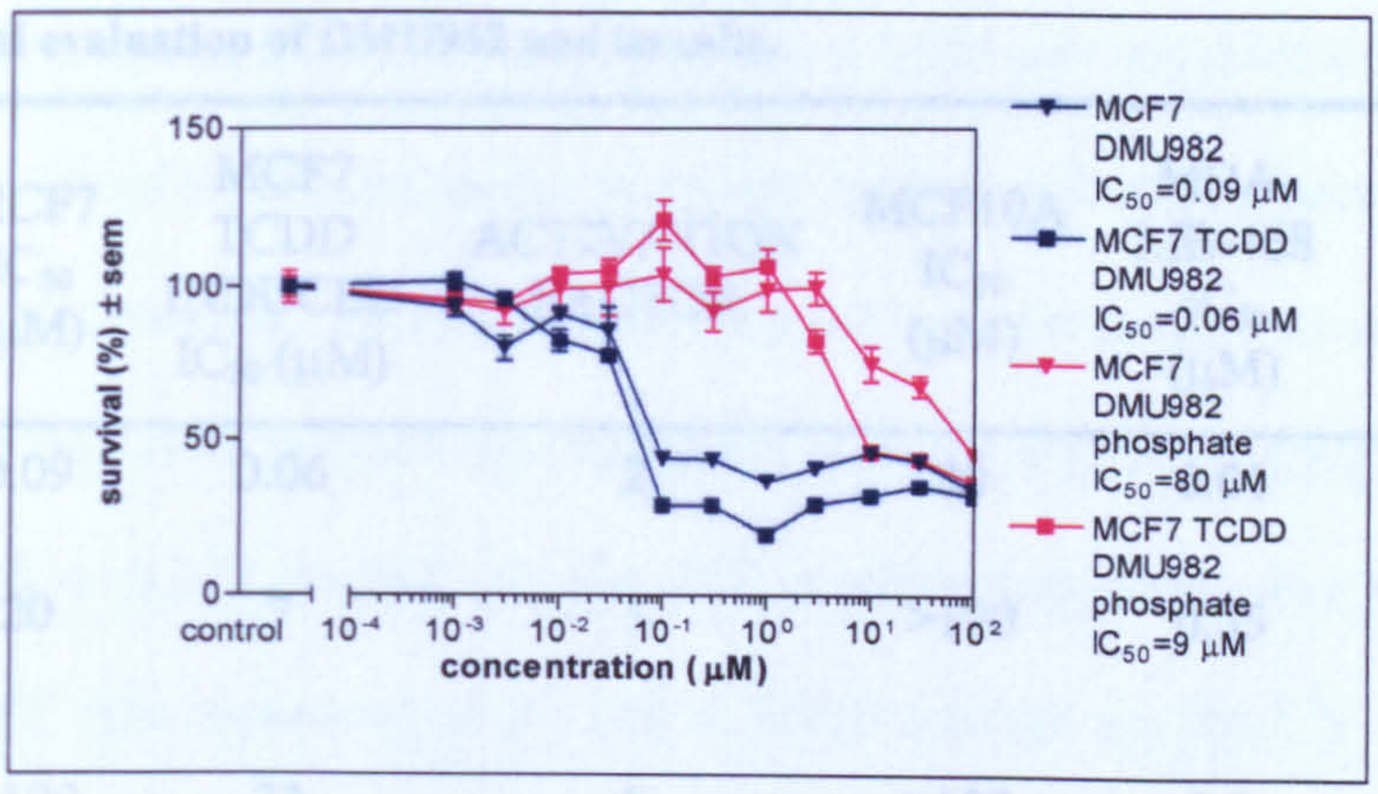

Figure 135. Cytotoxicity profile of DMU982 and DMU982 phosphate in MCF7 with and without TCDD induction.

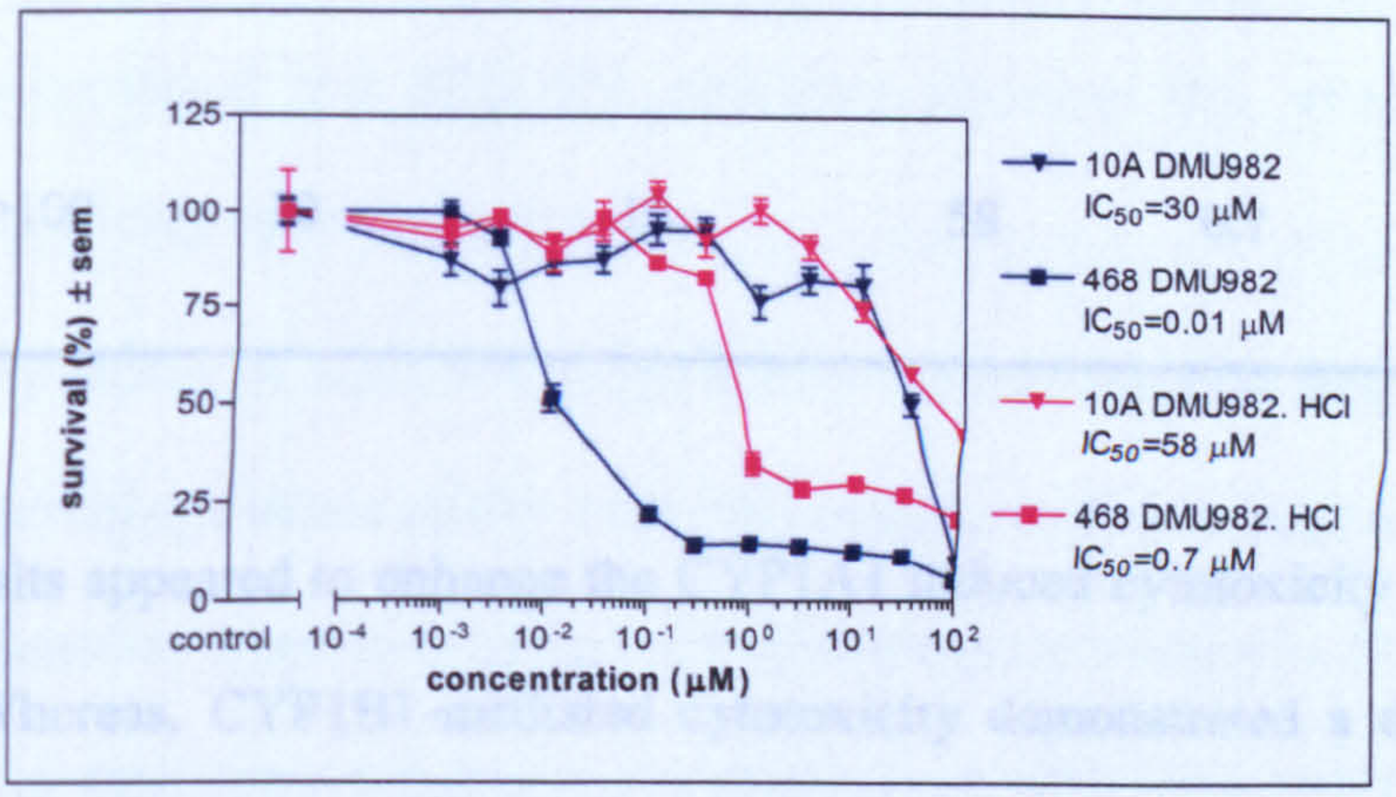

Figure 136. Cytotoxicity profile of DMU982 and DMU982 hydrochloride in MDA-MB-468 and MCF10A cell lines.

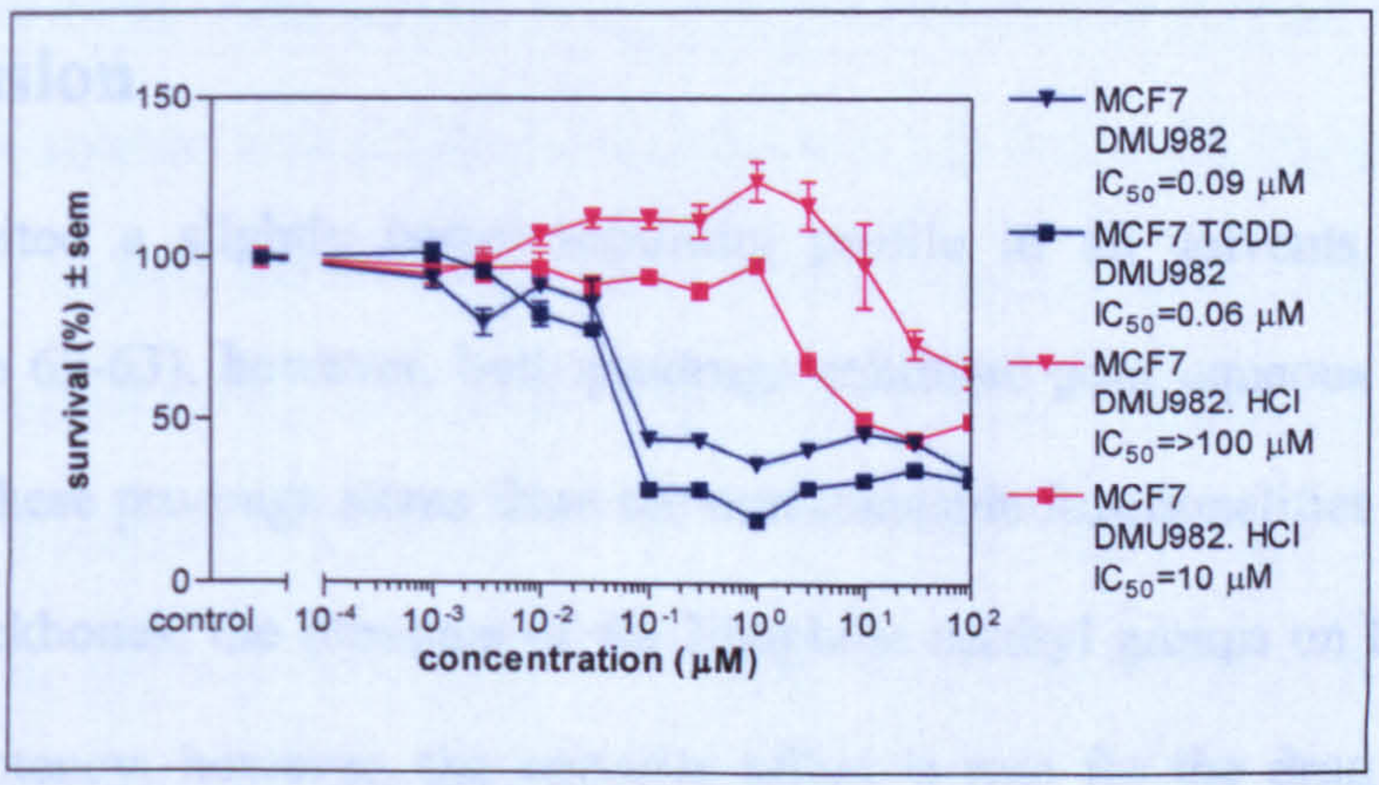

Figure 137. Cytotoxicity profile of DMU982 and DMU982 hydrochloride in MCF7 with and without TCDD induction.

Table 79. Biological evaluation of DMU982 and its salts.

DRUG	MCF7 IC_{50} (μM)	MCF7 TCDD INDUCED IC_{50} (μM)	ACTIVATION FACTOR	MCF10A IC_{50} (μM)	MDA-MB-468 IC_{50} (μM)	TUMOUR SELECTIVE FACTOR
DMU982	0.09	0.06	2	30	0.01	3000
DMU982 Sulphate	20	7	3	>100	0.35	286
DMU982 Maleate	>100	22	5	>100	0.3	333
DMU982 Phosphate	80	9	9	>100	0.4	250
DMU982 Hydrochloride	>100	10	10	58	0.7	83

The DMU982 salts appeared to enhance the CYP1A1 induced cytotoxicity of DMU982 in MCF7 cells. Whereas, CYP1B1-mediated cytotoxicity demonstrated a decrease in salt potency compared to the parent compound.

7.4 Discussion

DMU982 exhibited a slightly better solubility profile in all solvents compared with DMU949 (Table 62-63), however, both prodrugs exhibited poor aqueous solubility. The lipophilicity of these prodrugs stems from the non-ionisable functionalities on the pyridone and pyridine backbones, the presence of the lipophilic methyl groups on both prodrugs is important for potency; however, the opposite effect is true for the drug pharmaceutical properties [151]. Both prodrugs contain two methyl groups and five hydrogen bond

acceptor groups, however, DMU949 also contains a hydrogen bond donor group, which is reflected in the relative solubilites as the increased hydrogen bonding capacity of DMU949 slightly increases its polarity. Optimum solubility for both prodrugs was exhibited in NMP. The solubility of DMU949 in NMP was measured at *8.261 ± 0.348 mg/mL* on the UV plate reader and 8.094 ± 0.272 mg/mL on the UV spectrophotometer and the solubility of DMU982 in NMP was measured at 93.146 ± 1.909 mg/mL on the UV plate reader and 86.183 ± 5.766 mg/mL on the UV spectrophotometer. These results suggest that NMP may be the solvent/co-solvent of choice for future parenteral formulation and pharmacokinetic studies possibly combined with PEG 400, propylene glycol or IPA, which were the next best prodrug solubilizing agents respectively.

The pH-solubility profile of DMU949 (Figure 120) showed that it is non-ionisable, as the solubility did not change dramatically with pH as seen with conventional pH-solubility profiles where dramatic increases are observed when the drug is ionised. The non-ionisable nature of the drug could be attributed to the existence of DMU949 as a tautomer, where protonation causes the drug or its tautomer to revert to the 1-H-2-hydroxypyridine form of DMU949 (Figure 112). The pH-solubility profile of DMU982 (Figure 121) showed the drug to be most soluble at low pH values between pH 2-4, with the highest solubility measured at pH 2 on both the UV plate reader and spectrophotometer (Table 64), above pH 4 the solubility of DMU982 decreased. Using the aqueous solubility, the pH-solubility profile and Equation 6.4 the pKa of DMU982 was determined at 3.73 ± 0.002 on the UV plate reader (Figure 122) and 3.77 ± 0.09 on the UV spectrophotometer (Figure 123), thereby confirming the basic nature of the compound.

Overall, for both DMU949 and DMU982 pH modification did not alter the solubility as much as solvent modification, suggesting that co-solvation is the way forward for parenteral drug formulation.

Both DMU949 and DMU982 log *P* data suggest that the prodrugs are lipophilic, DMU982 exhibited the more favourable log *P* compared with DMU949 which is more lipophilic presenting greater barriers to drug aqueous solubility and adsorption. The log *P* of DMU949 determined by the UV spectrophotometer was 3.25 ± 0.28, compared to that determined on the fluorescent plate reader at 3.18 ± 0.14 and the log *P* of DMU982 determined by the UV spectrophotometer was 2.51 ± 0.12, comparable to the value determined on the fluorescent plate reader at 2.57 ± 0.20, thereby confirming the usefulness of the high-throughput method. The pH-log *P* profile of DMU982 showed that between pH 4.75-8.75 the log *P* was maintained at 2.39 ± 0.12 on the fluorescent plate reader and 2.40 ± 0.07 on the UV spectrophotometer (average of log *P* values between pH 4.75-8.75). These values are consistent with that determined for the unionised state of the drug using water as the aqueous phase. As the pH decreased below pH 4.75, partitioning into the octanol phase decreased, reflecting the ionisation of DMU982 in the aqueous phase. The inverse L-shaped pH-log *P* profile correlates well with the pH-solubility profile as do the pKa values determined for DMU982, with the log *P* lowest when the fraction of ionised DMU982 increases above pH 3.75.

DSC measurements for DMU982 did not show the presence of polymorphs, solvates and impurities, since a single melting point endotherm was detected with an onset temperature of 167.20°C and ΔH of 77.33 J/g. DSC measurements for DMU949 exhibited two melting

point endotherms with onset temperatures of 152.06°C and 254.51°C and ΔH values of 10.66 and 108.79 J/g respectively. These values correlate with the overall solubility of the two drugs; DMU982 requires less energy to overcome the intermolecular crystal lattice forces (i.e. ΔH) and as such was more soluble in all solvents compared with DMU949. The existence of two melting point endotherms for DMU949 is probably due to the polymorphic nature of the drug.

Immediately after the initial scan the samples were rapidly cooled and reheated to determine if any recrystallization was apparent and subsequently to determine the solid-state stability of the prodrugs. In the second DSC scan only one melting point endotherm was observed for DMU949 with an onset temperature of 261.09°C and ΔH of 107.10 J/g. These values indicate that upon immediate re-heat only one DMU949 polymorphic variant had recrystallized, suggesting that this is the more stable polymorph. With DMU982 a T_g was observed at 21.99°C, however, a recrystallization exotherm was also observed at 94.69°C with a ΔH of -57.25 J/g, as well as a melting point endotherm at 160.48°C with a ΔH of 64.66 J/g. This indicates that upon immediate re-heat some DMU982 crystals were in an amorphous state, some crystals were in the state of recrystallization, whereas some crystals had already recrystallized. The fact that both DMU949 and DMU982 exhibited recrystallization suggests that they have good solid-state stability.

SEM imaging of DMU949 showed the crystals system was triclinic with large compacts of agglomerated rods that have particle size of >40μM and a small surface area. DMU982 crystals were distinct with a particle size of approximately <20μM with a larger surface area and existed as orthorhombic blade crystals. The degree of agglomeration and the

relatively small surface area: volume ratio of DMU949 as opposed to DMU982 could account for its poorer solubility profile. The physicochemical properties of DMU949 and DMU982 have been evaluated and the core findings are summarised in Table 80:

Table 80. Comparison of some of the physicochemical properties of DMU949 and DMU982.

PROPERTY \ DRUG	DMU949	DMU982
Activation Factor	1	1.5
Tumour Selective Factor	2500	3000
Appearance	Terracotta, crystalline	Off-white, crystalline
Molecular Weight	367	351
Melting Point (°C)	152.06 254.51	167.20
Enthalpy of fusion ΔH (J/g)	10.66 108.79	77.33
Crystal System	Triclinic, aggregated rods	Orthorhombic, blades
Polymorphism	2 polymorphs detected	No evidence of polymorphs
Hydrogen Bond Acceptor Groups	5	5
Hydrogen Bond Donor Groups	1	0
Aqueous solubility (mg/mL)	0.003 ± 0.0004	0.001 ± 0.0004
Solubility in NMP (mg/mL)	8.094 ± 0.272	86.183 ± 5.766
Log *P*	3.25 ± 0.28	2.51 ± 0.12
pKa	-	3.77 ± 0.09

Generally, both DMU949 and DMU982 were found to be lipophilic, poorly soluble in water and greatly soluble in organic solvents such as NMP. The preformulation study conducted suggests that DMU982 has better development prospects compared to DMU982 with optimum solubility and log *P*. Although, thermodynamically DMU949 is more stable, the prodrug has two tautomers, which make it unsuitable for salt selection, whereas, salt

forms of DMU982 can be identified to potentially improve its physicochemical properties. Accrued with the cytotoxic data these physicochemical studies buttress the advancement of DMU982 to further drug development studies.

Initial salt screening studies with DMU982 using strong inorganic mineral acids (Table 40) yielded the sulphate, phosphate and hydrochloride salts, since the pKa of the respective conjugate acids were two pH units lower than DMU982. The second salt-forming group using organic aliphatic and olefinic acids yielded the maleate, mesylate, tartarate and oxalate salts. The conjugate acids used for these salts had pKa values lower than that of DMU982, moreover, the aliphatic and olefinic conjugate acids used which did not yield salts had pKa values higher than of DMU982. The final salt-forming group using organic aromatic acids yielded the besylate, tosylate and saccharinate salts. The conjugate acids used for these salts also had pKa values lower than that of DMU982. The aqueous solubility of all these salts was firstly measured to eliminate salts with the lowest solubility.

Overall, all of the salts had better aqueous solubility than DMU982 alone (Table 74). The salt with the lowest aqueous solubility was the saccharinate and the salts with the highest aqueous solubilities were the sulphate, maleate, phosphate and hydrochloride respectively, all of which were formed from strong low molecular weight conjugate acids. The most soluble salt form was 210 times more soluble compared with DMU982. Determination of the pH-solubility profile for these salts may provide an indication of the salt behaviour *in vivo* as well as providing valuable information for intravenous and oral formulations. The pH-solubility profile of DMU982 salts (Figures 127-128) showed all of the salts to be more soluble at low pH values between pH 2-4; the highest solubilities were observed at pH 2.

DMU982 sulphate was soluble over a wider pH range of pH 2-10 compared with the other salts (Table 75). The highest solubility at pH 2 was observed with DMU982 maleate. At pH 7 the highest solubility was with the DMU982 sulphate, followed by DMU982 maleate. The lowest solubility at pH 7 was with the DMU982 phosphate, followed by DMU982 hydrochloride.

DSC measurements for DMU982 maleate did not show the presence of polymorphs, solvates and impurities, since a single melting point endotherm was observed with an onset temperature of 138.78°C and a ΔH of 20.32 J/g, however, a small T_g was also observed at 106.97°C with a ΔC_p of 0.82 J/g.°C, suggesting that some of the maleate crystals had amorphous character. The DSC traces for DMU982 phosphate, hydrochloride and sulphate (Figure 129) showed more than one endotherm, suggesting the presence of solvates, polymorphs or hydrates. DSC measurements for DMU982 phosphate exhibited two melting point endotherms with onset temperatures of 231.76°C and 261.43°C and ΔH values of 19.55 and 59.10 J/g respectively. DSC measurements for DMU982 hydrochloride exhibited two melting point endotherms with onset temperatures of 175.25°C and 278.78°C and ΔH values of 17.61 and 50.89 J/g respectively. DSC measurements for DMU982 sulphate exhibited three melting point endotherms with onset temperatures of 129.66, 172.58°C and 247.89°C and ΔH values of 22.79, 4.79 and 98.31 J/g respectively. Immediately after the initial scan the samples were rapidly cooled and reheated to determine if any recrystallization was apparent and subsequently to determine the solid-state stability of the prodrugs. In the second DSC scan the melting point endotherms for the sulphate, maleate and phosphate were absent and the T_g's were observed at 95.10, 23.92

and 66.55 respectively, DMU982 hydrochloride exhibited two T_g's at 75.44 and 169.00°C suggesting that the crystals were in an amorphous state and no immediate recrystallization was apparent.

SEM imaging of DMU982 salts showed all of them to have a triclinic crystal system. The sulphate had agglomerated rod and plate shaped crystals, the maleate had agglomerated fibrous crystals, the phosphate existed as agglomerated rod shaped crystals and finally the hydrochloride existed as agglomerated needle and fibrous crystals. The particle size of the salts is difficult to assess as the aggregates have both *loosely and tightly bound particles [162]*. The degree of agglomeration and the relatively small surface area of all DMU982 salts would account for their poor aqueous solubility, compared with DMU590 and DMU2149 salts.

The biological data of DMU982 compared to DMU982 salts showed a significant reduction in CYP1B1 induced cytotoxicity (Table 79). Of the salts analysed DMU982 maleate showed the most useful CYP1B1 induced cytotoxicity, with a 333-fold tumour selectivity factor, although this was still lower than that seen for the parent compound DMU982 of 3000-fold. Nonetheless, a therapeutic window is retained. In the MCF-7 cell-line all of the salts enhanced the activation factor compared to the parent compound. DMU982 hydrochloride showed the greatest enhancement in CYP1A1 induced cytotoxicity with a 10-fold activation factor compared to 2-fold with DMU982. DMU982 sulphate showed the lowest enhancement in CYP1A1 induced cytotoxicity with a 3-fold activation factor.

Overall, DMU982 salt screening studies yielded ten crystalline salts, the sulphate, maleate, phosphate, hydrochloride, mesylate, tartarate, oxalate, besylate, tosylate and saccharinate.

Initially the aqueous solubility of the salts was determined to consider the feasibility for further development and the salts with the lowest solubility were eliminated. The optimum salt forms in terms of aqueous solubility were sulphate, maleate, phosphate and hydrochloride respectively. A preformulation study was conducted on each of these salts so as to select a salt with optimum physicochemical and biological properties. Table 81 lists the physicochemical properties of these salts and DMU982. The pH-solubility profiles of the sulphate and phosphate were better than DMU982, the sulphate being the best, with optimum buffering capacity. DSC measurements showed the sulphate, phosphate and hydrochloride to exist in more than one form and thus were discarded from future studies. The maleate exhibited no polymorphic variants; however, it did show some amorphous character. Biological evaluation of the salts showed the maleate to have the optimum CYP1B1-activation factor. Finally, SEM imaging of the salts showed all of the salts to have highly agglomerated crystals. On the basis of these results overall DMU982 maleate is recommended for further development.

Table 81. Comparison of some of the physicochemical properties of DMU982 and its salts.

PROPERTY \ DRUG	DMU982	DMU982 Sulphate	DMU982 Maleate	DMU982 Phosphate	DMU982 Hydrochloride
Activation Factor	2	3	5	9	10
Tumour Selective Factor	3000	286	333	250	83
Appearance	Off-white, crystalline	Yellow, crystalline	Yellow, crystalline	Yellow, crystalline	Yellow, crystalline
Molecular Weight	351	433	451	433	372
Melting Point (°C)	167.20	129.66 172.58 247.89	138.78	231.76 261.43	175.25 278.78
Enthalpy of fusion ΔH (J/g)	77.33	22.79 4.79 98.31	20.32	19.55 59.10	17.61 50.89
Glass Transition Temperature (°C)	-	-	106.97	-	-
Heat Capacity Increment ΔC_p (J/g°°C)	-	-	0.82	-	-
Crystal System	Orthorhombic, blades	Triclinic, aggregated rods and plates	Triclinic, aggregated fibrous	Triclinic, aggregated rods	Triclinic, aggregated needles and fibrous
Polymorphism	No evidence of polymorphs	At least 3 polymorphs detected	No evidence of polymorphs	At least 2 polymorphs detected	At least 2 polymorphs detected
Aqueous solubility (mg/mL)	0.001 ± 0.0004	0.202 ± 0.001	0.184 ± 0.005	0.087 ± 0.001	0.065 ± 0.0004
pKa	3.77 ± 0.09	-	-	-	-

DMU2297 and DMU2298 were designed as analogues of the CYP1B1 activated prodrug DMU949 in a double-prodrug strategy. These prodrugs were designed to enable salt selection and to be metabolically activated to DMU949 *in vivo*. This strategy should theoretically overcome the non-ionisable and lipophilic nature of DMU949. Both double-prodrugs were synthesised successfully by deprotonation of DMU949 followed by nucleophilic substitution with either 2-dimethylaminoethyl chloride hydrochloride (DMU2297) or 2-bromoacetamide (DMU2298). The overall reaction for both compounds proceeded fairly slowly with reaction times of 18 (DMU2297) and 26 hours (DMU2298). Both compounds were afforded as white solids; DMU2298 was afforded in a good yield (80%), whereas DMU2297 was afforded in a very poor yield (4%). The highest melting point was observed for DMU2298 (188°C) and the lowest was with DMU2297 (129°C).

Both compounds were analysed by ^{1}H-NMR, ^{13}C-NMR and infrared spectroscopy. The ^{1}H-NMR spectra confirmed the presence of the 3,4-methylenedioxy group by a characteristic singlet peak observed at δ 6.00, the methoxy groups were observed between δ 3.90-4.00 and the NH groups in DMU2298 were confirmed with broad peaks at δ 5.60 and δ 6.40. The ^{13}C-NMR spectra also demonstrated the presence of methoxy groups between δ 55.72-56.50, the NMe_2 groups in DMU2297 were observed between δ 45.71-45.83 and the spectra for DMU2298 showed a characteristic carbonyl peak at δ 170.76. Infrared spectroscopy for both compounds also demonstrated the presence of methoxy group peaks at 1607cm^{-1}. For DMU2297 a characteristic NC stretch was observed at 1506cm^{-1}, and for DMU2298 a characteristic carbonyl peak was observed at 1670cm^{-1} and NH peaks were

observed between 3367-3182 cm^{-1}. Mass spectrometry of the compounds showed that the desired compounds were synthesised as they both showed $M^{+}+1$ peaks.

The *in vitro* metabolism of DMU2297 was assessed by incubation with the CYP1 isozymes 1A1 and 1B1, PHLM and control microsomes. Apart from CYP1A1, DMU2297 was not metabolised by any of the other investigated enzymes (Figure 116). To ensure that the CYP1A1-mediated disappearance of DMU2297 was metabolism and not non-enzymatic degradation of the compound in the incubate; the stability of DMU2297 was assessed in the incubate. Control incubations prepared by exclusion of NADPH or removal of the active enzyme showed DMU2297 was stable under the incubation conditions (Figure 117). Furthermore, incubations of CYP1A1 without NADPH showed no drug metabolism, which indicates that DMU2297 metabolism is CYP-mediated; since NADPH is a necessary co-factor in CYP catalyzed reactions [40].

CYP1A1 catalysed metabolism of DMU2297 resulted in the formation of one primary metabolite (M1) at a retention time of 12.3 and a secondary metabolite (M2) at a retention time of 10.9. Co-elution studies of M1 with DMU949 showed that DMU2297 was not metabolised back to DMU949 (Figure 118), since the metabolite peak did not correlate with the DMU949 peak at a retention time of 12.5. The most probable route of metabolism for M1 is dealkylation of the 3,4-methylenedioxy functionality to generate the catechol motif on the A-ring of DMU2297 (Figure 138), since many similar CDDG prodrugs such as DMU135 undergo similar CYP1-mediated metabolism. The structure of the secondary metabolite M2 remains unknown.

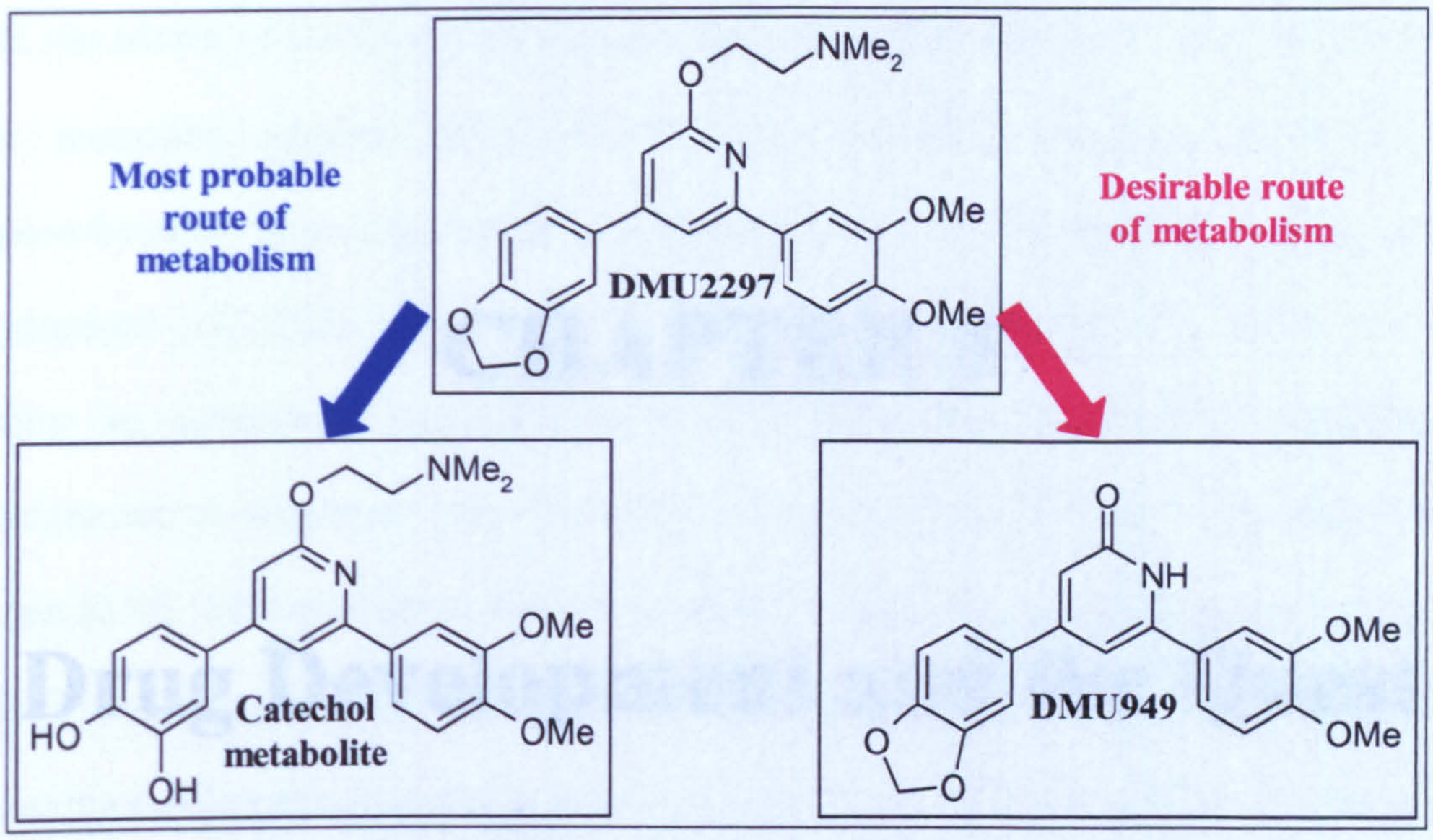

Figure 138. Proposed metabolism of DMU2297.

Regardless of the metabolic route, DMU2297 was not re-converted to DMU949 by PHLM, CYP1A1 or CYP1B1. Two metabolites were formed upon incubation with CYP1A1, none of which co-eluted with DMU949. In order to evaluate the clinical potential of DMU2297, which is beyond the realms of this study, further investigations need to be conducted with the metabolites formed.

The *in vitro* metabolism of DMU2298 was also assessed by incubation with the CYP1 isozymes 1A1 and 1B1, PHLM and control microsomes. DMU2298 was not metabolised by any of the investigated enzymes (Figure 119) and DMU949 was not detected after drug incubations and as such DMU2298 is not a candidate for further pre-clinical evaluation. On the whole, the double-prodrug strategy for both DMU2297 and DMU2298 was unsuccessful, since the *in vitro* re-conversion to DMU949 was not observed.

CHAPTER 8

Drug Development and the Quest for Tumour Selective Chemotherapy

With the advent of combinatorial chemistry and high-throughput screening techniques an ever increasing number of lead compounds are being identified, however the physicochemical properties of these compounds are not necessarily favourable for development [122, 123]. As a result, the assessment of drug pharmaceutical properties has become an increasingly important addition to traditional drug efficacy and toxicity measurement, to accelerate drug discovery and development in a time and cost-effective manner [234]. This strategy enables the early identification of the attributes and drawbacks of lead candidates before they enter the formal drug development process. Compounds presenting developmental challenges can be identified early and analogues can be evaluated to find the best candidate for lead nomination [235]. Ultimately lead candidates with both potency and desirable pharmaceutical properties will have a better chance of successfully completing the clinical programme and becoming therapeutic products to further the quest for tumour selective chemotherapy.

Development of compounds with desirable pharmaceutical properties has featured heavily in the evolutionary design of lead CDDG prodrugs (Figure *139*). *Initially* a series of stilbene (DMU212) and chalcone (DMU135) anticancer prodrugs was designed based on the pharmacophore of estradiol. These prodrugs favoured drug potency whilst compromising on drug pharmaceutical properties, with no derivatisable functional groups to enable manipulation of physicochemical properties through salt selection. Subsequently DMU590 was designed specifically as a morpholino prodrug so that salt forms could be formulated with more desirable physicochemical properties compared to DMU212. Ionisable chalcones were also designed (DMU762, DMU2145, DMU2146, DMU2147,

DMU2148, DMU2149 and DMU2306) with derivatisable functional groups so that salt forms could be formulated with more desirable physicochemical properties compared to DMU135. Another strategy used to overcome the lipophilic nature of chalcones was to incorporate the chalcone functionality into a nitrogen containing heterocycle, to form pyridone (DMU949) and pyridine (DMU982) anticancer prodrugs. Analogues of DMU949 (DMU2297 and DMU298) were also designed to overcome its tautomeric nature so that salt forms could be formulated with more desirable physicochemical properties compared to DMU949:

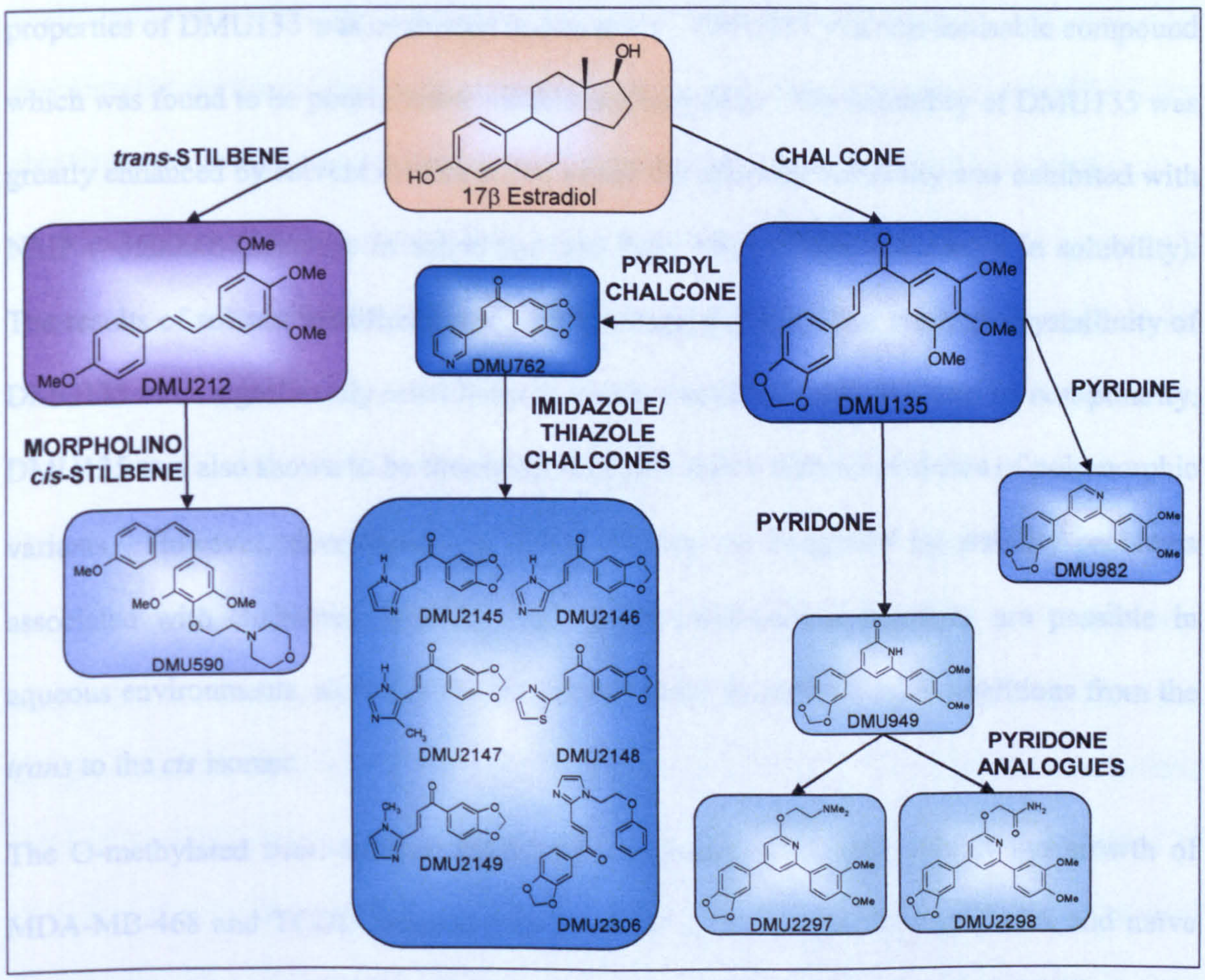

Figure 139. Evolution of CDDG prodrugs.

The ultimate aim of the strategies adopted by the CDDG was to design both a potent and developable CYP1B1 activated anticancer prodrug. The suitability for development of these prodrugs was investigated within the body of this work.

The 3,4-methylenedioxy chalcone DMU135 was found to be potently cytotoxic in MDA-MB-468 and TCDD induced MCF7 cancer cells with appreciably reduced cytotoxicity in MCF10A and naïve MCF7 cells (Table 9). Furthermore, DMU135 acts as a potent broad spectrum tyrosine kinase inhibitor [119] and is well tolerated in xenograft models of human cancer (MDA-MB-468) in nude mice [141]. In light of these findings the pharmaceutical properties of DMU135 was evaluated in this study. DMU135 is a non-ionisable compound which was found to be poorly water soluble and lipophilic. The solubility of DMU135 was greatly enhanced by solvent modification, where the optimum solubility was exhibited with NMP (>350000% increase in solubility) and PEG 400 (>35000% increase in solubility). The results of solvent modification and SEM imaging suggest that the high crystallinity of DMU135 more significantly contributes to its poor aqueous solubility than its non-polarity. DMU135 was also shown to be thermodynamically stable with no evidence of polymorphic variants. However, development of DMU135 may be hampered by stability problems associated with chalcones, whereby, retro-aldol condensation reactions are possible in aqueous environments, as well as photo-isomerization in ambient light conditions from the *trans* to the *cis* isomer.

The O-methylated *trans*-stilbene DMU212 was found to potently inhibit the growth of MDA-MB-468 and TCDD induced MCF7 cancer cells, compared to MCF10A and naïve MCF7 cells (Table 8). Furthermore, DMU212 has potent apoptotic activity [135], retards

the gastrointestinal adenoma formation in $Apc^{Min/+}$ mouse models [138] and is selectively bioactivated in human breast tumour clinical samples [103]. The clinical potential for DMU212 in tumour selective chemotherapy is being realised with imminent clinical trials in USA and as such the pharmaceutical properties of DMU212 was evaluated within the body of this work. DMU212 is a non-ionisable compound which was found to be poorly water soluble and lipophilic. The solubility of DMU212 was greatly enhanced by solvent modification, where the optimum solubility was exhibited with NMP (>150000% increase in solubility) and PEG 400 (>13000% increase in solubility). The results of solvent modification and SEM imaging again suggest that the high crystallinity of DMU212 more significantly contributes to its poor aqueous solubility than its non-polarity. DMU212 was also shown to be thermodynamically stable with no evidence of polymorphic variants.

It was also possible to formulate DMU212 in oral and topical preparations. Oral formulation studies led to development of a reliable *in vitro* dissolution method for DMU212 hard gelatine capsules using surfactant (SLS) containing dissolution medium at 37.5°C with physiological relevance to gastrointestinal conditions and an agitation speed of 100 rpm. The fastest dissolution rate of DMU212 was exhibited with capsules containing a drug particle size fraction of <150μM and sorbitol as the diluent. Topical formulation studies led to the development of a robust *in vitro* release test for DMU212 topical bases using a modified BP paddle-over-disk dissolution method [175] with an in-house release cell and dissolution medium of ethanol/water/IPM in a ratio of 80:10:10, agitation speed of 50 rpm and a cellulose acetate support membrane at 32°C. The fastest drug release of DMU212 was from an anionic o/w cream.

Although, DMU212 is a lipophilic prodrug with no derivatisable functional groups the aqueous solubility can be enhanced with solvent modification and additional drug permeability measurements may help to further predict its *in vivo* behaviour. Thermodynamically DMU212 was found to be stable; however, further studies using thermogravimetric and solution stability analysis may help to anticipate any stability issues before DMU212 enters the definitive drug development process. Overall, the lipophilicity of DMU212 does not appear to hamper its development as both DMU212 oral and topical formulations were identified with good drug release properties. The findings of this study indicate that the tumour specific prodrug DMU212 has both potency and desirable pharmaceutical properties and may satisfy the quest for tumour selective chemotherapy.

The morpholine *cis*-stilbene DMU590 was designed as an ionisable analogue of DMU212. It was found to be potently cytotoxic in MDA-MB-468 cancer cells with appreciably reduced cytotoxicity in MCF10A and MCF7 cells with and without TCDD induction (Table 38), and as such the pharmaceutical properties of DMU590 was investigated in this study. The aqueous solubility of DMU590 was greatly enhanced compared to DMU212 (120% increase in solubility). Its solubility increased by decreasing the pH below 5.5, particularly at pH 2 (500% increase in solubility); therefore, the use of low pH for parenteral formulations is preferred. Thermodynamic evaluation of DMU590 showed the drug to exist in an amorphous form. Another method used for increasing the drug solubility without altering the chemical structure of the drug was salt formation. Salt screening studies led to development of a crystalline phosphate salt with solubility higher than DMU590 (>8000% increase in solubility) and a clinically acceptable therapeutic

window. Although, DMU590 appears to have good development prospects recent *in vivo* studies have shown that it is not a candidate for further drug development, as a 24 hour transit period is required *in situ* before the drug can be bioactivated.

The 3,4-methylenedioxy pyridone DMU949 was found to be potently cytotoxic in MDA-MB-468 and TCDD induced MCF7 cancer cells with appreciably reduced cytotoxicity in MCF10A and naïve MCF7 cells (Table 60), and as such the pharmaceutical properties of DMU949 was investigated in this study. DMU949 is a non-ionisable compound which was found to be poorly water soluble and lipophilic. The solubility of DMU949 was greatly enhanced by solvent modification, where the optimum solubility was exhibited with NMP (>2500% increase in solubility) and PEG 400 (>150% increase in solubility). The results of solvent modification and SEM imaging suggest that the high crystallinity of DMU949 more significantly contributes to its poor aqueous solubility than its non-polarity. Thermodynamic evaluation of DMU949 showed it to have two polymorphic variants, which may present problems during drug development. To overcome the tautomeric nature of DMU949 whilst retaining its potency, analogues of the pyridone were designed in a double-prodrug strategy. However, metabolic evaluation of these analogues showed that the double-prodrug strategy was unsuccessful, since the *in vitro* re-conversion to DMU949 was not observed. Overall, the developmental challenges associated with DMU949 indicate that it is not a candidate for further drug development. However, use of the double-prodrug strategy for the rational design of other novel analogues may provide an opportunity for DMU949 in tumour selective chemotherapy.

The 3,4-methylenedioxy pyridine DMU982 was found to be potently cytotoxic in MDA-MB-468 and TCDD induced MCF7 cancer cells with appreciably reduced cytotoxicity in MCF10A and naïve MCF7 cells (Table 61), and as such the pharmaceutical properties of DMU982 was investigated in this study. DMU982 is an ionisable compound which was found to be poorly water soluble and lipophilic. The solubility of DMU982 was greatly enhanced by solvent modification, where the optimum solubility was exhibited with NMP (>90000% increase in solubility) and PEG 400 (>17000% increase in solubility). Its solubility increased by decreasing the pH below 4, particularly at pH 2 (175% increase in solubility). These results indicate that the use of a low pH for parenteral formulations is preferred, with the addition of co-solvents such as NMP and PEG 400. The results of solvent modification and SEM imaging suggest that the high crystallinity of DMU982 more significantly contributes to its poor aqueous solubility than its non-polarity. DMU982 was also shown to be thermodynamically stable with no evidence of polymorphic variants.

Another method used for increasing the drug solubility of DMU982 without altering the chemical structure of the drug was salt formation. DMU982 salt screening studies yielded ten crystalline salts, the sulphate, maleate, phosphate, hydrochloride, mesylate, tartarate, oxalate, besylate, tosylate and saccharinate. To aid in the selection of the best salt to progress with, the solubility of DMU982 salts was initially evaluated, where the salts with the lowest solubility were eliminated. The optimum salt forms in terms of aqueous solubility were the sulphate, maleate, phosphate and hydrochloride respectively. A preformulation study was conducted on each of these salts so as to select a salt with optimum physicochemical and biological properties, where the salts were evaluated by

solubility, pH-solubility profiles, polymorphism, morphology and cytotoxicity. Based on the results of this comparative physicochemical screening, the maleate salt was recommended for further development. However, further evaluation by solution stability, hygroscopicity, dissolution and thermogravimetry may help to further compare the optimum salt forms, to ensure that the optimum salt form is recommended for development.

Although, DMU982 is a lipophilic prodrug the aqueous solubility can be enhanced with both solvent modification and salt selection and additional drug permeability measurements may help to further predict its *in vivo* behaviour. Thermodynamically DMU982 was found to be stable; however, further studies using thermogravimetric and solution stability analysis may help to anticipate any stability issues before DMU982 enters the definitive drug development process. The findings of this study indicate that the tumour specific prodrug DMU982 has both potency and desirable pharmaceutical properties and may satisfy the quest for tumour selective chemotherapy.

The development challenges associated with non-ionisable chalcones were also addressed in this study with the design of CYP1B1 activated ionisable chalcones, based on the CDDG CYP1B1 pharmacophore model. Overall, a SAR was determined where the 2-imidazole position was found to be important for selective CYP1B1 bioactivation resulting from confirmation of a necessary hydrogen-bonding interaction near the aromatic 'A' ring hydroxylation hotspot (Figure 85). The 4-imidazole position does not associate with this hydrogen-bonding and thus does not allow CYP1B1 bioactivation. Optimum bioactivity was observed with the 2-imidaozle prodrug DMU2149. The potency observed with DMU2149 was significantly lower than the other lead prodrugs and as such it is not a

candidate for further drug development. However, since the imidazole prodrugs were specifically designed to enable salt selection, DMU2149 underwent salt screening and preformulation studies.

The aqueous solubility of DMU2149 was enhanced compared to the non-ionisable chalcone DMU135 (73% increase in solubility). Its solubility increased by decreasing the pH below 4, particularly at pH 2 (>50% increase in solubility); therefore, the use of low pH for parenteral formulations is preferred. Thermodynamic evaluation of DMU2149 showed the drug to be stable with no evidence of polymorphic variants. Another method used for increasing the drug solubility of DMU2149 without altering the chemical structure of the drug was salt formation. DMU2149 salt screening studies yielded eleven crystalline salts, the mesylate, phosphate, hydrochloride, sulphate, tartarate, besylate, oxalate, tosylate, maleate, fumarate and gentisate. To aid in the selection of the best salt to progress with, DMU2149 salts were initially evaluated by solubility, where the salts with the lowest solubility were eliminated. The optimum salt forms in terms of aqueous solubility were the mesylate, phosphate, hydrochloride and sulphate respectively. A preformulation study was conducted on each of these salts so as to select a salt with optimum physicochemical and biological properties, where the salts were evaluated by solubility, pH-solubility profiles, polymorphism, morphology and cytotoxicity. Based on the results of this comparative physicochemical screening, the sulphate salt would be recommended for further development, if DMU2149 were a lead drug candidate. However, further evaluation of solution stability, hygroscopicity, dissolution and thermogravimetry may help to further

compare the optimum salt forms, to ensure that the optimum salt form is recommended for development.

Another strategy implemented in this study was to reduce attrition rates in the later stages of drug development, by accelerating the assessment of drug pharmaceutical properties [146]. Where novel miniaturisation of high-throughput analytical technologies were implemented in the preformulation and formulation programmes, to identify potential physicochemical problems (solubility, pKa, log *P* and dissolution) at an early drug development stage [122, 124-127].

Several novel applications have been investigated. A high-throughput screening method using a 96-well fluorescent plate reader has been successfully implemented and validated for log *P* quantification to improve assay efficiency. Novel uses have also been successfully implemented and validated for the 96-well UV plate reader firstly in solubility and pKa quantification. Secondly, in high-throughput capsule formulation screening, from which optimum formulations may be ascertained. The MTT cytotoxicity assay was used as a novel application for determination of formulation effects on active drug cytotoxicity and CYP1 selectivity. Overall, high-throughput analytical technology can potentially accelerate the assessment of pharmaceutical properties. This enables the early identification of lead candidates with suboptimal biopharmaceutical properties, thereby reducing attrition rates in the later stages of drug development [146].

Over the past decade the increased understanding of the genomics and molecular pathology of cancer [14] has shifted the ethos of cancer drug development from an empirical to a mechanism based viewpoint, to potentially provide tumour specific therapy (Table 2). The

tumour specific expression of CYP1B1 in particular provides the opportunity for tumour selective chemotherapy. However, even with the recent advances in combinatorial chemistry and high-throughput screening techniques, the quest for tumour selective chemotherapy remains relatively unfulfilled. With the sole focus of most drug design being potency and selectivity, most chemotherapeutics agents lack the required pharmaceutical properties to ensure efficient progress through the drug development pipeline. As a result the assessment of drug pharmaceutical properties is becoming increasingly important in the identification of lead candidates, which will ultimately have both drug potency and desirable pharmaceutical properties.

The physicochemical properties of a range of novel anticancer prodrugs have been assessed within this study and are summarized in Table 82. The findings of this study indicate that the CYP1B1 activated anticancer prodrugs DMU212 and DMU982 have both potency and desirable pharmaceutical properties and may satisfy the quest for tumour selective chemotherapy and as such are recommended for further drug development.

Table 82. Comparison of physicochemical properties of lead CDDG anticancer prodrugs.

PROPERTY \ DRUG	DMU135	DMU212	DMU590	DMU949	DMU982
Activation Factor	90	22	9	1	2
Tumour Selective Factor	380	4300	5000	2500	3000
Appearance	Pale yellow, crystalline	Yellow, crystalline	Pale yellow oil	Terracotta, crystalline	Off-white, crystalline
Molecular Weight	342	300	399	367	351
Melting Point (°C)	138.27	164.96	-	152.06 254.51	167.20
Enthalpy of fusion ΔH (J/g)	83.79	107.27	-	10.66 108.79	77.33
Glass Transition Temperature (°C)	-	-	-15.88	-	-
Heat Capacity Increment ΔC_p (J/g°C)	-	-	0.30	-	-
Crystal System	Orthorhombic, aggregated blades	Triclinic, columnar	-	Triclinic, aggregated rods	Orthorhombic, blades
Polymorphism	No evidence of polymorphs	No evidence of polymorphs	No evidence of polymorphs	2 polymorphs detected	No evidence of polymorphs
Hydrogen Bond Acceptor Groups	6	4	6	6	5
Hydrogen Bond Donor Groups	0	0	0	1	0
Aqueous solubility (mg/mL)	0.001 ± 0.0001	0.001 ± 0.0001	0.120 ± 0.009	0.003 ± 0.0004	0.001 ± 0.0004
Solubility in NMP (mg/mL)	367.569 ± 4.286	152.727 ± 10.496	-	8.094 ± 0.272	86.183 ± 5.766
Log *P*	2.49 ± 0.01	2.93 ± 0.05	-	3.25 ± 0.28	2.51 ± 0.12
pKa	-	-	6.29 ± 0.02	-	3.77 ± 0.09

References

1. Alberts, B., et al., *Molecular biology of the cell.* Fourth ed. 2002, New York: Garland Publishing.
2. *Cancer: 1 in 3 develop cancer during their lives.* 2005, Office for National Statistics.
3. *Cancerstats mortality UK.* 2003, Cancer Research UK.
4. Doll, R. and J. Boreham, *Recent trends in cancer mortality in the UK.* British Journal of Cancer, 2005. **92**(7): p. 1329-1335.
5. Cozzi, P., N. Mongelli, and A. Suarato, *Recent anticancer cytotoxic agents.* Current Medicinal Chemistry - Anti-Cancer Agents, 2004. **4**(2): p. 93-121.
6. Hahn, W.C. and R.A. Weinberg, *Modelling the molecular circuitry of cancer.* Nature Reviews Cancer, 2002. **2**(5): p. 331-341.
7. Hanahan, D. and R.A. Weinberg, *The hallmarks of cancer.* Cell, 2000. **100**(1): p. 57-70.
8. Levine, A.J., *p53, the cellular gatekeeper for growth and division.* Cell, 1997. **88**(3): p. 323-331.
9. Vogelstein, B. and K.W. Kinzler, *Cancer genes and the pathways they control.* Nature Medicine, 2004. **10**(8): p. 789-799.
10. Blume-Jensen, P. and T. Hunter, *Oncogenic kinase signalling.* Nature, 2001. **411**(6835): p. 355-365.
11. Fabbro, D., et al., *Protein kinases as targets for anticancer agents: from inhibitors to useful drugs.* Pharmacology & Therapeutics, 2002. **93**(2-3): p. 79-98.
12. Hornberg, J.J., et al., *Cancer: A systems biology disease.* Biosystems, 2006. **83**(2-3): p. 81-90.
13. Renan, M.J., *How many mutations are required for tumorigenesis - implications from human cancer data.* Molecular Carcinogenesis, 1993. **7**(3): p. 139-146.
14. Workman, P. and S.B. Kaye, *Translating basic cancer research into new cancer therapeutics.* Trends in Molecular Medicine, 2002. **8**(4): p. S1-S9.
15. Goldspiel, B.R., *Future cancer therapies.* Highlights in Oncology Practice, 1998. **16**(1): p. 1-2.
16. Rooseboom, M., J.N.M. Commandeur, and N.P.E. Vermeulen, *Enzyme-catalyzed activation of anticancer prodrugs.* Pharmacological Reviews, 2004. **56**(1): p. 53-102.
17. Abou-Jawde, R., et al., *An overview of targeted treatments in cancer.* Clinical Therapeutics, 2003. **25**(8): p. 2121-2137.
18. Sorsa, M., K. Hemminki, and H. Vainio, *Occupational exposure to anticancer drugs - Potential and real hazards.* Mutation Research, 1985. **154**(2): p. 135-149.

19. Fuchs, J., et al., *DNA damage in nurses handling antineoplastic agents.* Mutation Research/Genetic Toxicology, 1995. **342**(1-2): p. 17-23.

20. Rang, H.P., M.M. Dale, and J.M. Ritter, *Pharmacology.* Fourth ed. 1999, London: Churchill Livingstone.

21. Beers, M.H., et al., *The merck manual of medical information.* Second Home Edition ed. 2004, New Jersey: Merck Research Laboratories.

22. Zwick, E., J. Bange, and A. Ullrich, *Receptor tyrosine kinases as targets for anticancer drugs.* Trends in Molecular Medicine, 2002. **8**(1): p. 17-23.

23. Guillemard, V. and H.U. Saragovi, *Novel approaches for targeted cancer therapy.* Current Cancer Drug Targets, 2004. **4**(4): p. 313-326.

24. Albert, A., *Chemical aspects of selective toxicity.* Nature, 1958. **182**: p. 421-423.

25. Sinhababu, A.K. and D.R. Thakker, *Prodrugs of anticancer agents.* Advanced Drug Delivery Reviews, 1996. **19**(2): p. 241-273.

26. Airley, R.E., J.E. Monaghan, and I.J. Stratford, *Hypoxia and disease: opportunities for novel diagnostic and therapeutic prodrug strategies.* The Pharmaceutical Journal, 2000. **264**(7094): p. 666-673.

27. Denny, W.A., *Hypoxia-activated anticancer prodrugs.* Expert Opinion on Therapeutic Patents, 2005. **15**(6): p. 635-646.

28. Jaffar, M., K.J. Williams, and I.J. Stratford, *Bioreductive and gene therapy approaches to hypoxic diseases.* Advanced Drug Delivery Reviews, 2001. **53**(2): p. 217-228.

29. Brown, J.M. and W.R. William, *Exploiting tumour hypoxia in cancer treatment.* Nature Reviews Cancer, 2004. **4**(6): p. 437-447.

30. Denny, W.A., *Tumor-activated prodrugs - A new approach to cancer therapy.* Cancer Investigation, 2004. **22**(4): p. 604-619.

31. Bagshawe, K.D., S.K. Sharma, and R.H.J. Begent, *Antibody-directed enzyme prodrug therapy for cancer.* Expert Opinion on Biological Therapy, 2004. **4**(11): p. 1777-1789.

32. Silva, A.T.D., et al., *Advances in prodrug design.* Mini-Reviews in Medicinal Chemistry, 2005. **5**(10): p. 893-914.

33. Xu, G. and H.L. McLeod, *Strategies for enzyme/prodrug cancer therapy.* Clin Cancer Res, 2001. **7**(11): p. 3314-3324.

34. Sherwood, R.F., *Advanced drug delivery reviews: enzyme prodrug therapy.* Advanced Drug Delivery Reviews, 1996. **22**(3): p. 269-288.

35. Kan, O., S. Kingsman, and S. Naylor, *Cytochrome P450-based cancer gene therapy: current status.* Expert Opinion on Biological Therapy, 2002. **8**(2): p. 857-868.

36. Doherty, M.M. and M. Michael, *Tumoral drug metabolism: Perspectives and therapeutic implications.* Current Drug Metabolism, 2003. **4**(2): p. 131-149.

37. Michael, M. and M.M. Doherty, *Tumoral drug metabolism: Overview and its implications for cancer therapy.* Journal of Clinical Oncology, 2005. **23**(1): p. 205-229.

38. Rendic, S., *Summary of information on human CYP enzymes: Human P450 metabolism data.* Drug Metabolism Reviews, 2002. **34**(1-2): p. 83-448.

39. Rooney, P.H., et al., *The role of cytochrome P450 in cytotoxic bioactivation: Future therapeutic directions.* Current Cancer Drug Targets, 2004. **4**(3): p. 257-265.

40. Omura, T., *Forty years of cytochrome P450.* Biochemical and Biophysical Research Communications, 1999. **266**(3): p. 690-698.

41. McFadyen, M.C.E., W.T. Melvin, and G.I. Murray, *Cytochrome P450 enzymes: Novel options for cancer therapeutics.* Molecular Cancer Therapeutics, 2004. **3**(3): p. 363-371.

42. Murray, G.I., *The role of cytochrome P450 in tumour development and progression and its potential in therapy.* Journal of Pathology, 2000. **192**(4): p. 419-426.

43. McFadyen, M.C., et al., *Cytochrome P450 CYP1B1 protein expression: A novel mechanism of anticancer drug resistance.* Biochemical Pharmacology, 2001. **62**(2): p. 207-12.

44. Scripture, C.D., A. Sparreboom, and W.D. Figg, *Modulation of cytochrome P450 activity: implications for cancer therapy.* Lancet Oncology, 2005. **6**(10): p. 780-789.

45. Patterson, L.H. and G.I. Murray, *Tumour cytochrome P450 and drug activation.* Current Pharmaceutical Design, 2002. **8**(15): p. 1335-1347.

46. Bradshaw, T.D., et al., *2-(4-aminophenyl)benzothiazoles: novel agents with selective profiles of in vitro anti-tumour activity.* British Journal of Cancer, 1998. **77**(5): p. 745-752.

47. Bradshaw, T.D., et al., *In vitro evaluation of amino acid prodrugs of novel antitumour 2-(4-amino-3-methylphenyl)benzothiazoles.* British Journal of Cancer, 2002. **86**(8): p. 1348-1354.

48. Downie, D., et al., *Pharmacogenomics of cytochrome P450 enzymes in tumours.* Current Pharmacogenomics, 2004. **2**(3): p. 243-254.

49. Bradshaw, T.D. and A.D. Westwell, *The development of the antitumour benzothiazole prodrug, Phortress, as a clinical candidate.* Current Medicinal Chemistry, 2004. **11**(8): p. 1009-1021.

50. Raleigh, S.M., et al., *Involvement of human cytochromes P450 (CYP) in the reductive metabolism of AQ4N, a hypoxia activated anthraquinone DI-N-oxide prodrug.* International Journal of Radiation Oncology*Biology*Physics, 1998. **42**(4): p. 763-767.

51. Patterson, L.H. and S.R. McKeown, *AQ4N: a new approach to hypoxia-activated cancer chemotherapy.* British Journal of Cancer, 2000. **83**(12): p. 1589-1593.

52. Roy, P. and D.J. Waxman, *Activation of oxazaphosphorines by cytochrome P450: Application to gene-directed enzyme prodrug therapy for cancer.* Toxicology in Vitro, 2006. **20**(2): p. 176-186.

53. Maecker, B., et al., *The shared tumor-associated antigen cytochrome P450 1B1 is recognized by specific cytotoxic T cells.* Blood, 2003. **102**(9): p. 3287-3294.

54. McFadyen, M.C.E. and G.I. Murray, *Cytochrome P450 1B1: a novel anticancer therapeutic target.* Future Oncology, 2005. **1**(2): p. 259-263.

55. Sutter, T.R., et al., *Complete Cdna sequence of a human dioxin-inducible messenger- rna identifies a new gene subfamily of cytochrome-P450 that maps to chromosome-2.* Journal of Biological Chemistry, 1994. **269**(18): p. 13092-13099.

56. Shimada, T., et al., *Metabolic activation of polycyclic aromatic hydrocarbons and other procarcinogens by cytochromes P450 1A1 and P450 1B1 allelic variants and other human cytochromes P450 in Salmonella typhimurium NM2009.* Drug Metabolism and Disposition, 2001. **29**(9): p. 1176-1182.

57. Tang, Y.M., et al., *Development of an antipeptide antibody that binds to the C-terminal region of human CYP1B1.* Drug Metabolism and Disposition, 1999. **27**(2): p. 274-280.

58. Tang, Y.M., et al., *Human CYP1B1 Leu432Val gene polymorphism: Ethnic distribution in African-Americans, Caucasians and Chinese; oestradiol hydroxylase activity; and distribution in prostate cancer cases and controls.* Pharmacogenetics, 2000. **10**(9): p. 761-766.

59. Muskhelishvili, L., et al., *In situ hybridization and immunohistochemical analysis of cytochrome P4501B1 expression in human normal tissues.* Journal of Histochemistry & Cytochemistry, 2001. **49**(2): p. 229-236.

60. Cheung, Y.L., et al., *Differential expression of CYP1A1, CYP1A2, CYP1B1 in human kidney tumours.* Cancer Letters, 1999. **139**(2): p. 199-205.

61. Spivack, S.D., et al., *CYP1B1 expression in human lung.* Drug Metabolism and Disposition, 2001. **29**(6): p. 916-922.

62. Rieder, C.R.M., et al., *Human brain cytochrome P4501B1: immunohistochemical localization in human temporal lobe and induction by dimethylbenz(a)anthracene in astrocytoma cell line (MOG-G-CCM).* Neuroscience Letters, 2000. **278**(3): p. 177-180.

63. Huang, Z., et al., *Expression of cytochromes P450 in human breast tissue and tumors.* Drug Metabolism and Disposition, 1996. **24**: p. 899-905.

64. Hakkola, J., et al., *Expression of CYP1B1 in human adult and fetal tissues and differential inducibility of CYP1B1 and CYP1A1 by Ah receptor ligands in human placenta and cultured cells.* Carcinogenesis, 1997. **18**: p. 391-7.

65. Zhang, Q.Y., et al., *Characterization of human small intestinal cytochromes P450.* Drug Metabolism and Disposition, 1999. **27**(7): p. 804-9.

66. Chang, T.K.H., et al., *Real-time polymerase chain reaction analysis of CYP1B1 gene expression in human liver.* Toxicological Sciences, 2003. **71**(1): p. 11-19.

67. Shehin, S.E., R.O. Stephenson, and W.F. Greenlee, *Transcriptional regulation of the human CYP1B1 gene: Evidence for involvement of an aryl hydrocarbon receptor response element in constitutive expression.* Journal of Biological Chemistry, 2000. **275**(10): p. 6770-6.

68. Murray, G.I., et al., *Tumor-specific expression of cytochrome P450 CYP1B1.* Cancer Research, 1997. **57**: p. 3026-31.

69. McFadyen, M.C., et al., *Immunohistochemical localization of cytochrome P450 CYP1B1 in breast cancer with monoclonal antibodies specific for CYP1B1.* Journal of Histochemistry & Cytochemistry, 1999. **47**: p. 1457-64.

70. McFadyen, M.C.E., et al., *Cytochrome P450 CYP1B1 overexpression in primary and metastatic ovarian cancer.* British Journal of Cancer, 2001. **85**(2): p. 242-246.

71. Murray, G.I., et al., *Regulation, function, and tissue-specific expression of cytochrome P450 CYP1B1.* Annual Review of Pharmacology and Toxicology, 2001. **41**: p. 297-316.

72. Gibson, P., et al., *Cytochrome P450 1B1 (CYP1B1) is overexpressed in human colon adenocarcinomas relative to normal colon: Implications for drug development.* Molecular Cancer Therapeutics, 2003. **2**(6): p. 527-534.

73. McKay, J.A., et al., *Expression of cytochrome P450 CYP1B1 in breast cancer.* Febs Letters, 1995. **374**(2): p. 270-2.

74. Carnell, D.M., et al., *Target validation of cytochrome P450 CYP1B1 in prostate carcinoma with protein expression in associated hyperplastic and premalignant tissue.* International Journal of Radiation Oncology*Biology*Physics, 2004. **58**(2): p. 500-509.

75. Edwards, R.J., et al., *Development of a comprehensive panel of antibodies against the major xenobiotic metabolising forms of cytochrome P450 in humans.* Biochemical Pharmacology, 1998. **56**(3): p. 377-387.

76. Stanley, L.A., et al., *CYP1B1 expression in human cevical abnormalities.* Drug Metabolism Reviews, 2001. **33**(Suppl.1): p. 77.

77. Stanley, L.A., et al., *Cytochrome P450 CYP1B1 in colon tumorigenesis.* Drug Metabolism Reviews, 2001. **33**(Suppl.1): p. 62.

78. Sheibani, N., et al., *CYP1B1 deficient mice exhibit reduced retinal vascular density and fail to respond to hypoxia-induced neovascularization.* ARVO Meeting Abstracts, 2003. 44(5): p. 2893.

79. Chan, W.K., et al., *Cross-talk between the Aryl Hydrocarbon Receptor and Hypoxia Inducible Factor Signaling Pathways.* J. Biol. Chem., 1999. **274**(17): p. 12115-12123.

80. Shimada, T., et al., *Oxidation of xenobiotics by recombinant human cytochrome P450 1B1.* Drug Metabolism and Disposition, 1997. **25**(5): p. 617-622.

81. Potter, G.A., et al., *The cancer preventative agent resveratrol is converted to the anticancer agent piceatannol by the cytochrome P450 enzyme CYP1B1.* British Journal of Cancer, 2002. **86**(5): p. 774-778.

82. Sesardic, D., et al., *Differential expression and regulation of members of the cytochrome-P450ia gene subfamily in human tissues.* Carcinogenesis, 1990. **11**(7): p. 1183-1188.

83. McKay, J.A., et al., *Xenobiotic metabolizing enzyme expression in colonic neoplasia.* Gut, 1993. **34**(9): p. 1234-1239.

84. Murray, G.I., et al., *Expression of xenobiotic metabolizing enzymes in breast cancer.* Journal of Pathology, 1993. **169**(3): p. 347-353.

85. Kim, J.H., et al., *Expression of cytochromes P450 1A1 and 1B1 in human lung from smokers, non-smokers, and ex-smokers.* Toxicology and Applied Pharmacology, 2004. **199**(3): p. 210-219.

86. Anttila, S., et al., *Smoking and peripheral type of cancer are related to high levels of pulmonary cytochrome P450IA in lung cancer patients.* International Journal of Cancer, 1991. **47**(5): p. 681-685.

87. Anttila, S., et al., *Immunohistochemical detection of pulmonary cytochrome P450IA and metabolic activities associated with P450IA1 and P450IA2 isozymes in lung cancer patients.* Environmental Health Perspectives, 1992. **98**: p. 179-182.

88. Beresford, A.P., *CYP1A1: Friend or foe?* Drug Metabolism Reviews, 1993. **25**: p. 503-17.

89. Doostdar, H., M.D. Burke, and R.T. Mayer, *Bioflavonoids: Selective substrates and inhibitors for cytochrome P450 CYP1A and CYP1B1.* Toxicology, 2000. **144**(1-3): p. 31-38.

90. Potter, G.A., et al., *Hydroxylation activated prodrugs for cancer chemotherapy.* PCT International Applications, 1999. **WO99/40056**.

91. Ciolino, H.P., C.J. MacDonald, and G.C. Yeh, *Inhibition of carcinogen-activating enzymes by 16 alpha-fluoro- 5-androsten-17-one.* Cancer Research, 2002. **62**(13): p. 3685-3690.

92. Rochat, B., et al., *Human CYP1B1 and anticancer agent metabolism: Mechanism for tumor-specific drug inactivation?* Journal of Pharmacology and Experimental Therapeutics, 2001. **296**(2): p. 537-41.

93. Tsuchiya, Y., M. Nakajima, and T. Yokoi, *Cytochrome P450-mediated metabolism of estrogens and its regulation in human.* Cancer Letters, 2005. **227**(2): p. 115-124.

94. Zhu, B.T. and A.H. Conney, *Functional role of estrogen metabolism in target cells: review and perspectives.* Carcinogenesis, 1998. **19**(1): p. 1-27.

95. Zhu, B.T., et al., *Conversion of estrone to 2- and 4-hydroxyestrone by hamster kidney and liver microsomes: implications for the mechanism of estrogen-induced carcinogenesis.* Endocrinology, 1994. **135**(5): p. 1772-1779.

96. Li, J.J. and S.A. Li, *Estrogen carcinogenesis in syrian-hamster tissues - role of metabolism.* Federation Proceedings, 1987. **46**(5): p. 1858-1863.

97. Spink, D.C., et al., *Induction of cytochrome P450 1B1 and catechol estrogen metabolism in ACHN human renal adenocarcinoma cells.* Journal of Steroid Biochemistry and Molecular Biology, 1997. **62**(2/3): p. 223-232.

98. Hayes, C.L., et al., *17β-Estradiol hydroxylation catalyzed by human cytochrome P450 1B1.* Proceedings of the National Academy of Sciences of the USA, 1996. **93**: p. 9776-81.

99. Potter, G.A. and R. McCague, *Highly stereoselective access to an (E)-vinyl bromide from an aryl ketone leads to short syntheses of (Z)-Tamoxifen and important substituted derivatives.* Journal of Organic Chemistry, 1990. **55**(25): p. 6184-6187.

100. Coombes, R.C., et al., *Idoxifene: Report of a phase I study in patients with metastatic breast cancer.* Cancer Research, 1995. **55**(5): p. 1070-1074.

101. Jang, M., et al., *Cancer chemopreventive activity of resveratrol, a natural product derived from grapes.* Science, 1997. **275**(5297): p. 218-220.

102. Geahlen, R.L. and J.L. McLaughlin, *Piceatannol (3,4,3',5'-Tetrahydroxy-Trans-Stilbene) is a naturally-occurring protein tyrosine kinase inhibitor.* Biochemical and Biophysical Research Communications, 1989. **165**(1): p. 241-245.

103. Wilsher, N.E., *CYP1B1 bioactivation of novel anticancer prodrugs and related natural products*, in *Pharmacy*. 2003, De Montfort University: Leicester.

104. Gazit, A., et al., *Tyrphostins .1. Synthesis and biological activity of protein tyrosine kinase inhibitors.* Journal of Medicinal Chemistry, 1989. **32**(10): p. 2344-2352.

105. Cushman, M., et al., *Synthesis and evaluation of stilbene and dihydrostilbene derivatives as potential anticancer agents that inhibit tubulin polymerization.* Journal of Medicinal Chemistry, 1991. **34**(8): p. 2579-2588.

106. Dark, G.G., et al., *Combretastatin A-4, an agent that displays potent and selective toxicity toward tumor vasculature.* Cancer Res, 1997. **57**(10): p. 1829-1834.

107. Hsieh, H.P., J.P. Liou, and N. Mahindroo, *Pharmaceutical design of antimitotic agents based on combretastatins.* Current Pharmaceutical Design, 2005. **11**(13): p. 1655-1677.

108. El-Zayat, A.A.E., et al., *In vitro evaluation of the antineoplastic activity of Combretastatin A4, a natural product from Combretum caffrum (arid shrub).* Anti-Cancer Drugs, 1993. **4**(1): p. 19-25.

109. Lin, C.M., et al., *Interactions of tubulin with potent natural and synthetic analogs of the antimitotic agent Combretastatin: A structure-activity study.* Molecular Pharmacology, 1988. **34**(2): p. 200-208.

110. Bibby, M.C., *Combretastatin anticancer drugs.* Drugs of the Future, 2002. **27**(5): p. 475-480.

111. Pettit, G.R., et al., *Antineoplastic Agents .145. Isolation and structure of the strong cell-growth and tubulin inhibitor combretastatin-A-4.* Experientia, 1989. **45**(2): p. 209-211.

112. Potter, G.A., et al., *DMU212: A novel CYP1B1 activated anticancer prodrug.* British Journal of Cancer, 2002. **86**: p. S117.

113. Ducki, S., et al., *Potent antimitotic and cell growth inhibitory properties of substituted chalcones.* Bioorganic & Medicinal Chemistry Letters, 1998. **8**(9): p. 1051-1056.

114. Lawrence, N.J., et al., *The interaction of chalcones with tubulin.* Anti-Cancer Drug Design, 2000. **15**(2): p. 135-141.

115. Lawrence, N.J., et al., *The synthesis of indanones related to combretastatin A-4 via microwave-assisted Nazarov cyclization of chalcones.* Tetrahedron Letters, 2006. **47**(10): p. 1637-1640.

116. Dimmock, J.R., et al., *Bioactivities of chalcones.* Current Medicinal Chemistry, 1999. **6**(12): p. 1125-1149.

117. Hadfield, J.A., et al., *Tubulin and microtubules as targets for anticancer drugs.* Progress in Cell Cycle Research, ed. D. Fabbro. Vol. 5. 2003. 309-25.

118. Potter, G.A. and P.C. Butler, *3,4-Methylenedioxy chalcones (DMU-135).* British Patent Appl., 2001. **GB 0123777.**

119. Butler, P.C., et al., *DMU135: A CYP1B1 activated tyrosine kinase inhibitor prodrug with tumour selective activity.* British Journal of Cancer, 2003. **87**: p. S33.

120. Gardner, C.R., et al., *Application of high throughput technologies to drug substance and drug product development.* Computers & Chemical Engineering, 2004. **28**(6-7): p. 943-953.

121. Gribbon, P. and S. Andreas, *High-throughput drug discovery: What can we expect from HTS?* Drug Discovery Today, 2005. **10**(1): p. 17-22.

122. Balbach, S. and C. Korn, *Pharmaceutical evaluation of early development candidates "the 100 mg-approach".* International Journal of Pharmaceutics, 2004. **275**(1-2): p. 1-12.

123. Almarsson, O. and C.R. Gardner, *Novel approaches to issues of developability.* Drug Discovery Today, 2003: p. 21-26.

124. Helen Chan, O. and B.H. Stewart, *Physicochemical and drug-delivery considerations for oral drug bioavailability.* Drug Discovery Today, 1996. 1(11): p. 461-473.

125. Kerns, E.H., *High throughput physicochemical profiling for drug discovery.* Journal of Pharmaceutical Sciences, 2001. **90**(11): p. 1838-1858.

126. Kerns, E.H. and L. Di, *Pharmaceutical profiling in drug discovery.* Drug Discovery Today, 2003. **8**(7): p. 316-323.

127. Kerns, E.H. and L. Di, *Physicochemical profiling: overview of the screens.* Drug Discovery Today: Technologies, 2004. **1**(4): p. 343-348.

128. Pettit, G.R., et al., *Antineoplastic agents-322 - Synthesis of combretastatin A-4 prodrugs.* Anti-Cancer Drug Design, 1995. **10**(4): p. 299-309.

129. Matsuda, H., et al., *Anti-allergic activity of stilbenes from Korean rhubarb (Rheum undulatum L.): structure requirements for inhibition of antigen-induced degranulation and their effects on the release of TNF-[alpha] and IL-4 in RBL-2H3 cells.* Bioorganic & Medicinal Chemistry, 2004. **12**(18): p. 4871-4876.

130. Gusman, J., H. Malonne, and G. Atassi, *A reappraisal of the potential chemopreventive and chemotherapeutic properties of resveratrol.* Carcinogenesis, 2001. **22**(8): p. 1111-1117.

131. Spink, D.C., et al., *Differential expression of CYP1A1 and CYP1B1 in human breast epithelial cells and breast tumor cells.* Carcinogenesis, 1998. **19**(2): p. 291-8.

132. Gordon, L.A., et al., *Breast cell invasive potential relates to the myoepithelial phenotype.* International Journal of Cancer, 2003. **106**(1): p. 8-16.

133. Collection, A.T.C., *http://www.atcc.org/*. 2003.

134. Mosmann, T., *Rapid colorimetric assay for cellular growth and survival: Application to proliferation and cytotoxicity assays.* Journal of Immunological Methods, 1983. **65**(1-2): p. 55-63.

135. Lu, J.B., et al., *Resveratrol analog, 3,4,5,4'-tetrahydroxystilbene, differentially induces pro-apoptotic p53/Bax gene expression and inhibits the growth of transformed cells but not their normal counterparts.* Carcinogenesis, 2001. **22**(2): p. 321-328.

136. Gosslau, A., et al., *A methoxy derivative of resveratrol analogue selectively induced activation of the mitochondrial apoptotic pathway in transformed fibroblasts.* British Journal of Cancer, 2005. **92**(3): p. 513-521.

137. Sale, S., et al., *Pharmacokinetics in mice and growth-inhibitory properties of the putative cancer chemopreventive agent resveratrol and the synthetic analogue trans 3,4,5,4 '-tetramethoxystilbene.* British Journal of Cancer, 2004. **90**(3): p. 736-744.

138. Sale, S., et al., *Comparison of the effects of the chemopreventive agent resveratrol and its synthetic analog trans 3,4,5,4 '-tetramethoxystilbene (DMU-212) on adenoma development in the Apc(Min+) mouse and cyclooxygenase-2 in human-derived colon cancer cells.* International Journal of Cancer, 2005. **115**(2): p. 194-201.

139. Anto, R.J., et al., *Anticancer and antioxidant activity of synthetic chalcones and related compounds.* Cancer Letters, 1995. 97(1): p. 33-37.

140. Le Bail, J., et al., *Chalcones are potent inhibitors of aromatase and 17[beta]-hydroxysteroid dehydrogenase activities.* Life Sciences, 2001. 68(7): p. 751-761.

141. Gibson, P., et al., *Bioavailability of novel anticancer chalcones in nude mice bearing xenografts.* British Journal of Cancer, 2003. 88: p. S27-S27.

142. Sale, S., et al., *Effects of the potential chemopreventive agent DMU-135 on adenoma development in the Apc$^{Min/+}$ mouse.* Investigational New Drugs, 2006.

143. Griffin, J.P. and J.G. O'Grady, *Pharmaceutical development*, in *Textbook of Pharmaceutical Medicine.* 2002, BMJ Books. p. 96-127.

144. Wells, J.I., *Pharmaceutical preformulation : the physicochemical properties of drug substances*. Pharmaceutical Technology. 1988, Chichester: Ellis Horwood.

145. van de Waterbeemd, H., *The fundamental variables of the biopharmaceutics classification system: a commentary.* European Journal of Pharmaceutical Sciences, 1998. 7(1): p. 1-3.

146. Wong, K.S., J. Kenseth, and R. Strasburg, *Validation and long-term assessment of an approach for the high throughput determination of lipophilicity (log P-OW) values using multiplexed, absorbance-based capillary electrophoresis.* Journal of Pharmaceutical Sciences, 2004. 93(4): p. 916-931.

147. Aulton, M.E., *Pharmaceutics: The science of dosage form design*. Second ed. 2002, London: Churchill Livingstone.

148. *Pharmaceutical technical information: Pharmasolve (N-Methyl-2-Pyrrolidone) code: PHARMSOLV/1000.* 2000, International Speciality Products.

149. Dehring, K.A., et al., *Automated robotic liquid handling/laser-based nephelometry system for high throughput measurement of kinetic aqueous solubility.* Journal of Pharmaceutical and Biomedical Analysis, 2004. 36(3): p. 447-456.

150. Glomme, A., J. Marz, and J.B. Dressman, *Comparison of a miniaturized shake-flask solubility method with automated potentiometric acid/base titrations and calculated solubilities.* Journal of Pharmaceutical Sciences, 2005. 94(1): p. 1-16.

151. Lipinski, C.A., et al., *Experimental and computational approaches to estimate solubility and permeability in drug discovery and development settings.* Advanced Drug Delivery Reviews, 1997. 23(1-3 SU): p. 3-25.

152. Bevan, C.D. and R.S. Lloyd, *A High-Throughput Screening Method for the Determination of Aqueous Drug Solubility Using Laser Nephelometry in Microtiter Plates.* Anal. Chem., 2000. 72(8): p. 1781-1787.

153. Avdeef, A., K. Tsinman, and O. Tsinman, *Solubility for today's chemist's needs: From discovery to preformulation*, www.pion-inc.com, 2004.

154. Huang, L. and W.Q. Tong, *Impact of solid state properties on developability assessment of drug candidates.* Advanced Drug Delivery Reviews, 2004. **56**(3): p. 321-334.

155. Chait, A., *Discovery ADMET profiling: solubility techniques*, in *Bioscience Technology*. 2003. **5**: p. 33-34.

156. Roy, D., et al., *Determination of the aqueous solubility of drugs using a convenient 96-well plate-based assay.* Drug Development and Industrial Pharmacy, 2001. **27**(1): p. 107-109.

157. Hansch, C. and T. Fujita, *ρ–σ–π Analysis. A method for the correlation of biological activity and chemical structure.* Journal of the American Chemical Society, 1964. **86**: p. 1616-26.

158. Florence, A.T. and D. Attwood, *Physicochemical principles of pharmacy*. Third ed. 1998, Basingstoke: Macmillan,.

159. Hitzel, L., A.P. Watt, and K.L. Locker, *An increased throughput method for the determination of partition coefficients.* Pharmaceutical Research, 2000. **17**(11): p. 1389-1395.

160. Buchwald, P. and N. Bodor, *Octanol-water partition: Searching for predictive models.* Current Medicinal Chemistry, 1998. **5**(5): p. 353-380.

161. Ahuja, S. and S. Scypinski, *Handbook of modern pharmaceutical analysis.* Separation science and technology, ed. S. Ahuja. Vol. 3. 2001, USA: Academic press. 566.

162. Lee, D.C. and M. Webb, *Pharmaceutical analysis*. Analytical Chemistry Series, ed. J.M. Chalmers and A.J. Handley. 2003: Blackwell Publishing Ltd.

163. Casella, R., D.A. Williams, and S.S. Jambhekar, *Solid-state [beta]-cyclodextrin complexes containing indomethacin, ammonia and water. II. Solubility studies.* International Journal of Pharmaceutics, 1998. **165**(1): p. 15-22.

164. Barratt, M.D., *Quantitative structure-activity relationships for skin permeability.* Toxicology in Vitro, 1995. **9**(1): p. 27-37.

165. Hansch, C. and A.J. Leo, *Substituent constants for correlation analysis in chemistry and biology*. 1979, New York: Wiley Interscience.

166. Leo, A.J., *Calculating log Poct from structures.* Chemical Reviews, 1993. **93**(4): p. 1281-1306.

167. Larsen, M., et al., *Conformationally restricted anti-plasmodial chalcones.* Bioorganic & Medicinal Chemistry Letters, 2005. **15**(21): p. 4858-4861.

168. DeMario, M.D. and M.J. Ratain, *Oral chemotherapy: rationale and future directions.* J Clin Oncol, 1998. **16**(7): p. 2557-2567.

169. Terwogt, J.M.M., et al., *Clinical pharmacology of anticancer agents in relation to formulations and administration routes.* Cancer Treatment Reviews, 1999. **25**(2): p. 83-101.

170. Allen, L.V., *Compounding capsules.* Secundum Artem. **4**(4):p. 1-6.

171. Cooper, J.W., *Powders and oral unit-dosage forms*, in *Title Cooper and Gunn's dispensing for pharmaceutical students*, S.J. Carter, Editor. 1975, Publisher Tunbridge Wells (etc.) : Pitman Medical.

172. Banakar, U.V., *Pharmaceutical dissolution testing*. Drugs and the pharmaceutical sciences, ed. J. Swarbrick. Vol. 49. 1991, New York: Marcel Dekker.

173. Hirayama, F. and K. Uekama, *Cyclodextrin-based controlled drug release system.* Advanced Drug Delivery Reviews, 1999. **36**(1 SU -): p. 125-141.

174. Ridgway, K., *Hard capsules : development and technology*. 1987, London: Pharmaceutical Press.

175. Great Britain, M.C., *British pharmacopoeia*. Vol. IV. 2003, London: HMSO.

176. Noyes, A.A. and W.R. Whitney, *The rate of solution of solid substances in their own solutions.* Journal of the American Chemical Society, 1897. **19**: p. 930–934.

177. Rohrs, B.R., *Dissolution method development for poorly soluble compounds.* Dissolution Technologies, 2001. **8**(3): p. 1-5.

178. FDA, *Guidance for industry: Dissolution testing of immediate release solid oral dosage forms*. 1997.

179. Noory, C., et al., *Steps for development of a dissolution test for sparingly water-soluble drug products.* Dissolution Technologies, 2000. **7**(1): p. 16-19.

180. Shah, V.P., et al., *In vitro dissolution of sparingly water-soluble drug dosage forms.* International Journal of Pharmaceutics, 1995. **125**(1): p. 99-106.

181. Brown, C.K., et al., *Acceptable analytical practices for dissolution testing of poorly soluble compounds.* Dissolution Technologies, 2005. **12**(4): p. 6-12.

182. Potter, G.A., et al., *Oscillating crystallization of (+) and (-) enantiomers during resolution by entrainment of 2-azabicyclo[2.2.1]hept-5-en-3-one.* Angewandte Chemie-International Edition in English, 1996. **35**(15): p. 1666-1668.

183. Luner, P.E. and D. VanDer Kamp, *Wetting characteristics of media emulating gastric fluids.* International Journal of Pharmaceutics, 2001. **212**(1): p. 81-91.

184. Sjokvist, E., C. Nystrom, and M. Alden, *Physicochemical aspects of drug release. XIII. The effect of sodium dodecyl sulphate additions on the structure and dissolution of a drug in solid dispersions.* International Journal of Pharmaceutics, 1991. **69**(1): p. 53-62.

185. Goette, D.K., *Topical chemotherapy with 5-Fluorouracil - a review.* Journal of the American Academy of Dermatology, 1981. 4(6): p. 633-649.

186. Williams, A.C., *Transdermal and topical drug delivery*. 2003, London: Pharmaceutical press.

187. Gupta, P. and S. Garg, *Recent advances in semisolid dosage forms for dermatological application.* Pharmaceutical Technology, 2002. p. 144-162.

188. Barry, B.W., *Dermatological formulations: Percutaneous absorption.* Drugs and the pharmaceutical sciences, ed. J. Swarbrick. Vol. 18. 1983, New York: Marcel Dekker Inc.

189. Allen, L.V., *Compounding topical dosage forms: ointments, creams, pastes and lotions.* Secundum Artem. **3**(2): p. 1-6.

190. Lopez, R.F.V., et al., *Photodynamic therapy of skin cancer: controlled drug delivery of 5-ALA and its esters.* Advanced Drug Delivery Reviews, 2004. **56**(1): p. 77-94.

191. Osborne, D.W. and A.H. Amann, *Topical drugs delivery formulations.* Drugs and the pharmaceutical sciences, ed. J. Swarbrick. Vol. 42. 1990, New York: Marcel Dekker.

192. Higuchi, T., *Physical chemical analysis of percutaneous absorption process from creams and ointments.* Journal of the Society of Cosmetic Chemists, 1960. **11**: p. 85-97.

193. Higuchi, T., *Analysis of data on medicament release from ointments.* Journal of Pharmaceutical Sciences, 1962. **51**: p. 802–804.

194. Poulsen, B.J., et al., *Effect of topical vehicle composition on the in vitro release of fluocinolone acetonide and its acetate esters.* Journal of Pharmaceutical Sciences, 1968. **57**(6): p. 928-933.

195. Rege, P.R., V.D. Vilivalam, and C.C. Collins, *Development in release testing of topical dosage forms: use of the Enhancer Cell(TM) with automated sampling.* Journal of Pharmaceutical and Biomedical Analysis, 1998. **17**(8): p. 1225-1233.

196. Hadgraft, J. and J.R. Guy, *Transdermal drug delivery: Developmental issues and research initiatives.* Drugs and the pharmaceutical sciences, ed. J. Swarbrick. Vol. 35. 1989, New York: Marcel Dekker Inc.

197. Shah, V.P., J.S. Elkins, and R.L. Williams, *Evaluation of the test system used for in vitro release of drugs for topical dermatological drug products.* Pharmaceutical Development and Technology, 1999. 4(3): p. 377-385.

198. Shah, V.P. and J.S. Elkins, *In vitro release from corticosteroid ointments.* Journal of Pharmaceutical Sciences, 1995. **84**(9): p. 1139-1140.

199. Shah, V.P., et al., *Determination of in vitro drug release from hydrocortisone creams.* International Journal of Pharmaceutics, 1989. **53**(1): p. 53-59.

200. Zatz, J.L., *Drug-Release from Semisolids - Effect of Membrane-Permeability on Sensitivity to Product Parameters.* Pharmaceutical Research, 1995. **12**(5): p. 787-789.

201. Zatz, J.L. and J.D. Segers, *Techniques for measuring in vitro release from semisolids.* Dissolution Technologies, 1998. **5**(1): p. 5-17.

202. Siewert, M., et al., *FIP/AAPS guidelines for dissolution/in vitro release testing of novel/special dosage froms.* Dissolution Technologies, 2003. **10**(1): p. 6-15.

203. FDA, *Guidance for industry: Nonsterile semisolid dosage forms. Scale-up and postapproval changes: chemistry, manufacturing and controls; In vitro release testing and in vivo bioequivalence documentation.* 1997.

204. Corbo, M., *Techniques for conducting in vitro release studies on semisolids formulations.* Dissolution Technologies, 1995. **2**(1): p. 3-6.

205. Sanghvi, P.P. and C.C. Collins, *Comparison of Diffusion Studies of Hydrocortisone between the Franz Cell and the Enhancer Cell.* Drug Development and Industrial Pharmacy, 1993. **19**(13): p. 1573-1585.

206. Fares, M. and J.L. Zatz, *Measurement of drug release from topical gels using two types of apparatus.* Pharmaceutical Technology, 1995. p. 52-58.

207. Refai, H. and C.C. Muller-Goymann, *Larvated incompatibilities of hydrocortisone cream preparations upon dilution with different cream bases.* Pharmazie, 1999. **54**(10): p. 754-758.

208. Shah, V.P., et al., *Invitro Release of Hydrocortisone from Topical Preparations and Automated Procedure.* Pharmaceutical Research, 1991. **8**(1): p. 55-59.

209. Guy, R.H. and J. Hadgraft, *Determination of Drug Release Rates from Topical Dosage Forms.* International Journal of Pharmaceutics, 1990. **60**(2): p. R1-R3.

210. Chang, Y.T., O.B. Stiffelman, and G.H. Loew, *Computer modeling of 3D structures of cytochrome P450s.* Biochimie, 1996. **78**(8-9): p. 771-779.

211. Williams, P.A., et al., *Mammalian microsomal cytochrome P450 monooxygenase: Structural adaptations for membrane binding and functional diversity.* Molecular Cell, 2000. **5**(1): p. 121-131.

212. Lewis, D.F.V., *Modelling human cytochromes P450 involved in drug metabolism from the CYP2C5 crystallographic template.* Journal of Inorganic Biochemistry, 2002. **91**(4): p. 502-514.

213. Rowland, P., et al., *Crystal structure of human cytochrome P450 2D6.* Journal of Biological Chemistry, 2006. **281**(11): p. 7614-7622.

214. Schoch, G.A., et al., *Structure of human microsomal cytochrome P4502C8 - Evidence for a peripheral fatty acid binding site.* Journal of Biological Chemistry, 2004. **279**(10): p. 9497-9503.

215. Yano, J.K., et al., *The structure of human microsomal cytochrome P450 3A4 determined by X-ray crystallography to 2.05-angstrom resolution.* Journal of Biological Chemistry, 2004. **279**(37): p. 38091-38094.

216. Kemp, C.A., J. Marechal, and M.J. Sutcliffe, *Progress in cytochrome P450 active site modeling.* Archives of Biochemistry and Biophysics, 2005. **433**(2): p. 361-368.

217. Lewis, D.F.V., et al., *Molecular modelling of human CYP1B1 substrate interactions and investigation of allelic variant effects on metabolism.* Chemico-Biological Interactions, 2003. **145**(3): p. 281-295.

218. Tan, H.L. and G.A. Potter, *Selective inhibitors of the cytochrome P450 enzyme CYP1B1*, in *School of Pharmacy*. 2006, De Montfort University: Leicester.

219. Dhar, D.N., *The chemistry of chalcones and related compounds*. 1981, New York: Wiley.

220. Forbes, R.T., P. York, and *J.R. Davidson, Dissolution kinetics and solubilities of p-aminosalicylic acid and its salts.* International Journal of Pharmaceutics, *1995.* **126**(1-2 SU): p. 199-208.

221. Heinrich Stahl, P. and C.G. Wermuth, *Handbook of pharmaceutical salts: Properties, selection, and use.* International Union of Pure and Applied Chemistry (IUPAC). 2002, Zurich: Wiley-VCH. 388.

222. Berge, S.M., L.D. Bighley, and D.C. Monkhouse, *Pharmaceutical salts.* Journal of Pharmaceutical Sciences, 1977. **66**(1 SU): p. 1-19.

223. Kramer, S.F. and G.L. Flynn, *Solubility of Organic Hydrochlorides.* Journal of Pharmaceutical Sciences, 1972. **61**(12): p. 1896-1904.

224. Tong, W.Q. and G. Whitesell, *In situ salt screening-a useful technique for discovery support and preformulation studies.* Pharmaceutical Development and Technology, 1998. **3**(2): p. 215-23.

225. Gould, P.L., *Salt selection for basic drugs.* International Journal of Pharmaceutics, 1986. **33**(1-3): p. 201-217.

226. Chaplin, D.A., et al., *Dynamic Diastereomeric Salt Resolution of Narwedine and its Transformation to (-)-Galanthamine.* Tetrahedron Letters, 1998. **39**(37): p. 6777-6780.

227. Wu, Z.M., et al., *Physicochernical characterization of ricobendazole: I. Solubility, lipophilicity, and ionization characteristics.* Journal of Pharmaceutical Sciences, 2005. **94**(5): p. 983-993.

228. Smith, A., et al., *Merck Index: An encyclopedia of chemicals, drugs, and biologicals*. 13th ed. 2001, New Jersey: John Wiley & Sons.

229. Kloog, Y. and A.D. Cox, *RAS inhibitors: potential for cancer therapeutics.* Molecular Medicine Today, 2000. **6**(10): p. 398-402.

230. Forlani, L., et al., *Reinvestigation of tautomerism of some substituted 2-hydroxypyridines.* ARKIVOC, 2002. **XI**: p. 198-215.

231. Bundgaard, H., *The double prodrug concept and its applications.* Advanced Drug Delivery Reviews, 1989. **3**(1): p. 39-65.

232. Top, S., et al., *Tamoxifen derivatives for delivery of the antitumoral (DACH)Pt group: Selective synthesis by McMurry coupling, and biochemical behaviour.* Chembiochem, 2003. **4**(8): p. 754-761.

233. Tyvorskii, V.I., et al., *Synthesis of 5-alkyl-4-amino-2-(trifluoromethyl)pyridines and their transformation into trifluoromethylated 1H-pyrazolo[4,3-c]pyridines.* Tetrahedron, 2001. **57**(10): p. 2051-2055.

234. Chen, X.Q., et al., *Discovery pharmaceutics - Challenges and opportunities.* Aaps Journal, 2006. **8**(2): p. E402-E408.

235. Lakings, D.B., *PROFILE: Developability: a science for lead candidate selection.* Pharmaceutical Science & Technology Today, 1998. **1**(6): p. 280-282.

Appendix

Table 83. Summary of compounds investigated or synthesized in this study.

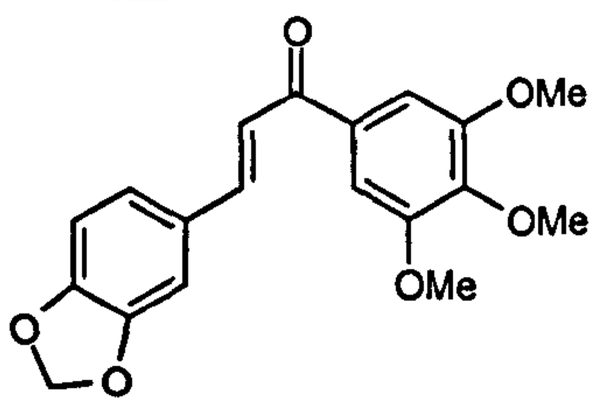

DMU135

3-Benzo[1,3]dioxol-5-yl-1-(3,4,5-trimethoxy-phenyl)-*propenone*

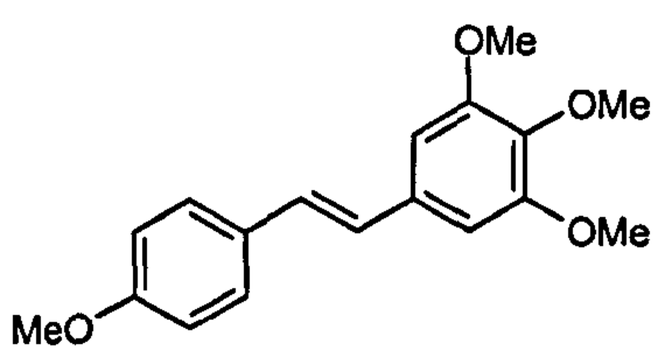

DMU212

trans 3,4,5,4'-tetramethoxystilbene

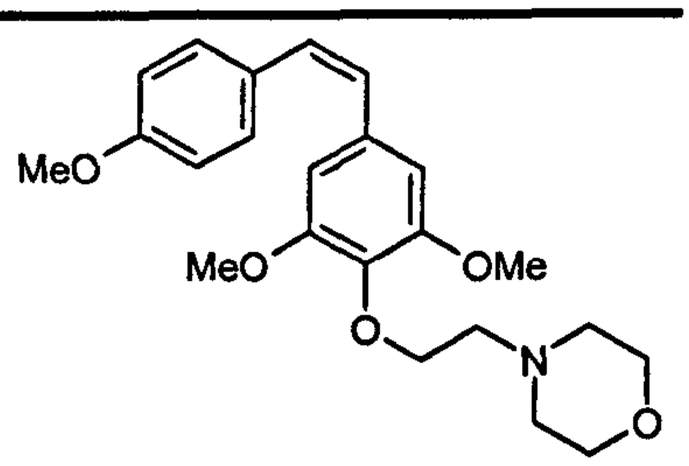

DMU590

4-(2-{2,6-Dimethoxy-4-[2-(4-methoxy-phenyl)-vinyl]-phenoxy}-ethyl)-morpholine

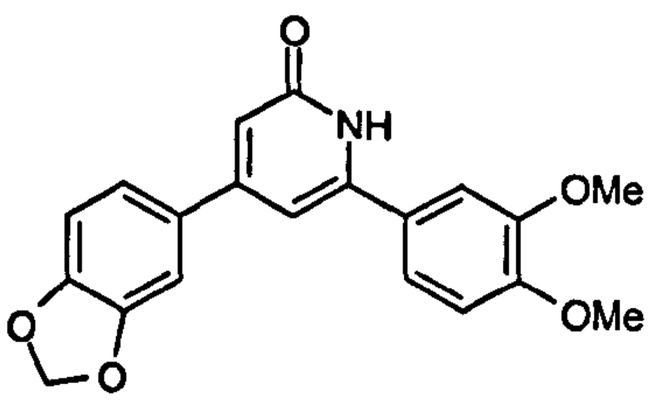

DMU949

4-Benzo[1,3]dioxol-5-yl-6-(3,4-dimethoxy-phenyl)-1H-pyridin-2-one

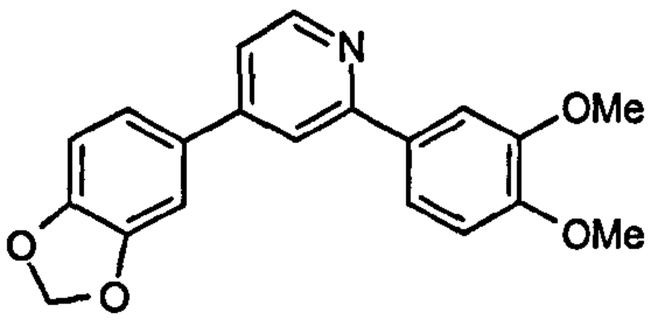

DMU982

4-Benzo[1,3]dioxol-5-yl-2-(3,4-dimethoxy-phenyl)-pyridine

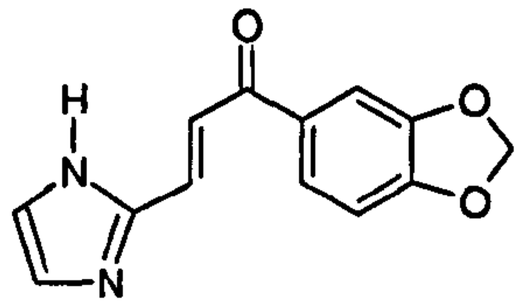

DMU2145

1-Benzo[1,3]dioxol-5-yl-3-(1H-imidazol-2-yl)-propenone

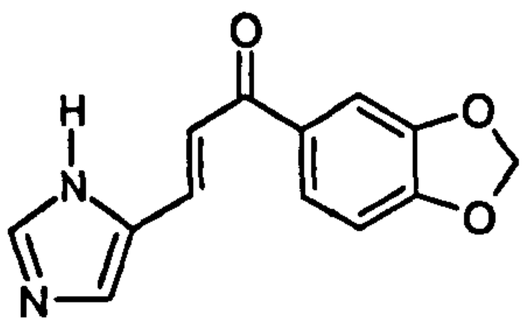

DMU2146

1-Benzo[1,3]dioxol-5-yl-3-(3H-imidazol-4-yl)-propenone

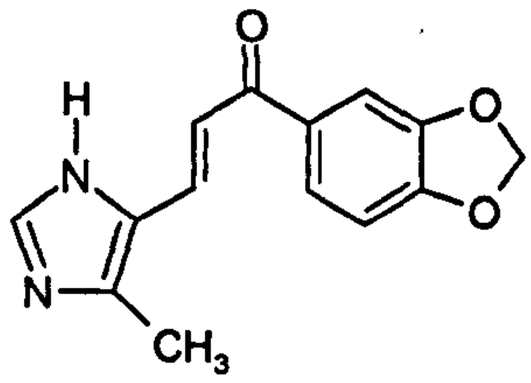

DMU2147

1-Benzo[1,3]dioxol-5-yl-3-(5-methyl-3H-imidazol-4-yl)-propenone

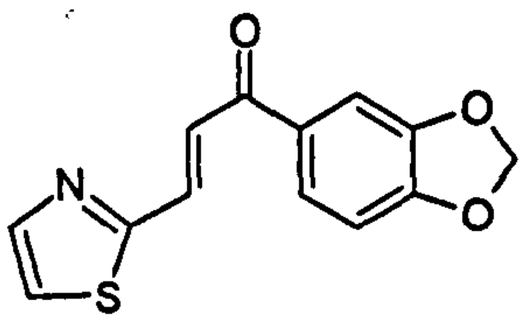

DMU2148

1-Benzo[1,3]dioxol-5-yl-3-thiazole-2-yl-propenone

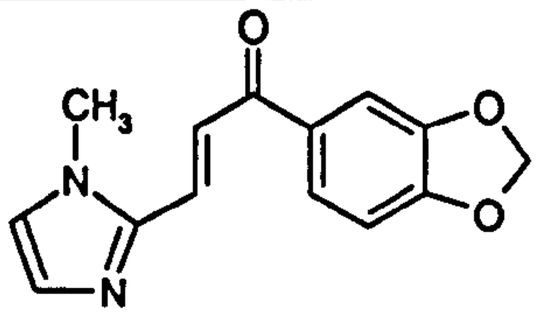

DMU2149

1-Benzo[1,3]dioxol-5-yl-3-(1-methyl-1H-imidazol-2-yl)-propenone

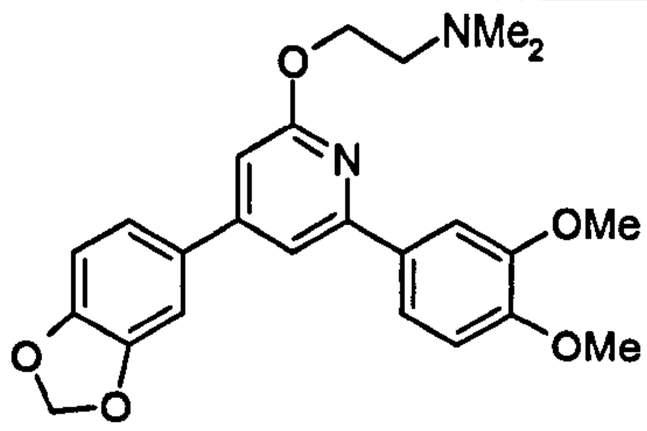

DMU2297

{2-[4-Benzo[1,3]dioxol-5-yl-6-(3,4-dimethoxy-phenyl)-pyridin-2-yloxy]-ethyl}-dimethyl-amine

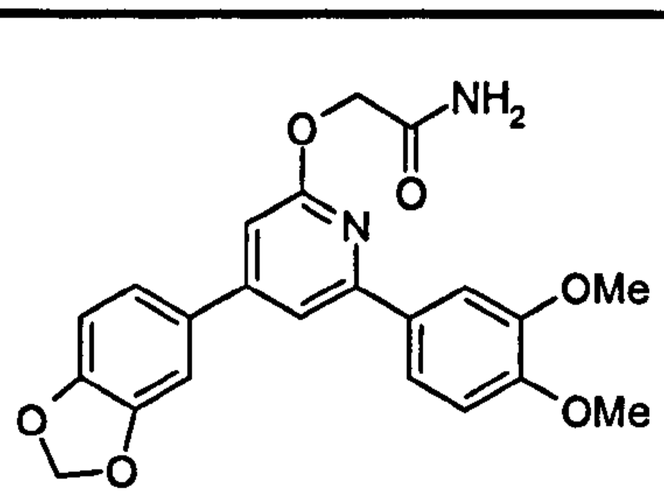

DMU2298

2-[4-Benzo[1,3]dioxol-5-yl-6-(3,4-dimethoxy-phenyl)-pyridin-2-yloxy]-acetamide

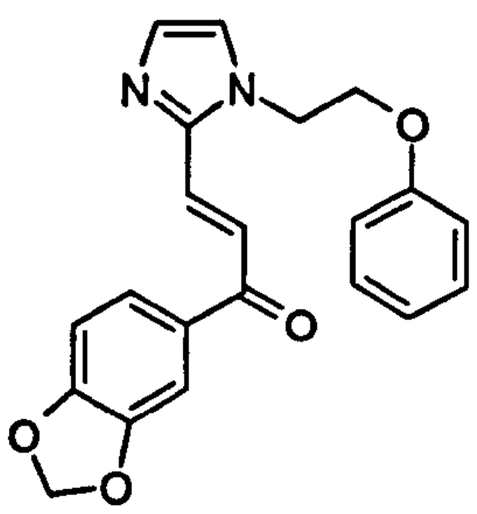

DMU2306

1-Benzo[1,3]dioxol-5-yl-3-[1-(2-phenoxy-ethyl)-1H-imidazol-2-yl)-propenone